Mathematical modelling and numerical simulation of elastic wave propagation in soft tissues with application to cardiac elastography

Federica Caforio

NNT : 2019SACLX001

THÈSE DE DOCTORAT

de

L'UNIVERSITÉ PARIS-SACLAY

École doctorale de mathématiques Hadamard (EDMH, ED 574)

Établissement d'inscription : Ecole polytechnique

Établissement d'accueil : Inria *Laboratoire d'accueil :* M3DISIM

Spécialité de doctorat : Mathématiques appliquées

Federica Caforio

Mathematical modelling and numerical simulation of elastic wave propagation in soft tissues with application to cardiac elastography

Date de soutenance : 24 Janvier 2019

Après avis des rapporteurs : XAVIER CLAEYS (Sorbonne Université)
BRUNO LOMBARD (CNRS)

Jury de soutenance :

ANNE-SOPHIE BONNET-BEN DHIA	(CNRS) President du jury
XAVIER CLAEYS	(Sorbonne Université) Rapporteur
BRUNO LOMBARD	(CNRS) Rapporteur
ALINE BEL-BRUNON	(INSA-Lyon) Examinateur
MATHIEU PERNOT	(INSERM) Examinateur
DOMINIQUE CHAPELLE	(Inria) Directeur de thèse
SÉBASTIEN IMPERIALE	(Inria) Codirecteur de thèse

Remerciements

Cette thèse a représenté pour moi une expérience inoubliable et très enrichissante, à la fois sur le plan professionnel et du point de vue personnel, car j'ai eu la chance d'être entourée par beaucoup de personnes merveilleuses que je souhaite remercier ici.

Mon premier remerciement va à mes deux encadrants de thèse. Je souhaite remercier profondément Sébastien Imperiale pour la confiance qu'il m'a accordée depuis le tout début, pour sa grande disponibilité et patience, et surtout pour m'avoir guidée et motivée dans ce parcours par son enthousiasme, sa rigueur et sa détermination. Travailler avec lui m'a permis d'évoluer sensiblement, et cela m'a stimulée à dépasser mes limites et analyser en profondeur les problèmes de différentes perspectives, dans la bonne humeur et dans la confiance qu'il m'a toujours distillée. Je souhaite aussi exprimer mes plus profonds remerciements à Dominique Chapelle, pour m'avoir tant apporté scientifiquement et m'avoir soutenue pendant ces années, avec une grande disponibilité et pédagogie. L'étendue de ses connaissances et sa capacité d'analyse et de compréhension profonde des problèmes seront toujours une grande source d'inspiration pour moi. Je me sens extrêmement honorée et fière d'avoir eu deux encadrants de thèse de cette valeur à mes côtés pendant ces années.

Je souhaite aussi remercier profondément Philippe Moireau pour m'avoir toujours soutenue et s'être intéressé aux différents sujets que j'ai abordés pendant la thèse avec grande énergie et passion, et en m'apportant de nombreux conseils et précieuses suggestions. En outre, j'ai eu l'opportunité de travailler avec lui pour divers aspects de la thèse (surtout liés aux applications cliniques et à l'implémentation), et cela a été très enrichissant et stimulant.

J'aimerais remercier vivement mes deux rapporteurs de thèse Bruno Lombard et Xavier Claeys, pour leur grande disponibilité et pour avoir lu avec beaucoup d'attention mon manuscrit. De plus, ils m'ont apporté de nombreux conseils qui m'ont permis d'améliorer le manuscrit. Je souhaite aussi remercier Anne-Sophie Bonnet-Ben Dhia pour avoir accepté de présider mon jury, et les autres membres du jury Aline Bel-Brunon et Mathieu Pernot. Ils ont dévoué un grand intérêt à mon travail de thèse, et cela a contribué à faire de ma soutenance de thèse une expérience très enrichissante et inoubliable.

Parmi les enjeux de cette thèse, ce qui m'a intrigué du début était l'aspect intrinsèquement multidisciplinaire et varié du problème à étudier. Cela m'a permis d'apprendre tous les jours dans différents domaines grâce à l'interaction avec les autres membres de l'équipe MΞDISIM, dont j'ai eu l'honneur de faire partie pendant ces années. Le grand dynamisme et la grande disponibilité de tous mes collègues, qui ont su me soutenir et supporter inconditionnellement pendant toutes les phases de ce parcours, professionnellement et personnellement, ont fait de cette thèse une expérience humaine simplement merveilleuse. Je dois cette thèse à toute l'équipe, pour leur apport sans égal. En particulier, je souhaite dire un grand merci à quelques collègues avec lesquels j'ai pu échanger le plus. D'abord, je voudrais

remercier Radek Chabiniok, pour m'avoir aidée dès mon arrivée avec grande disponibilité et générosité, et pour ses précieux conseils et contributions tout au long de la thèse. Je tiens à remercier profondément François Kimmig pour son dynamisme et sa proactivité dans l'équipe, qui ont contribué a créer un environnement de travail très agréable et productif, tout en resserrant les liens entre doctorants. En outre, je le remercie pour son grand soutien et complicité. Un énorme merci va à ma partenaire de bureau, sport et beaucoup plus Nicole Tueni. Partager ces moments avec elle m'a apporté beaucoup sur le plan humain et m'a beaucoup aidé, surtout pendant les derniers mois de la thèse. Un grand merci à Gautier Bureau, pour sa gentillesse et patience, et pour m'avoir toujours "secourue" quand j'avais des difficultés avec les différents codes. Je voudrais aussi remercier Arthur Le Gall pour avoir répondu à ma curiosité et soif de connaissances dans le domaine médical avec une énorme disponibilité, et pour nos échanges scientifiques, qui m'ont permis d'apprendre et d'appliquer mes aspirations didactiques. Mes remerciements vont aussi à Bruno Burtschell, que j'ai côtoyé pendant ma première année de thèse et avec qui une très belle amitié est née. Je souhaite remercier aussi Jessica Manganotti, pour son enthousiasme, sa curiosité et sa bonne humeur. Un grand merci aussi aux autres doctorants et stagiaires de l'équipe, avec qui j'ai passé de très très bons moments pendant et en dehors du temps de travail, et à qui je souhaite le meilleur pour la suite.

J'ai été très chanceuse de faire de très belles rencontres pendant ces années aussi en dehors de l'environnement de travail, qui ont donné lieu à des moments inoubliables. Pour cela, je suis très reconnaissante en particulier à Revekka et Chris, Elodie et Lindsey. Nous avons partagé tellement de belles expériences, et je suis sûre que ce ne sera que le début. Une place spéciale dans mon coeur est réservée aux personnes merveilleuses que j'ai connues pendant mon master à Trento et qui sont toujours très proches de moi : Alessia, qui représente une soeur pour moi ; Christian, qui m'étonne toujours pour son intelligence, son courage et sa générosité ; Qinghui, qui m'a constamment épaulée et inspirée par son caractère enthousiaste et chaleureux ; Francesco, qui m'a toujours stimulée et soutenue.

Mes pensées vont aussi aux amis avec qui j'ai grandi, qui sont à mes côtés depuis toujours malgré la distance et m'ont encouragée. Je dois un grand merci à mes proches, et surtout à ma cousine Carla, pour avoir toujours représenté une source d'inspiration pour moi, et m'avoir constamment motivée et encouragée dans mon parcours.

Je suis pour toujours reconnaissante à Thomas pour m'avoir pris par la main du tout début de ce chapitre de ma vie et m'avoir fait don de son amour inconditionnel, son âme gentille et sa compréhension. Je me sens bénie et fière de l'avoir à mes côtés, et j'ai hâte de partager encore de milliers d'expériences et nouveaux chapitres avec lui.

Enfin, mon dernier et plus important merci est pour ma famille, mon pilier et premier repère. Merci à mon frère Francesco, pour m'avoir toujours entourée de son affection et protection fraternelle, mon père Luigi pour m'avoir toujours encouragée dans tous mes choix sans réserve et pour sa bonté d'âme, et ma mère Gianna pour sa complicité et son support inconditionnel. Grazie di cuore per essere al mio fianco da sempre e per sempre. Nulla di tutto questo sarebbe accaduto senza il vostro sostegno. Mi avete insegnato a puntare sempre più in alto anche a costo di sacrifici e a dare sempre il massimo, circondandomi del vostro amore e del vostro supporto assoluto, e di questo vi sono immensamente grata.

Alone we can do so little;
together we can do so much.

Helen Keller

Table des matières

Introduction (English)

This PhD thesis was held in the Inria team MΞdisim, under the supervision of Dr. Dominique Chapelle and Dr. Sébastien Imperiale.

General context of the thesis

Cardiovascular diseases (CVD) represent one of the main causes of death in Europe and in the developed countries. Furthermore, early detection of cardiac pathologies is of crucial importance in order to profile a better diagnosis and reduce their incidence (prevalence) and mortality. At the present day, cardiologists have at their disposal numerous tools in order to retrieve information on the morphology and physiology of the cardiovascular system of the patients with a high spatial and temporal resolution. Most imaging modalities are based on Magnetic Resonance (MR), Ultrasound (US) and Computed Tomography (CT). These images allow to get useful information on the deformation of the heart throughout the cardiac cycle, and to retrieve information on the circulation. Another standard exam is the Electrocardiogram, to track the temporal evolution of the electric potential of the heart.
Nonetheless, none of these methods is able to access the intrinsic biomechanical properties of the myocardial tissue. At present, the standard clinical practice is to perform invasive catheterisation in the left ventricle or atrium, in order to collect direct measurements of pressure and volume and infer information on the structure of the tissue and internal stresses.

It has been extensively assessed that the estimation of the mechanical properties (e.g. stiffness) of soft tissues has a significant role in the early detection of pathologies, since such properties are highly sensitive to tissue structural changes associated with physiological and pathological processes [Sarvazyan et al., 2011]. The qualitative assessment of tissue stiffness of superficial organs by manual palpation has been used for centuries for breast cancer characterisation and hepatic fibrosis staging. However, the first technical approaches in elasticity imaging were developed only three decades ago, showing the feasibility of a quantitative assessment of tissue stiffness in soft tissues. Elastography techniques are mostly based on three steps:

- excitation of a Region of Interest (ROI) in the tissue;
- measurement of the induced perturbation;
- reconstruction of the biomechanical properties of the tissue.

Soft tissues are considered nearly-incompressible, due to the high content in water. The main factor responsible for that is the hydration phenomenon, i.e. the interaction of polar, charged and hydrophobic atomic groups of organic substances with molecules of water. For that reason, the bulk modulus – that mainly depends on the tissue molecular composition – is close to that of water and varies in a range of about 10% [Sarvazyan et al., 2011]. On the other hand, the shear modulus, that relies on other structural properties of the tissue, such as the degree of heterogeneity and anisotropy, on the cellular or higher levels of architecture, varies substantially (order of hundreds of percent) in physiological and pathological processes, and it differs of several orders of magnitude among different soft tissues.
The most standard relationship adopted to retrieve the shear modulus μ from the characteristics of shear wave propagation, assuming that the medium is homogeneous, linear,

isotropic and purely elastic, reads

$$\mu = \rho\, v_s^2,$$

where ρ represents the density of the tissue, and v_s is the velocity of the shear wave. However, note that this simple relationship does not hold in presence of tissue anisotropies, inhomogeneities and nonlinear behaviour of a medium like the myocardium. As a consequence, numerous experimental studies in the cardiac setting show an incorrect estimation of apparent mechanical properties that change significantly over the cardiac cycle.

We can identify two major elasticity imaging methods, based on the the underlying physical principles that are used to perform the measurement: Ultrasound (US) elasticity imaging and Magnetic Resonance Elastography (MRE). In the first ultrasonic methods (late 1980s), stresses in the tissue were generated by static loading or external vibrators. Later on, at the end of the 1990s, a new approach based on remote generation of elastic waves by Acoustic Radiation Force (ARF) was developed [Rudenko et al., 1996; Sarvazyan et al., 1998, 2010]. ARF can be defined as a time-averaged force exerted by an acoustic wave on an object, and it is generated by a change in the ultrasonic wave energy density of an incident acoustic field [Sarvazyan et al., 2011]. ARF-based techniques have raised a growing interest in the last years due to the fact that the induced strains are highly localised, since the generated elastic waves are fully attenuated after a few wavelengths. As a consequence, the local estimation of the biomechanical properties is simplified, since transparent boundary conditions can be assumed, i.e. the medium can be assumed to be infinite. Therefore, numerous ARF-driven imaging modalities have been developed and tested in the recent years. The main features of US elasticity imaging consist in an optimal spatial resolution (0.1 - 0.5 mm) and fast acquisition time (down to 4-30 µs). In general, two-dimensional elasticity maps are computed. However, by physically moving the US probe, or using 3D array probes, it is possible to obtain three-dimensional displacement data, thus elasticity maps.

In parallel to US-based techniques, numerous elasticity imaging modalities are based on MRI. The first experiments of MRE were performed in the early 1990s based on static loading [Fowlkes et al., 1992]. The first MRE studies involving dynamic loading, however, date back to 1995 [Muthupillai et al., 1995; Fowlkes et al., 1995]. In this imaging modality, an external vibrator is used to induce harmonic shear waves in the tissue, in a frequency range of 50-1000 Hz. Then, a motion-sensitising gradient is adopted, in order to measure the motion at a specific frequency and in a specified direction. This gradient is synchronised at the same frequency as the external vibrating source. The vibrational displacement field in the tissue is measured by MRI, and it is directly proportional to the phase shift in the acquired MR signal. Note that it is possible to acquire full three-dimensional displacement fields, by using gradients polarised in different directions. From the displacement field, a stiffness map – called *elastogram* – is computed, by an inversion algorithm [Arani et al., 2017; Sarvazyan et al., 2011]. The main advantages of MRE concern the absence of constraints on the imaging depth (since it is not limited by the presence of bone or gas) and the free orientation of the field of view, since no acoustic window is needed. Moreover, this technique is operator-independent, and whole organs can be mapped. However, MR scanners are more expensive and less easily accessible than US scanners. Moreover, a good spatial resolution (1-3 mm) is obtained at the price of the acquisition time, that ranges from seconds to minutes. This makes measurements more challenging for the cardiac settings, where data must be acquired at very high frame rate. Valuable progress in cardiac MRE is to be noted [Elgeti and Sack, 2014; Arani et al., 2017; Fovargue et al., 2018].

For the sake of completeness, we cite another elastography imaging method, based on optical techniques. The main advantage is the better spatial resolution (up to 5 µm) and signal-to-noise ratio than US or MRE techniques, allowing to explore phenomena occurring at an intermediate scale between cell and organ. The main underlying techniques are Optical Coherence Tomography (OCT) and Brillouin microscopy. The main drawbacks of optical methods are the constraint of an optical window to perform measurements and the considerably low imaging depth (0.1 - 3.0 mm), due to high optimal scattering and attenuation of soft tissues [Kennedy et al., 2017; Greenleaf et al., 2003].

The main clinical applications of Elastography imaging are breast mass evaluation and hepatic cirrhosis and fibrosis. However, recent developments show promising results in numerous applications, like prostate, thyroid, lymph nodes, arterial wall and atheromatous plaques evaluation, arterial and venous thrombosis, graft rejection, heart, skeletal muscles, lymphedema, brain and tumours in all major organs. Note that some applications are still at early stages of research, whereas other are already used in clinical practice. We refer to [Sarvazyan et al., 2011; Sigrist et al., 2017; Caenen, 2018] for further reading on elasticity imaging modalities and clinical applications.

Ultrasound elastography: an overview

We provide here a brief introduction on ultrasound-based elasticity imaging. We refer the reader to [Sarvazyan et al., 2011; Gennisson et al., 2013; Sigrist et al., 2017] for further details. The first approach in ultrasound elastography was Strain Elastography [Ophir et al., 1991]. It was developed at the beginning of the 1990s and it was was based on *static* compression. In more detail, a qualitative estimation of elasticity properties of the tissue was extrapolated by comparison of anatomical information before and after inducing a small deformation in the ROI by applying a constant stress. Usually, radiofrequency echo signals were used to retrieve the displacement field by correlation algorithms. Then, strain images could be obtained by computing the gradient of the displacement. The most widespread application is breast imaging. This method has been adopted on many commercial US devices, since it requires a simple implementation, even though it is not possible to retrieve a quantitative estimation of the stiffness of the tissue.

On the contrary, *dynamic* methods are based on the application of a time-varying force. We can further distinguish between *transient* methods, in which the tissue is excited by a short pulse, and *harmonic* methods, that are based on the application of an oscillatory force at a fixed frequency [Gennisson et al., 2013]. In both methods, the mechanical perturbation propagates in the form of elastic waves (pressure and shear) in the tissue. The family of transient methods relies on the characterisation of shear wave propagation; thus, it is possible to provide quantitative maps of the stiffness of the tissue, with a good spatial resolution, differently from quasi-static methods. However, the implementation of such techniques requires a more complex equipment, to induce shear waves and image the small perturbation related to shear wave propagation. Shear wave generation is realised via external excitation – by external vibrators – or internal excitation – by the Acoustic Radiation Force (ARF) of a focused ultrasound beam.

A widespread method based on surfacic excitation is **Transient Elastography (TE)**. The first technique was developed for a one-dimensional framework by the Langevin Institute in 1995 [Catheline, 1998]. This technique was based on the generation of a low-

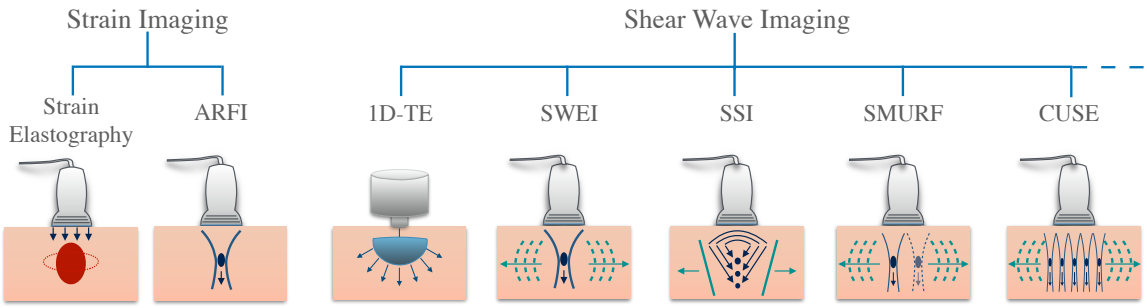

Figure 1 – Schematic illustration of some ultrasound-based elastography imaging methods.

frequency (10-500 Hz) transient mechanical impulse on the tissue, generating a spherical shear wave. The induced displacement was then measured by correlation algorithms and shear phase speed was retrieved, enabling the estimation of the stiffness, anisotropy, viscosity and non-linearity in soft tissue as the liver [Catheline et al., 2003; Sandrin et al., 2003; Catheline et al., 2004; Gennisson et al., 2013]. This technique was later extended to the two-dimensional framework in the same institute [Sandrin et al., 2002]. First in vivo results were promising, but this technique did not encounter great success, due to practical limitations of the device.

The idea to combine the internal excitation of the tissue by an acoustic pulse and the characterisation of the generated shear waves is due to Dr. Armen Sarvazyan [Sarvazyan et al., 1998]. Subsequently, numerous methods based on ARF were developed and applied in a great range of applications, e.g. liver fibrosis assessment, breast tumour detection, diagnosis of cardiac pathologies [Sarvazyan et al., 2011; Sigrist et al., 2017]. The main positive feature of internal methods is represented by the highly localised perturbation. Furthermore, shear waves are fully attenuated in a few wavelengths distance from the focal point of the ultrasonic beam. This induces a narrowing of the induced strain, and excludes interactions with longitudinal waves at the surface of the tissue. Hence, the elastic wave propagation only depends on the parameters of the acoustic excitation and the structural properties of the tissue. This enables a simpler reconstruction of the biomechanical properties of the tissue of interest, since the quality of reconstruction can be significantly affected by errors in the definition of boundary conditions [Sarvazyan et al., 2011]. In addition, the excitation energy is directly transferred in the tissue, whereas in external excitation techniques, there is a strong energy coupling at the surface of the body (skin and subcutaneous fat), that can considerably limit the induced tissue displacement in the organ, especially in obese subjects [Palmeri et al., 2008]. Note also that, since no compression is required, the technique is less operator-dependent than traditional US-based imaging methods [Nightingale, 2011].

We cite, among the ARF-driven elasticity imaging methods (see Figure 1):

- The **Acoustic Radiation Force Impulse (ARFI)** method [Nightingale et al., 2002]. This technique is based on tissue excitation via a short-duration, high intensity acoustic pulse (ARF) from focused ultrasound beams, and tracking of tissue motion in a region of interest via standard ultrasound imaging techniques. ARFI imaging measures longitudinal tissue displacement to determine relative differences in tissue stiffness, similar to the data generated with compressive strain imaging methods. The peak displacement is then displayed in an image, to estimate qualitatively the stiffness of the tissue.

- The **Shear Wave Elasticity Imaging (SWEI)** method, first described theoretically by Sarvazyan et al. [1998] and investigated in vivo in Nightingale et al. [2003]. It consists in remotely generating shear waves by a single acoustic push (about 100 µs), and measuring shear motion by focused ultrasound imaging; shear wave velocity is computed by standard Time Of Flight (TOF) methods, and tissue mechanical properties are derived by inversion algorithms.

- The **Supersonic Shear Imaging (SSI)** method [Bercoff et al., 2004], characterised by multiple ARF excitations at different focal locations, so that the shear waves generated at each push constructively interfere and generate a conical shear wave (Mach cone). In this way, the amplitude of tissue displacement is increased up to 100 µm in phantoms and 40 µm in vivo, compared to 10-20 µm obtained for a single push. The name "supersonic" is due to the fact that the radiation force focal point moves faster than the generated shear wave, inducing a quasi planar wavefront. A specificity of this method is the ability to image shear displacement at a very high frame rate (up to 12000 frames per second), since plane waves are transmitted for motion detection, instead of focused pulses. Thus, shear wave propagation can be measured in real-time and over a large field of view. Then, the shear wave speed is computed by inverting the wave equation, to infer the elastic properties of the medium.

- The **Spatially Modulated Ultrasound Radiation Force (SMURF)** technique [McAleavey et al., 2007]. It consists in exciting the tissue via single ARF pushes at two or more different locations in rapid succession, in order to generate a spatially-varying radiation force. The shear wave speed is retrieved from the difference in arrival times of the pulses, and the path length difference is taken as the offset in the push beam locations. The main feature of this method concerns the high spatial resolution of computed stiffness images.

- The **Comb-push Ultrasound Shear Elastography (CUSE)** method [Song et al., 2012], based on a combined push in order to generate a complex shear wave field propagating in the full field of view in 2D. Then, shear motion is tracked after transmission of plane waves. Directional filters are applied on the displacement data to extract the propagating shear waves, and shear wave velocity is inferred via TOF methods. This method allows to estimate elasticity properties in the whole ROI without problems of attenuation and with a very good SNR.

Among the *harmonic* elastography techniques, we cite the Shear wave Dispersion Ultrasound Vibrometry (SDUV) [Chen et al., 2009] and the Crawling Wave Sonoelastography (CWS) [Hah et al., 2010].
Henceforth, we will indicate by Shear Wave Elastography (SWE) the family of imaging methods based on shear wave generation at one location by acoustic radiation force (e.g. SWEI or SSI).

Modelling of the ARF

The main source of attenuation in soft tissues is absorption and the contribution associated with scattering can be neglected [Parker, 1983]. As a consequence, when an acoustic wave propagates in the medium, an energy gradient is formed in the medium, due to absorption. The ARF is related to the momentum transfer from the propagating ultrasound wave to the medium, that generates a modification in the acoustic energy density [Torr, 1984].

Under plane wave assumption, this force can be modelled as a body force in the direction of the wave propagation, distributed throughout the geometric shadow of the transducer aperture [Palmeri and Nightingale, 2011]. The ARF cannot be derived from the stress-strain relationship in purely elastic materials, since elastic models do not incorporate any energy-loss mechanism that could justify a change of momentum. Furthermore, we note that the viscoelastic properties of the tissues strongly depend on the frequency of the excitation: in fact, at low frequencies ($<$ 100 kHz), tissues can be modelled as soft tissues; however, at ultrasonic frequencies, tissues do not support shear stresses and acoustic wave attenuation generates heating and the ARF; thus, tissues are modelled as viscous fluids.

Numerous models to analyse the physical mechanisms responsible for ARF and remote generation of shear waves in water-like media have been proposed in the acoustics community. The first theoretical model of shear oscillations remotely generated by radiation force is presented by Rudenko et al. [1996] and Sarvazyan et al. [1998]. Subsequently, other authors [Zabolotskaya et al., 2004; Gennisson et al., 2007] have derived an evolution equation for shear waves in an isotropic soft medium, assuming plane shear waves. The role of inhomogeneity and viscosity in the generation of shear waves is first analysed in Ostrovsky et al. [2007]. In greater detail, it is proved that an acoustic field in a pure elastic (non-dissipative) homogeneous solid cannot generate shear motion.
However, to our best knowledge, no mathematical analysis has been provided yet to derive a complete formula for ARF and justify shear wave generation from ARF. In fact, for modelling purposes, some restrictive assumptions are made to derive a simple expression of the resulting body force. In particular, if the tissue is modelled as a linear viscous fluid, and under plane wave assumption, we can derive the following expression of the ARF, centred at the focal point (x_F, y_F, z_F): [Nightingale et al., 2002; Palmeri et al., 2005]

$$F(x,y,z,t) \coloneqq A_{\max} \exp^{-\left(\frac{(x-x_F)^2}{\sigma_x^2}+\frac{(y-y_F)^2}{\sigma_y^2}+\frac{(z-z_F)^2}{\sigma_z^2}\right)} \cdot \exp^{-\frac{(t-t_{pulse})^2}{\sigma_t^2}}, \tag{1}$$

with

$$A_{\max} = \frac{2\,\alpha\, I_{\max}}{v_p},$$

where α is the attenuation coefficient, $I_{\max}$ is a time-averaged intensity, and v_p is the longitudinal wave velocity. The direction of this force is the same as the orientation of the wave propagation, and it is called Poynting vector. It is usually oriented purely axially for locations in a range of $\pm 10\%$ from the focal depth. We refer the reader to Nightingale [2011]; Caenen [2018] for further reading on this modelling approximation.

Modelling of Shear Wave Elastography

The most suitable approach to model the underlying physics of Shear Wave Elastography in viscoelastic bounded media is by the Finite Element Method (FEM), due to its flexibility to the extension to more complex geometries, for example patient-specific. Numerous models of SWE have been developed in the last decade, mostly oriented toward the applications. The first models were based on the simplifying assumption of a linear and isotropic material, that could represent for example an approximation of the hepatic tissue or other isotropic soft tissues. One of the first FEM models of the dynamic response of the tissue to an impulsive radiation force excitation was presented by Palmeri et al. [2005]. The tissue modelled in this work was assumed to be isotropic, elastic and linear.

Among the first FE simulation in viscoelastic media we cite Lee et al. [2012]. In particular, they assumed a linear, viscoelastic, isotropic phantom with stiffer cylindrical inclusion. A similar numerical strategy was adopted by Caenen et al. [2017] to investigate shear wave physics in a viscoelastic, linear, isotropic medium. Results were compared with in vitro experimental data. More recently, Ye et al. [2017] proposed a 2D FE simulation of a visco-hyperelastic, isotropic, nearly-incompressible model. A fully explicit scheme was used for time discretisation, and simulations were performed in their in-house FE code.

One of the first anisotropic models was proposed by Rouze et al. [2013]. In greater detail, they proposed an FEM model of shear wave propagation in a quasi-incompressible, transversely isotropic, linear, elastic material undergoing impulsive ARF excitation, modelled with a 3D Gaussian distribution. More recently, Qiang et al. [2015] analysed shear wave propagation in the plane of symmetry of a transversely isotropic, viscoelastic, quasi-incompressible linear material. Ultimately, Caenen et al. [2018] studied an FEM model for shear wave mechanics in an orthotropic material, in combination with uniaxial mechanical loading. We highlight that all the aforementioned methods consider an approximation of the ARF source term as a body force with similar profile to Eq. (1). In particular, the acoustic intensity field was simulated with the software program FIELD II and/or modelled as a 3D Gaussian distribution.
In all the aforementioned works, fully explicit time discretisation was adopted and, except for the work by Ye et al. [2017], the software Abaqus was used to solve the resulting system of equations. In fact, the approach of the authors is more oriented towards the application rather than the development of adapted numerical schemes for this problems. However, this choice can introduce critical limitations on the time step due to the enforcement of incompressibility, as it is explained in what follows.

Treatment of incompressibility in elastodynamics

Numerous Finite Element Method (FEM) formulations for the approximation of elasticity in incompressible solids were developed in the last decades, due to their wide application in computational mechanics. However, the majority of the works proposed in the literature only treats a static configuration. The main contributions to date can be organised into two categories: pure displacement methods and mixed methods.

On the one hand, displacement-based FEM provide accurate solutions of quasi or pure incompressible elasticity problems; nonetheless, these methods can suffer of undesirable limitations, like ill-conditioning of the stiffness matrix, spurious or incorrect pressures and numerical locking (severe stiffening near the incompressible limit) [Sussman and Bathe, 1987], especially if low-order shape functions are adopted, due to the enforcement of the incompressibility constraint. Several methods have been proposed to improve accuracy of displacement-based methods [Malkus and Hughes, 1978; Hughes, 1980; Neto et al., 2005].

On the other hand, mixed finite element methods [Brezzi and Fortin, 2012] have proven effective to obtain accurate results in the resolution of incompressible fluid flows and incompressible elasticity. In these methods, the constrained problem is rewritten in form of an unconstrained saddle-point problem, and a second variable – the pressure – is introduced. However, not all mixed methods are stable. In fact, the convergence properties of this formulation are governed by stability considerations, involving ellipticity requirements and

the famous Ladyzhenskaya - Babŭska - Brezzi (LBB) inf-sup condition [Brezzi and Bathe, 1990; Brezzi and Falk, 1991]. If this stability condition is not satisfied, severe unphysical oscillations in the pressure field may appear. Stabilised methods have been proposed to overcome the limitations of classical mixed FE formulations in the field of incompressible fluid dynamics. These methods rely on the addition of artificial high-order differential terms to the discrete continuity equation, in order to circumvent the LBB condition (see [Quarteroni and Valli, 1994] for a thorough overview).

All the methods described before can be extended to dynamic equations using implicit time discretisation (e.g. Implicit Euler scheme or implicit Newmark schemes). However, at each time step, a matrix inversion is required for the computation of the velocity or the displacement field. A popular approach to increase the efficiency of dynamic solvers was first proposed in computational fluid dynamics by [Chorin, 1968, 1969] and [Temam, 1968, 2001] in the late 1960s, and it is called fractional-step projection. In this family of methods, time-discretisation in divided into two separate steps for viscosity and incompressibility, respectively. The first half-step corresponds to an elliptic Boundary Value Problem for an intermediate velocity, accounting for viscosity diffusion and advection, whereas the second half-step consists in an inviscid problem where the end-of-step, divergence-free velocity is computed, along with pressure distribution. In this way, at each time step two decoupled elliptic equations are solved, and this is very advantageous for large scale simulations [Guermond et al., 2006].

Less effort has been made to develop efficient methods for the treatment of the incompressibility constraint in elastodynamics. Since the underlying physics is wave propagation, fully explicit methods could be considered good candidates to obtain efficient schemes (in the case of nearly-incompressible media). However, the enforcement of incompressibility entails a drastic limit on the time step of the scheme, due to the stability condition. In order to circumvent the limitations of fully explicit methods, we propose to adopt the main ideas of the fractional-step projection algorithm to design an efficient scheme for incompressible elastodynamics, due to the efficiency of this method and the similarities with viscous incompressible fluids.

Structure of the thesis

This PhD thesis concerns the mathematical modelling and numerical approximation of impulsive ARF-driven SWE imaging in a prestressed soft tissue, with a specific reference to the cardiac setting.
The first part of the manuscript deals with the mathematical modelling of the ARF, the resulting shear wave propagation and the characterisation of shear wave velocity in a general constitutive law for the myocardial tissue. One of the main contributions of this work is the derivation of an original mathematical analysis of the acoustic radiation force phenomenon. In greater detail, we infer the governing equation of the pressure field and the shear wave field remotely induced by the ARF, and we compute an analytical expression of the source term responsible for the generation of shear waves from an acoustic pressure pulse. The approach we propose is based on asymptotic analysis.
In the second part of the PhD thesis, we present efficient numerical tools for a realistic numerical simulation of an SWE experiment. The numerical approximation of the elastodynamic equations is based on high-order Spectral Finite Elements for spatial discretisation. In addition, we show a novel method for time discretisation adapted to incompressible elas-

ticity. In particular, we construct a conservative time discretisation, and treat implicitly only the terms corresponding to "informations" travelling at infinite velocity, associated with the incompressibility constraint, by solving a scalar Poisson problem at each iteration of the algorithm. Furthermore, we provide a novel matrix-free, high-order, fast method to solve the Poisson partial differential equation in bounded domain.

Part I: Mathematical modelling

Extraction of mechanical properties of soft tissues from the shear wave velocity. The first goal of this thesis is to provide the description of a methodological approach to characterise elastographic shear wave propagation for a general constitutive behaviour of the myocardium. The equations governing shear wave propagation are derived from a biomechanical model accurately reflecting the complex behaviour of the myocardium and the organ. Then, shear wave velocities are computed based on the derivation of the so-called Christoffel tensor. We characterise shear wave propagation for different choices of constitutive law accounting for the passive behaviour. Furthermore, we study the contribution of active stress on the elastographic wave propagation, and we demonstrate that it is dominated by the prestress effect. We conclude the chapter by showing some applications to the extraction of fibre orientation throughout the myocardium and detection of "numerical pathologies" in a three-dimensional beating heart biomechanical model.

Modelling of the ARF and generation of shear waves. One of the aims of this PhD thesis is to provide an analytical expression of the excitation induced by the ARF in a nonlinear solid. In more detail, we want to propose a formulation valid for media undergoing large deformation, independently from the nature of the prestress. Furthermore, we aim at getting rid of the simplifying hypotheses that are usually made on the properties of the solution (e.g. plane wave assumption). To do so, we derive a mathematical model based on energy considerations and asymptotic analysis. Note also that in ARF-driven SWE applied to the cardiac setting, the wave propagation induced by the ARF is superposed to the nonlinear mechanics associated with the heart deformation during the cardiac cycle, that must be taken into account in the formulation. In Chapter 2, we provide a rigorous mathematical model that describes, in the context of an accurate nonlinear biomechanical model adequately representing the complex state of the myocardium:

- the expression of the surfacic source term (focused US beam);
- the pressure wave propagation induced by the ARF excitation;
- the shear wave propagation generated by the ARF.

A detailed expression of the source term responsible for shear wave propagation is provided, and it is shown that it is associated with the viscosity and the tissue nonlinearities. Furthermore, in Chapter 3 we provide a justification of our formulation, by deriving a proof of convergence of the approximation of the solution in a quasi-static linear configuration.

Part II: Numerical approximation

Numerical approximation of incompressible elastodynamic equations. In order to perform a suitable and efficient approximation of elastic wave propagation in incompressible solids, in Chapter 4 – which has the form of a paper already submitted for

publication in an international journal – we describe an adapted numerical framework that we have developed for the treatment of the incompressibility constraint. High-order conforming finite element with mass lumping are used for space discretisation and an implicit/explicit second-order, energy-preserving scheme is employed for time discretisation. The main feature of this method is that the time step is not governed by the pressure wave, that is travelling at "infinite" velocity, but only by the shear wave velocity. Furthermore, the incompressibility constraint is imposed by penalisation techniques and it consists in the resolution of a scalar Poisson problem at each iteration. Numerical analysis of the convergence order of the scheme is detailed in Chapter 5.

Numerical simulation of an SWE experiment. The second main aim of this thesis is to develop the computational framework for the realistic numerical simulation of an SWE experiment in a soft medium as the myocardium. To do so, Chapter 6 is devoted to the description of a complete three-dimensional mathematical model for propagation of elastic waves in a pre-stressed, hyperelastic, viscoelastic, heterogeneous, anisotropic medium, that is also subject to an active stress, under realistic conditions of an SWE experiment. The numerical approximation of this model consists in high-order Spectral Element method in space and the adapted implicit/explicit time discretisation described in Chapter 4. Proof of stability of the scheme is also detailed in this chapter.

A fast solver for the numerical resolution of the Poisson problem. In order to perform efficient numerical simulations of shear wave propagation in the myocardium, we developed an adapted method for the resolution of the Poisson problem that is introduced at every time step of the scheme proposed in Chapter 4. In particular, in Chapter 7 – which also has the form of a paper already submitted for publication in an international journal – we provide a novel, fast, matrix-free solver for the Poisson problem discretised with High-Order Spectral Element Methods (HO-SEM). This method relies on the use of Discrete Fourier Transform (DFT) to rewrite the problem as the inversion of the symbol of the operator in the frequency space. Since HO-SEM are adopted for space discretisation, an efficient implementation is required for the inversion of the symbol. The solver that we have developed is characterised by several features:

- it preserves the efficiency of standard fast Fourier transform algorithm for the linear case;
- the matrix storing is minimised;
- a pseudo-explicit Singular Value Decomposition (SVD) is used for inversion of the symbols;
- it is naturally extended to multiple dimensions by tensorisation, due to the underlying HO-SEM discretisation;
- it can be easily generalised to non-periodic boundary conditions by performing a periodic, symmetric extension of the source term. However, due to symmetry properties of the extended source term and intrinsic properties of the DFT, most computations are limited to the frequencies associated with the original (not extended) source term, preserving the efficiency of the algorithm.

This chapter is completed by numerical results and some remarks on the complexity of the solver – which is shown to be in $O(R^{d+1}\, N^d\, \log N)$ in dimension d – and its parallelisability.

Communications

Oral communications and poster presentations

- **Oral presentation at "Journée de Rentrée 2018 de l'EDMH".**
  IHES, Bures-sur-Yvette, 11.10.2018.
- **Oral presentation at VPH 2018 conference.**
  University of Zaragoza, Zaragoza, Spain, 05.09.2018.
- **Oral presentation at SIMAI 2018 national congress.**
  Università la Sapienza, Rome, Italy, 05.07.2018.
- **Oral presentation at INdAM Workshop "Mathematical and Numerical Modeling of the Cardiovascular System".**
  Istituto Nazionale di Alta Matematica (INdAM), Rome, Italy, 16.04.2018.
- **Oral presentation at Symposium CLIPS 2017: Coalition for Live Imaging Paris-Saclay, Multiscale Live Imaging in Human, Animal and Plant Health.**
  Campus CNRS Gif-sur-Yvette, France, 13.09.2017.
- **Oral presentation at the 5th International conference on Computational and Mathematical Biomedical Engineering (CMBE 2017).**
  University of Pittsburgh, Pittsburgh, PA, United States, 12.04.2017.
- **Poster presentation at the 7th Summer School on Biomechanics and Modeling in Mechanobiology**
  Institute of Biomechanics, Graz University of Technology, Graz, Austria, 06.07.2016.

Publications

- **A conservative penalisation strategy for the semi-implicit time discretisation of incompressible elastodynamic equations.** Caforio F. and Imperiale S., submitted.
- **High-order Discrete Fourier Transform for the resolution of the Poisson equation**. Caforio F. and Imperiale S., submitted.

Bibliography

Arani, A., Arunachalam, S. P., Chang, I. C., Baffour, F., Rossman, P. J., Glaser, K. J., Trzasko, J. D., McGee, K. P., Manduca, A., Grogan, M. et al. [2017], 'Cardiac MR elastography for quantitative assessment of elevated myocardial stiffness in cardiac amyloidosis', *Journal of Magnetic Resonance Imaging* **46**(5), 1361–1367.

Bercoff, J., Tanter, M. and Fink, M. [2004], 'Supersonic shear imaging: a new technique for soft tissue elasticity mapping', *IEEE transactions on ultrasonics, ferroelectrics, and frequency control* **51**(4), 396–409.

Brezzi, F. and Bathe, K.-J. [1990], 'A discourse on the stability conditions for mixed finite element formulations', *Computer methods in applied mechanics and engineering* **82**(1-3), 27–57.

Brezzi, F. and Falk, R. S. [1991], 'Stability of higher-order Hood–Taylor methods', *SIAM Journal on Numerical Analysis* **28**(3), 581–590.

Brezzi, F. and Fortin, M. [2012], *Mixed and hybrid finite element methods*, Vol. 15, Springer Science & Business Media.

Caenen, A. [2018], A biomechanical analysis of shear wave elastography in pediatric heart models, PhD thesis, Ghent University.

Caenen, A., Pernot, M., Peirlinck, M., Mertens, L., Swillens, A. and Segers, P. [2018], 'An in silico framework to analyze the anisotropic shear wave mechanics in cardiac shear wave elastography', *Physics in Medicine & Biology* **63**(7), 075005.

Caenen, A., Pernot, M., Shcherbakova, D. A., Mertens, L., Kersemans, M., Segers, P. and Swillens, A. [2017], 'Investigating shear wave physics in a generic pediatric left ventricular model via in vitro experiments and finite element simulations', *IEEE transactions on ultrasonics, ferroelectrics, and frequency control* **64**(2), 349–361.

Catheline, S. [1998], Interférométrie-Speckle ultrasonore: Application à la mesure d'élasticité, PhD thesis, Université Paris-Diderot-Paris VII.

Catheline, S., Gennisson, J.-L., Delon, G., Fink, M., Sinkus, R., Abouelkaram, S. and Culioli, J. [2004], 'Measurement of viscoelastic properties of homogeneous soft solid using transient elastography: An inverse problem approach', *The Journal of the Acoustical Society of America* **116**(6), 3734–3741.

Catheline, S., Gennisson, J.-L. and Fink, M. [2003], 'Measurement of elastic nonlinearity of soft solid with transient elastography', *The Journal of the Acoustical Society of America* **114**(6), 3087–3091.

Chen, S., Urban, M. W., Pislaru, C., Kinnick, R., Zheng, Y., Yao, A. and Greenleaf, J. F. [2009], 'Shearwave dispersion ultrasound vibrometry (SDUV) for measuring tissue elasticity and viscosity', *IEEE transactions on ultrasonics, ferroelectrics, and frequency control* **56**(1), 55–62.

Chorin, A. J. [1968], 'Numerical solution of the Navier–Stokes equations', *Mathematics of computation* **22**(104), 745–762.

Chorin, A. J. [1969], 'On the convergence of discrete approximations to the Navier–Stokes equations', *Mathematics of computation* **23**(106), 341–353.

Elgeti, T. and Sack, I. [2014], 'Magnetic resonance elastography of the heart', *Current Cardiovascular Imaging Reports* **7**(2), 9247.

Fovargue, D., Kozerke, S., Sinkus, R. and Nordsletten, D. [2018], 'Robust mr elastography stiffness quantification using a localized divergence free finite element reconstruction', *Medical image analysis* **44**, 126–142.

Fowlkes, J., Emelianov, S., Pipe, J., Skovoroda, A., Carson, P., Adler, R. and Sarvazyan, A. [1995], 'Magnetic-resonance imaging techniques for detection of elasticity variation', *Medical physics* **22**(11), 1771–1778.

Fowlkes, J., Yemelyanov, S., Pipe, J., Carson, P., Adler, R., Sarvazyan, A. and Skovoroda, A. [1992], 'Possibility of cancer detection by means of measurement of elastic properties', *Radiology* **185**(S), 206–207.

Gennisson, J.-L., Deffieux, T., Fink, M. and Tanter, M. [2013], 'Ultrasound elastography: principles and techniques', *Diagnostic and interventional imaging* **94**(5), 487–495.

Gennisson, J.-L., Rénier, M., Catheline, S., Barrière, C., Bercoff, J., Tanter, M. and Fink, M. [2007], 'Acoustoelasticity in soft solids: Assessment of the nonlinear shear modulus with the acoustic radiation force', *The Journal of the Acoustical Society of America* **122**(6), 3211–3219.

Greenleaf, J. F., Fatemi, M. and Insana, M. [2003], 'Selected methods for imaging elastic properties of biological tissues', *Annual review of biomedical engineering* **5**(1), 57–78.

Guermond, J.-L., Minev, P. and Shen, J. [2006], 'An overview of projection methods for incompressible flows', *Computer methods in applied mechanics and engineering* **195**(44-47), 6011–6045.

Hah, Z., Hazard, C., Cho, Y. T., Rubens, D. and Parker, K. [2010], 'Crawling waves from radiation force excitation', *Ultrasonic imaging* **32**(3), 177–189.

Hughes, T. J. [1980], 'Generalization of selective integration procedures to anisotropic and nonlinear media', *International Journal for Numerical Methods in Engineering* **15**(9), 1413–1418.

Kennedy, B. F., Wijesinghe, P. and Sampson, D. D. [2017], 'The emergence of optical elastography in biomedicine', *Nature Photonics* **11**(4), 215.

Lee, K. H., Szajewski, B. A., Hah, Z., Parker, K. J. and Maniatty, A. M. [2012], 'Modeling shear waves through a viscoelastic medium induced by acoustic radiation force', *International journal for numerical methods in biomedical engineering* **28**(6-7), 678–696.

Malkus, D. S. and Hughes, T. J. [1978], 'Mixed finite element methods. reduced and selective integration techniques: a unification of concepts', *Computer Methods in Applied Mechanics and Engineering* **15**(1), 63–81.

McAleavey, S. A., Menon, M. and Orszulak, J. [2007], 'Shear-modulus estimation by application of spatially-modulated impulsive acoustic radiation force', *Ultrasonic imaging* **29**(2), 87–104.

Muthupillai, R., Lomas, D., Rossman, P., Greenleaf, J. F., Manduca, A. and Ehman, R. [1995], 'Magnetic resonance elastography by direct visualization of propagating acoustic strain waves', *science* **269**(5232), 1854–1857.

Neto, E., Pires, F. and Owen, D. [2005], 'F-bar-based linear triangles and tetrahedra for finite strain analysis of nearly incompressible solids. part i: formulation and benchmarking', *International Journal for Numerical Methods in Engineering* **62**(3), 353–383.

Nightingale, K. [2011], 'Acoustic radiation force impulse (ARFI) imaging: a review', *Current medical imaging reviews* **7**(4), 328–339.

Nightingale, K., McAleavey, S. and Trahey, G. [2003], 'Shear-wave generation using acoustic radiation force: in vivo and ex vivo results', *Ultrasound in medicine & biology* **29**(12), 1715–1723.

Nightingale, K., Soo, M. S., Nightingale, R. and Trahey, G. [2002], 'Acoustic radiation force impulse imaging: in vivo demonstration of clinical feasibility', *Ultrasound in medicine & biology* **28**(2), 227–235.

Ophir, J., Cespedes, I., Ponnekanti, H., Yazdi, Y. and Li, X. [1991], 'Elastography: a quantitative method for imaging the elasticity of biological tissues', *Ultrasonic imaging* **13**(2), 111–134.

Ostrovsky, L., Sutin, A., Il'inskii, Y., Rudenko, O. and Sarvazyan, A. [2007], 'Radiation force and shear motions in inhomogeneous media', *The Journal of the Acoustical Society of America* **121**(3), 1324–1331.

Palmeri, M. L. and Nightingale, K. R. [2011], 'Acoustic radiation force-based elasticity imaging methods', *Interface focus* p. rsfs20110023.

Palmeri, M. L., Sharma, A. C., Bouchard, R. R., Nightingale, R. W. and Nightingale, K. R. [2005], 'A finite-element method model of soft tissue response to impulsive acoustic radiation force', *IEEE transactions on ultrasonics, ferroelectrics, and frequency control* **52**(10), 1699–1712.

Palmeri, M. L., Wang, M. H., Dahl, J. J., Frinkley, K. D. and Nightingale, K. R. [2008], 'Quantifying hepatic shear modulus in vivo using acoustic radiation force', *Ultrasound in medicine & biology* **34**(4), 546–558.

Parker, K. J. [1983], 'Ultrasonic attenuation and absorption in liver tissue', *Ultrasound in medicine & biology* **9**(4), 363–369.

Qiang, B., Brigham, J. C., Aristizabal, S., Greenleaf, J. F., Zhang, X. and Urban, M. W. [2015], 'Modeling transversely isotropic, viscoelastic, incompressible tissue-like materials with application in ultrasound shear wave elastography', *Physics in medicine and biology* **60**(3), 1289.

Quarteroni, A. and Valli, A. [1994], *Numerical Approximation of Partial Differential Equations*, Springer.

Rouze, N. C., Wang, M. H., Palmeri, M. L. and Nightingale, K. R. [2013], 'Finite element modeling of impulsive excitation and shear wave propagation in an incompressible, transversely isotropic medium', *Journal of biomechanics* **46**(16), 2761–2768.

Rudenko, O., Sarvazyan, A. and Emelianov, S. Y. [1996], 'Acoustic radiation force and streaming induced by focused nonlinear ultrasound in a dissipative medium', *The Journal of the Acoustical Society of America* **99**(5), 2791–2798.

Sandrin, L., Fourquet, B., Hasquenoph, J.-M., Yon, S., Fournier, C., Mal, F., Christidis, C., Ziol, M., Poulet, B., Kazemi, F. et al. [2003], 'Transient elastography: a new noninvasive method for assessment of hepatic fibrosis', *Ultrasound in medicine & biology* **29**(12), 1705–1713.

Sandrin, L., Tanter, M., Catheline, S. and Fink, M. [2002], 'Shear modulus imaging with 2-D transient elastography', *IEEE transactions on ultrasonics, ferroelectrics, and frequency control* **49**(4), 426–435.

Sarvazyan, A., J Hall, T., W Urban, M., Fatemi, M., R Aglyamov, S. and S Garra, B. [2011], 'An overview of elastography-an emerging branch of medical imaging', *Current medical imaging reviews* **7**(4), 255–282.

Sarvazyan, A. P., Rudenko, O. V. and Nyborg, W. L. [2010], 'Biomedical applications of radiation force of ultrasound: historical roots and physical basis', *Ultrasound in medicine & biology* **36**(9), 1379–1394.

Sarvazyan, A. P., Rudenko, O. V., Swanson, S. D., Fowlkes, J. B. and Emelianov, S. Y. [1998], 'Shear wave elasticity imaging: a new ultrasonic technology of medical diagnostics', *Ultrasound in medicine & biology* **24**(9), 1419–1435.

Sigrist, R. M., Liau, J., El Kaffas, A., Chammas, M. C. and Willmann, J. K. [2017], 'Ultrasound elastography: review of techniques and clinical applications', *Theranostics* **7**(5), 1303.

Song, P., Zhao, H., Manduca, A., Urban, M. W., Greenleaf, J. F. and Chen, S. [2012], 'Comb-push ultrasound shear elastography (CUSE): a novel method for two-dimensional shear elasticity imaging of soft tissues', *IEEE transactions on medical imaging* **31**(9), 1821–1832.

Sussman, T. and Bathe, K.-J. [1987], 'A finite element formulation for nonlinear incompressible elastic and inelastic analysis', *Computers & Structures* **26**(1-2), 357–409.

Temam, R. [1968], 'Une méthode d'approximation de la solution des équations de Navier-Stokes', *Bull. Soc. Math. France* **98**(4), 115–152.

Temam, R. [2001], *Navier-Stokes equations: theory and numerical analysis*, Vol. 343, American Mathematical Soc.

Torr, G. [1984], 'The acoustic radiation force', *American Journal of Physics* **52**, 402–408.

Ye, W., Bel-Brunon, A., Catheline, S., Combescure, A. and Rochette, M. [2017], 'Simulation of non-linear transient elastography: finite element model for the propagation of shear waves in homogeneous soft tissues', *International Journal for Numerical Methods in Biomedical Engineering* .

Zabolotskaya, E. A., Hamilton, M. F., Ilinskii, Y. A. and Meegan, G. D. [2004], 'Modeling of nonlinear shear waves in soft solids', *The Journal of the Acoustical Society of America* **116**(5), 2807–2813.

Introduction (Français)

Cette thèse a été effectuée au sein de l'équipe de recherche Inria MΞdisim, sous la supervision de Dominique Chapelle et Sébastien Imperiale.

Contexte général de la thèse

Les maladies cardiovasculaires représentent une des causes principales de décès en Europe et dans les pays développés. En outre, la détection précoce des pathologies cardiaques a une importance cruciale pour effectuer de meilleures diagnostics et réduire l'incidence (prévalence) et mortalité de ces pathologies. Actuellement, les cardiologues ont à leur disposition de nombreux outils pour obtenir des informations concernant la morphologie et la physiologie du système cardiovasculaire des patients avec une résolution spatiale et temporelle satisfaisante. La plupart des techniques d'imagerie biomédicale se basent sur la résonance magnétique (IRM), l'échographie (US) et tomographie computerisée (TC). Ces images permettent d'obtenir des informations très utiles sur la déformation du coeur à travers le cycle cardiaque, et sur la circulation sanguine. Un autre examen standard est l'électrocardiogramme (ECG), qui permet de tracer l'évolution temporelle du potentiel électrique dans le coeur.
Cependant, aucune de ces méthodes n'est capable d'accéder aux propriétés biomécaniques intrinsèques du tissu myocardique. Actuellement, la pratique clinique standard consiste en la cathéterisation invasive dans le ventricule ou l'oreillette gauche en combinaison avec l'échocardiographie, pour obtenir des mesures directes de pression et volume et recueillir des informations sur la structure du tissu et des contraintes internes.
Il a été largement validé que l'estimation des propriétés mécaniques (par ex. la raideur) des tissus mous joue un rôle décisif dans la détection précoce des pathologies, car ces propriétés sont très sensibles aux changements structurels qui sont associés aux processus physiologiques et pathologiques [Sarvazyan et al., 2011]. L'estimation qualitative de la raideur tissulaire des organes superficiels par palpation manuelle a été utilisée depuis des siècles pour la caractérisation du cancer au sein et l'évaluation du stade de fibrose hépatique. Toutefois, les premières approches techniques en imagerie d'élasticité ont été développées seulement depuis trente ans environ, démontrant la possibilité d'estimer quantitativement la raideur des tissus mous. Les techniques d'élastographie se basent surtout sur trois étapes :

- l'excitation d'une région d'interêt dans le tissu ;
- la mesure de la perturbation générée ;
- la reconstruction des propriétés biomécaniques du tissu.

Les tissus mous sont considérés quasi-incompressible, du fait de leur forte teneur d'eau. Le facteur principal pour cela est le phénomène d'hydration, i.e. l'interaction entre groupes atomiques de substances organiques polarisés, chargées et hydrophobes, avec les molécules d'eau. Pour cette raison, le module de compressibilité – qui dépend principalement de la composition moléculaire du tissu – est proche de celui de l'eau et varie dans un intervalle d'environ 10% [Sarvazyan et al., 2011]. Au contraire, le module de cisaillement, qui dépend d'autres propriétés du tissu, comme l'hétérogénéité et l'anisotropie, au niveau cellulaire ou à des niveaux supérieurs d'architecture, varie sensiblement (de l'ordre de centaines de pourcent) dans les processus physiologiques et pathologiques, et diffère de quelques ordres de grandeur parmi les différents tissus mous.
La relation la plus commune qui est adoptée pour estimer le module de cisaillement μ à partir de la caractérisation de la propagation des ondes de cisaillement, sous l'hypothèse

que le milieu soit homogène, linéaire, isotrope et purement élastique, est

$$\mu = \rho\, v_s^2,$$

où ρ représente la densité du milieu, et v_s est la vitesse des ondes de cisaillement. Cependant, cette relation simple n'est pas vraie en présence d'anisotropie du tissu, d'hétérogénéité ou d'un comportement nonlinéaire du milieu, comme le myocarde. Par conséquent, de nombreuses études expérimentales dans le contexte cardiaque présentent une estimation incorrecte des propriétés mécaniques. Plus en détails, ce qui est mesuré represente des propriétés apparentes qui changent considérablement pendant le cycle cardiaque.

Il est possible d'identifier deux méthodes principales d'imagerie d'élasticité. Cette distinction se base sur les principes physiques sous-jacents qui sont utilisés pour effectuer la mesure : imagerie d'élasticité ultrasonore (EUS) et élastographie par résonance magnétique (ERM).
Dans les premières méthodes ultrasonores (à la fin des années 1980), les déformations dans les tissus étaient générées par un chargement statique ou une vibration extérieure. Ensuite, à la fin des années 1990, une nouvelle approche basée sur la génération à distance d'ondes élastiques par force de radiation acoustique (FRA) a été développée [Rudenko et al., 1996; Sarvazyan et al., 1998, 2010]. La FRA peut être définie comme une force moyenne en temps exercée par une onde acoustique sur un objet, qui est générée par une modification de la densité d'énergie de l'onde ultrasonore du champ acoustique incident [Sarvazyan et al., 2011]. Les techniques basées sur la FRA ont obtenu un succès grandissant dans les dernières années, du fait que les déformations générées sont très localisées, car les ondes élastiques créées sont complètement atténuées après quelques longueurs d'ondes. Par conséquent, l'estimation locale des propriétés biomécaniques est simplifiée, car on peut faire l'hypothèse de conditions aux bords transparentes, i.e. le milieu peut être considéré comme infini. Ainsi, plusieurs méthodes basées sur la FRA ont été développées et testées récemment. Les caractéristiques principales de l'imagerie d'élasticité ultrasonore consistent en la résolution spatiale optimale (0.1 - 0.5 mm) et l'acquisition en temps très rapide (jusqu'à 4-30 µs). En général, des cartes bi-dimensionnelles d'élasticité sont calculées. De plus, si le capteur ultrasonore est déplacé, ou si des capteurs tri-dimensionnels sont utilisés, il est possible d'obtenir des données de déplacement tri-dimensionnelles, donc des cartes d'élasticité en trois dimensions.

En parallèle des techniques à base d'ultrasons, plusieurs modalités d'imagerie d'élasticité sont basées sur l'imagerie par résonance magnétique (IRM). Les premières expériences d'ERM ont été effectuées au début des années 1990 et se basaient sur un chargement statique [Fowlkes et al., 1992]. Par la suite, les premières études impliquant un chargement dynamique datent de 1995 [Muthupillai et al., 1995; Fowlkes et al., 1995]. Dans cette modalité d'imagerie, un vibrateur externe est utilisé pour générer des ondes de cisaillement harmoniques dans le tissu, dans un intervalle de fréquences de 50-1000 Hz. Puis, un gradient sensible au mouvement est adopté, afin de mesurer le mouvement à une fréquence et direction spécifiques. Ce gradient est synchronisé à la même fréquence que la source vibrante externe. Le champs de déplacement vibratoire dans le tissu est mesuré par IRM, et il est directement proportionnel au déphasage du signal IRM acquis. À noter qu'il est possible d'acquérir des champ de déplacement tri-dimensionnels en utilisant des gradients polarisés dans des directions différentes. À partir des champs de déplacement, une carte d'élasticité – appelée *élastogramme* – est calculée à travers un algorithme d'inversion [Arani et al., 2017; Sarvazyan et al., 2011]. Les avantages principaux de l'ERM sont l'absence de contraintes sur la profondeur d'image (car elle n'est pas limitée par la présence d'os ou de

gaz) et l'orientation libre du champ de vision, car il n'y a pas la nécessité d'une fenêtre acoustique. En outre, cette technique est opérateur-indépendante, et l'organe entier peut être pris en compte. Cependant, les scanners IRM sont plus chers et moins accessibles que les scanners ultrasonores. De plus, une bonne résolution spatiale (1-3 mm) peut être obtenue au prix du temps d'acquisition, qui peut varier de plusieurs secondes à plusieurs minutes. Cela rend les mesures plus compliquées à obtenir dans le contexte cardiaque, où les données doivent être acquises à une très haute fréquence. Des progrès appréciables sont à noter très récemment [Elgeti and Sack, 2014; Arani et al., 2017; Fovargue et al., 2018].

Par souci d'exhaustivité, une autre méthode d'imagerie élastographique est à citer, qui se base sur des techniques d'optique. L'avantage principal est la meilleure résolution en espace (jusqu'à 5 µm) et le meilleur rapport signal/bruit que l'US ou l'IRM, qui permet d'explorer des phénomènes à une échelle intermédiaire entre la cellule et l'organe. Les techniques sous-jacentes principales sont la tomographie par cohérence optique (TCO) et la microscopie de Brillouin. D'autre part, les inconvénients des méthodes optiques sont la contrainte d'une fenêtre optique pour effectuer les mesures et la profondeur d'image considérablement basse (0.1 - 3.0 mm), à cause de la grande dispersion et l'atténuation des tissus mous [Kennedy et al., 2017; Greenleaf et al., 2003].

Les applications cliniques principales de l'imagerie d'élastographie sont l'évaluation des masses tumorales du sein et les cirrhoses et fibroses hépatiques. Cependant, des développements récents sont à signaler dans de nombreuses applications, comme la prostate, la thyroïde, les noeuds lymphatiques, les parois artérielles, l'évaluation des plaques athéromateuses, des thromboses artérielles et veineuses, la rejection de greffes, le coeur, les muscles squelettiques, les lymphoedèmes, le cerveau et les tumeurs dans tous les organes majeurs. À noter que certaines applications sont encore à des états initiaux de recherche, alors que d'autres sont déjà utilisées dans la pratique clinique. Nous faisons référence à [Sarvazyan et al., 2011; Sigrist et al., 2017; Caenen, 2018] pour d'autres détails sur les méthodes d'imagerie d'élasticité et leurs applications cliniques.

Élastographie ultrasonore : un récapitulatif

Nous présentons ici une introduction rapide sur l'imagerie d'élasticité à base ultrasonore (EUS). Nous faisons référence à [Sarvazyan et al., 2011; Gennisson et al., 2013; Sigrist et al., 2017] pour des détails supplémentaires. La première approche en élastographie ultrasonore était l'élastographie de déformation (Strain Elastography) [Ophir et al., 1991]. Cette technique a été développée au début des années 1990 et était basée sur une compression *statique*. En particulier, une estimation qualitative des propriétés élastiques du tissu était déduite par comparaison des informations anatomiques avant et après avoir induit une petite déformation dans la région d'interêt à travers l'application d'une contrainte constante en temps. En général, des signaux écho de radiofréquence étaient utilisés pour extraire le champ de déplacement par des algorithmes de corrélation. Ensuite, des images de déformation pouvaient être obtenues par le calcul du gradient de déplacement. L'application la plus fréquente est l'imagerie du sein. Cette méthode a été adoptée par de nombreux dispositifs US commerciaux, puisqu'elle bénéficie d'une implémentation simple, même s'il n'est pas possible de recueillir des informations quantitatives de la raideur du tissu.

Au contraire, les méthodes *dynamiques* se basent sur l'application d'une force qui varie

en temps. Il est possible de distinguer ultérieurement entre les méthodes *impulsionnelles*, dans lesquelles le tissu est excité par une impulsion très rapide, et le méthodes *harmoniques*, qui sont basées sur l'application d'une force oscillatoire à une fréquence fixée [Gennisson et al., 2013]. Dans les deux méthodes, la perturbation mécanique se propage sous forme d'ondes élastiques (de pression et cisaillement) dans le tissu. La famille des méthodes impulsionnelles s'appuie sur la caractérisation de la propagation d'ondes ; par conséquent, il est possible d'extraire des cartes quantitatives de la raideur du tissu, avec une bonne résolution en espace, différemment des méthodes quasi-statiques. Cependant, l'implémentation de ces techniques demande un équipement plus complexe, pour induire des ondes de cisaillement et pour imager la petite perturbation associée à la propagation d'ondes de cisaillement. La génération d'ondes de cisaillement est réalisée à travers une excitation externe – par des vibrateurs externes – ou excitation interne – par la force de radiation acoustique (FRA) d'un faisceau ultrasonore focalisé.

Une méthode répandue qui se base sur une excitation surfacique est la **Transient Elastography (TE)**. La première technique a été développée en une dimension par l'Institut Langevin en 1995 [Catheline, 1998]. Cette technique se basait sur la génération d'une impulsion mécanique transitoire à basse fréquence (10-500 Hz) dans le tissu, générant une onde de cisaillement sphérique. Le déplacement induit était mesuré par des algorithmes de corrélation et la vitesse de phase de l'onde de cisaillement était extraite, permettant l'estimation de la raideur, l'anisotropie, la viscosité et la non-linéarité des tissus mous comme le foie [Catheline et al., 2003; Sandrin et al., 2003; Catheline et al., 2004; Gennisson et al., 2013]. Cette technique a été étendue depuis au cas bi-dimensionnel par le même institut [Sandrin et al., 2002]. Les premiers résultats in vivo étaient prometteurs, mais cette technique étendue n'a pas obtenu un grand succès, à cause des limitations pratiques du dispositif.

L'idée de combiner une excitation interne du tissu à travers une impulsion acoustique et la caractérisation des ondes de cisaillement générées est due au Dr. Armen Sarvazyan [Sarvazyan et al., 1998]. Depuis, plusieurs méthodes basées sur la FRA ont été développées et appliquées dans une large gamme d'applications, par ex. l'estimation des fibroses hépatiques, la détection des cancers du sein, des pathologies cardiaques [Sarvazyan et al., 2011; Sigrist et al., 2017]. L'avantage principal des méthodes internes est représenté par le caractère extrêmement localisé de la perturbation induite . De plus, les ondes de cisaillement sont complètement atténuées dans une distance de quelques longueurs d'onde à partir du point focal du faisceau ultrasonore. Cela induit un rétrécissement de la déformation générée et exclut l'interaction avec des ondes longitudinales à la surface du tissu. Par conséquent, la propagation d'ondes élastiques dépend seulement des paramètres de l'excitation acoustique et des propriétés structurelles du tissu. Cela permet une reconstruction plus simple des propriétés biomécaniques du tissu d'intérêt, car la qualité de la reconstruction peut être sensiblement affectée par des erreurs dans la définition des conditions au bord [Sarvazyan et al., 2011]. En outre, l'énergie d'excitation est transférée directement au tissu, alors que dans les techniques d'excitation externes il y a un couplage fort d'énergie à la surface du corps (peau ou graisse sous-cutanée), qui peut limiter considérablement le déplacement de tissu induit dans l'organe, spécialement dans les sujets obèses [Palmeri et al., 2008]. À noter que, à cause de l'absence de compression, cette technique est moins opérateur-dépendante des méthodes d'imagerie basées sur les ultrasons [Nightingale, 2011].
Nous citons, parmi les méthodes d'imagerie d'élasticité basées sur la FRA (en Figure 2) :

- La méthode **Acoustic Radiation Force Impulse (ARFI)** [Nightingale et al.,

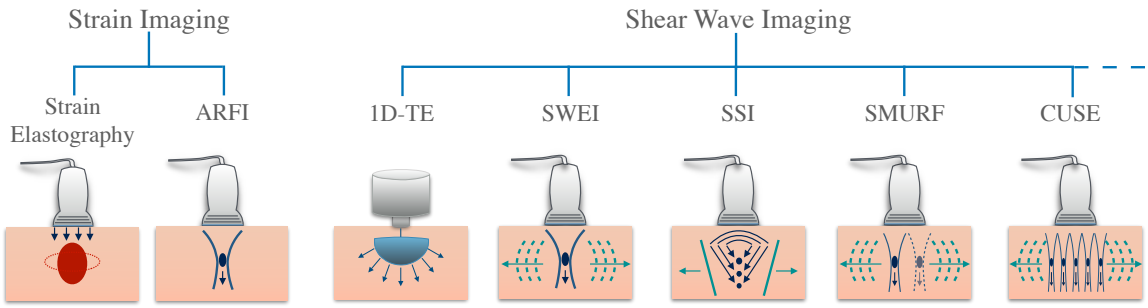

FIGURE 2 – Illustration schématique de quelques méthodes d'élastographie à base ultrasonore.

2002]. Cette technique se base sur l'excitation du tissu à travers une impulsion (FRA) rapide et à grande intensité à partir d'un faisceau ultrasonore focalisé, et le suivi du mouvement du tissu dans la région d'intérêt à travers des techniques d'imagerie ultrasonore standard. L'imagerie ARFI mesure les déplacements longitudinaux du tissu pour déterminer les différences relatives dans la raideur de tissu, de façon similaire aux données générées avec des méthodes d'imagerie de déformation de compression. Le pic de déplacement est affiché dans une image, pour estimer qualitativement la raideur du tissu.

- La méthode **Shear Wave Elasticity Imaging (SWEI)**, qui a été décrite théoriquement pour la première fois par Sarvazyan et al. [1998] et examinée in vivo par Nightingale et al. [2003]. Cette technique consiste en la génération à distance d'ondes de cisaillement par une impulsion acoustique (d'environ 100 µs) et dans la mesure du mouvement de cisaillement par imagerie d'ultrasons focalisés ; la vitesse des ondes de cisaillement est calculée par des méthodes standard de temps de vol, et les propriétés mécaniques du tissu sont obtenues par la résolution de problèmes inverses.

- La méthode **Supersonic Shear Imaging (SSI)** [Bercoff et al., 2004], caractérisée par plusieurs excitations de FRA à des positions différentes, de sorte que les ondes de cisaillement générées à chaque impulsion puissent interférer de façon constructive et générer une onde de cisaillement conique (cône de Mach). De cette façon, l'amplitude du déplacement du tissu est augmentée jusqu'à 100 µm dans les fantômes et 40 µm in vivo, contre 10-20 µm obtenus pour une impulsion simple. Le nom "supersonique" est dû au fait que le point focal de la force de radiation se déplace plus rapidement de l'onde de cisaillement générée, induisant un front d'onde quasi-plane. Une spécificité de cette méthode est la capacité d'imager le déplacement de cisaillement à une très haute fréquence d'images (jusqu'à 12000 images par seconde), car des ondes planes sont transmises pour la détection de mouvement au lieu d'impulsions focalisées. Pour cela, la propagation d'ondes de cisaillement peut être mesurée en temps-réel et sur un large champ de vision. La vitesse de l'onde de cisaillement peut être calculée par l'inversion de l'équation des ondes pour estimer les propriétés élastiques du milieu.

- La technique **Spatially Modulated Ultrasound Radiation Force (SMURF)** [McAleavey et al., 2007]. Cette technique consiste en l'excitation du tissu par une impulsion de FRA dans deux ou plusieurs positions différentes en succession rapide, afin de générer une force de radiation qui varie en espace. La vitesse de l'onde de cisaillement est estimée à partir de la différence dans les temps d'arrivée des impulsions, et la différence de longueur de trajet est prise comme le décalage dans les

emplacements du faisceau de l'impulsion. L'avantage principal de cette méthode est la haute résolution en espace des images de raideur qui sont calculées.

- La méthode **Comb-push Ultrasound Shear Elastography (CUSE)** [Song et al., 2012], qui se base sur une impulsion combinée afin de générer un champ d'onde de cisaillement complexe qui se propage dans le champ de vision complet en deux dimensions. Après, le mouvement de cisaillement est tracé à partir de la transmission d'ondes planes. Des filtres directionnels sont appliqués sur les données de déplacement pour extraire les ondes de cisaillement qui se propagent, et la vitesse des ondes de cisaillement est calculée par des méthodes de temps de vol. Cette technique permet l'estimation des propriétés élastiques de la région d'interêt entière sans problème d'atténuation et avec un très bon rapport signal/bruit.

Parmi les techniques d'élastographie *harmoniques*, nous citons la Shear wave Dispersion Ultrasound Vibrometry (SDUV) [Chen et al., 2009] et la Crawling Wave Sonoelastography (CWS) [Hah et al., 2010].
Dorénavant, nous indiquerons par élastographie par ondes de cisaillement, i.e. Shear Wave Elastography (SWE), la famille de méthodes d'imagerie basées sur la génération d'ondes de cisaillement à un endroit par la force de radiation acoustique (par exemple, SWEI ou SSI).

Modélisation de la FRA

La source principale d'atténuation dans les tissus mous est l'absorption, car la contribution liée à la diffusion peut être négligée [Parker, 1983]. Par conséquent, lorsqu'une onde acoustique se propage dans le milieu, un gradient d'énergie se forme dans le tissu, en raison de l'absorption. La FRA est liée au transfert de la quantité de mouvement de l'onde ultrasonore se propageant dans le milieu, ce qui génère une modification de la densité d'énergie acoustique [Torr, 1984]. Dans l'hypothèse d'ondes planes, cette force peut être modélisée comme une force volumique dans la direction de la propagation de l'onde, distribuée dans l'ombre géométrique de l'ouverture du transducteur [Palmeri and Nightingale, 2011]. La FRA ne peut pas être déduite de la relation contrainte-déformation dans des matériaux purement élastiques, car les modèles élastiques n'intègrent aucun mécanisme de perte d'énergie pouvant justifier un changement de la quantité de mouvement.

De plus, il est à noter que les propriétés viscoélastiques des tissus dépendent fortement de la fréquence de l'excitation : en fait, à des fréquences basses (<100 kHz), les tissus peuvent être modélisés comme des tissus mous ; toutefois, aux fréquences ultrasonores, les tissus ne supportent pas les contraintes de cisaillement et l'atténuation des ondes acoustiques génère un échauffement et la FRA ; ainsi, les tissus peuvent être modélisés comme des fluides visqueux.

De nombreux modèles pour analyser les mécanismes physiques responsables de la FRA et de la génération à distance d'ondes de cisaillement dans des milieux de type aqueux ont été proposés par la communauté acoustique. Le premier modèle théorique des oscillations de cisaillement générées à distance par la FRA a été présenté par Rudenko et al. [1996] et Sarvazyan et al. [1998]. Depuis, d'autres auteurs [Zabolotskaya et al., 2004; Gennisson et al., 2007] ont obtenu une équation d'évolution pour les ondes de cisaillement dans un milieu mou isotrope, en supposant des ondes de cisaillement planes. Le rôle de l'inhomogénéité et de la viscosité dans la génération des ondes de cisaillement a été d'abord analysé par Ostrovsky et al. [2007]. Plus en détail, il est prouvé qu'un champ acoustique dans un

solide homogène purement élastique (non dissipatif) ne peut pas générer de mouvements de cisaillement.
Cependant, à notre connaissance, aucune analyse mathématique n'a encore été fournie pour établir une expression analytique de la FRA et justifier la génération d'ondes de cisaillement à partir de la FRA. En fait, à des fins de modélisation, certaines hypothèses restrictives sont formulées pour dériver une expression simple de la force volumique résultante. En particulier, si le tissu est modélisé comme un fluide visqueux linéaire et dans l'hypothèse d'ondes planes, il est possible de déduire l'expression suivante de la FRA, centrée au point focal (x_F, y_F, z_F) : [Nightingale et al., 2002; Palmeri et al., 2005]

$$F(x,y,z,t) \coloneqq A_{\max} \exp^{-\left(\frac{(x-x_F)^2}{\sigma_x^2}+\frac{(y-y_F)^2}{\sigma_y^2}+\frac{(z-z_F)^2}{\sigma_z^2}\right)} \cdot \exp^{-\frac{(t-t_{pulse})^2}{\sigma_t^2}}, \tag{2}$$

avec

$$A_{\max} = \frac{2\,\alpha\, I_{\max}}{v_p},$$

où α est un coefficient d'atténuation, $I_{\max}$ est une intensité moyenne dans le temps et v_p est la vitesse de l'onde longitudinale. La direction de cette force est la même que l'orientation de la propagation de l'onde et elle est appelée vecteur de Poynting. Ce vecteur est généralement orienté dans le sens axial pour une plage de $\pm 10\%$ à partir de la profondeur focale. Nous renvoyons le lecteur à Nightingale [2011]; Caenen [2018] pour davantage de précisions sur cette approximation de modélisation.

Modélisation de l'élastographie par ondes de cisaillement

L'approche la plus appropriée pour modéliser la physique sous-jacente de l'élastographie par ondes de cisaillement dans un milieu fini viscoélastique est par la méthode des éléments finis (EF), en raison de sa flexibilité permettant l'extension à des géométries plus complexes, par exemple spécifiques au patient. De nombreux modèles de SWE ont été développés au cours de la dernière décennie, principalement orientés vers les applications. Les premiers modèles reposaient sur l'hypothèse simplificatrice d'un matériau linéaire et isotrope, pouvant représenter par exemple une approximation du tissu hépatique ou d'autres tissus mous isotropes. Un des premiers modèles EF de la réponse dynamique du tissu à une excitation par force de radiation ultrasonore a été présenté par Palmeri et al. [2005]. Le tissu modélisé dans ce travail est supposé isotrope, élastique et linéaire.

Parmi les premières simulations EF en milieu viscoélastique, nous citons Lee et al. [2012]. En particulier, ils ont considéré un fantôme linéaire viscoélastique, isotrope, avec une inclusion cylindrique plus rigide. Caenen et al. [2017] a adopté une stratégie numérique similaire pour étudier la physique des ondes de cisaillement dans un milieu viscoélastique, linéaire et isotrope. De plus, les résultats ont été comparés à des données expérimentales in vitro. Plus récemment, Ye et al. [2017] a proposé une simulation FE en 2D d'un modèle visco-hyperélastique, isotrope et quasi-incompressible.
Un des premiers modèles anisotropes a été proposé par Rouze et al. [2013]. Plus en détail, ils ont proposé un modèle EF de propagation d'ondes de cisaillement dans un matériau élastique, linéaire, quasi-incompressible et transverse isotrope, soumis à une excitation impulsive de la FRA, qui est modélisée avec une distribution gaussienne en 3D. Plus récemment, Qiang et al. [2015] ont analysé la propagation des ondes de cisaillement dans le plan de symétrie d'un matériau linéaire viscoélastique, isotrope transverse, et quasi incompressible. Très récemment, Caenen et al. [2018] ont étudié un modèle EF pour la mécanique

des ondes de cisaillement dans un matériau orthotrope, en combinaison avec un chargement mécanique uniaxial. Nous soulignons que toutes les méthodes mentionnées ci-dessus considèrent une approximation du terme source de FRA comme une force volumique ayant un profil similaire à celui de l'Eq. (2). En particulier, le champ d'intensité acoustique a été simulé avec le logiciel FIELD II et/ou modélisé sous forme d'une distribution 3D gaussienne.
Dans tous les travaux susmentionnés, une discrétisation temporelle totalement explicite a été adoptée et, à l'exception de Ye et al. [2017], le logiciel Abaqus a été utilisé pour résoudre le système d'équations obtenu. En fait, l'approche des auteurs est plus orientée vers l'application que vers le développement de schémas numériques adaptés à ces problèmes. Cependant, ce choix peut introduire des limitations critiques sur le pas de temps en raison de la contrainte d'incompressibilité, comme expliqué dans la suite.

Traitement de l'incompressibilité en élastodynamique

De nombreuses formulations de la méthode des éléments finis (EF) pour l'approximation de l'élasticité dans les solides incompressibles ont été développées au cours des dernières décennies, en raison de leur large application en mécanique numérique. Cependant, la majorité des travaux proposés dans la littérature prend en compte une configuration statique. Les principales contributions à ce jour peuvent être organisées en deux catégories : les méthodes de déplacement pur et les méthodes mixtes.

D'une part, les EF basés sur le déplacement fournissent des solutions satisfaisantes aux problèmes d'élasticité quasi- ou purement incompressibles ; néanmoins, ces méthodes peuvent présenter des limitations indésirables, telles qu'un mauvais conditionnement de la matrice de rigidité, des pressions parasites ou incorrectes et le verrouillage numérique (raidissement sévère près de la limite incompressible) [Sussman and Bathe, 1987], en raison de l'application de la contrainte d'incompressibilité. Plusieurs méthodes ont été proposées pour améliorer la précision des méthodes basées sur le déplacement [Malkus and Hughes, 1978; Hughes, 1980; Neto et al., 2005].

Par ailleurs, les méthodes mixtes par éléments finis [Brezzi and Fortin, 2012] se sont révélées efficaces pour obtenir des résultats précis dans la résolution des écoulements de fluides incompressibles et de l'élasticité incompressible. Dans ces méthodes, le problème sous contrainte est réécrit sous la forme d'un problème de point d'équilibre sans contrainte et une deuxième variable - la pression - est introduite. Cependant, toutes les méthodes mixtes ne sont pas stables. En fait, les propriétés de convergence de cette formulation sont régies par des considérations de stabilité, impliquant des exigences d'ellipticité et la fameuse condition Ladyzhenskaya - Babŭska - Brezzi (LBB) [Brezzi and Bathe, 1990; Brezzi and Falk, 1991]. Si cette condition de stabilité n'est pas satisfaite, des oscillations non physiques sévères peuvent apparaître dans le champ de pression. Des méthodes de stabilisation ont été proposées pour surmonter les limites des formulations classiques d'EF mixtes dans le domaine de la dynamique des fluides incompressibles. Ces méthodes reposent sur l'ajout de termes différentiels d'ordre élevé artificiels à l'équation de continuité discrète, afin de contourner la condition LBB (voir [Quarteroni and Valli, 1994] pour un aperçu complet).

Toutes les méthodes décrites précédemment peuvent être étendues à des équations dynamiques utilisant une discrétisation temporelle implicite (par exemple, schéma d'Euler implicite ou schémas de Newmark implicites). Cependant, à chaque pas de temps, une

inversion de matrice est requise pour le calcul de la vitesse ou du champ de déplacement. Une approche populaire pour augmenter l'efficacité des solveurs dynamiques a été proposée pour la première fois en calcul dynamique des fluides par [Chorin, 1968, 1969] et Temam [1968, 2001] à la fin des années 1960, et il est appelé projection à pas fractionnaire. Dans cette famille de méthodes, la discrétisation en temps est divisée en deux étapes distinctes pour la viscosité et l'incompressibilité, respectivement. La première demi-étape correspond à un problème elliptique pour une vitesse intermédiaire, tenant compte de la diffusion de la viscosité et de l'advection, tandis que la deuxième demi-étape consiste en un problème non visqueux où la vitesse à la fin du pas de temps, à divergence nulle, est calculée à partir de la distribution de pression. De cette manière, à chaque pas de temps, deux équations elliptiques découplées sont résolues, ce qui est très avantageux pour des simulations à grande échelle. [Guermond et al., 2006].

Des efforts moins importants ont été déployés pour développer des méthodes efficaces pour le traitement de la contrainte d'incompressibilité en élastodynamique. Étant donné que la physique sous-jacente est la propagation d'ondes, des méthodes totalement explicites pourraient être considérées comme de bons candidats pour obtenir des schémas efficaces (dans le cas de milieux quasi-incompressibles). Cependant, l'application de l'incompressibilité implique une limitation drastique du pas de temps du schéma, en raison de la condition de stabilité. Afin de contourner les limites des méthodes totalement explicites, nous proposons d'adopter les idées principales de l'algorithme de projection à pas fractionnaire pour concevoir un schéma efficace d'élastodynamique incompressible, en raison de l'efficacité de cette méthode et des similitudes avec les fluides incompressibles visqueux.

Structure de la thèse

La première partie du manuscrit traite de la modélisation mathématique de la FRA, de la propagation de l'onde de cisaillement résultante et de la caractérisation de la vitesse de l'onde de cisaillement dans une loi de comportement générale du tissu myocardique. L'une des contributions principales de ce travail est la mise au point d'une analyse mathématique originale du phénomène de la FRA. Plus en détail, nous déduisons l'équation dominante du champ de pression et du champ d'ondes de cisaillement induites à distance par la FRA, et nous calculons une expression analytique du terme source responsable de la génération d'ondes de cisaillement à partir d'une impulsion de pression acoustique. L'approche que nous proposons repose sur une analyse asymptotique.
Dans la deuxième partie de la thèse, nous présentons des outils numériques efficaces pour une simulation numérique réaliste d'une expérience de SWE. L'approximation numérique des équations de l'élastodynamique est basée sur des éléments finis spectraux d'ordre élevé pour la discrétisation spatiale. De plus, nous présentons une nouvelle méthode de discrétisation temporelle adaptée à l'élasticité incompressible. En particulier, nous construisons une discrétisation temporelle qui conserve l'énergie et ne traitons implicitement que les termes correspondant à des "informations" se déplaçant à une vitesse infinie, associées à la contrainte d'incompressibilité, en résolvant un problème scalaire de Poisson à chaque pas de temps de l'algorithme. De plus, nous proposons une nouvelle méthode rapide, sans stockage de matrice et d'ordre élevé pour résoudre l'équation différentielle partielle de Poisson dans le domaine fini.

Part I : Modélisation mathématique

Extraction des propriétés mécaniques des tissus mous à partir de la vitesse des ondes de cisaillement. Le premier objectif de cette thèse est de décrire une approche méthodologique permettant de caractériser la propagation élastographique des ondes de cisaillement pour une loi de comportement générale du myocarde. Les équations régissant la propagation des ondes de cisaillement sont obtenues à partir d'un modèle biomécanique reflétant avec précision le comportement complexe du myocarde et de l'organe entier. Ensuite, les vitesses des ondes de cisaillement sont calculées sur la base du calcul d'un tenseur dit de Christoffel. Nous caractérisons la propagation des ondes de cisaillement pour différents choix de loi de comportement associée à la contrainte passive. De plus, nous étudions la contribution de la contrainte active à la propagation de l'onde élastographique et démontrons qu'elle est dominée par l'effet de précontrainte. Nous conclurons ce chapitre en montrant quelques applications à l'extraction de l'orientation des fibres dans tout le myocarde et à la détection de "pathologies numériques" dans un modèle biomécanique tridimensionnel de coeur.

Modélisation de la FRA et génération d'ondes de cisaillement. L'un des objectifs de cette thèse est de fournir une expression analytique de l'excitation induite par la FRA dans un solide non linéaire. De manière plus détaillée, nous souhaitons proposer une formulation valable pour les milieux subissant une déformation importante, indépendamment de la nature de la précontrainte. De plus, nous visons à nous débarrasser des hypothèses simplificatrices habituellement faites sur les propriétés de la solution (par exemple, l'hypothèse d'onde plane). Pour ce faire, nous élaborons un modèle mathématique basé sur des considérations énergétiques et une analyse asymptotique. Il est à noter également que dans les méthodes d'élastographie basées sur la FRA appliquées au contexte cardiaque, la propagation des ondes induite par la FRA se superpose à la mécanique non linéaire associée à la déformation cardiaque pendant le cycle cardiaque, qui doit être prise en compte dans la formulation. Dans le Chapitre 2 nous fournissons un modèle mathématique rigoureux qui décrit, dans le contexte d'un modèle biomécanique non linéaire, représentant de manière adéquate l'état complexe du myocarde :

- l'expression du terme source surfacique (faisceau ultrasonore focalisé) ;
- la propagation d'ondes de pression induite par l'excitation de FRA ;
- la propagation d'ondes de cisaillement générée par la FRA.

Une expression détaillée du terme source responsable de la propagation de l'onde de cisaillement est fournie et il est montré qu'il est associé à la viscosité et aux non-linéarités du tissu. De plus, dans le Chapitre 3, nous fournissons une justification de notre formulation en présentant une preuve de convergence de l'approximation de la solution dans une configuration linéaire quasi-statique.

Partie II : Approximation numérique

Approximation numérique des équation d'élastodynamique en incompressible. Afin de réaliser une approximation appropriée et efficace de la propagation des ondes élastiques dans des solides incompressibles, nous décrivons dans le Chapitre 4 (qui prend la forme d'un article déjà soumis pour publication dans une revue internationale) un cadre numérique adapté que nous avons développé pour le traitement de la contrainte d'incom-

pressibilité. Des éléments finis conformes d'ordre élevé avec mass-lumping sont utilisés pour la discrétisation en espace et un schéma implicite/explicite de deuxième ordre, préservant l'énergie, est utilisé pour la discrétisation en temps. La caractéristique principale de cette méthode est que le pas de temps de l'algorithme n'est pas régi par l'onde de pression, qui se déplace à une vitesse "infinie", mais uniquement par la vitesse de l'onde de cisaillement. De plus, la contrainte d'incompressibilité est imposée par des techniques de pénalisation et consiste en la résolution d'un problème scalaire de Poisson à chaque pas de temps. L'analyse numérique de l'ordre de convergence du schéma est détaillée au Chapitre 5.

Simulation numérique d'une expérience de SWE . Le deuxième objectif principal de cette thèse est le développement d'un cadre computationnel pour la simulation numérique réaliste d'une expérience de SWE dans un tissu mou comme le myocarde. Pour ce faire, le Chapitre 6 est consacré à la description d'un modèle mathématique tridimensionnel complet pour la propagation des ondes élastiques dans un milieu précontraint, hyperélastique, viscoélastique, hétérogène, anisotrope, sujet à une contrainte active, dans des conditions réalistes d'une expérience de SWE. L'approximation numérique de ce modèle consiste en une méthode d'éléments spectraux d'ordre supérieur en espace et en une discrétisation temporelle implicite/explicite adaptée, décrite dans le Chapitre 4. Une preuve de la stabilité du schéma est également détaillée dans ce chapitre.

Un solveur rapide pour la résolution numérique du problème de Poisson. Afin de réaliser des simulations numériques efficaces de la propagation d'ondes élastiques dans le myocarde, nous avons développé une méthode adaptée à la résolution du problème de Poisson qui est introduit à chaque pas de temps du schéma proposé au Chapitre 4. En particulier, dans le Chapitre 7 (qui prend aussi la forme d'un article soumis pour publication dans une revue internationale), nous fournissons un nouveau solveur rapide, sans stockage de matrice, pour le problème de Poisson discrétisé avec les méthodes d'éléments spectraux d'ordre élevé (HO-SEM). Cette méthode repose sur l'utilisation de la transformation de Fourier discrète (TFD) pour réécrire le problème sous forme de l'inversion du symbole de l'opérateur dans l'espace des fréquences. Puisque des HO-SEM sont adoptés pour la discrétisation en espace, une implémentation efficace est requise pour l'inversion du symbole. Le solveur que nous avons développé se caractérise par plusieurs caractéristiques :

- il préserve l'efficacité de l'algorithme de transformée de Fourier rapide, qui est standard pour le cas linéaire ;
- le stockage de matrices est réduit sensiblement ;
- une décomposition en valeurs singulières (SVD) pseudo-explicite est utilisée pour l'inversion des symboles ;
- il est naturellement étendu à de multiples dimensions par tensorisation, en raison de la discrétisation HO-SEM sous-jacente ;
- il peut être facilement généralisé à des conditions aux bords non périodiques en effectuant une extension périodique symétrique du terme source. Cependant, en raison des propriétés de symétrie du terme source étendu et des propriétés intrinsèques de la TFD, la majeure partie des calculs est limitée aux fréquences associées au terme source d'origine (non étendu), préservant ainsi l'efficacité de l'algorithme.

Ce chapitre est complété par des résultats numériques et quelques remarques sur la complexité du solveur - qui se révèle être de l'ordre de $O(R^{d+1}\, N^d \log N)$ en dimension d - et

sa parallélisabilité.

Communications

Communications orales et présentations de posters

- **Présentation orale à la "Journée de Rentrée 2018 de l'EDMH".**
  IHES, Bures-sur-Yvette, 11.10.2018.
- **Présentation orale à la conférence VPH 2018.**
  University of Zaragoza, Zaragoza, Espagne, 05.09.2018.
- **Présentation orale à la conférence SIMAI 2018.**
  Università la Sapienza, Rome, Italie, 05.07.2018.
- **Présentation orale à la conférence INdAM "Mathematical and Numerical Modeling of the Cardiovascular System".**
  Istituto Nazionale di Alta Matematica (INdAM), Rome, Italie, 16.04.2018.
- **Présentation orale au symposium CLIPS 2017 : Coalition for Live Imaging Paris-Saclay, Multiscale Live Imaging in Human, Animal and Plant Health.**
  Campus CNRS Gif-sur-Yvette, France, 13.09.2017.
- **Présentation orale à la conférence CMBE 2017.**
  University of Pittsburgh, Pittsburgh, PA, États-Unis , 12.04.2017.
- **Présentation Poster à l'école d'été Biomechanics and Modeling in Mechanobiology**
  Institute of Biomechanics, Graz University of Technology, Graz, Autriche, 06.07.2016.

Publications

- **A conservative penalisation strategy for the semi-implicit time discretisation of incompressible elastodynamic equations.** Caforio F. and Imperiale S., soumis.
- **High-order Discrete Fourier Transform for the resolution of the Poisson equation**. Caforio F. and Imperiale S., soumis.

Bibliographie

Arani, A., Arunachalam, S. P., Chang, I. C., Baffour, F., Rossman, P. J., Glaser, K. J., Trzasko, J. D., McGee, K. P., Manduca, A., Grogan, M. et al. [2017], 'Cardiac MR elastography for quantitative assessment of elevated myocardial stiffness in cardiac amyloidosis', *Journal of Magnetic Resonance Imaging* **46**(5), 1361–1367.

Bercoff, J., Tanter, M. and Fink, M. [2004], 'Supersonic shear imaging : a new technique for soft tissue elasticity mapping', *IEEE transactions on ultrasonics, ferroelectrics, and frequency control* **51**(4), 396–409.

Brezzi, F. and Bathe, K.-J. [1990], 'A discourse on the stability conditions for mixed finite element formulations', *Computer methods in applied mechanics and engineering* **82**(1-3), 27–57.

Brezzi, F. and Falk, R. S. [1991], 'Stability of higher-order Hood–Taylor methods', *SIAM Journal on Numerical Analysis* **28**(3), 581–590.

Brezzi, F. and Fortin, M. [2012], *Mixed and hybrid finite element methods*, Vol. 15, Springer Science & Business Media.

Caenen, A. [2018], A biomechanical analysis of shear wave elastography in pediatric heart models, PhD thesis, Ghent University.

Caenen, A., Pernot, M., Peirlinck, M., Mertens, L., Swillens, A. and Segers, P. [2018], 'An in silico framework to analyze the anisotropic shear wave mechanics in cardiac shear wave elastography', *Physics in Medicine & Biology* **63**(7), 075005.

Caenen, A., Pernot, M., Shcherbakova, D. A., Mertens, L., Kersemans, M., Segers, P. and Swillens, A. [2017], 'Investigating shear wave physics in a generic pediatric left ventricular model via in vitro experiments and finite element simulations', *IEEE transactions on ultrasonics, ferroelectrics, and frequency control* **64**(2), 349–361.

Catheline, S. [1998], Interférométrie-Speckle ultrasonore : Application à la mesure d'élasticité, PhD thesis, Université Paris-Diderot-Paris VII.

Catheline, S., Gennisson, J.-L., Delon, G., Fink, M., Sinkus, R., Abouelkaram, S. and Culioli, J. [2004], 'Measurement of viscoelastic properties of homogeneous soft solid using transient elastography : An inverse problem approach', *The Journal of the Acoustical Society of America* **116**(6), 3734–3741.

Catheline, S., Gennisson, J.-L. and Fink, M. [2003], 'Measurement of elastic nonlinearity of soft solid with transient elastography', *The Journal of the Acoustical Society of America* **114**(6), 3087–3091.

Chen, S., Urban, M. W., Pislaru, C., Kinnick, R., Zheng, Y., Yao, A. and Greenleaf, J. F. [2009], 'Shearwave dispersion ultrasound vibrometry (SDUV) for measuring tissue elasticity and viscosity', *IEEE transactions on ultrasonics, ferroelectrics, and frequency control* **56**(1), 55–62.

Chorin, A. J. [1968], 'Numerical solution of the Navier–Stokes equations', *Mathematics of computation* **22**(104), 745–762.

Chorin, A. J. [1969], 'On the convergence of discrete approximations to the Navier–Stokes equations', *Mathematics of computation* **23**(106), 341–353.

Elgeti, T. and Sack, I. [2014], 'Magnetic resonance elastography of the heart', *Current Cardiovascular Imaging Reports* **7**(2), 9247.

Fovargue, D., Kozerke, S., Sinkus, R. and Nordsletten, D. [2018], 'Robust mr elastography stiffness quantification using a localized divergence free finite element reconstruction', *Medical image analysis* **44**, 126–142.

Fowlkes, J., Emelianov, S., Pipe, J., Skovoroda, A., Carson, P., Adler, R. and Sarvazyan, A. [1995], 'Magnetic-resonance imaging techniques for detection of elasticity variation', *Medical physics* **22**(11), 1771–1778.

Fowlkes, J., Yemelyanov, S., Pipe, J., Carson, P., Adler, R., Sarvazyan, A. and Skovoroda, A. [1992], 'Possibility of cancer detection by means of measurement of elastic properties', *Radiology* **185**(S), 206–207.

Gennisson, J.-L., Deffieux, T., Fink, M. and Tanter, M. [2013], 'Ultrasound elastography : principles and techniques', *Diagnostic and interventional imaging* **94**(5), 487–495.

Gennisson, J.-L., Rénier, M., Catheline, S., Barrière, C., Bercoff, J., Tanter, M. and Fink, M. [2007], 'Acoustoelasticity in soft solids : Assessment of the nonlinear shear modulus with the acoustic radiation force', *The Journal of the Acoustical Society of America* **122**(6), 3211–3219.

Greenleaf, J. F., Fatemi, M. and Insana, M. [2003], 'Selected methods for imaging elastic properties of biological tissues', *Annual review of biomedical engineering* **5**(1), 57–78.

Guermond, J.-L., Minev, P. and Shen, J. [2006], 'An overview of projection methods for incompressible flows', *Computer methods in applied mechanics and engineering* **195**(44-47), 6011–6045.

Hah, Z., Hazard, C., Cho, Y. T., Rubens, D. and Parker, K. [2010], 'Crawling waves from radiation force excitation', *Ultrasonic imaging* **32**(3), 177–189.

Hughes, T. J. [1980], 'Generalization of selective integration procedures to anisotropic and nonlinear media', *International Journal for Numerical Methods in Engineering* **15**(9), 1413–1418.

Kennedy, B. F., Wijesinghe, P. and Sampson, D. D. [2017], 'The emergence of optical elastography in biomedicine', *Nature Photonics* **11**(4), 215.

Lee, K. H., Szajewski, B. A., Hah, Z., Parker, K. J. and Maniatty, A. M. [2012], 'Modeling shear waves through a viscoelastic medium induced by acoustic radiation force', *International journal for numerical methods in biomedical engineering* **28**(6-7), 678–696.

Malkus, D. S. and Hughes, T. J. [1978], 'Mixed finite element methods. reduced and selective integration techniques : a unification of concepts', *Computer Methods in Applied Mechanics and Engineering* **15**(1), 63–81.

McAleavey, S. A., Menon, M. and Orszulak, J. [2007], 'Shear-modulus estimation by application of spatially-modulated impulsive acoustic radiation force', *Ultrasonic imaging* **29**(2), 87–104.

Muthupillai, R., Lomas, D., Rossman, P., Greenleaf, J. F., Manduca, A. and Ehman, R. [1995], 'Magnetic resonance elastography by direct visualization of propagating acoustic strain waves', *science* **269**(5232), 1854–1857.

Neto, E., Pires, F. and Owen, D. [2005], 'F-bar-based linear triangles and tetrahedra for finite strain analysis of nearly incompressible solids. part i : formulation and benchmarking', *International Journal for Numerical Methods in Engineering* **62**(3), 353–383.

Nightingale, K. [2011], 'Acoustic radiation force impulse (ARFI) imaging : a review', *Current medical imaging reviews* **7**(4), 328–339.

Nightingale, K., McAleavey, S. and Trahey, G. [2003], 'Shear-wave generation using acoustic radiation force : in vivo and ex vivo results', *Ultrasound in medicine & biology* **29**(12), 1715–1723.

Nightingale, K., Soo, M. S., Nightingale, R. and Trahey, G. [2002], 'Acoustic radiation force impulse imaging : in vivo demonstration of clinical feasibility', *Ultrasound in medicine & biology* **28**(2), 227–235.

Ophir, J., Cespedes, I., Ponnekanti, H., Yazdi, Y. and Li, X. [1991], 'Elastography : a quantitative method for imaging the elasticity of biological tissues', *Ultrasonic imaging* **13**(2), 111–134.

Ostrovsky, L., Sutin, A., Il'inskii, Y., Rudenko, O. and Sarvazyan, A. [2007], 'Radiation force and shear motions in inhomogeneous media', *The Journal of the Acoustical Society of America* **121**(3), 1324–1331.

Palmeri, M. L. and Nightingale, K. R. [2011], 'Acoustic radiation force-based elasticity imaging methods', *Interface focus* p. rsfs20110023.

Palmeri, M. L., Sharma, A. C., Bouchard, R. R., Nightingale, R. W. and Nightingale, K. R. [2005], 'A finite-element method model of soft tissue response to impulsive acoustic radiation force', *IEEE transactions on ultrasonics, ferroelectrics, and frequency control* **52**(10), 1699–1712.

Palmeri, M. L., Wang, M. H., Dahl, J. J., Frinkley, K. D. and Nightingale, K. R. [2008], 'Quantifying hepatic shear modulus in vivo using acoustic radiation force', *Ultrasound in medicine & biology* **34**(4), 546–558.

Parker, K. J. [1983], 'Ultrasonic attenuation and absorption in liver tissue', *Ultrasound in medicine & biology* **9**(4), 363–369.

Qiang, B., Brigham, J. C., Aristizabal, S., Greenleaf, J. F., Zhang, X. and Urban, M. W. [2015], 'Modeling transversely isotropic, viscoelastic, incompressible tissue-like materials with application in ultrasound shear wave elastography', *Physics in medicine and biology* **60**(3), 1289.

Quarteroni, A. and Valli, A. [1994], *Numerical Approximation of Partial Differential Equations*, Springer.

Rouze, N. C., Wang, M. H., Palmeri, M. L. and Nightingale, K. R. [2013], 'Finite element modeling of impulsive excitation and shear wave propagation in an incompressible, transversely isotropic medium', *Journal of biomechanics* **46**(16), 2761–2768.

Rudenko, O., Sarvazyan, A. and Emelianov, S. Y. [1996], 'Acoustic radiation force and streaming induced by focused nonlinear ultrasound in a dissipative medium', *The Journal of the Acoustical Society of America* **99**(5), 2791–2798.

Sandrin, L., Fourquet, B., Hasquenoph, J.-M., Yon, S., Fournier, C., Mal, F., Christidis, C., Ziol, M., Poulet, B., Kazemi, F. et al. [2003], 'Transient elastography : a new noninvasive method for assessment of hepatic fibrosis', *Ultrasound in medicine & biology* **29**(12), 1705–1713.

Sandrin, L., Tanter, M., Catheline, S. and Fink, M. [2002], 'Shear modulus imaging with 2-D transient elastography', *IEEE transactions on ultrasonics, ferroelectrics, and frequency control* **49**(4), 426–435.

Sarvazyan, A., J Hall, T., W Urban, M., Fatemi, M., R Aglyamov, S. and S Garra, B. [2011], 'An overview of elastography-an emerging branch of medical imaging', *Current medical imaging reviews* **7**(4), 255–282.

Sarvazyan, A. P., Rudenko, O. V. and Nyborg, W. L. [2010], 'Biomedical applications of radiation force of ultrasound : historical roots and physical basis', *Ultrasound in medicine & biology* **36**(9), 1379–1394.

Sarvazyan, A. P., Rudenko, O. V., Swanson, S. D., Fowlkes, J. B. and Emelianov, S. Y. [1998], 'Shear wave elasticity imaging : a new ultrasonic technology of medical diagnostics', *Ultrasound in medicine & biology* **24**(9), 1419–1435.

Sigrist, R. M., Liau, J., El Kaffas, A., Chammas, M. C. and Willmann, J. K. [2017], 'Ultrasound elastography : review of techniques and clinical applications', *Theranostics* **7**(5), 1303.

Song, P., Zhao, H., Manduca, A., Urban, M. W., Greenleaf, J. F. and Chen, S. [2012], 'Comb-push ultrasound shear elastography (CUSE) : a novel method for two-dimensional shear elasticity imaging of soft tissues', *IEEE transactions on medical imaging* **31**(9), 1821–1832.

Sussman, T. and Bathe, K.-J. [1987], 'A finite element formulation for nonlinear incompressible elastic and inelastic analysis', *Computers & Structures* **26**(1-2), 357–409.

Temam, R. [1968], 'Une méthode d'approximation de la solution des équations de Navier-Stokes', *Bull. Soc. Math. France* **98**(4), 115–152.

Temam, R. [2001], *Navier-Stokes equations : theory and numerical analysis*, Vol. 343, American Mathematical Soc.

Torr, G. [1984], 'The acoustic radiation force', *American Journal of Physics* **52**, 402–408.

Ye, W., Bel-Brunon, A., Catheline, S., Combescure, A. and Rochette, M. [2017], 'Simulation of non-linear transient elastography : finite element model for the propagation of shear waves in homogeneous soft tissues', *International Journal for Numerical Methods in Biomedical Engineering* .

Zabolotskaya, E. A., Hamilton, M. F., Ilinskii, Y. A. and Meegan, G. D. [2004], 'Modeling of nonlinear shear waves in soft solids', *The Journal of the Acoustical Society of America* **116**(5), 2807–2813.

Part I

Mechanical and mathematical modelling

CHAPTER 1

Elastodynamic equation in the cardiac setting

Summary

The aim of this chapter is to outline a methodological and numerical approach to characterise elastographic shear waves for a very general constitutive behaviour of the myocardium. To do so, we consider a biomechanical model that can accurately reflect the complex behaviour of the myocardium and of the organ, from which we derive the equations governing the shear wave propagation imaged in elastographic techniques. We also detail the derivation of the so-called Christoffel tensor, that is necessary to compute shear wave velocities, for different constitutive laws modelling the passive behaviour of the medium, and we analyse the contribution of active stress on the elastographic wave propagation. Furthermore, we show some results obtained with a three-dimensional beating heart biomechanical model, and compare the computed wave velocities with published experimental measurements.

Contents

1.1 Introduction

Elastography techniques have raised a growing interest in clinical applications for soft tissue characterisation over the past decades, the tissue stiffness being highly sensitive to structural changes associated with physiological and pathological processes [Sarvazyan et al., 2011; Gennisson, 2003]. In particular, very recent elastographic techniques, like Acoustic Radiation Force Imaging (ARFI) [Nightingale et al., 2002], Shear Wave Elasticity Imaging (SWEI) [Sarvazyan et al., 1998] and Supersonic Shear Imaging (SSI) [Bercoff et al., 2004], are based on the propagation of shear waves, the measurement of which is often referred to as "transient elastography". Experimental studies such as those presented in [Couade et al., 2011; Pernot et al., 2011, 2016] show the potential of the extension of transient elastography to cardiac imaging. Nevertheless, such studies often show an incorrect estimation of apparent mechanical properties that change significantly over the cardiac cycle. Hence, there is a clear need for associating this varying apparent stiffness with actual constitutive parameters – e.g. passive elastic moduli and active contractilities – that characterise the state of the myocardium.
The approach we outline in this chapter to model and analyse shear wave propagation in myocardium for elastography imaging can be summarised in three main steps:

- Consider an accurate biomechanical model adequately representing the complex behaviour of the myocardium;
- Derive the equations governing the shear wave propagation imaged in elastographic techniques;
- Apply a suitable methodological and numerical approach to a beating heart model to compute shear wave velocities.

Furthermore, the method we propose to compute elastographic shear wave propagation is valid for a general constitutive behaviour, since no restrictive assumption (e.g. small strains assumptions) is formulated for its derivation. The first part of this chapter (Section 1.2) focuses on the presentation of a complete biomechanical model for the heart deformation, following Chapelle et al. [2012]. Furthermore, the main aspects of elastic plane wave propagation in such media are outlined. Then, in Section 1.3 we present the main tools for the derivation of the equations governing shear wave propagation from the biomechanical model of the myocardium. Section 1.4 presents the derivation of the so-called Christoffel tensor, that is necessary to compute shear wave velocities, for different constitutive laws modelling the passive behaviour of the medium. The contribution of active stress on elastic wave propagation is analysed in Section 1.5. Then, some numerical applications are outlined in Section 1.6, concerning the extraction of fibre orientation and the analysis of the effect of local modification of the biomechanical properties of the tissue on elastographic wave propagation. Finally, Section 1.8 contains some mathematical considerations on the coercivity of the constitutive law adopted, parameter calibration and an alternative method for the computation of the Christoffel tensor in prestress-free configuration.

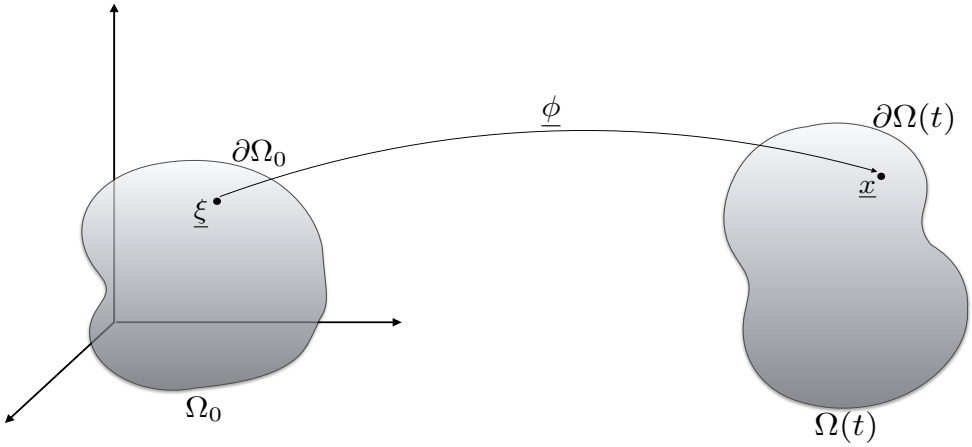

Figure 1.1 – Reference configuration Ω_0 and deformed configuration $\Omega(t)$, obtained by the deformation function $\underline{\phi}$.

1.2 Towards a model of elastic wave propagation in the heart

1.2.1 The equation of elastodynamics

Total Lagrangian formalism. The fundamental law of dynamics, or equilibrium equation, is the first step towards the formulation of the elastodynamic equations.
Let us consider a deformable solid occupying at time t the space domain $\Omega = \Omega(t) \in \mathbb{R}^3$, and let us assume that the boundary $\partial\Omega(t)$ exists and is piecewise C^1, so that the outward normal $\underline{\tau_1}$ is always defined in $\partial\Omega$ (Figure 1.1). We shall consider a Lagrangian formulation; therefore, we define the position of every point in $\Omega(t)$ with respect to a reference configuration Ω_0. We denote by $\underline{n_0}$ the outward normal on $\partial\Omega_0$. A deformation can be modelled as a bijective map $\underline{\phi} : \bar{\Omega}_0 \to \mathbb{R}^3$ from the reference to the deformed configuration, and it reads

$$\underline{\phi}\colon \underline{\xi} \mapsto \underline{x} = \underline{\phi}(\underline{\xi}, t).$$

Let us define the *displacement* $\underline{y}$ as

$$\underline{y}(\underline{\xi}, t) = \underline{x} - \underline{\xi} = \underline{\phi}(\underline{\xi}, t) - \underline{\xi},$$

and the *deformation gradient* $\underline{\underline{F}}$ as

$$\underline{\underline{F}}(\underline{\xi}, t) = \underline{\underline{\nabla}}_{\underline{\xi}} \underline{\phi} = \underline{\underline{\mathbb{1}}} + \underline{\underline{\nabla}}_{\underline{\xi}} \underline{y}. \tag{1.1}$$

For simplicity of notation, we denote in what follows $\underline{\underline{F}} = \underline{\underline{F}}(\underline{\xi}, t)$.

Transformation of surface and volume elements. From Eq. (1.2.1), the volume element $\mathrm{d}\underline{x}$ in the *deformed configuration* Ω is

$$\mathrm{d}\underline{x} = \det\left(\underline{\underline{\nabla}}_{\underline{\xi}} \underline{\phi}\right) \mathrm{d}\underline{\xi} = \det \underline{\underline{F}}\ \mathrm{d}\underline{\xi}.$$

Furthermore, given A_0 a measurable subset of the reference configuration Ω_0, we can define the volume of A_0 and $A = \underline{\phi}(A_0)$ as

$$\text{vol } A_0 \coloneqq \int_{A_0} \mathrm{d}\xi, \quad \text{vol } A \coloneqq \int_A \mathrm{d}x = \int_{A_0} det\left(\underline{\underline{F}}(\underline{\xi}, t)\right)\mathrm{d}\xi = \int_{A_0} J\mathrm{d}\xi,$$

where we have denoted $J = \det\left(\underline{\underline{F}}(\underline{\xi}, t)\right)$. If we consider a function $u : \underline{x} \in A \to \mathbb{R}$, it is $\mathrm{d}x$- integrable over the set A_0 if and only if the function

$$\underline{x} \in A \mapsto (u \circ \underline{\phi})(\underline{\xi})$$

is $\mathrm{d}\xi$- integrable over the set A_0, and in this case we can write

$$\int_A u(\underline{x})\mathrm{d}x = \int_{A_0} (u \circ \underline{\phi})(\underline{\xi}) J \mathrm{d}\xi.$$

In the same way, it is possible to define the transformation of an area element. If $\mathrm{d}S_0 \in \partial A_0$ is an infinitesimal area element on the boundary ∂A_0 of the subdomain A_0, the *deformed area element* $\mathrm{d}S = \underline{\phi}(\mathrm{d}S_0) \subset \partial A$ is obtained as

$$\underline{n}\,\mathrm{d}S = J\underline{\underline{F}}^{-T} \cdot \underline{n}_0\,\mathrm{d}S_0,$$

and

$$\text{area } S = \int_S \mathrm{d}S = \int_{S_0} J||\underline{\underline{F}}^{-T} \cdot \underline{n}_0||\mathrm{d}S_0.$$

Fundamental law of dynamics. Let us introduce the right *Cauchy-Green deformation tensor*

$$\underline{\underline{C}} = \underline{\underline{F}}^T \cdot \underline{\underline{F}}$$

and the *Green-Lagrange strain tensor* (or Green-Saint Venant strain tensor)

$$\underline{\underline{e}} = \frac{1}{2}(\underline{\underline{C}} - \underline{\underline{\mathbb{1}}}) = \frac{1}{2}(\underline{\underline{\nabla}}\,\underline{y} + \underline{\underline{\nabla}}\,\underline{y}^T + \underline{\underline{\nabla}}\,\underline{y}^T \cdot \underline{\underline{\nabla}}\,y).$$

Its linear part is given by

$$\underline{\underline{\varepsilon}} = \frac{1}{2}\left(\underline{\underline{\nabla}}_{\underline{\xi}}\underline{y} + (\underline{\underline{\nabla}}_{\underline{\xi}}\underline{y})^T\right).$$

The *equilibrium equation* is given by

$$\rho\left(\underline{\gamma} - \underline{f}\right) - \underline{\mathrm{div}}\,\underline{\underline{\sigma}} = 0, \quad \text{in } \Omega, \quad t > 0, \tag{1.2}$$

where $\underline{\gamma}$ is the acceleration, i.e. $\underline{\gamma} \circ \underline{\phi} = \frac{\partial^2 \underline{y}}{\partial t^2}$, $\underline{\underline{\sigma}}$ is the Cauchy stress tensor, ρ is the mass density of the solid and $\underline{f}$ is the external force per unit mass. We will consider for the moment zero initial condition, i.e. $\underline{y}(t = 0) = \underline{0}$.
The associated *weak formulation* reads

$$\forall \underline{w} \in \mathcal{X}, \quad \int_\Omega \rho\left(\underline{\gamma} - \underline{f}\right) \cdot \underline{w}\ \mathrm{d}\Omega + \int_\Omega \underline{\underline{\sigma}} : \underline{\underline{\nabla}}_{\underline{x}}\underline{w}\ \mathrm{d}\Omega = \int_{\Gamma_{N(t)}} \underline{\mathrm{t}} \cdot \underline{w}\ \mathrm{d}S, \tag{1.3}$$

where $\mathcal{X}$ is a space of admissible displacements to be defined, and $\underline{\mathrm{t}}$ is a surface-distributed load on the boundary $\Gamma_{N(t)} \subset \partial\Omega(t)$ where Neumann conditions apply. Note that $\underline{\mathrm{t}} = \underline{\underline{\sigma}} \cdot \underline{n}$ from Cauchy's theorem.
We can express Eq. (1.3) in a total Lagrangian formulation, i.e. with respect to Ω_0. Note

that we assume that each field $\underline{\gamma}$, $\underline{\underline{\sigma}}$, $\underline{w}$, $\underline{f}$, $\underline{\mathrm{t}}$ is defined in Eulerian framework. However, for simplicity of notation, in what follows we implicitly assume the composition with the deformation map $\underline{\phi}$ for each field when we express it in reference configuration.
First, note that we can rewrite

$$\underline{\underline{\nabla}}_{\underline{x}}\underline{w} = \underline{\underline{\nabla}}_{\underline{\xi}}\underline{w} \cdot \underline{\underline{\nabla}}_{\underline{x}}\underline{\xi} = \underline{\underline{\nabla}}_{\underline{\xi}}\underline{w} \cdot \underline{\underline{F}}^{-1},$$

Then, in the reference configuration we have

$$\forall \underline{w} \in \mathcal{X}, \quad \int_{\Omega_0} \rho\left(\underline{\gamma} - \underline{f}\right) \cdot \underline{w}\, J \, \mathrm{d}\Omega_0 + \int_{\Omega_0} \underline{\underline{\sigma}} : \underline{\underline{\nabla}}_{\underline{\xi}}\underline{w} \cdot \underline{\underline{F}}^{-1} J \, \mathrm{d}\Omega_0 = \int_{\Gamma_{N,0}} \underline{\mathrm{t}}_0 \cdot \underline{w} \, \mathrm{d}S_0, \tag{1.4}$$

with

$$\underline{\mathrm{t}}_0 = J||\underline{\underline{F}}^{-T} \cdot \underline{n}_0||\underline{\mathrm{t}}.$$

Let us define ρ_0 such that $\rho = \rho_0/J$ and introduce the *first Piola Kirchhoff stress tensor*

$$\underline{\underline{T}} = J\,\underline{\underline{\sigma}} \cdot \underline{\underline{F}}^{-T}.$$

Then, Eq. (1.4) can be rewritten as following:

$$\forall \underline{w} \in \mathcal{X}, \quad \int_{\Omega_0} \rho_0\big(\underline{\gamma} - \underline{f}\big) \cdot \underline{w} \, \mathrm{d}\Omega_0 + \int_{\Omega_0} \underline{\underline{T}} : \underline{\underline{\nabla}}_{\underline{\xi}}\underline{w} \, \mathrm{d}\Omega_0 = \int_{\Gamma_{N,0}} \underline{\mathrm{t}}_0 \cdot \underline{w} \, \mathrm{d}S_0, \tag{1.5}$$

from which we can derive the strong form:

$$\underline{\mathrm{div}}\,\underline{\underline{T}} - \rho_0\big(\underline{\gamma} - \underline{f}\big) = 0 \quad \text{in } \Omega_0.$$

In order to work with symmetric tensors, we introduce the *second Piola Kirchhoff stress tensor*

$$\underline{\underline{\Sigma}} = \underline{\underline{F}}^{-1} \cdot \underline{\underline{T}} = J\underline{\underline{F}}^{-1} \cdot \underline{\underline{\sigma}} \cdot \underline{\underline{F}}^{-T},$$

and we rewrite Eq. (1.5) as following:

$$\forall \underline{w} \in \mathcal{X}, \quad \int_{\Omega_0} \rho_0\big(\underline{\gamma} - \underline{f}\big) \cdot \underline{w} \, \mathrm{d}\Omega_0 + \int_{\Omega_0} \underline{\underline{\Sigma}} : (\underline{\underline{F}}^T \cdot \underline{\underline{\nabla}}_{\underline{\xi}}\underline{w}) \, \mathrm{d}\Omega_0 = \int_{\Gamma_{N,0}} \underline{\mathrm{t}}_0 \cdot \underline{w} \, \mathrm{d}S_0. \tag{1.6}$$

Using the fact that $\underline{\underline{\Sigma}}$ is a symmetric tensor, and that

$$\forall \underline{\underline{A}} \text{ s.t. } A_{ij} = A_{ji}, \ \forall \underline{\underline{B}}, \quad \underline{\underline{A}} : \underline{\underline{B}} = \underline{\underline{A}} : \frac{\underline{\underline{B}} + \underline{\underline{B}}^T}{2},$$

we can symmetrise the tensor $\underline{\underline{F}}^T \cdot \underline{\underline{\nabla}}_{\underline{\xi}}\underline{w}$ in Eq. (1.6). We define the derivative of the Green-Lagrange strain tensor with respect to displacements in $\mathcal{X}$ as

$$d_{\underline{y}}\underline{\underline{e}} \cdot \underline{w} = \frac{1}{2}\Big(\underline{\underline{\nabla}}^T_{\underline{\xi}}\underline{w} \cdot \underline{\underline{F}} + \underline{\underline{F}}^T \cdot \underline{\underline{\nabla}}_{\underline{\xi}}\underline{w}\Big) = \frac{1}{2}\Big((\mathrm{d}_{\underline{y}}\underline{\underline{F}} \cdot \underline{w})^T \cdot \underline{\underline{F}} + \underline{\underline{F}}^T \cdot \mathrm{d}_{\underline{y}}\underline{\underline{F}} \cdot \underline{w}\Big).$$

Then, we obtain the following formulation of the fundamental law of dynamics, that we will use from now on:

$$\forall \underline{w} \in \mathcal{X}, \quad \int_{\Omega_0} \rho_0\big(\underline{\gamma} - \underline{f}\big) \cdot \underline{w} \, \mathrm{d}\Omega_0 + \int_{\Omega_0} \underline{\underline{\Sigma}} : d_{\underline{y}}\underline{\underline{e}} \cdot \underline{w} \, \mathrm{d}\Omega_0 = \int_{\Gamma_{N,0}} \underline{\mathrm{t}}_0 \cdot \underline{w} \, \mathrm{d}S_0. \tag{1.7}$$

We note that the term $\underline{\underline{\Sigma}} : d_{\underline{y}}\underline{\underline{e}} \cdot \underline{w}$ depends on the specific constitutive law adopted.

1.2.2 The heart mechanical model in a nutshell

The heart dynamics cannot be described with sufficient precision by a linear constitutive law. This is due to the fact that, during the cardiac cycle, the maximum deformation rate of cardiac cells is about 20%. Consequently, a small deformation assumption is not correct. A more precise modelling of the stress-strain relationship can be found in the theory of hyperelasticity. Henceforth, we will give the main elements of hyperelastic theory, and refer the reader to Ciarlet [1988]; Le Tallec [1994]; Temam and Miranville [2005] for further reading on this subject.

Modelling of a hyperelastic medium. A material is said to be elastic if and only if the stress tensor $\underline{\underline{\Sigma}}$ only depends on the spatial variable $\underline{\xi}$ and the deformation gradient $\underline{\underline{F}}$. A hyperelastic material is defined as a homogeneous elastic material that does not dissipate energy during cyclic homogeneous deformations [Le Tallec, 1994], i.e. for every admissible deformation field $\underline{\phi}(\underline{\xi}, t) = \underline{\underline{F}}(t) \cdot \underline{\xi} + c(t)$, periodic in time with period T,

$$\int_0^T \int_{\Omega_0} \underline{\underline{T}}(\underline{\underline{F}}) : \dot{\underline{\underline{F}}} \, \mathrm{d}\Omega_0 \, \mathrm{d}t = \mathrm{vol}(\Omega_0) \int_{\underline{\underline{F}}(0)}^{\underline{\underline{F}}(T)} \underline{\underline{T}}(\underline{\underline{F}}) : \mathrm{d}\underline{\underline{F}} = 0. \tag{1.8}$$

Note that Eq. (1.8) corresponds in thermodynamics to the Clausius-Duhem inequality in absence of dissipation.
Consequently, we can define an elastic potential W^e s.t.

$$\underline{\underline{T}}(\underline{\underline{F}}) = \frac{\partial W^e}{\partial \underline{\underline{F}}}.$$

Let us now consider a rigid deformation $\underline{\underline{Q}}$. Then, the stored energy is not modified by this type of deformations, namely

$$W^e(\underline{\underline{F}}) = W^e(\underline{\underline{Q}} \cdot \underline{\underline{F}}), \quad \forall \underline{\underline{Q}} \in SO_3(\mathbb{R}).$$

If we take $\underline{\underline{Q}} = \sqrt{\underline{\underline{C}}} \cdot \underline{\underline{F}}^{-1}$, we see that W^e can be considered as a function of $\underline{\underline{C}}$.
At first, we take into account an isotropic material, i.e. a material for which the behaviour of the system does not depend on any rotation in Ω_0, that is to say

$$W^e(\underline{\underline{C}}) = W^e(\underline{\underline{Q}} \cdot \underline{\underline{C}} \cdot \underline{\underline{Q}}^T), \quad \forall \underline{\underline{Q}} \in SO_3(\mathbb{R}).$$

Then, if we take $\underline{\underline{Q}}$ as the matrix composed of the eigenvectors of the tensor $\underline{\underline{C}}$, we see that W^e can be expressed uniquely as a function of the eigenvalues of $\underline{\underline{C}}$, i.e. its invariants

$$I_1 = \mathrm{tr}(\underline{\underline{C}}), \quad I_2 = \mathrm{tr}(\mathrm{cof}\underline{\underline{C}}) = \frac{1}{2}\Big(\big(\mathrm{tr}(\underline{\underline{C}})\big)^2 - \mathrm{tr}(\underline{\underline{C}}^2) \Big), \quad I_3 = \det \underline{\underline{C}}.$$

As a consequence, there exists a relation for the energy W^e and $\underline{\underline{\Sigma}}$, specifically:

$$\exists W^e = W^e(I_1, I_2, I_3) \quad s.t. \quad \underline{\underline{\Sigma}}(\underline{\underline{e}}) = \frac{\partial W^e}{\partial \underline{\underline{e}}}(I_1, I_2, I_3), \tag{1.9}$$

where $\underline{\underline{e}}$ is the Green- Lagrange strain tensor previously defined.
Consequently, the stress tensor $\underline{\underline{\Sigma}}$ can be computed from the derivative of the strain energy

W^e with respect to the invariants I_i. In other words, from Eq. (1.9) we can derive the expression for the tensor $\underline{\underline{\Sigma}}$:

$$\underline{\underline{\Sigma}} = 2\sum_{i=1}^{4} \frac{\partial W^e}{\partial I_i} \cdot \frac{\partial I_i}{\partial \underline{\underline{C}}}, \tag{1.10}$$

with the identities:

$$\frac{\partial I_1}{\partial \underline{\underline{C}}} = \underline{\underline{\mathbb{1}}}, \quad \frac{\partial I_2}{\partial \underline{\underline{C}}} = (I_1 \underline{\underline{\mathbb{1}}} - \underline{\underline{C}}), \quad \frac{\partial I_3}{\partial \underline{\underline{C}}} = I_3 \underline{\underline{C}}^{-1}.$$

Hence, the constitutive law of the material is defined by the expression of the strain energy W^e. There exist several examples of isotropic, hyperelastic materials. We cite, as an illustration, the Mooney-Rivlin law, that reads

$$W^e := \chi_1(I_1 - 3) + \chi_2(I_2 - 3). \tag{1.11}$$

Alternatively, we can mention the energy potential proposed by Ciarlet and Geymonat [1982]

$$W^e = \chi_1(I_1 - 3) + \chi_2(I_2 - 3) + a(I_3 - 1) - (\chi_1 + 2\,\chi_2 + a)\log(I_3). \tag{1.12}$$

Note that, under small strain assumption, every isotropic hyperelastic constitutive law reduces to Hooke's law after linearisation, i.e. it can be formulated as

$$\underline{\underline{\Sigma}}(\underline{\underline{e}}) = \lambda\ \mathrm{tr}\big(\underline{\underline{e}}\big)\,\underline{\underline{\mathbb{1}}} + 2\,\mu\,\underline{\underline{e}}, \tag{1.13}$$

with (λ, μ) Lamé's coefficients.

Decomposition of the stress tensor. We now consider a standard decomposition of the stress tensor that is very useful in the case of incompressible materials. We define

$$\mathrm{p} = -\frac{1}{3\,J}\underline{\underline{\Sigma}} : \underline{\underline{C}}, \quad \text{and} \quad \underline{\underline{\Sigma}}_d = \underline{\underline{\Sigma}} + p\,J\,\underline{\underline{C}}^{-1}. \tag{1.14}$$

The following decomposition of the stress holds:

$$\underline{\underline{\Sigma}} = \underline{\underline{\Sigma}}_d - p\,J\,\underline{\underline{C}}^{-1}. \tag{1.15}$$

As a consequence, if we consider isotropic contraction-expansion deformations, for all test displacements $\underline{w} = \lambda\,\underline{x}$, we obtain

$$\mathrm{d}_{\underline{y}}\underline{\underline{e}} \cdot \underline{w} = \frac{1}{2}\mathrm{d}_{\underline{y}}\underline{\underline{C}} \cdot \underline{w} = \frac{1}{2}\big((\mathrm{d}_{\underline{y}}\underline{\underline{F}} \cdot \underline{w})^T \cdot \underline{\underline{F}} + \underline{\underline{F}}^T \cdot \mathrm{d}_{\underline{y}}\underline{\underline{F}} \cdot \underline{w}\big) = \frac{1}{2}\big((\underline{\underline{\nabla}}_{\underline{\xi}}\underline{w})^T \cdot \underline{\underline{F}} + \underline{\underline{F}}^T \cdot \underline{\underline{\nabla}}_{\underline{\xi}}\underline{w}\big) = \lambda\,\underline{\underline{C}}.$$

Hence, the deviatoric part of the stress tensor $\underline{\underline{\Sigma}}_d$ does not produce work on this type of deformations, i.e.

$$\underline{\underline{\Sigma}}_d : \mathrm{d}_{\underline{y}}\underline{\underline{e}} \cdot \underline{w} = \lambda\,\underline{\underline{\Sigma}} : \underline{\underline{C}} + \lambda\,p\,J\,\underline{\underline{C}}^{-1} : \underline{\underline{C}} = 0.$$

Reduced Invariants. More often, the strain energy is defined in terms of reduced invariants, since their use allows to simplify the decomposition of the stress tensor. We can define the reduced invariants as

$$J_1 = I_1 I_3^{-\frac{1}{3}}, \quad J_2 = I_2 I_3^{-\frac{2}{3}}, \quad J_3 = I_3^{\frac{1}{2}} = J. \tag{1.16}$$

In fact, since

$$\frac{\partial I_1}{\partial \underline{\underline{C}}} : \underline{\underline{C}} = I_1, \quad \frac{\partial I_2}{\partial \underline{\underline{C}}} : \underline{\underline{C}} = 2\, I_2, \quad \frac{\partial I_3}{\partial \underline{\underline{C}}} : \underline{\underline{C}} = 3\, I_3,$$

from Eq. (1.16) we obtain

$$\frac{\partial J_1}{\partial \underline{\underline{C}}} : \underline{\underline{C}} = 0, \quad \frac{\partial J_2}{\partial \underline{\underline{C}}} : \underline{\underline{C}} = 0, \quad \frac{\partial J_3}{\partial \underline{\underline{C}}} : \underline{\underline{C}} = \frac{3}{2} J.$$

Thus, using the definition (1.14), the decomposition (1.15) reduces to

$$\underline{\underline{\Sigma}}_d = 2\left(\frac{\partial W^e}{\partial J_1} \cdot \frac{\partial J_1}{\partial \underline{\underline{C}}} + \frac{\partial W^e}{\partial J_2} \cdot \frac{\partial J_2}{\partial \underline{\underline{C}}}\right), \quad \text{and} \quad p = -\frac{\partial W^e}{\partial J}. \tag{1.17}$$

Incompressibility. Incompressible materials are subject to the constraint that every deformation must preserve the volume at each point. Therefore, they satisfy

$$J = \det \underline{\underline{F}} = 1. \tag{1.18}$$

We emphasize the fact that, due to Eq. (1.18), the strain energy can be characterised as a function of the first two reduced invariants only, i.e.

$$W^e = W^e(J_1, J_2). \tag{1.19}$$

Note that, in static cases, Eq. (1.7) is a consequence of the minimisation problem

$$\min_{\underline{y}} (\mathcal{E}_m - \mathcal{W}^{\text{ext}}),$$

where $\mathcal{E}_m$ is the elastic energy of the system and it reads

$$\mathcal{E}_m = \int_{\Omega_0} W^e(\underline{\underline{e}})\, \mathrm{d}\Omega_0,$$

whereas $\mathcal{W}^{\text{ext}}$ represents the external work. In the case of incompressible materials, the incompressibility constraint is enforced by the introduction of a Lagrange multiplier p such that

$$\min_{\underline{y}, J=1} (\mathcal{E}_m - \mathcal{W}^{\text{ext}}) = \min_{\underline{y}} \max_{\mathrm{p}} \left(\int_{\Omega_0} \big(W^e(\underline{\underline{e}}) + p\,(1-J)\big) \mathrm{d}\Omega_0 - \mathcal{W}^{\text{ext}} \right).$$

Therefore, for all test displacement $\underline{w}$,

$$\int_{\Omega_0} \left(\frac{\partial W^e}{\partial \underline{\underline{e}}} - p\, \frac{\partial J}{\partial \underline{\underline{e}}}\right) : \mathrm{d}_{\underline{y}} \underline{\underline{e}} \cdot \underline{w}\, \mathrm{d}\Omega_0 - \mathrm{d}_y \mathcal{W}^{\text{ext}} \cdot \underline{w} = 0.$$

Hence, if we identify the stress tensor

$$\underline{\underline{\Sigma}} = \frac{\partial W^e}{\partial \underline{\underline{e}}} - p\, \frac{\partial J}{\partial \underline{\underline{e}}} = \frac{\partial W^e}{\partial \underline{\underline{e}}} - p\, J\, \underline{\underline{C}}^{-1}.$$

and considering Eqs. (1.19), (1.15) and (1.17), we retrieve that the multiplier p coincides with the pressure introduced in the decomposition of the stress tensor. The so-called mixed formulation must be solved:
Find $(\underline{y}, p) \in \mathcal{X} \times \mathcal{L}$ such that, $\forall\, (\underline{w}, q) \in \mathcal{X} \times \mathcal{L}$

$$\begin{cases} \displaystyle\int_{\Omega_0} \rho_0 \big(\ddot{\underline{y}} - \underline{f}\big) \cdot \underline{w}\, \mathrm{d}\Omega_0 + \int_{\Omega_0} \underline{\underline{\Sigma}}\big(\underline{y}, \mathrm{p}\big) : d_{\underline{y}} \underline{\underline{e}} \cdot \underline{w}\, \mathrm{d}\Omega_0 = \int_{\Gamma_{N,0}} \mathrm{t}_0 \cdot \underline{w}\, \mathrm{d}S_0 \\ \displaystyle\int_{\Omega_0} \rho_0 \Big(\det\big(\underline{\underline{F}}(\underline{y})\big) - 1\Big)\, q\, \mathrm{d}\Omega_0 = 0, \end{cases}$$

with $\mathcal{L}$ space of admissible pressures.
In the case of nearly-incompressible media, a penalisation formulation is derived. As an example, one can choose

$$W^e(\underline{\underline{e}}) = W^e(J_1, J_2) + \frac{\kappa}{2}(1-J)^2,$$

with κ bulk modulus, assumed very large in order to penalise the term $(1-J)^2$. Another choice for the penalisation term is the one proposed in the model by Ciarlet and Geymonat [1982], that reads, in reduced invariants,

$$W^e(\underline{\underline{e}}) = \chi_1(J_1 - 3) + \chi_2(J_2 - 3) + \kappa(J-1) - \kappa \log(J).$$

This formulation also implies $J > 0$ by hypothesis.

Anisotropy. Until now, we have detailed a constitutive law for an isotropic material. However, the myocardial tissue cannot be modelled as such, due to the fibered structure of this tissue. In fact, it has been experimentally validated that muscle fibres are wound as in a coil and arranged in parallel laminar structures, denoted sheets, of three to four muscle fibres in the thickness, that are oriented transversely to the heart wall [Streeter et al., 1969; Lee et al., 2012]. Moreover, the fibre orientation in human left ventricle myocardium changes smoothly throughout the wall thickness. Their direction goes from $-60°$ to $-70°$ in sub-epicardial region (outer layer), to orthoradial orientation in mid-wall regions, and finally to $+60°$ to $+70°$ in sub-endocardial regions (inner layer) [Sommer et al., 2015]. This type of anisotropy can be well captured by considering the medium as transversely isotropic. This means that at every point there exists a privileged direction $\underline{\tau_1}(\underline{\xi})$. In this case, more invariants are needed in order to express the elastic potential [Raoult, 2009]

$$I_4 = \underline{\tau_1} \cdot \underline{\underline{C}} \cdot \underline{\tau_1}, \quad I_5 = \underline{\tau_1} \cdot \underline{\underline{C}}^2 \cdot \underline{\tau_1}.$$

The strain energy W^e becomes a function of five invariants, giving the following expression for the stress tensor $\underline{\underline{\Sigma}}$:

$$\underline{\underline{\Sigma}}(\underline{\underline{e}}) = 2\sum_{i=1}^{3} \frac{\partial W^e}{\partial I_i} \cdot \frac{\partial I_i}{\partial \underline{\underline{C}}} + \frac{\partial W^e}{\partial I_4} \underline{\tau_1} \otimes \underline{\tau_1} + \frac{\partial W^e}{\partial I_5} \Big((\underline{\underline{C}} \cdot \underline{\tau_1}) \otimes \underline{\tau_1} + \underline{\tau_1} \otimes \underline{\underline{C}} \cdot (\underline{\tau_1}) \Big).$$

Recent works also consider another privileged direction, transverse to the fibre axis within the sheet, denoted sheet axis. Therefore, at every material point, a right-handed orthogonal set of axes is defined, composed of the fibre axis, the sheet axis, and the sheet-normal axis. In this case, the material is denoted as orthotropic, and the strain energy can be a function of 6 to 8 invariants [Holzapfel and Ogden, 2009; Sommer et al., 2015].
In what follows, we will consider a transversely isotropic constitutive law. This is justified by the fact that the characterisation of sheet direction is limited by the physiological data available. Moreover, for our purposes, the description of the myocardium as a composite of multiple transversely isotropic thin media is detailed enough for capturing the main features of shear wave propagation in the myocardium. In fact, it is experimentally established that shear waves propagate faster along than across the fibre direction [Royer and Dieulesaint, 2000]. Furthermore, we will choose an exponential constitutive law, since it has been shown in multiple experimental studies [Guccione et al., 1995; Costa et al., 2001; Holzapfel and Ogden, 2009] that this type of law suits well the material nonlinearities of the myocardium. In more detail, if we define a fourth reduced invariant as

$$J_4 = I_4 \, I_3^{-\frac{1}{3}},$$

we can describe the passive elastic potential of the myocardium as

$$W^e(\underline{\underline{e}}) = \kappa_1 e^{\kappa_2(J_1-3)^2} + \kappa_3 e^{\kappa_4(J_4-1)^2} + \chi_2(J_2-3) + \kappa(J-1) - \kappa\,\log(J).$$

This definition consists in a combination of a transversely isotropic exponential law with a penalisation term for incompressibility and a linear, isotropic term. This term is inserted in order to ensure overall numerical stability of the system, whereas the exponential component dominates in large deformations. In what follows, we will justify this choice of constitutive law.

Viscoelasticity. Biological soft tissues are known to be viscoelastic [Fung, 1973]. This implies that the shape of the stress-strain curve depends on the strain rate at which the traction is performed. In order to take into account viscosity, the equality (1.8) is generalised into the Clausius-Duhem inequality

$$\left(\underline{\underline{\Sigma}} - \frac{\partial W^e}{\partial \underline{\underline{e}}}\right) : \dot{\underline{\underline{e}}} \geq 0, \quad \forall\, \underline{\underline{e}},\, \dot{\underline{\underline{e}}}. \tag{1.20}$$

As a consequence, in any thermomechanical process the dissipation must be nonnegative. Eq. (1.20) is satisfied if we introduce a scalar viscous pseudo-potential $W^{\mathrm{VS}}(\dot{\underline{\underline{e}}})$ that verifies $\frac{\partial W^{\mathrm{VS}}}{\partial \dot{\underline{\underline{e}}}}(\underline{\underline{0}}) = \underline{\underline{0}}$ and is convex with respect to $\dot{\underline{\underline{e}}}$. In this case, we can define

$$\underline{\underline{\Sigma}} = \frac{\partial W^e}{\partial \underline{\underline{e}}} + \frac{\partial W^{\mathrm{VS}}}{\partial \dot{\underline{\underline{e}}}}.$$

A simple choice for W^{VS} is represented by

$$W^{\mathrm{VS}} = \frac{\zeta}{2}\left(\mathrm{tr}\left(\dot{\underline{\underline{e}}}\right)\right)^2,$$

so that the associated stress tensor $\underline{\underline{\Sigma}}^{\mathrm{VS}}$ is given by

$$\underline{\underline{\Sigma}}^{\mathrm{VS}} = \zeta\,\mathrm{tr}\left(\dot{\underline{\underline{e}}}\right)\underline{\underline{\mathbb{1}}}.$$

Active stress. A more realistic constitutive law of the heart takes into account the contribution of the active stress. In this regard, we follow the model proposed by Chapelle et al. [2012]. The complete constitutive law is composed of passive and active elements, and it is constructed based on a non-linear rheological scheme, as depicted in Figure 1.2. It consists of:

- An active component that describes the active behaviour of the sarcomere with the Bestel-Clément-Sorine model [Bestel et al., 2001]

  $$\sigma_c = \tau_c + \mu \dot{e}_c,$$

  where e_c and σ_c are the strain and stress of the active element, τ_c is the contraction stress and μ deals with the friction of the sarcomere.

- An elastic element accounting for the passive endings of the filament, set in series with the active component. The introduction of this element is crucial to let the active element contract ($\dot{e}_c < 0$) without any deformation of the entire fibre ($e = 0$).

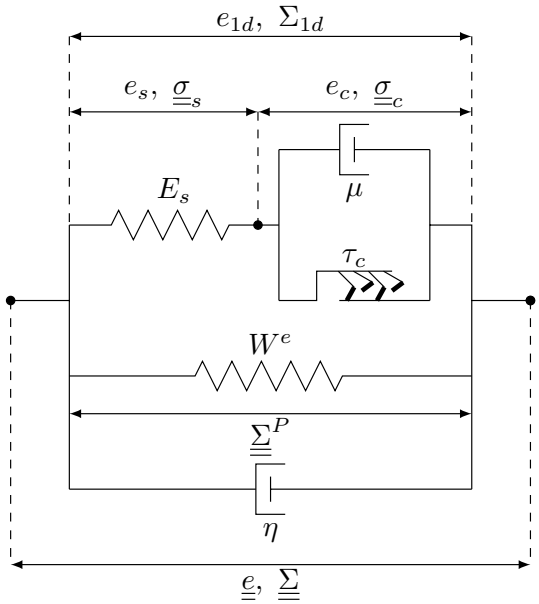

Figure 1.2 – Complete rheological model for the active law (in the direction $\underline{\tau_1}$). Inspired by [Caruel et al., 2014].

Let us denote by (e_s, σ_s) the one-dimensional strain and stress of the elastic element, and assume $\sigma_s = E_s e_s$ (Hooke's law). From the rheological model we obtain

$$(1 + 2e_{1d}) = (1 + 2e_s)(1 + 2e_c).$$

Consequently, indicating by $e_{1d} = \underline{\tau_1} \cdot \underline{\underline{e}} \cdot \underline{\tau_1}$ the strain in the fibre direction $\underline{\tau_1}$, the total stress of the fibre reads

$$\Sigma_{1d} = \frac{\sigma_c}{(1 + 2e_s)} = \frac{\sigma_s}{(1 + 2e_c)} \implies \Sigma_{1d} = \frac{E_s}{(1 + 2e_c)^2}(e_{1d} - e_c),$$

As a consequence, we obtain

$$\sigma_c = \tau_c + \mu_c \dot{e}_c = E_s \frac{e_{1d} - e_c}{(1 + 2e_c)^3}(1 + 2e_{1d}).$$

- An additional element representing the collagen and elastin extracellular matrix, set in parallel. This element follows the passive constitutive law presented above.

We refer the reader to [Chapelle et al., 2012] for a throughout analysis of this active model.

The complete constitutive law for the myocardium. The total stress tensor can be defined as

$$\underline{\underline{\Sigma}} := \underline{\underline{\Sigma}}^P + \underline{\underline{\Sigma}}^A,$$

with $\underline{\underline{\Sigma}}^P$ given by

$$\begin{cases} \underline{\underline{\Sigma}}^P = \underline{\underline{\Sigma}}^e + \underline{\underline{\Sigma}}^{\mathrm{VS}} = \dfrac{\partial W^e}{\partial \underline{\underline{e}}} + \dfrac{\partial W^{\mathrm{VS}}}{\partial \underline{\underline{\dot{e}}}} \\ W^e = \kappa_1 e^{\kappa_2 (J_1 - 3)^2} + \kappa_3 e^{\kappa_4 (J_4 - 1)^2} + \chi(J_2 - 3) + \kappa\big((J - 1) - \log(J)\big) \\ W^{\mathrm{VS}} = \frac{\zeta}{2} \operatorname{tr}\big(\underline{\underline{\dot{e}}}\big)^2, \end{cases} \tag{1.21}$$

whereas $\underline{\underline{\Sigma}}^A$ is defined as

$$\underline{\underline{\Sigma}}^A = \Sigma_{1d}(e_{1d})\, \underline{\tau_1} \otimes \underline{\tau_1},$$

with specific stress of the sarcomere

$$\Sigma_{1d} = \frac{\sigma_c}{1+2\,e_s} = \frac{\sigma_s}{1+2\,e_c}.$$

1.2.3 Elastic wave propagation in a hyperelastic medium

Most recent elastography imaging techniques consist in the remote generation of shear waves (by acoustic radiation force) in a biological tissue. In fact, there is experimental evidence that the velocity of propagation of the induced shear waves is strictly correlated with biomechanical properties that are highly sensitive to structural changes associated with physiological and pathological processes. As a consequence, by analysing the induced shear wave propagation, it is possible to have an non-invasive insight on some biomechanical properties of great clinical interest.
From a physical perspective, the elastic wave propagation corresponds to a small perturbation of the dynamics described in Eq. (1.7) on a small time scale, for which we can assume that the domain Ω is static.
With this assumption, we can rewrite the solution as

$$\underline{y}(\underline{x},t) = \underline{y}_0(\underline{x},t) + \delta\tilde{\underline{y}}\Big(\underline{x},\frac{t}{\delta}\Big),$$

with δ small.
The governing equation of the perturbation $\tilde{\underline{y}}$ can be then recovered by linearising Eq. (1.7) around a reference configuration, given by the moving domain. In particular, under the assumption of a hyperelastic medium, we can rewrite the second Piola-Kirchhoff tensor $\underline{\underline{\Sigma}}$ as

$$\underline{\underline{\Sigma}} = \underline{\underline{\Sigma}}_0 + \delta\frac{\partial\underline{\underline{\Sigma}}}{\partial\underline{\underline{e}}} : \big(d_{\underline{y}_0}\underline{\underline{e}}\cdot\tilde{\underline{y}}\big) + O(\delta^2) = \underline{\underline{\Sigma}}_0 + \delta\tilde{\underline{\underline{\Sigma}}} + O(\delta^2).$$

We also observe that

$$\begin{aligned} d_{\underline{y}}\underline{\underline{e}}\cdot\underline{w} &= \varepsilon(\underline{w}) + \frac{1}{2}(\underline{\underline{\nabla}}_{\underline{\xi}}\,\underline{w}^T\cdot\underline{\underline{\nabla}}_{\underline{\xi}}\,\underline{y}_0 + \underline{\underline{\nabla}}_{\underline{\xi}}\,\underline{y}_0^T\cdot\underline{\underline{\nabla}}_{\underline{\xi}}\,\underline{w}) + \frac{\delta}{2}(\underline{\underline{\nabla}}_{\underline{\xi}}\,\underline{w}^T\cdot\underline{\underline{\nabla}}_{\underline{\xi}}\,\tilde{\underline{y}} + \underline{\underline{\nabla}}_{\underline{\xi}}\,\tilde{\underline{y}}^T\cdot\underline{\underline{\nabla}}_{\underline{\xi}}\,\underline{w}) + O(\delta^2) \\ &= d_{\underline{y}_0}\underline{\underline{e}}\cdot\underline{w} + \frac{\delta}{2}(\underline{\underline{\nabla}}_{\underline{\xi}}\,\underline{w}^T\cdot\underline{\underline{\nabla}}_{\underline{\xi}}\,\tilde{\underline{y}} + \underline{\underline{\nabla}}_{\underline{\xi}}\,\tilde{\underline{y}}^T\cdot\underline{\underline{\nabla}}_{\underline{\xi}}\,\underline{w}) + O(\delta^2). \end{aligned}$$

Consequently,

$$\begin{aligned} \underline{\underline{\Sigma}} : (d_{\underline{y}}\underline{\underline{e}}\cdot\underline{w}) &= \underline{\underline{\Sigma}}_0 : d_{\underline{y}_0}\underline{\underline{e}}\cdot\underline{w} + \delta\Big(\tilde{\underline{\underline{\Sigma}}} : d_{\underline{y}_0}\underline{\underline{e}}\cdot\underline{w} + \underline{\underline{\Sigma}}_0 : \frac{1}{2}\big(\underline{\underline{\nabla}}_{\underline{\xi}}\,\underline{w}^T\cdot\underline{\underline{\nabla}}\,\tilde{\underline{y}} + \underline{\underline{\nabla}}_{\underline{\xi}}\,\tilde{\underline{y}}^T\cdot\underline{\underline{\nabla}}_{\underline{\xi}}\,\underline{w}\big)\Big) + O(\delta^2) \\ &= \underline{\underline{\Sigma}}_0 : d_{\underline{y}_0}\underline{\underline{e}}\cdot\underline{w} + \delta\Big(d_{\underline{y}_0}\underline{\underline{e}}\cdot\tilde{\underline{y}} : \frac{\partial\underline{\underline{\Sigma}}}{\partial\underline{\underline{e}}} : d_{\underline{y}_0}\underline{\underline{e}}\cdot\underline{w} + \underline{\underline{\Sigma}}_0 : \big(\underline{\underline{\nabla}}_{\underline{\xi}}\,\tilde{\underline{y}}^T\cdot\underline{\underline{\nabla}}_{\underline{\xi}}\,\underline{w}\big)\Big) + O(\delta^2), \end{aligned}$$

due to the definition of $\tilde{\underline{\underline{\Sigma}}}$ and for symmetry reasons.
Consequently, the linear problem associated with the perturbation $\tilde{\underline{y}}$ reads $\forall\underline{w}\in\mathcal{X}$

$$\int_{\Omega_0}\rho_0\,\ddot{\tilde{\underline{y}}}\cdot\underline{w}\,\mathrm{d}\Omega_0 + \int_{\Omega_0} d_{\underline{y}_0}\underline{\underline{e}}\cdot\tilde{\underline{y}} : \frac{\partial\underline{\underline{\Sigma}}}{\partial\underline{\underline{e}}} : d_{\underline{y}_0}\underline{\underline{e}}\cdot\underline{w}\,\mathrm{d}\Omega_0 + \int_{\Omega_0}\underline{\underline{\Sigma}}_0 : \big(\underline{\underline{\nabla}}_{\underline{\xi}}\tilde{\underline{y}}^T\cdot\underline{\underline{\nabla}}_{\underline{\xi}}\underline{w}\big)\,\mathrm{d}\Omega_0 = 0. \quad (1.22)$$

The last two integrals account for *material stiffness* and *prestress effect*, respectively. We can rewrite Eq. (1.22) in a compact form:

$$\text{find } \underline{\tilde{y}} \text{ s.t. } m(\underline{\ddot{\tilde{y}}}, \underline{w}) + a(t; \underline{\tilde{y}}, \underline{w}) = 0 \quad \forall \underline{w} \in V(\Omega_0), \tag{1.23}$$

where we have introduced the bilinear forms

$$m(\underline{\ddot{\tilde{y}}}, \underline{w}) = \int_{\Omega_0} \rho_0 \underline{\ddot{\tilde{y}}} \cdot \underline{w} \, \mathrm{d}\Omega_0,$$
$$a(t; \underline{\tilde{y}}, \underline{w}) = \int_{\Omega_0} d_{\underline{y}_0} \underline{\underline{e}} \cdot \underline{\tilde{y}} : \frac{\partial \underline{\underline{\Sigma}}}{\partial \underline{\underline{e}}} : d_{\underline{y}_0} \underline{\underline{e}} \cdot \underline{w} \, \mathrm{d}\Omega_0 + \int_{\Omega_0} \underline{\underline{\Sigma}}_0 : \left(\underline{\underline{\nabla}}_{\underline{\xi}} \underline{\tilde{y}}^T \cdot \underline{\underline{\nabla}}_{\underline{\xi}} \underline{w} \right) \mathrm{d}\Omega_0.$$

Furthermore, in terms of a total tangent stiffness operator, we can rewrite Eq. (1.22) as

$$\forall \underline{w} \in \mathcal{X}, \quad \int_{\Omega_0} \rho_0 \, \underline{\ddot{\tilde{y}}} \cdot \underline{w} \, \mathrm{d}\Omega_0 + \int_{\Omega_0} \underline{\underline{\nabla}}_{\underline{\xi}} \underline{\tilde{y}} : \underline{\underline{\mathbf{C}}}^{\mathrm{Lag}} : \underline{\underline{\nabla}}_{\underline{\xi}} \underline{w} \, \mathrm{d}\Omega_0 = 0. \tag{1.24}$$

However, elastic wave propagation is measured in the deformed configuration. Consequently, Eq. (1.24) must be reformulated as

$$\forall \underline{w} \in \mathcal{X}, \quad \int_{\Omega} \rho \, \underline{\ddot{\tilde{y}}} \cdot \underline{w} \, \mathrm{d}\Omega + \int_{\Omega} J^{-1} \left(\underline{\underline{\nabla}}_{\underline{x}} \underline{\tilde{y}} \cdot \underline{\underline{F}} \right) : \underline{\underline{\mathbf{C}}}^{\mathrm{Lag}} : \left(\underline{\underline{\nabla}}_{\underline{x}} \underline{w} \cdot \underline{\underline{F}} \right) \mathrm{d}\Omega = 0. \tag{1.25}$$

If we define

$$\underline{\underline{\mathbf{C}}}^{\mathrm{Eul}} = J^{-1} \, \underline{\underline{F}} \cdot \underline{\underline{\mathbf{C}}}^{\mathrm{Lag}} \cdot \underline{\underline{F}}^T,$$

we can rewrite Eq. (1.25) as

$$\forall \underline{w} \in \mathcal{X}, \quad \int_{\Omega} \rho \, \underline{\ddot{\tilde{y}}} \cdot \underline{w} \, \mathrm{d}\Omega + \int_{\Omega} \underline{\underline{\nabla}}_{\underline{x}} \underline{\tilde{y}} : \underline{\underline{\mathbf{C}}}^{\mathrm{Eul}} : \underline{\underline{\nabla}}_{\underline{x}} \underline{w} \, \mathrm{d}\Omega = 0. \tag{1.26}$$

All the information of the elastic wave propagation can be retrieved by analysing the fourth-order tensor $\underline{\underline{\mathbf{C}}}^{\mathrm{Eul}}$. For our purposes, we shall choose with care the expression for the stress tensor $\underline{\underline{\Sigma}}$, in order to capture realistic values of the physical parameters that we want to estimate.

1.2.4 Plane wave propagation in homogeneous media

Let us define $\Omega = \mathbb{R}^{\mathrm{d}}$, $\underline{\underline{\mathbf{C}}} = \underline{\underline{\mathbf{C}}}^{\mathrm{Eul}}$. The elastodynamic equation (1.26) can be rewritten as

$$\rho \frac{\partial^2 \tilde{y}_i}{\partial t^2} = C_{ij\ell m} \frac{\partial^2 \tilde{y}_\ell}{\partial x_j \partial x_m}, \quad \forall \, i = 1, 2, .., \mathrm{d}. \tag{1.27}$$

We highlight that we have used the Einstein summation convention for repeated indices. Following the assumption that the domain can be considered "fixed" with respect to elastic wave propagation, we can consider that the fourth-order tensor $\underline{\underline{\mathbf{C}}}$ is "locally" constant in time and space. Therefore, Eq. (1.27) reads in weak formulation
$\forall \, \underline{w} = (w_1, w_2, ..., w_{\mathrm{d}}) \in V(\Omega)$

$$\int_{\Omega} \rho \, \underline{\ddot{y}}_i \, w_i \, \mathrm{d}\Omega = \int_{\Omega} C_{ij\ell m} \frac{\partial y_\ell}{\partial x_m} \frac{\partial w_i}{\partial x_j} \, \mathrm{d}\Omega \overset{(*)}{=} \int_{\Omega} C_{ij\ell m} \, \varepsilon_{\ell m}(\underline{y}) \, \varepsilon_{ij}(\underline{w}) \, \mathrm{d}\Omega, \quad \forall k = 1, 2, .., \mathrm{d}, \tag{1.28}$$

with

$$\varepsilon_{\ell m}(\underline{y}) = \frac{1}{2} \left(\frac{\partial y_\ell}{\partial x_m} + \frac{\partial y_m}{\partial x_\ell} \right).$$

The last equality $(*)$ is verified if $\underline{\underline{\mathbf{C}}}$ is symmetric, i.e. $C_{ij\ell m} = C_{jim\ell}$, $\forall\, i,j,\ell,m = 1,2,..,\mathrm{d}$ [Joly, 2008].

Let us assume that the solution of Eq. (1.27) is a plane wave, i.e. a particular wave in the following form:

$$\underline{y}(x,t) = \underline{d}e^{i(\underline{k}\cdot\underline{x}-\omega t)}, \tag{1.29}$$

where $\underline{k} \in \mathbb{R}^{\mathrm{d}}$ is the wave vector, $\omega \in \mathbb{R}$ is the angular frequency and $\underline{d} \in \mathbb{R}^{\mathrm{d}}$ is the displacement vector (or polarisation vector).
The solution $\underline{y}$ of (1.29) represents a plane wave propagating in the direction $\underline{\nu} = \frac{\underline{k}}{|\underline{k}|}$ at the so-called *phase velocity*

$$V = \frac{\omega}{|\underline{k}|}.$$

Then, $\underline{y}$ is solution of Eq. (1.27) iff $\underline{d}$, $\underline{k}$ and ω satisfy

$$\underline{\underline{\Gamma}}(\underline{k})\,\underline{d} = \rho\,\omega^2\underline{d}, \tag{1.30}$$

where we have introduced the Christoffel tensor $\underline{\underline{\Gamma}}(\underline{k})$, that is a $\mathrm{d}\times\mathrm{d}$ symmetric matrix defined as

$$\Gamma_{i\,\ell}(\underline{k}) = \sum_{j,m=1}^{d} C_{ij\ell m}\,k_j\,k_m.$$

Consequently, the eigenvalue problem (1.30) reads

$$\left(C_{ij\ell m}\,k_j\,k_m - \rho\,\omega^2\,\delta_{i\ell}\right)d_\ell = 0 \quad \forall \ell = 1,2,..,\mathrm{d}. \tag{1.31}$$

The symmetry of $\underline{\underline{\Gamma}}(\underline{k})$ is a direct consequence of the symmetry of $\underline{\underline{\mathbf{C}}}$.
Furthermore, the Christoffel tensor is positive definite if $\underline{\underline{\mathbf{C}}}$ is coercive [Joly, 2008]. Therefore, if $\underline{\underline{\mathbf{C}}}$ is coercive, $\underline{\underline{\Gamma}}$ has only real positive eigenvalues (consequently, Eq. (1.27) is hyperbolic) and it is diagonalisable in an orthonormal basis of $\mathbb{R}^d$.
Moreover, as $\underline{\underline{\Gamma}}(\underline{k})$ is a homogeneous polynomial of degree two with respect to the wave vector $\underline{k}$, there exist d smooth functions

$$V_j(\underline{\nu}) : S^{d-1} \to \mathbb{R}^+,$$

where $S^{d-1} = \{\underline{\nu} \in \mathbb{R}^d \,|\, |\underline{\nu}| = 1\}$ is the unit sphere in $\mathbb{R}^d$ such that the spectrum of the Christoffel matrix $\underline{\underline{\Gamma}}(\underline{k})$ reads

$$\mathrm{sp}\,\underline{\underline{\Gamma}}(\underline{k}) = \{\rho|\underline{k}|^2 V_j^2(\underline{\nu}), j = 1,2,..,d\}.$$

As a consequence, for every direction $\underline{\nu} \in S^{d-1}$ there exists an orthonormal basis $p_j(\underline{\nu})_{j=1}^d$ (composed of the polarisation vectors) such that

$$\underline{\underline{\Gamma}}(\underline{k})\,p_j(\underline{\nu}) = \rho\,|\underline{k}|^2 V_j(\underline{\nu})^2 p_j(\underline{\nu}).$$

From Eq. (1.30) we can consider $\underline{d}$ as an eigenvector of $\underline{\underline{\Gamma}}(\underline{k})$ associated with the eigenvalue $\rho\omega^2$. This means that $\underline{y}$ is a non-trivial solution of the elastodynamic equation (1.27) iff

$$\exists\, j \in \{1,2,..,d\} \text{ s.t. } \omega = \pm\omega_j(\underline{k}) = |\underline{k}|V_j(\underline{\nu}),$$

and $\underline{d}$ belongs to the eigenspace of $\underline{\underline{\Gamma}}(\underline{k})$ associated with $\rho|\underline{k}|^2V_j^2(\underline{\nu})$, i.e. $\underline{d}$ is collinear to $p_j(\underline{\nu})$.
The elastic medium satisfies the *dispersion relation*

$$D(\omega,\underline{k}) \coloneqq \rho^d \prod_{j=1}^{d}(\omega_j(\underline{k})^2 - \omega^2) = 0, \tag{1.32}$$

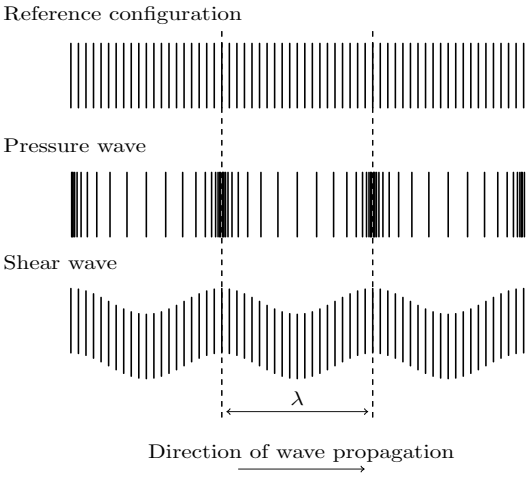

Figure 1.3 – Illustration of longitudinal and transverse waves.

namely

$$D(\omega, \underline{k}) \equiv \det\big(\underline{\underline{\Gamma}}(\underline{k}) - \rho\omega^2 I\big) = 0.$$

In particular, let us consider a plane wave satisfying the dispersion relation

$$\omega = \omega_j(\underline{k}).$$

Then, the corresponding *group velocity* is defined as:

$$\underline{V}_j^g(\underline{k}) = \underline{\nabla}\omega_j(\underline{k}).$$

From the homogeneity property

$$\omega_j(\alpha\,\underline{k}) = \alpha\,\omega_j(\underline{k}), \quad \forall j = 1, 2, .., d, \ \forall\,\alpha \in \mathbb{R},$$

we can define, if $\omega \neq 0$,

$$\hat{D}(\underline{s}) = D(1, \underline{s}) \equiv \rho^d \prod_{j=1}^{d} (\omega_j(\underline{s})^2 - 1),$$

where $\underline{s} = \frac{\underline{k}}{\omega}$ is called slowness vector.
Consequently, Eq. (1.32) holds iff $\hat{D}(\underline{s}) = 0$, and the solutions of this equation in the $\underline{s}$-plane are called *slowness curves*.
The *wavefronts* are the curves defined by the extremities of the group velocity vectors $V_j(\underline{\nu})$, with $\underline{\nu} \in S^{d-1}$. We note that the wavefronts geometrically represent the polar reciprocal curves of the slowness curves.
In homogenous isotropic media, there are two types of plane waves:

- The pressure waves or P waves, whose polarisation is collinear to the direction of propagation $\underline{\nu}$,
- The shear waves or S waves, whose polarisation is orthogonal to the direction $\underline{\nu}$.

See Figure 1.3 for a graphical illustration of pressure and transverse waves. If we denote by V_P and V_S the phase velocities of P waves and S waves, respectively, then $V_P > V_S$. In homogeneous isotropic media V_P and V_S do not depend on the propagation direction $\underline{\nu}$. Furthermore, the wavefronts are two circles of radius V_P and V_S, and the corresponding

slowness curves are circles of radius V_P^{-1} and V_S^{-1}, respectively.
In anisotropic media, shear plane waves have a polarisation orthogonal to the propagation direction, but they do not propagate at the same (phase) velocity, since it depends on the propagation direction. Consequently, these waves are denoted as quasi-shear waves. Furthermore, longitudinal waves have polarisation direction almost equal to propagation direction, and they are denoted quasi-pressure waves. In three-dimensional anisotropic media, it is possible to distinguish three waves: one quasi-pressure wave, one quasi-transverse wave; and a coupling term of lower amplitude [Bercoff et al., 2004].

1.3 Linearisation of mechanical quantities around a prestressed configuration

The aim of this chapter is to derive the expression of the linearised equation (1.22) for a realistic constitutive law of the myocardium and derive the corresponding Christoffel tensor, in order to retrieve the main features of elastic wave propagation in the medium. To do so, we first perform a linearisation of strain tensors, stress tensors and invariants, in order to compute a first-order approximation of the second Piola-Kirchhoff stress tensor $\underline{\underline{\Sigma}}$.
In the simplest linearised formulation, small displacements from the reference configuration are assumed. Therefore, only the first order of each quantity in the principle of virtual work is retained, in particular:

$$\underline{\underline{e}} \approx \underline{\underline{\varepsilon}} := \frac{1}{2}(\underline{\underline{\nabla}}\,\underline{y} + \underline{\underline{\nabla}}\,\underline{y}^T).$$

Our purpose is to generalise this approach, linearising along a time-dependent deformed configuration denoted $\Omega_0(t)$, related to the intrinsic movement of the heart.

1.3.1 Hypothesis

Let us consider the domain $\Omega_0(t)$, representing the moving configuration of the heart. We rewrite the displacement vector, according to our assumptions,

$$\underline{y}(t,x) = \underline{y}_0(t,x) + \delta\underline{\tilde{y}}(\tau,x),$$

with $\tau := \frac{t}{\delta}$, δ small. Consequently,

$$\underline{\underline{\nabla}}\,\underline{y} = \underline{\underline{\nabla}}\,\underline{y}_0 + \delta\underline{\underline{\nabla}}\,\underline{\tilde{y}},$$

and the deformation tensor becomes

$$\underline{\underline{F}} = \underline{\underline{\mathbb{1}}} + \underline{\underline{\nabla}}\,\underline{y} = \underline{\underline{\mathbb{1}}} + \underline{\underline{\nabla}}\,\underline{y}_0 + \delta\underline{\underline{\nabla}}\,\underline{\tilde{y}}.$$

For simplicity of notation, we define

$$\underline{\underline{F}}_0 := \underline{\underline{\mathbb{1}}} + \underline{\underline{\nabla}}\,\underline{y}_0.$$

1.3.2 Linearisation of strain and stress tensors

The Green-Lagrange strain tensor $\underline{\underline{e}}$ linearises as

$$\begin{aligned}\underline{\underline{e}} &= \frac{1}{2}(\underline{\underline{\nabla}}\,\underline{y} + \underline{\underline{\nabla}}\,\underline{y}^T + \underline{\underline{\nabla}}\,\underline{y}^T \cdot \underline{\underline{\nabla}}\,\underline{y}) \\ &= \frac{1}{2}\big(\underline{\underline{\nabla}}\,(\underline{y}_0 + \delta\underline{\tilde{y}}) + \underline{\underline{\nabla}}\,(\underline{y}_0^T + \delta\underline{\tilde{y}}^T) + \underline{\underline{\nabla}}\,(\underline{y}_0^T + \delta\underline{\tilde{y}}^T) \cdot \underline{\underline{\nabla}}\,(\underline{y}_0 + \delta\underline{\tilde{y}})\big) \\ &= \underline{\underline{e}}_0 + \delta\underline{\underline{e}}_0(\underline{\tilde{y}}) + O(\delta^2) \approx \underline{\underline{e}}_0 + \delta\underline{\underline{e}}_0(\underline{\tilde{y}}),\end{aligned}$$

where

$$\begin{aligned}\underline{\underline{e}}_0 &= \frac{1}{2}(\underline{\underline{\nabla}}\,\underline{y}_0 + \underline{\underline{\nabla}}\,\underline{y}_0^T + \underline{\underline{\nabla}}\,\underline{y}_0^T \cdot \underline{\underline{\nabla}}\,\underline{y}_0), \\ \underline{\underline{e}}_0(\underline{\tilde{y}}) &= \frac{1}{2}(\underline{\underline{\nabla}}\,\underline{\tilde{y}} + \underline{\underline{\nabla}}\,\underline{\tilde{y}}^T + \underline{\underline{\nabla}}\,\underline{y}_0^T \cdot \underline{\underline{\nabla}}\,\underline{\tilde{y}} + \underline{\underline{\nabla}}\,\underline{\tilde{y}}^T \cdot \underline{\underline{\nabla}}\,\underline{y}_0) = \frac{1}{2}(\underline{\underline{F}}_0^T \cdot \underline{\underline{\nabla}}\,\underline{\tilde{y}} + \underline{\underline{\nabla}}\,\underline{\tilde{y}}^T \cdot \underline{\underline{F}}_0).\end{aligned}$$

Therefore, the Cauchy-Green tensor can be reformulated as

$$\begin{aligned}\underline{\underline{C}} &= \underline{\underline{F}}^T\underline{\underline{F}} = (\underline{\underline{\mathbb{1}}} + \underline{\underline{\nabla}}\,\underline{y}_0^T + \delta\underline{\underline{\nabla}}\,\underline{\tilde{y}}^T)(\underline{\underline{\mathbb{1}}} + \underline{\underline{\nabla}}\,\underline{y}_0 + \delta\underline{\underline{\nabla}}\,\underline{\tilde{y}}) \\ &= \underline{\underline{\mathbb{1}}} + \underline{\underline{\nabla}}\,\underline{y}_0 + \delta\underline{\underline{\nabla}}\,\underline{\tilde{y}} + \underline{\underline{\nabla}}\,\underline{y}_0^T + \delta\underline{\underline{\nabla}}\,\underline{\tilde{y}}^T + \underline{\underline{\nabla}}\,\underline{y}_0^T \cdot \underline{\underline{\nabla}}\,\underline{y}_0 + \delta\underline{\underline{\nabla}}\,\underline{y}_0^T \cdot \underline{\underline{\nabla}}\,\underline{\tilde{y}} + \delta\underline{\underline{\nabla}}\,\underline{\tilde{y}}^T \cdot \underline{\underline{\nabla}}\,\underline{y}_0 + O(\delta^2) \\ &= \underline{\underline{\mathbb{1}}} + 2\,\underline{\underline{e}}_0 + 2\,\delta\underline{\underline{e}}_0(\underline{\tilde{y}}) + O(\delta^2) \approx \underline{\underline{C}}_0 + \delta\,\underline{\underline{\tilde{C}}},\end{aligned}$$

with

$$\underline{\underline{C}}_0 \coloneqq \underline{\underline{\mathbb{1}}} + 2\underline{\underline{e}}_0, \quad \underline{\underline{\tilde{C}}} \coloneqq 2\,\underline{\underline{e}}_0(\underline{\tilde{y}})$$

and factors of δ^2 are neglected according to the usual assumption of δ small. Furthermore, the inverse of $\underline{\underline{C}}$ reads

$$\underline{\underline{C}}^{-1}(\underline{y}) = \Big(\underline{\underline{C}}_0 + \delta\,\underline{\underline{\tilde{C}}}\Big)^{-1} + O(\delta^2) = \Big(\underline{\underline{\mathbb{1}}} + \delta\,\underline{\underline{C}}_0^{-1} \cdot \underline{\underline{\tilde{C}}}\Big)^{-1} \cdot \underline{\underline{C}}_0^{-1} + O(\delta^2).$$

In addition, we recall that

$$(\underline{\underline{\mathbb{1}}} + \delta\,\underline{\underline{A}})^{-1} = \underline{\underline{\mathbb{1}}} - \delta\,\underline{\underline{A}} + O(\delta^2).$$

Hence, we can define

$$\underline{\underline{C}}^{-1} \coloneqq \underline{\underline{C}}^{-1}(\underline{y}) = \underline{\underline{C}}_0^{-1} + \delta\,\underline{\underline{\tilde{G}}} + O(\delta^2),$$

where

$$\underline{\underline{C}}_0^{-1} \coloneqq (\underline{\underline{\mathbb{1}}} + 2\,\underline{\underline{e}}_0)^{-1}, \quad \underline{\underline{\tilde{G}}} \coloneqq -\underline{\underline{C}}_0^{-1} \cdot \underline{\underline{\tilde{C}}} \cdot \underline{\underline{C}}_0^{-1} = -2\,\underline{\underline{C}}_0^{-1} \cdot \underline{\underline{e}}_0(\underline{\tilde{y}}) \cdot \underline{\underline{C}}_0^{-1}.$$

1.3.3 Linearisation of invariants and reduced invariants

We can now proceed to linearise the invariants I_i, $i \in \{1,2,3,4\}$. The first invariant I_1 reads

$$\begin{aligned}I_1 &= \operatorname{tr}(\underline{\underline{C}}) = 3 + 2\operatorname{tr}\Big(\underline{\underline{e}}_0\Big) + 2\,\delta\ \operatorname{tr}\Big(\underline{\underline{e}}_0(\underline{\tilde{y}})\Big) + O(\delta^2) \\ &\approx I_{1,0} + \delta\tilde{I}_1,\end{aligned}$$

with

$$I_{1,0} \coloneqq 3 + 2\operatorname{tr}\Big(\underline{\underline{e}}_0\Big), \quad \tilde{I}_1 \coloneqq 2\operatorname{tr}\Big(\underline{\underline{e}}_0(\underline{\tilde{y}})\Big).$$

Analogously, we can reformulate the second invariant I_2 as

$$\begin{aligned}
I_2 &= \frac{1}{2}\big((\operatorname{tr}(\underline{\underline{C}}))^2 - \operatorname{tr}(\underline{\underline{C}}^2)\big) \\
&= \frac{1}{2}\Big(3 + 2\operatorname{tr}\Big(\underline{\underline{e}}_0\Big) + 2\,\delta\ \operatorname{tr}\Big(\underline{\underline{e}}_0(\underline{\tilde{y}})\Big) + O(\delta^2)\Big)^2 \\
&\quad - \frac{1}{2}\operatorname{tr}\Big(\underline{\underline{\mathbb{1}}} + 4\underline{\underline{e}}_0^2 + 8\delta\underline{\underline{e}}_0 \cdot \underline{\underline{e}}_0(\underline{\tilde{y}}) + 4\underline{\underline{e}}_0 + 4\,\delta\,\underline{\underline{e}}_0(\underline{\tilde{y}}) + O(\delta^2)\Big) \\
&= 3 + 4\operatorname{tr}\Big(\underline{\underline{e}}_0\Big) + 2\operatorname{tr}^2(\underline{\underline{e}}_0) - 2\operatorname{tr}\Big(\underline{\underline{e}}_0^2\Big) \\
&\quad + 4\delta\Big(\operatorname{tr}\Big(\underline{\underline{e}}_0(\underline{\tilde{y}})\Big) + \operatorname{tr}\Big(\underline{\underline{e}}_0\Big)\operatorname{tr}\Big(\underline{\underline{e}}_0(\underline{\tilde{y}})\Big) - \operatorname{tr}\Big(\underline{\underline{e}}_0 \cdot \underline{\underline{e}}_0(\underline{\tilde{y}})\Big)\Big) + O(\delta^2) \\
&\approx I_{2,0} + \delta\tilde{I}_2,
\end{aligned}$$

with

$$\begin{aligned}
I_{2,0} &\coloneqq 3 + 4\operatorname{tr}\Big(\underline{\underline{e}}_0\Big) + 2\operatorname{tr}^2(\underline{\underline{e}}_0) - 2\operatorname{tr}\Big(\underline{\underline{e}}_0^2\Big), \\
\tilde{I}_2 &\coloneqq 4\operatorname{tr}\Big(\underline{\underline{e}}_0(\underline{\tilde{y}})\Big) + 4\operatorname{tr}\Big(\underline{\underline{e}}_0\Big)\operatorname{tr}\Big(\underline{\underline{e}}_0(\underline{\tilde{y}})\Big) - 4\operatorname{tr}\Big(\underline{\underline{e}}_0 \cdot \underline{\underline{e}}_0(\underline{\tilde{y}})\Big).
\end{aligned}$$

As far as I_3 is concerned, we use the following property, valid for every scalar $A, B \in \mathbb{R}$:

$$\begin{aligned}
\det\big(\underline{\underline{A}} + \delta\underline{\underline{B}}\big) &= \det\underline{\underline{A}}\det\big(\underline{\underline{\mathbb{1}}} + \delta\underline{\underline{A}}^{-1} \cdot \underline{\underline{B}}\big) \\
&= \det\underline{\underline{A}}\big(1 + \delta\operatorname{tr}\big(\underline{\underline{A}}^{-1} \cdot \underline{\underline{B}}\big) + O(\delta^2)\big) \\
&= \det\underline{\underline{A}} + \delta\det\underline{\underline{A}}\operatorname{tr}\big(\underline{\underline{A}}^{-1} \cdot \underline{\underline{B}}\big) + O(\delta^2),
\end{aligned}$$

valid if δ small. Consequently, we can linearise the third invariant I_3 as

$$\begin{aligned}
I_3 = \det\underline{\underline{C}} &= \det\Big(\underline{\underline{\mathbb{1}}} + 2\underline{\underline{e}}_0 + 2\,\delta\,\underline{\underline{e}}_0(\underline{\tilde{y}})\Big) + O(\delta^2) \\
&= \det\underline{\underline{C}}_0 + 2\,\delta\ \det\underline{\underline{C}}_0\operatorname{tr}\Big(\underline{\underline{C}}_0^{-1} \cdot \underline{\underline{e}}_0(\underline{\tilde{y}})\Big) + O(\delta^2) \\
&\approx I_{3,0} + \delta\,\tilde{I}_3,
\end{aligned}$$

with

$$\begin{aligned}
I_{3,0} &\coloneqq \det\underline{\underline{C}}_0, \\
\tilde{I}_3 &\coloneqq 2\det\underline{\underline{C}}_0\operatorname{tr}\Big(\underline{\underline{C}}_0^{-1} \cdot \underline{\underline{e}}_0(\underline{\tilde{y}})\Big).
\end{aligned}$$

At last, the invariant I_4, introduced to model transversely isotropic media, linearises as

$$\begin{aligned}
I_4 &= \underline{\tau_1} \cdot \underline{\underline{C}} \cdot \underline{\tau_1} = \underline{\tau_1} \cdot \underline{\tau_1} + 2\underline{\tau_1} \cdot \underline{\underline{e}}_0 \cdot \underline{\tau_1} + 2\,\delta\,\underline{\tau_1} \cdot \underline{\underline{e}}_0(\underline{\tilde{y}}) \cdot \underline{\tau_1} + O(\delta^2) \\
&\approx I_{4,0} + \delta\tilde{I}_4,
\end{aligned}$$

with

$$I_{4,0} \coloneqq 1 + 2\,\underline{\tau_1} \cdot \underline{\underline{e}}_0 \cdot \underline{\tau_1}, \quad \tilde{I}_4 \coloneqq 2\,\underline{\tau_1} \cdot \underline{\underline{e}}_0(\underline{\tilde{y}}) \cdot \underline{\tau_1}.$$

As far as the *reduced invariants* are regarded, we recall their expression:

$$J_1 = I_1\,I_3^{-\frac{1}{3}}, \quad J_2 = I_2\,I_3^{-\frac{2}{3}}, \quad J_3 = I_3^{\frac{1}{2}}, \quad J_4 = I_4\,I_3^{-\frac{1}{3}}.$$

We recall that, for every scalar $A \in \mathbb{R}$ and $\alpha \in \mathbb{R}$ we can write

$$(1 + \delta\,A)^\alpha = 1 + \alpha\,\delta\,A + O(\delta^2).$$

In order to compute the linearised expression for these invariants, we first linearise the scalar $I_3^{-\frac{1}{3}}$:

$$\begin{aligned} I_3^{-\frac{1}{3}} &= \big(I_{3,0} + \delta\tilde{I}_3\big)^{-\frac{1}{3}} + O(\delta^2) = (I_{3,0})^{-\frac{1}{3}}\big(1 + \delta\, I_{3,0}^{-1}\,\tilde{I}_3\big)^{-\frac{1}{3}} + O(\delta^2) \\ &= (I_{3,0})^{-\frac{1}{3}}\Big(1 - \frac{1}{3}\delta\, I_{3,0}^{-1}\,\tilde{I}_3\Big) + O(\delta^2). \end{aligned}$$

Then, we can find the new expression for J_1:

$$\begin{aligned} J_1 = I_1 I_3^{-\frac{1}{3}} &= \big(I_{1,0} + \delta\tilde{I}_1\big)\big(I_{3,0} + \delta\,\tilde{I}_3\big)^{-\frac{1}{3}} + O(\delta^2) \\ &= \big(I_{1,0} + \delta\,\tilde{I}_1\big)\left(I_{3,0}^{-\frac{1}{3}} - \frac{1}{3}\delta\, I_{3,0}^{-\frac{4}{3}}\tilde{I}_3\right) + O(\delta^2) \\ &= I_{1,0}\, I_{3,0}^{-\frac{1}{3}} + \delta\left(\tilde{I}_1\, I_{3,0}^{-\frac{1}{3}} - \frac{1}{3} I_{1,0}\, I_{3,0}^{-\frac{4}{3}}\tilde{I}_3\right) + O(\delta^2) \\ &\approx J_{1,0} + \delta\tilde{J}_1, \end{aligned}$$

with

$$J_{1,0} \coloneqq I_{1,0}\, I_{3,0}^{-\frac{1}{3}}, \quad \tilde{J}_1 \coloneqq \tilde{I}_1\, I_{3,0}^{-\frac{1}{3}} - \frac{1}{3} I_{1,0}\, I_{3,0}^{-\frac{4}{3}}\tilde{I}_3.$$

Analogously, the invariant J_2 linearises as

$$J_2 \approx J_{2,0} + \delta\tilde{J}_2,$$

where we have defined

$$J_{2,0} \coloneqq I_{2,0} I_{3,0}^{-\frac{1}{3}}, \quad \tilde{J}_2 \coloneqq \tilde{I}_2\, I_{3,0}^{-\frac{1}{3}} - \frac{1}{3} I_{2,0}\, I_{3,0}^{-\frac{4}{3}}\tilde{I}_3.$$

The invariant J_3 can be rewritten as

$$J_3 \approx J_{3,0} + \delta\tilde{J}_3,$$

with

$$J_{3,0} \coloneqq I_{3,0}^{\frac{1}{2}}, \quad \tilde{J}_3 \coloneqq \frac{1}{2} I_{3,0}^{-1}\,\tilde{I}_3.$$

Similarly, for J_4 we obtain the following expression:

$$\begin{aligned} J_4 = I_4 I_3^{-\frac{1}{3}} &= \big(I_{4,0} + \delta\tilde{I}_4\big)\big(I_{3,0} + \delta\tilde{I}_3\big)^{-\frac{1}{3}} + O(\delta^2) \\ &= \big(I_{4,0} + \delta\tilde{I}_4\big)\left(I_{3,0}^{-\frac{1}{3}} - \frac{1}{3}\delta I_{3,0}^{-\frac{4}{3}}\tilde{I}_3\right) + O(\delta^2) \\ &= I_{4,0} I_{3,0}^{-\frac{1}{3}} + \delta\left(\tilde{I}_4 I_{3,0}^{-\frac{1}{3}} - \frac{1}{3} I_{4,0} I_{3,0}^{-\frac{4}{3}}\tilde{I}_3\right) + O(\delta^2) \\ &\approx J_{4,0} + \delta\tilde{J}_4, \end{aligned}$$

with

$$J_{4,0} \coloneqq I_{4,0}\, I_{3,0}^{-\frac{1}{3}}, \quad \tilde{J}_4 \coloneqq \tilde{I}_4\, I_{3,0}^{-\frac{1}{3}} - \frac{1}{3} I_{4,0}\, I_{3,0}^{-\frac{4}{3}}\tilde{I}_3.$$

We are now able to linearise the stress tensor $\underline{\underline{\Sigma}}$ around the deformed configuration and derive the expression of the Christoffel tensor associated with it.

1.4 Illustration on some constitutive laws for passive stress

Henceforth, we derive the expression of the Christoffel tensor for different constitutive laws. In particular, we start by deriving the Christoffel tensor associated with an exponential transversely isotropic constitutive law, and we discuss the properties of the wavefronts and slowness curves that correspond to this model. Then, we add in the constitutive law the contribution of a penalisation term accounting for nearly-incompressibility, and comment the effects of this term on the Christoffel tensor and slowness curves. Subsequently, we include an isotropic, linear term depending on the invariant I_2, that corresponds to the trace of the adjoint of the stress tensor $\underline{\underline{C}}$. We show that this term is fundamental to regularise the values in the Christoffel tensor and, as a consequence, the wavefronts and the slowness curves associated with the shear wave. We do not take into account viscosity in our analysis, since the introduction of the stress tensor associated with viscosity generates complex angular frequencies. As a consequence, the slowness curves and wavefronts do not have a clear meaning in this case. Furthermore, we consider dimension $d = 2$ for the sake of clarity.

1.4.1 An anisotropic model

First, we consider a transversely isotropic stress-strain law in the parallel element, and define $\underline{\tau_1}$ the privileged direction that corresponds to the muscle fibre for cardiac modelling. A possible choice for the energy W^e consists in

$$W^e(\underline{\underline{e}}) = W^{\mathrm{TI}}(J_1, J_4) \coloneqq \kappa_1\, e^{\kappa_2 (J_1-3)^2} + \kappa_3\, e^{\kappa_4 (J_4-1)^2}, \tag{1.33}$$

with $\kappa_i \in \mathbb{R}^+$, for all $i \in \{1,2,3,4\}$. We linearise the first exponential term in W^{TI}, assuming δ small, as following:

$$\begin{aligned} e^{\kappa_2\,(J_1-3)^2} &= e^{\kappa_2\,(J_{1,0}+\delta\,\tilde{J}_1-3)^2} + O(\delta^2) = e^{\kappa_2 (J_{1,0}-3)^2} e^{2\,\delta\,\kappa_2\,\tilde{J}_1\,(J_{1,0}-3)} + O(\delta^2) \\ &\approx e^{\kappa_2 (J_{1,0}-3)^2}\big(1 + 2\,\delta\,\kappa_2\,\tilde{J}_1 (J_{1,0}-3)\big) + O(\delta^2). \end{aligned}$$

The second term $e^{\kappa_4\,(J_4-1)^2}$ can be linearised in an analogous manner.
In order to retrieve the specific expression of the stress tensor $\underline{\underline{\Sigma}}$ for this constitutive law, following Eq. (1.10), we need to compute

$$\underline{\underline{\Sigma}}^{\mathrm{TI}} = 2\Big(\frac{\partial W^{\mathrm{TI}}}{\partial J_1} \cdot \frac{\partial J_1}{\partial \underline{\underline{C}}} + \frac{\partial W^{\mathrm{TI}}}{\partial J_4} \cdot \frac{\partial J_4}{\partial \underline{\underline{C}}}\Big). \tag{1.34}$$

First, we evaluate the partial derivative of W^{TI} with respect to the invariants J_1 and J_4 . We get

$$\begin{aligned} \frac{\partial W^{\mathrm{TI}}}{\partial J_1} &= 2\,\kappa_1\,\kappa_2 (J_1-3)\, e^{\kappa_2\,(J_1-3)^2} \\ &= 2\,\kappa_1 \kappa_2 e^{\kappa_2 (J_{1,0}-3)^2} (J_{1,0}-3) + 2\,\delta\,\kappa_1\,\kappa_2 e^{\kappa_2 (J_{1,0}-3)^2}\big(\tilde{J}_1 + 2\,\kappa_2\,\tilde{J}_1 (J_{1,0}-3)^2\big) + O(\delta^2), \\ \frac{\partial W^{\mathrm{TI}}}{\partial J_4} &= 2\,\kappa_3\,\kappa_4 (J_4-1) e^{\kappa_4 (J_4-1)^2} \\ &= 2\,\kappa_3\,\kappa_4 e^{\kappa_4 (J_{4,0}-1)^2} (J_{4,0}-1) + 2\,\delta\,\kappa_3\,\kappa_4 e^{\kappa_4 (J_{4,0}-1)^2}\big(\tilde{J}_4 + 2\,\kappa_4 \tilde{J}_4 (J_{4,0}-1)^2\big) + O(\delta^2). \end{aligned}$$

Moreover, the derivatives of J_1 and J_4 with respect to $\underline{\underline{C}}$ read, after some algebra,

$$\begin{aligned}
\frac{\partial J_1}{\partial \underline{\underline{C}}} &= I_3^{-\frac{1}{3}}\Big(\underline{\underline{\mathbb{1}}} - \frac{1}{3} I_1 \underline{\underline{C}}^{-1}\Big) = I_3^{-\frac{1}{3}}\underline{\underline{\mathbb{1}}} - \frac{1}{3} J_1 \underline{\underline{C}}^{-1} \\
&= I_{3,0}^{-\frac{1}{3}}\underline{\underline{\mathbb{1}}} + \delta\, \tilde{I}_3^{-\frac{1}{3}}\underline{\underline{\mathbb{1}}} - \frac{1}{3}\Big(J_{1,0}\,\underline{\underline{C}}_0^{-1} + \delta\, J_{1,0}\underline{\underline{\tilde{G}}} + \delta\, \tilde{J}_1 \underline{\underline{C}}_0^{-1}\Big) + O(\delta^2), \\
\frac{\partial J_4}{\partial \underline{\underline{C}}} &= I_3^{-\frac{1}{3}}\Big(\underline{\tau}_1 \otimes \underline{\tau}_1 - \frac{1}{3} I_4 \underline{\underline{C}}^{-1}\Big) = I_3^{-\frac{1}{3}}\underline{\tau}_1 \otimes \underline{\tau}_1 - \frac{1}{3} J_4 \underline{\underline{C}}^{-1} \\
&= I_{3,0}^{-\frac{1}{3}}\,\underline{\tau}_1 \otimes \underline{\tau}_1 + \delta\, \tilde{I}_3^{-\frac{1}{3}}\underline{\tau}_1 \otimes \underline{\tau}_1 - \frac{1}{3}\Big(J_{4,0}\,\underline{\underline{C}}_0^{-1} + \delta\, J_{4,0}\,\underline{\underline{\tilde{G}}} + \delta\, \tilde{J}_4\,\underline{\underline{C}}_0^{-1}\Big) + O(\delta^2),
\end{aligned}$$

where we have approximated

$$\begin{aligned}
I_3^{-\frac{1}{3}} &= \Big(I_{3,0} + 2\,\delta\, I_{3,0}\,\mathrm{tr}\big(\underline{\underline{C}}_0^{-1}\cdot \underline{\underline{e}}_0(\underline{\tilde{y}})\big)\Big)^{-\frac{1}{3}} + O(\delta^2) \\
&= I_{3,0}^{-\frac{1}{3}}\Big(1 - \frac{2}{3}\delta\,\mathrm{tr}\big(\underline{\underline{C}}_0^{-1}\cdot \underline{\underline{e}}_0(\underline{\tilde{y}})\big)\Big) + O(\delta^2) \\
&\approx I_{3,0}^{-\frac{1}{3}} + \delta \tilde{I}_3^{-\frac{1}{3}},
\end{aligned}$$

with

$$I_{3,0}^{-\frac{1}{3}} = \det \underline{\underline{C}}_0^{-\frac{1}{3}}, \quad \tilde{I}_3^{-\frac{1}{3}} = -\frac{2}{3}\, I_{3,0}^{-\frac{1}{3}}\ \mathrm{tr}\Big(\underline{\underline{C}}_0^{-1}\cdot \underline{\underline{e}}_0(\underline{\tilde{y}})\Big).$$

Under the assumption $\underline{y}_0 = 0$, after some algebra we get

$$\begin{aligned}
\frac{\partial W^{\mathrm{TI}}}{\partial J_1} &= 2\,\delta\,\kappa_1\,\kappa_2\,\tilde{J}_1 = 0 + O(\delta^2), \\
\frac{\partial W^{\mathrm{TI}}}{\partial J_4} &= 2\,\delta\,\kappa_3\,\kappa_4\,\tilde{J}_4 = 4\,\delta\,\kappa_3\,\kappa_4\Big(\underline{\tau}_1\cdot \underline{\underline{e}}_0(\underline{\tilde{y}})\cdot \underline{\tau}_1 - \frac{1}{3}\,\mathrm{tr}\Big(\underline{\underline{e}}_0(\underline{\tilde{y}})\Big)\Big) + O(\delta^2),
\end{aligned}$$

and

$$\begin{aligned}
\frac{\partial J_1}{\partial \underline{\underline{C}}} &= -\frac{2}{3}\delta\ \mathrm{tr}\Big(\underline{\underline{e}}_0(\underline{\tilde{y}})\Big)\,\underline{\underline{\mathbb{1}}} + 2\,\delta\,\underline{\underline{e}}_0(\underline{\tilde{y}}) + O(\delta^2), \\
\frac{\partial J_4}{\partial \underline{\underline{C}}} &= \underline{\tau}_1 \otimes \underline{\tau}_1 - \frac{1}{3}\underline{\underline{\mathbb{1}}} - \frac{2}{3}\delta\ \mathrm{tr}\Big(\underline{\underline{e}}_0(\underline{\tilde{y}})\Big)\,\underline{\tau}_1 \otimes \underline{\tau}_1 + \frac{2}{3}\delta\,\underline{\underline{e}}_0(\underline{\tilde{y}}) \\
&\quad - \frac{2}{3}\delta\,\underline{\tau}_1\cdot \underline{\underline{e}}_0(\underline{\tilde{y}})\cdot \underline{\tau}_1 + \frac{2}{9}\delta\ \mathrm{tr}\Big(\underline{\underline{e}}_0(\underline{\tilde{y}})\Big) + O(\delta^2).
\end{aligned}$$

Note that in prestressed-free configuration $\underline{\underline{e}}_0(\underline{\tilde{y}}) = \underline{\underline{\varepsilon}}(\underline{\tilde{y}})$. At this point, we are able to evaluate Eq. (1.34). The resulting Piola-Kirchhoff tensor $\underline{\underline{\Sigma}}^{\mathrm{TI}}$ in a prestress-free configuration reads

$$\begin{aligned}
\underline{\underline{\Sigma}}^{\mathrm{TI}} &= \delta\, c(\underline{\tau}_1\cdot \underline{\underline{\varepsilon}}(\underline{\tilde{y}})\cdot \underline{\tau}_1)\underline{\tau}_1 \otimes \underline{\tau}_1 - \frac{1}{3}\delta\, c\ \mathrm{tr}\big(\underline{\underline{\varepsilon}}(\underline{\tilde{y}})\big)\underline{\tau}_1 \otimes \underline{\tau}_1 - \frac{1}{3}\delta\, c(\underline{\tau}_1\cdot \underline{\underline{\varepsilon}}(\underline{\tilde{y}})\cdot \underline{\tau}_1)\underline{\underline{\mathbb{1}}} \\
&\quad + \frac{1}{9}\delta\, c\,\mathrm{tr}\big(\underline{\underline{\varepsilon}}(\underline{\tilde{y}})\big)\underline{\underline{\mathbb{1}}} + O(\delta^2) \\
&= \delta c\Big(\underline{\underline{\tilde{\Sigma}}}_1^{\mathrm{TI}} - \frac{1}{3}\underline{\underline{\tilde{\Sigma}}}_2^{\mathrm{TI}} - \frac{1}{3}\underline{\underline{\tilde{\Sigma}}}_3^{\mathrm{TI}} + \frac{1}{9}\underline{\underline{\tilde{\Sigma}}}_4^{\mathrm{TI}}\Big) + O(\delta^2),
\end{aligned} \tag{1.35}$$

with

$$\begin{aligned}
\underline{\underline{\tilde{\Sigma}}}_1^{\mathrm{TI}} &= (\underline{\tau}_1\cdot \underline{\underline{\varepsilon}}(\underline{\tilde{y}})\cdot \underline{\tau}_1)\,\underline{\tau}_1 \otimes \underline{\tau}_1, \\
\underline{\underline{\tilde{\Sigma}}}_2^{\mathrm{TI}} &= \mathrm{tr}\big(\underline{\underline{\varepsilon}}(\underline{\tilde{y}})\big)\underline{\tau}_1 \otimes \underline{\tau}_1, \\
\underline{\underline{\tilde{\Sigma}}}_3^{\mathrm{TI}} &= (\underline{\tau}_1\cdot \underline{\underline{\varepsilon}}(\underline{\tilde{y}})\cdot \underline{\tau}_1)\underline{\underline{\mathbb{1}}}, \\
\underline{\underline{\tilde{\Sigma}}}_4^{\mathrm{TI}} &= \mathrm{tr}\big(\underline{\underline{\varepsilon}}(\underline{\tilde{y}})\big)\underline{\underline{\mathbb{1}}}
\end{aligned} \tag{1.36}$$

and

$$c = 8\,\kappa_3\,\kappa_4.$$

We define $\tilde{\underline{\underline{\Sigma}}}^{\mathrm{TI}} = \delta^{-1}\,\underline{\underline{\Sigma}}^{\mathrm{TI}}$, in order to make explicit the dependence on δ.
We recall that for elastographic purposes, we need to perform our analysis in deformed configuration. To this end, we consider the stress tensor in deformed configuration

$$\underline{\underline{\sigma}}^{\mathrm{TI}} = J^{-1}\underline{\underline{F}} \cdot \underline{\underline{\Sigma}}^{\mathrm{TI}} \cdot \underline{\underline{F}}^{T},$$

and we define $\tilde{\underline{\underline{\sigma}}}^{\mathrm{TI}} = \delta^{-1}\underline{\underline{\sigma}}^{\mathrm{TI}}$. As a consequence, the fourth-order tensor $\underline{\underline{\mathbf{C}}}$ in Eulerian configuration is given by

$$\underline{\underline{\mathbf{C}}} \equiv \underline{\underline{\mathbf{C}}}^{\mathrm{Eul}} = J^{-1}\underline{\underline{F}} \cdot \underline{\underline{\mathbf{C}}}^{\mathrm{Lag}} \cdot \underline{\underline{F}}^{T}.$$

In prestress-free configuration, however, $\underline{\underline{F}} = \underline{\underline{\mathbb{1}}} + O(\delta)$ and $J = 1 + O(\delta)$. As a consequence, for this choice of constitutive law, $\underline{\underline{\mathbf{C}}}^{\mathrm{Eul}} = \underline{\underline{\mathbf{C}}}^{\mathrm{Lag}} + O(\delta)$.

Christoffel tensor in prestress-free configuration. We assume $\underline{y}_0 = \underline{0}$. We can define the fourth-order symmetric tensor $\underline{\underline{\mathbf{C}}}$ such that $\tilde{\underline{\underline{\sigma}}}^{\mathrm{TI}} = \underline{\underline{\mathbf{C}}}\,\underline{\underline{e}}_0(\tilde{\underline{y}})$. Hence, it reads

$$\begin{aligned}\underline{\underline{\mathbf{C}}} &= c\Big(\underline{\tau}_1 \otimes \underline{\tau}_1 \otimes \underline{\tau}_1 \otimes \underline{\tau}_1 - \frac{1}{3}\,(\underline{\tau}_1 \otimes \underline{\tau}_1) \otimes \underline{\underline{\mathbb{1}}} - \frac{1}{3}\underline{\underline{\mathbb{1}}}\ \otimes (\underline{\tau}_1 \otimes \underline{\tau}_1) + \frac{1}{9}\underline{\underline{\mathbb{1}}} \otimes \underline{\underline{\mathbb{1}}}\Big) \\ &= c\Big(\underline{\tau}_1 \otimes \underline{\tau}_1 - \frac{1}{3}\,\underline{\underline{\mathbb{1}}}\Big) \otimes \Big(\underline{\tau}_1 \otimes \underline{\tau}_1 - \frac{1}{3}\,\underline{\underline{\mathbb{1}}}\Big).\end{aligned} \tag{1.37}$$

It is easy to see that $\underline{\underline{\mathbf{C}}}$ is symmetric and semi-definite positive. In fact, for every $\underline{\underline{e}}$ symmetric and admissible we get

$$\underline{\underline{\mathbf{C}}}\,\underline{\underline{e}} : \underline{\underline{e}} = c\Big(\underline{\tau}_1 \cdot \underline{\underline{e}} \cdot \underline{\tau}_1 - \frac{1}{3}\,\mathrm{tr}\big(\underline{\underline{e}}\big)\Big)^2 \geq 0,$$

as c is a positive constant by hypothesis. Our aim is to compute

$$\tilde{\Gamma}_{i\,\ell}(\underline{k}) = \sum_{j,m}^{2} C_{ij\ell m} k_j\, k_m, \quad \forall i\,\ell \in \{1,2\}. \tag{1.38}$$

First, we compute the explicit expression of $\underline{\underline{\mathbf{C}}}$. First, we detail each term of the sum in Eq. (1.37). We obtain

$$
\begin{aligned}
(\underline{\tau_1} \otimes \underline{\tau_1}) \otimes (\underline{\tau_1} \otimes \underline{\tau_1}) &= \begin{bmatrix} \tau_{1,1}^4 & \tau_{1,1}^3\,\tau_{1,2} & \tau_{1,1}^3\,\tau_{1,2} & \tau_{1,1}^2\,\tau_{1,2}^2 \\ \tau_{1,1}^3\,\tau_{1,2} & \tau_{1,1}^2\,\tau_{1,2}^2 & \tau_{1,1}^2\,\tau_{1,2}^2 & \tau_{1,1}\,\tau_{1,2}^3 \\ \tau_{1,1}^3\,\tau_{1,2} & \tau_{1,1}^2\,\tau_{1,2}^2 & \tau_{1,1}^2\,\tau_{1,2}^2 & \tau_{1,1}\,\tau_{1,2}^3 \\ \tau_{1,1}^2\,\tau_{1,2}^2 & \tau_{1,1}\,\tau_{1,2}^3 & \tau_{1,1}\,\tau_{1,2}^3 & \tau_{1,2}^4 \end{bmatrix} \\
(\underline{\tau_1} \otimes \underline{\tau_1}) \otimes \underline{\underline{\mathbb{1}}} &= \begin{bmatrix} \tau_{1,1}^2 & 0 & \tau_{1,1}\,\tau_{1,2} & 0 \\ 0 & \tau_{1,1}^2 & 0 & \tau_{1,1}\,\tau_{1,2} \\ \tau_{1,1}\,\tau_{1,2} & 0 & \tau_{1,2}^2 & 0 \\ 0 & \tau_{1,1}\,\tau_{1,2} & 0 & \tau_{1,2}^2 \end{bmatrix} \\
\underline{\underline{\mathbb{1}}} \otimes (\underline{\tau_1} \otimes \underline{\tau_1}) &= \begin{bmatrix} \tau_{1,1}^2 & \tau_{1,1}\,\tau_{1,2} & 0 & 0 \\ \tau_{1,1}\,\tau_{1,2} & \tau_{1,2}^2 & 0 & 0 \\ 0 & 0 & \tau_{1,1}^2 & \tau_{1,1}\,\tau_{1,2} \\ 0 & 0 & \tau_{1,1}\,\tau_{1,2} & \tau_{1,2}^2 \end{bmatrix} \\
\underline{\underline{\mathbb{1}}} \otimes \underline{\underline{\mathbb{1}}} &= \begin{bmatrix} 1 & 0 & 0 & 0 \\ 0 & 1 & 0 & 0 \\ 0 & 0 & 1 & 0 \\ 0 & 0 & 0 & 1 \end{bmatrix}.
\end{aligned}
\tag{1.39}
$$

By combining Eqs. (1.37), (1.38) and (1.39), after some algebra we obtain the expression of the Christoffel tensor

$$
\underline{\underline{\tilde{\Gamma}}}(\underline{k}) = c \begin{bmatrix} \tilde{\Gamma}_{11} & \tilde{\Gamma}_{12} \\ \tilde{\Gamma}_{12} & \tilde{\Gamma}_{22} \end{bmatrix}
$$

with

$$
\tilde{\Gamma}_{11} = \left(\tau_{1,1}^2 - \frac{1}{3}\right)^2 k_1^2 + 2\tau_{1,1}\,\tau_{1,2}\left(\tau_{1,1}^2 - \frac{1}{3}\right) k_1\,k_2 + \tau_{1,1}^2\,\tau_{1,2}^2\,k_2^2,
$$

$$
\tilde{\Gamma}_{12} = \left(\tau_{1,1}^2 - \frac{1}{3}\right)\tau_{1,1}\,\tau_{1,2} k_1^2 + \left(2\tau_{1,1}^2\,\tau_{1,2}^2 - \frac{1}{3}\tau_{1,1}^2 - \frac{1}{3}\tau_{1,2}^2 + \frac{1}{9}\right) k_1\,k_2 + \left(\tau_{1,2}^2 - \frac{1}{3}\right)\tau_{1,1}\,\tau_{1,2}\,k_2^2,
$$

$$
\tilde{\Gamma}_{22} = \tau_{1,1}^2\,\tau_{1,2}^2\,k_1^2 + 2\,\tau_{1,1}\,\tau_{1,2}\left(\tau_{1,2}^2 - \frac{1}{3}\right) k_1\,k_2 + \left(\tau_{1,2}^2 - \frac{1}{3}\right)^2 k_2^2.
$$

In the simple case $\underline{\tau_1} = \underline{e}_1 \equiv (1,0)$, we obtain

$$
\underline{\underline{\tilde{\Gamma}}}(\underline{k}) = c \begin{bmatrix} \frac{4}{9}k_1^2 & -\frac{2}{9}k_1\,k_2 \\ -\frac{2}{9}k_1\,k_2 & \frac{1}{9}k_2^2 \end{bmatrix}. \tag{1.40}
$$

On the contrary, if $\underline{\tau_1} = \underline{e}_2 \equiv (0,1)$, we get

$$
\underline{\underline{\tilde{\Gamma}}}(\underline{k}) = c \begin{bmatrix} \frac{1}{9}k_1^2 & -\frac{2}{9}k_1\,k_2 \\ -\frac{2}{9}k_1\,k_2 & \frac{4}{9}k_2^2 \end{bmatrix}.
$$

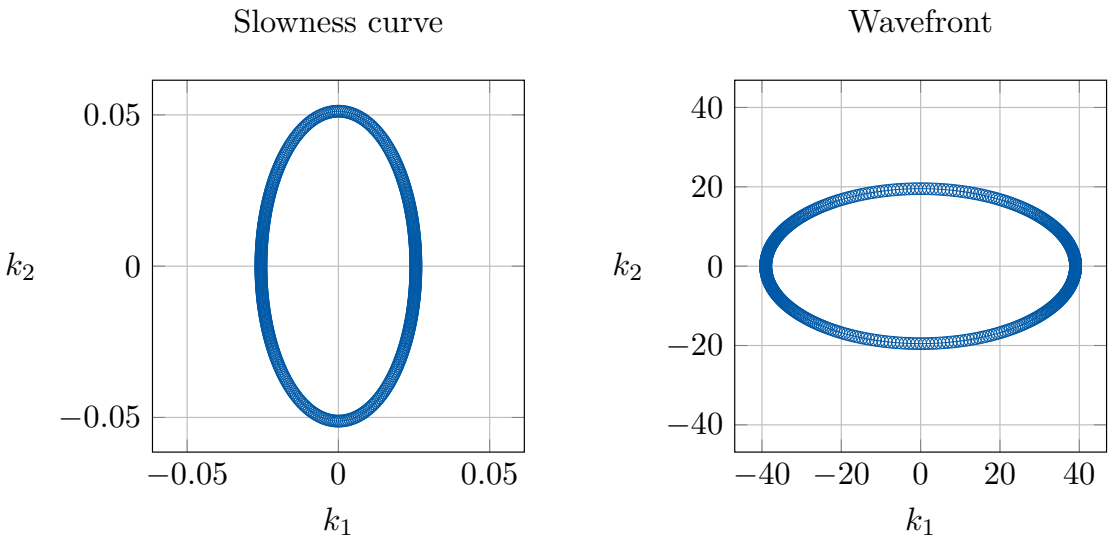

Figure 1.4 – Slowness curve (left) and wavefront (right) associated with the quasi-longitudinal wave in a transversely isotropic medium. $\kappa_3 = 170\,\mathrm{Pa}$, $\kappa_4 = 2.5$.

It is interesting to note that $\det\left(\underline{\underline{\tilde{\Gamma}}}(\underline{k})\right) = 0$. The resulting *dispersion relation* for the case $\underline{\tau_1} = e_1 \equiv (1,0)$ reads

$$0 = \det\left(\underline{\underline{\tilde{\Gamma}}}(\underline{k}) - \rho\,\omega^2 I\right) = \rho^2\omega^4 - \frac{1}{9}c\,(4\,k_1^2 + k_2^2)\,\rho\,\omega^2. \tag{1.41}$$

We shall consider Eq. (1.41) as an equation for a given value of the wave vector $\underline{k}$ at the frequency ω. Then, we get four solutions

$$\omega = \pm\,\omega_{QP}(\underline{k}), \quad \omega = \pm\,\omega_{QS}(\underline{k}),$$

where QP and QS stand for quasi-pressure and quasi-shear, since we are considering an anisotropic medium. $\underline{\underline{\Gamma}}(\underline{k})$ has two eigenvalues, associated with eigenvectors $D_{QP}(\underline{k})$ and $D_{QS}(\underline{k})$, respectively, that read

$$\gamma_{QP} = \rho\,\omega_{QP}^2(\underline{k}) = \frac{1}{9}c\,(4k_1^2 + k_2^2), \quad \gamma_{QS} = \rho\,\omega_{QS}^2(\underline{k}) = 0. \tag{1.42}$$

We notice from Eq. (1.42) that the quasi-transverse wave has zero velocity, while the quasi-longitudinal wave has angular frequency

$$\omega_{QP}(\underline{k}) = \pm\,\frac{1}{3}\sqrt{\frac{c\,(4\,k_1^2 + k_2^2)}{\rho}}.$$

We choose $\kappa_3 = 170\mathrm{Pa}$, $\kappa_4 = 2.5$ (see Section 1.8.2 for further details on calibration). Consequently, we obtain $c = 3400\,\mathrm{Pa}$. Figure 1.4 depicts the resulting slowness curves and wavefronts for the quasi-longitudinal wave. We observe that they are finite and well describe the anisotropic character of the model. In fact, since we set $\underline{\tau_1} = \underline{e}_1$, the wave propagates faster along this direction. On the contrary, the curves related to the quasi-transverse wave are not well-defined, because the eigenvalue corresponding to this wave is zero. The first extension of the model will consist in the inclusion of a penalisation term to enforce nearly-incompressibility.

1.4.2 Nearly-incompressible material

In order to take account for a nearly-incompressible material, the penalisation term W^{NI} is added to the elastic potential W^e, namely

$$W^e = W^{\mathrm{TI}} + W^{\mathrm{NI}}. \tag{1.43}$$

We define the term W^{NI} as

$$W^{\mathrm{NI}} = \kappa(J-1) - \kappa \log(J). \tag{1.44}$$

This also ensures $J > 0$.
If we consider this additional term, the stress tensor becomes

$$\underline{\underline{\Sigma}}^e = \underline{\underline{\Sigma}}^{\mathrm{TI}} + \underline{\underline{\Sigma}}^{\mathrm{NI}} = \frac{\partial W^{\mathrm{TI}}}{\partial e} - p\frac{\partial J}{\partial e} = \frac{\partial W^{\mathrm{TI}}}{\partial e}(J_1, J_4) - pJ\underline{\underline{C}}^{-1},$$

where p is the *hydrostatic* pressure and, due to Eq. (1.44), it has the following expression:

$$p = \kappa\frac{1-J}{J}.$$

After linearisation, the term $\underline{\underline{\Sigma}}^{\mathrm{NI}}$ reads

$$\underline{\underline{\Sigma}}^{\mathrm{NI}} = -p\,J\underline{\underline{C}}^{-1} = \kappa\Big((J_0\,\underline{\underline{C}}_0^{-1} - \underline{\underline{C}}_0^{-1}) + \delta(J_0\,\underline{\underline{\tilde{G}}} + \tilde{J}\,\underline{\underline{C}}_0^{-1} - \underline{\underline{\tilde{G}}})\Big) + O(\delta^2).$$

Christoffel tensor in prestress-free configuration. First, note that with the simplifying prestress-free assumption $\underline{y}_0 = 0$, we obtain the following expression for this additional term:

$$\underline{\underline{\Sigma}}^{\mathrm{NI}} = \delta\kappa\,\mathrm{tr}\big(\underline{\underline{\varepsilon}}(\underline{\tilde{y}})\big)\underline{\underline{\mathbb{1}}} + O(\delta^2).$$

Note that here again, due to the assumption $\underline{y}_0 = 0$, we can approximate the tensor $\underline{\underline{\sigma}}^{\mathrm{NI}}$ in deformed configuration as

$$\underline{\underline{\sigma}}^{\mathrm{NI}} = \underline{\underline{\Sigma}}^{\mathrm{NI}} + O(\delta).$$

Let us define $\underline{\underline{\tilde{\sigma}}}^{\mathrm{NI}} = \delta^{-1}\underline{\underline{\sigma}}^{\mathrm{NI}}$. Then, we can define the fourth-order tensor $\underline{\underline{\mathbf{C}}}$ such that $\underline{\underline{\tilde{\sigma}}}^{\mathrm{NI}} = \underline{\underline{\mathbf{C}}}^{\mathrm{NI}}\,\underline{\underline{e}}_0(\underline{\tilde{y}})$ and it reads

$$\underline{\underline{\mathbf{C}}} = \kappa\,\underline{\underline{\mathbb{1}}} \otimes \underline{\underline{\mathbb{1}}}. \tag{1.45}$$

Consequently, using Eqs. (1.38), (1.39) and (1.45), we compute the Christoffel tensor $\underline{\underline{\tilde{\Gamma}}}(\underline{k})$ as

$$\underline{\underline{\tilde{\Gamma}}}(\underline{k}) = \kappa\begin{bmatrix} k_1^2 & k_1\,k_2 \\ k_1\,k_2 & k_2^2 \end{bmatrix}. \tag{1.46}$$

From Eqs. (1.40) and (1.46), the *dispersion relation* associated with the complete constitutive law (1.43), for $\underline{\tau}_1 = \underline{e}_1$, reads

$$0 = \det\Big(\underline{\underline{\tilde{\Gamma}}}(\underline{k}) - \gamma\underline{\underline{\mathbb{1}}}\Big) = \det\left(\begin{bmatrix} \Big(\frac{4}{9}c+\kappa\Big)k_1^2 - \gamma & \Big(-\frac{2}{9}c+\kappa\Big)k_1k_2 \\ \Big(-\frac{2}{9}c+\kappa\Big)k_1k_2 & \Big(\frac{1}{9}c+\kappa\Big)k_2^2 - \gamma \end{bmatrix}\right),$$

with the usual assumption $\gamma = \rho\omega^2$. We can compute the eigenvalues

$$\gamma_{QP} = \frac{1}{2}\Big(\beta + \sqrt{\beta^2 - \frac{4}{9}c\,\kappa\,k_1^2\,k_2^2}\Big), \qquad \gamma_{QS} = \frac{1}{2}\Big(\beta - \sqrt{\beta^2 - \frac{4}{9}c\,\kappa\,k_1^2\,k_2^2}\Big), \tag{1.47}$$

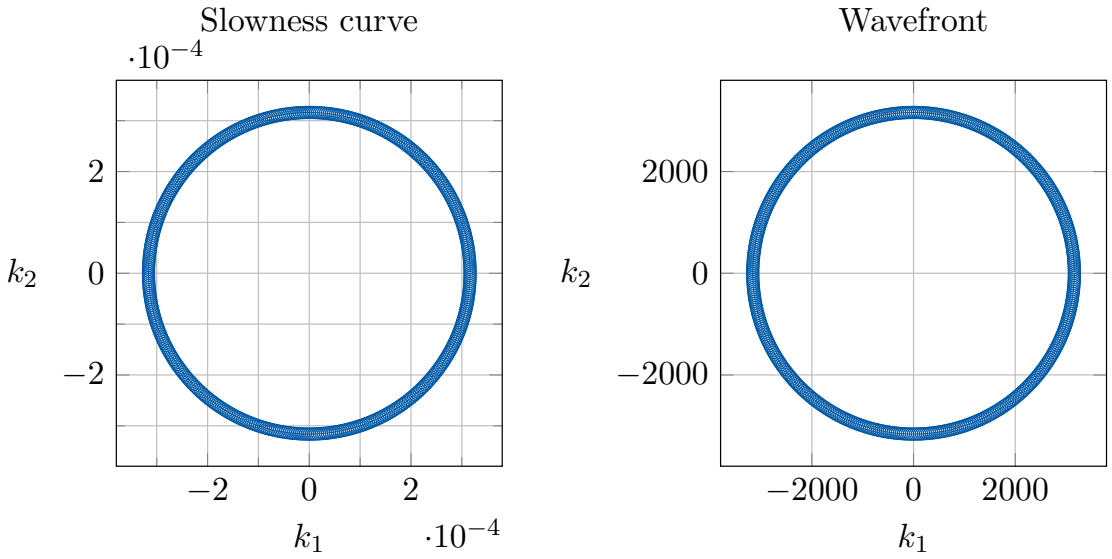

Figure 1.5 – Slowness curve (left) and wavefront (right) associated with the quasi-longitudinal wave in a transversely isotropic, nearly-incompressible medium. $\kappa_3 = 170\,\mathrm{Pa}$, $\kappa_4 = 2.5$, $\kappa = 10\,\mathrm{MPa}$.

with

$$\beta = \left(\frac{4}{9}c + \kappa\right)k_1^2 + \left(\frac{1}{9}c + \kappa\right)k_2^2.$$

The angular frequency corresponding to the quasi-longitudinal and quasi-transverse wave can be derived from Eq. (1.47).
Note that, in order to obtain two real solutions of the *dispersive relation*, we need to ensure that the discriminant $\det\left(\underline{\underline{\tilde{\Gamma}}}(\underline{k})\right)$ is strictly positive. After some algebra, we get the necessary condition

$$c\,\kappa\,k_1^2\,k_2^2 > 0. \tag{1.48}$$

Eq. (1.48) implies that the eigenvalue related to the quasi-transverse wave approaches zero at the axes ($k_1 \to 0$ or $k_2 \to 0$).
For the numerical simulation we adopt $\kappa = 10\,\mathrm{MPa}$. The resulting slowness curves and wavefronts associated with this constitutive law are depicted in Figures 1.5 and 1.6. The inclusion of the term accounting for compressibility has a considerable influence on the elastic wave propagation, due to the large value of κ. The slowness curve and the wavefront related to the quasi-longitudinal wave reproduce the features of an isotropic medium. Furthermore, as a consequence of this additional term, the quasi-longitudinal wave propagates faster than in a compressible medium (Figure 1.4). On the other hand, as far as the quasi-transverse wave is concerned, this model is still not sufficient to generate a well-defined slowness curve, because the eigenvalue associated with this wave tends to zero for $k_1 \to 0$ or $k_2 \to 0$. Consequently, the slowness vector (that is proportional to the inverse of the phase velocity) tends to infinity when $\underline{k}$ approaches to the axes, as illustrated in Figure 1.6. Note that the slowness curve and wavefront are depicted for every (k_1, k_2), with $k_1 \neq 0$, $k_2 \neq 0$, for the sake of clarity.
It is clear that, in order to obtain higher regularity on the quasi-transverse wave propagation, we need to include other terms to the constitutive law.

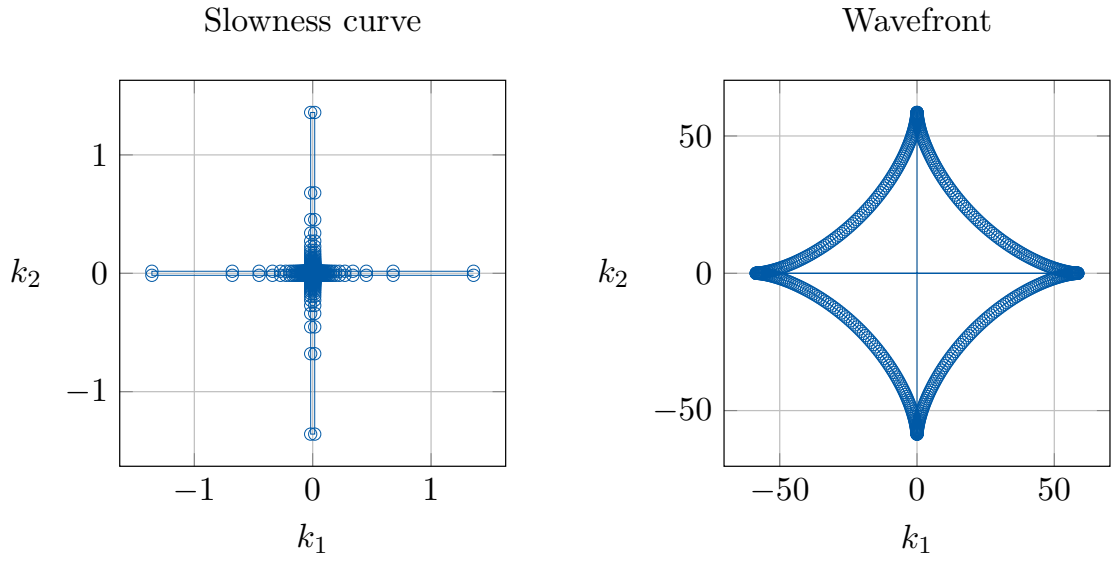

Figure 1.6 – Slowness curve (left) and wavefront (right) associated with the quasi-transverse wave in a transversely isotropic, nearly incompressible medium. $\kappa_3 = 170\,\text{Pa}$, $\kappa_4 = 2.5$, $\kappa = 10\,\text{MPa}$. View of the solution except for $k_1 = 0$, $k_2 = 0$.

1.4.3 A more complex constitutive law

A suitable constitutive law can be obtained by adding an isotropic term depending on the reduced invariant J_2 to the strain energy W^e, inspired by the classical Mooney-Rivlin constitutive law [Rivlin and Ericksen, 1997; Chapelle et al., 2012]:

$$W^{ISO} = \chi_2(J_2 - 3).$$

This choice is justified by stability and coercivity requirements [Ciarlet and Geymonat, 1982; Rivlin and Ericksen, 1997]. The first derivative of W^{ISO} with respect to the invariant J_2 is simply χ_2. In addition, the first derivative of the invariant J_2 with respect to $\underline{\underline{C}}$ reads

$$\begin{aligned}
\frac{\partial J_2}{\partial \underline{\underline{C}}} &= I_3^{-\frac{2}{3}} I_1\, \underline{\underline{\mathbb{1}}} - I_3^{-\frac{2}{3}} \underline{\underline{C}} - \frac{2}{3} I_3^{-\frac{2}{3}} I_2\, \underline{\underline{C}}^{-1} \\
&= I_{3,0}^{-\frac{2}{3}} I_{1,0}\, \underline{\underline{\mathbb{1}}} - I_{3,0}^{-\frac{2}{3}} \underline{\underline{C}}_0 - \frac{2}{3} I_{3,0}^{-\frac{2}{3}} I_{2,0}\, \underline{\underline{C}}_0^{-1} + \delta(I_{3,0}^{-\frac{2}{3}} \tilde{I}_1\, \underline{\underline{\mathbb{1}}} + \tilde{I}_3^{-\frac{2}{3}} I_{1,0}\, \underline{\underline{\mathbb{1}}}) \\
&\quad - \delta\left(\tilde{I}_3^{-\frac{2}{3}}\, \underline{\underline{C}}_0 + I_{3,0}^{-\frac{2}{3}}\, \underline{\underline{\tilde{C}}}\right) - \frac{2}{3}\,\delta\Big(I_{3,0}^{-\frac{2}{3}} I_{2,0}\, \underline{\underline{\tilde{G}}} + I_{3,0}^{-\frac{2}{3}} \tilde{I}_2\, \underline{\underline{C}}_0^{-1} + \tilde{I}_3^{-\frac{2}{3}} I_{2,0}\, \underline{\underline{C}}_0^{-1}\Big) + O(\delta^2).
\end{aligned}$$

Under the assumption $\underline{y}_0 = 0$, we obtain

$$\begin{aligned}
\frac{\partial J_2}{\partial \underline{\underline{C}}} &= -2\,\delta\ \mathrm{tr}\big(\underline{\underline{\varepsilon}}(\tilde{\underline{y}})\big)\, \underline{\underline{\mathbb{1}}} + \frac{4}{3}\delta\ \mathrm{tr}\big(\underline{\underline{\varepsilon}}(\tilde{\underline{y}})\big)\, \underline{\underline{\mathbb{1}}} - 2\,\delta \underline{\underline{\varepsilon}}(\tilde{\underline{y}}) + 4\,\delta\, \underline{\underline{\varepsilon}}(\tilde{\underline{y}}) + O(\delta^2) \\
&= 2\,\delta\, \underline{\underline{\varepsilon}}(\tilde{\underline{y}}) - \delta \frac{2}{3}\,\mathrm{tr}\big(\underline{\underline{\varepsilon}}(\tilde{\underline{y}})\big)\, \underline{\underline{\mathbb{1}}} + O(\delta^2).
\end{aligned}$$

The decomposition of the stress tensor is then

$$\begin{aligned}
\underline{\underline{\Sigma}}^{ISO} &= 2\,\frac{\partial W^{ISO}}{\partial J_2} \cdot \frac{\partial J_2}{\partial \underline{\underline{C}}} = 4\,\delta\,\chi_2\Big(\underline{\underline{\varepsilon}}(\tilde{\underline{y}}) - \frac{1}{3}\,\mathrm{tr}\big(\underline{\underline{\varepsilon}}(\tilde{\underline{y}})\big)\underline{\underline{\mathbb{1}}}\Big) + O(\delta^2) \\
&= 4\,\delta\,\chi_2\, \underline{\underline{\varepsilon}}(\tilde{\underline{y}}) - \frac{4}{3}\delta\,\chi_2\ \mathrm{tr}\big(\underline{\underline{\varepsilon}}(\tilde{\underline{y}})\big)\underline{\underline{\mathbb{1}}} + O(\delta^2).
\end{aligned} \tag{1.49}$$

In what follows, we will use $\chi := 4\,\chi_2$. As usual, under the assumption $\underline{y}_0 = 0$, we can approximate the stress tensor $\underline{\underline{\sigma}}^{ISO}$ as

$$\underline{\underline{\sigma}}^{ISO} = \underline{\underline{\Sigma}}^{ISO} + O(\delta).$$

Christoffel tensor in prestress-free configuration. We define $\underline{\underline{\tilde{\sigma}}}^{ISO} = \delta^{-1}\underline{\underline{\sigma}}^{ISO}$. We define the fourth-order tensor $\underline{\underline{\mathbf{C}}}^{ISO}$ such that $\underline{\underline{\tilde{\sigma}}}^{ISO} = \underline{\underline{\mathbf{C}}}^{ISO}\,\underline{\underline{e}}_0(\underline{\tilde{y}})$, given by

$$C^{ISO}_{ij\ell m} = \frac{1}{2}\chi\big(\delta_{i\ell}\delta_{jm} + \delta_{im}\delta_{jl}\big) - \frac{1}{3}\chi\delta_{ij}\delta_{\ell m} \quad i,j,\ell,m \in \{1,2\}. \tag{1.50}$$

Therefore, the tensor $\underline{\underline{\mathbf{C}}}^{ISO}$ reads:

$$\underline{\underline{\mathbf{C}}}^{ISO} = \frac{1}{2}\chi\begin{bmatrix}2&0&0&1\\0&0&1&0\\0&1&0&0\\1&0&0&2\end{bmatrix} - \frac{1}{3}\chi\begin{bmatrix}1&0&0&0\\0&1&0&0\\0&0&1&0\\0&0&0&1\end{bmatrix} = \chi\begin{bmatrix}\frac{2}{3}&0&0&\frac{1}{2}\\0&-\frac{1}{3}&\frac{1}{2}&0\\0&\frac{1}{2}&-\frac{1}{3}&0\\\frac{1}{2}&0&0&\frac{2}{3}\end{bmatrix}.$$

As a consequence, using Eqs. (1.38), (1.39) and (1.50), we can derive the expression of $\underline{\underline{\tilde{\Gamma}}}^{ISO}$ as

$$\underline{\underline{\tilde{\Gamma}}}^{ISO}(\underline{k}) = \chi\begin{bmatrix}\frac{2}{3}k_1^2 + \frac{1}{2}k_2^2 & \frac{1}{6}k_1\,k_2\\ \frac{1}{6}k_1\,k_2 & \frac{1}{2}k_1^2 + \frac{2}{3}k_2^2\end{bmatrix}.$$

The full stress tensor reads

$$\begin{aligned}\underline{\underline{\Sigma}}^{e} &= \underline{\underline{\Sigma}}^{\mathrm{TI}} + \underline{\underline{\Sigma}}^{\mathrm{NI}} + \underline{\underline{\Sigma}}^{ISO} = \delta\Big(\underline{\underline{\tilde{\Sigma}}}^{\mathrm{TI}} + \underline{\underline{\tilde{\Sigma}}}^{\mathrm{NI}} + \underline{\underline{\tilde{\Sigma}}}^{ISO}\Big) + O(\delta^2)\\ &= \delta c\Big(\underline{\underline{\Sigma}}^{\mathrm{TI}}_4 - \frac{1}{3}\underline{\underline{\Sigma}}^{\mathrm{TI}}_2 - \frac{1}{3}\underline{\underline{\Sigma}}^{\mathrm{TI}}_3 + \frac{1}{9}\underline{\underline{\Sigma}}^{\mathrm{TI}}_4\Big) + \delta\,\kappa\,\mathrm{tr}\big(\underline{\underline{\varepsilon}}(\underline{\tilde{y}})\big)\underline{\underline{\mathbb{1}}}\\ &\quad + \delta\,\chi\,\underline{\underline{\varepsilon}}(\underline{\tilde{y}}) - \frac{1}{3}\delta\,\chi\,\mathrm{tr}\big(\underline{\underline{\varepsilon}}(\underline{\tilde{y}})\big)\underline{\underline{\mathbb{1}}} + O(\delta^2),\end{aligned} \tag{1.51}$$

with $\underline{\underline{\Sigma}}^{\mathrm{TI}}_i$, for $i \in \{1,2,3,4\}$, defined in Eq. (1.36).
The dispersion relation for this model, with the standard assumption $\underline{\tau_1} = \underline{e}_1$, is

$$\begin{aligned}0 &= \det\Big(\underline{\underline{\tilde{\Gamma}}}(\underline{k}) - \gamma\underline{\underline{\mathbb{1}}}\Big)\\ &= \det\left(\begin{bmatrix}\Big(\frac{4}{9}c + \kappa + \frac{2}{3}\chi\Big)k_1^2 + \frac{1}{2}\chi k_2^2 - \gamma & \Big(-\frac{2}{9}c + \kappa + \frac{1}{6}\chi\Big)k_1\,k_2\\ \Big(-\frac{2}{9}c + \kappa + \frac{1}{6}\chi\Big)k_1\,k_2 & +\frac{1}{2}\chi k_1^2 + \Big(\frac{1}{9}c + \kappa + \frac{2}{3}\chi\Big)k_2^2 - \gamma\end{bmatrix}\right).\end{aligned}$$

Considering the usual assumption $\gamma = \rho\omega^2$, we compute

$$\gamma_{QP} = \frac{1}{2}\Big(\beta_* + \sqrt{\beta_*^2 - 4\alpha_*}\Big), \qquad \gamma_{QS} = \frac{1}{2}\Big(\beta_* - \sqrt{\beta_*^2 - 4\alpha_*}\Big),$$

with

$$\begin{aligned}\alpha_* &:= \frac{1}{2}\chi\,\zeta_1\,k_1^4 + \frac{1}{2}\chi\,\zeta_2\,k_2^4 + \zeta_3\,(k_1^2\,k_2^2),\\ \beta_* &:= \zeta_1\,k_1^2 + \frac{1}{2}\chi\,k_1^2 + \zeta_2\,k_2^2 + \frac{1}{2}\,\chi\,k_2^2,\end{aligned}$$

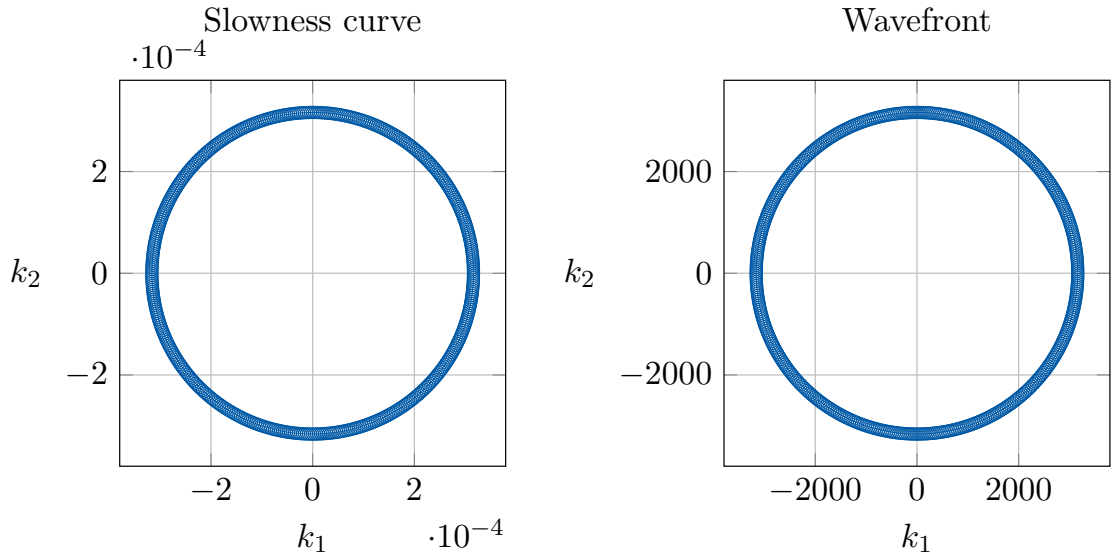

Figure 1.7 – Slowness curve (left) and wavefront (right) associated with the quasi-longitudinal wave in a transversely isotropic, nearly-incompressible medium. $\kappa_3 = 170\,\text{Pa}$, $\kappa_4 = 2.5$, $\kappa = 10\,\text{MPa}$, $\chi = 80\,\text{Pa}$.

and

$$\begin{aligned}\zeta_1 &:= \frac{4}{9}c + \kappa + \frac{2}{3}\chi,\\ \zeta_2 &:= \frac{1}{9}c + \kappa + \frac{2}{3}\chi,\\ \zeta_3 &:= c\,\kappa + \frac{4}{9}c\,\chi + \chi\,\kappa + \frac{2}{3}\chi^2.\end{aligned}$$

The sufficient condition to ensure that the determinant $\det\big(\underline{\underline{\Gamma}}(\underline{k})\big)$ is greater than zero is

$$\frac{1}{2}\chi\,\zeta_1\,k_1^4 + \frac{1}{2}\,\chi\,\zeta_2\,k_2^4 + \zeta_3\,k_1^2\,k_2^2 > 0. \tag{1.52}$$

Eq. (1.52) is always satisfied, except at the origin ($k_1 = k_2 = 0$). Thus, we can observe that the introduction of this term in the model adds regularity to our analysis. The value of the parameter χ is set equal to 80 Pa, in order to preserve physiological results (see Section 1.8.2 for further details on parameter calibration). In Figure 1.7 it is possible to observe that the profile of the slowness curve and wavefront corresponding to the quasi-longitudinal wave has similar features to wave propagation in isotropic media. On the contrary, Figure 1.8 depicts the slowness curves and the wavefronts associated with the quasi-longitudinal and transverse wave, reproducing the classical features of propagation in an anisotropic medium.

1.5 Active stress

In this section we take into account the contribution associated with active stress in the Christoffel tensor. From our analysis, we will be able to justify the need for a very simple expression for the active stress to retrieve information on the active contractility of the tissue.

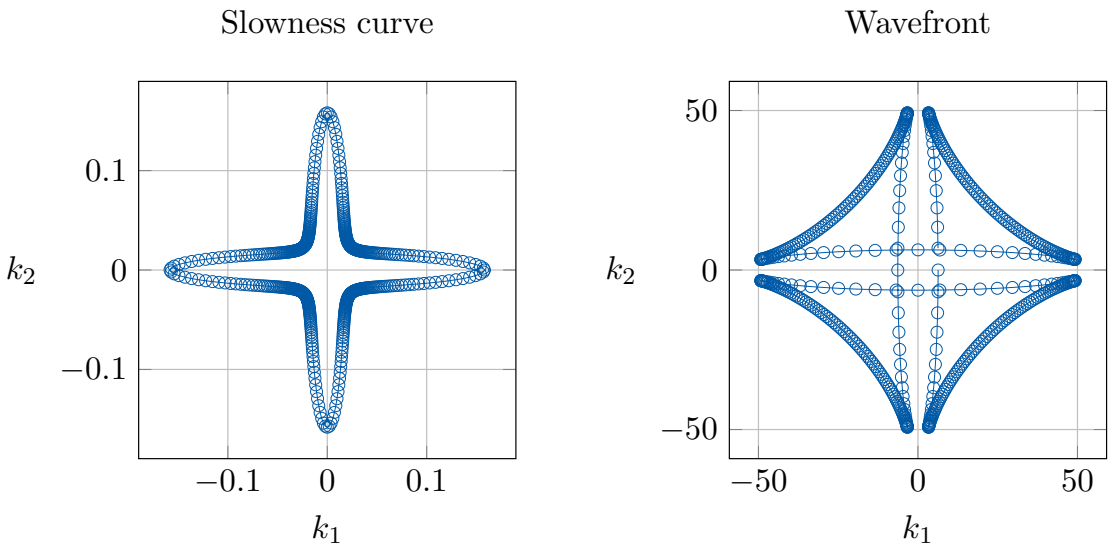

Figure 1.8 – Slowness curve (left) and wavefront (right) associated with the quasi-transverse wave in a transversely isotropic, nearly-incompressible medium. $\kappa_3 = 170\,\text{Pa}$, $\kappa_4 = 2.5$, $\kappa = 10\,\text{MPa}$, $\chi = 80\,\text{Pa}$.

First, taking into account the contribution of the active stress, we define the total stress tensor as

$$\underline{\underline{\Sigma}} = \underline{\underline{\Sigma}}^P + \underline{\underline{\Sigma}}^A,$$

where

$$\underline{\underline{\Sigma}}^P = \underline{\underline{\Sigma}}^e = \underline{\underline{\Sigma}}^{\text{TI}} + \underline{\underline{\Sigma}}^{ISO} + \underline{\underline{\Sigma}}^{\text{NI}} = \frac{\partial W^e}{\partial e}(J_1, J_2, J_4) + \kappa(J-1)\underline{\underline{C}}^{-1}, \tag{1.53}$$

$$\underline{\underline{\Sigma}}^A = \Sigma_{1d}\big(e_{1d}\big)\,\underline{\tau_1} \otimes \underline{\tau_1}, \tag{1.54}$$

and we have defined

$$e_{1d} = \underline{\underline{e}} : (\underline{\tau_1} \otimes \underline{\tau_1}) = \underline{\tau_1} \cdot \underline{\underline{e}} \cdot \underline{\tau_1}.$$

From Eqs. (1.22) and (1.54), the active stress gives the following contribution:

$$\int_{\Omega_0} \frac{\partial \Sigma_{1d}}{\partial e_{1d}} \big(d_{\underline{y}_0} e_{1d} \cdot \tilde{\underline{y}}\big)\big(d_{\underline{y}_0} e_{1d} \cdot \underline{w}\big)\ \mathrm{d}\Omega_0 + \int_{\Omega_0} \underline{\underline{\Sigma}}^A : \big(\underline{\underline{\nabla}}_{\underline{\xi}}\, \tilde{\underline{y}}^T \cdot \underline{\underline{\nabla}}_{\underline{\xi}}\, \underline{w}\big)\ \mathrm{d}\Omega_0. \tag{1.55}$$

We will analyse the two terms separately.

1.5.1 Stiffness associated with prestress

Let us first consider the term

$$\int_{\Omega_0} \underline{\underline{\Sigma}}^A : \big(\underline{\underline{\nabla}}_{\underline{\xi}}\, \tilde{\underline{y}}^T \cdot \underline{\underline{\nabla}}_{\underline{\xi}}\, \underline{w}\big)\ \mathrm{d}\Omega_0$$

in Eq. (1.55). We can rewrite this term in the deformed configuration, considering that

$$\begin{aligned}\underline{\underline{\Sigma}}^A : \big(\underline{\underline{\nabla}}_{\underline{\xi}}\, \tilde{\underline{y}}^T \cdot \underline{\underline{\nabla}}_{\underline{\xi}}\, \underline{w}\big)\,\mathrm{d}\Omega_0 &= J\underline{\underline{F}}^{-1} \cdot \underline{\underline{\sigma}}^A \cdot \underline{\underline{F}}^{-T} : \big(\underline{\underline{\nabla}}_{\underline{\xi}}\, \tilde{\underline{y}}^T \cdot \underline{\underline{\nabla}}_{\underline{\xi}}\, \underline{w}\big)\,\mathrm{d}\Omega_0 \\ &= J\underline{\underline{\sigma}}^A : \big(\underline{\underline{\nabla}}_{\underline{x}}\, \tilde{\underline{y}}^T \cdot \underline{\underline{\nabla}}_{\underline{x}}\, \underline{w}\big)\,\mathrm{d}\Omega_0 = \underline{\underline{\sigma}}^A : \big(\underline{\underline{\nabla}}_{\underline{x}}\, \tilde{\underline{y}}^T \cdot \underline{\underline{\nabla}}_{\underline{x}}\, \underline{w}\big)\,\mathrm{d}\Omega.\end{aligned}$$

Following Eq. (1.54), we can define

$$\underline{\underline{\sigma}}^A = J^{-1}\underline{\underline{F}}\cdot\left(\Sigma_{1d}\,\underline{\tau_1}\otimes\underline{\tau_1}\right)\cdot\underline{\underline{F}}^T = J^{-1}\Sigma_{1d}\left(\underline{\underline{F}}\cdot\underline{\tau_1}\right)\otimes\left(\underline{\underline{F}}\cdot\underline{\tau_1}\right) = \sigma_{1d}\,\underline{\tau_1}'\otimes\underline{\tau_1}',$$

with

$$\sigma_{1d} = J^{-1}\Sigma_{1d}\left\|\underline{\underline{F}}\cdot\underline{\tau_1}\right\|^2 \quad\text{and}\quad \underline{\tau_1}' = \frac{\underline{\underline{F}}\cdot\underline{\tau_1}}{\left\|\underline{\underline{F}}\cdot\underline{\tau_1}\right\|}.$$

Note that if $\underline{y}_0 = 0$, then $\underline{\underline{F}}$ can be approximated by the identity $\underline{\underline{\mathbb{1}}}$, and $\underline{\tau_1}' \equiv \underline{\tau_1}$.
Now, since $\underline{\underline{\mathbf{C}}}$ is symmetric, we obtain

$$C_{ij\ell m} = \delta_{i\ell}\,\sigma_{jm}, \quad \forall\, i,j,\ell,m = 1,2,..,\mathrm{d}.$$

Therefore, the Christoffel eigenvalue problem (1.31) becomes

$$\left(\sigma_{jm}k_jk_m - \rho\,\omega^2\right)d_\ell = 0 \quad \forall\ell = 1,2,..,\mathrm{d}.$$

By definition, the term $\sigma_{jm}\,k_jk_m$ reads

$$\sigma_{jm}\,k_jk_m = \sigma_{1d}\left(\underline{\tau_1}'\otimes\underline{\tau_1}'\right)_{jm}k_jk_m = \sigma_{1d}\,\tau'_{1j}\tau'_{1m}k_jk_m = \sigma_{1d}\left(\underline{\tau_1}'\cdot\underline{k}\right)^2 = \sigma_{1d}\,k_1^2,$$

with $k_1 \coloneqq \underline{\tau_1}'\cdot\underline{k}$. Thus, we get

$$\left(\sigma_{1d}\,k_1^2 - \rho\,\omega^2\right)d_\ell = 0 \quad \forall\ell = 1,2,..,\mathrm{d}. \tag{1.56}$$

This implies that for every polarisation $\underline{d}$, the wave associated with the eigenvector $\underline{d}$ has phase velocity

$$\boxed{V = \frac{\omega}{|\underline{k}|} = \frac{k_1}{|\underline{k}|}\sqrt{\frac{\sigma_{1d}}{\rho}}.} \tag{1.57}$$

From Eq. (1.57) we can observe that the phase velocity V gives a direct measure of the active contractility of the tissue. In fact, during the systolic phase, the active contribution strikingly prevails on the passive term. Consequently, in this phase the active contribution is the only responsible for the heart contraction, and we can approximate $\underline{\underline{\Sigma}} = \underline{\underline{\Sigma}}^A$. Hence, from the properties of the elastic wave propagation it is possible to have a direct insight on the active behaviour of the myocardium.
The expression of the Christoffel tensor can be directly retrieved from Eq. (1.56), and it reads

$$\underline{\underline{\tilde{\Gamma}}}^A(\underline{k}) = \sigma_{1d}\,k_1^2\begin{bmatrix}1 & 0\\ 0 & 1\end{bmatrix}. \tag{1.58}$$

1.5.2 Stiffness associated with material nonlinearity

Now, let us analyse the contribution

$$\int_{\Omega_0}\frac{\partial\Sigma_{1d}}{\partial e_{1d}}\left(d_{\underline{y}_0}e_{1d}\cdot\underline{\tilde{y}}\right)\left(d_{\underline{y}_0}e_{1d}\cdot\underline{w}\right)\,\mathrm{d}\Omega_0$$

in Eq. (1.55). First, we note that

$$\begin{aligned} d_{\underline{y}}e_{1d}\cdot\underline{w} &= \left(d_{\underline{y}}\underline{\underline{e}}\cdot\underline{w}\right):\left(\underline{\tau_1}\otimes\underline{\tau_1}\right) = \left(\underline{\underline{F}}^T\cdot\underline{\underline{\nabla}}_{\underline{\xi}}\underline{w}\right):\left(\underline{\tau_1}\otimes\underline{\tau_1}\right) = \left(\underline{\underline{F}}^T\cdot\underline{\underline{\nabla}}_{\underline{\xi}}\underline{w}\cdot\underline{\underline{F}}^{-1}\cdot\underline{\underline{F}}\right):\left(\underline{\tau_1}\otimes\underline{\tau_1}\right)\\ &= \left(\underline{\underline{\nabla}}_{\underline{x}}\underline{w}\right):\left(\underline{\underline{F}}\cdot\underline{\tau_1}\otimes\underline{\underline{F}}\cdot\underline{\tau_1}\right) = \left\|\underline{\underline{F}}\cdot\underline{\tau_1}\right\|^2\left(\underline{\underline{\nabla}}_{\underline{x}}\underline{w}\right):\left(\underline{\tau_1}'\otimes\underline{\tau_1}'\right)\\ &= \left\|\underline{\underline{F}}\cdot\underline{\tau_1}\right\|^2\underline{\tau_1}'\cdot\underline{\underline{\nabla}}_{\underline{x}}\underline{w}\cdot\underline{\tau_1}' \coloneqq \left\|\underline{\underline{F}}\cdot\underline{\tau_1}\right\|^2\varepsilon_{11}(\underline{w}). \end{aligned}$$

Therefore, the term accounting for the material stiffness becomes

$$\frac{\partial \Sigma_{1d}}{\partial e_{1d}} \left(d_{\underline{y}_H} e_{1d} \cdot \underline{\tilde{y}}\right) \left(d_{\underline{y}_H} e_{1d} \cdot \underline{w}\right) = \frac{\partial \Sigma_{1d}}{\partial e_{1d}} \left\| \underline{\underline{F}} \cdot \underline{\tau_1} \right\|^4 \varepsilon_{11}\left(\underline{\tilde{y}}\right) \varepsilon_{11}\left(\underline{w}\right).$$

From Eq. (1.28) we get

$$\int_\Omega C_{ij\ell m}\, \varepsilon_{\ell m}\left(\underline{\tilde{y}}\right) \varepsilon_{ij}\left(\underline{w}\right)\, \mathrm{d}\Omega = \int_\Omega J^{-1} \frac{\partial \Sigma_{1d}}{\partial e_{1d}} \left\| \underline{\underline{F}} \cdot \underline{\tau_1} \right\|^4 \varepsilon_{11}\left(\underline{\tilde{y}}\right) \varepsilon_{11}\left(\underline{w}\right) \mathrm{d}\Omega$$

$$\iff \begin{cases} C_{1111} = J^{-1} \frac{\partial \Sigma_{1d}}{\partial e_{1d}} \left\| \underline{\underline{F}} \cdot \underline{\tau_1} \right\|^4, \\ C_{ij\ell m} = 0 \qquad i,j,\ell,m \in [2,3,..,\mathrm{d}]. \end{cases}$$

The Christoffel eigenvalue problem reads

$$\begin{cases} \left(C_{1111} k_1^2 - \rho\, \omega^2\right) d_1 = 0, \\ \left(0 - \rho\, \omega^2\right) d_\ell = 0 \qquad \forall \ell = 2,3,..,\mathrm{d}. \end{cases} \tag{1.59}$$

We recall that the muscle fibres are arranged in parallel laminar structures, denoted sheets, oriented transversely to the heart wall, and that their orientation varies throughout the wall thickness. In transient elastography imaging of the myocardium, the ultrasound probe is positioned orthogonally to the heart wall, in order to investigate the directions of propagation that lie in the sheets. Thus, from Eq. (1.59) we can assert that, given a propagation direction $\underline{k}$ in the sheet, only if the polarisation of the wave is along the fibre direction $\underline{\tau_1}'$, then the phase velocity is non-zero, and it reads

$$V = \frac{\omega}{|\underline{k}|} = \frac{k_1}{|\underline{k}|} \sqrt{\frac{C_{1111}}{\rho}}.$$

Consequently, in elastographic applications in cardiac setting, where shear wave propagation is analysed (transverse polarisation), the contribution given by the material stiffness is negligible, and a simple model for the active stress can be considered, such as

$$\underline{\underline{\Sigma}}^A = \Sigma_{1d}\, \underline{\tau_1} \otimes \underline{\tau_1},$$

with Σ_{1d} constant, i.e. independent from $\underline{\underline{e}}_{1d}$, since the only contribution to the shear wave is represented by the active prestress.
Furthermore, we have shown that the wavespeed associated with the shear wave gives a measure of the contractility of the tissue.

1.5.3 Christoffel tensor

The complete dispersion relation, taking into account isotropic term, transversely isotropic term, nearly-incompressibility and active stress, reads

$$\begin{aligned} 0 &= \det\left(\underline{\underline{\tilde{\Gamma}}}(\underline{k}) - \gamma \underline{\underline{\mathbb{1}}}\right) \\ &= \det\left(\begin{bmatrix} \left(\zeta_1 + \sigma_{1d}\right) k_1^2 + \frac{1}{2}\chi k_2^2 - \gamma & \left(-\frac{2}{9}c + \kappa + \frac{1}{6}\chi\right) k_1\, k_2 \\ \left(-\frac{2}{9}c + \kappa + \frac{1}{6}\chi\right) k_1\, k_2 & +\left(\frac{1}{2}\chi + \sigma_{1d}\right) k_1^2 + \zeta_2\, k_2^2 - \gamma \end{bmatrix}\right). \end{aligned} \tag{1.60}$$

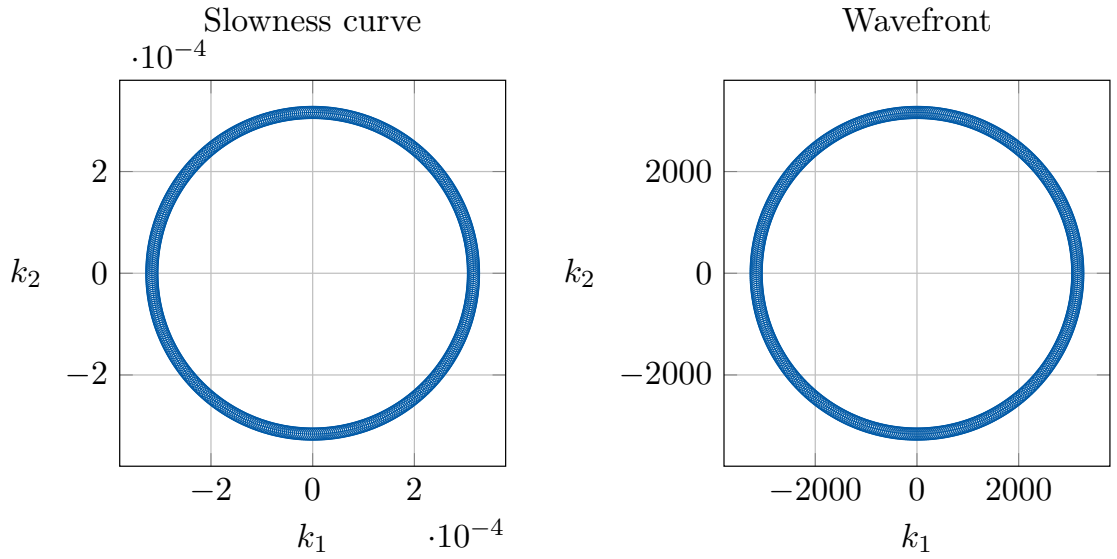

Figure 1.9 – Slowness curve (left) and wavefront (right) associated with the quasi-longitudinal wave in a transversely isotropic, nearly-incompressible medium, including active stress. $\kappa_3 = 170\,\text{Pa}$, $\kappa_4 = 2.5$, $\kappa = 10\,\text{MPa}$, $\chi = 80\,\text{Pa}$, $\Sigma_{1d} = 10\,\text{Pa}$.

The two solutions of Eq. (1.60) are

$$\gamma_{QP} = \frac{1}{2}\Big(\beta_* + \sqrt{\beta_*^2 - 4\alpha_*}\Big), \qquad \gamma_{QS} = \frac{1}{2}\Big(\beta_* - \sqrt{\beta_*^2 - 4\alpha_*}\Big),$$

with

$$\alpha_* = \Big(\frac{1}{2}\chi + \sigma_{1d}\Big)(\zeta_1 + \sigma_{1d})k_1^4 + \frac{1}{2}\chi\,\zeta_2 k_2^4 + k_1^2\,k_2^2\Big(\zeta_3 + \sigma_{1d}\,\zeta_2 + \frac{1}{2}\sigma_{1d}\chi\Big),$$
$$\beta_* = (\zeta_1 + \sigma_{1d})k_1^2 + \Big(\frac{1}{2}\chi + \sigma_{1d}\Big)k_1^2 + \zeta_2\,k_2^2 + \frac{1}{2}\chi\,k_2^2,$$

with the usual definition for ζ_1, ζ_2 and ζ_3.
As an illustration, we investigate the elastic wave propagation in a transversely isotropic, nearly-incompressible medium under active stress, with $\underline{\tau_1} = \underline{e}_1$, $\kappa_3 = 170\,\text{Pa}$, $\kappa_4 = 2.5$, $\chi = 80\,\text{Pa}$, $\kappa = 10\,\text{MPa}$ and Σ_{1d} ranging in $[10, 1e5]$ Pa. The propagation of the quasi-longitudinal wave is very slightly affected by the contribution of the active stress, as shown in Figures 1.9 and 1.10. On the contrary, Figures 1.11, 1.12 and 1.13 show that the increasing contribution of the active term implies a faster propagation of the quasi-transverse wave in the direction $\underline{k} = \underline{\tau_1} \equiv \underline{e}_1$, as expected. For the sake of clarity, we also depict in Figure 1.14 the results associated with $\Sigma_{1d} = 1e5\,\text{Pa}$ on a different axis scaling.

1.6 Some numerical applications

We recall that the problem of elastic wave propagation consists is solving

$$\forall \underline{w} \in \mathcal{X}, \quad \int_{\Omega_0} \rho_0\, \ddot{\underline{y}} \cdot \underline{w}\, \mathrm{d}\Omega_0 + \int_{\Omega_0} \underline{\underline{\nabla}}_{\underline{\xi}} \tilde{\underline{y}} : \underline{\underline{\mathbf{C}}}^{\text{Lag}} : \underline{\underline{\nabla}}_{\underline{\xi}} \underline{w}\, \mathrm{d}\Omega_0 = 0.$$

where $\underline{\underline{\mathbf{C}}}^{\text{Lag}}$ represents the tangent constitutive relation defined in the Lagrangian framework. From a practical point of view, in a finite element code this tensor is usually

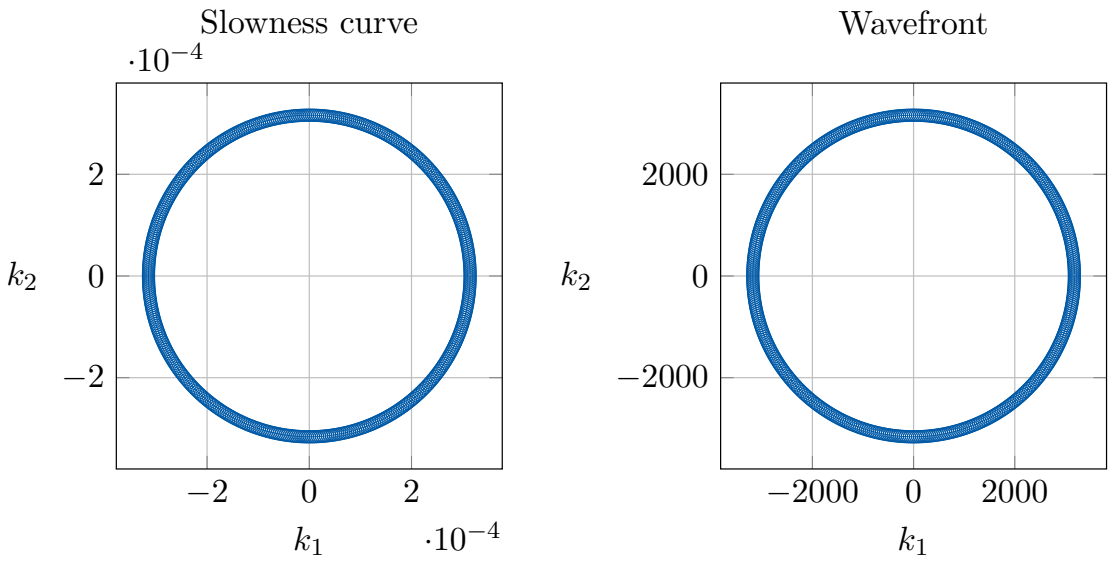

Figure 1.10 – Slowness curve (left) and wavefront (right) associated with the quasi-longitudinal wave in a transversely isotropic, nearly-incompressible medium, including active stress. $\kappa_3 = 170\,\mathrm{Pa}$, $\kappa_4 = 2.5$, $\kappa = 10\,\mathrm{MPa}$, $\chi = 80\,\mathrm{Pa}$, $\Sigma_{1d} = 1e5\,\mathrm{Pa}$.

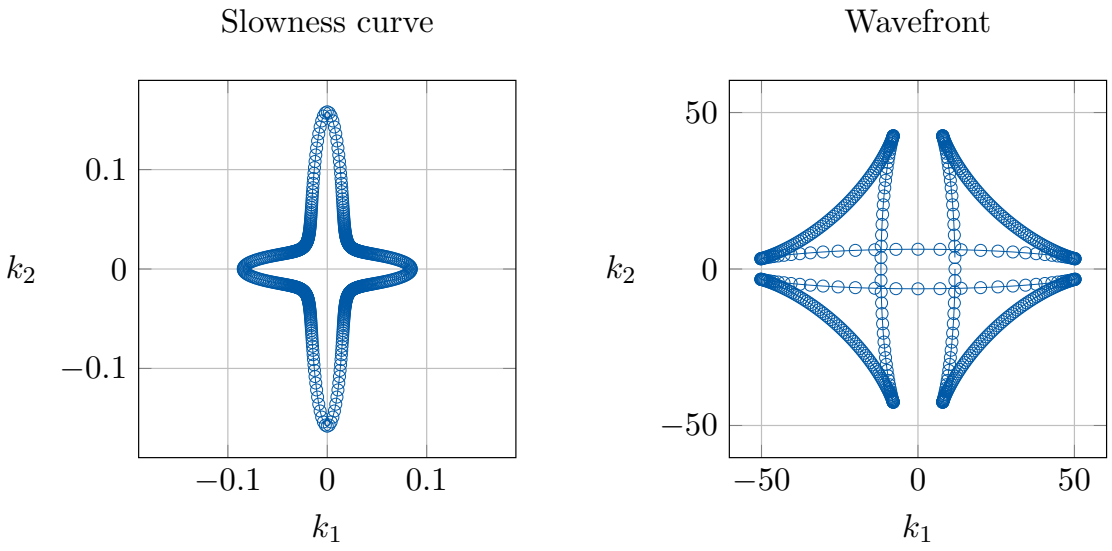

Figure 1.11 – Slowness curve (left) and wavefront (right) associated with the quasi-transverse wave in a transversely isotropic, nearly-incompressible medium. $\kappa_3 = 170\,\mathrm{Pa}$, $\kappa_4 = 2.5$, $\kappa = 10\,\mathrm{MPa}$, $\chi = 80\,\mathrm{Pa}$, $\Sigma_{1d} = 10\,\mathrm{Pa}$.

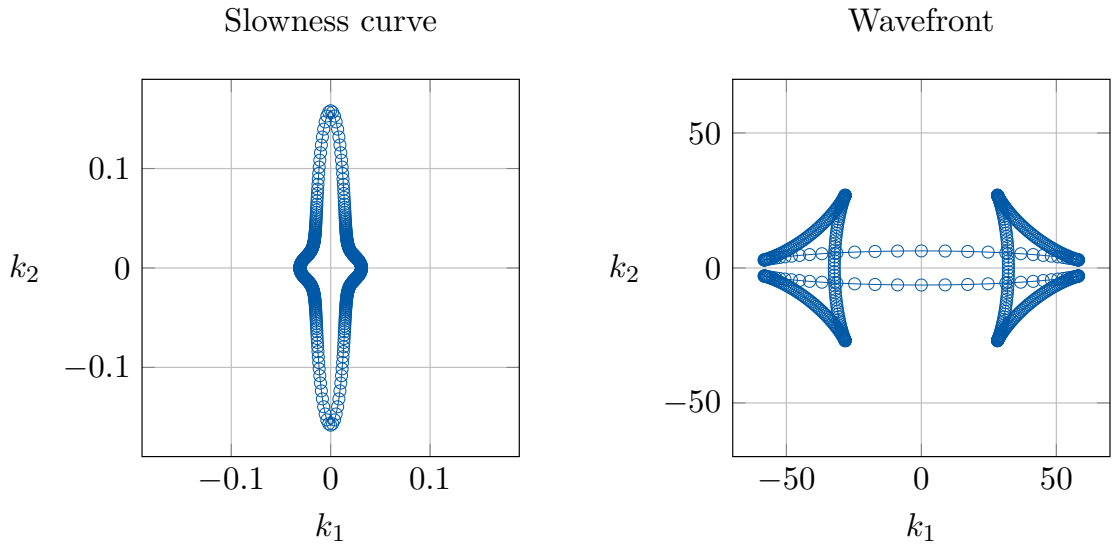

Figure 1.12 – Slowness curve (left) and wavefront (right) associated with the quasi-transverse wave in a transversely isotropic, nearly-incompressible medium. $\kappa_3 = 170\,\mathrm{Pa}$, $\kappa_4 = 2.5$, $\kappa = 10\,\mathrm{MPa}$, $\chi = 80\,\mathrm{Pa}$, $\Sigma_{1d} = 1e3\,\mathrm{Pa}$.

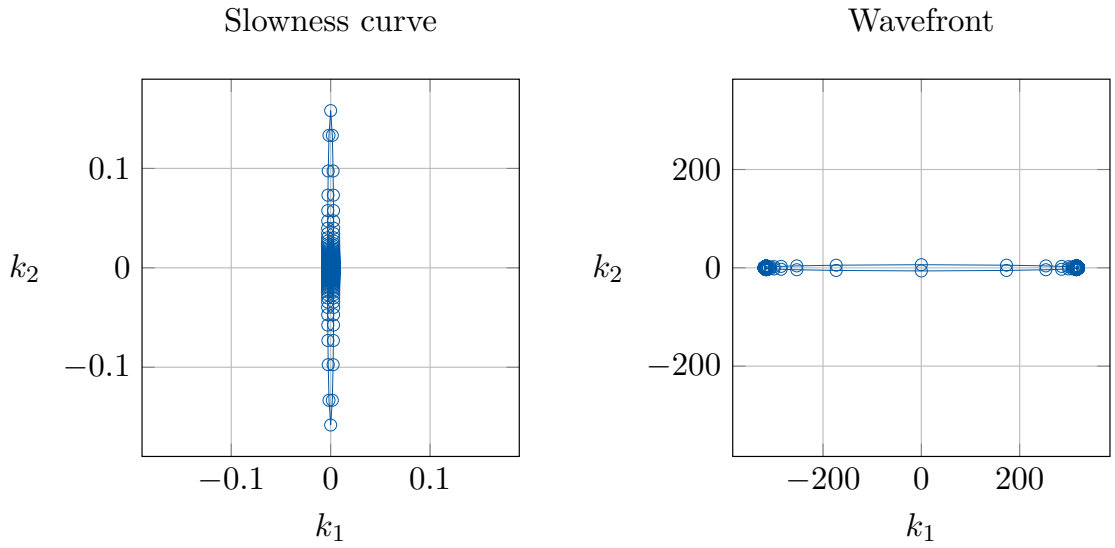

Figure 1.13 – Slowness curve (left) and wavefront (right) associated with the quasi-transverse wave in a transversely isotropic, nearly-incompressible medium. $\kappa_3 = 170\,\mathrm{Pa}$, $\kappa_4 = 2.5$, $\kappa = 10\,\mathrm{MPa}$, $\chi = 80\,\mathrm{Pa}$, $\Sigma_{1d} = 1e5\,\mathrm{Pa}$. Equal scaling on x and y axis.

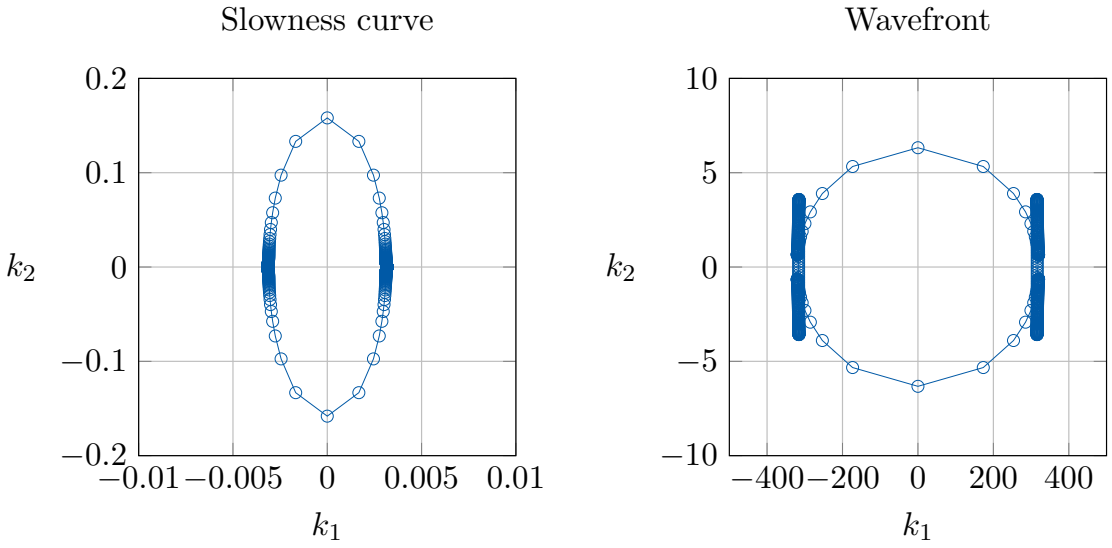

Figure 1.14 – Slowness curve (left) and wavefront (right) associated with the quasi-transverse wave in a transversely isotropic, nearly-incompressible medium. $\kappa_3 = 170\,\text{Pa}$, $\kappa_4 = 2.5$, $\kappa = 10\,\text{MPa}$, $\chi = 80\,\text{Pa}$, $\Sigma_{1d} = 1e5\,\text{Pa}$. Different scaling on x and y axis.

computed as part of the Newton algorithm when solving the nonlinear problem associated with the solution $\underline{y}$ of Eq. (1.7). Nevertheless we recall that, since elastographic waves are measured in the actual (deformed) object, the problem needs to be analysed in the deformed configuration $\Omega(t)$, i.e.

$$\forall \underline{w} \in \mathcal{X}, \quad \int_\Omega \rho\, \ddot{\underline{y}} \cdot \underline{w}\, \mathrm{d}\Omega + \int_\Omega J^{-1} \left(\underline{\underline{\nabla}}_{\underline{x}} \tilde{\underline{y}} \cdot \underline{\underline{F}}\right) : \underline{\underline{\mathbf{C}}}^{\text{Lag}} : \left(\underline{\underline{\nabla}}_{\underline{x}} \underline{w} \cdot \underline{\underline{F}}\right) \mathrm{d}\Omega = 0.$$

where $\underline{\underline{\mathbf{C}}}^{\text{Eul}}$ corresponds to the tangent constitutive relation in the Eulerian frame, and it is given by

$$\underline{\underline{\mathbf{C}}}^{\text{Eul}} = J^{-1}\, \underline{\underline{F}} \cdot \underline{\underline{\mathbf{C}}}^{\text{Lag}} \cdot \underline{\underline{F}}^T.$$

The tensor $\underline{\underline{\mathbf{C}}}^{\text{Eul}}$ can be computed as a by-product of the dynamical equation solution, once the Newton algorithm has converged at each time step, for each quadrature point. From this tensor, the Christoffel tensor can be derived to calculate the velocity of shear wave propagation in the medium, as it is experimentally measured in transient elastography.
In this chapter we have outlined a methodological and numerical approach to characterise elastographic shear waves in a general mechanical model. To do so, we have extended the standard derivation of the Christoffel tensor for a general constitutive law, dispensing with the usual "small strain" assumption. Additionally, we have derived the expression of the Christoffel tensor for a complex nonlinear constitutive law for the heart mechanics. Henceforth, we will show some detailed results obtained when applying this approach with the heart model proposed in Chapelle et al. [2012] and compare the computed wave velocities with published experimental measurements.

1.6.1 Detection of fibre orientation

The first application consists in the assessment of the fibre orientation in the myocardium from the analysis of shear wave propagation in the medium. This example is inspired by an experiment proposed by Lee et al. [2012]. The aim of the paper was to validate the

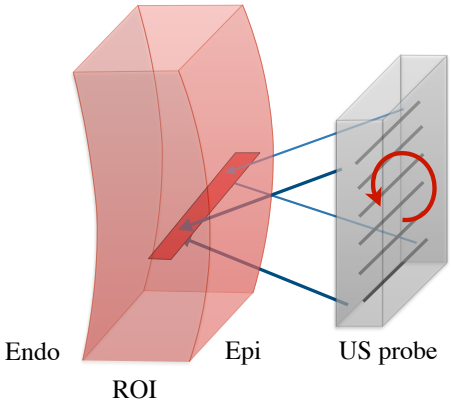

Figure 1.15 – Experimental framework: Counterclockwise rotation of the ultrasound probe from $-90°$ to $+90°$ with respect to circumferential axis.

the feasibility of Shear Wave Imaging (SWI) for real-time assessment of transmural fibre orientation of the myocardium in vivo. The estimation of fibre arrangement in the myocardial tissue is of great clinical interest. In fact, the transmural variation in fibre orientation is directly related to myocardial deformation and electrical activation [Costa et al., 1999; Hooks et al., 2007]. Furthermore, fibrosis and myocardial fibre disruption usually characterise hypertrophic cardiomyopathy and post-infarction remodelling. As a consequence, the non-invasive assessment of fibre organisation would benefit to the understanding of cardiac function in physiological and pathological states.

Experimental framework. In Lee et al. [2012] the authors performed one-dimensional SWI [Couade et al., 2011; Pernot et al., 2011] on five in vitro porcine hearts and three in vivo ovine hearts. In more detail, in order to acquire the SWI data, an ultrasound probe was firstly aligned with the longitudinal axis of the region of interest (ROI) located in the anterior wall at the middle left-ventricular level, and then rotated from $-90°$ to $+90°$, as shown in Figure 1.15. In the in vivo acquisitions, the images were acquired at the same phase of the cardiac cycle, namely at midsystolic phase (the synchronisation was ensured by electrocardiogram gating). At each depth of interest z, the shear wave group velocity v was estimated by standard speckle tracking methods as a function of myocardial depth z and probe angle θ at the centre of the region of interest. In this way, a measure of shear wave velocity was collected and mapped at each depth of the myocardial wall and each probe angle. Then, since maximum shear wave speed corresponds to a propagation longitudinal to the fibre orientation, at each depth the maximum velocity over the fibre angle was estimated, i.e.

$$\tilde{\theta}(z) = \underset{\theta\in[-90°,90°]}{\arg\max}\ v(z,\theta).$$

At each depth, the angle $\tilde{\theta}(z)$ was identified as fibre angle. The authors found a counterclockwise transmural change of fibre orientation from the sub-epicardial region to the sub-endocardial region which was consistent with the literature. Furthermore, SWE estimations of porcine in vitro models were also validated against histologic measurements. The midsystolic phase was selected for two main reasons:

- The highest wave speed is registered in this phase, due to the active contribution, increasing the signal-to-noise ratio;

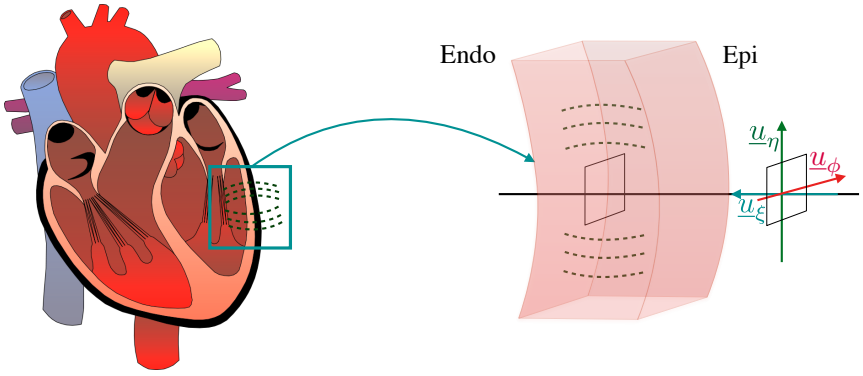

Figure 1.16 – In silico framework: region of interest selected at the middle left-ventricular level and definition of a local basis.

- In this phase it is possible to infer information on the active properties of the myocardium, whose alteration is associated with several major myocardial pathologies, e.g. ischemia induced by stenosis of the coronary arteries.

We refer the reader to Lee et al. [2012] for further details on the experimental framework.

Modelling of shear wave propagation and extraction of fibre arrangement. In order to reproduce in silico the experiment performed in Lee et al. [2012], we developed a numerical framework in the context of our in-house code for the resolution of the nonlinear, three-dimensional problem of heart mechanics. The algorithm consists of the following steps:

- A region of interest at the middle left-ventricular level is considered;
- A virtual line connecting the endocardium to the epicardium is traced, and a local basis $(\underline{u}_\xi, \underline{u}_\phi, \underline{u}_\eta)$ is defined, as depicted in Figure 1.16;
- At every discrete time step and for each location crossed by this line, the tensor $\underline{\underline{\mathbf{C}}}^{\mathrm{Eul}}(\underline{x}, t)$ is computed;
- Multiple directions $\underline{k}_\theta$, for all $\theta \in [-90°, +90°]$ in the plane $(\underline{u}_\phi, \underline{u}_\eta)$ are considered (see Figure 1.17), and for each of them we compute the Christoffel tensor

$$\Gamma_{i\ell}(\underline{x}, t, \underline{k}_\theta) = \sum_{j,m=1}^{3} C^{\mathrm{Eul}}_{ij\ell m}(\underline{x}, t)\, k_{\theta,j}\, k_{\theta,m};$$

- Then, the eigenvalues λ_j and eigenvectors $\underline{u}_j$ of the Christoffel tensor are obtained along with the corresponding wavespeed, that is given by

$$V_j = \sqrt{\frac{\lambda_j}{\rho}}.$$

- Consequently, in order to retrieve the quasi-shear wave propagating in the medium, we need to track the wave with polarisation orthogonal to the direction of propagation, that lies in the plane $(\underline{u}_\phi, \underline{u}_\eta)$ by hypothesis. Hence, we need to find the eigenvector almost collinear to $\underline{u}_\xi$.

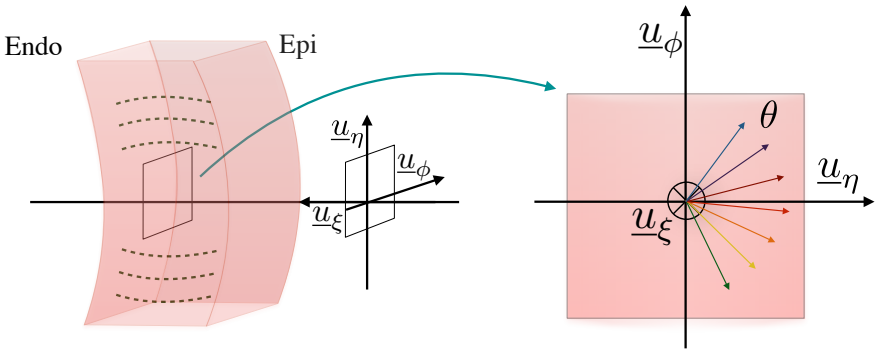

Figure 1.17 – In silico framework: evaluation of different directions of propagation ranging in $[-90°, +90°]$ in the plane $(\underline{u}_\phi, \underline{u}_\eta)$.

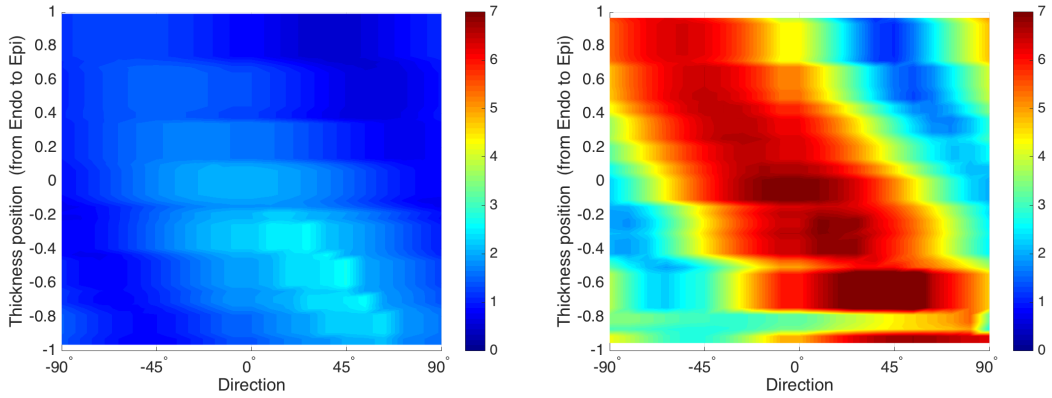

Figure 1.18 – Two-dimensional plots of shear wave velocity as a function of probe angle and depth in the medium, from sub-epicardial to sub-endocardial. Left: diastolic phase. Right: isovolumic contraction phase . Velocity is depicted in $\mathrm{m\,s^{-1}}$.

- Once the eigenvector is identified, we collect the corresponding shear wavespeed.

With this procedure we obtain a map of shear wave velocity at each discrete time step, at every probe angle and depth in the region of interest. We recall that the fibre orientation corresponds to the angle where the velocity is the highest. In Figure 1.18 we show the two-dimensional maps obtained at two time steps, corresponding to diastole and isovolumic contraction (during systole). We can observe that, from the simulation, the arrangement of the fibres could already be deduced during the diastolic phase, even though the only contribution is given by the passive stress and, consequently, the velocity ranges in $[0, 3]\mathrm{m\,s^{-1}}$. In an experimental framework this is not suitable yet, since the signal is too weak to provide an accurate measure of shear wave and allow a correct extraction of fibre direction. During systole the velocity of the shear wave is significantly increased, since the largest contribution to the signal is given by the active stiffness, i.e. the myocardial contractility (as we have shown theoretically in Section 1.5). In practice, this enables a more accurate extraction of the transmural fibre orientation. In our in silico framework, the algorithm correctly predicted a fibre variation from $-60°$ to $+60°$ with respect to the circumferential axis, as it was prescribed in the definition of the computational domain. As a proof of concept, we show in Figure 1.19 a comparison with the data published in Lee et al. [2012]. We highlight that this is only a preliminary result, and the model was not calibrated on the ovine heart adopted in the experiment. As a consequence, we do

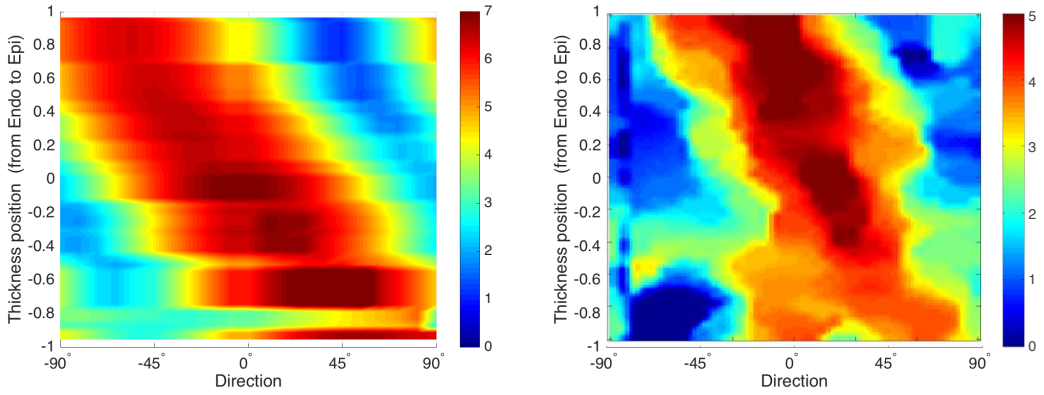

Figure 1.19 – Two-dimensional plots of shear wave velocity as a function of probe angle and depth in the medium, from sub-epicardial to sub-endocardial. Left: numerical simulation. Right: SWI experiment (edited from Lee et al. [2012]). Velocity is depicted in $\mathrm{m\,s^{-1}}$.

not have a perfect matching in the transmural fibre orientation. However, our aim was to prove that the result was qualitatively and quantitatively consistent with the experiment. The calibration of case-specific biomechanical models for complete comparison with experimental data represents one of the future aims of this study.

1.6.2 Local modification of mechanical properties by induced "numerical pathologies"

The second application concerns the analysis of the effect of local alteration of the biomechanical properties of the medium on the elastic wave propagation. This example is inspired by the fact that several pathologies, like ischemic cardiomyopathy and heart failure, are associated with a local variation in myocardial passive stiffness and active contractility. As a consequence, the non-invasive estimation of the local biomechanical properties and the analysis of the variation of such parameters in a small time-scale (a cardiac cycle) and a large time-scale (months) would be of crucial clinical interest for the assessment of physiological and pathological conditions, as well as tissue remodelling induced by cardiac pathologies or after surgical interventions, providing a new unique tool of diagnosis and monitoring.
The in silico framework is developed in the context of our in-house code for the resolution of the nonlinear, three-dimensional problem of heart mechanics, and it consists in the following steps:

- First, we consider the constitutive law defined in Eq. (1.21). Then, a region of in the septum (membrane separating left and right ventricle) is selected, and the biomechanical properties associated with this region are modified with respect to the rest of the computational domain. The passive elastic modulus κ_3 is increased by a factor of 5 with respect to the reference value, whereas the active contractility is reduced by a factor of 5;

- Then, at each discrete time step of the evolution problem, the fourth-order tensor $\underline{\underline{\mathbf{C}}}^{\mathrm{Eul}}(\underline{x}, t)$ is computed;

- The fibre direction $\underline{\tau_1}$ is selected as propagation direction;

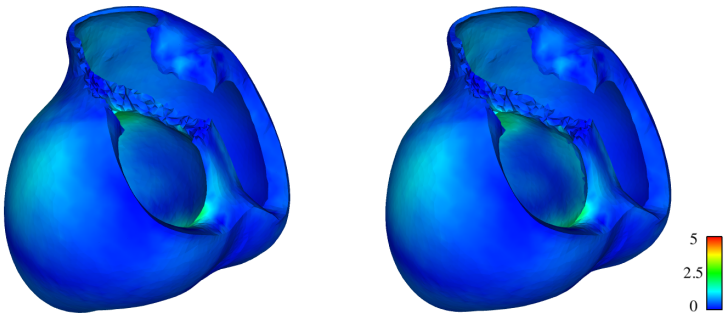

Figure 1.20 – Numerical simulation of shear wave propagation during diastolic phase. Left: healthy case; Right: Local modification of passive elastic moduli and active contractility in the septum. Velocities are depicted in $\mathrm{m\,s^{-1}}$.

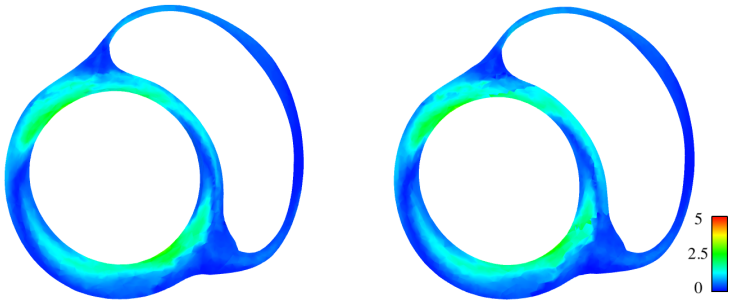

Figure 1.21 – Numerical simulation of shear wave propagation during diastolic phase. Left: healthy case; Right: Local modification of passive elastic moduli and active contractility in the septum. Velocities are depicted in $\mathrm{m\,s^{-1}}$. Transverse view.

- The Christoffel tensor $\underline{\underline{\Gamma}}(\underline{x}, t)$ is computed, along with its eigenvalues λ_j and eigenvectors $\underline{u}_j$;

- The second highest wavespeed is selected, which corresponds to the quasi-shear wave with polarisation orthogonal to the local plane of the fibres.

With this algorithm, it is possible to have a measure of shear wave velocity as function of the position in the computational domain and the phase of the cardiac cycle. Consequently, it is possible to assess the variation of shear wave velocity along the cycle associated with physiological conditions in the whole heart, and detect the local modification of biomechanical properties in the myocardium induced by a "numerical pathology", that imitates what occurs in patients presenting ischemic scars. Figures 1.20 to 1.23 show that the septal region is characterised by a negligible increase in shear wave velocity during the diastolic phase, due to the augmentation of the passive elastic modulus, accounting for passive stress. However, a more substantial variation can be appreciated at the beginning of the isovolumic contraction, due to the fact that the leading term is represented by the active stress, and it has been reduced by a factor of 5 in this area. As a consequence, shear wave propagation reflects well the local variation in space of the biomechanical properties of the tissue.

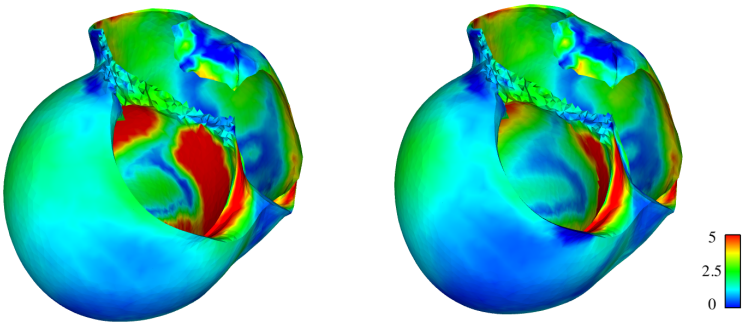

Figure 1.22 – Numerical simulation of shear wave propagation during early-systolic phase. Left: healthy case; Right: Local modification of passive elastic moduli and active contractility in the septum. Velocities are depicted in $\mathrm{m\,s^{-1}}$.

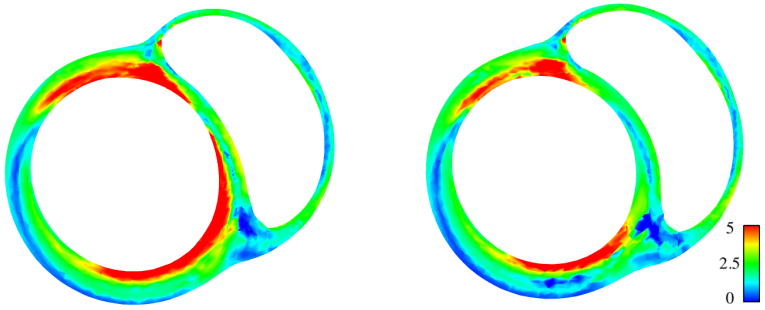

Figure 1.23 – Numerical simulation of shear wave propagation during early-systolic phase. Left: healthy case; Right: Local modification of passive elastic moduli and active contractility in the septum. Velocities are depicted in $\mathrm{m\,s^{-1}}$. Transverse view.

1.7 Conclusions

In this chapter we have outlined a methodological and numerical approach to characterise elastographic shear waves in a general mechanical model, that extends the classical derivation of the Christoffel tensor. Furthermore, we have shown some detailed results obtained when applying this approach with the heart model and compared the computed wave velocities with published experimental measurements.
We highlight the fact that the variation of shear wave velocity over the cardiac cycle is only due to the different contributions of the active stress associated with the different phases of the heartbeat. This could lead to a incorrect estimation of apparent mechanical properties that change significantly over the cardiac cycle, as it is often done in SWE experiments. However, the measured time-varying apparent stiffness is given by the current (transient) tangent stiffness operator and is associated with passive elastic moduli and active contractilities, constant in time. Hence, there is a crucial need to relate the measured apparent stiffness to actual constitutive parameters, such as passive elastic moduli and active contractility.
The approach that we have proposed in this chapter to solve this problem can be summarised in three main steps:

- Consider an accurate biomechanical model adequately representing the complex state of the myocardium;
- Derive the equations governing the shear wave propagation imaged in elastographic techniques;
- Apply a suitable methodological and numerical approach to a beating heart model to compute shear wave velocities.

Note that the methodological and numerical approach developed to compute elastographic shear wave propagation is valid for a general constitutive behaviour, since no restrictive assumption (e.g. small strains assumptions) was formulated for its derivation.
In addition, we have deduced in our analysis that the active contractility can be directly retrieved from shear wave velocity measurements during the systolic phase, providing a valuable biomarker of the heart function.
The model correctly depicted the impact of non-linearity and anisotropy in shear wave propagation, and demonstrated the feasibility of extracting the fibre orientation by SWE. The estimation of fibre arrangement is of great clinical impact, since local modification in fibre arrangement is frequently related to myocardial fibrosis.
Future perspectives include further model validation with SWE experiments.

1.8 Appendix

1.8.1 Coercivity of the bilinear form associated with the constitutive law in a linearised static configuration

In order to compute the bilinear form $a(t;\tilde{\underline{y}},\underline{w})$ in Eq. (1.23), we shall consider the following expression for $\underline{\underline{\Sigma}}$:

$$\underline{\underline{\Sigma}} = \underline{\underline{\Sigma}}^P + \underline{\underline{\Sigma}}^A = \underline{\underline{\Sigma}}_0^P + \underline{\underline{\Sigma}}^A + \delta\tilde{\underline{\underline{\Sigma}}}^P + O(\delta)^2,$$

with

$$\underline{\underline{\Sigma}}^P = \underline{\underline{\Sigma}}^{\mathrm{TI}} + \underline{\underline{\Sigma}}^{ISO} + \underline{\underline{\Sigma}}^{\mathrm{NI}}.$$

This decomposition holds with the assumption that the stress tensor corresponding to the active stress $\underline{\underline{\Sigma}}^A$ does not depend on $\underline{y}$. In particular, we can identify in this decomposition a nonlinear term $\underline{\underline{\Sigma}}_0^P + \underline{\underline{\Sigma}}^A$, and the linear contribution $\tilde{\underline{\underline{\Sigma}}}^P$. In a prestress-free configuration ($\underline{y}_0 = \underline{0}$), we obtain $\underline{y} = \delta\tilde{\underline{y}}$. As a consequence, we can show that the nonlinear part of the passive stress tensor is zero. If we consider a complex constitutive law, including isotropic, transversely isotropic, nearly-incompressible and active terms, we obtain the following expression for $\underline{\underline{\Sigma}}$:

$$\begin{aligned}\underline{\underline{\Sigma}} &= \underline{\underline{\Sigma}}^A + \delta\,\tilde{\underline{\underline{\Sigma}}}^P + O(\delta^2) = \underline{\underline{\Sigma}}^A + \delta\Big(\tilde{\underline{\underline{\Sigma}}}^{\mathrm{TI}} + \tilde{\underline{\underline{\Sigma}}}^{ISO} + \tilde{\underline{\underline{\Sigma}}}^{\mathrm{NI}}\Big) + O(\delta^2)\\ &= \Sigma_{1D}\,\underline{\tau}_1 \otimes \underline{\tau}_1 + \delta\, c\Big(-\frac{1}{3}\underline{\underline{\Sigma}}_1^e - \frac{1}{3}\underline{\underline{\Sigma}}_2^e + \frac{1}{9}\underline{\underline{\Sigma}}_3^e + \underline{\underline{\Sigma}}_4^e\Big) + \delta\,\chi\Big(\underline{\underline{e}}_0(\tilde{\underline{y}}) - \frac{1}{3}\underline{\underline{\mathbb{1}}} : \underline{\underline{e}}_0(\tilde{\underline{y}})\ \underline{\underline{\mathbb{1}}}\Big)\\ &\quad + \delta\,\kappa\,\underline{\underline{\mathbb{1}}} : \underline{\underline{e}}_0(\tilde{\underline{y}})\ \underline{\underline{\mathbb{1}}} + O(\delta^2),\end{aligned} \tag{1.61}$$

with $\underline{\underline{\Sigma}}^{\mathrm{TI}}$, for $i = \{1, 2, 3, 4\}$, defined as in Eq. (1.36).
By hypothesis, we assume $c \geq 0$, $\Sigma_{1D} \geq 0$, $\lambda \geq 0$.
We recall that we can rewrite the term $d_{\underline{y}}\underline{\underline{e}} \cdot \underline{w}$ as following:

$$d_{\underline{y}}\underline{\underline{e}} \cdot \underline{w} = \underline{\underline{\varepsilon}}(\underline{w}) + \delta\frac{1}{2}\Big(\underline{\underline{\nabla}}\,\tilde{\underline{y}}^T \cdot \underline{\underline{\nabla}}\,\underline{w} + \underline{\underline{\nabla}}\,\underline{w}^T \cdot \underline{\underline{\nabla}}\,\tilde{\underline{y}}\Big) + O(\delta^2), \tag{1.62}$$

where $\underline{\underline{\varepsilon}}(\underline{w}) = \frac{1}{2}\big(\underline{\underline{\nabla}}\,\underline{w} + (\underline{\underline{\nabla}}\,\underline{w})^T\big)$. Furthermore, the simplifying hypothesis $\underline{y}_0 = 0$ implies

$$\underline{\underline{e}}_0(\tilde{\underline{y}}) = \underline{\underline{\varepsilon}}(\tilde{\underline{y}}).$$

Due to Eqs. (1.61) and (1.62), we get

$$\underline{\underline{\Sigma}} : d_{\underline{y}}\underline{\underline{e}} \cdot \underline{w} = \underline{\underline{\Sigma}}^A : \underline{\underline{\varepsilon}}(\underline{w}) + \delta\,\tilde{\underline{\underline{\Sigma}}}^P : \underline{\underline{\varepsilon}}(\underline{w}) + \underline{\underline{\Sigma}}^A : \frac{1}{2}\delta\Big(\underline{\underline{\nabla}}\,\tilde{\underline{y}}^T \cdot \underline{\underline{\nabla}}\,\underline{w} + \underline{\underline{\nabla}}\,\underline{w}^T \cdot \underline{\underline{\nabla}}\,\tilde{\underline{y}}\Big) + O(\delta)^2.$$

We emphasize that the term $\underline{\underline{\Sigma}}^A : \underline{\underline{\varepsilon}}(\underline{w})$ shall be considered a source term, since it is independent of $\tilde{\underline{y}}$. Therefore, it is not included in the bilinear form $a(t;\cdot,\cdot)$.
Hence, the bilinear form $a(t;\cdot,\cdot)$ reduces to

$$a(t;\tilde{\underline{y}},\underline{w}) = \int_{\Omega_0} \tilde{\underline{\underline{\Sigma}}}^P : \underline{\underline{\varepsilon}}(\underline{w})\ \mathrm{d}\Omega_0 + \int_{\Omega_0} \underline{\underline{\Sigma}}^A : \Big(\underline{\underline{\nabla}}_{\underline{\xi}}\,\tilde{\underline{y}}^T \cdot \underline{\underline{\nabla}}_{\underline{\xi}}\,\underline{w}\Big)\ \mathrm{d}\Omega_0. \tag{1.63}$$

We can prove the following proposition, that is fundamental to ensure existence of solution of the elastodynamic problem (1.22).

Proposition 1.1. *Let Eq. (1.61) hold. Then, in a prestress-free configuration, the bilinear form $a(t;\cdot,\cdot) : C^1([0,T] \times H^1(\Omega) \times H^1(\Omega) \to \mathbb{R}$ in Eq. (1.63) is symmetric and coercive, with coercivity constant $\alpha = 2\mu$.*

Proof. Let $(\tilde{\underline{y}}, \underline{w}) \in H^1(\Omega) \times H^1(\Omega)$. First, we prove the symmetry of $a(t;\tilde{\underline{y}},\underline{w})$. We develop each term in Eq. (1.61) accounting for passive stress. We obtain

$$\begin{aligned}\tilde{\underline{\underline{\Sigma}}}^{\mathrm{TI}} : \underline{\underline{\varepsilon}}(\underline{w}) &= c\Big(-\frac{1}{3}\underline{\underline{\mathbb{1}}} : \underline{\underline{\varepsilon}}(\tilde{\underline{y}})\ \underline{\tau}_1 \otimes \underline{\tau}_1 : \underline{\underline{\varepsilon}}(\underline{w}) - \frac{1}{3}\underline{\underline{\mathbb{1}}} : \underline{\underline{\varepsilon}}(\underline{w})\ \underline{\tau}_1 \otimes \underline{\tau}_1 : \underline{\underline{\varepsilon}}(\tilde{\underline{y}})\\ &\qquad + \frac{1}{9}\underline{\underline{\mathbb{1}}} : \underline{\underline{\varepsilon}}(\tilde{\underline{y}})\ \underline{\underline{\mathbb{1}}} : \underline{\underline{\varepsilon}}(\underline{w}) + \underline{\tau}_1 \otimes \underline{\tau}_1 : \underline{\underline{\varepsilon}}(\tilde{\underline{y}})\ \underline{\tau}_1 \otimes \underline{\tau}_1 : \underline{\underline{\varepsilon}}(\underline{w})\Big)\\ \tilde{\underline{\underline{\Sigma}}}^{ISO} : \underline{\underline{\varepsilon}}(\underline{w}) &= \chi\Big(\underline{\underline{\varepsilon}}(\tilde{\underline{y}}) : \underline{\underline{\varepsilon}}(\underline{w}) - \frac{1}{3}\underline{\underline{\mathbb{1}}} : \underline{\underline{\varepsilon}}(\tilde{\underline{y}})\ \underline{\underline{\mathbb{1}}} : \underline{\underline{\varepsilon}}(\underline{w})\Big)\\ \tilde{\underline{\underline{\Sigma}}}^{\mathrm{NI}} : \underline{\underline{\varepsilon}}(\underline{w}) &= \kappa\,\underline{\underline{\mathbb{1}}} : \underline{\underline{\varepsilon}}(\tilde{\underline{y}})\ \underline{\underline{\mathbb{1}}} : \underline{\underline{\varepsilon}}(\underline{w}).\end{aligned} \tag{1.64}$$

Consequently,

$$\begin{aligned}\tilde{\underline{\underline{\Sigma}}}^P : \underline{\underline{\varepsilon}}(\underline{w}) = \Big(\frac{1}{9}c - \frac{1}{3}\chi + \kappa\Big)\underline{\underline{\mathbb{1}}} : \underline{\underline{\varepsilon}}(\tilde{\underline{y}})\ \underline{\underline{\mathbb{1}}} : \underline{\underline{\varepsilon}}(\underline{w}) - \frac{1}{3}c\,\underline{\underline{\mathbb{1}}} : \underline{\underline{\varepsilon}}(\tilde{\underline{y}})\ \underline{\tau}_1 \otimes \underline{\tau}_1 : \underline{\underline{\varepsilon}}(\underline{w}) \\ - \frac{1}{3}c\,\underline{\underline{\mathbb{1}}} : \underline{\underline{\varepsilon}}(\underline{w})\ \underline{\tau}_1 \otimes \underline{\tau}_1 : \underline{\underline{\varepsilon}}(\tilde{\underline{y}}) + c\,\underline{\tau}_1 \otimes \underline{\tau}_1 : \underline{\underline{\varepsilon}}(\tilde{\underline{y}})\ \underline{\tau}_1 \otimes \underline{\tau}_1 : \underline{\underline{\varepsilon}}(\underline{w}).\end{aligned} \tag{1.65}$$

From Eq. (1.65) it is evident that $\tilde{\underline{\underline{\Sigma}}}^P : \underline{\underline{\varepsilon}}(\underline{w})$ is symmetric and linear with respect to $\tilde{\underline{y}}$ and $\underline{w}$.
The term accounting for the active stress reads

$$\underline{\underline{\Sigma}}^A : \frac{1}{2}\Big(\underline{\underline{\nabla}}\,\tilde{\underline{y}}^T \cdot \underline{\underline{\nabla}}\,\underline{w} + \underline{\underline{\nabla}}\,\underline{w}^T \cdot \underline{\underline{\nabla}}\,\tilde{\underline{y}}\Big) \tag{1.66}$$

and is symmetric by definition. Therefore, the bilinear form $a(t; \tilde{\underline{y}}, \underline{w})$ is symmetric.
Let us now prove coercivity. First, we prove that there exists $\alpha > 0$ such that

$$\tilde{\underline{\underline{\Sigma}}}^P(\underline{\underline{\varepsilon}}) : \underline{\underline{\varepsilon}} \geq \alpha \left|\underline{\underline{\varepsilon}}\right|^2 \quad \forall\, \underline{\underline{\varepsilon}} \in \mathcal{L}_s(\mathbb{R}^d).$$

We consider as test displacement $\underline{w} = \tilde{\underline{y}}$ in Eq. (1.64). . Thus, we obtain

$$\begin{aligned}\tilde{\underline{\underline{\Sigma}}}^{\mathrm{TI}} : \underline{\underline{\varepsilon}}(\tilde{\underline{y}}) &= c\Big(-\frac{2}{3}\underline{\underline{\mathbb{1}}} : \underline{\underline{\varepsilon}}(\tilde{\underline{y}})\ \underline{\tau}_1 \otimes \underline{\tau}_1 : \underline{\underline{\varepsilon}}(\tilde{\underline{y}}) + \frac{1}{9}\big(\underline{\underline{\mathbb{1}}} : \underline{\underline{\varepsilon}}(\tilde{\underline{y}})\big)^2 + \big(\underline{\tau}_1 \otimes \underline{\tau}_1 : \underline{\underline{\varepsilon}}(\tilde{\underline{y}})\big)^2\Big) \\ &= c\Big(\underline{\tau}_1 \otimes \underline{\tau}_1 : \underline{\underline{\varepsilon}}(\tilde{\underline{y}}) - \frac{1}{3}\underline{\underline{\mathbb{1}}} : \underline{\underline{\varepsilon}}(\tilde{\underline{y}})\Big)^2, \\ \tilde{\underline{\underline{\Sigma}}}^e_{MR} : \underline{\underline{\varepsilon}}(\tilde{\underline{y}}) &= \chi\Big(\underline{\underline{\varepsilon}}(\tilde{\underline{y}}) : \underline{\underline{\varepsilon}}(\tilde{\underline{y}}) - \frac{1}{3}\big(\underline{\underline{\mathbb{1}}} : \underline{\underline{\varepsilon}}(\tilde{\underline{y}})\big)^2\Big), \\ \tilde{\underline{\underline{\Sigma}}}^{\mathrm{NI}} : \underline{\underline{\varepsilon}}(\tilde{\underline{y}}) &= \kappa\,\underline{\underline{\mathbb{1}}} : \underline{\underline{\varepsilon}}(\tilde{\underline{y}})\ \underline{\underline{\mathbb{1}}} : \underline{\underline{\varepsilon}}(\tilde{\underline{y}}).\end{aligned}$$

Let us introduce the Lamé constants $\lambda = \kappa - \frac{1}{3}\chi$ and $\mu = \frac{1}{2}\chi$. Note that they are positive by hypothesis in a bulky medium ($\kappa > \chi$).
Thus, we obtain

$$\tilde{\underline{\underline{\Sigma}}}^P : \underline{\underline{\varepsilon}}(\tilde{\underline{y}}) = c\Big(\underline{\tau}_1 \otimes \underline{\tau}_1 : \underline{\underline{\varepsilon}}(\tilde{\underline{y}}) - \frac{1}{3}\operatorname{tr}\big(\underline{\underline{\varepsilon}}(\tilde{\underline{y}})\big)\Big)^2 + 2\,\mu\,\underline{\underline{\varepsilon}}(\tilde{\underline{y}}) : \underline{\underline{\varepsilon}}(\tilde{\underline{y}}) + \lambda \operatorname{tr}\big(\underline{\underline{\varepsilon}}(\tilde{\underline{y}})\big)^2.$$

Note that all the terms are quadratic, thus non-negative. As a consequence we obtain, due to Korn's inequality,

$$\tilde{\underline{\underline{\Sigma}}}^P : d_{\underline{y}}\underline{\underline{e}} \cdot \tilde{\underline{y}} = \tilde{\underline{\underline{\Sigma}}}^P : \underline{\underline{\varepsilon}}(\tilde{\underline{y}}) + O(\delta) \geq 2\,\mu\,\underline{\underline{\varepsilon}}(\tilde{\underline{y}}) : \underline{\underline{\varepsilon}}(\tilde{\underline{y}}) \geq 2\,\mu\,|\underline{\underline{\varepsilon}}(\tilde{\underline{y}})|^2,$$

proving that the tensor $\tilde{\underline{\underline{\Sigma}}}^P$ is coercive with constant $\alpha = 2\,\mu$. We now take into account the active term in the bilinear form. We rewrite, considering Eq. (1.66),

$$\begin{aligned}\underline{\underline{\Sigma}}^A : \big(\underline{\underline{\nabla}}\,\tilde{\underline{y}}^T \cdot \underline{\underline{\nabla}}\,\tilde{\underline{y}}\big) &= \Sigma_{1D}\,\underline{\tau}_1 \otimes \underline{\tau}_1 : \frac{1}{2}\Big(\underline{\underline{\nabla}}\,\tilde{\underline{y}}^T \cdot \underline{\underline{\nabla}}\,\tilde{\underline{y}} + \underline{\underline{\nabla}}\,\tilde{\underline{y}}^T \cdot \underline{\underline{\nabla}}\,\tilde{\underline{y}}\Big) \\ &= \Sigma_{1D}\Big(\big(\tau_{1,1}\partial_1\tilde{y}_1 + \tau_{1,2}\partial_2\tilde{y}_1\big)^2 + \big(\tau_{1,1}\partial_1\tilde{y}_2 + \tau_{1,2}\partial_2\tilde{y}_2\big)^2\Big).\end{aligned}$$

Hence, this term is quadratic, thus non-negative. As a consequence, the bilinear form $a(t; \tilde{\underline{y}}, \underline{w})$ in Eq. (1.63) is coercive with constant $\alpha = 2\,\mu$. □

1.8.2 Parameter calibration on a reduced-order cardiac model

In this section we show some results concerning the calibration of the passive parameters in the proposed constitutive laws. To do so, we used a in-house reduced-order cardiac model, based on a "zero-dimensional" formulation of the cardiac cavity [Caruel et al., 2014]. The 0-D model is derived by assuming spherical symmetry. As a consequence, the simplified geometry is univocally determined by the radius R_0 and the thickness d_0 in the reference configuration, and R and d in a deformed configuration. The material is assumed to be purely incompressible ($\det \underline{\underline{C}} = 1$). In addition to the spherical symmetry assumption, it is assumed that the radial stress can be neglected compared to the orthoradial components, leading to the elimination of the hydrostatic pressure. Hence, the system of equation to be solved is drastically simplified. In particular, the equilibrium equation reads

$$\rho\, d_0 \ddot{y} + \frac{d_0}{R_0}\left(1 + \frac{y}{R_0}\right)\Sigma_{sph} = P_v \left(1 + \frac{y}{R_0}\right)^2,$$

where P_v is the internal pressure in the ventricle, and the second Piola-Kirchhoff stress tensor Σ_{sph} is given by

$$\Sigma_{sph} = \sigma_{1d} + 4(1 - C^{-3})\left(\frac{\partial W_e}{\partial J_1} + C\frac{\partial W_e}{\partial J_2}\right) + 2\frac{\partial W_e}{\partial J_4} + 2\,\eta\,\dot{C}(1 - 2\,C^{-6}),$$

with η accounting for the viscous contribution.
Inflows and outflows are generated by opening and closing of valves, and flow is modelled as:

$$-\dot{V} = Q = q\,(P_v, P_{ar}, P_{at}),$$

with P_{ar} pressure in the aorta or in the pulmonary artery and P_{at} atrial pressure.
The system of equations is closed by a two-stage Windkessel model for the external circulation, given by

$$\begin{cases} C_p \dot{P}_{ar} + \dfrac{P_{ar} - P_d}{R_p} = Q, \\ C_d \dot{P}_d + \dfrac{P_{ar} - P_d}{R_p} = (P_{vs} - P_d)/R_d, \end{cases}$$

where C_p, R_p, C_d and R_d represent the capacitances and resistances of the proximal and distal circulations, P_d represents the distal pressure and P_{vs} denotes the venous system pressure. We refer the reader to [Caruel et al., 2014] for further details on the model.
As demonstrated in the previous section, the simple constitutive law Eq. (1.35) is not sufficient to satisfy the coercivity requirements and, thus, regularity of elastic wave propagation in the medium. Consequently, we proposed to include in the constitutive law an isotropic term - defined in Eq. (1.49) - that is a function of the reduced invariant J_2, that is sufficient to regularise the solution of the elastic wave propagation. However, we do not want that this term affects the underlying cardiac mechanics. The main objective of our calibration is to find a value of χ that does not perturb the overall behaviour of heart deformation. To do so, we first consider as reference simulation an instance of the model corresponding to a transversely isotropic medium described by Eq. (1.35), with $\kappa_3 = 170\,\text{Pa}$, $\kappa_4 = 2.5$. Physiological curves associated with this simulation are shown in Figure 1.24. This simulation satisfies all physiological requirements, since all the cardiac and haemodynamic parameters are in a physiological range. Then, we test our model against different choices for χ and we analyse two physiological curves that characterise the passive properties of the myocardium:

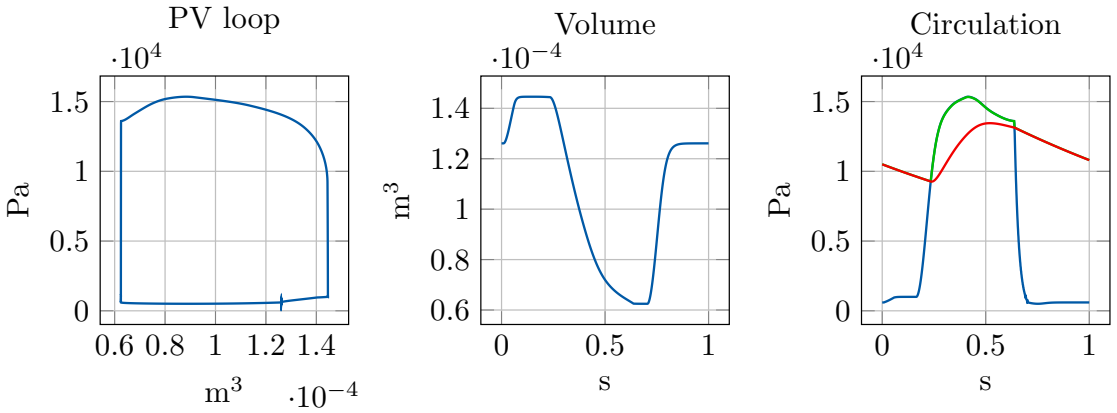

Figure 1.24 – Left: Pressure-volume loop; Centre: volume evolution in the cavity in a cardiac cycle; Right: pressure evolution in the cavity (blue), in proximal arteries (green) and distal arteries (red) in a cardiac cycle.

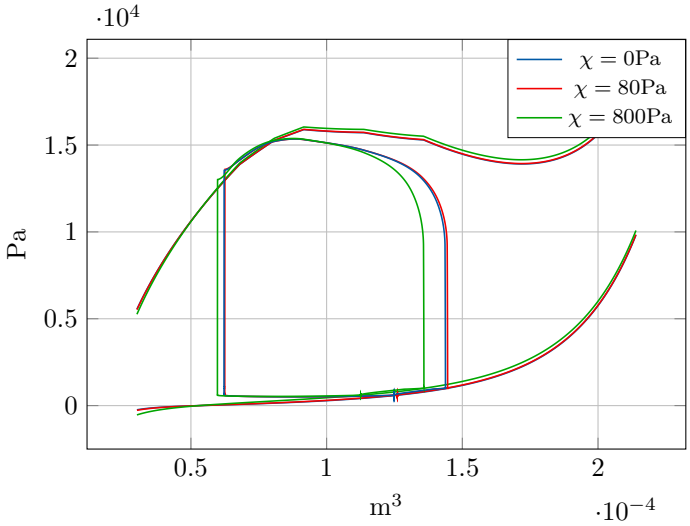

Figure 1.25 – Volume-pressure loop, ESPVR and EDPVR associated with transversely isotropic constitutive law for different values of the parameter χ. Blue line: $\chi = 0\,\text{Pa}$ (reference simulation); Red line: $\chi = 80\,\text{Pa}$; Green line: $\chi = 800\,\text{Pa}$.

- Pressure-volume (PV) loop, from which numerous physiologically relevant haemodynamic parameters can be derived;
- End diastolic pressure-volume relationship (EDPVR), describing the passive filling curve for the ventricle.

For the sake of completeness, we show in the results also the curves corresponding to the end-systolic pressure-volume relationship (ESPVR), that is associated with the systolic function. As shown in Figure 1.25, a suitable choice is represented by $\chi = 80\,\text{Pa}$. In fact, both the PV-loop and the EDPVR are not affected by the inclusion of this term in the constitutive law, and their profile is almost superposed to the PV loop and EDPVR corresponding to the reference simulation ($\chi = 0\,\text{Pa}$). On the contrary, if we consider larger values, i.e. $\chi = 800\,\text{Pa}$, the dynamics is consistently modified, affecting PV loop and EDPVR.

1.8.3 Alternative method to compute the Christoffel tensor in prestress-free configuration

Christoffel tensor associated with transversely isotropic term. In order to compute the Christoffel tensor associated with Eq. (1.37), we first compute $\underline{\mathrm{div}}\left(\tilde{\underline{\underline{\Sigma}}}^{\mathrm{TI}}\right)$. From the tensor theory:

$$\underline{\mathrm{div}}\left(\tilde{\underline{\underline{\Sigma}}}^{\mathrm{TI}}\right) = \frac{\partial \tilde{\Sigma}^{\mathrm{TI}}_{ji}}{\partial x_j} e_i,$$

where e_i, for $i = 1, 2$, are basis vectors in a Cartesian coordinate system, and we adopt the Einstein summation notation.
For simplicity of notation, we introduce in what follows the scalars

$$\zeta_{1\,2} = \tau_{1,1}\,\tau_{1,2}, \quad \eta_{1\,2} = (\partial_1 \tilde{y}_2 + \partial_2 \tilde{y}_1).$$

We first compute $\tilde{\underline{\underline{\Sigma}}}^{\mathrm{TI}}_1$ in matrix form. It reads

$$\tilde{\underline{\underline{\Sigma}}}^{\mathrm{TI}}_1 = \begin{bmatrix} \tau^4_{1,1}\,\partial_1\tilde{y}_1 + \tau^3_{1,1}\,\tau_{1,2}\,\eta_{1\,2} + \zeta^2_{1\,2}\,\partial_2\tilde{y}_2 & \tau^3_{1,1}\,\tau_{1,2}\partial_1\tilde{y}_1 + \zeta^2_{1\,2}\,\eta_{1\,2} + \tau_{1,1}\,\tau^3_{1,2}\,\partial_2\tilde{y}_2 \\ \tau^3_{1,1}\,\tau_{1,2}\,\partial_1\tilde{y}_1 + \zeta^2_{1\,2}\,\eta_{1\,2} + \tau_{1,1}\,\tau^3_{1,2}\,\partial_2\tilde{y}_2 & \zeta^2_{1\,2}\,\partial_1\tilde{y}_1 + \tau_{1,1}\,\tau^3_{1,2}\,\eta_{1\,2} + \tau^4_{1,2}\,\partial_2\tilde{y}_2 \end{bmatrix}.$$

If we compute its divergence, we get

$$\underline{\mathrm{div}}\left(\tilde{\underline{\underline{\Sigma}}}^{\mathrm{TI}}_1\right) = \begin{bmatrix} \varsigma_{1,1} & \varsigma_{1,2} \\ \varsigma_{2,1} & \varsigma_{2,2} \end{bmatrix} \cdot \begin{bmatrix} \tilde{y}_1 \\ \tilde{y}_2 \end{bmatrix}$$

with

$$\begin{aligned} \varsigma_{1,1} &\coloneqq \tau^4_{1,1}\partial_{11} + 2\tau^3_{1,1}\,\tau_{1,2}\,\partial_{12} + \zeta^2_{1\,2}\,\partial_{22} & \varsigma_{1,2} &\coloneqq \tau^3_{1,1}\,\tau_{1,2}\,\partial_{11} + 2\,\zeta^2_{1\,2}\,\partial_{12} + \tau_{1,1}\,\tau^3_{1,2}\,\partial_{22} \\ \varsigma_{2,1} &\coloneqq \tau^3_{1,1}\,\tau_{1,2}\,\partial_{11} + 2\,\zeta^2_{1\,2}\,\partial_{12} + \tau_{1,1}\,\tau^3_{1,2}\,\partial_{22} & \varsigma_{2,2} &\coloneqq \zeta^2_{1\,2}\,\partial_{11} + 2\,\tau_{1,1}\,\tau^3_{1,2}\,\partial_{12} + \tau^4_{1,2}\partial_{22}. \end{aligned}$$

Let us consider the term $\tilde{\underline{\underline{\Sigma}}}^{\mathrm{TI}}_2$. It reads

$$\tilde{\underline{\underline{\Sigma}}}^{\mathrm{TI}}_2 = \begin{bmatrix} \tau^2_{1,1}\,(\partial_1\tilde{y}_1 + \partial_2\tilde{y}_2) & \zeta_{1\,2}\,(\partial_1\tilde{y}_1 + \partial_2\tilde{y}_2) \\ \zeta_{1\,2}\,(\partial_1\tilde{y}_1 + \partial_2\tilde{y}_2) & \tau^2_{1,2}\,(\partial_1\tilde{y}_1 + \partial_2\tilde{y}_2) \end{bmatrix}.$$

If we compute the divergence of $\tilde{\underline{\underline{\Sigma}}}^{\mathrm{TI}}_2$, we get

$$\underline{\mathrm{div}}\left(\tilde{\underline{\underline{\Sigma}}}^{\mathrm{TI}}_2\right) = \begin{bmatrix} \tau^2_{1,1}\,\partial_{11} + \zeta_{1\,2}\,\partial_{12} & \tau^2_{1,1}\,\partial_{12} + \zeta_{1\,2}\,\partial_{22} \\ \zeta_{1\,2}\,\partial_{11} + \tau^2_{1,2}\,\partial_{12} & \zeta_{1\,2}\,\partial_{12} + \tau^2_{1,2}\,\partial_{22} \end{bmatrix} \cdot \begin{bmatrix} \tilde{y}_1 \\ \tilde{y}_2 \end{bmatrix}.$$

Let us now analyse the tensor $\tilde{\underline{\underline{\Sigma}}}^{\mathrm{TI}}_3$. It reads, in matrix form,

$$\tilde{\underline{\underline{\Sigma}}}^{\mathrm{TI}}_3 = \begin{bmatrix} \tau^2_{1,1}\,\partial_1\tilde{y}_1 + \zeta_{1\,2}\,\eta_{1\,2} + \tau^2_{1,2}\,\partial_2\tilde{y}_2 & 0 \\ 0 & \tau^2_{1,1}\,\partial_1\tilde{y}_1 + \zeta_{1\,2}\,\eta_{1\,2} + \tau^2_{1,2}\,\partial_2\tilde{y}_2. \end{bmatrix}.$$

Thus, the divergence of $\tilde{\underline{\underline{\Sigma}}}^{\mathrm{TI}}_3$ is

$$\underline{\mathrm{div}}\left(\tilde{\underline{\underline{\Sigma}}}^{\mathrm{TI}}_3\right) = \begin{bmatrix} \tau^2_{1,1}\,\partial_{11} + \zeta_{1\,2}\,\partial_{12} & \zeta_{1\,2}\,\partial_{11} + \tau^2_{1,2}\,\partial_{12} \\ \tau^2_{1,1}\,\partial_{12} + \zeta_{1\,2}\,\partial_{22} & \zeta_{1\,2}\,\partial_{12} + \tau^2_{1,2}\,\partial_{22} \end{bmatrix} \cdot \begin{bmatrix} \tilde{y}_1 \\ \tilde{y}_2 \end{bmatrix}.$$

As far as the fourth stress tensor is concerned, we have

$$\tilde{\underline{\underline{\Sigma}}}^{\mathrm{TI}}_4 = \begin{bmatrix} \partial_1\tilde{y}_1 + \partial_2\tilde{y}_2 & 0 \\ 0 & \partial_1\tilde{y}_1 + \partial_2\tilde{y}_2 \end{bmatrix}.$$

Consequently, we obtain

$$\underline{\mathrm{div}}\Big(\underline{\underline{\tilde{\Sigma}}}_4^{\mathrm{TI}}\Big) = \begin{bmatrix} \partial_{11} & \partial_{12} \\ \partial_{12} & \partial_{22} \end{bmatrix} \cdot \begin{bmatrix} \tilde{y}_1 \\ \tilde{y}_2 \end{bmatrix}.$$

Summing all the four addends, we obtain

$$\underline{\mathrm{div}}\Big(\underline{\underline{\Sigma}}^{\mathrm{TI}}\Big) = \delta\, c \begin{bmatrix} D_{11} & D_{12} \\ D_{12} & D_{22} \end{bmatrix} \cdot \begin{bmatrix} \tilde{y}_1 \\ \tilde{y}_2 \end{bmatrix}, \tag{1.67}$$

with

$$D_{11} = \Big(\tau_{1,1}^2 - \frac{1}{3}\Big)^2 \partial_{11} + 2\tau_{1,1}\,\tau_{1,2}\Big(\tau_{1,1}^2 - \frac{1}{3}\Big)\partial_{12} + \tau_{1,1}^2\,\tau_{1,2}^2\,\partial_{22},$$

$$D_{12} = \Big(\tau_{1,1}^2 - \frac{1}{3}\Big)\tau_{1,1}\,\tau_{1,2}\partial_{11} + \Big(2\tau_{1,1}^2\,\tau_{1,2}^2 - \frac{1}{3}\tau_{1,1}^2 - \frac{1}{3}\tau_{1,2}^2 + \frac{1}{9}\Big)\partial_{12} + \Big(\tau_{1,2}^2 - \frac{1}{3}\Big)\tau_{1,1}\,\tau_{1,2}\partial_{22},$$

$$D_{22} = \tau_{1,1}^2\,\tau_{1,2}^2\,\partial_{11} + 2\,\tau_{1,1}\,\tau_{1,2}\Big(\tau_{1,2}^2 - \frac{1}{3}\Big)\partial_{12} + \Big(\tau_{1,2}^2 - \frac{1}{3}\Big)^2\partial_{22}.$$

Let us now assume that the solution of the fundamental equation in elastodynamic is a plane wave, i.e. a particular wave in the following form:

$$\underline{y}(\underline{x}, t) = \underline{d} e^{i(\underline{k}\cdot\underline{x} - \omega t)},$$

where $\underline{k} = (k_1, k_2) \in \mathbb{R}^2$ is the wave vector, $\omega \in \mathbb{R}$ is the angular frequency and $\underline{d} \in \mathbb{R}^2$ is the polarisation vector. In order to analyse the wave propagation in this medium, we derive the slowness curves and the wavefronts associated with this model. We start by computing the Christoffel matrix. In practice, we just need to substitute in Eq. (1.67) the terms ∂_i by the component k_i , for $i = 1, 2$.
In the simple case in which $\underline{\tau_1} = \underline{e}_1 \equiv (1, 0)$, we obtain the following Christoffel matrix:

$$\underline{\underline{\tilde{\Gamma}}}(\underline{k}) = \begin{bmatrix} \frac{4}{9} c\, k_1^2 & -\frac{2}{9} c\, k_1\, k_2 \\ -\frac{2}{9} c\, k_1\, k_2 & \frac{1}{9} c\, k_2^2 \end{bmatrix}. \tag{1.68}$$

On the other hand, if $\underline{\tau_1} = \underline{e}_2 \equiv (0, 1)$, we get

$$\underline{\underline{\tilde{\Gamma}}}^{\mathrm{TI}}(\underline{k}) = \begin{bmatrix} \frac{1}{9} c\, k_1^2 & -\frac{2}{9} c\, k_1\, k_2 \\ -\frac{2}{9} c\, k_1\, k_2 & \frac{4}{9} c\, k_2^2 \end{bmatrix}. \tag{1.69}$$

Christoffel tensor for the nearly-incompressible term. First, note that with the simplifying prestress-free assumption $\underline{\underline{y}}_0 = 0$, we obtain the following expression for the additional term accounting for nearly-incompressibility:

$$\underline{\underline{\Sigma}}^{\mathrm{NI}} = \delta\kappa\, \mathrm{tr}\Big(\underline{\underline{e}}_0(\underline{\tilde{y}})\Big)\underline{\underline{\mathbb{1}}} + O(\delta^2).$$

Let us define $\underline{\underline{\Sigma}}^{\mathrm{NI}} := \delta\underline{\underline{\tilde{\Sigma}}}^{\mathrm{NI}}$. In order to retrieve the expression of $\underline{\underline{\Gamma}}$ associated with this contribution, we compute the divergence of $\underline{\underline{\tilde{\Sigma}}}^{\mathrm{NI}}$.

$$\underline{\underline{\tilde{\Sigma}}}^{\mathrm{NI}} = \kappa \begin{bmatrix} \partial_1\tilde{y}_1 + \partial_2\tilde{y}_2 & 0 \\ 0 & \partial_1\tilde{y}_1 + \partial_2\tilde{y}_2 \end{bmatrix} \implies \underline{\mathrm{div}}\Big(\underline{\underline{\tilde{\Sigma}}}^{\mathrm{NI}}\Big) = \kappa \begin{bmatrix} \partial_{11} & \partial_{12} \\ \partial_{12} & \partial_{22} \end{bmatrix} \cdot \begin{bmatrix} \tilde{y}_1 \\ \tilde{y}_2 \end{bmatrix}.$$

Consequently, the Christoffel tensor corresponding to this contribution is simply given by

$$\underline{\underline{\tilde{\Gamma}}}^{\mathrm{NI}}(\underline{k}) = \kappa \begin{bmatrix} k_1^2 & k_1\, k_2 \\ k_1\, k_2 & k_2^2 \end{bmatrix}.$$

Christoffel tensor associated with isotropic term. As usual, we define $\underline{\underline{\Sigma}}^{ISO} := \delta\underline{\underline{\tilde{\Sigma}}}^{ISO}$. The divergence of the stress tensor $\underline{\underline{\tilde{\Sigma}}}^{ISO}$ is

$$\begin{aligned}\underline{\mathrm{div}}\left(\underline{\underline{\tilde{\Sigma}}}^{ISO}\right) &= \chi\left(\begin{bmatrix}\partial_1^2+\frac{1}{2}\partial_{22} & \frac{1}{2}\partial_1\partial_2\\ \frac{1}{2}\partial_1\partial_2 & \frac{1}{2}\partial_{11}+\partial_2^2\end{bmatrix}\cdot\begin{bmatrix}\tilde{y}_1\\ \tilde{y}_2\end{bmatrix} - \frac{1}{3}\begin{bmatrix}\partial_{11} & \partial_{12}\\ \partial_{12} & \partial_{22}\end{bmatrix}\cdot\begin{bmatrix}\tilde{y}_1\\ \tilde{y}_2\end{bmatrix}\right)\\ &= \chi\begin{bmatrix}\frac{2}{3}\partial_{11}+\frac{1}{2}\partial_{22} & \frac{1}{6}\partial_1\partial_2\\ \frac{1}{6}\partial_1\partial_2 & \frac{1}{2}\partial_{11}+\frac{2}{3}\partial_{22}\end{bmatrix}\cdot\begin{bmatrix}\tilde{y}_1\\ \tilde{y}_2\end{bmatrix}.\end{aligned}$$

As a consequence, the Christoffel tensor corresponding to $\underline{\underline{\tilde{\Sigma}}}^{ISO}$ reads

$$\underline{\underline{\tilde{\Gamma}}}^{ISO}(\underline{k}) = \chi\begin{bmatrix}\frac{2}{3}k_1^2+\frac{1}{2}k_2^2 & \frac{1}{6}k_1\,k_2\\ \frac{1}{6}k_1\,k_2 & \frac{1}{2}k_1^2+\frac{2}{3}k_2^2\end{bmatrix}.$$

Christoffel associated with active stress. For our applications, we will only consider the contribution associated with the prestress, i.e.

$$\int_\Omega \underline{\underline{\sigma}}^A : \left(\underline{\underline{\nabla}}_{\underline{x}}\,\underline{\tilde{y}}^T\cdot\underline{\underline{\nabla}}_{\underline{x}}\,\underline{w}\right)\mathrm{d}\Omega = \int_\Omega \sigma_{1d}\,\underline{\tau_1}'\otimes\underline{\tau_1}' : \left(\underline{\underline{\nabla}}_{\underline{x}}\,\underline{\tilde{y}}^T\cdot\underline{\underline{\nabla}}_{\underline{x}}\,\underline{w}\right)\mathrm{d}\Omega\ .$$

First, we recall that

$$\underline{\underline{\nabla}}\,\underline{w} = \begin{bmatrix}\partial_1 w_1 & \partial_2 w_1\\ \partial_1 w_2 & \partial_2 w_2\end{bmatrix}.$$

The tensor $\underline{\underline{M}} := \underline{\underline{\nabla}}_{\underline{x}}\,\underline{\tilde{y}}^T\cdot\underline{\underline{\nabla}}_{\underline{x}}\,\underline{w}$ reads

$$\underline{\underline{M}} = \begin{bmatrix}\partial_1\tilde{y}_1\,\partial_1 w_1+\partial_1\tilde{y}_2\,\partial_1 w_2 & \partial_1\tilde{y}_1\,\partial_2 w_1+\partial_1\tilde{y}_2\,\partial_2 w_2\\ \partial_2\tilde{y}_1\,\partial_1 w_1+\partial_2\tilde{y}_2\,\partial_1 w_2 & \partial_2\tilde{y}_1\,\partial_2 w_1+\partial_2\tilde{y}_2\,\partial_2 w_2\end{bmatrix}.$$

The dyadic product $\underline{\tau_1}\otimes\underline{\tau_1}$ can be rewritten in matrix form as

$$\underline{\tau_1}\otimes\underline{\tau_1} = \begin{bmatrix}\tau_{1,1}^2 & \tau_{1,1}\,\tau_{1,2}\\ \tau_{1,1}\,\tau_{1,2} & \tau_{1,2}^2\end{bmatrix}.$$

If we only consider the active term, the problem to solve reads in weak formulation

$$\int_\Omega(\ddot{\tilde{y}}_1\,w_1+\ddot{\tilde{y}}_2\,w_2)\,\mathrm{d}\Omega + \sigma_{1d}\int_\Omega \underline{\tau_1}\otimes\underline{\tau_1} : \underline{\underline{M}}\,\mathrm{d}\Omega = 0,$$

where the contribution due to the tensor product $\underline{\tau_1}\otimes\underline{\tau_1} : \underline{\underline{M}}$ is given by

$$\begin{aligned}\int_\Omega \underline{\tau_1}\otimes\underline{\tau_1} : \underline{\underline{M}}\,\mathrm{d}\Omega = \int_\Omega\Big(&\tau_{1,1}^2(\partial_1 w_1\partial_1\tilde{y}_1+\partial_1 w_2\partial_1\tilde{y}_2)+\tau_{1,1}\,\tau_{1,2}(\partial_1 w_1\partial_2\tilde{y}_1+\partial_1 w_2\partial_2\tilde{y}_2)+\\ &\tau_{1,1}\,\tau_{1,2}(\partial_2 w_1\partial_1\tilde{y}_1+\partial_2 w_2\partial_1\tilde{y}_2)+\tau_{1,2}^2(\partial_2 w_1\partial_2\tilde{y}_1+\partial_2 w_2\partial_2\tilde{y}_2)\Big)\,\mathrm{d}\Omega.\end{aligned}$$

By integrating by parts (and considering homogeneous Dirichlet boundary conditions) we get

$$\begin{aligned}\int_\Omega(\underline{\tau_1}\otimes\underline{\tau_1} : \underline{\underline{M}})\,\mathrm{d}\Omega = -\int_\Omega\Big(&(\tau_{1,1}^2\,\partial_{11}\tilde{y}_1+\tau_{1,2}^2\,\partial_{22}\tilde{y}_1+2\tau_{1,1}\,\tau_{1,2}\,\partial_{12}\tilde{y}_1)w_1\\ &+(2\tau_{1,1}\,\tau_{1,2}\,\partial_{12}\tilde{y}_2+\tau_{1,1}^2\,\partial_{11}\tilde{y}_2+\tau_{1,2}^2\,\partial_{22}\tilde{y}_2)w_2\Big)\,\mathrm{d}\Omega.\end{aligned}$$

Therefore, in strong form we can write

$$\begin{bmatrix} \ddot{\tilde{y}}_1 \\ \ddot{\tilde{y}}_2 \end{bmatrix} = \sigma_{1d} \begin{bmatrix} \tau_{1,1}^2\,\partial_{11} + 2\tau_{1,1}\,\tau_{1,2}\,\partial_{12} + \tau_{1,2}^2\,\partial_{22} & 0 \\ 0 & \tau_{1,1}^2\,\partial_{11} + 2\tau_{1,1}\,\tau_{1,2}\,\partial_{12} + \tau_{1,2}^2\,\partial_{22} \end{bmatrix} \begin{bmatrix} y_1 \\ y_2 \end{bmatrix},$$

from which we can recover the symbol of the operator associated with the active stress:

$$\sigma_{1d} \begin{bmatrix} k_1^2\tau_{1,1}^2 + 2k_1k_2\tau_{1,1}\,\tau_{1,2} + k_2^2\tau_{1,2}^2 & 0 \\ 0 & k_1^2\tau_{1,1}^2 + 2k_1k_2\tau_{1,1}\,\tau_{1,2} + k_2^2\tau_{1,2}^2 \end{bmatrix}.$$

If we redefine $k_1 = \underline{\tau_1} \cdot \underline{k}$, or we simply take $\underline{\tau_1} = \underline{e}_1$, we obtain

$$\sigma_{1d}\, k_1^2 \begin{bmatrix} 1 & 0 \\ 0 & 1 \end{bmatrix}.$$

Bibliography

Bercoff, J., Tanter, M. and Fink, M. [2004], 'Supersonic shear imaging: a new technique for soft tissue elasticity mapping', *IEEE transactions on ultrasonics, ferroelectrics, and frequency control* **51**(4), 396–409.

Bestel, J., Clément, F. and Sorine, M. [2001], A biomechanical model of muscle contraction, *in* 'International Conference on Medical Image Computing and Computer-Assisted Intervention', Springer, pp. 1159–1161.

Caruel, M., Chabiniok, R., Moireau, P., Lecarpentier, Y. and Chapelle, D. [2014], 'Dimensional reductions of a cardiac model for effective validation and calibration', *Biomechanics and modeling in mechanobiology* **13**(4), 897–914.

Chapelle, D., Le Tallec, P., Moireau, P. and Sorine, M. [2012], 'An energy-preserving muscle tissue model: formulation and compatible discretizations', *International Journal for Multiscale Computational Engineering* **10**(2), 189–211.

Ciarlet, P. G. [1988], 'Mathematical elasticity. vol. i, volume 20 of studies in mathematics and its applications'.

Ciarlet, P. G. and Geymonat, G. [1982], 'Sur les lois de comportement en élasticité non linéaire compressible', *CR Acad. Sci. Paris Sér. II* **295**, 423–426.

Costa, K. D., Holmes, J. W. and McCulloch, A. D. [2001], 'Modelling cardiac mechanical properties in three dimensions', *Philosophical Transactions of the Royal Society of London A: Mathematical, Physical and Engineering Sciences* **359**(1783), 1233–1250.

Costa, K. D., Takayama, Y., McCulloch, A. D. and Covell, J. W. [1999], 'Laminar fiber architecture and three-dimensional systolic mechanics in canine ventricular myocardium', *American Journal of Physiology-Heart and Circulatory Physiology* **276**(2), H595–H607.

Couade, M., Pernot, M., Messas, E., Bel, A., Ba, M., Hagege, A., Fink, M. and Tanter, M. [2011], 'In vivo quantitative mapping of myocardial stiffening and transmural anisotropy during the cardiac cycle', *IEEE transactions on medical imaging* **30**(2), 295–305.

Fung, Y.-C. B. [1973], 'Biorheology of soft tissues', *Biorheology* **10**(2), 139–155.

Gennisson, J.-L. [2003], Le palpeur acoustique: un nouvel outils d'investigation des tissus biologiques, PhD thesis, Université Pierre et Marie Curie-Paris VI.

Guccione, J. M., Costa, K. D. and McCulloch, A. D. [1995], 'Finite element stress analysis of left ventricular mechanics in the beating dog heart', *Journal of biomechanics* **28**(10), 1167–1177.

Holzapfel, G. A. and Ogden, R. W. [2009], 'Constitutive modelling of passive myocardium: a structurally based framework for material characterization', *Philosophical Transactions of the Royal Society of London A: Mathematical, Physical and Engineering Sciences* **367**(1902), 3445–3475.

Hooks, D. A., Trew, M. L., Caldwell, B. J., Sands, G. B., LeGrice, I. J. and Smaill, B. H. [2007], 'Laminar arrangement of ventricular myocytes influences electrical behavior of the heart', *Circulation Research* **101**(10), e103–e112.

Joly, P. [2008], *The mathematical model for elastic wave propagation. In "Effective Computational Methods for Wave Propagation"*, Numerical Insights, CRC Press.

Le Tallec, P. [1994], 'Numerical methods for nonlinear three-dimensional elasticity', *Handbook of numerical analysis* **3**, 465–622.

Lee, W.-N., Pernot, M., Couade, M., Messas, E., Bruneval, P., Bel, A., Hagege, A. A., Fink, M. and Tanter, M. [2012], 'Mapping myocardial fiber orientation using echocardiography-based shear wave imaging', *IEEE transactions on medical imaging* **31**(3), 554–562.

Nightingale, K., Soo, M. S., Nightingale, R. and Trahey, G. [2002], 'Acoustic radiation force impulse imaging: in vivo demonstration of clinical feasibility', *Ultrasound in medicine & biology* **28**(2), 227–235.

Pernot, M., Couade, M., Mateo, P., Crozatier, B., Fischmeister, R. and Tanter, M. [2011], 'Real-time assessment of myocardial contractility using shear wave imaging', *Journal of the American College of Cardiology* **58**(1), 65–72.

Pernot, M., Lee, W.-N., Bel, A., Mateo, P., Couade, M., Tanter, M., Crozatier, B. and Messas, E. [2016], 'Shear wave imaging of passive diastolic myocardial stiffness: stunned versus infarcted myocardium', *JACC: Cardiovascular Imaging* **9**(9), 1023–1030.

Raoult, A. [2009], 'Symmetry groups in nonlinear elasticity: An exercise in vintage mathematics', *Communications on Pure and Applied Mathematics* **8**(1), 435–456.

Rivlin, R. S. and Ericksen, J. L. [1997], *Stress-Deformation Relations for Isotropic Materials*, Springer New York, New York, NY, pp. 911–1013.

Royer, D. and Dieulesaint, E. [2000], 'Elastic waves in solids i: Free and guided propagation, translated by DP Morgan', *Springer-Verlag, New York* .

Sarvazyan, A., J Hall, T., W Urban, M., Fatemi, M., R Aglyamov, S. and S Garra, B. [2011], 'An overview of elastography-an emerging branch of medical imaging', *Current medical imaging reviews* **7**(4), 255–282.

Sarvazyan, A. P., Rudenko, O. V., Swanson, S. D., Fowlkes, J. B. and Emelianov, S. Y. [1998], 'Shear wave elasticity imaging: a new ultrasonic technology of medical diagnostics', *Ultrasound in medicine & biology* **24**(9), 1419–1435.

Sommer, G., Schriefl, A. J., Andrä, M., Sacherer, M., Viertler, C., Wolinski, H. and Holzapfel, G. A. [2015], 'Biomechanical properties and microstructure of human ventricular myocardium', *Acta biomaterialia* **24**, 172–192.

Streeter, D. D., Spotnitz, H. M., Patel, D. P., Ross, J. and Sonnenblick, E. H. [1969], 'Fiber orientation in the canine left ventricle during diastole and systole', *Circulation research* **24**(3), 339–347.

Temam, R. and Miranville, A. [2005], *Mathematical modeling in continuum mechanics*, Cambridge University Press.

CHAPTER 2

Mathematical modelling of transient shear wave elastography in the heart

Summary

The aim of this chapter is to mathematically justify an original expression of the excitation induced by the Acoustic Radiation Force (ARF) of a focused ultrasound beam generated by piezoelectric probes in nonlinear solids, based on energy considerations and asymptotic analysis.

To this end, we consider a family of problems, parametrised by a small parameter ε related to the velocity ratio between pressure and shear wave propagation, the high frequency of the piezoelectric source term and viscosity. We derive a simplified model for the expression of the ARF by investigating the limit behaviour of the solution for $\varepsilon \to 0$. By formal asymptotic analysis – an asymptotic expansion of the solution is used – we show that the leading-order term of the expansion is the underlying nonlinear cardiac mechanics, having as a source term the electrical activation of the heart. Subsequently, two corrector terms are computed. The first is a fast-oscillating pressure wave generated by the probes, solution of a Helmholtz equation at every time instant. The second corrector term consists in an elastic field with prescribed divergence, with a function of the first corrector as a source term. This field corresponds to the shear acoustic wave induced by the ARF. We also show that, in prestressed media, the presence of viscosity is essential to produce shear waves with ARF, and that they are related to the nonlinearity of the partial differential equation. *This chapter is in the form of a paper – coauthored by F. Caforio and S. Imperiale – already submitted for publication in an international journal.*

Contents

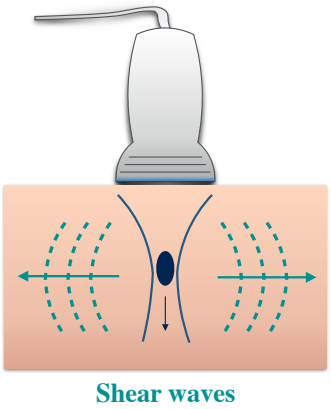

Figure 2.1 – Schematic description of shear wave generation.

2.1 Introduction

Shear acoustic waves remotely induced by the acoustic radiation force (ARF) of a focused ultrasound beam have raised a growing interest in biomedical applications, mainly in elasticity imaging. In fact, by measuring the velocity of propagation of the generated shear waves, it is possible to locally assess biomechanical properties highly sensitive to structural changes associated with physiological and pathological processes. The development of the first ARF-based shear wave elastography (SWE) technique dates back to late 1990s and was proposed by Sarvazyan et al. [1998] under the name of Shear Wave Elastography Imaging (SWEI). Thereafter, several techniques based on impulsive acoustic radiation force were introduced, e.g. Acoustic Radiation Force Imaging (ARFI) [Nightingale et al., 2003], Supersonic Shear Imaging (SSI) [Bercoff et al., 2004], Spatially Modulated Ultrasound Radiation Force (SMURF) [McAleavey et al., 2007] and Comb-push Ultrasound Shear Elastography (CUSE) [Song et al., 2012].
ARF-driven SWE techniques are based on three main steps. First, an acoustic radiation force source is used to remotely induce shear wave propagation in the tissue (Figure 2.1). We recall that in nearly-incompressible soft media, such as biological tissues, the propagation velocity of shear waves (1–10 $\mathrm{m\,s^{-1}}$) is much smaller than the velocity of pressure waves (1500 $\mathrm{m\,s^{-1}}$). ARF is obtained from the emission of a high-intensity acoustic pressure pulse at a specific tissue depth by a conventional ultrasound transducer. Shear motion is then tracked by ultrasound imaging, by emission of low-intensity pulses. Finally, tissue properties are quantitatively estimated by post-processing techniques and inversion algorithms.

The ARF phenomenon is caused by the transfer of momentum from the focused ultrasound to the medium, mainly due to wave absorption [Torr, 1984; Nightingale et al., 2002; Sarvazyan et al., 2010]. It is generally defined as a time-averaged force applied to a medium by a sound wave. The main orientation of this body force (also known as radiation pressure) is perpendicular to the probe surface. Tissue displacements are first localised close to the focus, then start propagating in the medium. Particle displacements are then oriented along the direction of propagation of the wave (pressure waves), or perpendicular to it (shear waves). Two relevant advantages of ARF-driven SWE are the highly localised motion and the full attenuation of shear waves in a few wavelengths distance from the focal point of the ultrasonic beam. This induces a narrowing of the induced strain, and excludes coupling phenomena at the surface of the tissue. Furthermore, the dynamics of the localised motion

is only defined by the parameters of acoustic excitation and the mechanical properties of the tissue, and it is not necessary to incorporate complicated modelling ingredients (e.g. specific boundary conditions), that take into account far-field interactions, to solve the forward problem. This represents a great simplification in reconstruction methods, since the quality of reconstruction can be significantly affected by errors in the definition of boundary conditions [Sarvazyan et al., 2011].

Various models to analyse the physical mechanisms responsible for ARF and remote generation of shear waves in water-like media have been proposed in the acoustics community. The first theoretical models of shear oscillations remotely induced by radiation force were presented by Rudenko et al. [1996] and Sarvazyan et al. [1998]. The models are derived in the paraxial regime from the Khokhlov-Zabolotskaya-Kuznetsov (KZK) equation. In that context, we refer to Zabolotskaya et al. [2004]; Gennisson et al. [2007] for a derivation of an evolution equation for shear waves in an isotropic soft medium. A substantial contribution in this subject is also due to E. Dontsov and B. B. Guzina. In more detail, they have derived an expression of the body force generated by a high-intensity, focused ultrasound signal, modulated by a low-frequency signal, induced in a Newtonian fluid Dontsov and Guzina [2011], or and isotropic, viscoelastic, homogeneous solid with heat conduction Dontsov and Guzina [2012]. To do so, they split the temporal variable into a "fast" (associated with the high-frequency pulse) and "slow" component (related to the ultrasound modulation), they consider that the pressure wave has a specific structure, it is a quasi-plane wave or a focused-beam and they perform a linearisation around an equilibrium state. Moreover, assuming some a-priori properties of the solution, they derive the nonlinear acoustic ARF source term. Furthermore, they have analysed the discrepancy of the solution with respect to the classical solution of the KZK equation, due to the effects of modulation Dontsov and Guzina [2013]. The role of inhomogeneity and viscosity in the generation of shear waves is analysed in Ostrovsky et al. [2007], and a theoretical model for shear stress and shear motion in an isotropic solid is presented, under the hypothesis of quasi-longitudinal, quasi-harmonic wave, with varying amplitude and phase, due to inhomogeneity. It is also proved that an acoustic field in a purely elastic (non-dissipative) homogeneous and nonlinear solid cannot generate shear motion.

Nonetheless, there is still a lack of a complete mathematical analysis of all the phenomena involved in the ARF and the related shear wave generation, in particular when complex soft tissues are considered, such as a fibered muscle tissue. In fact, for finite element computations – as [Palmeri et al., 2005; Caenen, 2018] – , some restrictive assumptions are made to derive a simple expression for the resulting body force. In particular, if the tissue is modelled as a linear viscous fluid and under plane wave assumption, the expression for the ARF is approximated as a gaussian profile centred around a focalisation point, namely

$$\underline{F}(x,y,z,t) \coloneqq A_{\max}\, \underline{g}(x,y,z,t),$$

with

$$A_{\max} = \frac{2\,\alpha_p\, I_{\max}}{v_p}, \tag{2.1}$$

where α_p is a coefficient accounting for acoustic attenuation, $I_{\max}$ is a time-averaged acoustic intensity, and v_p is the longitudinal wave velocity. The field $\underline{g}$ is a smooth function with compact support centred at the focal point (x_F, y_F, z_F) multiplied by a smooth function with compact support in time; most often, a Gaussian profile is used for both functions:

$$\underline{g}(x,y,z,t) \coloneqq \exp^{-\left(\frac{(x-x_F)^2}{\sigma_x^2}+\frac{(y-y_F)^2}{\sigma_y^2}+\frac{(z-z_F)^2}{\sigma_z^2}\right)} \cdot \exp^{-\frac{(t-t_{pulse})^2}{\sigma_t^2}} \underline{e}_z,$$

with $\underline{e}_z = (0, 0, 1)$. In this chapter, we introduce a new methodology to analyse the ARF and provide a new perspective on the understanding and practical simulation of this phenomenon. Our aim is to formally derive and justify by asymptotic analysis the expression of the excitation induced by the ARF in a nonlinear solid. The proposed formulation is valid for media undergoing large deformation, independently from the nature of the prestress. Furthermore, one originality of this work lies in the absence of simplifying hypotheses on the properties of the emitted pressure waves. For example, in [Rudenko et al., 1996; Sarvazyan et al., 1998; Zabolotskaya et al., 2004; Gennisson et al., 2007] the expression of the ARF is deduced from the KZK equation under the assumption that a specific paraxial approximation is valid. We refer to [Destrade et al., 2010] for a derivation of these equations from the nonlinear elastodynamics equation. Note that in cardiac elastography the wave propagation induced by the ARF is superposed to the nonlinear mechanics associated with the heart deformation during the cardiac cycle.
In particular, in the context of an accurate nonlinear biomechanical model adequately representing the complex state of the myocardium, we provide a rigorous model for

- the expression of the surface source term (focused ultrasound beam);
- the pressure wave propagation induced by the ARF excitation;
- the shear wave propagation generated by the ARF.

The approach we propose consists in considering a family of problems, parametrised by a small parameter ε inversely proportional to the excitation frequency of the probes, the viscosity and the velocity of pressure wave propagation. We formulate a stability estimate, based on energy considerations, from which we retrieve some useful properties of the solution, that lead to further simplifications of its expression. Subsequently, a regular asymptotic expansion of the solution is proposed, and each term of the expansion is further decomposed into a potential - curl-free - and a rotational - divergence-free - component, and into a fast-oscillating and slow-varying term. We assume, indeed, that two time variables can be distinguished: one slow, related to the nonlinear mechanics and the shear wave propagation, and a fast one, associated with the pressure wave induced by the ARF excitation. In order to derive a simplified model for the expression of ARF, we approximate the solution by the first terms of the asymptotic expansion, and we insert this approximation in the elastodynamics equation. Then, we identify and solve the equations proportional to the same order of ε.
By doing so, we show that the leading-order term of the expansion is the underlying nonlinear cardiac mechanics, the electrical activation of the heart being the corresponding source term. Afterwards, two corrector terms are computed. The first consists in a fast-oscillating pressure wave excited by the probes, and we show that it is the solution of a Helmholtz equation at every time. The second corrector term is an elastic field with prescribed divergence, having as a source term a function of the first corrector. This field corresponds to the shear acoustic wave induced by the ARF. As a by-product of our analysis, we prove that, in prestressed media, the presence of viscosity is essential to produce shear waves with ARF. Furthermore, they are related to the nonlinearity of the partial differential equation (PDE).

Note that the approach adopted is based on 2-scale homogenisation techniques – that are standard for the space variable – for the time variable. The use of 2 time scales is not original for this problem (see Dontsov and Guzina [2012]). Furthermore, we emphasise that the results are obtained by considering a family of problems parametrised by ε, that is inversely proportional to the excitation frequency of the probes, the viscosity and the velocity of pressure wave propagation. To our knowledge, this corresponds to the

minimal set of assumptions necessary to understand, by asymptotic methods, the ARF phenomenon. By doing so, we avoid the standard simplifying hypotheses on the properties of the emitted pressure waves. For instance, in [Sarvazyan et al., 1998; Rudenko et al., 1996; Zabolotskaya et al., 2004; Gennisson et al., 2007] the expression of the ARF is deduced under the assumption that paraxial approximations are valid. In addition, we consider a general constitutive law for hyperelastic, nonlinear soft tissues that can be heterogeneous and anisotropic, and the formulation proposed in this work is valid for media undergoing large deformation, independently from the nature of the prestress. Since one of our applications is the cardiac setting, we also consider the electric activation of the muscle fibres responsible for the heart contraction. Finally, we also derive an original expression of the ARF that is compatible with standard Finite Element (FE) computations, allowing to overcome the standard assumptions that are made on the resulting body force: typically, a gaussian profile centred around a focalisation point (see [Palmeri et al., 2005; Caenen, 2018]). More precisely, we show that the computation of the ARF source term involves the solution of a scalar Helmholtz problem in the frequency domain at each time instant of the shear wave propagation.

The chapter is organised as follows. First, some preliminary notions on the elastodynamic problem and our mathematical approach are provided in Section 2.2. In more detail, the constitutive law of an anisotropic, viscoelastic, quasi-incompressible, hyperelastic medium is introduced in terms of its invariants in Section 2.2.1. Then, a family of problems is proposed in Section 2.2.2. A stability estimate is proved for such problems in Section 2.3. Section 2.4.1 is devoted to the definition of a regular asymptotic expansion of the solution, and in Section 2.4.3 the nonlinear equation for the limit term of the expansion and the equation for the higher-order correctors are derived by linearisation in a general framework. The main contributions of this work are summarised in Section 2.4.4. The methodological approach used to retrieve our formulation is detailed in Section 2.5. In particular, some preliminary algebraic manipulations and considerations are outlined in Section 2.5.1. Then, the terms corresponding to the same order of ε are identified and solved, leading to the derivation of the equation satisfied by the leading-order term in the expansion, associated with the nonlinear mechanics (Section 2.5.4), and the governing equation for the higher-order terms, that correspond to the fast-oscillating pressure waves (Section 2.5.5) and slow-oscillating shear waves generated by the ARF excitation (Section 2.5.7). A detailed expression of the source term responsible for shear wave propagation is provided, and it is shown that it is associated with the viscosity and the tissue nonlinearities. Section 2.6 is devoted to further considerations and detail on some theoretical results.

2.2 A 3D nonlinear model for ARF and elastic wave propagation in a prestressed soft tissue

The starting point of our analysis is the fundamental equation of elastodynamics in the cardiac setting. For simplicity of analysis, we consider a smooth, bounded, convex, domain $\Omega_0 \subset \mathbb{R}^3$, that corresponds to some region of the domain under investigation. As given in Chapelle et al. [2012], we use the following variational formulation to describe the nonlinear cardiac mechanics in the Lagrangian framework: Given an admissible functional space $\mathcal{X}$,

for all $t \in [0,T]$, find $\underline{y}(t) \in \mathcal{X}$ such that $\forall \underline{w} \in \mathcal{X}$

$$\begin{cases} \displaystyle\int_{\Omega_0} \rho_0\, \partial_t^2 \underline{y} \cdot \underline{w}\, \mathrm{d}\Omega_0 + \int_{\Omega_0} \underline{\underline{\Sigma}} : d_{\underline{y}} \underline{\underline{e}} \cdot \underline{w}\, \mathrm{d}\Omega_0 = \int_{\Gamma_{N,0}} \underline{\mathrm{t}} \cdot \underline{w}\, \mathrm{d}S_0 + \int_{\Omega_0} \rho_0\, \underline{f} \cdot \underline{w}\, \mathrm{d}\Omega_0, \\ \underline{y}\big|_{\Gamma_{0,D}} = \underline{0}, \\ \underline{y}(0) = \underline{0}, \quad \partial_t \underline{y}(0) = \underline{0}. \end{cases} \tag{2.2}$$

We recall that $\underline{\underline{e}}$ is the Green-Lagrange strain tensor and it reads

$$\underline{\underline{e}} = \frac{1}{2}\Big(\underline{\underline{\nabla}}\, \underline{y} + \big(\underline{\underline{\nabla}}\, \underline{y}\big)^T + \big(\underline{\underline{\nabla}}\, \underline{y}\big)^T \cdot \underline{\underline{\nabla}}\, \underline{y} \Big).$$

Furthermore, $d_{\underline{y}} \underline{\underline{e}}$ is the derivative of the Green-Lagrange tensor with respect to the displacement and is given by

$$d_{\underline{y}} \underline{\underline{e}} \cdot \underline{w} = \frac{1}{2}\Big(\big(\underline{\underline{\nabla}}\, \underline{w}\big)^T \cdot \underline{\underline{F}} + \underline{\underline{F}}^T \cdot \underline{\underline{\nabla}}\, \underline{w} \Big),$$

where $\underline{\underline{F}}$ is the deformation gradient $\underline{\underline{F}} = \underline{\underline{\mathbb{1}}} + \underline{\underline{\nabla}}\, \underline{y}$. Moreover, $\underline{\underline{\Sigma}}$ is the Second Piola-Kirchhoff stress tensor accounting for total stress, and $\underline{\mathrm{t}}_0$ accounts for the surface excitation on the boundary $\Gamma_{N,0}$, due to the piezoelectric probes. The operator "$\cdot$" corresponds to scalar product, whereas ":" stands for dyadic product. Note that $\underline{f}$ represents generic external volume forces (e.g. gravity) per unit volume, and we set it to zero for the sake of simplicity.

2.2.1 Constitutive law

For muscle tissues, it is standard to consider a constitutive law that is composed of two contributions, accounting for passive and active stress. Therefore, we define

$$\underline{\underline{\Sigma}} = \underline{\underline{\Sigma}}^P + \underline{\underline{\Sigma}}^A.$$

As far as the passive term is concerned, we consider a visco-hyperelastic medium, and therefore we can express

$$\underline{\underline{\Sigma}}^P = \frac{\partial W^e}{\partial \underline{\underline{e}}} + \frac{\partial W^{\mathrm{VS}}}{\partial \dot{\underline{\underline{e}}}}, \tag{2.3}$$

with W^e the hyperelastic potential and W^{VS} the viscous pseudo-potential. For cardiac modelling, we take into account a hyperelastic potential composed of a term accounting for a transversely isotropic (TI) law, and a penalisation term related to nearly-incompressibility (NI) [Chapelle et al., 2012]. If we define the jacobian of the deformation $J = \det \underline{\underline{F}}$ and the right *Cauchy-Green deformation tensor* $\underline{\underline{C}} = \underline{\underline{F}}^T \cdot \underline{\underline{F}} = \underline{\underline{\mathbb{1}}} + 2\,\underline{\underline{e}}$, we introduce

$$W^e := W^{\mathrm{TI}} + W^{\mathrm{NI}}, \tag{2.4}$$

where W^{TI} and W^{NI} read

$$W^{\mathrm{TI}} = \kappa_1\, e^{\kappa_2 (I_1 - 3)^2} + \kappa_3\, e^{\kappa_4 (I_4 - 1)^2} + \kappa_5 \big(I_2 - 2\log(J^2) - 3\big), \tag{2.5}$$

$$W^{\mathrm{NI}} = \frac{\kappa}{2}\big((J^2 - 1) - \log\big(J^2\big)\big) = \frac{\kappa}{2}\big((I_3 - 1) - \log(I_3)\big). \tag{2.6}$$

We recall that the *invariants* concerned in Eq. (2.5) and (2.6) read

$$I_1 = \left|\underline{\underline{F}}\right|^2 = \mathrm{tr}\left(\underline{\underline{C}}\right), \quad I_2 = \left|\mathrm{adj}\,\underline{\underline{F}}\right|^2 = \mathrm{tr}\left(\mathrm{adj}\,\underline{\underline{C}}\right) = \frac{1}{2}\Big(\left(\mathrm{tr}\left(\underline{\underline{C}}\right)\right)^2 - \mathrm{tr}\left(\underline{\underline{C}}^2\right)\Big)$$
$$I_3 = \det\,\underline{\underline{C}} = \left(\det\,\underline{\underline{F}}\right)^2, \quad I_4 = \underline{\tau_1}\cdot\underline{\underline{C}}\cdot\underline{\tau_1}, \tag{2.7}$$

where $\underline{\tau_1}(\underline{\xi})$ is the – space-dependent – fibre direction. Note that the norm operator $|\cdot|$ denotes the euclidean norm in $\mathbb{R}^d$ or the Frobenius norm $\mathbb{R}^{d\times d}$, accordingly. Note that we consider here a slightly different expression for W^{TI} and W^{NI} than in Chapter 1. This choice is justified by stability requirements, as we will show in what follows. Finally, the viscous pseudo-potential reads

$$W^{\mathrm{VS}} := \frac{\zeta}{2}\,\mathrm{tr}\left(\underline{\underline{C}}^{-1}\cdot\underline{\underline{\dot{e}}}\right)^2, \quad \text{with} \quad \underline{\underline{\dot{e}}} := d_{\underline{y}}\underline{\underline{e}}\cdot\partial_t\underline{y} = \frac{1}{2}\Big(\left(\underline{\underline{\nabla}}\partial_t\underline{y}\right)^T\cdot\underline{\underline{F}} + \underline{\underline{F}}^T\cdot\underline{\underline{\nabla}}\partial_t\underline{y}\Big). \tag{2.8}$$

We emphasize that the expression of W^{VS} in Eq. (2.8) implies that the viscous effects only affect the pressure wave (in the deformed configuration it is a contribution on the divergence of $\underline{\dot{y}}$), for the sake of simplicity. However, the contribution of viscosity could be extended to the shear wave, and in this case more complex effects would impact shear wave propagation. Then, we define

$$\underline{\underline{\Sigma}}^{\mathrm{TI}} := \frac{\partial W^{\mathrm{TI}}}{\partial\,\underline{\underline{e}}}, \quad \underline{\underline{\Sigma}}^{\mathrm{NI}} := \frac{\partial W^{\mathrm{NI}}}{\partial\,\underline{\underline{e}}}, \quad \text{and} \quad W^{\mathrm{VS}} := \frac{\partial W^{\mathrm{VS}}}{\partial\,\underline{\underline{\dot{e}}}}.$$

For the active term, we define a simple constitutive law, and suppose that the stress tensor is only oriented along the fibre direction. Namely, we set

$$\underline{\underline{\Sigma}}^{A} = \sigma_a\,\underline{\tau_1}\otimes\underline{\tau_1}. \tag{2.9}$$

Note that $\underline{\underline{\Sigma}}^{A}$ does not depend on the displacement $\underline{y}$ and it represents a nonlinear source term for Problem 2.2. Henceforth, we provide a stability estimate of the solution $\underline{y}$ of Eq. (2.2).

2.2.2 Definition of a parametric family of problems

In nearly-incompressible soft media, such as biological tissues, the propagation velocity of shear waves (1–10 $\mathrm{m\,s^{-1}}$) is much smaller than the velocity of pressure waves (1500 $\mathrm{m\,s^{-1}}$). As a result, we can consider a family of problems, parametrised by a small parameter ε related to the ratio between the two wave velocities.
First, we rewrite the bulk modulus as

$$\kappa = \varepsilon^{-2}\hat{\kappa}, \tag{2.10}$$

where $\hat{\kappa}$ is a normalised parameter and ε is dimensionless. Since experimental evidence suggests that pressure waves are also localised, we also hypothesise that the viscosity coefficient satisfies

$$\zeta = \varepsilon^{-1}\,\hat{\zeta},$$

where $\hat{\zeta}$ is a normalised parameter.
Moreover, our asymptotic analysis of the ARF relies on the assumption that the source term - generated by the piezoelectric sensors - is of high frequency ω. From experimental

evidence, we set the ultrasound frequency proportional to the viscosity coefficient [Ostrovsky et al., 2007]. In particular, given a normalised frequency $\hat{\omega}$, such that $\hat{\omega} = \varepsilon\,\omega > 0$, we define

$$\underline{\mathrm{t}}_\varepsilon(\underline{\xi}, t) \coloneqq p(\underline{\xi}, t)\,\cos(\hat{\omega}\,t/\varepsilon)\,J\,\big|\underline{\underline{F}}^{-T}\cdot\underline{n}_0\big|\underline{\underline{F}}^{-T}\cdot\underline{n}_0, \tag{2.11}$$

where $\underline{n}_0$ is the outward unitary normal of Ω_0 and $p \in C^0\big([0,T]; H^{\frac{1}{2}}(\Gamma_0)\big)$ is a smooth, space and time-dependent pressure term representing the action of the probes at the boundary and

$$\omega = \varepsilon^{-1}\,\hat{\omega}.$$

Note that the vector $\underline{\mathrm{t}}_0$ is collinear with $\underline{\underline{F}}^{-T}\cdot\underline{n}_0$, that corresponds to the outward normal of the domain $\Omega(t)$.
We denote by $\underline{y}_\varepsilon$ the family of solutions in $\mathcal{X}$ associated with Eq. (2.2) with the definitions above, and we define the deformation gradient $\underline{\underline{F}}_\varepsilon$, the Cauchy-Green stress tensor $\underline{\underline{C}}_\varepsilon$, the invariant J_ε and the second Piola-Kirchhoff stress tensor $\underline{\underline{\Sigma}}_\varepsilon$ associated with the solution $\underline{y}_\varepsilon$.
We also assume that $\underline{f} \in C^0\big([0,T]; (L^2(\Omega_0))^3\big)$. Then, the variational formulation reads: Find, for all $t \in [0,T]$, a function $\underline{y}_\varepsilon(t) \in \mathcal{X}$ such that for all $\underline{w} \in \mathcal{X}$

$$\begin{aligned}
&\int_{\Omega_0} \rho_0\,\partial_t^2\underline{y}_\varepsilon\cdot\underline{w}\,\mathrm{d}\Omega_0 + \int_{\Omega_0}\big(\underline{\underline{\Sigma}}_\varepsilon^{\mathrm{TI}} + \underline{\underline{\Sigma}}_\varepsilon^{\mathrm{NI}} + \underline{\underline{\Sigma}}_\varepsilon^{\mathrm{VS}}\big) : d_{\underline{y}_\varepsilon}\underline{\underline{e}}\cdot\underline{w}\;\mathrm{d}\Omega_0 \\
&= -\int_{\Omega_0}\underline{\underline{\Sigma}}^A : d_{\underline{y}_\varepsilon}\underline{\underline{e}}\cdot\underline{w}\;\mathrm{d}\Omega_0 + \int_{\Omega_0}\rho_0\,\underline{f}\cdot\underline{w}\;\mathrm{d}\Omega_0 + \int_{\Gamma_{N,0}}\underline{\mathrm{t}}_\varepsilon\cdot\underline{w}\,\mathrm{d}S_0,
\end{aligned} \tag{2.12}$$

with vanishing initial conditions

$$\begin{cases}
\underline{y}_\varepsilon\big|_{\Gamma_{0,D}} = \underline{0}, \\
\underline{y}_\varepsilon(0) = \underline{0}, \quad \partial_t\underline{y}_\varepsilon(0) = \underline{0}.
\end{cases}$$

Assumption 2.1. *For all $\varepsilon > 0$ sufficiently small, there exists a unique smooth solution $\underline{y}_\varepsilon$ to Eq. (2.12) satisfying*

$$\underline{y}_\varepsilon \in \Big(C^2\big([0,T]\times\overline{\Omega_0}\big)\Big)^3, \qquad \det\big(\underline{\underline{\mathbb{1}}} + \underline{\underline{\nabla}}_{\underline{\xi}}\,\underline{y}_\varepsilon\big) > 0.$$

Note that this assumption may not be optimal. One could expect a similar result in a less regular space, as

$$\mathcal{X} \coloneqq \{\underline{v} \in \big(W^{1,p}(\Omega_0)\big)^3 \mid \underline{v} = 0 \text{ in } \Gamma_{0,D}\},\ p > 2.$$

However, for the sake of simplicity, we choose to state Assumption 2.1 in order to derive our main results.

2.3 Stability estimates

In this section, we retrieve some energy estimates allowing to derive some interesting properties of the solution $\underline{y}_\varepsilon$. Choosing the actual velocity $\partial_t\underline{y}_\varepsilon$ as a test function, we obtain the following energy balance (see Chapelle et al. [2012])

$$\frac{\mathrm{d}\mathcal{E}_\varepsilon^{tot}}{\mathrm{d}t} + \mathcal{E}_\varepsilon^{\mathrm{VS}} + \mathcal{E}_\varepsilon^{A} = \mathcal{P}_\varepsilon^{ext} + \mathcal{P}_\varepsilon^{A}, \tag{2.13}$$

where the total energy $\mathcal{E}_\varepsilon^{tot}$ reads

$$\mathcal{E}_\varepsilon^{tot} = \mathcal{K}_\varepsilon + \mathcal{E}_\varepsilon^{\mathrm{TI}} + \mathcal{E}_\varepsilon^{\mathrm{NI}},$$

and the kinetic and potential energy associated with the hyperelastic term and nearly-incompressibility are given by

$$\begin{aligned}\mathcal{K}_\varepsilon &= \frac{\rho_0}{2}\int_{\Omega_0} |\underline{\dot{y}}_\varepsilon|^2 \,\mathrm{d}\Omega_0, \qquad \mathcal{E}_\varepsilon^{\mathrm{TI}} = \int_{\Omega_0} W_\varepsilon^{\mathrm{TI}} \,\mathrm{d}\Omega_0,\\ \mathcal{E}_\varepsilon^{\mathrm{NI}} &= \varepsilon^{-2}\frac{\hat{\kappa}}{2}\int_{\Omega_0} \left((J_\varepsilon^2 - 1) - \log\left(J_\varepsilon^2\right)\right) \mathrm{d}\Omega_0.\end{aligned}$$

The contribution related to viscous losses reads

$$\mathcal{E}_\varepsilon^{\mathrm{VS}} = \varepsilon^{-1}\,\hat{\zeta}\int_{\Omega_0} \mathrm{tr}\left(\underline{\underline{C}}_\varepsilon^{-1}\cdot\underline{\underline{\dot{e}}}_\varepsilon\right)^2 \mathrm{d}\Omega_0 = \varepsilon^{-1}\,\hat{\zeta}\int_{\Omega_0} \mathrm{tr}\left(\underline{\underline{F}}_\varepsilon^{-1}\cdot\underline{\underline{\nabla}}_{\underline{\xi}}\,\underline{\dot{y}}_\varepsilon\right)^2 \mathrm{d}\Omega_0,$$

whereas the source term contributions are given by

$$\begin{aligned}\mathcal{P}_\varepsilon^{ext} &= \int_{\Gamma_{N,0}} \underline{\mathrm{t}}_\varepsilon\cdot\underline{\dot{y}}_\varepsilon \,\mathrm{d}S_0 = \int_{\Gamma_{N,0}} p\,\cos(\hat{\omega}\,t/\varepsilon)\,J_\varepsilon\left|\underline{\underline{F}}_\varepsilon^{-T}\cdot\underline{n}_0\right|\underline{\underline{F}}_\varepsilon^{-T}\cdot\underline{n}_0\cdot\underline{\dot{y}}_\varepsilon\,\mathrm{d}S_0,\\ \mathcal{P}_\varepsilon^{A} &= \sigma_a\int_{\Omega_0}\underline{\tau_1}\cdot\underline{\underline{\dot{e}}}\cdot\underline{\tau_1}\,\mathrm{d}\Omega_0,\end{aligned}$$

In order to demonstrate that the energy $\mathcal{E}_\varepsilon^{tot}$ is uniformly bounded with respect to ε, we first need to formulate an estimate for the term $\mathcal{P}_\varepsilon^{ext}$. To do so, we assume extra regularity on p and the domain $\overline{\Omega_0}$ to be able to define a smooth lifting operator of p. More precisely, we do the following assumption.

Assumption 2.2. *We assume that there exists $\ell \in C^0\big([0,T];\mathcal{W}^{1,\infty}(\Omega_0)\big)$ i.e.*

$$|||\ell||| \coloneqq \sup_{t\in[0,T]}\ \operatorname*{ess\,sup}_{\underline{\xi}\in\overline{\Omega_0}}\left(\left|\ell(\underline{\xi},t)\right| + \left|\underline{\nabla}_{\underline{\xi}}\,\ell(\underline{\xi},t)\right|\right) < +\infty$$

such that

$$\forall t\in[0,T]\quad \ell(\cdot,t)|_{\Gamma_0} = p(\cdot,t). \tag{2.14}$$

In order to have an estimate on $\mathcal{P}_\varepsilon^{ext}$, we first need to rewrite this term as a volume integral. To do so, we apply Green's formula, and obtain the result of the following lemma.

Lemma 2.3. *If Assumption 2.2 holds, then the term $\mathcal{P}_\varepsilon^{ext}$ accounting for the surface source term can be rewritten as*

$$\begin{aligned}\mathcal{P}_\varepsilon^{ext} = &\int_{\Omega_0} J_\varepsilon\,\cos(\hat{\omega}\,t/\varepsilon)\ \mathrm{tr}\left(\underline{\underline{F}}_\varepsilon^{-1}\cdot\underline{\underline{\nabla}}_{\underline{\xi}}\,\underline{\dot{y}}_\varepsilon\right)\ell\,\mathrm{d}\Omega_0\\ &+\int_{\Omega_0} J_\varepsilon\,\cos(\hat{\omega}\,t/\varepsilon)\,\underline{\dot{y}}_\varepsilon\cdot\left(\underline{\underline{F}}_\varepsilon^{-T}\cdot\underline{\nabla}_{\underline{\xi}}\ell\right)\mathrm{d}\Omega_0.\end{aligned} \tag{2.15}$$

We can now state the following stability estimate.

Proposition 2.4. *Let ε small enough. Then, there exists a constant $C > 0$ independent of ε such that*

$$\mathcal{E}_\varepsilon^{tot}(t) \leq C \quad \forall t \in [0, T].$$

In particular, $\forall t \in [0, T]$,

$$\int_{\Omega_0} \left((J_\varepsilon^2 - 1) - \log\left(J_\varepsilon^2\right) \right) \mathrm{d}\Omega_0 \leq \varepsilon^2 C, \tag{2.16}$$

$$\int_0^t \left\| \mathrm{tr}\left(\underline{\underline{C}}_\varepsilon^{-1} \cdot \dot{\underline{\underline{e}}}_\varepsilon \right) \right\|^2_{L^2(\Omega_0)} \mathrm{d}s \leq \varepsilon C. \tag{2.17}$$

Proofs of Lemma 2.3 and Proposition 2.4 can be found in Sections 2.6.1 and 2.6.2. As a consequence of Proposition 2.4, we deduce that at the limit $\varepsilon \to 0$, we obtain that J_ε tends to one in Ω.

2.4 Asymptotic expansion of the solution

2.4.1 Definition of a power series expansion

We look for a regular asymptotic expansion of the solution of Eq. (2.12), i.e. we assume that $\underline{y}_\varepsilon$ can be written using a power series expansion in ε. We suppose that there exists $N \in \mathbb{N}$ such that the solution $\underline{y}_\varepsilon$ can be decomposed, for all ε sufficiently small, as

$$\underline{y}_\varepsilon(\underline{\xi}, t) = \sum_{i=0}^{N} \varepsilon^i \, \underline{y}_i(\underline{\xi}, t, t/\varepsilon) + \varepsilon^N \, \underline{r}_\varepsilon, \qquad \forall \underline{\xi} \in \Omega_0, \ \forall t \in [0, T], \tag{2.18}$$

with

$$\lim_{\varepsilon \to 0} \sup_{\underline{\xi}, t} \left(\|\underline{r}_\varepsilon\| + \|\partial_t \underline{r}_\varepsilon\| + \left\|\underline{\underline{\nabla}}_{\underline{\xi}} \underline{r}_\varepsilon\right\| \right) = 0,$$

with $\underline{r}_\varepsilon$ is smooth and $\lim_{\varepsilon \to 0} \|\underline{r}_\varepsilon\|$ for an adequate norm $\|\cdot\|$. We assume that every term $\underline{y}_i$ of the power series is periodic in $\tau = t/\varepsilon$, with period $2\,\pi/\hat{\omega}$ (this is suggested by the structure of the source term). Furthermore, we assume that all components $\underline{y}_i(\underline{\xi}, t, \tau)$ are regular enough in τ and, as a consequence, all $\partial \underline{y}_i / \partial \tau$ are periodic in τ.
The idea is to approximate the solution $\underline{y}_\varepsilon$ by the first terms of expansion (2.18). By doing so, we recover the limit (asymptotic) behaviour of the solution $\underline{y}_\varepsilon$ for $\varepsilon \to 0$. In practice, we substitute the expression of $\underline{y}_\varepsilon$ presented in Eq. (2.18) in Problem (2.12). To do so, all mechanical quantities must be rewritten in series form, accordingly. Furthermore, we shall use the following expansion of the second derivative in time for every term in Eq. (2.18):

$$\partial_t^2 \underline{y}_i(\underline{\xi}, t, t/\varepsilon) = \left(\varepsilon^{-2} \, \partial_\tau^2 \underline{y}_i + 2\varepsilon^{-1} \partial_{t\tau}^2 \underline{y}_i + \varepsilon^0 \, \partial_t^2 \underline{y}_i\right)(\underline{\xi}, t, t/\varepsilon).$$

Once all the terms of the expansion are obtained and inserted in Eq. (2.12), the equations proportional to the same order of ε are identified. Note that this approach represents an application of a methodology for homogenisation which is standard in the spatial domain [Lions et al., 1978].

We show that the ARF is a nonlinear phenomenon that occurs at a higher order of approximation. More precisely, we will show that the leading-order term in Eq. (2.18) corresponds to the underlying nonlinear mechanical behaviour of the solution. Then, the first two correctors are computed, and they correspond to:

- a fast-oscillating pressure wave generated by the piezoelectric probes, solution of a Helmholtz equation at every time;
- an elastic field with prescribed divergence, having as a source term a function of the first corrector. This field corresponds to the shear acoustic wave induced by the ARF (and it is divergence-free in case of no prestress).

2.4.2 Expansion of mechanical quantities

Henceforth, we introduce several definitions that are related to the linearisation of nonlinear mechanics, in order to state our main results and according to our hypothesis defined in Eq. (2.18). In particular, we derive a series expansion for all the deformation and stress tensors involved in Eq. (2.12), accordingly. For the sake of simplicity, we assume that the operations $\underline{\underline{\nabla}}$, $\underline{\nabla}$, Δ, div and $\underline{\mathrm{div}}$ are performed in the reference configuration, if not specified.

Deformation tensors. From Eq. (2.18), we can rewrite the deformation gradient

$$\underline{\underline{F}}_\varepsilon := \underline{\underline{\mathbb{1}}} + \underline{\underline{\nabla}}\,\underline{y}_\varepsilon = \underline{\underline{F}}_0 + \sum_{i=1}^{N} \varepsilon^i \underline{\underline{\nabla}}\,\underline{y}_i + o(\varepsilon^N), \quad \text{with} \quad \underline{\underline{F}}_0 := \underline{\underline{\mathbb{1}}} + \underline{\underline{\nabla}}\,\underline{y}_0.$$

Consequently, the Green-Lagrange tensor reads

$$\underline{\underline{e}}_\varepsilon := \frac{1}{2}\Big(\underline{\underline{\nabla}}\,\underline{y}_\varepsilon + \big(\underline{\underline{\nabla}}\,\underline{y}_\varepsilon\big)^T + \big(\underline{\underline{\nabla}}\,\underline{y}_\varepsilon\big)^T \cdot \underline{\underline{\nabla}}\,\underline{y}_\varepsilon\Big) = \underline{\underline{e}}_0 + \sum_{i=1}^{N} \varepsilon^i \underline{\underline{e}}_0(\underline{y}_i) + \sum_{\substack{i+j=2 \\ i,j>0}}^{N} \varepsilon^{i+j} \big(\underline{\underline{\nabla}}\,\underline{y}_i\big)^T \cdot \underline{\underline{\nabla}}\,\underline{y}_j + o(\varepsilon^N),$$

with

$$\underline{\underline{e}}_0 := \frac{1}{2}\big(\underline{\underline{F}}_0^T \cdot \underline{\underline{F}}_0 - \underline{\underline{\mathbb{1}}}\big) = \frac{1}{2}\big(\underline{\underline{\nabla}}\,\underline{y}_0 + \big(\underline{\underline{\nabla}}\,\underline{y}_0\big)^T + \big(\underline{\underline{\nabla}}\,\underline{y}_0\big)^T \cdot \underline{\underline{\nabla}}\,\underline{y}_0\big),$$

and, for any vector field $\underline{w}$,

$$\underline{\underline{e}}_0(\underline{w}) := \frac{1}{2}\big(\underline{\underline{F}}_0^T \cdot \underline{\underline{\nabla}}\,\underline{w} + \big(\underline{\underline{\nabla}}\,\underline{w}\big)^T \cdot \underline{\underline{F}}_0\big) = \frac{1}{2}\big(\underline{\underline{\nabla}}\,\underline{w} + \big(\underline{\underline{\nabla}}\,\underline{w}\big)^T + \big(\underline{\underline{\nabla}}\,\underline{y}_0\big)^T \cdot \underline{\underline{\nabla}}\,\underline{w} + \big(\underline{\underline{\nabla}}\,\underline{w}\big)^T \cdot \underline{\underline{\nabla}}\,\underline{y}_0\big).$$

With the same assumptions, we obtain for any vector field $\underline{w}$

$$d_{\underline{y}_\varepsilon}\underline{\underline{e}} \cdot \underline{w} = \frac{1}{2}\Big(\big(\underline{\underline{\nabla}}\,\underline{w}\big)^T \cdot \underline{\underline{F}}_\varepsilon + \underline{\underline{F}}_\varepsilon^T \cdot \underline{\underline{\nabla}}\underline{w}\Big) := \underline{\underline{e}}_0(\underline{w}) + \sum_{i=1}^{N} \varepsilon^i\, \underline{\underline{e}}_i(\underline{w}) + o(\varepsilon^N),$$

where

$$\underline{\underline{e}}_i(\underline{w}) := \frac{1}{2}\big(\big(\underline{\underline{\nabla}}\,\underline{y}_i\big)^T \cdot \underline{\underline{\nabla}}\,\underline{w} + \big(\underline{\underline{\nabla}}\,\underline{w}\big)^T \cdot \underline{\underline{\nabla}}\,\underline{y}_i\big).$$

Analogously, the Cauchy-Green deformation tensor reads

$$\underline{\underline{C}}_\varepsilon := \underline{\underline{\mathbb{1}}} + 2\,\underline{\underline{e}}_\varepsilon = \underline{\underline{C}}_0 + \sum_{i=1}^{N} \varepsilon^i\, \underline{\underline{C}}_i + o(\varepsilon^N),$$

with

$$\underline{\underline{C}}_0 := (\underline{\underline{\mathbb{1}}} + 2\,\underline{\underline{e}}_0), \qquad \underline{\underline{C}}_1 := 2\,\underline{\underline{e}}_0(\underline{y}_1),$$

and we do not give the expression of the higher-order terms for the moment, for the sake of simplicity. The inverse of the Cauchy-Green deformation tensor can be rewritten, at the limit as ε tends to zero, as

$$\underline{\underline{C}}_{\varepsilon}^{-1} = \underline{\underline{C}}_{0}^{-1} + \sum_{i=1}^{N} \varepsilon^{i}\, \underline{\underline{G}}_{i} + o(\varepsilon^{N}), \qquad \text{with} \quad \underline{\underline{C}}_{0}^{-1} := (\underline{\underline{\mathbb{1}}} + 2\,\underline{\underline{e}}_{0})^{-1},$$

and we do not detail for the moment the expression of $\underline{\underline{G}}_{i}$ for $i \geq 1$.
Furthermore, the invariant J_{ε} can be rewritten as

$$J_{\varepsilon} := J_{0} + O(\varepsilon), \qquad \text{with} \quad J_{0} = \big(\det \underline{\underline{C}}_{0}\big)^{\frac{1}{2}}.$$

Finally, we also have

$$\underline{\mathrm{t}}_{\varepsilon} = \cos(\hat{\omega}\, t/\varepsilon)\, \underline{\mathrm{t}}_{0} + \cos(\hat{\omega}\, t/\varepsilon) \sum_{i=0}^{N} \varepsilon^{i}\, \underline{\mathrm{t}}_{i} + o\big(\varepsilon^{N}\big),$$

where the leading-order boundary source term is given by

$$\underline{\mathrm{t}}_{0}\big(\underline{\xi}, t\big) := p\big(\underline{\xi}, t\big)\, J_{0}\, \big|\underline{\underline{F}}_{0}^{-T} \cdot \underline{n}_{0}\big|\, \underline{\underline{F}}_{0}^{-T} \cdot \underline{n}_{0}.$$

Note that $\underline{\mathrm{t}}_{0}$ does not depend on ε. However, the expansion of the source term $\underline{\mathrm{t}}_{\varepsilon}$ is not polynomial in ε.

Stress tensors. The second Piola-Kirchhoff stress tensor accounting for transverse isotropy, nearly-incompressibility and viscosity can be rewritten in terms of a power series expansion, following Eq. (2.18). In more detail, $\underline{\underline{\Sigma}}_{\varepsilon}^{\mathrm{NI}}$ reads, from Eq. (2.4),

$$\underline{\underline{\Sigma}}_{\varepsilon}^{\mathrm{NI}} = \varepsilon^{-2} \frac{\hat{\kappa}}{2} (J_{\varepsilon}^{2} - 1) \underline{\underline{C}}_{\varepsilon}^{-1} = \varepsilon^{-2}\, \frac{\hat{\kappa}}{2}\, (J_{0}^{2} - 1) \underline{\underline{C}}_{0} + \frac{\hat{\kappa}}{2} \sum_{i=1}^{N} \varepsilon^{i-2}\, \underline{\underline{\Sigma}}_{i}^{\mathrm{NI}} + o(\varepsilon^{N}).$$

In a similar way, we derive the power series expansion in ε of $\underline{\underline{\Sigma}}_{\varepsilon}^{\mathrm{TI}}$

$$\underline{\underline{\Sigma}}_{\varepsilon}^{\mathrm{TI}} = \underline{\underline{\Sigma}}_{0}^{\mathrm{TI}} + \sum_{i=1}^{N} \varepsilon^{i}\, \underline{\underline{\Sigma}}_{i}^{\mathrm{TI}} + o(\varepsilon^{N}), \qquad \text{with} \quad \underline{\underline{\Sigma}}_{0}^{\mathrm{TI}} := \underline{\underline{\Sigma}}^{\mathrm{TI}}\big(\underline{\underline{e}}_{0}\big),$$

where $\underline{\underline{\Sigma}}_{0}^{\mathrm{TI}}$ is given in the Appendix. The expansion of the second Piola-Kirchhoff stress tensor $\underline{\underline{\Sigma}}_{\varepsilon}^{\mathrm{VS}}$ related to viscosity

$$\underline{\underline{\Sigma}}_{\varepsilon}^{\mathrm{VS}} = \varepsilon^{-1}\, \hat{\zeta}\, \mathrm{tr}\Big(\underline{\underline{C}}_{\varepsilon}^{-1} \cdot \dot{\underline{\underline{e}}}_{\varepsilon}\big(\underline{y}\big)\Big)\, \underline{\underline{C}}_{\varepsilon}^{-1} = \hat{\zeta} \sum_{i=0}^{N} \varepsilon^{i-2}\, \underline{\underline{\Sigma}}_{i}^{\mathrm{VS}} + o(\varepsilon^{N}).$$

Note that the series above behaves as a $O(\varepsilon^{-2})$, due to the fact that differentiation with respect to the fast time variable τ introduces another factor ε^{-1} in the expression. Finally, the stress stress tensor $\underline{\underline{\Sigma}}^{A}$ given by (2.9) is independent of ε.

The full expression of the tensors $\underline{\underline{\Sigma}}_{i}^{\mathrm{TI}}$, $\underline{\underline{\Sigma}}_{i}^{\mathrm{TI}}$ and $\underline{\underline{\Sigma}}_{i}^{\mathrm{VS}}$ is not detailed here, for the sake of compactness. In fact, we will show that their expression can be considerably simplified, due to the properties of the first terms in the expansion (2.18). More precisely, we will show that $\partial_{\tau} \underline{y}_{0} = \underline{0}$, $J_{0} = 1$ and $\underline{y}_{1} = \underline{0}$.

2.4.3 The incompressible, nonlinear heart mechanics and its linearisation

In Shear Wave Elastography, the propagation of elastic waves in a prestressed soft medium like the myocardium can be modelled as a perturbation of the underlying nonlinear incompressible heart mechanics. Henceforth, we formulate the nonlinear problem and its linearisation that govern some of the terms in the asymptotic expansion (2.18). More precisely, we will show that the perturbation associated with the shear wave propagation satisfies an equation that can be recovered by linearisation of Eq. (2.12) around a reference, time-dependent deformation state. The well-posedness properties of the two problems considered (existence/uniqueness/regularity of solutions) are not analysed but assumed instead.

Nonlinear mechanical model of heart deformation. The nonlinear, incompressible cardiac mechanics is described as follows, given an adequate function space $\mathcal{L}$:
For all $t \in [0,T]$, find $\big(\underline{y}_0(t), \mathrm{p}_0(t)\big) \in \mathcal{X} \times \mathcal{L}$ such that $\forall \underline{w} \in \mathcal{X}$

$$\begin{cases} \displaystyle\int_{\Omega_0} \rho_0\, \partial_t^2 \underline{y}_0 \cdot \underline{w}\, \mathrm{d}\Omega_0 + \int_{\Omega_0} \mathrm{p}_0\, \underline{\underline{C}}_0^{-1} : \underline{\underline{e}}_0\big(\underline{w}\big) \mathrm{d}\Omega_0 + \int_{\Omega_0} \underline{\underline{\Sigma}}_0^{\mathrm{TI}} : \underline{\underline{e}}_0\big(\underline{w}\big) \mathrm{d}\Omega_0 \\ \qquad\qquad = -\displaystyle\int_{\Omega_0} \underline{\underline{\Sigma}}^{A} : \underline{\underline{e}}_0\big(\underline{w}\big)\ \mathrm{d}\Omega_0, \\ \underline{y}_0(0) = \underline{0}, \quad \partial_t\, \underline{y}_0(0) = \underline{0}, \\ J_0 = 1, \end{cases} \tag{2.19}$$

with p_0 a Lagrange multiplier to enforce incompressibility. Typically, the space $\mathcal{L}$ is the space of square integrable zero-average scalar functions. The analysis of the existence and uniqueness of solution to Eq. (2.19) is a well-known difficult problem; as a consequence, we will state the following assumption.

Assumption 2.5. *There exists a unique couple* $(\underline{y}_0, \mathrm{p}_0)$ *solution to Eq.* (2.19) *satisfying*

$$\underline{y}_0 \in C^2\big([0,T] \times \overline{\Omega_0}\big), \qquad \det\big(\underline{\underline{\mathbb{1}}} + \underline{\underline{\nabla}}\, \underline{y}_0\big) > 0, \quad \mathrm{p}_0 \in C^0\big([0,T] \times \overline{\Omega_0}\big).$$

Furthermore, we will show that the perturbation associated with the shear wave propagation satisfies an equation that can be recovered by linearisation of Eq. (2.12) around a reference, time-dependent deformation state.

Linearised problem for the elastic perturbation. The linearisation of (2.12) around a time-dependent solution $\underline{y}_0(t)$ leads to the following linear problem: given an admissible functional space for the linearised problem $\mathcal{X}_\ell$ and $\mathcal{L}_\ell$, find, for all $t \in [0,T]$, a couple $\big(\tilde{\underline{y}}(t), \tilde{\mathrm{p}}(t)\big) \in \mathcal{X}_\ell \times \mathcal{L}_\ell$ such that for all $\underline{w} \in \mathcal{X}_\ell$ and for all $q \in \mathcal{L}_\ell$

$$\begin{cases} \displaystyle\int_{\Omega_0} \rho_0\, \partial_t^2 \tilde{\underline{y}} \cdot \underline{w}\, \mathrm{d}\Omega_0 + \int_{\Omega_0} \tilde{\mathrm{p}}\, \underline{\underline{C}}_0^{-1} : \underline{\underline{e}}_0\big(\underline{w}\big)\, \mathrm{d}\Omega_0 + a(\tilde{\underline{y}}, \underline{w}) = s(t, \underline{w}), \\ \displaystyle\int_{\Omega_0} \underline{\underline{C}}_0^{-1} : \underline{\underline{e}}_0\big(\tilde{\underline{y}}\big)\, q\, \mathrm{d}\Omega_0 = r(t,q), \\ \tilde{\underline{y}}(0) = \underline{0}, \quad \partial_t\, \tilde{\underline{y}}(0) = \underline{0}, \end{cases} \tag{2.20}$$

with

$$a(\underline{\tilde{y}},\underline{w}) = \int_{\Omega_0} \underline{\underline{e}}_0(\underline{\tilde{y}}) : \frac{\partial \underline{\underline{\Sigma}}^{\mathrm{TI}}}{\partial \underline{\underline{e}}}(\underline{y}_0) : \underline{\underline{e}}_0(\underline{w})\,\mathrm{d}\Omega_0 - 2\int_{\Omega_0} \mathrm{p}_0\,\underline{\underline{C}}_0^{-1}\cdot\underline{\underline{e}}_0(\underline{\tilde{y}}) : \underline{\underline{C}}_0^{-1}\cdot\underline{\underline{e}}_0(\underline{w})\,\mathrm{d}\Omega_0$$
$$+\int_{\Omega_0} \left(\underline{\underline{\Sigma}}_0^{\mathrm{TI}} + \underline{\underline{\Sigma}}^{A} + \mathrm{p}_0\,\underline{\underline{C}}_0^{-1}\right) : \left(\underline{\underline{\nabla}}\,\underline{\tilde{y}}\right)^T\cdot\underline{\underline{\nabla}}\,\underline{w}\,\mathrm{d}\Omega_0,$$

where $s(t,\cdot)$ and $r(t,\cdot)$ are some linear forms yet unspecified and $\tilde{\mathrm{p}}$ is a Lagrange multiplier enforcing compressibility and $\frac{\partial \underline{\underline{\Sigma}}^{\mathrm{TI}}}{\partial \underline{\underline{e}}}(\underline{y}_0)$ is a fourth-order tensor corresponding to the derivative of the second Piola-Kirchoff stress tensor $\underline{\underline{\Sigma}}^{\mathrm{TI}}$ with respect to the Green-Lagrange strain tensor $\underline{\underline{e}}$, evaluated at $\underline{y}_0$. We refer the reader to Section 2.6.4 for the detailed expression of the tensor $\underline{\underline{e}}_0(\underline{\tilde{y}}) : \frac{\partial \underline{\underline{\Sigma}}^{\mathrm{TI}}}{\partial \underline{\underline{e}}}(\underline{y}_0)$. Finally, note that we typically have

$$\mathcal{L} \subset \mathcal{L}_\ell = \left\{ q \in L^2(\Omega) \mid \int_\Omega q\,\mathrm{d}\Omega = 0 \right\} \quad \text{and} \quad \mathcal{X} \subset \mathcal{X}_\ell = H^1(\Omega_0)^3.$$

In general, the well-posedeness of linear elastodynamic problem is not given (for instance, buckling may occur). However, in our context, it is reasonable to do the following assumption.

Assumption 2.6. *For every $s(t,\underline{w})$ and $r(t,q)$, there exists a unique couple $(\underline{\tilde{y}}(t),\tilde{\mathrm{p}}(t))$ solution of Eq. (2.20) satisfying*

$$\underline{\tilde{y}} \in C^2\big([0,T]\times\overline{\Omega_0}\big), \quad \tilde{\mathrm{p}} \in C^0\big([0,T]\times\overline{\Omega_0}\big).$$

One of the aims of this work is to derive a rigorous expression of the source term $s(t,\underline{w})$. We will demonstrate that the shear wave generated by ARF is solution of Eq. (2.20), with a source term that depends on the viscous effects and the tissue nonlinearity. The presented analysis is formal, a complete analysis would require to turn most of the assumptions we made into mathematical results and to specify in which functional spaces the various quantities introduced before belong. However, this is a difficult task, since it involves the analysis of the nonlinear elastodynamics problem, that we did not want to address in this work.

2.4.4 Statement of main results

Preliminarily, we define the deformation map as the bijective map $\underline{\phi}_0 : \overline{\Omega}_0 \to \overline{\Omega}(t) \subset \mathbb{R}^3$ from the *reference* to the *deformed* configuration that reads $\underline{\phi}_0 \colon \underline{\xi} \mapsto \underline{x} = \underline{\phi}_0(\underline{\xi},t)$. Then, the displacement $\underline{y}_0$ reads $\underline{y}_0(\underline{\xi},t) = \underline{x} - \underline{\xi} = \underline{\phi}_0(\underline{\xi},t) - \underline{\xi}$. We remind that we assume that the operators $\underline{\underline{\nabla}}$, $\underline{\nabla}$, Δ, div, $\underline{\mathrm{div}}$ and $\underline{\underline{H}}$ (Hessian matrix) correspond to differential operators in the reference configuration, and we use the same symbols with the subscript $\underline{x}$ when considering differentiation in the deformed configuration. Finally, note that by definition $\underline{\underline{F}}_0 \coloneqq \underline{\underline{\nabla}}\,\underline{\phi}_0$ and, for any function $h \in L^2(\Gamma_0)$, we have

$$\int_{\Gamma_0} h\,J_0\left|\underline{\underline{F}}_0^{-T}\cdot\underline{n}_0\right|\underline{\underline{F}}_0^{-T}\cdot\underline{n}_0\,\mathrm{d}\Gamma_0 = \int_{\Gamma(t)} \left(h\circ\underline{\phi}_0^{-1}\right)\underline{n}(t)\,\mathrm{d}\Gamma,$$

where $n(t)$ is the outward unitary normal of $\Omega(t)$ and $\Gamma(t) = \underline{\phi}_0(\Gamma_0)$. Henceforth, if not specified, we will implicitly assume the composition with the deformation map $\underline{\phi}_0$ when we consider a field in the reference configuration that is defined in the deformed configuration, and reciprocally for $\underline{\phi}_0^{-1}$.

Proposition 2.7. *Let us assume that the asymptotic expansion (2.18) of the solution $\underline{y}_\varepsilon$ holds. Then,*

- *the leading-order term $\underline{y}_0(\underline{\xi}, t)$ is solution of the nonlinear heart mechanics with prescribed activation, given by Eq. (2.19); we emphasize that is satisfies*

$$\lim_{\varepsilon \to 0} \underline{y}_\varepsilon = \underline{y}_0;$$

- *the first-order corrector term $\underline{y}_1(\underline{\xi}, t)$ is such that the couple $(\underline{y}_1, \mathrm{p}_1)$ is solution of Eq. (2.20) with $s(t, \underline{w}) = 0$, $r(t, q) = 0$ and null initial conditions. As a consequence, it is a null field;*

- *the second-order corrector $\underline{y}_2$ can be further decomposed into two terms*

$$\underline{y}_2(\underline{\xi}, t, \tau) = \underline{y}_2^f(\underline{\xi}, t, \tau) + \underline{y}_2^S(\underline{\xi}, t),$$

where $\underline{y}_2^f$ is a fast-oscillating, irrotational (pressure) wave, and it is solution of the mixed problem

$$\begin{cases} \rho_0 \, \partial_\tau^2 \underline{y}_2^f - (\hat{\kappa} + \hat{\zeta} \, \partial_\tau) \underline{\nabla}_{\underline{x}} p_2^f = 0 & \text{in} \quad \Omega(t), \\ p_2^f = \mathrm{div}_{\underline{x}} \, \underline{y}_2^f & \text{in} \quad \Omega(t), \\ \underline{y}_2^f = \underline{0} & \text{in} \quad \Gamma_D(t), \\ (\hat{\kappa} + \hat{\zeta} \, \partial_\tau) p_2^f = p \, \cos(\hat{\omega} \, \tau) & \text{on} \quad \Gamma_N(t); \end{cases} \tag{2.21}$$

- *the corrector $\underline{y}_2^S$ is a slowly varying component with prescribed divergence, corresponding to the nonlinear contribution associated with the ARF; the couple $(\underline{y}_2^S, \mathrm{p}_2)$ satisfies Eq. (2.20), with $s(t, \underline{w})$ depending nonlinearly on $\underline{y}_2^f$. It reads, in the deformed configuration:*

$$s(t, \underline{w}) = \frac{\hat{\omega}}{2\pi} \int_0^{\frac{2\pi}{\hat{\omega}}} \int_{\Omega(t)} \mathrm{div}_{\underline{x}} \Big(\big(\hat{\kappa} + \hat{\zeta} \partial_\tau \big) \, \underline{y}_2^f \Big) \, \big(\underline{\underline{\nabla}}_{\underline{x}} \, \underline{y}_2^f \big)^T : \underline{\underline{\nabla}}_{\underline{x}} \, \underline{w} \, \mathrm{d}\Omega \, \mathrm{d}\tau. \tag{2.22}$$

The term $r(t, q)$ is given by

$$r(t, q) = \frac{1}{\hat{\kappa}} \int_{\Omega_0} \mathrm{p}_0 \, q \, \mathrm{d}\Omega_0. \tag{2.23}$$

Note that $\underline{y}_2^f$ solution of (2.21) satisfies at each time $t \in [0, T]$ a periodic problem in τ. Since the source term of Problem (2.21) is a cosine at a single frequency, $\underline{y}_2^f$ can be computed from the solution of a frequency problem. Furthermore, since $\underline{y}_2^f$ is irrotational, its computation can be reduced to the resolution of a scalar problem, namely a Helmholtz problem. As shown in the following corollary, these observations can be used to provide a better interpretation of the source term accounting for the ARF phenomenon.

Corollary 2.1. *The vector field p_2^f solution of (2.21) satisfies*

$$p_2^f(\underline{\xi}, t, \tau) = \mathrm{Re} \left(e^{-i\hat{\omega}\tau} \hat{p}_2^f \right)$$

where $\hat{p}_2^f$ *satisfies at each time* t *the Helmholtz equation*

$$\begin{cases} \Delta_{\underline{x}}\, \hat{p}_2^f + \alpha\, \hat{p}_2^f = 0 & \text{in} \quad \Omega(t), \\ \underline{\nabla}_{\underline{x}}\, \hat{p}_2^f \cdot \underline{n} = 0 & \text{on} \quad \Gamma_D(t), \\ (\hat{\kappa} - i\,\hat{\omega}\,\hat{\zeta})\, \hat{p}_2^f(\underline{x}, t) = p(\underline{x}, t) & \text{on} \quad \Gamma_N(t), \end{cases}$$

with

$$\alpha := \frac{\rho_0\, \hat{\omega}^2}{\hat{\kappa} - i\,\hat{\omega}\,\hat{\zeta}} \in \mathbb{C}.$$

Moreover, there exists another scalar field $\tilde{p}_2$ *such that the couple* $(\underline{y}_2^S, \tilde{p}_2)$ *is solution of Eq.* (2.20) *with*

$$s(t, \underline{w}) = -\frac{\hat{\zeta}\,\hat{\omega}}{2} \int_{\Omega(t)} \mathrm{Im}\left(\hat{p}_2^f\, \underline{\nabla}_{\underline{x}} \overline{\hat{p}_2^f} \right) \cdot \underline{w}\, \mathrm{d}\Omega - \frac{\rho_0\, \hat{\omega}^2}{2|\alpha|^2} \int_{\Gamma_N(t)} \left(\mathrm{Re}\left(\hat{p}_2^f\, \underline{\underline{H}}_{\underline{x}}\big(\overline{\hat{p}_2^f}\big) \right) \cdot \underline{n} \right) \cdot \underline{w}\, \mathrm{d}\Gamma$$
$$+ \frac{1}{4|\alpha|^2} \int_{\Gamma_N(t)} \left(\rho_0\, \hat{\omega}^2 |\underline{\nabla}_{\underline{x}} \hat{p}_2^f|^2 - \hat{\kappa}\, |\alpha|^2\, |\hat{p}_2^f|^2 \right) \underline{w} \cdot \underline{n}\, \mathrm{d}\Gamma. \tag{2.24}$$

Note that $\hat{p}_2^f$ corresponds to the pushing pressure associated with the ARF. The term $s(t, \underline{w})$ is composed of a volume integral accounting for the ARF and a surface term. Furthermore, observe that for small values of $\hat{\zeta}$, one can expect that the volume integral in $s\big(t, \underline{w}\big)$ behaves linearly with respect to attenuation, in accordance with Eq. (2.1). Therefore, viscosity is essential for the generation of shear waves from ARF. Note also that the pressure term p_2 in Proposition 2.7 differs from the term $\tilde{\mathrm{p}}_2$ in Corollary 2.1. Indeed, the definition of $s\big(t, \underline{w}\big)$ given in Eq. (2.22) only differs from the one given in Eq. (2.24) by a contribution that is of the form

$$-\int_{\Omega_0} \check{\mathrm{p}}_2\, \underline{\underline{C}}_0^{-1} : \underline{\underline{e}}_0\big(\underline{w}\big)\, \mathrm{d}\Omega_0$$

and therefore $\tilde{\mathrm{p}}_2 = \mathrm{p}_2 + \check{\mathrm{p}}_2$.

2.5 Proof of main results

In this section, we detail the procedure used to establish Proposition 2.7 and Corollary 2.1. As we have already introduced above, our approach is based on the approximation of $\underline{y}_\varepsilon$ by the first terms of the series expansion in Eq. (2.18). Then, by injecting this expression in Eq. (2.12), we obtain a cascade of equations, and by identification of the equations proportional to the same order of ε, we retrieve the desired results. Henceforth, we will

- prove that the leading term $\underline{y}_0$ does not depend on τ;
- demonstrate that $\underline{y}_1$ does not depend on τ as well;
- describe a system of equations on $\underline{y}_0$ and a new variable p_0 that corresponds to the incompressible nonlinear mechanical system (2.19), from which we will obtain an expression for $\underline{y}_0$;
- find the equation satisfied by $\underline{y}_2^f$ (Eq. (2.21)), that represents the pressure field associated with the ARF;

- describe a system of equations on $\underline{y}_1$ and a new variable p_1 similar to Eq. (2.20), with zero source terms and null initial conditions, that will imply $\underline{y}_1 = \underline{0}$;
- describe a system of equations on $\underline{y}_2^S$ and a new variable p_2 similar to Eq. (2.20), with source terms as in Eqs. (2.22) and (2.23), from which we will obtain an expression for $\underline{y}_2^S$; the shear wave propagation generated by the ARF is observed at this stage.

2.5.1 Preliminaries

Before detailing our approach, we introduce a decomposition that will be used in what follows to split each term $\underline{y}_i$ of the expansion (2.18) into more simple terms. Moreover, we derive some first properties based on the energy estimates (2.16) and (2.17).

Helmholtz decomposition. First, we provide a result that is a straightforward application of the Helmholtz decomposition [Monk et al., 2003].

Proposition 2.8. *Let $\underline{w}(\underline{x})$ be a vector field in $L^2\big(\Omega(t)\big)^3$, $t \in [0,T]$, with $\Omega(t)$ bounded, Lipschitz domain and simply connected. Then, there exist*

$$\Phi \in H_0^1(\Omega), \quad \underline{\Psi} \in \{\underline{v} \in H(curl, \Omega(t)) \,|\, \mathrm{div}_{\underline{x}}(\underline{v}) = 0 \text{ in } \Omega(t),\ \underline{n} \cdot \underline{v} = 0 \text{ on } \partial\Omega\},$$

such that

$$\underline{w}(\underline{x}) = \underline{\nabla}_{\underline{x}} \Phi\big(\underline{x}\big) + \underline{\nabla}_{\underline{x}} \times \underline{\Psi}\big(\underline{x}\big). \tag{2.25}$$

Proposition 2.8 is a standard result in functional analysis. The reader may refer e.g. to Monk et al. [2003] for a proof of the proposition. An analogous decomposition can be derived with respect to the reference domain Ω_0, as asserted in the following Corollary. The proof is omitted again, since the result is directly derived from Proposition 2.8 by applying a change of variable.

Corollary 2.2. *For every $t \in [0,T]$, let $\underline{\tilde{w}}(t)$ be a vector field in $L^2\big(\Omega_0\big)^3$, Then, there exist*

$$\tilde{\Phi}(t) \in H_0^1(\Omega_0), \quad \underline{\tilde{\Psi}}(t) \in H\big(curl, \Omega_0\big)$$

such that

$$\underline{\tilde{w}} = \underline{\underline{F}}_0^{-T} \cdot \underline{\nabla}\, \tilde{\Phi} + J_0^{-1}\, \underline{\underline{F}}_0 \cdot \Big(\underline{\nabla} \times \underline{\tilde{\Psi}}\Big). \tag{2.26}$$

Moreover, if we define $\underline{w}$ such that $\underline{w} \circ \underline{\phi}_0 = \underline{\tilde{w}}$, then

$$\mathrm{tr}\left(\underline{\underline{F}}_0^{-1} \cdot \underline{\nabla}\, \underline{\tilde{w}}\right) = 0 \quad \text{in } \Omega_0 \iff \mathrm{div}_{\underline{x}}\big(\,\underline{w}\,\big) = 0 \quad \text{in } \Omega(t) \iff \tilde{\Phi} = 0 \quad \text{in } \Omega_0.$$

Proof. From Proposition 2.8 it is straightforward to derive Eq. (2.26) by applying a change of variable and by setting $\Phi \circ \underline{\phi}_0 = \tilde{\Phi}$ and $\underline{\Psi} \circ \underline{\phi}_0 = \underline{\underline{F}}_0^{-T}\, \underline{\tilde{\Psi}}$. Then, it is straightforward to prove that (see Monk et al. [2003, Section 3.9])

$$\mathrm{div}_{\underline{x}}\big(\,\underline{w}\,\big) \circ \underline{\phi}_0 = J_0^{-1} \mathrm{div}\, \underline{\tilde{w}} = J_0^{-1} \mathrm{div}\Big(J_0\, \underline{\underline{F}}_0^{-1} \cdot \underline{\tilde{w}}\Big).$$

This divergence can be expressed as

$$\mathrm{div}\Big(J_0\, \underline{\underline{F}}_0^{-1} \cdot \underline{\tilde{w}}\Big) = J_0 \underline{\underline{F}}_0^{-1} : \underline{\nabla} \cdot \underline{\tilde{w}} + \underline{\mathrm{div}}\Big(J_0 \underline{\underline{F}}_0^{-1}\Big) \cdot \underline{\tilde{w}}.$$

However, using the fact that $J_0\underline{\underline{F}}_0^{-1} = \text{Cof F}_0^T$ has divergence-free columns (see Evans [2010, Section 8.1]), we can infer that $\underline{\text{div}}\Big(J_0\underline{\underline{F}}_0^{-1}\Big) = 0$ and, as a consequence,

$$\text{div}_{\underline{x}}\big(\underline{w}\big) \circ \underline{\phi}_0 = \underline{\underline{F}}_0^{-1} : \underline{\underline{\nabla}} \cdot \underline{\tilde{w}} = \text{tr}\,\Big(\underline{\underline{F}}_0^{-1} \cdot \underline{\underline{\nabla}}\,\underline{\tilde{w}}\Big),$$

which concludes the proof. □

Henceforth, we will implicitly assume the composition with the deformation map $\underline{\phi}$ when we consider in the reference configuration a field that is defined in the deformed configuration, for the sake of simplicity.

Decomposition into fast- and slow-oscillating terms. Let us decompose $\underline{y}_i\big(\underline{\xi}, t, \tau\big)$, for $i \geq 0$, into two components, namely

$$\underline{y}_i\big(\underline{\xi}, t, \tau\big) \coloneqq \underline{y}_i^F\big(\underline{\xi}, t, \tau\big) + \underline{y}_i^S\big(\underline{\xi}, t\big), \qquad \text{with} \quad \underline{y}_i^S\big(\underline{\xi}, t\big) = \frac{\hat{\omega}}{2\pi}\int_0^{\frac{2\pi}{\hat{\omega}}} \underline{y}_i(\underline{\xi}, t, \tau)\,\mathrm{d}\tau. \tag{2.27}$$

Subsequently, let us consider the Helmholtz decomposition (2.26) for each component, and define

$$\phi_i^F,\ \phi_i^S,\ \underline{\psi}_i^F,\ \underline{\psi}_i^S,\ i \geq 0,$$

such that

$$\begin{aligned}\underline{y}_i^F\big(\underline{\xi}, t, \tau\big) &= \underline{y}_i^f\big(\underline{\xi}, t, \tau\big) + \underline{y}_i^r\big(\underline{\xi}, t, \tau\big),\\ \underline{y}_i^S\big(\underline{\xi}, t\big) &= \underline{y}_i^p\big(\underline{\xi}, t\big) + \underline{y}_i^s\big(\underline{\xi}, t\big),\end{aligned}$$

with

$$\begin{aligned}\underline{y}_i^f\big(\underline{\xi}, t, \tau\big) &\coloneqq \underline{\underline{F}}^{-T}(\underline{\xi}, t) \cdot \underline{\nabla}_{\underline{\xi}}\phi_i^F\big(\underline{\xi}, t, \tau\big) \qquad & \underline{y}_i^r\big(\underline{\xi}, t, \tau\big) &\coloneqq J^{-1}\,\underline{\underline{F}} \cdot \underline{\nabla}_{\underline{\xi}} \times \underline{\psi}_i^F\big(\underline{\xi}, t, \tau\big)\\ \underline{y}_i^p\big(\underline{\xi}, t\big) &\coloneqq \underline{\underline{F}}^{-T}(\underline{\xi}, t) \cdot \underline{\nabla}_{\underline{\xi}}\phi_i^S\big(\underline{\xi}, t\big) & \underline{y}_i^s\big(\underline{\xi}, t\big) &\coloneqq J^{-1}\,\underline{\underline{F}} \cdot \underline{\nabla}_{\underline{\xi}} \times \underline{\psi}_i^S\big(\underline{\xi}, t\big),\end{aligned}$$

and the superscripts denote focusing, residual, pressure and shear wave, respectively. For simplicity of notation, we explicitly denote only the dependence on τ henceforth, and we implicitly assume that all $\underline{y}_i$'s (and their components) depend on $\underline{\xi}$ and t.

Properties of the limit displacement field from the energy estimate. From Proposition 2.4 it is possible to retrieve some preliminary properties of the leading-order term $\underline{y}_0$. First, we note that the power series expansion of $I_{3,\varepsilon} \equiv J_\varepsilon^2 = \det\big(\underline{\underline{C}}_\varepsilon\big)$ reads

$$I_{3,\varepsilon} \coloneqq I_{3,0} + \sum_{i=1}^{N} \varepsilon^i\, I_{3,i} + o(\varepsilon^N), \tag{2.28}$$

with

$$\begin{aligned}I_{3,0} &\coloneqq \det\big(\underline{\underline{C}}_0\big) = \det\Big(\underline{\underline{\mathbb{1}}} + 2\,\underline{\underline{e}}_0\Big),\\ I_{3,1} &\coloneqq 2\,\det\big(\underline{\underline{C}}_0\big)\ \text{tr}\Big(\big(\underline{\underline{\mathbb{1}}} + 2\,\underline{\underline{e}}_0\big)^{-1} \cdot \underline{\underline{e}}_0\big(\underline{y}_1\big)\Big) = 2\,I_{3,0}\ \text{tr}\Big(\underline{\underline{C}}_0^{-1} \cdot \underline{\underline{e}}_0\big(\underline{y}_1\big)\Big),\end{aligned}$$

and we do not detail the expression of $I_{3,i}$ for the moment for higher-order of approximation for the sake of conciseness. If we substitute in Eq. (2.16) the expansion of $I_{3,\varepsilon}$ given in Eq. (2.28), we obtain

$$\int_{\Omega_0} \big((I_{3,0}-1)-\log(I_{3,0})\big)\,\mathrm{d}\Omega_0 + \varepsilon \int_{\Omega_0} (I_{3,0}-1) I_{3,1}\, I_{3,0}^{-1}\,\mathrm{d}\Omega_0 + o(\varepsilon^2) \leq \varepsilon^2\, C.$$

Hence, we can assert

$$(I_{3,0}-1)-\log(I_{3,0}) = 0 \implies I_{3,0} = 1. \tag{2.29}$$

Consequently, the leading term $\underline{y}_0$ is incompressible. Furthermore, from Eq. (2.29) and Jacobi's formula, we obtain

$$I_{3,0} = \det\Big(\underline{\underline{C}}_0\Big) = 1 \implies 0 = \partial_t I_{3,0} = I_{3,0}\ \mathrm{tr}\left(\underline{\underline{C}}_0^{-1}\cdot\partial_t\underline{\underline{C}}_0\right) = 2\, I_{3,0}\ \mathrm{tr}\left(\underline{\underline{C}}_0^{-1}\cdot\partial_t\underline{\underline{e}}_0\right). \tag{2.30}$$

Analogously,

$$0 = \partial_\tau I_{3,0} = I_{3,0}\ \mathrm{tr}\left(\underline{\underline{C}}_0^{-1}\cdot\partial_\tau\underline{\underline{C}}_0\right) = 2\, I_{3,0}\ \mathrm{tr}\left(\underline{\underline{C}}_0^{-1}\cdot\partial_\tau\underline{\underline{e}}_0\right). \tag{2.31}$$

Notations. We denote the power series expansion of $I_{i,\varepsilon}$, $i = 1, 2, 4$ by

$$I_{i,\varepsilon} = I_{i,0} + \sum_{k=1}^{2} \varepsilon^k\, I_{i,k} + o(\varepsilon^2). \tag{2.32}$$

In what follows, the explicit expression of the terms $I_{i,k}$ will be provided when required.

Detailed expansion of some stress tensors. For the sake of clarity, we provide here the first terms of the expansion of the stress tensor $\underline{\underline{\Sigma}}_\varepsilon^{\mathrm{NI}}$ associated with nearly-incompressibility. They read, due to Eq. (2.29),

$$\underline{\underline{\Sigma}}_0^{\mathrm{NI}} = (I_{3,0}-1)\underline{\underline{C}}_0^{-1} = \underline{\underline{0}}, \qquad \underline{\underline{\Sigma}}_1^{\mathrm{NI}} = (I_{3,0}-1)\underline{\underline{G}}_1 + I_{3,1}\underline{\underline{C}}_0^{-1} = I_{3,1}\underline{\underline{C}}_0^{-1}. \tag{2.33}$$

Due to Eq. (2.31), the first term of the stress tensor $\underline{\underline{\Sigma}}_\varepsilon^{\mathrm{VS}}$ related to the viscous contribution is given by

$$\underline{\underline{\Sigma}}_0^{\mathrm{VS}} = \underline{\underline{C}}_0^{-1}\ \mathrm{tr}\Big(\underline{\underline{C}}_0^{-1}\cdot\partial_\tau\underline{\underline{e}}_0\Big) = \underline{\underline{0}}. \tag{2.34}$$

In addition, due to Eqs. (2.30) and (2.31), the viscous stress tensor $\underline{\underline{\Sigma}}_1^{\mathrm{VS}}$ reduces to

$$\begin{aligned}\underline{\underline{\Sigma}}_1^{\mathrm{VS}} &= \underline{\underline{C}}_0^{-1}\ \mathrm{tr}\Big(\underline{\underline{C}}_0^{-1}\cdot\partial_t\underline{\underline{e}}_0\Big) + \underline{\underline{C}}_0^{-1}\ \mathrm{tr}\Big(\underline{\underline{C}}_0^{-1}\cdot\partial_\tau\underline{\underline{e}}_0(\underline{y}_1) + \underline{\underline{G}}_1\cdot\partial_\tau\underline{\underline{e}}_0\Big) + \underline{\underline{G}}_1\ \mathrm{tr}\Big(\underline{\underline{C}}_0^{-1}\cdot\partial_\tau\underline{\underline{e}}_0\Big)\\ &= \underline{\underline{C}}_0^{-1}\ \mathrm{tr}\Big(\underline{\underline{C}}_0^{-1}\cdot\partial_\tau\underline{\underline{e}}_0(\underline{y}_1)\Big),\end{aligned}$$

with

$$\underline{\underline{G}}_1 \coloneqq -2\,\underline{\underline{C}}_0^{-1}\cdot\underline{\underline{e}}_0(\underline{y}_1)\cdot\underline{\underline{C}}_0^{-1}.$$

2.5.2 Time dependence of the leading term

First, we take into account the equation proportional to ε^{-2} in problem (2.12). It reads

$$\int_{\Omega_0} \rho_0 \, \partial_\tau^2 \underline{y}_0 \cdot \underline{w} \, \mathrm{d}\Omega_0 + \frac{\hat{\kappa}}{2} \int_{\Omega_0} \underline{\underline{\Sigma}}_0^{\mathrm{NI}} : \underline{\underline{e}}_0(\underline{w}) \, \mathrm{d}\Omega_0 + \hat{\zeta} \int_{\Omega_0} \underline{\underline{\Sigma}}_0^{\mathrm{VS}} : \underline{\underline{e}}_0(\underline{w}) \, \mathrm{d}\Omega_0 = 0. \tag{2.35}$$

From Eq. (2.35) and using the energy estimates provided in Section 2.5.1, it is possible to prove that the term $\underline{y}_0$ does not depend on the fast time variable τ, as stated in the following proposition.

Proposition 2.9. *The leading-order term of the expansion $\underline{y}_0$ satisfies*

$$\partial_\tau \underline{y}_0 = 0. \tag{2.36}$$

Proof. Using Eqs. (2.33) and (2.34), we obtain

$$\underline{\underline{\Sigma}}_0^{\mathrm{NI}} = \underline{\underline{0}} \quad \text{and} \quad \underline{\underline{\Sigma}}_0^{\mathrm{VS}} = \underline{\underline{0}}.$$

Hence, Eq. (2.35) reduces to

$$\int_{\Omega_0} \partial_\tau^2 \underline{y}_0 \cdot \underline{w} \, \mathrm{d}\Omega_0 = 0.$$

Since $\underline{w}$ is arbitrary, $\underline{y}_0$ is regular and periodic, and $\partial_\tau \underline{y}_0$ is also periodic, we obtain the desired result. □

2.5.3 Properties of the first-order corrector

In this section, we prove that the corrector $\underline{y}_1$ does not depend on the fast time variable, and it is divergence-free. To this end, we consider the equation associated with ε^{-1} in problem (2.12). After some simplifications due to the properties that we have proved on $\underline{y}_0$ (namely, $\partial_\tau \underline{y}_0 = \underline{0}$, $\underline{\underline{\Sigma}}_0^{\mathrm{NI}} = \underline{\underline{0}}$ and $\underline{\underline{\Sigma}}_0^{\mathrm{VS}} = \underline{\underline{0}}$), it reads

$$\int_{\Omega_0} \rho_0 \, \partial_\tau^2 \underline{y}_1 \cdot \underline{w} \, \mathrm{d}\Omega_0 + \frac{\hat{\kappa}}{2} \int_{\Omega_0} \underline{\underline{\Sigma}}_1^{\mathrm{NI}} : \underline{\underline{e}}_0(\underline{w}) \, \mathrm{d}\Omega_0 + \hat{\zeta} \int_{\Omega_0} \underline{\underline{\Sigma}}_1^{\mathrm{VS}} : \underline{\underline{e}}_0(\underline{w}) \, \mathrm{d}\Omega_0 = 0. \tag{2.37}$$

Note that, due to Proposition 2.9, $\underline{\underline{\Sigma}}_1^{\mathrm{VS}}$ is given by

$$\underline{\underline{\Sigma}}_1^{\mathrm{VS}} = \underline{\underline{C}}_0^{-1} \, \mathrm{tr}\Big(\underline{\underline{C}}_0^{-1} \cdot \partial_\tau \underline{\underline{e}}_0(\underline{y}_1)\Big).$$

The main result of this section is in the following proposition.

Proposition 2.10. *The first-order corrector $\underline{y}_1$ satisfies*

$$\underline{\underline{\Sigma}}_1^{NI} = \underline{\underline{\Sigma}}_1^{VS} = \underline{\underline{0}} \quad \textit{and} \quad \partial_\tau \underline{y}_1 = \underline{0}.$$

Proof. First, we simplify expression (2.37). Note that we can approximate

$$\mathrm{tr}\Big(\underline{\underline{C}}_\varepsilon^{-1} \cdot \dot{\underline{\underline{e}}}_\varepsilon\Big) = \mathrm{tr}\Big(\underline{\underline{C}}_0^{-1} \cdot \partial_\tau \underline{\underline{e}}_0(\underline{y}_1)\Big) + O(\varepsilon).$$

As a consequence, from the energy estimation (2.17), $\underline{y}_1$ satisfies

$$\mathrm{tr}\Big(\underline{\underline{C}}_0^{-1} \cdot \partial_\tau \underline{\underline{e}}_0(\underline{y}_1)\Big) = 0, \tag{2.38}$$

that implies $\underline{\underline{\Sigma}}_1^{\mathrm{VS}} = \underline{\underline{0}}$. Now, let us decompose $\underline{y}_1$ into two components as in Eq. (2.27):

$$\underline{y}_1 = \underline{y}_1^F(\tau) + \underline{y}_1^S.$$

Since $\partial_\tau \underline{y}_0 = 0$, we get:

$$0 \overset{(2.38)}{=} \mathrm{tr}\Big(\underline{\underline{C}}_0^{-1} \cdot \partial_\tau \underline{\underline{e}}_0\big(\underline{y}_1^F(\tau)\big)\Big) = \partial_\tau \,\mathrm{tr}\Big(\underline{\underline{C}}_0^{-1} \cdot \underline{\underline{e}}_0\big(\underline{y}_1^F(\tau)\big)\Big).$$

As $\underline{y}_1^F(\tau)$ has zero mean, it must satisfy

$$\mathrm{tr}\Big(\underline{\underline{C}}_0^{-1} \cdot \underline{\underline{e}}_0\big(\underline{y}_1^F(\tau)\big)\Big) = 0. \tag{2.39}$$

On the other hand, if we take $\underline{w} = \underline{y}_1^S$ in Eq. (2.37) and we integrate on τ over its period, due to the periodicity assumption of all the terms $\partial_\tau \underline{y}_i$ and $\underline{y}_i$ with respect to τ in $[0, 2\,\pi/\hat{\omega}]$, we obtain

$$\int_0^{\frac{2\pi}{\hat{\omega}}} \int_{\Omega_0} \mathrm{tr}\Big(\underline{\underline{C}}_0^{-1} \cdot \underline{\underline{e}}_0\big(\underline{y}_1^S\big)\Big)^2 \,\mathrm{d}\Omega_0 \,\mathrm{d}\tau = 0 \implies \mathrm{tr}\Big(\underline{\underline{C}}_0^{-1} \cdot \underline{\underline{e}}_0\big(\underline{y}_1^S\big)\Big) = 0. \tag{2.40}$$

Therefore, from Eqs. (2.39) and (2.40) and by linearity,

$$\mathrm{tr}\Big(\underline{\underline{C}}_0^{-1} \cdot \underline{\underline{e}}_0\big(\underline{y}_1\big)\Big) = 0 \implies I_{3,1} = 0. \tag{2.41}$$

Hence, $\underline{\underline{\Sigma}}_1^{\mathrm{NI}} = \underline{\underline{0}}$. Finally, from Eq. (2.37) and the periodicity and regularity of $\underline{y}_1$, we can assert

$$\int_{\Omega_0} \partial_\tau^2 \underline{y}_1 \cdot \underline{w} \,\mathrm{d}\Omega_0 = 0 \implies \partial_\tau^2 \underline{y}_1 = 0 \implies \partial_\tau \underline{y}_1 = 0 \implies \underline{y}_1^F\big(\underline{\xi}, t, \tau\big) = 0,$$

thus concluding the proof. □

Furthermore, note that Eq. (2.41) implies that the field $\underline{y}_1$ is divergence-free. Consequently, we can infer that

$$\underline{y}_1\big(\underline{\xi}, t\big) = \underline{y}_1^S\big(\underline{\xi}, t\big) = \underline{y}_1^s\big(\underline{\xi}, t\big).$$

This corresponds to a shear wave generated by the source term, independent of the rapid time variable τ.

2.5.4 The governing equation of the leading term: the underlying nonlinear problem

The next step of our procedure consists in analysing the equation corresponding to ε^0 in the expansion of the elastodynamic problem (2.12). Taking into account the results above (namely, $I_{3,0} = 1$, $I_{3,1} = 0$, $\partial_\tau \underline{y}_1 = \partial_\tau \underline{y}_0 = \underline{0}$), its expression reads

$$\int_{\Omega_0} \rho_0 \left(\partial_\tau^2 \underline{y}_2 + \partial_t^2 \underline{y}_0\right) \cdot \underline{w} \,\mathrm{d}\Omega_0 + \frac{\hat{\kappa}}{2} \int_{\Omega_0} \underline{\underline{\Sigma}}_2^{\mathrm{NI}} : \underline{\underline{e}}_0\big(\underline{w}\big) \,\mathrm{d}\Omega_0 + \int_{\Omega_0} \left(\underline{\underline{\Sigma}}_0^{\mathrm{TI}} + \underline{\underline{\Sigma}}^A\right) : \underline{\underline{e}}_0\big(\underline{w}\big) \,\mathrm{d}\Omega_0$$
$$+\hat{\zeta} \int_{\Omega_0} \underline{\underline{\Sigma}}_2^{\mathrm{VS}} : \underline{\underline{e}}_0\big(\underline{w}\big) \,\mathrm{d}\Omega_0 = cos(\hat{\omega}\,\tau) \int_{\Gamma_{N,0}} \underline{\mathrm{t}}_0 \cdot \underline{w} \,\mathrm{d}S_0, \tag{2.42}$$

with the stress tensor

$$\underline{\underline{\Sigma}}_2^{\mathrm{NI}} = I_{3,1}\underline{\underline{G}}_1 + I_{3,2}\underline{\underline{C}}_0^{-1} = I_{3,2}\underline{\underline{C}}_0^{-1},$$

where we recall that $\underline{\underline{G}}_1 \coloneqq -2\,\underline{\underline{C}}_0^{-1} \cdot \underline{\underline{e}}_0\Big(\underline{y}_1\Big) \cdot \underline{\underline{C}}_0^{-1}$, and the expression of $\underline{\underline{\Sigma}}_0^{\mathrm{TI}}$ is given in Section 2.6.4. We highlight that, by definition, $\underline{\underline{\Sigma}}_0^{\mathrm{TI}}$ depends only on $\underline{y}_0$. Hence, it is independent of τ. Taking into account the fact that $\partial_\tau \underline{y}_1 = \underline{0}$, the viscous contribution is given by

$$\underline{\underline{\Sigma}}_2^{\mathrm{VS}} = \underline{\underline{C}}_0^{-1}\ \mathrm{tr}\Big(\underline{\underline{G}}_1 \cdot \partial_t \underline{\underline{e}}_0\Big) + \underline{\underline{C}}_0^{-1}\ \mathrm{tr}\Big(\underline{\underline{C}}_0^{-1} \cdot \partial_t \underline{\underline{e}}_0(\underline{y}_1)\Big) + \underline{\underline{C}}_0^{-1}\ \mathrm{tr}\Big(\underline{\underline{C}}_0^{-1} \cdot \partial_\tau \underline{\underline{e}}_0(\underline{y}_2)\Big).$$

We can further simplify the viscous contribution. This is the result of the following lemma.

Lemma 2.11. *The term* $\underline{\underline{\Sigma}}_2^{VS}$ *satisfies*

$$\underline{\underline{\Sigma}}_2^{VS} = \underline{\underline{C}}_0^{-1}\ \mathrm{tr}\Big(\underline{\underline{C}}_0^{-1} \cdot \partial_\tau \underline{\underline{e}}_0(\underline{y}_2)\Big).$$

Proof. Our aim is to prove

$$\mathrm{tr}\Big(\underline{\underline{G}}_1 \cdot \partial_t \underline{\underline{e}}_0\Big) + \mathrm{tr}\left(\underline{\underline{C}}_0^{-1} \cdot \partial_t \underline{\underline{e}}_0(\underline{y}_1)\right) = 0. \tag{2.43}$$

First, note that from Eq. (2.41) we have

$$\partial_t\ \mathrm{tr}\left(\underline{\underline{C}}_0^{-1} \cdot \underline{\underline{e}}_0(\underline{y}_1)\right) = 0 \implies \mathrm{tr}\left(\partial_t\, \underline{\underline{C}}_0^{-1} \cdot \underline{\underline{e}}_0(\underline{y}_1)\right) + \mathrm{tr}\left(\underline{\underline{C}}_0^{-1} \cdot \partial_t \underline{\underline{e}}_0(\underline{y}_1)\right) = 0. \tag{2.44}$$

Now, by definition,

$$\mathrm{tr}\Big(\underline{\underline{G}}_1 \cdot \partial_t \underline{\underline{e}}_0\Big) = \mathrm{tr}\left(-2\,\underline{\underline{C}}_0^{-1} \cdot \underline{\underline{e}}_0(\underline{y}_1) \cdot \underline{\underline{C}}_0^{-1} \cdot \partial_t \underline{\underline{e}}_0\right) = \mathrm{tr}\left(-2\,\underline{\underline{C}}_0^{-1} \cdot \partial_t \underline{\underline{e}}_0 \cdot \underline{\underline{C}}_0^{-1} \cdot \underline{\underline{e}}_0(\underline{y}_1)\right).$$

Moreover, note that

$$\begin{aligned} -2\,\underline{\underline{C}}_0^{-1} \cdot \partial_t \underline{\underline{e}}_0 \cdot \underline{\underline{C}}_0^{-1} &= \left(\underline{\underline{F}}_0^{-1} \cdot \dot{\underline{\underline{F}}}_0 \cdot \underline{\underline{F}}_0^{-1} \cdot \underline{\underline{F}}_0^{-T} + \underline{\underline{F}}_0^{-1} \cdot \underline{\underline{F}}_0^{-T} \cdot \dot{\underline{\underline{F}}}_0^{T} \cdot \underline{\underline{F}}_0^{-T}\right) \\ &= \partial_t\left(\underline{\underline{F}}_0^{-1} \cdot \underline{\underline{F}}_0^{-T}\right) = \partial_t\left(\underline{\underline{C}}_0^{-1}\right), \end{aligned} \tag{2.45}$$

therefore, we can state

$$\mathrm{tr}\Big(\underline{\underline{G}}_1 \cdot \partial_t \underline{\underline{e}}_0\Big) = \mathrm{tr}\left(\partial_t\, \underline{\underline{C}}_0^{-1} \cdot \underline{\underline{e}}_0(\underline{y}_1)\right). \tag{2.46}$$

Combining Eqs. (2.44) and (2.46), we obtain Eq. (2.43), which concludes the proof. □

We are now able to state the main result of this subsection.

Proposition 2.12. *There exists a scalar field* p_0 *depending on time* t *such that the couple* $(\underline{y}_0, \mathrm{p}_0)$ *is solution of Eq.* (2.19) *and*

$$\frac{\hat{\omega}\,\hat{\kappa}}{2\pi} \int_0^{\frac{2\pi}{\hat{\omega}}} \frac{1}{2} I_{3,2}\, \mathrm{d}\tau = \mathrm{p}_0. \tag{2.47}$$

Proof. In order to derive an expression for the governing equation of $\underline{y}_0$, we need to discard the terms depending of the fast time variable τ in Eq. (2.42). Therefore, we integrate it on τ over its period. Since $\underline{y}_2(\tau)$ is smooth and periodic, and $\underline{\mathrm{t}}_0$ has zero mean value on the same period, we derive Eq. (2.19) using the expression of the stress tensors, as desired. □

Remark Note that the viscous term does not give any contribution at this stage. Furthermore, (2.47) relates higher-order corrector terms to p_0. In what follows, we will show that it is a constraint on the divergence of the (slowly varying) second-order corrector $\underline{y}_2$.

2.5.5 The governing equation of the fast-oscillating second-order corrector: the ARF pressure field

The second main result of this chapter concerns the derivation of the governing equation of the pressure wave propagation associated with the ARF. To do so, we still consider the term corresponding to ε^0 in the expansion of problem (2.12). More precisely, if we inject Eq. (2.19) in Eq. (2.42), we obtain

$$\begin{aligned}&\int_{\Omega_0} \rho_0\, \partial_\tau^2 \underline{y}_2 \cdot \underline{w}\, \mathrm{d}\Omega_0 + \int_{\Omega_0} \left(\frac{\hat{\kappa}}{2}\underline{\underline{\Sigma}}_2^{\mathrm{NI}} - \mathrm{p}_0\, \underline{\underline{C}}_0^{-1}\right) : \underline{\underline{e}}_0(\underline{w})\, \mathrm{d}\Omega_0 + \hat{\zeta} \int_{\Omega_0} \underline{\underline{\Sigma}}_2^{\mathrm{VS}} : \underline{\underline{e}}_0(\underline{w})\, \mathrm{d}\Omega_0 \\ &\quad = \int_{\Gamma_{N,0}} \underline{\mathrm{t}}_0 \cdot \underline{w}\ \mathrm{d}S_0.\end{aligned} \tag{2.48}$$

First, note that

$$\frac{\hat{\kappa}}{2}\underline{\underline{\Sigma}}_2^{\mathrm{NI}} - \mathrm{p}_0\, \underline{\underline{C}}_0^{-1} = \frac{\hat{\kappa}}{2}\left(I_{3,2} - \frac{\hat{\omega}}{2\pi}\int_0^{\frac{2\pi}{\hat{\omega}}} I_{3,2}\, \mathrm{d}\tau\right)\underline{\underline{C}}_0^{-1}. \tag{2.49}$$

Now, to go further in our analysis, we need to decompose $\underline{y}_2$ as in Eq. (2.27):

$$\underline{y}_2 = \underline{y}_2^F(\tau) + \underline{y}_2^S. \tag{2.50}$$

Using Eq. (2.41), the invariant $I_{3,2}$ is given by

$$I_{3,2} = 2\ \mathrm{tr}\left(\underline{\underline{C}}_0^{-1}\, \underline{\underline{e}}_0(\underline{y}_2)\right) - \mathrm{tr}\Big(\underline{\underline{C}}_0^{-1}\underline{\underline{e}}_0(\underline{y}_1)\, \underline{\underline{C}}_0^{-1}\underline{\underline{e}}_0(\underline{y}_1)\Big).$$

Hence, since $\underline{y}_1$ does not depend on τ, and using Eqs. (2.49) and (2.50), we can see that

$$\frac{\hat{\kappa}}{2}\underline{\underline{\Sigma}}_2^{\mathrm{NI}} - \mathrm{p}_0\, \underline{\underline{C}}_0^{-1} = \hat{\kappa}\ \mathrm{tr}\left(\underline{\underline{C}}_0^{-1} \cdot \underline{\underline{e}}_0\big(\underline{y}_2^F(\tau)\big)\right)\underline{\underline{C}}_0^{-1}. \tag{2.51}$$

The main result of this section is the following proposition.

Proposition 2.13. *There exist a time-dependent, irrotational field $\underline{y}_2^f$ and a scalar field p_2^f such that $\underline{y}_2^f = \underline{y}_2^F$ and the couple $(\underline{y}_2^f, p_2^f)$ satisfies Eq. (2.21).*

Proof. Let us consider Eq. (2.48). If we use Eq. (2.51) and the definition of the stress tensor $\underline{\underline{\Sigma}}_2^{\mathrm{VS}}$, we obtain the following equation on $\underline{y}_2^F(\tau)$:

$$\begin{aligned}&\int_{\Omega_0} \rho_0\, \partial_\tau^2 \underline{y}_2^F \cdot \underline{w}\, \mathrm{d}\Omega_0 + \hat{\kappa}\int_{\Omega_0} \mathrm{tr}\Big(\underline{\underline{C}}_0^{-1} \cdot \underline{\underline{e}}_0\big(\underline{y}_2^F\big)\Big)\, \mathrm{tr}\Big(\underline{\underline{C}}_0^{-1} \cdot \underline{\underline{e}}_0(\underline{w})\Big)\, \mathrm{d}\Omega_0 \\ &\quad + \hat{\zeta}\int_{\Omega_0} \mathrm{tr}\Big(\underline{\underline{C}}_0^{-1} \cdot \partial_\tau \underline{\underline{e}}_0\big(\underline{y}_2^F\big)\Big)\, \mathrm{tr}\Big(\underline{\underline{C}}_0^{-1} \cdot \underline{\underline{e}}_0(\underline{w})\Big)\, \mathrm{d}\Omega_0 \\ &\quad = \int_{\Gamma_{N,0}} \cos(\hat{\omega}\,\tau)\, p(\underline{\xi}, t)\, \big(\underline{\underline{F}}^{-T}\underline{n}_0\big) \cdot \underline{w}\, \big|\underline{\underline{F}}^{-T}\underline{n}_0\big|\, \mathrm{d}S_0.\end{aligned} \tag{2.52}$$

Eq. (2.52) can be rewritten in the deformed configuration as

$$\begin{aligned}&\int_{\Omega(t)} \rho_0\, \partial_\tau^2 \underline{y}_2^F \cdot \underline{w}\, \mathrm{d}\Omega + \hat{\kappa}\int_{\Omega(t)} \mathrm{div}_{\underline{x}}\, \underline{y}_2^F \cdot \mathrm{div}_{\underline{x}}\, \underline{w}\, \mathrm{d}\Omega + \hat{\zeta}\int_{\Omega(t)} \mathrm{div}_{\underline{x}}\, \partial_t\, \underline{y}_2^F \cdot \mathrm{div}_{\underline{x}}\, \underline{w}\, \mathrm{d}\Omega \\ &\quad = \int_{\Gamma_N(t)} \cos(\hat{\omega}\,\tau)\, p(\underline{\xi}, t)\, \underline{n} \cdot \underline{w}\ \mathrm{d}S,\end{aligned} \tag{2.53}$$

since $J_0 = 1$. In strong form, Eq. (2.53) reads

$$\begin{cases} \rho_0\, \partial_\tau^2 \underline{y}_2^F - \hat{\kappa}\, \underline{\nabla}_{\underline{x}}\, \mathrm{div}_{\underline{x}}\, \underline{y}_2^F - \hat{\zeta}\, \underline{\nabla}_{\underline{x}}\, \mathrm{div}_{\underline{x}}\, \partial_\tau \underline{y}_2^F = 0 & \text{in} \quad \Omega(t), \\ \underline{y}_2^F = \underline{0} & \text{on} \quad \Gamma_D(t), \\ \big(\hat{\kappa} + \hat{\zeta}\, \partial_\tau\big) \mathrm{div}_{\underline{x}}\, \underline{y}_2^F \cdot \underline{n} = p\, \cos(\hat{\omega}\, \tau)\, \underline{n} & \text{on} \quad \Gamma_N(t). \end{cases} \tag{2.54}$$

This shows that $\underline{y}_2^F$ is indeed irrotational. Consequently, by performing a Helmholtz decomposition as detailed in Section 2.5.1, we can assert that

$$\underline{y}_2^F = \underline{y}_2^f.$$

Moreover, Eq. (2.54) can be recast as the mixed problem (2.21). □

2.5.6 The governing equation of the first-order corrector: a null field

We are now interested in the equation associated with ε^1 in problem (2.12). It reads, using the fact that $I_{3,0} = 1$, $I_{3,1} = 0$ and $\partial_\tau \underline{y}_0 = \partial_\tau \underline{y}_1 = \underline{0}$,

$$\begin{aligned} &\int_{\Omega_0} \rho_0 \left(\partial_\tau^2 \underline{y}_3 + \partial_{t\tau} \underline{y}_2 + \partial_t^2 \underline{y}_1\right) \cdot \underline{w}\, \mathrm{d}\Omega_0 + \frac{\hat{\kappa}}{2} \int_{\Omega_0} \Big(\underline{\underline{\Sigma}}_2^{\mathrm{NI}} : \underline{\underline{e}}_1(\underline{w}) + \underline{\underline{\Sigma}}_3^{\mathrm{NI}} : \underline{\underline{e}}_0(\underline{w})\Big) \mathrm{d}\Omega_0 \\ &+ \int_{\Omega_0} \Big(\big(\underline{\underline{\Sigma}}_0^{\mathrm{TI}} + \underline{\underline{\Sigma}}^A\big) : \underline{\underline{e}}_1(\underline{w}) + \underline{\underline{\Sigma}}_1^{\mathrm{TI}} : \underline{\underline{e}}_0(\underline{w})\Big) \mathrm{d}\Omega_0 \\ &+ \hat{\zeta} \int_{\Omega_0} \Big(\underline{\underline{\Sigma}}_2^{\mathrm{VS}} : \underline{\underline{e}}_1^s(\underline{w}) + \underline{\underline{\Sigma}}_3^{\mathrm{VS}} : \underline{\underline{e}}_0(\underline{w})\Big) \mathrm{d}\Omega_0 = \cos(\hat{\omega}\, \tau) \int_{\Gamma_0} \underline{\mathrm{t}}_1 \cdot \underline{w}\ \mathrm{d}\Gamma_0. \end{aligned} \tag{2.55}$$

After some algebra, the terms $\underline{\underline{\Sigma}}_3^{\mathrm{NI}}$ and $\underline{\underline{\Sigma}}_3^{\mathrm{VS}}$ read:

$$\begin{aligned} \underline{\underline{\Sigma}}_3^{\mathrm{NI}} &= I_{3,1} \underline{\underline{G}}_2 + I_{3,2} \underline{\underline{G}}_1 + I_{3,3} \underline{\underline{C}}_0^{-1} = I_{3,2} \underline{\underline{G}}_1 + I_{3,3}\, \underline{\underline{C}}_0^{-1}, \\ \underline{\underline{\Sigma}}_3^{\mathrm{VS}} &= \underline{\underline{C}}_0^{-1}\, \mathrm{tr}\left(\underline{\underline{D}}_3\right) + \underline{\underline{G}}_1\, \mathrm{tr}\left(\underline{\underline{C}}_0^{-1} \cdot \partial_\tau \underline{\underline{e}}_0\big(\underline{y}_2\big)\right), \end{aligned}$$

where $\underline{\underline{D}}_3$ is a tensor depending on $\left(\underline{y}_0, \underline{y}_1, \underline{y}_2, \underline{y}_3\right)$, whose expression is of no practical interest. The detailed expression of the tensor $\underline{\underline{\Sigma}}_1^{\mathrm{TI}}$ can be found in Section 2.6.4 by substituting $\underline{y}_1 = \underline{w}$. For the sake of completeness, we recall here that it corresponds to

$$\underline{\underline{\Sigma}}_1^{\mathrm{TI}} = \frac{\partial \underline{\underline{\Sigma}}^{\mathrm{TI}}}{\partial \underline{\underline{e}}}(\underline{y}_0) : \underline{\underline{e}}_0(\underline{y}_1).$$

Therefore, it does not depend on τ. Similarly to Eq. (2.47), we can see that there exists a scalar field p_1 depending on time t such that

$$\frac{\hat{\omega}}{2\pi} \int_0^{\frac{2\pi}{\hat{\omega}}} \left(\frac{\hat{\kappa}}{2}\, I_{3,3} + \hat{\zeta}\ \mathrm{tr}\left(\underline{\underline{D}}_3\right)\right) \mathrm{d}\tau = \mathrm{p}_1. \tag{2.56}$$

Since we want to derive the governing equation for $\underline{y}_1$ (that does not depend on τ), it is natural to integrate Eq. (2.55) on τ over $[0, \hat{\omega}/(2\pi)]$. Using similar arguments to the

previous section (namely, the periodicity of the quantities depending on τ), one can show that

$$\begin{aligned}&\int_{\Omega_0} \rho_0\, \partial_t^2 \underline{y}_1 \cdot \underline{w}\, \mathrm{d}\Omega_0 + \int_{\Omega_0} \mathrm{p}_1\, \underline{\underline{C}}_0^{-1} : \underline{\underline{e}}_0(\underline{w})\mathrm{d}\Omega_0 + \int_{\Omega_0} \underline{\underline{\Sigma}}_1^{\mathrm{TI}} : \underline{\underline{e}}_0(\underline{w})\mathrm{d}\Omega_0 \\ &\quad + \int_{\Omega_0} \mathrm{p}_0\, \underline{\underline{G}}_1 : \underline{\underline{e}}_0(\underline{w})\, \mathrm{d}\Omega_0 + \int_{\Omega_0} \left(\underline{\underline{\Sigma}}_0^{\mathrm{TI}} + \underline{\underline{\Sigma}}^A + \mathrm{p}_0\, \underline{\underline{C}}_0^{-1}\right) : \underline{\underline{e}}_1(\underline{w})\mathrm{d}\Omega_0 = 0.\end{aligned} \tag{2.57}$$

We are now able to prove the following proposition concerning the field $\underline{y}_1$.

Proposition 2.14. *The first-order corrector $\underline{y}_1$ satisfies*

$$\underline{y}_1 = \underline{0}.$$

Proof. The proof consists in showing that the couple $(\underline{y}_1, \mathrm{p}_1)$ satisfies problem (2.20) with no source terms. First, by algebraic manipulations and using the definition of the stress tensors, it is easy to see that Eq. (2.57) corresponds to the first equation of Eq. (2.20) with $\tilde{\underline{y}} = \underline{y}_1$, $\tilde{p} = \mathrm{p}_1$, and $s(t, \underline{w}) = 0$.
Then, since we have shown previously that $I_{3,1} = 0$, we can write

$$\int_{\Omega_0} \underline{\underline{C}}_0^{-1} : \underline{\underline{e}}_0(\underline{y}_1)\, q\, \mathrm{d}\Omega_0 = 0,$$

retrieving the second equation in (2.20), with $r(t, q)$ equal to zero.
Finally, since initial conditions are assumed to be zero, and problem (2.20) is well-posed, the only solution of our problem is

$$\underline{y}_1 = \underline{0}, \quad \mathrm{p}_1 = 0,$$

completing the proof. □

Remark Since $\underline{y}_1$ vanishes, numerous simplifications can be deduced in the expansion of the mechanical quantities in Section 2.4.2. Among them, one can deduce

$$I_{3,2} = 2\,\mathrm{tr}\left(\underline{\underline{C}}_0^{-1} \cdot \underline{\underline{e}}_0(\underline{y}_2)\right), \quad \underline{\underline{G}}_2 = -2\,\underline{\underline{C}}_0^{-1} \cdot \underline{\underline{e}}_0(\underline{y}_2) \cdot \underline{\underline{C}}_0^{-1}, \quad \underline{\mathrm{t}}_1 = \underline{0},$$

and

$$\underline{\underline{e}}_\varepsilon = \underline{\underline{e}}_0 + \sum_{i=2}^{3} \varepsilon^i\, \underline{\underline{e}}_0(\underline{y}_i) + o(\varepsilon^3).$$

2.5.7 The governing equation of the slow-oscillating second-order corrector: the shear wave propagation

At last, we give an explicit expression of the governing equation of the second-order corrector $\underline{y}_2^S$ as defined in Eq. (2.50). To this end, we need to evaluate the term corresponding to ε^2 in the expansion of the problem (2.12). Using the results above, namely, $I_{3,0} = 1$, $\partial_\tau \underline{y}_0 = \underline{0}$, $\underline{y}_1 = \underline{0}$, it reads

$$\begin{aligned}&\int_{\Omega_0} \rho_0 \left(\partial_\tau^2 \underline{y}_4 + \partial_{t\tau} \underline{y}_3^F + \partial_t^2 \underline{y}_2\right) \cdot \underline{w}\, \mathrm{d}\Omega_0 + \frac{\hat{\kappa}}{2} \int_{\Omega_0} \left(\underline{\underline{\Sigma}}_2^{\mathrm{NI}} : \underline{\underline{e}}_2(\underline{w}) + \underline{\underline{\Sigma}}_4^{\mathrm{NI}} : \underline{\underline{e}}_0(\underline{w})\right)\mathrm{d}\Omega_0 \\ &+ \int_{\Omega_0} \left(\underline{\underline{\Sigma}}_2^{\mathrm{TI}} : \underline{\underline{e}}_0(\underline{w}) + \left(\underline{\underline{\Sigma}}_0^{\mathrm{TI}} + \underline{\underline{\Sigma}}^A\right) : \underline{\underline{e}}_2(\underline{w})\right)\mathrm{d}\Omega_0 \\ &+ \hat{\zeta} \int_{\Omega_0} \left(\underline{\underline{\Sigma}}_2^{\mathrm{VS}} : \underline{\underline{e}}_2(\underline{w}) + \underline{\underline{\Sigma}}_4^{\mathrm{VS}} : \underline{\underline{e}}_0(\underline{w})\right)\mathrm{d}\Omega_0 = \cos(\hat{\omega}\,\tau) \int_{\Gamma_0} \underline{\mathrm{t}}_2 \cdot \underline{w}\ \mathrm{d}\Gamma_0.\end{aligned} \tag{2.58}$$

Note that, since $\underline{y}_1 = \underline{0}$, the equation above only involves even terms of the expansion of the stress tensors. The term $\underline{\underline{\Sigma}}_2^{\mathrm{TI}}$ is defined as

$$\underline{\underline{\Sigma}}_2^{\mathrm{TI}} = \frac{\partial \underline{\underline{\Sigma}}^{\mathrm{TI}}}{\partial \underline{\underline{e}}}(\underline{y}_0) : \underline{\underline{e}}_0(\underline{y}_2).$$

The full expression of this term is detailed in Section 2.6.4 by substituting $\underline{y}_2 = \underline{w}$, for the sake of completeness. We just highlight here that it is linear in $\underline{y}_2$. Moreover, since $\underline{y}_1 = 0$, the terms $\underline{\underline{\Sigma}}_2^{\mathrm{NI}}$ and $\underline{\underline{\Sigma}}_2^{\mathrm{VS}}$ reduce to

$$\underline{\underline{\Sigma}}_2^{\mathrm{NI}} = I_{3,2}\,\underline{\underline{C}}_0^{-1} = 2\ \mathrm{tr}\left(\underline{\underline{C}}_0^{-1} \cdot \underline{\underline{e}}_0(\underline{y}_2)\right)\underline{\underline{C}}_0^{-1}, \quad \underline{\underline{\Sigma}}_2^{\mathrm{VS}} = \underline{\underline{C}}_0^{-1}\ \mathrm{tr}\left(\underline{\underline{C}}_0^{-1} \cdot \partial_\tau \underline{\underline{e}}_0(\underline{y}_2)\right).$$

whereas the terms $\underline{\underline{\Sigma}}_4^{\mathrm{NI}}$ and $\underline{\underline{\Sigma}}_4^{\mathrm{VS}}$ read

$$\underline{\underline{\Sigma}}_4^{\mathrm{NI}} = I_{3,2}\underline{\underline{G}}_2 + I_{3,4}\underline{\underline{C}}_0^{-1}, \quad \underline{\underline{\Sigma}}_4^{\mathrm{VS}} = \underline{\underline{C}}_0^{-1}\,\mathrm{tr}\left(\underline{\underline{D}}_4\right) + \underline{\underline{G}}_2\,\mathrm{tr}\left(\underline{\underline{C}}_0^{-1} \cdot \partial_\tau \underline{\underline{e}}_0(\,\underline{y}_2\,)\right),$$

where $\underline{\underline{D}}_4$ is a tensor field and $I_{3,4}$ a scalar field and their exact expressions are not needed. Note that from Eq. (2.47), we deduce

$$\mathrm{p}_0 = \frac{\hat{\omega}\,\hat{\kappa}}{2\pi}\int_0^{\frac{2\pi}{\hat{\omega}}} \frac{1}{2} I_{3,2}\,\mathrm{d}\tau = \hat{\kappa}\,\underline{\underline{C}}_0^{-1} : \underline{\underline{e}}_0(\underline{y}_2^S). \tag{2.59}$$

We can state now the main result of this section.

Proposition 2.15. *There exists a scalar field* p_2 *depending on time* t *such that the couple* $(\underline{y}_2^S, \mathrm{p}_2)$ *is solution of Eq.* (2.20) *and*

$$\begin{aligned} s(t,\underline{w}) &= \frac{\hat{\omega}}{2\pi}\int_0^{\frac{2\pi}{\hat{\omega}}}\int_{\Omega(t)} \mathrm{div}_{\underline{x}}\Big(\left(\hat{\kappa} + \hat{\zeta}\partial_\tau\right)\underline{y}_2^f\Big)\left(\underline{\underline{\nabla}}_{\underline{x}}\,\underline{y}_2^f\right)^T : \underline{\underline{\nabla}}_{\underline{x}}\,\underline{w}\,\mathrm{d}\Omega\,\mathrm{d}\tau, \\ r(t,q) &= \frac{1}{\hat{\kappa}}\int_{\Omega_0} \mathrm{p}_0\,q\,\mathrm{d}\Omega_0. \end{aligned} \tag{2.60}$$

Proof. First, since we want to derive the governing equation of the slowly varying vector field $\underline{y}_2^S$, we integrate Eq. (2.58) on τ over its period. If we also take into account Eq. (2.59), we obtain the system of equations satisfied by $(\underline{y}_2^S, \mathrm{p}_2)$:

$$\begin{cases} \displaystyle\int_{\Omega_0} \rho_0\,\partial_t^2 \underline{y}_2^S \cdot \underline{w}\,\mathrm{d}\Omega_0 + \int_{\Omega_0} \mathrm{p}_2\,\underline{\underline{C}}_0^{-1} : \underline{\underline{e}}_0(\underline{w})\,\mathrm{d}\Omega_0 + a(\underline{y}_2^S, \underline{w}) = s(t,\underline{w}) \\ \displaystyle\hat{\kappa}\int_{\Omega_0} \underline{\underline{C}}_0^{-1} : \underline{\underline{e}}_0(\underline{y}_2^S)\,q\,\mathrm{d}\Omega_0 = \int_{\Omega_0} \mathrm{p}_0\,q\,\mathrm{d}\Omega_0, \end{cases} \tag{2.61}$$

where

$$\frac{\hat{\omega}}{2\pi}\int_0^{\frac{2\pi}{\hat{\omega}}} \left(\frac{\hat{\kappa}}{2} I_{3,4} + \hat{\zeta}\ \mathrm{tr}\left(\underline{\underline{D}}_4\right)\right)\mathrm{d}\tau = \mathrm{p}_2, \tag{2.62}$$

and

$$\begin{aligned} a(\underline{y}_2^S, \underline{w}) = &\int_{\Omega_0} \underline{\underline{\Sigma}}_{2,S}^{\mathrm{TI}} : \underline{\underline{e}}_0(\underline{w})\,\mathrm{d}\Omega_0 - 2\int_{\Omega_0} \mathrm{p}_0\,\underline{\underline{C}}_0^{-1} \cdot \underline{\underline{e}}_0(\underline{y}_2^S) : \underline{\underline{C}}_0^{-1} \cdot \underline{\underline{e}}_0(\underline{w})\,\mathrm{d}\Omega_0 \\ &+ \int_{\Omega_0} \left(\underline{\underline{\Sigma}}_0^{\mathrm{TI}} + \underline{\underline{\Sigma}}^A + \mathrm{p}_0\,\underline{\underline{C}}_0^{-1}\right) : \left(\underline{\underline{\nabla}}\,\underline{y}_2^S\right)^T \cdot \underline{\underline{\nabla}}\,\underline{w}\,\mathrm{d}\Omega_0. \end{aligned}$$

The tensor $\underline{\underline{\Sigma}}^{\mathrm{TI}}_{2,S}$ is obtained from $\underline{\underline{\Sigma}}^{\mathrm{TI}}_{2}$ by substituting $\underline{y}^S_2$ for $\underline{y}_2$ in the expression of the tensor. Furthermore, the term $s(t,\underline{w})$ reads

$$\begin{aligned} s(t,\underline{w}) \coloneqq &-\frac{\hat{\omega}}{2\pi}\int_0^{\frac{2\pi}{\hat{\omega}}}\int_{\Omega_0}\hat{\kappa}\,\mathrm{tr}\Big(\underline{\underline{C}}_0^{-1}\cdot\underline{\underline{e}}_0\big(\underline{y}_2^f\big)\Big)\,\mathrm{tr}\Big(\underline{\underline{C}}_0^{-1}\cdot\underline{\underline{e}}_2^f\big(\underline{w}\big)+\underline{\underline{G}}_2^f\cdot\underline{\underline{e}}_0\big(\underline{w}\big)\Big)\mathrm{d}\Omega_0\,\mathrm{d}\tau \\ &-\frac{\hat{\omega}}{2\pi}\int_0^{\frac{2\pi}{\hat{\omega}}}\int_{\Omega_0}\hat{\zeta}\,\mathrm{tr}\Big(\underline{\underline{C}}_0^{-1}\cdot\partial_\tau\underline{\underline{e}}_0\big(\underline{y}_2^f\big)\Big)\,\mathrm{tr}\Big(\underline{\underline{C}}_0^{-1}\cdot\underline{\underline{e}}_2^f\big(\underline{w}\big)+\underline{\underline{G}}_2^f\cdot\underline{\underline{e}}_0\big(\underline{w}\big)\Big)\mathrm{d}\Omega_0\,\mathrm{d}\tau, \end{aligned} \tag{2.63}$$

with

$$\underline{\underline{e}}_2^f\big(\underline{w}\big)\coloneqq\frac{1}{2}\Big(\big(\underline{\underline{\nabla}}\,\underline{y}_2^f\big)^T\cdot\underline{\underline{\nabla}}\,\underline{w}+\big(\underline{\underline{\nabla}}\,\underline{w}\big)^T\cdot\underline{\underline{\nabla}}\,\underline{y}_2^f\Big),\qquad \underline{\underline{G}}_2^f=-2\,\underline{\underline{C}}_0^{-1}\cdot\underline{\underline{e}}_0\big(\underline{y}_2^f\big)\cdot\underline{\underline{C}}_0^{-1}.$$

We can see that it is a nonlinear (quadratic) contribution only depending on $\underline{y}_2^f(\tau)$. As a consequence, it is a source term (accounting for the ARF contribution) and, although $\underline{y}_2^f(\tau)$ has zero mean, it gives a non-zero contribution in the equation, due to nonlinearity. We can rewrite Eq. (2.63) in the deformed configuration. It becomes

$$s(t,\underline{w})\coloneqq\frac{\hat{\omega}}{2\pi}\int_0^{\frac{2\pi}{\hat{\omega}}}\int_{\Omega(t)}\Big(\hat{\kappa}\,\mathrm{tr}\Big(\underline{\underline{\nabla}}_{\underline{x}}\,\underline{y}_2^f\Big)+\hat{\zeta}\,\mathrm{tr}\Big(\partial_\tau\,\underline{\underline{\nabla}}_{\underline{x}}\,\underline{y}_2^f\Big)\Big)\,\mathrm{tr}\Big(\underline{\underline{\nabla}}_{\underline{x}}\,\underline{y}_2^f\cdot\underline{\underline{\nabla}}_{\underline{x}}\,\underline{w}\Big)\mathrm{d}\Omega\,\mathrm{d}\tau, \tag{2.64}$$

since

$$\mathrm{tr}\Big(\underline{\underline{C}}_0^{-1}\cdot\underline{\underline{e}}_2^f\big(\underline{w}\big)+\underline{\underline{G}}_2^f\cdot\underline{\underline{e}}_0\big(\underline{w}\big)\Big)=-\,\mathrm{tr}\Big(\underline{\underline{\nabla}}_{\underline{\xi}}\,\underline{y}_2^f\cdot\underline{\underline{F}}_0^{-1}\cdot\underline{\underline{\nabla}}_{\underline{\xi}}\,\underline{w}\cdot\underline{\underline{F}}_0^{-1}\Big)=-\,\mathrm{tr}\Big(\underline{\underline{\nabla}}_{\underline{x}}\,\underline{y}_2^f\cdot\underline{\underline{\nabla}}_{\underline{x}}\,\underline{w}\Big).$$

As a consequence, we derive

$$s(t,\underline{w})=\frac{\hat{\omega}}{2\pi}\int_0^{\frac{2\pi}{\hat{\omega}}}\int_{\Omega(t)}\mathrm{div}_{\underline{x}}\Big(\big(\hat{\kappa}+\hat{\zeta}\partial_\tau\big)\,\underline{y}_2^f\Big)\,\big(\underline{\underline{\nabla}}_{\underline{x}}\,\underline{y}_2^f\big)^T:\underline{\underline{\nabla}}_{\underline{x}}\,\underline{w}\,\mathrm{d}\Omega\,\mathrm{d}\tau. \tag{2.65}$$

Therefore, it is easy to see that the couple $(\underline{y}_2^S,\mathrm{p}_2)$ is solution of Eq. (2.20) with $\tilde{\underline{y}}=\underline{y}_2^S$ and $\tilde{p}=\mathrm{p}_2$, $s(t,\underline{w})$ and $r(t,q)$ defined as in Eq. (2.63), thus concluding the proof. □

Remark Note that p_2 represents a Lagrange multiplier for the solution $\underline{y}_2^S$. Due to Eq. (2.62) and the definition of $I_{3,4}$, p_2 also contains some terms that depend on $\underline{y}_2^f$ and do not vanish after integration, since they are quadratic in $\underline{y}_2^f$.
We also emphasize that, if the solution of the nonlinear problem $\underline{y}_0$ is zero, then the Lagrangian multiplier p_0 is also zero due to Eq. (2.61). This implies that, in this case, the term $\underline{y}_2^S$ is divergence-free.

In order to further simplify the expression of $s(t,\underline{w})$ we need to take into account the governing equation of $\underline{y}_2^f$, namely Eq. (2.54), as discussed in the following section.

2.5.8 Proof of Corollary 2.1

Governing equation of the pressure field induced by ARF. Due to the periodic structure of the surface source term, Eq. (2.54) can be recast in the frequency domain. First, we can rewrite the scalar field $\mathrm{p}_2^f=\mathrm{div}_{\underline{x}}\underline{y}_2^f$ as

$$p_2^f(\underline{\xi},t,\tau)=\mathrm{Re}\left(e^{-i\hat{\omega}\tau}\hat{p}_2^f(\underline{\xi},t)\right) \tag{2.66}$$

where $\hat{p}_2^f$ satisfies

$$\begin{cases} \Delta_{\underline{x}}\,\hat{p}_2^f + \alpha\,\hat{p}_2^f = 0 & \text{in} \quad \Omega(t), \\ \underline{\nabla}_{\underline{x}}\,\hat{p}_2^f \cdot \underline{n} = 0 & \text{on} \quad \Gamma_D(t), \\ (\hat{\kappa} - i\,\hat{\omega}\,\hat{\zeta})\,\hat{p}_2^f(\underline{x},t) = p(\underline{x},t) & \text{on} \quad \Gamma_N(t), \end{cases} \tag{2.67}$$

with

$$\alpha := \frac{\rho_0\,\hat{\omega}^2}{\hat{\kappa} - i\,\hat{\omega}\,\hat{\zeta}} \in \mathbb{C}. \tag{2.68}$$

Remark Eq. (2.67) represents for each time t a Helmholtz equation governing the propagation of the pushing pressure wave corresponding to the ARF. Note that t plays the role of a parameter in this equation, due to Eq. (2.66). Problem (2.67) is well-posed, for all time t, because $\mathrm{Im}(\alpha) \neq 0$. To continue in the simplification process we introduce the function $\underline{\hat{y}}_2^f$ such that $\underline{\hat{y}}_2^f = -\alpha^{-1}\underline{\nabla}_{\underline{x}}\hat{p}_2^f$. By definition of $\hat{p}_2^f$, we retrieve that $\mathrm{div}_{\underline{x}}\,\underline{\hat{y}}_2^f = \hat{p}_2^f$. In addition, the function $\underline{y}_2^f$ satisfies

$$\underline{y}_2^f = \mathrm{Re}\left(\underline{\hat{y}}_2^f e^{-i\hat{\omega}\tau}\right). \tag{2.69}$$

Remark Note that if the surface source term was defined in the deformed configuration as

$$\underline{\mathrm{t}}(\underline{n}) = \hat{p}_c\,\cos(\hat{\omega}\,\tau)\,\underline{n} + \,\hat{p}_s\,\sin(\omega\,\tau)\,\underline{n},$$

Eq. (2.67) would be easily modified as

$$\begin{cases} \Delta_{\underline{x}}\,\hat{p}_2^f + \alpha\,\hat{p}_2^f = 0 & \text{in} \quad \Omega(t), \\ \underline{\nabla}_{\underline{x}}\,\hat{p}_2^f \cdot \underline{n} = 0 & \text{on} \quad \Gamma_D(t), \\ (\hat{\kappa} - i\,\hat{\omega}\,\hat{\zeta})\,\hat{p}_2^f(\underline{x},t) = \hat{p}_c(\underline{x},t) + i\,\hat{p}_s(\underline{x},t) & \text{on} \quad \Gamma_N(t), \end{cases} \tag{2.70}$$

and α defined as in Eq. (2.68).

Simplified expression of the source term for shear wave propagation generated by ARF. The expression of the source term $s(t,\underline{w})$ in Eq. (2.65) can be drastically simplified due to Eq. (2.67). In more detail, after some algebra, we obtain the following lemma:

Lemma 2.16. *Let us define*

$$\begin{aligned} q_\alpha &:= \frac{\alpha}{2|\alpha|^2}\left|\underline{\nabla}_{\underline{x}}\hat{p}_2^f\right|^2 - \frac{1}{2}\left|\hat{p}_2^f\right|^2, \\ \underline{l}_\alpha &:= i\,\frac{\alpha}{|\alpha|^2}\Big(- \underline{\underline{H}}_{\underline{x}}\big(\mathrm{Im}\,(\hat{p}_2^f)\big)\,\underline{\nabla}_{\underline{x}}\,\mathrm{Re}\,(\hat{p}_2^f) + \underline{\underline{H}}_{\underline{x}}\big(\mathrm{Re}\,(\hat{p}_2^f)\big)\,\underline{\nabla}_{\underline{x}}\,\mathrm{Im}\,(\hat{p}_2^f)\Big) \\ &\quad - i\,\mathrm{Im}\left(\hat{p}_2^f\,\underline{\nabla}_{\underline{x}}\Big(\overline{\hat{p}_2^f}\Big)\right). \end{aligned} \tag{2.71}$$

with $\underline{\underline{H}}_{\underline{x}}\big(\hat{p}_2^f\big)$ *the Hessian matrix of* $\hat{p}_2^f$. *Then the source term reads, in the deformed*

configuration,

$$
\begin{aligned}
s\big(t,\underline{w}\big) \coloneqq & \frac{1}{2}\int_{\Omega(t)} \underline{\nabla}_{\underline{x}}\left(\hat{\kappa}\ \mathrm{Re}(q_\alpha)+\hat{\zeta}\,\hat{\omega}\ \mathrm{Im}(q_\alpha)\right)\cdot\underline{w}\,\mathrm{d}\Omega \\
& + \frac{1}{2}\int_{\Omega(t)} \left(\hat{\kappa}\ \mathrm{Re}\left(\underline{l}_\alpha\right)+\hat{\zeta}\,\hat{\omega}\,Im\big(\underline{l}_\alpha\big)\right)\cdot\underline{w}\,\mathrm{d}\Omega \\
& - \frac{\rho_0\,\hat{\omega}^2}{2\,|\alpha|^2}\int_{\Gamma_N(t)} \left(\mathrm{Re}\left(\hat{p}_2^f\,\underline{\underline{H}}_{\underline{x}}\big(\overline{\hat{p}_2^f}\big)\right)\cdot\underline{n}\right)\cdot\underline{w}\,\mathrm{d}\Gamma.
\end{aligned}
\tag{2.72}
$$

The proof of Lemma 2.16 can be found in Section 2.6.1. Furthermore, note that the first term in Eq. (2.72) can be considered a "compression" term, since it is associated with a gradient. As a consequence, we can rewrite the result of Proposition 2.15 as follows.

Proposition 2.17. *There exists a scalar field* p_2 *depending on time* t *such that the couple* $(\underline{y}_2^S,\mathrm{p}_2)$ *is solution of Eq.* (2.20) *and*

$$
\begin{aligned}
s\big(t,\underline{w}\big) = & -\frac{\hat{\zeta}\,\hat{\omega}}{2}\int_{\Omega(t)} \mathrm{Im}\left(\hat{p}_2^f\,\underline{\nabla}_{\underline{x}}\Big(\overline{\hat{p}_2^f}\Big)\right)\cdot\underline{w}\,\mathrm{d}\Omega - \frac{\rho_0\,\hat{\omega}^2}{2\,|\alpha|^2}\int_{\Gamma_N(t)} \left(\mathrm{Re}\left(\hat{p}_2^f\,\underline{\underline{H}}_{\underline{x}}\big(\overline{\hat{p}_2^f}\big)\right)\cdot\underline{n}\right)\cdot\underline{w}\,\mathrm{d}\Gamma, \\
& + \frac{1}{4|\alpha|^2}\int_{\Gamma(t)} \big(\,\rho_0\,\hat{\omega}^2|\underline{\nabla}_{\underline{x}}\hat{p}_2^f|^2 - \hat{\kappa}\,|\alpha|^2\,|\hat{p}_2^f|^2\,\big)\underline{w}\cdot\underline{n}\,\mathrm{d}\Gamma. \\
r(t,q) = & \frac{1}{\hat{\kappa}}\int_{\Omega_0} \mathrm{p}_0\,q\,\mathrm{d}\Omega_0,
\end{aligned}
$$

with $\hat{p}_2^f \coloneqq \mathrm{div}_{\underline{x}}\,\underline{\hat{y}}_2^f$ *solution of Eq.* (2.67).

Proof. We start the proof by considering the result given in Proposition 2.15. In order to simplify the expression of the source term, we consider Eq. (2.72). First, we apply the Green formula on the first term of $s\big(t,\underline{w}\big)$:

$$
\begin{aligned}
\frac{1}{2}\int_{\Omega(t)} \underline{\nabla}_{\underline{x}}\left(\hat{\kappa}\ \mathrm{Re}(q_\alpha)+\hat{\zeta}\,\hat{\omega}\ \mathrm{Im}(q_\alpha)\right)\cdot\underline{w}\,\mathrm{d}\Omega = & -\frac{1}{2}\int_{\Omega(t)} \left(\hat{\kappa}\ \mathrm{Re}(q_\alpha)+\hat{\zeta}\,\hat{\omega}\ \mathrm{Im}(q_\alpha)\right)\mathrm{div}_{\underline{x}}\underline{w}\,\mathrm{d}\Omega \\
& + \frac{1}{2}\int_{\Gamma(t)} \left(\hat{\kappa}\ \mathrm{Re}(q_\alpha)+\hat{\zeta}\,\hat{\omega}\ \mathrm{Im}(q_\alpha)\right)\underline{w}\cdot\underline{n}\,\mathrm{d}\Gamma
\end{aligned}
$$

is a "compression" term, this contribution can be naturally included in p_2:

$$
\begin{aligned}
& \frac{\hat{\omega}\,\hat{\zeta}}{2\pi}\int_0^{\frac{2\pi}{\hat{\omega}}} \left(\mathrm{tr}\left(\underline{\underline{C}}_0^{-1}\cdot\partial_t\underline{\underline{e}}_0\big(\underline{y}_3\big)+\underline{\underline{G}}_3\cdot\partial_t\underline{\underline{e}}_0+\underline{\underline{G}}_2\cdot\partial_\tau\underline{\underline{e}}_0\big(\underline{y}_2\big)+\hat{\omega}\ \mathrm{Im}(q_\alpha)\right)\mathrm{d}\tau\right. \\
& \left. + \frac{\hat{\omega}\,\hat{\kappa}}{2\pi}\int_0^{\frac{2\pi}{\hat{\omega}}} \left(\frac{1}{2}I_{3,4}+\mathrm{Re}(q_\alpha)\right)\mathrm{d}\tau = \mathrm{p}_2.\right.
\end{aligned}
$$

On the other hand, after some algebra, it is possible to retrieve from Lemma 2.16:

$$
\frac{1}{2}\int_{\Gamma(t)} \big(\hat{\kappa}\ \mathrm{Re}(q_\alpha)+\hat{\zeta}\,\hat{\omega}\ \mathrm{Im}(q_\alpha)\big)\underline{w}\cdot\underline{n}\,\mathrm{d}\Gamma = \frac{1}{4|\alpha|^2}\int_{\Gamma(t)} \big(\,\rho_0\,\hat{\omega}^2|\underline{\nabla}_{\underline{x}}\hat{p}_2^f|^2 - \hat{\kappa}\,|\alpha|^2\,|\hat{p}_2^f|^2\,\big)\underline{w}\cdot\underline{n}\,\mathrm{d}\Gamma.
$$

Then, our aim is to simplify the second term in Eq. (2.72), that reads

$$
\frac{1}{2}\int_{\Omega(t)} \left(\hat{\kappa}\ \mathrm{Re}\left(\underline{l}_\alpha\right)+\hat{\zeta}\,\hat{\omega}\,Im\big(\underline{l}_\alpha\big)\right)\cdot\underline{w}\,\mathrm{d}\Omega.
$$

To do so, we consider the vector field $\underline{l}_\alpha$ in (2.71). It can be decomposed into

$$\underline{l}_\alpha = i\,\alpha\,R + i\,S,$$

with

$$R := \frac{1}{|\alpha|^2}\Big(-\underline{\underline{H}}_{\underline{x}}\big(\mathrm{Im}\,(\hat{p}_2^f)\big)\,\underline{\nabla}_{\underline{x}}\,\mathrm{Re}\,(\hat{p}_2^f)+\underline{\underline{H}}_{\underline{x}}\big(\mathrm{Re}\,(\hat{p}_2^f)\big)\,\underline{\nabla}_{\underline{x}}\,\mathrm{Im}\,(\hat{p}_2^f)\Big),\ S := -\,\mathrm{Im}\left(\hat{p}_2^f\,\underline{\nabla}_{\underline{x}}\left(\overline{\hat{p}_2^f}\right)\right).$$

Then, we obtain that

$$\mathrm{Re}(\underline{l}_\alpha) = -\,\mathrm{Im}(\alpha)\,R, \quad \mathrm{Im}(\underline{l}_\alpha) = \mathrm{Re}(\alpha)\,R + S.$$

Furthermore, by the definition (2.68), we can derive

$$\mathrm{Re}(\alpha) = \rho_0\,\hat{\omega}^2\frac{\hat{\kappa}}{|\hat{\kappa}|^2 + \left|\hat{\omega}\,\hat{\zeta}\right|^2}, \quad \mathrm{Im}(\alpha) = \rho_0\,\hat{\omega}^2\frac{\hat{\omega}\,\hat{\zeta}}{|\hat{\kappa}|^2 + \left|\hat{\omega}\,\hat{\zeta}\right|^2}.$$

As a consequence, we can rewrite

$$\hat{\kappa}\ \mathrm{Re}\,(\underline{l}_\alpha) + \hat{\zeta}\,\hat{\omega}\,Im(\underline{l}_\alpha) = -\hat{\kappa}\ \mathrm{Im}(\alpha)\,R + \hat{\zeta}\,\hat{\omega}\ \mathrm{Re}(\alpha)\,R + \hat{\zeta}\,\hat{\omega}\,S = \hat{\zeta}\,\hat{\omega}\,S.$$

Hence, from Eq. (2.72), we deduce that the only source term contributing in the generation of shear waves reads

$$s(t,\underline{w}) = -\frac{\hat{\zeta}\,\hat{\omega}}{2}\int_{\Omega(t)}\mathrm{Im}\left(\hat{p}_2^f\,\underline{\nabla}_{\underline{x}}\left(\overline{\hat{p}_2^f}\right)\right)\cdot\underline{w}\,\mathrm{d}\Omega - \frac{\rho_0\,\hat{\omega}^2}{2\,|\alpha|^2}\int_{\Gamma_N(t)}\left(\mathrm{Re}\left(\hat{p}_2^f\,\underline{\underline{H}}_{\underline{x}}\big(\overline{\hat{p}_2^f}\big)\right)\cdot\underline{n}\right)\cdot\underline{w}\,\mathrm{d}\Gamma$$
$$+\frac{1}{4|\alpha|^2}\int_{\Gamma(t)}\big(\,\rho_0\,\hat{\omega}^2|\underline{\nabla}_{\underline{x}}\hat{p}_2^f|^2 - \hat{\kappa}\,|\alpha|^2\,|\hat{p}_2^f|^2\,\big)\underline{w}\cdot\underline{n}\,\mathrm{d}\Gamma.$$

that was to be demonstrated. □

Note that $s(t,\underline{w})$ is quadratic in $\hat{p}_2^f$, and it consists of a volume term, accounting for the ARF phenomenon, and a surface term. Furthermore, observe that for small values of $\hat{\zeta}$, one can expect that the volume integral in $s(t,\underline{w})$ behaves linearly with respect to attenuation, in accordance with Eq. (2.1). Hence, viscosity is essential for the generation of shear waves from ARF.

2.6 Appendix - Further details on theoretical results

2.6.1 Proof of Lemma 2.3

Proof. Our objective is to rewrite $\mathcal{P}_\varepsilon^{ext}$ as a volume integral, as in Eq. (2.15). First, let us take into account Eq. (2.14), and rewrite $\mathcal{P}_\varepsilon^{ext}$ as

$$\begin{aligned}\mathcal{P}_\varepsilon^{ext} &= \int_{\Gamma_{N,0}} J_\varepsilon\,\cos(\hat{\omega}\,t/\varepsilon)\,p\,\underline{\dot{y}}_\varepsilon\cdot\underline{\underline{F}}_\varepsilon^{-T}\cdot\underline{n}_0\left|\underline{\underline{F}}_\varepsilon^{-T}\cdot\underline{n}_0\right|\mathrm{d}S_0\\ &= \int_{\Gamma_{N,0}} J_\varepsilon\,\cos(\hat{\omega}\,t/\varepsilon)\,\ell\,\underline{\dot{y}}_\varepsilon\cdot\underline{\underline{F}}_\varepsilon^{-T}\cdot\underline{n}_0\left|\underline{\underline{F}}_\varepsilon^{-T}\cdot\underline{n}_0\right|\mathrm{d}S_0.\end{aligned} \tag{2.73}$$

We now consider Eq. (2.73) in the deformed domain $\Omega(t)$, with the usual convention of implicit composition with the deformation map $\underline{\phi}$. Applying the divergence theorem, since $\underline{\dot{y}}_\varepsilon = \underline{0}$ on $\Gamma_D(t)$, we have

$$\begin{aligned}\int_{\Gamma_N(t)} \ell\, \underline{\dot{y}}_\varepsilon \cdot \underline{n}\, \mathrm{d}S = \int_{\Gamma(t)} \ell\, \underline{\dot{y}}_\varepsilon \cdot \underline{n}\, \mathrm{d}S &= \int_{\Omega(t)} \underline{\nabla}_{\underline{x}} \cdot \underline{\dot{y}}_\varepsilon\, \ell\, \mathrm{d}\Omega + \int_{\Omega(t)} \underline{\dot{y}}_\varepsilon \cdot \underline{\nabla}_{\underline{x}} \ell\, \mathrm{d}\Omega \\ &= \int_{\Omega(t)} \mathrm{tr}\Big(\underline{\underline{\nabla}}_{\underline{x}} \cdot \underline{\dot{y}}_\varepsilon\Big)\, \ell\, \mathrm{d}\Omega + \int_{\Omega(t)} \underline{\dot{y}}_\varepsilon \cdot \underline{\nabla}_{\underline{x}} \ell\, \mathrm{d}\Omega.\end{aligned} \tag{2.74}$$

Eq. (2.74) can be rewritten in Lagrangian formulation, leading to

$$\begin{aligned}\int_{\Gamma_{N,0}} J_\varepsilon\, \ell\, \underline{\dot{y}}_\varepsilon \cdot \underline{\underline{F}}_\varepsilon^{-T} \cdot \underline{n}_0 \Big| \underline{\underline{F}}_\varepsilon^{-T} \cdot \underline{n}_0 \Big|\, \mathrm{d}S_0 = \int_{\Omega_0} J_\varepsilon\ \mathrm{tr}\left(\underline{\underline{F}}_\varepsilon^{-1} \cdot \underline{\underline{\nabla}}_{\underline{\xi}}\, \underline{\dot{y}}_\varepsilon\right) \ell\, \mathrm{d}\Omega_0 \\ + \int_{\Omega_0} J_\varepsilon \underline{\dot{y}}_\varepsilon \cdot \underline{\underline{F}}_\varepsilon^{-T} \cdot \underline{\nabla}_{\underline{\xi}} \ell\, \mathrm{d}\Omega_0.\end{aligned} \tag{2.75}$$

If we multiply Eq. (2.75) by $\cos(\hat{\omega}\, t/\varepsilon)$, we obtain Eq. (2.15), thus concluding the proof. □

2.6.2 Proof of Proposition 2.4

As preliminary results, we provide the following propositions.

Proposition 2.18. *For any $\kappa_* > 2$, there exists $c \in \mathbb{R}$ such that for all $\kappa > \kappa_*$ we have*

$$W^{NI} \geq J^2 + c.$$

Proof. For the sake of simplicity, we set $k := \kappa/2$ in Eq. (2.6) and define $I := J^2$. Our objective is to prove the following inequality:

$$k\,(I-1) - k\,\log(I) \geq I + c, \quad c \in \mathbb{R}. \tag{2.76}$$

We define $\mathcal{L}(I) \coloneqq (k-1)\,I - k\,\log I$. Then, Eq. (2.76) reads

$$\mathcal{L}(I) \geq k + c. \tag{2.77}$$

Note that, since $k > 1$, we have

$$\lim_{I\to 0} \mathcal{L}(I) = +\infty, \qquad \lim_{I\to+\infty} \mathcal{L}(I) = +\infty,$$

and therefore the minimum I^* of the function $\mathcal{L}(I)$ can be found in the interval $]0, +\infty[$ by imposing

$$\mathcal{L}'(I^*) = 0 \implies (k-1) - \frac{k}{I^*} = 0 \implies I^* = \frac{k}{k-1}.$$

Now

$$\min_{I\in]0,+\infty[} \mathcal{L}(I) = \mathcal{L}(I^*) = k - k\,\log\left(\frac{k}{k-1}\right),$$

thus Eq. (2.77) is satisfied if and only if

$$k\,\log\left(\frac{k}{k-1}\right) \leq -c. \tag{2.78}$$

In addition, since $k > \kappa^*/2 > 1$, then we can show that there exists $c^* > 1$ such that

$$\lim_{k\to\kappa^*/2} k\,\log\left(\frac{k}{k-1}\right) = c^*.$$

Moreover, the left-hand side of Eq. (2.78) is monotone decreasing, and

$$\lim_{k\to+\infty} k\,\log\left(\frac{k}{k-1}\right) = 1.$$

Consequently, Eq. (2.78) is verified with $-c = c^*$, thus concluding the proof. □

Proposition 2.19. *For any $\kappa_* > 2$, there exists $c \in \mathbb{R}$, depending on $\{\kappa_*, \kappa_1, \kappa_2, \kappa_3, \kappa_4, \kappa_5\}$ only, such that for all $\kappa > \kappa_*$,*

$$W^{TI}+\kappa_5\,W^{NI} \geq \kappa_5 I_2+c,\ W^{TI}+\kappa_5\,W^{NI} \geq \frac{\kappa_3\kappa_4}{2}\,I_4^2+c \ \text{ and } \ W^{TI}+\kappa_5\,W^{NI} \geq \kappa_3\sqrt{\kappa_4}\,I_4+c.$$

Proof. We first recall the definition of the potential W^{TI}. It reads

$$W^{\mathrm{TI}} = \kappa_1\,e^{\kappa_2(I_1-3)^2} + \kappa_3\,e^{\kappa_4(I_4-1)^2} + \kappa_5\big(I_2 - 2\log(J^2) - 3\big).$$

Now, let us prove the first inequality of the Proposition. We have, since $\log x \leq x/e$ and thanks to Proposition 2.18,

$$c + \kappa_5 I_2 \leq W^{\mathrm{TI}} + 2\,\kappa_5\log(J^2) \leq W^{\mathrm{TI}} + \frac{2}{e}\,\kappa_5\,J^2 \Rightarrow c + \kappa_5 I_2 \leq W^{\mathrm{TI}} + \kappa_5\,W^{\mathrm{NI}}.$$

Now, observing that $e^{\,x} \geq x$, and using the fact that $I_2 \geq 0$, we get

$$W^{\mathrm{TI}} + \kappa_5\,W^{\mathrm{NI}} \geq \kappa_3\kappa_4(I_4^2 - 2I_4 + 1) - 3\kappa_5.$$

Using the inequality $2I_4 \leq I_4^2/2 + 2$, we obtain the second inequality of the proposition. Finally, using the property that $e^{\,c^*x^2} \geq x$ with $c^* = e^{-1}/2 < 1$, and using this inequality with $x = \sqrt{\kappa_3}\,|I_4 - 1|\,/\sqrt{c^*}$, we retrieve

$$W^{\mathrm{TI}} + \kappa_5\,W^{\mathrm{NI}} \geq \kappa_3\frac{\sqrt{\kappa_4}}{\sqrt{c^*}}\,|I_4 - 1| - 3\kappa_5.$$

The third inequality then follows straightforwardly. Note that I_1 could be estimated in a similar way, but such estimate is not used in what follows. □

Note that, if we consider the stress tensors associated with the parametric family of solutions $\underline{y}_\varepsilon$:

$$W_\varepsilon^{\mathrm{TI}} = \kappa_1\,e^{\kappa_2(I_{1,\varepsilon}-3)^2} + \kappa_3\,e^{\kappa_4(I_{4,\varepsilon}-1)^2} + \kappa_5\big(I_{2,\varepsilon} - 2\log(J_\varepsilon^2) - 3\big),$$
$$W_\varepsilon^{\mathrm{NI}} = \frac{\hat{\kappa}\varepsilon^{-2}}{2}\Big((J_\varepsilon^2 - 1) - \log\big(J_\varepsilon^2\big)\Big),\ W_\varepsilon^{\mathrm{VS}} = \frac{\zeta}{2}\,\mathrm{tr}\left(\underline{\underline{C}}_\varepsilon^{-1}\cdot\underline{\underline{\dot{e}}}_\varepsilon\right)^2,$$

then we can state that, assuming $\varepsilon > 0$ small enough, that there exists $c \in \mathbb{R}$ depending on $\{\kappa_1, \kappa_2, \kappa_3, \kappa_4, \kappa_5\}$ such that we have

$$W_\varepsilon^{\mathrm{NI}} \geq J_\varepsilon^2 + c.$$

and

$$W_\varepsilon^{\mathrm{TI}}+\kappa_5\,W_\varepsilon^{\mathrm{NI}} \geq \kappa_5 I_{2,\varepsilon}+c,\ W_\varepsilon^{\mathrm{TI}}+\kappa_5\,W_\varepsilon^{\mathrm{NI}} \geq \frac{\kappa_3\kappa_4}{2}\,I_{4,\varepsilon}^2+c \ \text{ and } \ W_\varepsilon^{\mathrm{TI}}+\kappa_5\,W_\varepsilon^{\mathrm{NI}} \geq \kappa_3\sqrt{\kappa_4}\,I_{4,\varepsilon}+c.$$

We also need another expression of the source term $\mathcal{P}_\varepsilon^A$. We can rewrite, by definition of the tensor $\underline{\underline{\dot{e}}}_\varepsilon$,

$$\mathcal{P}_\varepsilon^A = -\int_{\Omega_0}\sigma_a\underline{\tau_1}\cdot\underline{\underline{\dot{e}}}_\varepsilon\cdot\underline{\tau_1}\,\mathrm{d}\Omega_0 = -\frac{1}{2}\int_{\Omega_0}\sigma_a\,\underline{\tau_1}\cdot\partial_t\left(\underline{\underline{F}}_\varepsilon^T\underline{\underline{F}}_\varepsilon\right)\cdot\underline{\tau_1}\,\mathrm{d}\Omega_0.$$

Hence, by integrating over time, we find

$$\int_0^t \mathcal{P}_\varepsilon^A(s)\,\mathrm{d}s = \frac{1}{2}\int_0^t \int_{\Omega_0} \partial_t \sigma_a(\underline{\xi},s)\, I_{4,\varepsilon}(\underline{\xi},s)\,\mathrm{d}\Omega_0\,\mathrm{d}s - \frac{1}{2}\int_{\Omega_0} \sigma_a(\underline{\xi},t)\, I_{4,\varepsilon}(\underline{\xi},t)\,\mathrm{d}\Omega_0. \quad (2.79)$$

where $I_{4,\varepsilon} = \underline{\tau_1}\cdot\left(\underline{\underline{F}}_\varepsilon^T\cdot\underline{\underline{F}}_\varepsilon\right)\cdot\underline{\tau_1}$. Now we are able to prove Proposition 2.4.

Proof. We want to prove that the total internal energy $\mathcal{E}_\varepsilon^{tot}$ is bounded at every time $t\in[0,T]$, namely there exists a finite constant $C\in\mathbb{R}$ independent of ε such that

$$\mathcal{E}_\varepsilon^{tot}(t)\le C \quad \forall t\in[0,T].$$

Note that the value of C will change along every line of the proof, for the sake of simplicity. In order to retrieve this estimate, we need to control the source term contributions. First, let us integrate with respect to time equation (2.13). We obtain

$$\tilde{\mathcal{E}}_\varepsilon^{tot}(t) = \int_0^t \mathcal{P}_\varepsilon^{ext}(s)\,\mathrm{d}s + \int_0^t \mathcal{P}_\varepsilon^A(s),\mathrm{d}s, \quad \tilde{\mathcal{E}}_\varepsilon^{tot}(t) := \mathcal{E}_\varepsilon^{tot}(t) + \int_0^t \mathcal{E}_\varepsilon^{\mathrm{VS}}(s)\,\mathrm{d}s. \quad (2.80)$$

Now, we find an estimate for the term $\mathcal{P}_\varepsilon^{ext}$. We recall that, by Assumption 2.2, $|||\ell|||$ is a finite quantity. Therefore, we can assume that $|||\ell|||\le C$. Starting from Lemma 2.3 and applying the Cauchy-Schwarz inequality, Eq. (2.15) gives

$$\left|\mathcal{P}_\varepsilon^{ext}\right| \le C\,\|J_\varepsilon\|_{L^2(\Omega_0)}\left\|\mathrm{tr}\left(\underline{\underline{F}}_\varepsilon^{-1}\cdot\underline{\underline{\nabla}}_{\underline{\xi}}\,\underline{\dot{y}}_\varepsilon\right)\right\|_{L^2(\Omega_0)} + C\left\|\mathrm{adj}\,\underline{\underline{F}}_\varepsilon\right\|_{L^2(\Omega_0)}\left\|\underline{\dot{y}}_\varepsilon\right\|_{L^2(\Omega_0)},$$

since $\mathrm{adj}\,\underline{\underline{F}}_\varepsilon = J_\varepsilon\underline{\underline{F}}_\varepsilon^{-1}$, and $|\cos(\hat{\omega}\,t/\varepsilon)|\le 1$. Furthermore, from the Young inequality,

$$\left|\mathcal{P}_\varepsilon^{ext}\right| \le C\left(\|J_\varepsilon\|^2_{L^2(\Omega_0)} + \left\|\mathrm{tr}\left(\underline{\underline{F}}_\varepsilon^{-1}\cdot\underline{\underline{\nabla}}_{\underline{\xi}}\,\underline{\dot{y}}_\varepsilon\right)\right\|^2_{L^2(\Omega_0)}\right) + C\left(\left\|\mathrm{adj}\,\underline{\underline{F}}_\varepsilon\right\|^2_{L^2(\Omega_0)} + \left\|\underline{\dot{y}}_\varepsilon\right\|^2_{L^2(\Omega_0)}\right).$$

We now estimate each term using the energy. From Proposition 2.18, we can state that

$$\|J_\varepsilon\|^2_{L^2(\Omega_0)} - c \le \mathcal{E}_\varepsilon^{\mathrm{NI}} \le \mathcal{E}_\varepsilon^{tot}.$$

From Proposition 2.19 (first inequality) we have

$$\left\|\mathrm{adj}\,\underline{\underline{F}}_\varepsilon\right\|^2_{L^2(\Omega_0)} - C = \|I_{2,\varepsilon}\|_{L^1(\Omega_0)} - C \le \frac{1}{\kappa_5}\mathcal{E}_\varepsilon^{\mathrm{TI}} + \mathcal{E}_\varepsilon^{\mathrm{NI}} \le \left(\frac{1}{\kappa_5}+1\right)\mathcal{E}_\varepsilon^{tot}(t),$$

and

$$\rho_0\left\|\partial_t \underline{y}_\varepsilon\right\|^2_{L^2(\Omega_0)} \le \mathcal{K}_\varepsilon \le \mathcal{E}_\varepsilon^{tot}(t).$$

Finally, we have

$$\int_0^t \left\|\mathrm{tr}\left(\underline{\underline{F}}_\varepsilon^{-1}\cdot\underline{\underline{\nabla}}\,\partial_t\underline{y}_\varepsilon\right)\right\|^2_{L^2(\Omega_0)}\mathrm{d}s = \frac{\varepsilon}{\hat{\zeta}}\int_0^t \mathcal{E}_\varepsilon^{\mathrm{VS}}(s)\,\mathrm{d}s.$$

Collecting the results above, we find

$$\int_0^t \mathcal{P}_\varepsilon^{ext}(s)\,\mathrm{d}s \le C\left(1+\varepsilon\int_0^t \mathcal{E}_\varepsilon^{\mathrm{VS}}(s)\,\mathrm{d}s + \int_0^t \mathcal{E}_\varepsilon^{tot}(s)ds\right). \quad (2.81)$$

We now find an estimate for the term $\mathcal{P}_\varepsilon^A$. From Eq. (2.79) we have

$$\int_0^t \mathcal{P}_\varepsilon^A(s)\,\mathrm{d}s \leq \frac{1}{2}\|\partial_t\sigma_a\|_{L^\infty((0,T)\times\Omega)} \int_0^t \|I_{4,\varepsilon}(\cdot,s)\|_{L^1(\Omega_0)}\mathrm{d}s \\ + \frac{1}{2}\|\sigma_a\|_{L^\infty((0,T);L^2(\Omega_0))}\,\|I_{4,\varepsilon}(\cdot,t)\|_{L^2(\Omega_0)}$$

Therefore, using Proposition 2.19 (second and third inequalities), we get

$$\int_0^t \mathcal{P}_\varepsilon^A(s)\,\mathrm{d}s \leq C\left(\sqrt{\mathcal{E}_\varepsilon^{tot}(t)} + \int_0^t \mathcal{E}_\varepsilon^{tot}(s)\,\mathrm{d}s\right). \tag{2.82}$$

Injecting Eq. (2.81) and Eq. (2.82) into (2.80) we obtain the energy estimate

$$\mathcal{E}_\varepsilon^{tot}(t) + (1-C\varepsilon)\int_0^t \mathcal{E}_\varepsilon^{\mathrm{VS}}(s)\,\mathrm{d}s \leq C\left(1+\sqrt{\mathcal{E}_\varepsilon^{tot}(t)} + \int_0^t \mathcal{E}_\varepsilon^{tot}(s)\,\mathrm{d}s\right).$$

Then, using the Young inequality and assuming ε small enough, one can show that

$$\tilde{\mathcal{E}}_\varepsilon^{tot}(t) = \mathcal{E}_\varepsilon^{tot}(t) + \int_0^t \mathcal{E}_\varepsilon^{\mathrm{VS}}(s)\,\mathrm{d}s \leq C\left(1+\int_0^t \tilde{\mathcal{E}}_\varepsilon^{tot}(s)\,\mathrm{d}s\right),$$

thus, by the Grönwall inequality in integral form, we can state that

$$\tilde{\mathcal{E}}_\varepsilon^{tot}(t) \leq C\exp\left(\int_0^t C\,\mathrm{d}s\right).$$

As a consequence, $\mathcal{E}_\varepsilon^{tot}(t) \leq \tilde{\mathcal{E}}_\varepsilon^{tot}(t) \leq C$, thus concluding the proof. □

2.6.3 Proof of Lemma 2.16

Proof. Our aim is to derive the expression for the source term $s(t,\underline{w})$ in Eq. (2.72). Let us consider Eq. (2.65), that we recall here:

$$s(t,\underline{w}) = \frac{\hat{\omega}}{2\pi}\int_0^{\frac{2\pi}{\hat{\omega}}}\int_{\Omega(t)} \mathrm{div}_{\underline{x}}\Big(\big(\hat{\kappa}+\hat{\zeta}\partial_\tau\big)\,\underline{y}_2^f\Big)\,\big(\underline{\underline{\nabla}}_{\underline{x}}\,\underline{y}_2^f\big)^T : \underline{\underline{\nabla}}_{\underline{x}}\,\underline{w}\,\mathrm{d}\Omega\,\mathrm{d}\tau.$$

As a consequence, we can rewrite, by using the divergence theorem and Eq. (2.54),

$$\begin{aligned} s(t,\underline{w}) = &-\frac{\hat{\omega}}{2\pi}\int_0^{\frac{2\pi}{\hat{\omega}}}\int_{\Omega(t)} \underline{\mathrm{div}}_{\underline{x}}\Big(\mathrm{div}_{\underline{x}}\Big(\big(\hat{\kappa}+\hat{\zeta}\partial_\tau\big)\,\underline{y}_2^f\Big)\,\big(\underline{\underline{\nabla}}_{\underline{x}}\,\underline{y}_2^f\big)^T\Big)\cdot\underline{w}\,\mathrm{d}\Omega\,\mathrm{d}\tau \\ &+\frac{\hat{\omega}}{2\pi}\int_0^{\frac{2\pi}{\hat{\omega}}}\int_{\Gamma_N(t)} \Big(\mathrm{div}_{\underline{x}}\Big(\big(\hat{\kappa}+\hat{\zeta}\partial_\tau\big)\,\underline{y}_2^f\Big)\,\big(\underline{\underline{\nabla}}_{\underline{x}}\,\underline{y}_2^f\big)^T\cdot\underline{n}\Big)\cdot\underline{w}\,\mathrm{d}\Gamma\,\mathrm{d}\tau \\ = &-\frac{\hat{\omega}}{2\pi}\int_0^{\frac{2\pi}{\hat{\omega}}}\int_{\Omega(t)} \underline{\mathrm{div}}_{\underline{x}}\Big(\mathrm{div}_{\underline{x}}\Big(\big(\hat{\kappa}+\hat{\zeta}\partial_\tau\big)\,\underline{y}_2^f\Big)\,\big(\underline{\underline{\nabla}}_{\underline{x}}\,\underline{y}_2^f\big)^T\Big)\cdot\underline{w}\,\mathrm{d}\Omega\,\mathrm{d}\tau \\ &+\frac{\hat{\omega}}{2\pi}\int_0^{\frac{2\pi}{\hat{\omega}}}\int_{\Gamma_N(t)} \Big(\mathrm{div}_{\underline{x}}\Big(\big(\hat{\kappa}+\hat{\zeta}\partial_\tau\big)\,\underline{y}_2^f\Big)\,\big(\underline{\underline{\nabla}}_{\underline{x}}\,\underline{y}_2^f\big)^T\cdot\underline{n}\Big)\cdot\underline{w}\,\mathrm{d}\Gamma\,\mathrm{d}\tau. \end{aligned}$$

Using Eq. (2.69) and by integration over τ, we derive

$$\begin{aligned} s(t,\underline{w}) = &-\frac{1}{2}\int_{\Omega(t)} \underline{\mathrm{div}}_{\underline{x}}\Big(\mathrm{div}_{\underline{x}}\Big(\hat{\kappa}\ \mathrm{Re}\left(\underline{\hat{y}}_2^f\right) + \hat{\zeta}\hat{\omega}\ \mathrm{Im}\left(\underline{\hat{y}}_2^f\right)\Big)\left(\underline{\underline{\nabla}}_{\underline{x}}\ \mathrm{Re}\left(\underline{\hat{y}}_2^f\right)\right)^T\Big)\cdot\underline{w}\,\mathrm{d}\Omega \\ &-\frac{1}{2}\int_{\Omega(t)} \underline{\mathrm{div}}_{\underline{x}}\Big(\mathrm{div}_{\underline{x}}\Big(\hat{\kappa}\ \mathrm{Im}\left(\underline{\hat{y}}_2^f\right) - \hat{\zeta}\hat{\omega}\ \mathrm{Re}\left(\underline{\hat{y}}_2^f\right)\Big)\left(\underline{\underline{\nabla}}_{\underline{x}}\ \mathrm{Im}\left(\underline{\hat{y}}_2^f\right)\right)^T\Big)\cdot\underline{w}\,\mathrm{d}\Omega \\ &+\frac{\rho_0\hat{\omega}^2}{2}\int_{\Gamma_N(t)}\Big(\mathrm{Re}\left(\alpha^{-1}\mathrm{div}_{\underline{x}}(\underline{\hat{y}}_2^f)(\underline{\underline{\nabla}}_{\underline{x}}\,\overline{\underline{\hat{y}}_2^f}\right)^T\cdot\underline{n}\Big)\cdot\underline{w}\,\mathrm{d}\Gamma, \end{aligned} \tag{2.83}$$

since we have used the standard properties of sine and cosine

$$\int_0^{\frac{2\pi}{\hat{\omega}}}\cos(\hat{\omega}\tau)\,\sin(\hat{\omega}\tau)\,\mathrm{d}\tau = 0, \qquad \int_0^{\frac{2\pi}{\hat{\omega}}}\cos^2(\hat{\omega}\tau)\,\mathrm{d}\tau = \int_0^{\frac{2\pi}{\hat{\omega}}}\sin^2(\hat{\omega}\tau)\,\mathrm{d}\tau = \frac{\pi}{\hat{\omega}}.$$

In order to further simplify Eq. (2.83), we note that

$$\begin{aligned} \mathrm{div}_{\underline{x}}(\underline{\hat{y}}_2^f)\underline{\underline{\nabla}}_{\underline{x}}\overline{\underline{\hat{y}}_2^f} = &\ \mathrm{div}_{\underline{x}}\,\mathrm{Re}\left(\underline{\hat{y}}_2^f\right)\left(\underline{\underline{\nabla}}_{\underline{x}}\ \mathrm{Re}\left(\underline{\hat{y}}_2^f\right)\right)^T + \mathrm{div}_{\underline{x}}\,\mathrm{Im}\left(\underline{\hat{y}}_2^f\right)\left(\underline{\underline{\nabla}}_{\underline{x}}\ \mathrm{Im}\left(\underline{\hat{y}}_2^f\right)\right)^T \\ &+ i\Big(\mathrm{div}_{\underline{x}}\,\mathrm{Im}\left(\underline{\hat{y}}_2^f\right)\left(\underline{\underline{\nabla}}_{\underline{x}}\ \mathrm{Re}\left(\underline{\hat{y}}_2^f\right)\right)^T - \mathrm{div}_{\underline{x}}\,\mathrm{Re}\left(\underline{\hat{y}}_2^f\right)\left(\mathrm{Im}\left(\underline{\hat{y}}_2^f\right)\right)^T\Big). \end{aligned}$$

Consequently, the source term can be decomposed into

$$s(t,\underline{w}) = s_\Omega(t,\underline{w}) + s_\Gamma(t,\underline{w}),$$

with

$$\begin{aligned} s_\Omega(t,\underline{w}) \coloneqq &-\frac{\hat{\kappa}}{2}\int_{\Omega(t)}\underline{\mathrm{div}}_{\underline{x}}\Big(\mathrm{Re}\left(\mathrm{div}_{\underline{x}}(\underline{\hat{y}}_2^f)\,\underline{\underline{\nabla}}_{\underline{x}}\overline{\underline{\hat{y}}_2^f}\right)\Big)\cdot\underline{w}\,\mathrm{d}\Omega \\ &\frac{-\hat{\omega}\,\hat{\zeta}}{2}\int_{\Omega(t)}\underline{\mathrm{div}}_{\underline{x}}\Big(\mathrm{Im}\left(\mathrm{div}_{\underline{x}}(\underline{\hat{y}}_2^f)\,\underline{\underline{\nabla}}_{\underline{x}}\overline{\underline{\hat{y}}_2^f}\right)\Big)\cdot\underline{w}\,\mathrm{d}\Omega, \\ s_\Gamma(t,\underline{w}) \coloneqq &\frac{\rho_0\hat{\omega}^2}{2}\int_{\Gamma_N(t)}\Big(\mathrm{Re}\left(\alpha^{-1}\mathrm{div}_{\underline{x}}(\underline{\hat{y}}_2^f)(\underline{\underline{\nabla}}_{\underline{x}}\,\overline{\underline{\hat{y}}_2^f}\right)^T\cdot\underline{n}\Big)\cdot\underline{w}\,\mathrm{d}\Gamma \end{aligned} \tag{2.84}$$

Now, from Eq. (2.69) to Eq. (2.68), we can suppose that there exist $\alpha\in\mathbb{C}$ and $\hat{p}_2^f\in\mathbb{C}$ such that $\hat{p}_2^f \coloneqq \mathrm{div}_{\underline{x}}\,\underline{\hat{y}}_2^f$, and $\hat{p}_2^f$ satisfies the Helmholtz equation

$$\begin{cases} \Delta_{\underline{x}}\,\hat{p}_2^f + \alpha\,\hat{p}_2^f = 0 & \text{in } \Omega(t), \\ \underline{\nabla}_{\underline{x}}\,\hat{p}_2^f\cdot\underline{n} = 0 & \text{on } \Gamma_D(t), \\ \frac{\rho_0\,\hat{\omega}^2}{\alpha}\,\hat{p}_2^f = p & \text{in } \Gamma_N(t). \end{cases} \tag{2.85}$$

As a consequence, we retrieve

$$s_\Gamma(t,\underline{w}) = -\frac{\rho_0\,\hat{\omega}^2}{2|\alpha|^2}\int_{\Gamma_N(t)}\Big(\mathrm{Re}\left(\hat{p}_2^f\,\underline{\underline{H}}_{\underline{x}}(\overline{\hat{p}_2^f})\right)\cdot\underline{n}\Big)\cdot\underline{w}\,\mathrm{d}\Gamma.$$

We now derive a simplified expression for the term $s_\Omega(t,\underline{w})$. First, we can reformulate

$$\mathrm{div}_{\underline{x}}(\underline{\hat{y}}_2^f)\,\underline{\underline{\nabla}}_{\underline{x}}\overline{\underline{\hat{y}}_2^f} = -(\overline{\alpha})^{-1}\,\hat{p}_2^f\,\underline{\underline{\nabla}}_{\underline{x}}\Big(\underline{\nabla}_{\underline{x}}\overline{\hat{p}_2^f}\Big) = -\frac{\alpha}{|\alpha|^2}\,\hat{p}_2^f\,\underline{\underline{H}}_{\underline{x}}\Big(\overline{\hat{p}_2^f}\Big).$$

Consequently, we obtain

$$\begin{aligned}\underline{\mathrm{div}}_{\underline{x}}\Big(\mathrm{div}_{\underline{x}}(\underline{\hat{y}}_2^f)\,\underline{\nabla}_{\underline{x}}\overline{\hat{y}_2^f}\Big) &= -\frac{\alpha}{|\alpha|^2}\,\underline{\mathrm{div}}_{\underline{x}}\Big(\hat{p}_2^f\,\underline{\underline{H}}_{\underline{x}}\Big(\overline{\hat{p}_2^f}\Big)\Big)\\ &= -\frac{\alpha}{|\alpha|^2}\,\underline{\underline{H}}_{\underline{x}}\Big(\overline{\hat{p}_2^f}\Big)\cdot\underline{\nabla}_{\underline{x}}(\hat{p}_2^f) - \frac{\alpha}{|\alpha|^2}\,\hat{p}_2^f\,\underline{\nabla}_{\underline{x}}\Big(\Delta_{\underline{x}}\overline{\hat{p}_2^f}\Big)\\ &= -\frac{\alpha}{|\alpha|^2}\,\underline{V} + \underline{W},\end{aligned} \tag{2.86}$$

with

$$\underline{V} \coloneqq \underline{\underline{H}}_{\underline{x}}\Big(\overline{\hat{p}_2^f}\Big)\cdot\underline{\nabla}_{\underline{x}}(\hat{p}_2^f), \qquad \underline{W} \coloneqq \hat{p}_2^f\,\underline{\nabla}_{\underline{x}}\Big(\overline{\hat{p}_2^f}\Big),$$

and we have used Eq. (2.85). We now retrieve a simpler expression for Eq. (2.86). On the one hand, we can rewrite

$$\begin{aligned}\underline{V} = \underline{\underline{H}}_{\underline{x}}\Big(\overline{\hat{p}_2^f}\Big)\cdot\underline{\nabla}_{\underline{x}}(\hat{p}_2^f) &= \underline{\underline{H}}_{\underline{x}}\Big(\mathrm{Re}\,(\hat{p}_2^f)\Big)\cdot\underline{\nabla}_{\underline{x}}\,\mathrm{Re}\,(\hat{p}_2^f) + \underline{\underline{H}}_{\underline{x}}\Big(\mathrm{Im}\,(\hat{p}_2^f)\Big)\cdot\underline{\nabla}_{\underline{x}}\,\mathrm{Im}\,(\hat{p}_2^f)\\ &\quad + i\,\Big(\underline{\underline{H}}_{\underline{x}}\Big(\mathrm{Re}\,(\hat{p}_2^f)\Big)\cdot\underline{\nabla}_{\underline{x}}\,\mathrm{Im}\,(\hat{p}_2^f) - \underline{\underline{H}}_{\underline{x}}\Big(\mathrm{Im}\,(\hat{p}_2^f)\Big)\cdot\underline{\nabla}_{\underline{x}}\,\mathrm{Re}\,(\hat{p}_2^f)\Big).\end{aligned}$$

Now, since

$$\underline{\underline{H}}_{\underline{x}}\Big(\mathrm{Re}\,(\hat{p}_2^f)\Big)\cdot\underline{\nabla}_{\underline{x}}\,\mathrm{Re}\,(\hat{p}_2^f) = \sum_j \frac{\partial^2\,\mathrm{Re}\,(\hat{p}_2^f)}{\partial x_i\,\partial x_j}\,\frac{\partial\,\mathrm{Re}\,(\hat{p}_2^f)}{\partial x_j} = \frac{1}{2}\sum_j \underline{\nabla}_{\underline{x}}\Big(\frac{\partial\,\mathrm{Re}\,(\hat{p}_2^f)}{\partial x_j}\Big)^2,$$

and analogously for $\underline{\underline{H}}_{\underline{x}}\big(\mathrm{Im}\,(\hat{p}_2^f)\big)\cdot\underline{\nabla}_{\underline{x}}\,\mathrm{Im}\,(\hat{p}_2^f)$, we can simplify $\underline{V}$ as

$$\underline{V} = \frac{1}{2}\underline{\nabla}_{\underline{x}}\Big|\underline{\nabla}_{\underline{x}}\hat{p}_2^f\Big|^2 + i\,\Big(\underline{\underline{H}}_{\underline{x}}\Big(\mathrm{Re}\,(\hat{p}_2^f)\Big)\,\underline{\nabla}_{\underline{x}}\,\mathrm{Im}\,(\hat{p}_2^f) - \underline{\underline{H}}_{\underline{x}}\Big(\mathrm{Im}\,(\hat{p}_2^f)\Big)\,\underline{\nabla}_{\underline{x}}\,\mathrm{Re}\,(\hat{p}_2^f)\Big). \tag{2.87}$$

On the other hand, we can express

$$\begin{aligned}\underline{W} = \hat{p}_2^f\,\underline{\nabla}_{\underline{x}}\Big(\overline{\hat{p}_2^f}\Big) &= \underline{\nabla}_{\underline{x}}\,\mathrm{Re}\,(\hat{p}_2^f)\;\mathrm{Re}\,(\hat{p}_2^f) + \underline{\nabla}_{\underline{x}}\,\mathrm{Im}\,(\hat{p}_2^f)\;\mathrm{Im}\,(\hat{p}_2^f)\\ &\quad + i\,\Big(\underline{\nabla}_{\underline{x}}\,\mathrm{Re}\,(\hat{p}_2^f)\;\mathrm{Im}\,(\hat{p}_2^f) - \underline{\nabla}_{\underline{x}}\,\mathrm{Im}\,(\hat{p}_2^f)\;\mathrm{Re}\,(\hat{p}_2^f)\Big).\end{aligned}$$

As a consequence, we can reformulate $\underline{W}$ as

$$\underline{W} = \frac{1}{2}\,\underline{\nabla}_{\underline{x}}\Big|\hat{p}_2^f\Big|^2 + i\,\Big(\underline{\nabla}_{\underline{x}}\,\mathrm{Re}\,(\hat{p}_2^f)\;\mathrm{Im}\,(\hat{p}_2^f) - \underline{\nabla}_{\underline{x}}\,\mathrm{Im}\,(\hat{p}_2^f)\;\mathrm{Re}\,(\hat{p}_2^f)\Big). \tag{2.88}$$

Therefore, using Eqs. (2.87) and (2.88), we can rewrite Eq. (2.86) as

$$\begin{aligned}\underline{\mathrm{div}}_{\underline{x}}\Big(\mathrm{div}_{\underline{x}}(\underline{\hat{y}}_2^f)\,\underline{\nabla}_{\underline{x}}\overline{\hat{y}_2^f}\Big) &= \underline{\nabla}_{\underline{x}}\Big(-\frac{\alpha}{2|\alpha|^2}\,\Big|\underline{\nabla}_{\underline{x}}\hat{p}_2^f\Big|^2 + \frac{1}{2}\,\Big|\hat{p}_2^f\Big|^2\Big)\\ &\quad + i\frac{\alpha}{|\alpha|^2}\,\Big(\underline{\underline{H}}_{\underline{x}}\Big(\mathrm{Im}\,(\hat{p}_2^f)\Big)\,\underline{\nabla}_{\underline{x}}\,\mathrm{Re}\,(\hat{p}_2^f) - \underline{\underline{H}}_{\underline{x}}\Big(\mathrm{Re}\,(\hat{p}_2^f)\Big)\,\underline{\nabla}_{\underline{x}}\,\mathrm{Im}\,(\hat{p}_2^f)\Big) + i\;\mathrm{Im}\,\Big(\hat{p}_2^f\,\underline{\nabla}_{\underline{x}}\Big(\overline{\hat{p}_2^f}\Big)\Big).\end{aligned}$$

Let us introduce the variables q_α, $\underline{l}_\alpha$ such that

$$-\underline{\mathrm{div}}_{\underline{x}}\Big(\mathrm{div}_{\underline{x}}(\underline{\hat{y}}_2^f)\,\underline{\nabla}_{\underline{x}}\overline{\hat{y}_2^f}\Big) = \underline{\nabla}_{\underline{x}}\,q_\alpha + \underline{l}_\alpha,$$

with

$$\begin{aligned} q_\alpha &:= \frac{\alpha}{2|\alpha|^2}\left|\underline{\nabla}_{\underline{x}}\hat{p}_2^f\right|^2 - \frac{1}{2}\left|\hat{p}_2^f\right|^2, \\ \underline{l}_\alpha &:= i\,\frac{\alpha}{|\alpha|^2}\Big(-\underline{\underline{H}}_{\underline{x}}\Big(\operatorname{Im}\big(\hat{p}_2^f\big)\Big)\,\underline{\nabla}_{\underline{x}}\operatorname{Re}\big(\hat{p}_2^f\big) + \underline{\underline{H}}_{\underline{x}}\Big(\operatorname{Re}\big(\hat{p}_2^f\big)\Big)\,\underline{\nabla}_{\underline{x}}\operatorname{Im}\big(\hat{p}_2^f\big)\Big) \\ &\quad - i\,\operatorname{Im}\Big(\hat{p}_2^f\,\underline{\nabla}_{\underline{x}}\Big(\overline{\hat{p}_2^f}\Big)\Big). \end{aligned}$$

Then, the source term $s_\Omega(t,\underline{w})$ in Eq. (2.84) can be rewritten as

$$s_\Omega(t,\underline{w}) = \frac{1}{2}\int_{\Omega(t)}\underline{\nabla}_{\underline{x}}\left(\hat{\kappa}\,\operatorname{Re}(q_\alpha)+\hat{\zeta}\,\hat{\omega}\,\operatorname{Im}(q_\alpha)\right)\cdot\underline{w}\,\mathrm{d}\Omega + \frac{1}{2}\int_{\Omega(t)}\Big(\hat{\kappa}\,\operatorname{Re}\big(\underline{l}_\alpha\big)+\hat{\zeta}\,\hat{\omega}\,Im\big(\underline{l}_\alpha\big)\Big)\cdot\underline{w}\,\mathrm{d}\Omega,$$

that was to be demonstrated. □

2.6.4 Full expression of a linearised stress tensor term

We define the transversely isotropic potential associated to the displacement $\underline{y}_0$ as

$$W_0^{\mathrm{TI}} = \kappa_1\, e^{\kappa_2(I_{1,0}-3)^2} + \kappa_3\, e^{\kappa_4(I_{4,0}-1)^2} + \kappa_5\big(I_{2,0} - 2\log(J_0^2) - 3\big),$$

with

$$I_{1,0} = 3{+}2\,\operatorname{tr}\big(\underline{\underline{e}}_0\big), \quad I_{4,0} = 1{+}2\,\underline{\tau}_1{\cdot}\underline{\underline{e}}_0{\cdot}\underline{\tau}_1, \quad I_{2,0} = |\operatorname{adj}\underline{\underline{F}}_0|^2 = 3{+}4\,\operatorname{tr}\big(\underline{\underline{e}}_0\big){+}2\,\operatorname{tr}^2\big(\underline{\underline{e}}_0\big){-}2\,\operatorname{tr}\big(\underline{\underline{e}}_0^2\big).$$

The corresponding stress tensor is given by

$$\underline{\underline{\Sigma}}_0^{\mathrm{TI}} = \frac{\partial W_0^{\mathrm{TI}}}{\partial \underline{\underline{e}}_0} = K_{1,0}\,\big(I_{1,0}-3\big)\,\underline{\underline{\mathbb{1}}} + K_{4,0}\,\big(I_{4,0}-1\big)\,\underline{\tau}_1\otimes\underline{\tau}_1 + 2\,\kappa_5\Big(\,I_{1,0}\underline{\underline{\mathbb{1}}} - \underline{\underline{C}}_0 - 2\,\underline{\underline{C}}_0^{-1}\,\Big),$$

with

$$K_{1,0} := 4\kappa_1\kappa_2 e^{\kappa_2(I_{1,0}-3)^2}, \quad K_{4,0} := 4\kappa_3\kappa_4 e^{\kappa_4(I_{4,0}-1)^2}.$$

One can observe that $\underline{\underline{\Sigma}}_0^{\mathrm{TI}}$ vanishes if $\underline{\underline{e}}_0 = \underline{\underline{0}}$. Furthermore, for any test function $\underline{w}$ we can define

$$\begin{aligned} \underline{\underline{\mathbf{A}}}_0 : \underline{\underline{e}}_0(\underline{w}) &:= \frac{\partial \underline{\underline{\Sigma}}^{\mathrm{TI}}}{\partial \underline{\underline{e}}}(\underline{y}_0) : \underline{\underline{e}}_0(\underline{w}) \\ &= Q_{1,0}\,\operatorname{tr}\Big(\underline{\underline{e}}_0(\underline{w})\Big)\,\underline{\underline{\mathbb{1}}} + Q_{4,0}\big(\underline{\tau}_1\cdot\underline{\underline{e}}_0(\underline{w})\cdot\underline{\tau}_1\big)\,\underline{\tau}_1\otimes\underline{\tau}_1 + 4\,\kappa_5\Big(2\,\underline{\underline{C}}_0^{-1}\cdot\underline{\underline{e}}_0(\underline{w})\cdot\underline{\underline{C}}_0^{-1} - \underline{\underline{e}}_0(\underline{w})\Big) \end{aligned}$$

with

$$Q_{1,0} = 2\,K_{1,0}\left(1 + 2\,\kappa_2(I_{1,0}-3)^2\right) + 4\,\kappa_5, \quad Q_{4,0} = 2K_{4,0}\big(1 + 2\,\kappa_2(I_{4,0}-1)^2\big).$$

If $\underline{\underline{e}}_0 = \underline{\underline{0}}$, then

$$\underline{\underline{\mathbf{A}}}_0 : \underline{\underline{e}}_0\big(\,\underline{w}\,\big) = \underline{\underline{\mathbf{A}}}_0 : \underline{\underline{\varepsilon}}\big(\,\underline{w}\,\big) = (8\,\kappa_1\,\kappa_2{+}4\kappa_5)\,\operatorname{tr}\big(\,\underline{\underline{\varepsilon}}(\underline{w})\big)\underline{\underline{\mathbb{1}}}{+}8\,\kappa_3\,\kappa_4\big(\underline{\tau}_1{\cdot}\underline{\underline{\varepsilon}}(\underline{w}){\cdot}\underline{\tau}_1\big)\;\underline{\tau}_1{\otimes}\underline{\tau}_1{+}4\kappa_5\underline{\underline{\varepsilon}}(\underline{w}),$$

with $\underline{\underline{\varepsilon}}(\underline{w}) = \underline{\underline{\nabla}}\,\underline{w} + (\underline{\underline{\nabla}}\,\underline{w})^T$. The expression above shows that $\underline{\underline{\mathbf{A}}}_0$ is a positive fourth-order tensor for small values of $\underline{\underline{e}}_0$. Indeed, for all $\underline{\underline{\varepsilon}} \in \mathcal{L}_s(\mathbb{R}^d)$, we can show that there exists a positive constant α such that

$$\big(\underline{\underline{\mathbf{A}}}_0 : \underline{\underline{\varepsilon}}\big) : \underline{\underline{\varepsilon}} = (8\,\kappa_1\,\kappa_2 + 4\kappa_5)\,\operatorname{tr}\big(\,\underline{\underline{\varepsilon}}\big)^2 + 8\,\kappa_3\,\kappa_4\big(\underline{\tau}_1\cdot\underline{\underline{\varepsilon}}\cdot\underline{\tau}_1\big)^2 + 4\kappa_5\underline{\underline{\varepsilon}} : \underline{\underline{\varepsilon}} > \alpha\big|\,\underline{\underline{\varepsilon}}\,\big|^2.$$

Bibliography

Bercoff, J., Tanter, M. and Fink, M. [2004], 'Supersonic shear imaging: a new technique for soft tissue elasticity mapping', *IEEE transactions on ultrasonics, ferroelectrics, and frequency control* **51**(4), 396–409.

Caenen, A. [2018], A biomechanical analysis of shear wave elastography in pediatric heart models, PhD thesis, Ghent University.

Chapelle, D., Le Tallec, P., Moireau, P. and Sorine, M. [2012], 'An energy-preserving muscle tissue model: formulation and compatible discretizations', *International Journal for Multiscale Computational Engineering* **10**(2), 189–211.

Destrade, M., Goriely, A. and Saccomandi, G. [2010], 'Scalar evolution equations for shear waves in incompressible solids: a simple derivation of the z, zk, kzk and kp equations', *Proceedings of the Royal Society A: Mathematical, Physical and Engineering Sciences* **467**(2131), 1823–1834.

Dontsov, E. and Guzina, B. B. [2011], 'Effect of low-frequency modulation on the acoustic radiation force in newtonian fluids', *SIAM Journal on Applied Mathematics* **71**(1), 356–378.

Dontsov, E. V. and Guzina, B. B. [2012], 'Acoustic radiation force in tissue-like solids due to modulated sound field', *Journal of the Mechanics and Physics of Solids* **60**(10), 1791–1813.

Dontsov, E. V. and Guzina, B. B. [2013], 'On the kzk-type equation for modulated ultrasound fields', *Wave Motion* **50**(4), 763–775.

Evans, L. C. [2010], 'Partial differential equations'.

Gennisson, J.-L., Rénier, M., Catheline, S., Barrière, C., Bercoff, J., Tanter, M. and Fink, M. [2007], 'Acoustoelasticity in soft solids: Assessment of the nonlinear shear modulus with the acoustic radiation force', *The Journal of the Acoustical Society of America* **122**(6), 3211–3219.

Lions, J.-L., Papanicolaou, G. and Bensoussan, A. [1978], *Asymptotic analysis for periodic structures*, North-Holland.

McAleavey, S. A., Menon, M. and Orszulak, J. [2007], 'Shear-modulus estimation by application of spatially-modulated impulsive acoustic radiation force', *Ultrasonic imaging* **29**(2), 87–104.

Monk, P. et al. [2003], *Finite element methods for Maxwell's equations*, Oxford University Press.

Nightingale, K., McAleavey, S. and Trahey, G. [2003], 'Shear-wave generation using acoustic radiation force: in vivo and ex vivo results', *Ultrasound in medicine & biology* **29**(12), 1715–1723.

Nightingale, K., Soo, M. S., Nightingale, R. and Trahey, G. [2002], 'Acoustic radiation force impulse imaging: in vivo demonstration of clinical feasibility', *Ultrasound in medicine & biology* **28**(2), 227–235.

Ostrovsky, L., Sutin, A., Il'inskii, Y., Rudenko, O. and Sarvazyan, A. [2007], 'Radiation force and shear motions in inhomogeneous media', *The Journal of the Acoustical Society of America* **121**(3), 1324–1331.

Palmeri, M. L., Sharma, A. C., Bouchard, R. R., Nightingale, R. W. and Nightingale, K. R. [2005], 'A finite-element method model of soft tissue response to impulsive acoustic radiation force', *IEEE transactions on ultrasonics, ferroelectrics, and frequency control* **52**(10), 1699–1712.

Rudenko, O., Sarvazyan, A. and Emelianov, S. Y. [1996], 'Acoustic radiation force and streaming induced by focused nonlinear ultrasound in a dissipative medium', *The Journal of the Acoustical Society of America* **99**(5), 2791–2798.

Sarvazyan, A., J Hall, T., W Urban, M., Fatemi, M., R Aglyamov, S. and S Garra, B. [2011], 'An overview of elastography-an emerging branch of medical imaging', *Current medical imaging reviews* **7**(4), 255–282.

Sarvazyan, A. P., Rudenko, O. V. and Nyborg, W. L. [2010], 'Biomedical applications of radiation force of ultrasound: historical roots and physical basis', *Ultrasound in medicine & biology* **36**(9), 1379–1394.

Sarvazyan, A. P., Rudenko, O. V., Swanson, S. D., Fowlkes, J. B. and Emelianov, S. Y. [1998], 'Shear wave elasticity imaging: a new ultrasonic technology of medical diagnostics', *Ultrasound in medicine & biology* **24**(9), 1419–1435.

Song, P., Zhao, H., Manduca, A., Urban, M. W., Greenleaf, J. F. and Chen, S. [2012], 'Comb-push ultrasound shear elastography (CUSE): a novel method for two-dimensional shear elasticity imaging of soft tissues', *IEEE transactions on medical imaging* **31**(9), 1821–1832.

Torr, G. [1984], 'The acoustic radiation force', *American Journal of Physics* **52**, 402–408.

Zabolotskaya, E. A., Hamilton, M. F., Ilinskii, Y. A. and Meegan, G. D. [2004], 'Modeling of nonlinear shear waves in soft solids', *The Journal of the Acoustical Society of America* **116**(5), 2807–2813.

CHAPTER 3

Analysis of a quasi-static method for the computation of the acoustic radiation force

Summary

The objective of this chapter is to present a preliminary study aimed at investigating the quasi-static assumption that is performed to decouple pressure and shear waves. The purpose is to further justify the asymptotic approach proposed in Chapter 2 for the approximation of the solution of the elastodynamic equation with impulsive source term for a nearly-incompressible medium. To do so, we consider the simplifying assumption of a linear constitutive law and we perform a quasi-static approximation. In particular, we outline a proof of convergence of the approximation of the solution.

Contents

3.1 Introduction

The remote generation of shear acoustic waves is based on the radiation force of a focused ultrasound beam induced by a conventional transducer. ARF is obtained from the emission of a high-intensity acoustic pressure pulse (of the order of $100 - 500\,\mu s$) at a specific tissue location by a conventional ultrasound transducer [Pernot et al., 2016; Correia et al., 2017]. The generation of shear waves from an impulsive pressure excitation relies on a non-linear effect: additional specific stresses are generated in regions where pressure is high [Sarvazyan et al., 2010].
The aim of this chapter is to further justify the asymptotic approach proposed in Chapter 2 to approximate the solution of the elastodynamic equation with impulsive source term for a nearly-incompressible medium, with the simplifying assumption of a linear constitutive law. We recall that the asymptotic approach is motivated by the great difference that is experimentally observed in soft media in the velocity of propagation between shear waves (1–$10\,m\,s^{-1}$) and pressure waves ($1500\,m\,s^{-1}$). Therefore, we assume that the bulk modulus, associated with quasi-incompressibility, is two orders of magnitude greater than the elastic moduli in the constitutive law. Furthermore, we hypothesise that the source term, composed of piezoelectric sensors, is high frequency and of small amplitude, therefore we can decouple the fast timescale of the pressure wave generated by the sensors from the slow timescale associated with elastic wave propagation. Note that we incorporate viscosity in the constitutive law of the solid. Since in real tissues the dissipation is proportional to the ultrasound frequency [Ostrovsky et al., 2007], we rescale the viscosity coefficient accordingly. We define a family of problems parametrised by a small parameter ε related to the velocity ratio between shear and pressure wave propagation phenomena, the high frequency of the piezoelectric source term and viscosity. We assume that a solution exists for every ε, and we formulate a stability estimate, based on energy considerations, from which we retrieve some useful properties of the solution, and further simplify its expression. Subsequently, a regular asymptotic expansion of the solution is proposed.
In analogy to Chapter 2, in order to derive a simplified model for the expression of ARF, the solution is approximated by the first terms of the asymptotic expansion. This approximation is inserted in the elastodynamic equation, and the equations proportional to the same order of ε are identified and solved. For each order of ε, we average the corresponding equation over the period of the high frequency wave, in order to retrieve the equation for the average displacement (that is a slow-oscillating term). By doing so, we obtain that the leading term of the expansion is related to the underlying nonlinear mechanics, and it is zero in the absence of volumic source terms. Furthermore, we show that the first-order corrector is zero, and we present the governing equations of the higher correctors (along with the corresponding Helmholtz problem). Finally, we outline a proof of convergence of the approximation of the solution. Our objective is to present a preliminary study aimed at investigating the quasi-static assumption that is performed to decouple pressure and shear waves. Hence, the end-goal of this work is to study when the principle of limiting amplitude takes place, i.e. when it is reasonable to consider that, at every time of the slow time scale, we can solve a Helmholtz equation associated with the fast time scale of the pressure field. However, we emphasize that, due to the absence of non-linear effects, there is no generation of shear waves in the problem considered.

The chapter is organised as follows. First, in Section 3.2.1 we introduce the elastodynamic problem and we give the constitutive law of an isotropic, quasi-incompressible linear elastic medium, in terms of its invariants. Then, a family of problems is created in Section 3.2.2 and a stability estimate is proved for such problem in Section 3.2.3. Section 3.3 deals with

the definition of a regular asymptotic expansion of the solution. Then, it is proved that both the leading-order term and the first corrector are zero, and the governing equations for the higher correctors are retrieved. In Section 3.4 we derive the approximation properties of the correctors. In particular, the proof of convergence for the k^{th} corrector is given in Section 3.4.2.

3.2 Definition of a parametrised family of problems

3.2.1 Constitutive laws

Let us start from the definition of the **elastodynamic equation** in strong formulation. We define a regular domain $\Omega \subset \mathbb{R}^d$, $d > 2$, fixed in time by hypothesis. The problem reads
Find $\underline{y} \in \mathcal{X}$ such that

$$\begin{cases} \rho(\ddot{\underline{y}} - \underline{f}) - \underline{\operatorname{div}}\,\underline{\underline{\sigma}} = 0, & \text{in } \Omega, \quad t \in (0,T], \\ \underline{\underline{\sigma}} \cdot \underline{n} = \underline{\mathrm{t}}, & \text{in } \Gamma_N, \quad t \in (0,T], \\ \underline{y} = \underline{0}, & \text{in } \Gamma_D, \quad t \in (0,T], \\ \underline{y}(t=0) = \underline{0}, \quad \dot{\underline{y}}(t=0) = \underline{0} & \text{in } \Omega, \end{cases} \tag{3.1}$$

where ρ is the mass density of the solid, $\ddot{\underline{y}}$ is the acceleration, $\underline{\underline{\sigma}}$ is the Cauchy stress tensor, and $\underline{\mathrm{t}}$ is a surfacic source term. $\mathcal{X}$ is the space of admissible displacements, to be defined. The *weak formulation* associated with Eq. (3.1) reads
Find $\underline{y} \in \mathcal{X}$ such that $\forall \underline{w} \in \mathcal{X}$

$$\int_\Omega \rho\big(\ddot{\underline{y}}(\underline{x},t) - \underline{f}(\underline{x},t)\big) \cdot \underline{w}(\underline{x})\, \mathrm{d}\Omega + \int_\Omega \underline{\underline{\sigma}}(\underline{x}) : \underline{\underline{\nabla}}\, \underline{w}(\underline{x})\, \mathrm{d}\Omega = \int_{\Gamma_N} \underline{\mathrm{t}}(\underline{x},t) \cdot \underline{w}(\underline{x})\, \mathrm{d}S. \tag{3.2}$$

Henceforth, we make the following assumptions for the sake of simplicity.
Assumption 3.1. *The constitutive law of the medium is given by*

$$\underline{\underline{\sigma}} = \kappa\, \mathrm{tr}\big(\underline{\underline{\varepsilon}}(\underline{y}(\underline{x},t))\big)\, \underline{\underline{\mathbb{1}}} + 2\,\mu\, \underline{\underline{\varepsilon}}\big(\underline{y}(\underline{x},t)\big) + \zeta\, \mathrm{tr}\big(\underline{\underline{\varepsilon}}(\dot{\underline{y}}(\underline{x},t))\big)\, \underline{\underline{\mathbb{1}}},$$

where κ is the bulk modulus, μ is the second Lamé coefficient, and ζ is a viscosity coefficient. Furthermore, no external volumic forces are imposed, i.e. $\underline{f} = 0$.

Under Assumption 3.1, Problem (3.2) reads
Find $\underline{y} \in \mathcal{X}$ such that $\forall\, \underline{w} \in \mathcal{X}$

$$\begin{cases} \displaystyle\int_\Omega \rho\, \ddot{\underline{y}}(\underline{x},t)\, \underline{w}(\underline{x})\, \mathrm{d}\Omega + \kappa \int_\Omega \operatorname{div} \underline{y}(\underline{x},t) \operatorname{div} \underline{w}(\underline{x})\, \mathrm{d}\Omega + 2\,\mu \int_\Omega \underline{\underline{\varepsilon}}\big(\underline{y}(\underline{x},t)\big) : \underline{\underline{\varepsilon}}\big(\underline{w}(\underline{x})\big)\, \mathrm{d}\Omega \\ \qquad\qquad + \zeta \displaystyle\int_\Omega \operatorname{div} \dot{\underline{y}}(\underline{x},t) \operatorname{div} \underline{w}(\underline{x})\, \mathrm{d}\Omega = \int_{\Gamma_N} \underline{\mathrm{t}}(\underline{x},t) \cdot \underline{w}(\underline{x})\, \mathrm{d}S, \\ \underline{y}(\underline{x},t)\big|_{\Gamma_D} = \underline{0}, \\ \underline{y}(\underline{x},0) = \underline{0}, \quad \dot{\underline{y}}(\underline{x},0) = \underline{0}. \end{cases} \tag{3.3}$$

3.2.2 Definition of a parametric family of problems

Under the assumption that the medium is nearly-incompressible, we define a family of problems parametrised by ε, associated with the ratio between the pressure and the shear wave velocities. First, we rewrite the bulk modulus as

$$\kappa = \varepsilon^{-2}\hat{\kappa},$$

where $\hat{\kappa}$ is a normalised parameter.We also hypothesize that the viscosity coefficient satisfies

$$\zeta = \varepsilon^{-1}\,\hat{\zeta},$$

where $\hat{\zeta}$ is a normalised parameter. Furthermore, our asymptotic analysis relies on the hypothesis that the source term is high-frequency and of small amplitude. Therefore, we set

$$\underline{\mathrm{t}}(\underline{x},t) \coloneqq p(\underline{x},t)\,\cos(\hat{\omega}\,t/\varepsilon)\,\underline{n},$$

where p is a pressure and it is a regular function with compact support in $[0,T]$, and

$$\omega = \varepsilon^{-1}\,\hat{\omega}.$$

We denote by $\underline{y}_\varepsilon$ the family of solutions associated with Eq. (3.3) with the definition above. Then, problem (3.3) reads:
Find $\underline{y}_\varepsilon \in \mathcal{X}$ such that $\forall \underline{w} \in \mathcal{X}$

$$\begin{cases} \displaystyle\int_\Omega \rho\,\ddot{\underline{y}}_\varepsilon(\underline{x},t)\cdot\underline{w}(\underline{x})\,\mathrm{d}\Omega + \varepsilon^{-2}\hat{\kappa}\int_\Omega \operatorname{div}\underline{y}_\varepsilon(\underline{x},t)\operatorname{div}\underline{w}(\underline{x})\,\mathrm{d}\Omega \\ \qquad + 2\,\mu\displaystyle\int_\Omega \underline{\underline{\varepsilon}}\big(\underline{y}(\underline{x},t)\big) : \underline{\underline{\varepsilon}}\big(\underline{w}(\underline{x})\big)\,\mathrm{d}\Omega + \varepsilon^{-1}\hat{\zeta}\displaystyle\int_\Omega \operatorname{div}\dot{\underline{y}}_\varepsilon(\underline{x},t)\operatorname{div}\underline{w}(\underline{x})\,\mathrm{d}\Omega \\ \qquad = \displaystyle\int_{\Gamma_N} p(\underline{x},t)\cos(\hat{\omega}\,t/\varepsilon)\,\underline{n}\cdot\underline{w}\,\mathrm{d}S, \\ \underline{y}\big|_{\Gamma_D} = \underline{0}, \\ \underline{y}_\varepsilon(\underline{x},0) = \underline{0}, \quad \dot{\underline{y}}_\varepsilon(\underline{x},0) = \underline{0}. \end{cases} \tag{3.4}$$

3.2.3 Stability estimates

In this section, we retrieve some energy estimates allowing to derive some useful properties of the solution $\underline{y}_\varepsilon$. Choosing the velocity $\dot{\underline{y}}_\varepsilon(t)$ as a test function, we obtain the energy balance

$$\frac{\mathrm{d}}{\mathrm{d}t}\mathcal{E}_\varepsilon^{tot}(t) + \mathcal{E}_\varepsilon^{\mathrm{VS}}(t) = \mathcal{P}_\varepsilon^{ext}(t),$$

where the total energy $\mathcal{E}_\varepsilon^{tot}(t)$ is defined as

$$\mathcal{E}_\varepsilon^{tot}(t) = \mathcal{K}_\varepsilon(t) + \mathcal{E}_\varepsilon^{\mathrm{NI}}(t) + \mathcal{E}_\varepsilon^{ISO}(t),$$

and the kinetic energy and internal energy terms are given by

$$\begin{aligned} \mathcal{K}_\varepsilon(t) &= \frac{1}{2}\int_\Omega \rho\,|\dot{\underline{y}}_\varepsilon(t)|^2\,\mathrm{d}\Omega = \frac{1}{2}\rho\Big\|\dot{\underline{y}}_\varepsilon(t)\Big\|_0^2, \\ \mathcal{E}_\varepsilon^{\mathrm{NI}}(t) &= \frac{1}{2}\varepsilon^{-2}\,\hat{\kappa}\int_\Omega \Big|\operatorname{div}\underline{y}_\varepsilon(t)\Big|^2\,\mathrm{d}\Omega = \frac{1}{2}\varepsilon^{-2}\,\hat{\kappa}\Big\|\operatorname{div}\underline{y}_\varepsilon(t)\Big\|_0^2, \\ \mathcal{E}_\varepsilon^{ISO}(t) &= \mu\int_\Omega \underline{\underline{\varepsilon}}\big(\underline{y}_\varepsilon(t)\big) : \underline{\underline{\varepsilon}}\big(\underline{y}_\varepsilon(t)\big)\,\mathrm{d}\Omega = \mu\sum_{i,k=1}^{3}\Big\|\varepsilon_{ik}\big(\underline{y}_\varepsilon(t)\big)\Big\|_0^2. \end{aligned} \tag{3.5}$$

Note that we denote by $\|\cdot\|_0$ the standard norm on $L^2(\Omega)$, and $\dot{\underline{y}}_\varepsilon$ stands for total derivative in time.
The contribution associated with the viscous losses reads

$$\mathcal{E}_\varepsilon^{\mathrm{VS}}(t) = \varepsilon^{-1}\,\hat{\zeta}\int_\Omega \left|\operatorname{div}\dot{\underline{y}}_\varepsilon(t)\right|^2 \mathrm{d}\Omega = \varepsilon^{-1}\,\hat{\zeta}\left\|\operatorname{div}\dot{\underline{y}}_\varepsilon(t)\right\|_0^2, \tag{3.6}$$

whereas the source term contribution is given by

$$\mathcal{P}_\varepsilon^{ext}(t) = \int_{\Gamma_N} p(\underline{x},t)\cos(\hat{\omega}\,t/\varepsilon)\,\underline{n}\cdot\dot{\underline{y}}_\varepsilon\;\mathrm{d}S.$$

In order to demonstrate that the energy $\mathcal{E}_\varepsilon^{tot}$ is uniformly bounded with respect to ε, we first provide an estimate for the term $\mathcal{P}_\varepsilon^{ext}$.
To do so, we assume that there exists $C>0$ s.t. $\|p\|_{H^{\frac{1}{2}}(\Gamma)} \le C$. Then, using the Cauchy-Schwarz inequality, the definition of the norm in $H(\operatorname{div};\Omega)$ and the Young inequality, we derive the estimation

$$\begin{aligned}\left|\mathcal{P}_\varepsilon^{ext}(t)\right| &\le \int_{\Gamma_N}\left|p(\underline{x},t)\,\underline{n}\cdot\dot{\underline{y}}_\varepsilon(t)\right|\,\mathrm{d}S \le \|p(t)\|_{H^{\frac{1}{2}}(\Gamma)}\left\|\underline{n}\cdot\dot{\underline{y}}_\varepsilon(t)\right\|_{H^{-\frac{1}{2}}(\Gamma)} \le C\left\|\dot{\underline{y}}_\varepsilon(t)\right\|_{H(\operatorname{div};\Omega)}\\ &\le C\left(1+\left\|\dot{\underline{y}}_\varepsilon(t)\right\|_0^2+\left\|\operatorname{div}\dot{\underline{y}}_\varepsilon(t)\right\|_0^2\right).\end{aligned} \tag{3.7}$$

We are now able to retrieve the following result:
Proposition 3.2. *Let $\varepsilon>0$ small enough. Then, there exists a constant $C>0$ independent of ε such that*

$$\mathcal{E}_\varepsilon^{tot}(t) \le C \quad \forall t\in[0,T].$$

In particular,

$$\boxed{\sup_{t\in[0,T]}\left\|\operatorname{div}\underline{y}_\varepsilon(t)\right\|_0^2 + \varepsilon\int_0^T\left\|\operatorname{div}\dot{\underline{y}}_\varepsilon(t)\right\|_0^2\mathrm{d}t \le \varepsilon^2\,C.}$$

Proof. We want to prove that the total internal energy $\mathcal{E}_\varepsilon^{tot}$ is uniformly bounded in time. In order to retrieve this estimate, we need to control the source term contributions. Note that the value of C will change along the proof, for the sake of simplicity. First, we recall that, from Eq. (3.7), we have

$$|P_{ext}| \le C\left(1+\left\|\dot{\underline{y}}_\varepsilon(t)\right\|_0^2+\left\|\operatorname{div}\dot{\underline{y}}_\varepsilon(t)\right\|_0^2\right).$$

As a consequence, using also the definition of the total energy $\mathcal{E}_\varepsilon^{tot}(t)$ and Eq. (3.6), we can derive

$$\frac{\mathrm{d}}{\mathrm{d}t}\mathcal{E}_\varepsilon^{tot}(t) \le -\left(\varepsilon^{-1}\hat{\zeta}-C\right)\left\|\operatorname{div}\dot{\underline{y}}_\varepsilon(t)\right\|_0^2 + C\left\|\dot{\underline{y}}_\varepsilon(t)\right\|_0^2 + C.$$

By definition of the kinetic energy term in Eq. (3.5), we obtain the estimation

$$\left\|\dot{\underline{y}}_\varepsilon(t)\right\|_0^2 \le C\,\mathcal{K}_\varepsilon(t) \le C\,\mathcal{E}_\varepsilon^{tot}(t).$$

Since ε is small by hypothesis, we can assert the following inequality:

$$\frac{\mathrm{d}}{\mathrm{d}t}\mathcal{E}_\varepsilon^{tot}(t) \le -\varepsilon^{-1}\,C\left\|\operatorname{div}\dot{\underline{y}}_\varepsilon(t)\right\|_0^2 + C\,\mathcal{E}_\varepsilon^{tot}(t) + C.$$

By integrating w.r.t. time, we retrieve

$$\mathcal{E}_\varepsilon^{tot}(t) + \varepsilon^{-1} C \int_0^t \left\| \mathrm{div} \underline{\dot{y}}_\varepsilon(s) \right\|_0^2 \mathrm{d}s \leq \mathcal{E}_\varepsilon^{tot}(0) + \int_0^t C\, \mathcal{E}_\varepsilon^{tot}(s)\, \mathrm{d}s + C\, t.$$

Note that $\mathcal{E}_\varepsilon^{tot}(0) = 0$ due to the null initial conditions. Let us now define a new total energy function $\tilde{\mathcal{E}}_\varepsilon^{tot}(t)$, given by

$$\tilde{\mathcal{E}}_\varepsilon^{tot}(t) \coloneqq \mathcal{E}_\varepsilon^{tot}(t) + \varepsilon^{-1} C \int_0^t \left\| \mathrm{div} \underline{\dot{y}}_\varepsilon(s) \right\|_0^2 \mathrm{d}s.$$

Then, we obtain, for all $t \in [0, T]$,

$$\tilde{\mathcal{E}}_\varepsilon^{tot}(t) \leq C\, T + \int_0^t C \tilde{\mathcal{E}}_\varepsilon^{tot}(s)\, \mathrm{d}s,$$

since we assume by hypothesis that $\underline{y}$ and $\dot{\underline{y}}$ vanish at time $t = 0$. We highlight that both C and $\mathcal{E}_\varepsilon^{tot}(s)$ are positive. Then, by the Grönwall inequality in integral form, we can state that

$$\tilde{\mathcal{E}}_\varepsilon^{tot}(t) \leq C \exp\Big(\int_0^t C\, \mathrm{d}s \Big). \tag{3.8}$$

As a consequence, there exists $C > 0$ such that

$$\mathcal{E}_\varepsilon^{tot}(t) \leq \tilde{\mathcal{E}}_\varepsilon^{tot}(t) \leq C \quad \forall t \in [0, T],$$

thus concluding the proof. □

Note that estimate (3.8) may not be optimal, but here our objective is to retrieve a bound independent of ε. Due to the structure of the surfacic source term, we expect the solution to oscillate. As a consequence, we expect that its primitive in time is small. This is the object of the following corollaries. First, let us define

$$\underline{Y}_\varepsilon(t) \coloneqq \int_0^t \underline{y}_\varepsilon(s)\, \mathrm{d}s, \quad \forall t \in [0, T]. \tag{3.9}$$

Corollary 3.1. *There exists a constant $C > 0$ such that*

$$\boxed{\sup_{t \in [0,T]} \left(\| \mathrm{div}\, \underline{Y}_\varepsilon(t) \|_0^2 + \varepsilon^2 \left\| \underline{y}_\varepsilon(t) \right\|_0^2 \right) + \varepsilon \int_0^T \left\| \mathrm{div}\, \underline{y}_\varepsilon(t) \right\|_0^2 \mathrm{d}t \leq \varepsilon^4\, C.}$$

Furthermore, we can assert that there exists $C > 0$ such that

$$\boxed{\sup_{t \in [0,T]} \left(\left\| \underline{y}_\varepsilon \right\|_{H(\mathrm{div};\Omega)}^2 \right) \leq \varepsilon^2\, C.} \tag{3.10}$$

Proof. Let us integrate Eq. (3.4) w.r.t. time and substitute

$$\underline{w} = \int_0^t \dot{\underline{y}}_\varepsilon(s)\, \mathrm{d}s = \underline{y}_\varepsilon.$$

We obtain

$$\frac{\mathrm{d}}{\mathrm{d}t} \hat{\mathcal{E}}_\varepsilon^{tot}(t) + \hat{\zeta}\, \varepsilon^{-1} \left\| \mathrm{div}\, \underline{y}_\varepsilon \right\|_0^2 = \int_{\Gamma_N} \left| \left(\int_0^t \cos\left(\frac{\hat{\omega}\, s}{\varepsilon} \right) p(\underline{x}, s)\, \mathrm{d}s \right) \underline{n} \cdot \underline{y}_\varepsilon(t) \right| \mathrm{d}S, \tag{3.11}$$

where we have used Eq. (3.9), whereas the energy function $\hat{\mathcal{E}}_\varepsilon^{tot}(t)$ is given by

$$\hat{\mathcal{E}}_\varepsilon^{tot}(t) := \left(\frac{1}{2}\rho\left\|\underline{y}_\varepsilon(t)\right\|_0^2 + \frac{1}{2}\hat{\kappa}\,\varepsilon^{-2}\left\|\operatorname{div}\underline{Y}_\varepsilon(t)\right\|_0^2 + \mu\sum_{i,k=1}^{3}\left\|\varepsilon_{ik}\big(\underline{Y}_\varepsilon(t)\big)\right\|_0^2\right).$$

Let us further analyse the surfacic source term: it can be rewritten as

$$\begin{aligned}
&\int_{\Gamma_N}\left|\left(\int_0^t \cos\left(\frac{\hat{\omega}\,s}{\varepsilon}\right)p(\underline{x},s)\mathrm{d}s\right)\underline{n}\cdot\underline{y}_\varepsilon(t)\right|\,\mathrm{d}S\\
&= \frac{\varepsilon}{\hat{\omega}}\int_{\Gamma_N}\left(\left|\sin\left(\frac{\hat{\omega}\,t}{\varepsilon}\right)p(\underline{x},t)\,\underline{n}\cdot\underline{y}_\varepsilon(t)\right| + \left|\left(\int_0^t \sin\left(\frac{\hat{\omega}\,s}{\varepsilon}\right)\frac{\partial}{\partial s}p(\underline{x},s)\,\mathrm{d}s\right)\underline{n}\cdot\underline{y}_\varepsilon(t)\right|\right)\mathrm{d}S\\
&\leq 2\,\frac{\varepsilon}{\hat{\omega}}\|p\|_{H^{\frac{1}{2}}(\Gamma)}\left\|\underline{n}\cdot\underline{y}_\varepsilon(t)\right\|_{H^{-\frac{1}{2}}(\Gamma)} \leq \varepsilon\,C\left\|\underline{y}_\varepsilon(t)\right\|_{H(\mathrm{div};\Omega)}\\
&\leq C\left(1+\varepsilon^2\left\|\underline{y}_\varepsilon(t)\right\|_0^2 + \varepsilon^2\left\|\operatorname{div}\underline{y}_\varepsilon(t)\right\|_0^2\right).
\end{aligned}$$

We recall that by definition of the energy $\hat{\mathcal{E}}_\varepsilon^{tot}(t)$, there exists $C>0$ such that

$$\left\|\underline{y}_\varepsilon(t)\right\|_0^2 \leq C\,\hat{\mathcal{E}}_\varepsilon^{tot}(t).$$

Hence, we obtain

$$\frac{\mathrm{d}}{\mathrm{d}t}\hat{\mathcal{E}}_\varepsilon^{tot}(t) + (\varepsilon^{-1}\,\hat{\zeta} - \varepsilon^2\,C)\left\|\operatorname{div}\underline{y}_\varepsilon(t)\right\|_0^2 \leq C\,\varepsilon^2\hat{\mathcal{E}}_\varepsilon^{tot}(t).$$

By integrating w.r.t. t, we retrieve

$$\hat{\mathcal{E}}_\varepsilon^{tot}(t) + \varepsilon^{-1}\,C\int_0^t\left\|\operatorname{div}\underline{y}_\varepsilon(s)\right\|_0^2\mathrm{d}s \leq \hat{\mathcal{E}}_\varepsilon^{tot}(0) + \varepsilon^2\int_0^t C\,\hat{\mathcal{E}}_\varepsilon^{tot}(s)\,\mathrm{d}s,$$

with $\hat{\mathcal{E}}_\varepsilon^{tot}(0) = 0$ due to the null initial conditions. Then, by similar arguments to the previous proof, we can obtain that there exists $c>0$ such that

$$\hat{\mathcal{E}}_\varepsilon^{tot}(t) + \varepsilon^{-1}\,C\int_0^t\left\|\operatorname{div}\underline{y}_\varepsilon(s)\right\|_0^2\mathrm{d}s \leq \varepsilon^2 c \quad \forall t\in[0,T],$$

Finally, using the definition of $\hat{\mathcal{E}}_\varepsilon^{tot}(t)$, we retrieve the desired result. □

Corollary 3.2. *There exists a strictly positive constant C such that*

$$\boxed{\varepsilon\sup_{t\in[0,T]}\|\underline{Y}_\varepsilon(t)\|_0^2 + \int_0^T\|\operatorname{div}\underline{Y}_\varepsilon(t)\|_0^2\,\mathrm{d}t \leq \varepsilon^5\,C.}$$

Furthermore,

$$\sup_{t\in[0,T]}\|\underline{Y}_\varepsilon(t)\|_{H(\mathrm{div};\Omega)}^2 \leq \varepsilon^4\,C.$$

The proof of this corollary is omitted for the sake of conciseness. The main idea is to integrate twice Eq. (3.4) w.r.t. t, and substitute

$$\underline{w} = \int_0^t \underline{y}_\varepsilon(s)\,\mathrm{d}s = \underline{Y}_\varepsilon.$$

Then, by similar considerations to the previous proofs, and using Corollary 3.1, we obtain the desired result.

3.3 Asymptotic expansion of the solution

We recall here the main elements of the asymptotic approach outlined in Chapter 2. Recall that we look for a regular asymptotic expansion of the solution of Problem (3.4), i.e. we assume that y_ε can be written using a power series expansion in ε. We suppose that there exists $N \in \mathbb{N}$ such that the solution y_ε can be decomposed, for all ε sufficiently small, as

$$\underline{y}_\varepsilon(\underline{x}, t) = \sum_{i=0}^{N} \varepsilon^i \, \underline{y}_i(\underline{x}, t, t/\varepsilon) + o(\varepsilon^N). \tag{3.12}$$

We assume that every term $\underline{y}_i$ of the power series is periodic on $\tau = t/\varepsilon$, with period $2\,\pi/\hat{\omega}$, and regular enough. Hence, we assume that all $\partial_\tau \underline{y}_i$ are periodic. We approximate the solution $\underline{y}_\varepsilon$ by the first terms of the expansion (3.12). By doing so, we recover the limit (asymptotic) behaviour of the solution y_ε for $\varepsilon \to 0$.
In practice, we substitute the expression of y_ε presented in Eq. (3.12) in the problem (3.4). To do so, all mechanical quantities must be rewritten in series form, accordingly. We use the following expansion of the second derivative in time for every term in Eq. (3.12):

$$\ddot{\underline{y}}_i(\underline{x}, t, t/\varepsilon) = \left(\varepsilon^{-2}\, \partial^2_\tau \underline{y}_i + 2\varepsilon^{-1} \partial^2_{t\tau} \underline{y}_i + \varepsilon^0\, \partial^2_t \underline{y}_i\right)(\underline{x}, t, t/\varepsilon). \tag{3.13}$$

Once all the terms of the expansion are obtained and inserted in Eq. (3.4), the equations proportional to the same order of ε are identified. For simplicity of notation, we explicitly denote only the dependence on τ in what follows, and we implicitly assume that all $\underline{y}_i$'s (and their components) depend on $\underline{x}$ and t. Note that $\underline{y}_i(\underline{x}, 0, 0) = \underline{0}$, for all $i \in \{0, 1, .., N\}$, due to the fact that the pressure field has compact support in $[0, T]$.

Henceforth, we identify the equations proportional to the same order of ε. Based on the properties retrieved by energy arguments, we are able to demonstrate that the leading term of the expansion $\underline{y}_0$ and the first corrector $\underline{y}_1$ are zero. Then, we outline the governing equations for the higher correctors. The next section will be devoted to the description of a proof of convergence for this approximation.

Properties of the solution from the energy estimate. Let the expansion (3.12) hold. Then, if we substitute in Eq. (3.10) the proposed expansion, we obtain

$$\int_\Omega \left|\underline{y}_0\right|^2 \mathrm{d}\Omega \leq \varepsilon^2\, C \implies \underline{y}_0 = 0.$$

In addition, from Proposition 3.2 and Corollary 3.2, we get that there exists $C > 0$ such that

$$\int_0^T \left\|\operatorname{div} \dot{\underline{y}}_\varepsilon\right\|_0^2 \mathrm{d}t \leq \varepsilon\, C \implies \int_0^T \left\|\operatorname{div} \partial_\tau \underline{y}_1\right\|_0^2 \mathrm{d}t = 0 \implies \left\|\operatorname{div} \partial_\tau \underline{y}_1\right\|_0 = 0, \tag{3.14}$$

Properties of the first-order corrector: a null field. Assume that the expansion (3.12) hold. In this section, we prove that the corrector $\underline{y}_1$ is null. To this end, we consider the equation associated with ε^{-1} in problem (3.4). This term reads accordingly for all t and all τ

$$\begin{cases} \displaystyle\int_\Omega \rho\, \partial^2_\tau \underline{y}_1 \cdot \underline{w}\, \mathrm{d}\Omega + \hat{\kappa} \int_\Omega \operatorname{div} \underline{y}_1 \operatorname{div} \underline{w}\, \mathrm{d}\Omega = 0, \ \forall \underline{w} \in \mathfrak{X} \\ \underline{y}_1\big|_{\Gamma_D} = \underline{0}, \end{cases} \tag{3.15}$$

due to Eq. (3.14). First, we can notice that, if we differentiate Eq. (3.15) w.r.t. τ, we obtain

$$\int_\Omega \rho\, \partial_\tau^3 \underline{y}_1 \cdot \underline{w}\, \mathrm{d}\Omega = 0 \quad \forall \underline{w} \in \mathcal{X} \implies \partial_\tau^3 \underline{y}_1 = 0,$$

that implies that $\underline{y}_1$ should be a second-order polynomial in τ and, due to the regularity and periodicity of $\underline{y}_1$,

$$\partial_\tau \underline{y}_1 = 0.$$

Moreover, from Corollary 3.2, we have that

$$\int_\Omega \left| \int_0^T \underline{y}_\varepsilon \, \mathrm{d}t \right|^2 \mathrm{d}\Omega \leq \varepsilon^4 C \implies \int_0^T \underline{y}_1(\underline{x}, s)\, \mathrm{d}s = 0, \quad \text{in} \Omega. \tag{3.16}$$

As a consequence, the only solution

$$\underline{y}_1 = 0.$$

Equation for the second-order corrector. The governing equation for the second-order corrector y_2 corresponds to the term of order ε^0 in Eq. (3.4), that reads

$$\begin{cases} \displaystyle\int_\Omega \rho\, \partial_\tau^2 \underline{y}_2 \cdot \underline{w}\, \mathrm{d}\Omega + \hat{\kappa} \int_\Omega \mathrm{div}\, \underline{y}_2\, \mathrm{div}\, \underline{w}\, \mathrm{d}\Omega + \hat{\zeta} \int_\Omega \partial_\tau \mathrm{div}\, \underline{y}_2\, \mathrm{div}\, \underline{w}\, \mathrm{d}\Omega \\ \qquad\qquad = \displaystyle\int_{\Gamma_N} \cos(\hat{\omega}\,\tau)\, p(\underline{x}, t)\, \underline{n} \cdot \underline{w}\, \mathrm{d}S, \\ \underline{y}_2\big|_{\Gamma_D} = \underline{0}. \end{cases} \tag{3.17}$$

In strong form, Eq. (3.17) reads

$$\begin{cases} \rho_0\, \partial_\tau^2 \underline{y}_2 - \hat{\kappa}\, \underline{\nabla}\, \mathrm{div}_{\underline{x}}\, \underline{y}_2 - \hat{\zeta}\, \underline{\nabla}\, \mathrm{div}_{\underline{x}}\, \partial_\tau \underline{y}_2 = 0 & \text{in} \quad \Omega, \\ \underline{y}_2 = \underline{0} & \text{on} \quad \Gamma_D, \\ \left(\hat{\kappa} + \hat{\zeta}\, \partial_\tau\right) \mathrm{div}_{\underline{x}}\, \underline{y}_2 \cdot \underline{n} = p\, \cos(\hat{\omega}\,\tau)\, \underline{n} & \text{on} \quad \Gamma_N. \end{cases} \tag{3.18}$$

Due to the periodic structure of the surfacic source term, Eq. (3.18) can be recast in the frequency domain. First, we rewrite the solution as a linear combination of periodic functions, i.e.

$$\underline{y}_2(\underline{\xi}, t, \tau) = \mathrm{Re}\left(\underline{\hat{y}}_2(\underline{\xi}, t)\right) \cos(\hat{\omega}\,\tau) + \mathrm{Im}\left(\underline{\hat{y}}_2(\underline{\xi}, t)\right) \sin(\hat{\omega}\,\tau), \tag{3.19}$$

where $\underline{\hat{y}}_2 = \mathrm{Re}\left(\underline{\hat{y}}_2\right) + i\, \mathrm{Im}\left(\underline{\hat{y}}_2\right) \in \mathbb{C}$.
Then, using (3.19) and identifying in the first equation in (3.18) the terms in $\cos(\hat{\omega}\,\tau)$ and $\sin(\hat{\omega}\,\tau)$, we obtain

$$-\rho_0\, \hat{\omega}^2\, \mathrm{Re}\left(\underline{\hat{y}}_2\right) - \hat{\kappa}\, \underline{\nabla}\, \mathrm{div}_{\underline{x}}\, \mathrm{Re}\left(\underline{\hat{y}}_2\right) - \hat{\omega}\, \hat{\zeta}\, \underline{\nabla}\, \mathrm{div}_{\underline{x}}\, \mathrm{Im}\left(\underline{\hat{y}}_2\right) = 0,$$

$$-\rho_0\, \hat{\omega}^2\, \mathrm{Im}\left(\underline{\hat{y}}_2\right) - \hat{\kappa}\, \underline{\nabla}\, \mathrm{div}_{\underline{x}}\, \mathrm{Im}\left(\underline{\hat{y}}_2\right) + \hat{\omega}\, \hat{\zeta}\, \underline{\nabla}\, \mathrm{div}_{\underline{x}}\, \mathrm{Re}\left(\underline{\hat{y}}_2\right) = 0.$$

Therefore, $\underline{\hat{y}}_2$ is solution of

$$\begin{cases} -\rho_0\, \hat{\omega}^2\, \underline{\hat{y}}_2 - \hat{\kappa}\, \underline{\nabla}_{\underline{x}}\, \mathrm{div}_{\underline{x}}\, \underline{\hat{y}}_2 + i\, \hat{\omega}\, \hat{\zeta}\, \underline{\nabla}_{\underline{x}}\, \mathrm{div}_{\underline{x}}\, \underline{\hat{y}}_2 = 0 & \text{in} \quad \Omega, \\ \underline{\hat{y}}_2 = \underline{0} & \text{on} \quad \Gamma_D, \\ \left(\hat{\kappa} - i\, \hat{\omega}\, \hat{\zeta}\right) \mathrm{div}_{\underline{x}}\, \underline{\hat{y}}_2(\underline{x}, t) = p(\underline{x}, t) & \text{on} \quad \Gamma_N. \end{cases} \tag{3.20}$$

Let us define $\hat{p}_2 \coloneqq \operatorname{div}_{\underline{x}} \underline{\hat{y}}_2$. Then, $\underline{\hat{y}}_2$ is solution of

$$\underline{\hat{y}}_2 = -\frac{1}{\alpha} \underline{\nabla} \hat{p}_2, \quad \text{in} \quad \Omega, \tag{3.21}$$

where $\hat{p}_2$ satisfies

$$\begin{cases} \Delta \hat{p}_2 + \alpha \hat{p}_2 = 0 & \text{in} \quad \Omega, \\ \underline{\nabla}_{\underline{x}} \hat{p}_2 \cdot \underline{n} = 0 & \text{on} \quad \Gamma_D, \\ (\hat{\kappa} - i\,\hat{\omega}\,\hat{\zeta})\,\hat{p}_2(\underline{x}, t) = p(\underline{x}, t) & \text{on} \quad \Gamma_N, \end{cases} \tag{3.22}$$

with

$$\alpha \coloneqq \frac{\rho_0\,\hat{\omega}^2}{\hat{\kappa} - i\,\hat{\omega}\,\hat{\zeta}} \in \mathbb{C}. \tag{3.23}$$

In fact, on Γ_D we have by hypothesis $\underline{\hat{y}}_2 = \underline{0}$. Therefore,

$$\underline{\hat{y}}_2 \cdot \underline{n} = 0 \implies \underline{\nabla}_{\underline{x}} \hat{p} \cdot \underline{n} = 0.$$

Eq. (3.22) represents for each time t a Helmholtz equation governing the propagation of the pressure wave. Note that t plays the role of a parameter in this equation, thanks to Eq. (3.19).

Equation for the corrector of order k. In order to retrieve the governing equation for the corrector y_k, we consider the term of order ε^{k-2} in Eq. (3.4). The problem satisfied by y_k is given by

$$\begin{cases} \displaystyle\int_\Omega \rho \left(\partial_\tau^2 \underline{y}_k + 2\,\partial_\tau \partial_t \underline{y}_{k-1} + \partial_t^2 \underline{y}_{k-2}\right) \underline{w}\,\mathrm{d}\Omega + \hat{\kappa} \int_\Omega \operatorname{div} \underline{y}_k \operatorname{div} \underline{w}\,\mathrm{d}\Omega \\ \qquad + \hat{\zeta} \displaystyle\int_\Omega \left(\partial_\tau \operatorname{div} \underline{y}_k + \partial_t \operatorname{div} \underline{y}_{k-1}\right) \operatorname{div} \underline{w}\,\mathrm{d}\Omega + 2\mu \int_\Omega \underline{\underline{\varepsilon}}(\underline{y}_{k-2}) : \underline{\underline{\varepsilon}}(\underline{w})\,\mathrm{d}\Omega = 0, \\ \underline{y}_k\big|_{\Gamma_D} = \underline{0}. \end{cases} \tag{3.24}$$

Note that $y_{k-1}(\underline{x}, t, \tau)$ and $y_{k-2}(\underline{x}, t, \tau)$ are computed at the previous steps, therefore they represent source terms.

3.4 Approximation properties

3.4.1 Approximation property of the second corrector

Henceforth, we formulate an estimate of the error associated with the approximation of the solution $\underline{y}_\varepsilon$ with the second corrector $\underline{y}_2$.

Proposition 3.3. *Let the corrector $\underline{y}_2$ regular enough. Then, there exists $C > 0$ such that*

$$\boxed{\forall t \in [0, T], \quad \left\| \underline{y}_\varepsilon(t) - \varepsilon^2 \underline{y}_2\left(t, \frac{t}{\varepsilon}\right) \right\|_0 \leq \varepsilon^2\, C.}$$

Remark Note that by Proposition 3.3, we trivially obtain $\left\|\underline{y}_\varepsilon(t)\right\|_0 \leq \varepsilon^2$, $\forall t \in [0,T]$, that confirms *a posteriori* that the solution $\underline{y}_\varepsilon$ is at least of the order of ε^2, i.e. the first two terms of the expansion are zero.

Proof. Note that the value of the constant C will change along the proof, for simplicity of notation. Let us first define the error

$$\underline{e}_2 \equiv \underline{e}_2(t) = \underline{y}_\varepsilon(t) - \varepsilon^2\, \underline{y}_2\Big(t, \frac{t}{\varepsilon}\Big).$$

If we subtract Eq. (3.4) by Eqs. (3.15), we can deduce

$$\begin{aligned}
&\int_\Omega \rho\, \ddot{\underline{e}}_2(\underline{x},t)\ \cdot \underline{w}(\underline{x})\, \mathrm{d}\Omega + \varepsilon^{-2}\hat{\kappa} \int_\Omega \operatorname{div} \underline{e}_2(\underline{x},t) \operatorname{div} \underline{w}(\underline{x})\ \mathrm{d}\Omega \\
&\quad + 2\,\mu \int_\Omega \underline{\underline{\varepsilon}}\big(\underline{y}(\underline{x},t)\big) : \underline{\underline{\varepsilon}}\big(\underline{w}(\underline{x})\big)\, \mathrm{d}\Omega + \varepsilon^{-1}\hat{\zeta} \int_\Omega \operatorname{div} \dot{\underline{e}}_2(\underline{x},t) \operatorname{div} \underline{w}(\underline{x})\, \mathrm{d}\Omega = \\
&\varepsilon^2 \int_\Omega \rho\, \partial_t^2 \underline{y}_2 \cdot \underline{w}\, \mathrm{d}\Omega + 2\,\varepsilon \int_\Omega \rho\, \partial_t \partial_\tau \underline{y}_2 \cdot \underline{w}\, \mathrm{d}\Omega + \varepsilon \int_\Omega \hat{\zeta}\, \partial_t \operatorname{div} \underline{y}_2 \cdot \operatorname{div} \underline{w}\, \mathrm{d}\Omega \\
&\quad + 2\,\varepsilon^2\,\mu \int_\Omega \underline{\underline{\varepsilon}}(\underline{y}_2) : \underline{\underline{\varepsilon}}(\underline{w})\, \mathrm{d}\Omega.
\end{aligned} \tag{3.25}$$

Let us formally define the energy associated with $\underline{e}_2$. It reads:

$$\mathcal{E}^{tot}\big(\underline{e}_2\big) = \mathcal{K}\big(\underline{e}_2\big) + \mathcal{E}^{\mathrm{NI}}\big(\underline{e}_2\big) + \mathcal{E}^{ISO}\big(\underline{e}_2\big),$$

with kinetic energy and internal energy given by

$$\mathcal{K}\big(\underline{e}_2\big) = \int_\Omega \rho\, |\dot{\underline{e}}_2|^2\, \mathrm{d}\Omega = \rho \|\dot{\underline{e}}_2\|_0^2,$$

$$\mathcal{E}^{\mathrm{NI}}\big(\underline{e}_2\big) = \varepsilon^{-2}\, \hat{\kappa} \int_\Omega |\operatorname{div} \underline{e}_2|^2\, \mathrm{d}\Omega = \varepsilon^{-2}\, \hat{\kappa} \|\operatorname{div} \underline{e}_2\|_0^2,$$

$$\mathcal{E}^{ISO}\big(\underline{e}_2\big) = 2\,\mu \int_\Omega \underline{\underline{\varepsilon}}\big(\underline{e}_2\big) : \underline{\underline{\varepsilon}}\big(\underline{e}_2\big)\, \mathrm{d}\Omega = 2\,\mu \sum_{i,k=1}^{3} \big\|\varepsilon_{ik}\big(\underline{e}_2\big)\big\|_0^2.$$

The contribution associated with the viscous losses reads

$$\mathcal{E}^{\mathrm{VS}}\big(\underline{e}_2\big) = \varepsilon^{-1}\, \hat{\zeta} \int_\Omega |\operatorname{div} \dot{\underline{e}}_2|^2\, \mathrm{d}\Omega = \varepsilon^{-1}\, \hat{\zeta} \|\operatorname{div} \dot{\underline{e}}_2\|_0^2.$$

On the other hand, the energy associated with Eq. (3.25) reads

$$\begin{aligned}
\frac{\mathrm{d}}{\mathrm{d}\,t}\mathcal{E}^{tot}\big(\underline{e}_2\big) + \mathcal{E}^{\mathrm{VS}}\big(\underline{e}_2\big) &= \varepsilon^2 \int_\Omega \rho\, \partial_t^2 \underline{y}_2 \cdot \dot{\underline{e}}_2\, \mathrm{d}\Omega + 2\,\varepsilon \int_\Omega \rho\, \partial_t \partial_\tau \underline{y}_2 \cdot \dot{\underline{e}}_2\, \mathrm{d}\Omega \\
&\quad + \varepsilon \int_\Omega \hat{\zeta}\, \partial_t \operatorname{div} \underline{y}_2 \cdot \operatorname{div} \dot{\underline{e}}_2\, \mathrm{d}\Omega + 2\,\varepsilon^2\,\mu \int_\Omega \underline{\underline{\varepsilon}}(\underline{y}_2) : \underline{\underline{\varepsilon}}(\dot{\underline{e}}_2)\, \mathrm{d}\Omega.
\end{aligned}$$

Hence, we can derive, using the Cauchy-Schwarz inequality,

$$\begin{aligned}
\frac{\mathrm{d}}{\mathrm{d}\,t}\mathcal{E}^{tot}\big(\underline{e}_2\big) + \mathcal{E}^{\mathrm{VS}}\big(\underline{e}_2\big) &\leq \varepsilon\Big(\varepsilon\,\rho \Big\|\partial_t^2 \underline{y}_2\Big\|_0 + \rho \Big\|\partial_t \partial_\tau \underline{y}_2\Big\|_0\Big) \|\dot{\underline{e}}_2\|_0 \\
&\quad + \varepsilon\, \hat{\zeta} \Big\|\partial_t \operatorname{div} \underline{y}_2\Big\|_0 \|\operatorname{div} \dot{\underline{e}}_2\|_0 + 2\,\varepsilon^2\,\mu \int_\Omega \underline{\underline{\varepsilon}}(\underline{y}_2) : \underline{\underline{\varepsilon}}(\dot{\underline{e}}_2)\, \mathrm{d}\Omega.
\end{aligned}$$

Due to the regularity assumption on $\underline{y}_2$, we can assume that there exists $A > 0$ such that

$$\varepsilon\,\rho\left\|\partial_t^2\underline{y}_2\right\|_0 + \rho\left\|\partial_t\partial_\tau\underline{y}_2\right\|_0 + \hat{\zeta}\left\|\partial_t \mathrm{div}\,\underline{y}_2\right\|_0 \leq A.$$

Then, we retrieve

$$\begin{aligned}\frac{\mathrm{d}}{\mathrm{d}\,t}\mathcal{E}^{tot}(\underline{e}_2) + \mathcal{E}^{\mathrm{VS}}(\underline{e}_2) &\leq \varepsilon\,A\sqrt{\mathcal{E}^{tot}(\underline{e}_2)} + \varepsilon\,A\sqrt{\varepsilon\mathcal{E}^{\mathrm{VS}}(\underline{e}_2)} + 2\,\varepsilon^2\mu\int_\Omega \underline{\underline{\varepsilon}}(\underline{y}_2) : \underline{\underline{\varepsilon}}(\dot{\underline{e}}_2)\,\mathrm{d}\Omega \\ &\leq \varepsilon\,A\sqrt{\mathcal{E}^{tot}(\underline{e}_2)} + \frac{1}{2}\varepsilon^2\,A^2 + \frac{1}{2}\varepsilon\mathcal{E}^{\mathrm{VS}}(\underline{e}_2) + 2\,\varepsilon^2\mu\int_\Omega \underline{\underline{\varepsilon}}(\underline{y}_2) : \underline{\underline{\varepsilon}}(\dot{\underline{e}}_2)\,\mathrm{d}\Omega.\end{aligned} \tag{3.26}$$

The next step consists in integrating (3.26) with respect to the time variable in $[0, t]$. We retrieve that there exists a constant $c > 0$ such that

$$\begin{aligned}&\mathcal{E}^{tot}\big(\underline{e}_2(t)\big) + \int_0^t \mathcal{E}^{\mathrm{VS}}(\underline{e}_2(s))\,\mathrm{d}s \\ &\qquad\leq \varepsilon\,c\int_0^t \sqrt{\mathcal{E}^{tot}(\underline{e}_2(s))}\,\mathrm{d}s + \varepsilon^2\,c\,t + 2\,\varepsilon^2\,c\,\mu\int_\Omega \underline{\underline{\varepsilon}}(\underline{y}_2) : \underline{\underline{\varepsilon}}(\dot{\underline{e}}_2)\,\mathrm{d}\Omega.\end{aligned} \tag{3.27}$$

Observe that we consider a finite time interval $[0, T]$. Hence, we can introduce a positive constant C such that $\varepsilon^2\,c\,t \leq \varepsilon^2\,C$. Furthermore, if we integrate with respect to time the last integral in Eq. (3.26), we obtain:

$$\begin{aligned}&\int_0^t\int_\Omega \underline{\underline{\varepsilon}}\big(\underline{y}_2(s)\big) : \underline{\underline{\varepsilon}}\big(\dot{\underline{e}}_2(s)\big)\,\mathrm{d}\Omega\,\mathrm{d}s \\ &= \Big[\int_\Omega \underline{\underline{\varepsilon}}\big(\underline{y}_2(s)\big) : \underline{\underline{\varepsilon}}\big(\underline{e}_2(s)\big)\,\mathrm{d}\Omega\Big]_0^t - \int_0^t\int_\Omega \underline{\underline{\varepsilon}}\big(\dot{\underline{y}}_2(s)\big) : \underline{\underline{\varepsilon}}\big(\underline{e}_2(s)\big)\,\mathrm{d}\Omega\,\mathrm{d}s \\ &= \sum_{i,k=1}^3\int_\Omega \varepsilon_{ik}\big(\underline{y}_2(t)\big)\varepsilon_{ik}\big(\underline{e}_2(t)\big)\,\mathrm{d}\Omega - \int_0^t\sum_{i,k=1}^3\Big(\int_\Omega \varepsilon_{ik}\big(\dot{\underline{y}}_2(s)\big)\varepsilon_{ik}\big(\underline{e}_2(s)\big)\,\mathrm{d}\Omega\Big)\,\mathrm{d}s.\end{aligned}$$

Due to the regularity of $\underline{y}_2$, we can assume that there exists $A > 0$ such that for all $s \in [0, t]$

$$\begin{aligned}&\max_{i,k}\left\|\varepsilon_{ik}\big(\underline{y}_2(s)\big)\right\|_0 \leq A, \\ &\max_{i,k}\left\|\varepsilon_{ik}\big(\dot{\underline{y}}_2(s)\big)\right\|_0 \leq \max_{i,k}\left(\varepsilon^{-1}\left\|\partial_\tau\varepsilon_{ik}\big(\underline{y}_2(s)\big)\right\|_0 + \left\|\partial_t\varepsilon_{ik}\big(\underline{y}_2(s)\big)\right\|_0\right) \leq \varepsilon^{-1}A.\end{aligned}$$

Hence, we retrieve

$$\begin{aligned}&\int_0^t\int_\Omega \underline{\underline{\varepsilon}}\big(\underline{y}_2(s)\big) : \underline{\underline{\varepsilon}}\big(\dot{\underline{e}}_2(s)\big)\,\mathrm{d}\Omega\,\mathrm{d}s \\ &\leq A\Big(\sum_{i,k=1}^3\int_\Omega \big|\varepsilon_{ik}\big(\underline{e}_2(t)\big)\big|^2\,\mathrm{d}\Omega\Big)^{\frac{1}{2}} + \varepsilon^{-1}A\int_0^t\Big(\sum_{i,k=1}^3\int_\Omega \big|\varepsilon_{ik}\big(\underline{e}_2(s)\big)\big|^2\,\mathrm{d}\Omega\Big)^{\frac{1}{2}}\mathrm{d}s \\ &\leq A\sqrt{\mathcal{E}^{ISO}\big(\underline{e}_2(t)\big)} + \varepsilon^{-1}A\int_0^t\sqrt{\mathcal{E}^{ISO}\big(\underline{e}_2(s)\big)}\mathrm{d}s \\ &\leq A\sqrt{\mathcal{E}^{tot}\big(\underline{e}_2(t)\big)} + \varepsilon^{-1}A\int_0^t\sqrt{\mathcal{E}^{tot}\big(\underline{e}_2(s)\big)}\mathrm{d}s \\ &\leq \frac{1}{2}A^2 + \frac{1}{2}\mathcal{E}^{tot}\big(\underline{e}_2(t)\big) + \varepsilon^{-1}A\int_0^t\sqrt{\mathcal{E}^{tot}\big(\underline{e}_2(s)\big)}\mathrm{d}s.\end{aligned} \tag{3.28}$$

Hence, from Eq. (3.27) we can deduce that there exists a positive constant C such that

$$\mathcal{E}^{tot}\big(\underline{e}_2(t)\big) + \int_0^t \mathcal{E}^{\mathrm{VS}}(\underline{e}_2(s))\,\mathrm{d}s \le \varepsilon^2\, C + \varepsilon\, C \int_0^t \sqrt{\mathcal{E}^{tot}(\underline{e}_2(s))}\,\mathrm{d}s.$$

Since $\mathcal{E}^{\mathrm{VS}}(\underline{e}_2(s))$ is positive by definition, we now define the energy $\tilde{\mathcal{E}}^{tot}\big(\underline{e}_2(t)\big)$:

$$\tilde{\mathcal{E}}^{tot}\big(\underline{e}_2(t)\big) \coloneqq \mathcal{E}^{tot}\big(\underline{e}_2(t)\big) + \int_0^t \mathcal{E}^{\mathrm{VS}}(\underline{e}_2(s))\,\mathrm{d}s.$$

As a consequence, using Eq. (3.28) we can state that there exists a constant $C > 0$ such that

$$\tilde{\mathcal{E}}^{tot}\big(\underline{e}_2(t)\big) \le \varepsilon^2\, C + \varepsilon\, C \int_0^t \sqrt{\tilde{\mathcal{E}}^{tot}(\underline{e}_2(s))}\,\mathrm{d}s,$$

since $\mathcal{E}^{tot}(\underline{e}_2(0)) = 0$. that entails, from the Grönwall lemma, that there exists a positive constant C such that

$$\tilde{\mathcal{E}}^{tot}\big(\underline{e}_2(t)\big) \le \varepsilon^2 C.$$

Hence, there exists $C > 0$ satisfying

$$\varepsilon \sup_{t\in[0,T]} \left(\|\dot{\underline{e}}_2(t)\|_0^2 + \varepsilon^{-2} \|\mathrm{div}\, \underline{e}_2(t)\|_0^2 \right) + \int_0^T \int_\Omega |\mathrm{div}\, \dot{\underline{e}}_2(t)|^2\,\mathrm{d}\Omega\,\mathrm{d}t \le \varepsilon^3\, C.$$

Due to the structure of the source term, we are allowed to define

$$y_2(\underline{x}, t) = \hat{\underline{y}}_2(\underline{x})\, h(t)\, \cos(\hat{\omega} t/\varepsilon),$$

with $\hat{\underline{y}}_2(\underline{x})$ bounded in $L^2(\Omega)$. Then, we can introduce

$$\underline{Y}_2(t) \coloneqq \int_0^t \underline{y}_2\,\mathrm{d}s = \int_0^t \hat{\underline{y}}_2(\underline{x})\, h(s)\, \cos(\hat{\omega} s/\varepsilon)\mathrm{d}s.$$

By integration by parts, we can rewrite

$$\underline{Y}_2(t) = -\frac{\varepsilon}{\hat{\omega}} \int_0^t \hat{\underline{y}}_2(\underline{x})\, h'(s)\, \sin(\hat{\omega} s/\varepsilon)\mathrm{d}s + \left[\frac{\varepsilon}{\hat{\omega}} h(s)\, \sin(\hat{\omega} s/\varepsilon) \right]_0^t. \tag{3.29}$$

Therefore, if we consider the term $\left\|\partial_t^2 \underline{Y}_2\right\|$, we can assert that there exists $A > 0$ s.t.

$$\begin{aligned}
\|\partial_t^2 \underline{Y}_2\| &= \left\| \partial_t^2 \int_0^t \underline{y}_2(\underline{x}, s)\,\mathrm{d}s \right\| \\
&= \varepsilon \left\| \partial_t^2 \left(-\frac{1}{\hat{\omega}} \int_0^t \hat{\underline{y}}_2(\underline{x})\, h'(s)\, \sin(\hat{\omega} s/\varepsilon)\mathrm{d}s + \left[\frac{1}{\hat{\omega}} h(t)\, \sin(\hat{\omega} t/\varepsilon) \right]_0^t \right) \right\| \\
&\le \varepsilon A,
\end{aligned}$$

since $\hat{\underline{y}}_2(\underline{x})$ is bounded in $L^2(\Omega)$ by hypothesis, $h(s)$ is assumed regular and $|\sin(\hat{\omega} s/\varepsilon)| \le 1$. We can make analogous remarks concerning the terms $\|\partial_t \partial_\tau \underline{Y}_2\|$ and $\|\partial_t \mathrm{div}\, \underline{Y}_2\|$, and we can assert that there exists another $A > 0$ s.t.

$$\varepsilon\, \rho \left\|\partial_t^2 \underline{Y}_2\right\| + \rho \|\partial_t \partial_\tau \underline{Y}_2\| + \hat{\zeta} \|\partial_t \mathrm{div}\, \underline{Y}_2\| \le \varepsilon\, A.$$

Then, if we define $\underline{E}_2 \equiv \underline{E}_2(t) = \int_0^t \underline{e}_2 \,\mathrm{d}s$, by similar arguments we obtain

$$\begin{aligned}
&\frac{\mathrm{d}}{\mathrm{d}t}\mathcal{E}^{tot}(\underline{E}_2) + \mathcal{E}^{\mathrm{VS}}(\underline{E}_2) = \frac{1}{2}\frac{\mathrm{d}}{\mathrm{d}t}\Big(\rho\Big\|\dot{\underline{E}}_2\Big\|^2 + \varepsilon^{-2}\,\hat{\kappa}\|\mathrm{div}\,\underline{E}_2\|^2\Big) + \varepsilon^{-1}\,\hat{\zeta}\Big\|\mathrm{div}\,\dot{\underline{E}}_2\Big\|^2 \\
&\leq \varepsilon\Big(\varepsilon\,\rho\big\|\partial_t^2\underline{Y}_2\big\| + \rho\|\partial_t\partial_\tau\underline{Y}_2\|\Big)\Big\|\dot{\underline{E}}_2\Big\| + \varepsilon\,\hat{\zeta}\|\partial_t\mathrm{div}\,\underline{Y}_2\|\,\Big\|\mathrm{div}\dot{\underline{E}}_2\Big\| + 2\,\varepsilon^2\mu\int_\Omega \underline{\underline{\varepsilon}}(\underline{Y}_2) : \underline{\underline{\varepsilon}}(\dot{\underline{E}}_2)\,\mathrm{d}\Omega \\
&\leq \varepsilon^2\,A\sqrt{\mathcal{E}^{tot}(\underline{E}_2)} + \varepsilon^2\,A\sqrt{\varepsilon\,\mathcal{E}^{\mathrm{VS}}(\underline{E}_2)} + 2\,\varepsilon^2\mu\int_\Omega \underline{\underline{\varepsilon}}(\underline{Y}_2) : \underline{\underline{\varepsilon}}(\dot{\underline{E}}_2)\,\mathrm{d}\Omega \\
&\leq \varepsilon^2\,A\sqrt{\mathcal{E}^{tot}(\underline{E}_2)} + \frac{1}{2}\varepsilon^4\,A^2 + \frac{1}{2}\varepsilon\,\mathcal{E}^{\mathrm{VS}}(\underline{E}_2) + 2\,\varepsilon^2\mu\int_\Omega \underline{\underline{\varepsilon}}(\underline{Y}_2) : \underline{\underline{\varepsilon}}(\dot{\underline{E}}_2)\,\mathrm{d}\Omega.
\end{aligned} \tag{3.30}$$

Then, we integrate Eq. (3.30) with respect to time. As previously, we have that

$$\begin{aligned}
\int_0^t\int_\Omega \underline{\underline{\varepsilon}}\big(\underline{Y}_2(s)\big) : \underline{\underline{\varepsilon}}\big(\dot{\underline{E}}_2(s)\big)\,\mathrm{d}\Omega\,\mathrm{d}s &= \sum_{i,k=1}^{3}\int_\Omega \varepsilon_{ik}\big(\underline{Y}_2(t)\big)\varepsilon_{ik}\big(\underline{E}_2(t)\big)\,\mathrm{d}\Omega \\
&\quad - \int_0^t \sum_{i,k=1}^{3}\left(\int_\Omega \varepsilon_{ik}\big(\underline{y}_2(s)\big)\varepsilon_{ik}\big(\underline{E}_2(s)\big)\,\mathrm{d}\Omega\right)\mathrm{d}s.
\end{aligned}$$

Now, due to Eq. (3.29) and the regularity assumptions on $\underline{y}_2$, we can assume that there exists $A > 0$ such that for all $s \in [0,T]$

$$\max_{i,k}\big\|\varepsilon_{ik}\big(\underline{Y}_2(s)\big)\big\|_0 \leq \varepsilon\,A,$$

then, similarly to Eq. (3.28), we deduce

$$\begin{aligned}
\int_0^t\int_\Omega \underline{\underline{\varepsilon}}\big(\underline{Y}_2(s)\big) : \underline{\underline{\varepsilon}}\big(\dot{\underline{E}}_2(s)\big)\,\mathrm{d}\Omega\,\mathrm{d}s &\leq \varepsilon\,A\sqrt{\mathcal{E}^{tot}\big(\underline{E}_2(t)\big)} + A\int_0^t\sqrt{\mathcal{E}^{tot}\big(\underline{E}_2(s)\big)}\,\mathrm{d}s. \\
&\leq \frac{1}{2}\varepsilon^2\,A^2 + \frac{1}{2}\mathcal{E}^{tot}\big(\underline{E}_2(t)\big) + A\int_0^t\sqrt{\mathcal{E}^{tot}\big(\underline{E}_2(s)\big)}\,\mathrm{d}s.
\end{aligned} \tag{3.31}$$

At last, we define the energy $\tilde{\mathcal{E}}^{tot}\big(\underline{E}_2(t)\big)$:

$$\tilde{\mathcal{E}}^{tot}\big(\underline{E}_2(t)\big) \coloneqq \mathcal{E}^{tot}\big(\underline{E}_2(t)\big) + \int_0^t \mathcal{E}^{\mathrm{VS}}\big(\underline{E}_2(s)\big)\,\mathrm{d}s$$

and using Eq. (3.31) we can derive, similarly to the previous case, that

$$\tilde{\mathcal{E}}^{tot}\big(\underline{E}_2(t)\big) \leq \varepsilon^4\,C + \varepsilon^2\,C\int_0^t\sqrt{\mathcal{E}^{tot}\big(\underline{e}_2(s)\big)}\,\mathrm{d}s.$$

Again, using the Grönwall lemma, we can assert that

$$\tilde{\mathcal{E}}^{tot}\big(\underline{E}_2(t)\big) \leq C\,\varepsilon^4.$$

Therefore, there exists $C > 0$ s.t.

$$\varepsilon\sup_{t\in[0,T]}\Big(\|\underline{e}_2(t)\|_0^2 + \varepsilon^{-2}\|\mathrm{div}\,\underline{E}_2(t)\|_0\Big) + \int_0^T\int_\Omega |\mathrm{div}\,\underline{e}_2(t)|^2\,\mathrm{d}\Omega\,\mathrm{d}t \leq \varepsilon^5\,C. \tag{3.32}$$

Eq. (3.32) implies that

$$\sup_{t\in[0,T]}\|\underline{e}_2(t)\|_0 \leq \varepsilon^2\,C.$$

Since we defined $\underline{e}_2(t) = \underline{y}_\varepsilon(t) - \varepsilon^2\underline{y}_2(t)$, we directly obtain the desired results using (3.32). □

3.4.2 Approximation property of the corrector of order k

In what follows, we formulate an estimate for the error associated with the approximation of the solution $\underline{y}_\varepsilon$ with the first k correctors.

Proposition 3.4. *Let $k > 2$, and let $\underline{y}_i$ regular enough, for all $i \leq k$. Then, there exists a strictly positive constant C such that*

$$\boxed{\forall t \in [0,T], \quad \left\| \underline{y}_\varepsilon(t) - \sum_{i=2}^{k-2} \varepsilon^i \, \underline{y}_i\Big(t, \frac{t}{\varepsilon}\Big) \right\|_0 \leq \varepsilon^{k-1}.}$$

Proof. We first define

$$e_k \equiv e_k(t) = \underline{y}_\varepsilon(t) - \sum_{i=2}^{k} \varepsilon^i \, \underline{y}_i\Big(t, \frac{t}{\varepsilon}\Big).$$

We now inject $y_\varepsilon = e_k$ in Eq. (3.4). Then, using Eq. (3.4) and Eq. (3.24), for $i \in \{1, 2, .., k-2\}$, we obtain, for $\underline{w} = \underline{\dot{e}}_k$,

$$\begin{aligned}
&\int_\Omega \rho \, \underline{\ddot{e}}_k(\underline{x}, t) \cdot \underline{w}(\underline{x}) \, \mathrm{d}\Omega + \varepsilon^{-2} \hat{\kappa} \int_\Omega \operatorname{div} \underline{e}_k(\underline{x}, t) \operatorname{div} \underline{w}(\underline{x}) \, \mathrm{d}\Omega \\
&\quad + 2\,\mu \int_\Omega \underline{\underline{\varepsilon}}\big(\underline{y}(\underline{x}, t)\big) : \underline{\underline{\varepsilon}}\big(\underline{w}(\underline{x})\big) \, \mathrm{d}\Omega + \varepsilon^{-1} \hat{\zeta} \int_\Omega \operatorname{div} \underline{\dot{e}}_k(\underline{x}, t) \operatorname{div} \underline{w}(\underline{x}) \, \mathrm{d}\Omega = \\
&\varepsilon^k \int_\Omega \rho \, \partial_t^2 \underline{y}_k \cdot \underline{\dot{e}}_k \, \mathrm{d}\Omega + 2\varepsilon^k \, \mu \int_\Omega \underline{\underline{\varepsilon}}(\underline{y}_k) : \underline{\underline{\varepsilon}}(\underline{\dot{e}}_k) \, \mathrm{d}\Omega + \varepsilon^{k-1} \int_\Omega \rho \, (\partial_t^2 \underline{y}_{k-1} + 2\,\partial_t \partial_\tau \underline{y}_k) \cdot \underline{\dot{e}}_k \, \mathrm{d}\Omega \\
&\quad + \varepsilon^{k-1} \int_\Omega \hat{\zeta} \, \partial_t \operatorname{div} \underline{y}_{k-1} \operatorname{div} \underline{\dot{e}}_{k-1} \, \mathrm{d}\Omega + 2\varepsilon^{k-1} \mu \int_\Omega \underline{\underline{\varepsilon}}(\underline{y}_k) : \underline{\underline{\varepsilon}}(\underline{\dot{e}}_k) \, \mathrm{d}\Omega.
\end{aligned}$$

Therefore, we obtain

$$\begin{aligned}
\frac{\mathrm{d}}{\mathrm{d}\,t} \mathcal{E}^{tot}(\underline{e}_k) + \mathcal{E}^{\mathrm{VS}}(\underline{e}_k) &\leq \varepsilon^{k-1} \Big(\varepsilon \, \rho \Big\| \partial_t^2 \underline{y}_k \Big\|_0 + 2\,\rho \Big\| \partial_t \partial_\tau \underline{y}_k \Big\|_0 + \rho \Big\| \partial_t^2 \underline{y}_{k-1} \Big\|_0 \Big) \| \underline{\dot{e}}_k \|_0 \\
&\quad + \varepsilon^{k-1} \, \hat{\zeta} \Big\| \partial_t \operatorname{div} \underline{y}_k \Big\|_0 \, \| \operatorname{div} \underline{\dot{e}}_k \|_0 + 2\varepsilon^k \mu \int_\Omega \underline{\underline{\varepsilon}}(\underline{y}_k) : \underline{\underline{\varepsilon}}(\underline{\dot{e}}_k) \, \mathrm{d}\Omega + 2\varepsilon^{k-1} \mu \int_\Omega \underline{\underline{\varepsilon}}(\underline{y}_{k-1}) : \underline{\underline{\varepsilon}}(\underline{\dot{e}}_k) \, \mathrm{d}\Omega.
\end{aligned}$$

Due to the regularity assumption on the correctors $\underline{y}_k$ and $\underline{y}_{k-1}$, we can assume that there exists a constant $A > 0$ such that

$$\varepsilon \, \rho \Big\| \partial_t^2 \underline{y}_k \Big\|_0 + 2\,\rho \Big\| \partial_t \partial_\tau \underline{y}_k \Big\|_0 + \rho \Big\| \partial_t^2 \underline{y}_{k-1} \Big\|_0 + \hat{\zeta} \Big\| \partial_t \operatorname{div} \underline{y}_k \Big\|_0 \leq A.$$

As a consequence, we derive the following estimation on the energy:

$$\begin{aligned}
\frac{\mathrm{d}}{\mathrm{d}t} \mathcal{E}^{tot}(\underline{e}_k) + \mathcal{E}^{\mathrm{VS}}(\underline{e}_k) &\leq \varepsilon^{k-1} \, A \sqrt{\mathcal{E}^{tot}(\underline{e}_K)} + \varepsilon^{k-1} \, A \sqrt{\varepsilon \, \mathcal{E}^{\mathrm{VS}}(\underline{e}_k)} \\
&\quad + 2\,\varepsilon^k \mu \int_\Omega \underline{\underline{\varepsilon}}(\underline{y}_k) : \underline{\underline{\varepsilon}}(\underline{\dot{e}}_k) \, \mathrm{d}\Omega + 2\,\varepsilon^{k-1} \mu \int_\Omega \underline{\underline{\varepsilon}}(\underline{y}_{k-1}) : \underline{\underline{\varepsilon}}(\underline{\dot{e}}_k) \, \mathrm{d}\Omega.
\end{aligned} \tag{3.33}$$

Observe that, as usual, we can estimate by the Young inequality

$$\varepsilon^{k-1} \, A \sqrt{\varepsilon \, \mathcal{E}^{\mathrm{VS}}(\underline{e}_k)} \leq \frac{1}{2} \varepsilon^{2(k-1)} \, A^2 + \frac{1}{2} \varepsilon \, \mathcal{E}^{\mathrm{VS}}(\underline{e}_k).$$

Note that the term $2\varepsilon^{k-1}\mu \int_\Omega \underline{\underline{\varepsilon}}(\underline{y}_{k-1}) : \underline{\underline{\varepsilon}}(\underline{\dot{e}}_k)\,\mathrm{d}\Omega$ are zero for $k \leq 2$.
As usual, we now integrate Eq. (3.33) in time. Note that, due to the regularity of the correctors $\underline{y}_k(s)$ and $\underline{y}_{k-1}(s)$, we can also assume that there exists $A > 0$ such that

$$\begin{aligned}
&\max_{i,k} \left\| \varepsilon_{ik}(\underline{y}_k(s)) \right\|_0 \leq A,\\
&\max_{i,k} \left\| \varepsilon_{ik}(\underline{\dot{y}}_k(s)) \right\|_0 \leq \max_{i,k} \left(\varepsilon^{-1} \left\| \partial_\tau \varepsilon_{ik}(\underline{y}_k(s)) \right\|_0 + \left\| \partial_t \varepsilon_{ik}(\underline{y}_k(s)) \right\|_0 \right) \leq \varepsilon^{-1} A,\\
&\max_{i,k} \left\| \varepsilon_{ik}(\underline{\dot{y}}_{k-1}(s)) \right\|_0 \leq \max_{i,k} \left(\varepsilon^{-1} \left\| \partial_\tau \varepsilon_{ik}(\underline{y}_{k-1}(s)) \right\|_0 + \left\| \partial_t \varepsilon_{ik}(\underline{y}_{k-1}(s)) \right\|_0 \right) \leq \varepsilon^{-1} A,
\end{aligned}$$

Hence, we retrieve

$$\begin{aligned}
&\int_0^t \int_\Omega \underline{\underline{\varepsilon}}\big(\underline{y}_k(s)\big) : \underline{\underline{\varepsilon}}\big(\underline{\dot{e}}_k(s)\big)\,\mathrm{d}\Omega\,\mathrm{d}s + \int_0^t \int_\Omega \underline{\underline{\varepsilon}}\big(\underline{y}_{k-1}(s)\big) : \underline{\underline{\varepsilon}}\big(\underline{\dot{e}}_k(s)\big)\,\mathrm{d}\Omega\,\mathrm{d}s\\
&\quad \leq A\sqrt{\mathcal{E}^{tot}\big(\underline{e}_k(t)\big)} + \varepsilon^{-1} A \int_0^t \sqrt{\mathcal{E}^{tot}\big(\underline{e}_k(s)\big)}\,\mathrm{d}s \qquad (3.34)\\
&\quad \leq \frac{1}{2}A^2 + \frac{1}{2}\mathcal{E}^{tot}\big(\underline{e}_k(t)\big) + \varepsilon^{-1} A \int_0^t \sqrt{\mathcal{E}^{tot}\big(\underline{e}_k(s)\big)}\,\mathrm{d}s.
\end{aligned}$$

Hence, we can estimate

$$\mathcal{E}^{tot}(\underline{e}_k)(t) + \int_0^t \mathcal{E}^{\mathrm{VS}}(\underline{e}_k(s))\,\mathrm{d}s \leq \varepsilon^{k-1}\, C + \varepsilon^{k-2} C \int_0^t \sqrt{\mathcal{E}^{tot}\big(\underline{e}_k(s)\big)}\,\mathrm{d}s.$$

If we define

$$\tilde{\mathcal{E}}^{tot}\big(\underline{e}_k(t)\big) := \mathcal{E}^{tot}\big(\underline{e}_k(t)\big) + \int_0^t \mathcal{E}^{\mathrm{VS}}(\underline{e}_k(s))\,\mathrm{d}s,$$

then we obtain, using Eqs. (3.33) and (3.34), and by the Grönwall inequality,

$$\tilde{\mathcal{E}}^{tot}\big(\underline{e}_k(t)\big) \leq \varepsilon^{2(k-2)} C,$$

since $\mathcal{E}^{tot}(\underline{e}_k(0)) = 0$. Consequently, there exists $C > 0$ satisfying

$$\varepsilon \sup_{t\in[0,T]} \left(\|\underline{\dot{e}}_k(t)\|_0^2 + \varepsilon^{-2} \|\mathrm{div}\, \underline{e}_k(t)\|_0^2 \right) + \int_0^T \int_\Omega |\mathrm{div}\, \underline{\dot{e}}_k(t)|^2\,\mathrm{d}\Omega\,\mathrm{d}t \leq \varepsilon^{2k-3}\, C.$$

Analogously, if we define $\underline{E}_k \equiv \underline{E}_k(t) = \int_0^t \underline{e}_k(s)\,\mathrm{d}s$, we obtain

$$\begin{aligned}
\frac{\mathrm{d}}{\mathrm{d}t}\mathcal{E}^{tot}(\underline{E}_k) + \mathcal{E}^{\mathrm{VS}}(\underline{E}_k) = \varepsilon^{k-1} &\Big(\varepsilon\,\rho \left\| \partial_t^2 \underline{Y}_k \right\|_0 + 2\,\rho \|\partial_t \partial_\tau \underline{Y}_k\|_0 + \rho \left\| \partial_t^2 \underline{Y}_{k-1} \right\|_0 \Big) \left\| \underline{\dot{E}}_k \right\|_0\\
&+ \varepsilon^{k-1}\,\hat{\zeta} \|\partial_t \mathrm{div}\, \underline{Y}_k\|_0 \left\| \mathrm{div}\, \underline{\dot{E}}_k \right\|_0 + 2\varepsilon^k \mu \int_\Omega \underline{\underline{\varepsilon}}(\underline{Y}_k) : \underline{\underline{\varepsilon}}(\underline{\dot{E}}_k)\,\mathrm{d}\Omega\\
&+ 2\varepsilon^{k-1}\mu \int_\Omega \underline{\underline{\varepsilon}}(\underline{Y}_{k-1}) : \underline{\underline{\varepsilon}}(\underline{\dot{e}}_k)\,\mathrm{d}\Omega.
\end{aligned}$$

As a consequence, we derive the following estimation on the energy:

$$\begin{aligned}\frac{\mathrm{d}}{\mathrm{d}t}\mathcal{E}^{tot}(\underline{E}_k) + \mathcal{E}^{\mathrm{VS}}(\underline{E}_k) \leq \varepsilon^k\, A\sqrt{\mathcal{E}^{tot}(\underline{E}_K)} + \varepsilon^{k-1}\, A\,\sqrt{\varepsilon\,\mathcal{E}^{\mathrm{VS}}(\underline{E}_k)} \\ + 2\,\varepsilon^k\mu\int_\Omega \underline{\underline{\varepsilon}}(\underline{Y}_k) : \underline{\underline{\varepsilon}}(\dot{\underline{E}}_k)\,\mathrm{d}\Omega + 2\,\varepsilon^{k-1}\mu\int_\Omega \underline{\underline{\varepsilon}}(\underline{Y}_{k-1}) : \underline{\underline{\varepsilon}}(\dot{\underline{E}}_k)\,\mathrm{d}\Omega.\end{aligned} \tag{3.35}$$

Once again, we integrate Eq. (3.35) in time. We can assume that there exists $A > 0$ such that

$$\max_{i,k} \|\varepsilon_{ik}(\underline{Y}_k(s))\|_0 + \max_{i,k} \left\|\varepsilon_{ik}(\underline{Y}_{k-1}(s))\right\|_0 \leq \varepsilon\, A.$$

Hence, we have the following estimations:

$$\begin{aligned}\int_0^t\int_\Omega \underline{\underline{\varepsilon}}(\underline{Y}_k(s)) : \underline{\underline{\varepsilon}}(\dot{\underline{E}}_k(s))\,\mathrm{d}\Omega\,\mathrm{d}s + \int_0^t\int_\Omega \underline{\underline{\varepsilon}}(\underline{Y}_{k-1}(s)) : \underline{\underline{\varepsilon}}(\dot{\underline{E}}_k(s))\,\mathrm{d}\Omega\,\mathrm{d}s \\ \leq \varepsilon\, A\,\sqrt{\mathcal{E}^{tot}\big(\underline{E}_k(t)\big)} + A\int_0^t \sqrt{\mathcal{E}^{tot}\big(\underline{E}_k(s)\big)}\,\mathrm{d}s,\end{aligned} \tag{3.36}$$

At last, if we define

$$\tilde{\mathcal{E}}^{tot}\big(\underline{e}_k(t)\big) \coloneqq \mathcal{E}^{tot}\big(\underline{e}_k(t)\big) + \int_0^t \mathcal{E}^{\mathrm{VS}}(\underline{E}_k(s))\,\mathrm{d}s$$

using Eqs. (3.35) and (3.36), we retrieve

$$\tilde{\mathcal{E}}^{tot}\big(\underline{e}_k(t)\big) \leq \varepsilon^{k+1}C + \varepsilon^{k-1}\,C\int_0^t \sqrt{\mathcal{E}^{tot}\big(\underline{E}_k(s)\big)}\,\mathrm{d}s.$$

Hence, using again the Grönwall lemma, we can assert that

$$\tilde{\mathcal{E}}^{tot}\big(\underline{E}_k(t)\big) \leq C\,\varepsilon^{2(k-1)}.$$

Therefore, there exists $C > 0$ s.t.

$$\varepsilon \sup_{t\in[0,T]}\left(\|\underline{e}_k(t)\|_0^2 + \varepsilon^{-2}\|\mathrm{div}\,\underline{E}_k(t)\|_0^2\right) + \int_0^T\int_\Omega |\mathrm{div}\,\underline{e}_k(t)|^2\,\mathrm{d}\Omega\,\mathrm{d}t \leq \varepsilon^{2k-1}\,C. \tag{3.37}$$

Since we defined $\underline{e}_k(t) = \underline{y}_\varepsilon(t) - \sum_{i=2}^{k}\varepsilon^i\,\underline{y}_i(t)$, with $k > 2$, Eq. (3.37) implies that

$$\forall t \geq 0, \quad \left\|\underline{y}_\varepsilon(t) - \sum_{i=2}^{k}\varepsilon^i\,\underline{y}_i(t)\right\|_0 \leq \varepsilon^{k-1}\,C \implies \left\|\underline{y}_\varepsilon(t) - \sum_{i=2}^{k-2}\varepsilon^i\,\underline{y}_i(t)\right\|_0 \leq \varepsilon^{k-1},$$

thus concluding the proof. □

Remark Note that the regularity assumption on the corrector terms, that is necessary to retrieve Proposition 3.4, is valid under some regularity assumptions on the source term. However, in practice, in ARF-based Shear Wave Elastography, there are some short intervals (of the order of some µs) in which the source term is singular, namely at the very beginning of the pulse, that lasts about $100-500$ µs, and right before its end, as illustrated in Figure 3.1. As a consequence, there is an open question concerning the best procedure to adopt. One solution could be to simulate the solution in these short time intervals, or to approximate the source term by a continuous function.

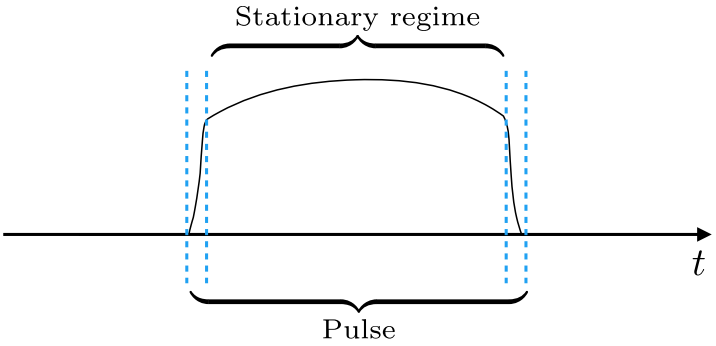

Figure 3.1 – Graphical illustration of the envelope of the ultrasound pulse in ARF-based Shear Wave Elastography.

Bibliography

Correia, M., Podetti, I., Villemain, O., Baranger, J., Tanter, M. and Pernot, M. [2017], 'Non-invasive myocardial shear wave elastography device for clinical applications in cardiology', *IRBM* **38**(6), 357–362.

Ostrovsky, L., Sutin, A., Il'inskii, Y., Rudenko, O. and Sarvazyan, A. [2007], 'Radiation force and shear motions in inhomogeneous media', *The Journal of the Acoustical Society of America* **121**(3), 1324–1331.

Pernot, M., Lee, W.-N., Bel, A., Mateo, P., Couade, M., Tanter, M., Crozatier, B. and Messas, E. [2016], 'Shear wave imaging of passive diastolic myocardial stiffness: stunned versus infarcted myocardium', *JACC: Cardiovascular Imaging* **9**(9), 1023–1030.

Sarvazyan, A. P., Rudenko, O. V. and Nyborg, W. L. [2010], 'Biomedical applications of radiation force of ultrasound: historical roots and physical basis', *Ultrasound in medicine & biology* **36**(9), 1379–1394.

Part II

Numerical approximation

CHAPTER 4

Numerical schemes for wave propagation in incompressible media: a conservative penalisation strategy for semi-implicit time discretisation

Summary

The principal aim of this chapter is to provide an adapted numerical scheme for elastic wave propagation in incompressible solids. High-order finite elements are used for space discretisation and an implicit/explicit second order, energy-preserving scheme is employed for time discretisation. The time step restriction only depends on the shear wave velocity and at each iteration a Poisson problem is solved to account for the incompressibility constraint, that is imposed by penalisation techniques. *This chapter is in the form of a paper – coauthored by F. Caforio and S. Imperiale – already accepted for publication in an international journal.*

Contents

4.1 Introduction

Since large applications in computational mechanics concern nearly and pure incompressible elasticity (living tissues, biomaterials), a great effort has been made in the last forty years to provide accurate Finite Element Method (FEM) formulations for the approximation of elasticity in incompressible solids. However, the majority of the works proposed in the literature only deals with static computations. The main contributions to date can be mainly divided into two categories: pure displacement methods and mixed methods.
On the one hand, displacement-based FEM can provide accurate solutions of quasi or pure incompressible elasticity problems; nonetheless, the space resolution necessary to provide an accurate solution is far greater than the one required for a compressible material [Bathe, 2006; Sussman and Bathe, 1987]. Indeed, these methods can suffer of undesirable limitations, such as ill-conditioning of the stiffness matrix, spurious or incorrect pressures and numerical locking (severe stiffening near the incompressible limit) [Sussman and Bathe, 1987], especially if low-order shape functions are adopted, due to the enforcement of the incompressibility constraint – i.e. the requirement that the displacement field is divergence-free. Locking is due to the fact that, in case of incompressible materials, volumetric strains approach zero, while the pressure field is of the order of the boundary traction, therefore it cannot be computed from strains, but it must be calculated directly from the equilibrium equations [Sussman and Bathe, 1987; Chapelle and Bathe, 1993]. Several methods have been proposed to improve accuracy of displacement-based methods. Among them, we cite the reduced/selective integration method proposed in [Malkus and Hughes, 1978], the B-bar method [Hughes, 1980] and the F-bar method [Neto et al., 2005]. These methods circumvent volumetric locking by reducing the number of discrete incompressibility constraints enforced at the quadrature points [Hughes, 2012]. We also cite a method adapted to nearly-incompressible materials with volumetric energy penalty function in the framework of the continuum-based absolute nodal coordinate formulation (ANCF) [Orzechowski and Frączek, 2015].
On the other hand, mixed finite element methods [Brezzi and Fortin, 2012] have proven effective and even necessary to obtain accurate results in the resolution of incompressible fluid flows and incompressible elasticity. In these methods, the constrained problem is rewritten in form of an unconstrained saddle-point problem, due to the introduction of a second variable (namely, the pressure). However, not all mixed methods are stable. In fact, the convergence properties of this formulation are governed by stability considerations, involving ellipticity requirements and the famous Ladyzenskaya - Babŭska - Brezzi (LBB) inf-sup condition [Brezzi and Bathe, 1990; Brezzi and Falk, 1991]. For example, equal-order interpolation both for displacement and pressure field does not satisfy the LBB condition for classical mixed FEM [Brezzi and Fortin, 2012]. If this stability condition is not satisfied, severe unphysical oscillations in the pressure field can appear, named "spurious pressure modes". Stabilised methods have been proposed to overcome the limitations of classical mixed FE formulations in the field of incompressible fluid dynamics (see [Franca and Frey, 1992; Tezduyar, 1991; Boffi et al., 2013] and references therein for throughout reviews on the subject). Brezzi and collaborators [Brezzi and Pitkäranta, 1984] proposed to extend the equation accounting for incompressibility in Stokes flows by adding a Laplacian of the pressure field. Other methods are based on the addition of artificial high-order differential terms to the discrete continuity equation, in order to let the formulation satisfy the LBB condition (for more details, see [Quarteroni and Valli, 1994]). We cite for example the Streamline Upwind Petrov-Galerkin method [Brooks and Hughes, 1982; Hughes et al., 1986; Franca et al., 1988]. Similar stabilised methods have been recently extended to the context of linear elasticity [Klaas et al., 1999; Maniatty et al., 2002; Chiumenti et al., 2002;

Masud and Truster, 2013; Zienkiewicz et al., 2000].
All the aforementioned methods can be straightforwardly extended to the discretisation of dynamic equations using implicit time discretisation (e.g. Implicit Euler scheme or implicit Newmark schemes). However, at each time step, the resolution of the resulting linear system is required for the computation of the velocity field (or most often the displacement field in elasticity). We highlight that, in linear elasticity, this could be done in practice by performing a factorisation of the matrices to invert, since they are constant in time. However, for large scale problems, it is not possible to store any factorisation of the matrices and it is even difficult to store preconditioners. A popular approach to increase the efficiency of dynamic solvers was first proposed in computational fluid dynamics in the late 1960s [Chorin, 1968, 1969; Temam, 1968, 2001], and it is called fractional-step projection. This family of methods aims at accurately solving the equation governing viscous incompressible fluids by performing a time-discretisation in which viscosity and incompressibility are treated in two separate steps. In more detail, the first half-step (Burgers step) corresponds to an elliptic Boundary Value Problem (BVP) for an intermediate velocity, accounting for viscosity diffusion and advection. The second half-step (projection step) represents an inviscid problem where the end-of-step, divergence-free velocity is computed, along with pressure distribution. This step essentially consists in solving a Poisson problem. In this way, at each time step two decoupled elliptic equations are solved, and this is very advantageous for large scale simulations [Guermond and Quartapelle, 1998*b*,*a*; Guermond et al., 2006].
Less effort has been made to develop efficient methods for the treatment of the incompressibility constraint in elastodynamics. Since the underlying physics is wave propagation, fully explicit methods seem to be good candidates to obtain efficient schemes (this is possible for nearly-incompressible media). We cite in this context a recent method for quasi-incompressible elastodynamics [Scovazzi et al., 2016] with linear finite elements, extended in [Rossi et al., 2016] to the purely incompressible case. Furthermore, a recent velocity/stress formulation for the simulation of linear elastodynamics in nearly-incompressible solids with weakly enforced boundary conditions was proposed by Scovazzi and collaborators [Scovazzi et al., 2017]. However, the stability constraint (CFL condition) is drastically limited by the enforcement of incompressibility. In this regard, the efficiency of the fractional-step projection algorithm mentioned above, along with the similarities with viscous incompressible fluids, suggests the possibility to adopt the main ideas of this method to design an efficient scheme for incompressible elastodynamics.
A first method that integrates a fractional time-step method for Lagrangian formulations of elastodynamics problems has been proposed by Lahiri and collaborators [Lahiri et al., 2005]. In this paper, the authors use variational integrators that take advantage of the Hamilton variational principle to construct a discrete approximation of the integral of the Lagrangian over a given interval, and they adopt linear finite element discretisation in space.
We have developed a numerical scheme that carefully takes into account the intrinsic properties of the wave equation. Namely, we construct a conservative time discretisation, and treat implicitly only the terms corresponding to "informations" travelling at infinite velocity (i.e. the incompressibility constraint) by solving a Poisson problem. The fully discrete scheme that we propose to efficiently solve the incompressible elastodynamic problem is

$$\begin{cases} \dfrac{\underline{\tilde{y}}_{\alpha,h}^{n+1} - 2\,\underline{\tilde{y}}_{\alpha,h}^{n} + \underline{\tilde{y}}_{\alpha,h}^{n-1}}{\Delta t^2} + A_h\,\underline{\tilde{y}}_{\alpha,h}^{n} + B_h^T\,\tilde{p}_{\alpha,h}^{n} = \underline{f}_h^n, \\ B_h\,\underline{\tilde{y}}_{\alpha,h}^{n} = \alpha\,\Delta t^2\,C_h\,C_h^T\,\tilde{p}_{\alpha,h}^{n}, \end{cases} \tag{4.1}$$

where A_h denotes a stiffness operator (independent of the compressibility parameters), B_h^T and B_h correspond to discrete gradient and divergence operators, and $C_h C_h^T$ represents a discrete laplacian operator. The coefficient α corresponds to a penalisation parameter and $(\underline{\tilde{y}}^n_{\alpha,h}, \tilde{p}^n_{\alpha,h}, \underline{f}^n_h)$ denote respectively the displacement field, the pressure and the source term.
Therefore, if effective methods for explicit time-discretisation are used, our algorithm requires at each time step the resolution of a scalar Poisson problem (that can be done by several, efficient algorithms) and few matrix-vector multiplications for the explicit methods.
Note that the stability condition for scheme (4.1) reads

$$\Delta t^2 \leq 4 \left\| A_h \right\|^{-1} \frac{4\alpha - 1}{4\alpha}, \quad \alpha > 1/4.$$

for some operator norm $\| \cdot \|$ that we define later. Contrarily to the standard results one could expect (i.e. $\Delta t^2 \leq 4 \left\| A_h \right\|^{-1}$, see [Joly, 2008]), the stability condition is slightly more constraining due to the factor $(4\alpha - 1)/4\alpha$.

Our approach is a strategy to approximate elastic wave propagation in quasi-incompressible media. In order to do that, we introduce a first good approximation: the pure incompressible formulation. Then, we construct a penalised formulation to approximate the pure incompressible problem. Our procedure is justified by arguments of stability, computational cost and numerical convergence of the resulting schemes. Finally, the work we propose is closely related to the Selective Mass Scaling Method (SMS) developed in Ye et al. [2017] for wave propagation in quasi-incompressible materials. In this method, the mass matrix is modified: artificial mass is added, hence obtaining very good stability properties at the cost of computing a mass matrix that cannot be lumped anymore. The problem is then implicit for the displacement field, and thus it not possible to use fast solvers (like FFT solvers) for the inversion of a scalar Poisson problem.
The chapter is organised as follows. In Section 4.2 we provide two standard formulations of the continuous elastodynamic problem for quasi-incompressible and pure incompressible media along with a novel formulation for the treatment of incompressibility by penalisation. Furthermore, we derive the variational formulation associated with each problem. Section 4.3 deals with the abstract framework for space discretisation of the incompressible elastodynamics equation by Spectral Element Method. In Section 4.4 we provide the time discretisations for each formulation by finite difference. Then, a stability analysis based on energy considerations is performed for each scheme in 4.4.2 and pros and cons are discussed. Numerical results, including convergence curves to the solution of the incompressible elastodynamics equations for different choices of materials, are shown in Section 4.5. Finally, a three-dimensional illustration in a more realistic test case for elastography imaging is shown in Section 4.7.

4.2 Continuous framework

4.2.1 The equation of elastodynamics

Given a domain $\Omega \subset \mathbb{R}^d$ smooth enough, with $d = 2$ or $d = 3$, we introduce the following notations to define Hilbert spaces for the elastic displacements

$$\mathcal{H} \coloneqq \left\{ \underline{v} \in L^2(\Omega)^d \right\}, \quad \mathcal{X} \coloneqq H_0^1(\Omega)^d, \quad \mathcal{X}' = H^{-1}(\Omega)^d.$$

For the sake of simplicity, we consider homogenous Dirichlet condition on the boundary of the propagation domain. We also need to consider divergence-free displacements. Hence, we introduce the following subspace of $\mathcal{X}$

$$\mathcal{V} \coloneqq \{\underline{v} \in \mathcal{X} \mid \operatorname{div} \underline{v} = 0\}.$$

Pressure is a variable of interest, and is sought in the spaces

$$\mathcal{L} \coloneqq L^2_0(\Omega) = \left\{ q \in L^2(\Omega) \mid \int_\Omega q = 0 \right\}, \quad \mathcal{M} = \{q \in H^1(\Omega) \mid q \in \mathcal{L}\}.$$

As usual, we identify $\mathcal{L}$ and $\mathcal{H}$ with their dual in what follows. Moreover, for the sake of conciseness, we define, given a function space A on Ω,

$$C^k(A) \coloneqq C^k([0,T]; A), \quad k \in \{0, 1, 2, ..\},$$

where $T > 0$ is a given final time of observation. Furthermore, we introduce $\Omega_T \coloneqq [0,T] \times \Omega$. Our aim is to analyse the propagation of elastic waves in heterogenous, anisotropic, incompressible solids and we consider as a reference model the following partial differential equation (PDE) system:
For $\underline{f}$ given and sufficiently regular, find $\underline{y}_\lambda \in C^2(\mathcal{H}) \cap C^1(\mathcal{X})$ such that

$$\begin{cases} \rho\, \partial_t^2 \underline{y}_\lambda - \underline{\operatorname{div}} \left(\underline{\underline{\mathbf{C}}} \underline{\varepsilon}(\underline{y}_\lambda) \right) - \lambda\, \underline{\nabla} \operatorname{div} \underline{y}_\lambda = \underline{f} & \text{in } \Omega_T, \\ \underline{y}_\lambda(t=0) = \underline{0}, \quad \partial_t \underline{y}_\lambda(t=0) = \underline{0} & \text{in } \Omega, \end{cases} \tag{QI}$$

with $\lambda \in \mathbb{R}^+$ the bulk modulus, that is assumed to be large, due to nearly-incompressibility, $\rho(\underline{x})$ the strictly positive density of the medium and $\underline{\underline{\mathbf{C}}}(\underline{x})$ the elasticity tensor which is symmetric, coercive and bounded, i.e. there exist two positive scalars c, C such that

$$c \left| \underline{\underline{\varepsilon}} \right|^2 \leq \underline{\underline{\mathbf{C}}}(\underline{x}) \underline{\underline{\varepsilon}} : \underline{\underline{\varepsilon}} \leq C \left| \underline{\underline{\varepsilon}} \right|^2, \quad \forall \underline{\underline{\varepsilon}}. \tag{4.2}$$

4.2.2 Non-dimensionalisation

Since we are going to consider a limit process where the bulk modulus tends to infinity, a first step is to non-dimensionalise our system of equations. To do so, we introduce a typical length scale L of the domain Ω, a typical observation time τ and a shear modulus μ, and we define a non-dimensionalised displacement as follows:

$$\underline{\hat{y}}_{\hat{\lambda}}(t, \underline{x}) \coloneqq L^{-1} \underline{y}_\lambda(\tau\, t, L\, \underline{x}), \quad t \in [0, \widehat{T}], \quad \underline{x} \in \widehat{\Omega},$$

where $\widehat{\Omega}$ is a rescaled domain and $\widehat{T} = T/\tau$ is of the order of unity. Note that t and $\underline{x}$ refer now to non-dimensionalised variables. We also introduce the non-dimensionalised quantities

$$\hat{\rho} = \frac{L^2 \rho}{\tau^2 \mu}, \quad \underline{\underline{\widehat{\mathbf{C}}}} = \mu^{-1}\, \underline{\underline{\mathbf{C}}}, \quad \hat{\lambda} = \frac{\lambda}{\mu}, \quad \underline{\hat{f}} = \frac{L}{\mu} \underline{f}.$$

Then, the equation of elastodynamics can be recast as

$$\begin{cases} \hat{\rho}\, \partial_t^2 \underline{\hat{y}}_{\hat{\lambda}} - \underline{\operatorname{div}} \left(\underline{\underline{\widehat{\mathbf{C}}}} \underline{\varepsilon}(\underline{\hat{y}}_{\hat{\lambda}}) \right) - \hat{\lambda}\, \underline{\nabla} \operatorname{div} \underline{\hat{y}}_{\hat{\lambda}} = \underline{\hat{f}} & \text{in } [0, \widehat{T}] \times \widehat{\Omega}, \\ \underline{\hat{y}}_{\hat{\lambda}}(t=0) = \underline{0}, \quad \partial_t \underline{\hat{y}}_{\hat{\lambda}}(t=0) = \underline{0} & \text{in } \widehat{\Omega}. \end{cases}$$

We also introduce here the pressure field p_λ associated with the displacement field $\underline{y}_\lambda$. Its non-dimensionalised counterpart is given by

$$\hat{p}_{\hat{\lambda}}(t, \underline{x}) \coloneqq \mu^{-1} p_\lambda(\tau\, t, L\, \underline{x}), \quad t \in [0, \widehat{T}], \quad \underline{x} \in \widehat{\Omega}.$$

For the sake of simplicity, we drop the notation $\hat{\cdot}$ throughout the rest of the chapter.

4.2.3 The mixed and penalised formulations

Existence and uniqueness results for problem (QI) are well-known (see [Joly, 2008]). An alternative, equivalent formulation to (QI) is obtained by introducing the scalar function $p_\lambda := \lambda \operatorname{div} \underline{y}_\lambda$. The couple $(\underline{y}_\lambda, p_\lambda) \in C^2(\mathcal{H}) \cap C^1(\mathcal{X}) \times C^0(\mathcal{L})$ satisfies

$$\begin{cases} \rho\, \partial_t^2 \underline{y}_\lambda - \underline{\operatorname{div}}\,(\underline{\underline{\mathbf{C}}}(\underline{x})\underline{\underline{\varepsilon}}(\underline{y}_\lambda)) - \underline{\nabla}\, p_\lambda = \underline{f} & \text{in } \Omega_T, \\ \operatorname{div} \underline{y}_\lambda = \lambda^{-1}\, p_\lambda & \text{in } \Omega_T, \\ \underline{y}_\lambda(t=0) = \underline{0}, \quad \partial_t \underline{y}_\lambda(t=0) = \underline{0} & \text{in } \Omega. \end{cases} \tag{QIM}$$

Since λ is large, it is natural to approximate the solution of (QIM) by the solution obtained at the limit as λ goes to infinity. More precisely, if one defines $(\underline{y}, p)$ and some corrector functions $(\underline{y}_1, p_1)$ and $(\underline{y}_2, p_2)$ such that

$$\underline{y}_\lambda = \underline{y} + \lambda^{-1}\underline{y}_1 + \lambda^{-2}\underline{y}_2 + \cdots, \quad p_\lambda = p + \lambda^{-1} p_1 + \lambda^{-2} p_2 + \cdots,$$

then a standard asymptotic analysis procedure shows that $(\underline{y}, p)$ satisfies a pure incompressible problem. This formulation reads
Find $(\underline{y},\, p) \in C^2(\mathcal{H}) \cap C^1(\mathcal{V}) \times C^0(\mathcal{L})$ such that

$$\begin{cases} \rho\, \partial_t^2 \underline{y} - \underline{\operatorname{div}}\,(\underline{\underline{\mathbf{C}}}(\underline{x})\underline{\underline{\varepsilon}}(\underline{y})) - \underline{\nabla}\, p = \underline{f} & \text{in } \Omega_T, \\ \operatorname{div} \underline{y} = 0 & \text{in } \Omega_T, \\ \underline{y}(t=0) = \underline{0}, \quad \partial_t \underline{y}(t=0) = \underline{0} & \text{in } \Omega. \end{cases} \tag{IM}$$

Observe that the function p in (IM) acts as a Lagrange multiplier to enforce incompressibility. If we assume that (IM) is the standard problem to solve, then Eq. (QIM) can be seen as an approximate penalised formulation of (IM). Existence, uniqueness and regularity results of problem (IM) can also be induced from (QI) by a limit process as $\lambda \to \infty$.
We now introduce another formulation by penalisation of the problem (IM), inspired from existing formulations for the Stokes problem [Boffi et al., 2013]. It reads
Find $(\tilde{\underline{y}}_\alpha, \tilde{p}_\alpha) \in C^2(\mathcal{H}) \cap C^1(\mathcal{X}) \times C^0(\mathcal{M})$ such that

$$\begin{cases} \rho\, \partial_t^2 \tilde{\underline{y}}_\alpha - \underline{\operatorname{div}}\,(\underline{\underline{\mathbf{C}}}(\underline{x})\underline{\underline{\varepsilon}}(\tilde{\underline{y}}_\alpha)) - \underline{\nabla}\, \tilde{p}_\alpha = \underline{f} & \text{in } \Omega_T, \\ \operatorname{div} \tilde{\underline{y}}_\alpha = -\alpha\, \Delta \tilde{p}_\alpha & \text{in } \Omega_T, \\ \tilde{\underline{y}}_\alpha(t=0) = \underline{0}, \quad \partial_t \tilde{\underline{y}}_\alpha(t=0) = \underline{0} & \text{in } \Omega. \end{cases} \tag{QIP}$$

First, note that (QIP) is different from (QIM) due to the introduction of the laplacian operator in the second equation. Furthermore, one can observe that (QIP) differs from the other formulations by several important but subtle aspects. First, the pressure $\tilde{p}_\alpha$ is sought in a more regular space, namely $C^0(\mathcal{M})$, that is mandatory to give an appropriate meaning to the introduced Laplace operator. Second, system (QIP) is not a closed set of equations. Indeed, a boundary condition is required for the second equation for the pressure, that now has a trace (we recall that we use homogeneous Dirichlet conditions on the displacement). A standard choice is to use homogenous Neumann boundary conditions

$$\underline{\nabla}\, \tilde{p}_\alpha \cdot \underline{n} = 0 \quad \text{on } [0,T] \times \partial\Omega. \tag{4.3}$$

Then, using the same arguments as before, i.e., writing

$$\underline{\tilde{y}}_\alpha = \underline{y} + \alpha\,\underline{\tilde{y}}_1 + \alpha^2\,\underline{\tilde{y}}_2 + \cdots, \quad \tilde{p}_\alpha = p + \alpha\,\tilde{p}_1 + \alpha^2\,\tilde{p}_2 + \cdots, \tag{4.4}$$

one can see that $(\underline{\tilde{y}}_\alpha, \tilde{p}_\alpha)$ can be approximated by $(\underline{y}, p)$, solution of the pure incompressible mixed formulation (IM). Reciprocally, $(\underline{\tilde{y}}_\alpha, \tilde{p}_\alpha)$ represents another approximation of the pure incompressible mixed formulation (IM). Moreover, eliminating the unknown $\tilde{p}_\alpha$, it is possible to rewrite (QIP) as

$$\rho\,\partial_t^2 \underline{\tilde{y}}_\alpha - \underline{\mathrm{div}}\left(\underline{\underline{\mathbf{C}}}\underline{\underline{\varepsilon}}(\underline{\tilde{y}}_\alpha)\right) - \alpha^{-1}\underline{\nabla}(-\Delta)^{-1}\mathrm{div}\underline{\tilde{y}}_\alpha = \underline{f}, \tag{4.5}$$

where $\Delta^{-1} : \mathcal{L} \to \mathcal{M}$ stands for the inverse Laplace operator equipped with a homogeneous Neumann boundary condition. It is possible to prove that the operator $-\underline{\mathrm{div}}\left(\underline{\underline{\mathbf{C}}}\underline{\underline{\varepsilon}}(\cdot)\right) - \alpha^{-1}\underline{\nabla}(-\Delta)^{-1}\mathrm{div}(\cdot)$ defines a self-adjoint coercive bilinear form. Consequently, existence and uniqueness of the solution can be retrieved from (4.5) by standard theory.

Remark Note that the choice (4.3) is arbitrary. In the context of the Stokes equations it was observed (see [Guermond et al., 2006] and reference therein) that it results in a boundary layer that deteriorates the approximation of the gradient of the solution. Correcting terms can be introduced in specific cases (see again [Guermond et al., 2006]) but their analysis is more difficult.

4.2.4 Weak formulation of the continuous PDE

Let us first consider the weak formulation associated with (IM). Given $\underline{f}$ sufficiently regular, it reads:
Find $(\underline{y}, p) \in C^2(\mathcal{H}) \cap C^1(\mathcal{X}) \times C^0(\mathcal{L})$ such that for all $\underline{w} \in \mathcal{X},\ q \in \mathcal{L}$

$$\begin{cases} m(\partial_t^2 \underline{y}, \underline{w}) + a(\underline{y}, \underline{w}) + b(p, \underline{w}) = (\underline{f}, \underline{w}), \\ b(q, \underline{y}) = 0, \\ \underline{y}(t=0) = \underline{0},\ \partial_t \underline{y}(t=0) = \underline{0}, \end{cases} \tag{4.6}$$

where we have defined the bilinear forms $m : \mathcal{X} \times \mathcal{X} \to \mathbb{R}$, $a : \mathcal{X} \times \mathcal{X} \to \mathbb{R}$ and $b : \mathcal{L} \times \mathcal{X} \to \mathbb{R}$ such that

$$m(\underline{y}, \underline{w}) \coloneqq \int_\Omega \rho\,\underline{y} \cdot \underline{w}\,\mathrm{d}\Omega, \quad a(\underline{y}, \underline{w}) \coloneqq \int_\Omega \underline{\underline{\mathbf{C}}}\,\underline{\underline{\varepsilon}}(\underline{y}) : \underline{\underline{\varepsilon}}(\underline{w})\mathrm{d}\Omega,$$

$$b(p, \underline{w}) \coloneqq \int_\Omega p\,\mathrm{div}\,\underline{w}\,\mathrm{d}\Omega.$$

Note that the bilinear form $m(\cdot,\cdot)$ is symmetric and positive. Furthermore, due to Eq. (4.2) and the Korn inequality, the bilinear form $a(\cdot,\cdot)$ is symmetric and coercive in $\mathcal{X}$. We can write (4.6) as a set of equations written in $\mathcal{X}' \times \mathcal{L}$ for all $t \in [0, T]$. To do so, we introduce the linear continuous operators $M : \mathcal{X} \to \mathcal{X}'$, $A : \mathcal{X} \to \mathcal{X}'$, such that $\forall\ (\underline{y}, \underline{w}) \in \mathcal{X} \times \mathcal{X}$

$$\langle M\underline{y}, \underline{w}\rangle = m(\underline{y}, \underline{w}), \quad \langle A\underline{y}, \underline{w}\rangle = a(\underline{y}, \underline{w}),$$

and we define the divergence operator $B : \mathcal{X} \to \mathcal{L}$ and its transpose $B^T : \mathcal{L} \to \mathcal{X}'$ such that, $\forall\ (\underline{y}, q) \in \mathcal{X} \times \mathcal{L}$,

$$(B\underline{y}, q)_\mathcal{L} = b(q, \underline{y}) = \langle B^T q, \underline{y}\rangle,$$

where $(\cdot,\cdot)_\mathcal{L}$ denotes the standard scalar product of $L^2(\Omega)$. Note that the operator M can be continuously extended to an operator from $\mathcal{H}$ to $\mathcal{H}$ and, if $\rho \equiv 1$, then it is the identity

operator. Finally, the variational formulation can be equivalently rewritten
Find $(\underline{y}, p) \in C^2(\mathcal{H}) \cap C^1(\mathcal{X}) \times C^0(\mathcal{L})$ such that for all $t \in [0, T]$

$$\begin{cases} M\, \partial_t^2 \underline{y} + A\, \underline{y} + B^T p = \underline{f} & \text{in } \mathcal{X}', \\ B\, \underline{y} = 0 & \text{in } \mathcal{L}, \end{cases} \tag{IMv}$$

and

$$\underline{y}(t=0) = 0,\ \partial_t \underline{y}(t=0) = 0.$$

Analogously, the variational formulation associated with system (QIM) reads, equivalently,
Find $(\underline{y}_\lambda, p_\lambda) \in C^2(\mathcal{H}) \cap C^1(\mathcal{X}) \times C^0(\mathcal{L})$ such that for all $t \in [0, T]$

$$\begin{cases} M\, \partial_t^2 \underline{y}_\lambda + A\, \underline{y}_\lambda + B^T p_\lambda = \underline{f} & \text{in } \mathcal{X}', \\ B\, \underline{y}_\lambda = \lambda^{-1} I\, p_\lambda & \text{in } \mathcal{L}, \end{cases} \tag{QIMv}$$

and

$$\underline{y}_\lambda(t=0) = 0,\ \partial_t \underline{y}_\lambda(t=0) = 0,$$

where I is the identity operator from $\mathcal{L}$ to $\mathcal{L}$. Concerning the problem (QIP) with the boundary condition (4.3), we propose a variational formulation that reads
Find $(\tilde{\underline{y}}_\alpha, \tilde{p}_\alpha) \in C^2(\mathcal{H}) \cap C^1(\mathcal{X}) \times C^0(\mathcal{M})$ such that for all $(\underline{w}, q) \in \mathcal{X} \times \mathcal{M}$

$$\begin{cases} m(\partial_t^2 \tilde{\underline{y}}_\alpha, \underline{w}) + a(\tilde{\underline{y}}_\alpha, \underline{w}) + b(\tilde{p}_\alpha, \underline{w}) = (\underline{f}, \underline{w}), \\ b(q, \tilde{\underline{y}}_\alpha) = \alpha\, (\nabla \tilde{p}_\alpha, \nabla q)_{\mathcal{L}}, \end{cases} \tag{4.7}$$

and

$$\tilde{\underline{y}}_\alpha(t=0) = \underline{0},\ \partial_t \tilde{\underline{y}}_\alpha(t=0) = \underline{0}.$$

It is not straightforward to write equations in dual spaces from the variational formulation (4.7). This is due to the fact that we have changed the functional space in which the pressure is sought. To do so, we introduce the divergence operator $C : \mathcal{H} \to \mathcal{M}'$ and its transpose $C^T : \mathcal{M} \to \mathcal{H}$ defined by

$$c(q, \underline{w}) = -\int_\Omega \underline{\nabla}\, q \cdot \underline{w}\, \mathrm{d}\Omega \qquad \langle C\underline{w}, q \rangle = (C^T q, \underline{w})_{\mathcal{H}} = c(q, \underline{w}),$$

where $(\cdot, \cdot)_{\mathcal{H}}$ denotes the standard scalar product on $L^2(\Omega)^d$. Then, by identification of the operator B as an operator from $\mathcal{X}$ to $\mathcal{M}'$ (instead of an operator from $\mathcal{X}$ to $\mathcal{L}$), one can show that (4.7) is equivalent to
Find $(\tilde{\underline{y}}_\alpha, \tilde{p}_\alpha) \in C^2(\mathcal{H}) \cap C^1(\mathcal{X}) \times C^0(\mathcal{M})$ such that, for all $t \in [0, T]$,

$$\begin{cases} M\, \partial_t^2 \tilde{\underline{y}}_\alpha + A\, \tilde{\underline{y}}_\alpha + B^T \tilde{p}_\alpha = \underline{f} & \text{in } \mathcal{X}', \\ B\, \tilde{\underline{y}}_\alpha = \alpha C\, C^T \tilde{p}_\alpha & \text{in } \mathcal{M}', \end{cases} \tag{QIPv}$$

and

$$\tilde{\underline{y}}_\alpha(t=0) = 0,\ \partial_t \tilde{\underline{y}}_\alpha(t=0) = 0.$$

Note that the operator C corresponds to an extension of the operator B. Inversely, the gradient operator B^T represents the extension of C^T in a larger space. This distinction in the notation is not relevant in the continuous framework, but it will be fundamental at the discrete level.

4.3 Space discretisation

Let us now consider a regular finite-dimensional space $\mathcal{X}_h \subset \mathcal{X}$ for the discretisation of the displacement field and $\mathcal{M}_h \subset \mathcal{M}$ for the discretisation of the pressure field. These spaces are obtained by finite element approximation of $\mathcal{X}$ and $\mathcal{M}$, respectively. Furthermore, inspired by [Guermond and Quartapelle, 1998*b*], in order to discretise accordingly the variational formulation (4.7) that we propose, we introduce a third finite-dimensional space denoted $\mathcal{Y}_h \subset \mathcal{H}$ that should satisfy, for the sake of simplicity,

$$\mathcal{X}_h \subset \mathcal{Y}_h \text{ and } \nabla\mathcal{M}_h \subset \mathcal{Y}_h.$$

We define the embedding $i_h : \mathcal{X}_h \to \mathcal{Y}_h$ and its transpose $i_h^T : \mathcal{Y}_h \to \mathcal{X}_h$ such that for all $(\underline{y}_h, \underline{w}_h) \in \mathcal{X}_h \times \mathcal{Y}_h$

$$(\underline{y}_h, i_h^T \underline{w}_h)_{\mathcal{H}} := (i_h \underline{y}_h, \underline{w}_h)_{\mathcal{Y}_h} := (\underline{y}_h, \underline{w}_h)_{\mathcal{Y}_h}, \tag{4.8}$$

where $(\cdot,\cdot)_{\mathcal{Y}_h}$ stands for the approximation of the scalar product in $\mathcal{H}$ that is defined using quadrature formulae (it is a symmetric coercive and continuous bilinear form in $\mathcal{Y}_h$ for the norm in $\mathcal{H}$). In a more general way, we assume that quadrature formulae do not corrupt symmetry and positivity properties of the bilinear forms. We introduce the discrete divergence operator $C_h : \mathcal{Y}_h \to \mathcal{M}_h$ and the discrete gradient operator $C_h^T : \mathcal{M}_h \to \mathcal{Y}_h$ such that for all $(p_h, \underline{w}_h) \in \mathcal{M}_h \times \mathcal{Y}_h$

$$(p_h, C_h \underline{w}_h)_{\mathcal{L}} := (C_h^T p_h, \underline{w}_h)_{\mathcal{Y}_h} := -(\nabla p_h, \underline{w}_h)_{\mathcal{Y}_h}.$$

Observe that C_h^T corresponds to the operator $C^T \equiv -\nabla$ applied to functions in $\mathcal{M}_h$, considering the resulting functions in the larger space $\mathcal{Y}_h$. Then, we define another discrete divergence operator $B_h : \mathcal{X}_h \to \mathcal{M}_h$ and another discrete gradient operator $B_h^T : \mathcal{M}_h \to \mathcal{X}_h$ as

$$B_h := C_h\, i_h \quad \text{and} \quad B_h^T := i_h^T\, C_h^T.$$

One can observe that, for all $(p_h, \underline{w}_h) \in \mathcal{M}_h \times \mathcal{X}_h$, we have

$$\begin{aligned}(B_h\, \underline{w}_h, p_h)_{\mathcal{L}} &= (C_h\, i_h\, \underline{w}_h, p_h)_{\mathcal{L}} = (i_h\, \underline{w}_h, C_h^T p_h)_{\mathcal{Y}_h} \\ &= (\underline{w}_h, i_h^T\, C_h^T p_h)_{\mathcal{H}} = (\underline{w}_h, B_h^T p_h)_{\mathcal{H}}.\end{aligned} \tag{4.9}$$

Note also that the following commutative diagrams (taken from [Guermond and Quartapelle, 1998*b*]) hold

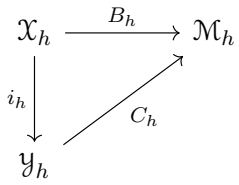

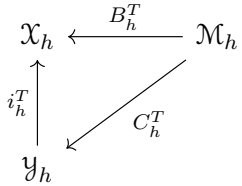

We introduce the linear continuous operators $M_h : \mathcal{X}_h \to \mathcal{X}_h$ and $A_h : \mathcal{X}_h \to \mathcal{X}_h$ such that for all $(\underline{v}_h, \underline{w}_h) \in \mathcal{X}_h \times \mathcal{X}_h$

$$(M_h \underline{v}_h, \underline{w}_h)_{\mathcal{H}} = m_h(\underline{v}_h, \underline{w}_h), \quad (A_h \underline{v}_h, \underline{w}_h)_{\mathcal{H}} = a_h(\underline{v}_h, \underline{w}_h).$$

where the subscript h in the notation of the bilinear forms stands for the use of quadrature rule in the computation of integrals. The finite element approximation of (IMv) reads
Find $(\underline{y}_h, p_h) \in C^2(\mathcal{X}_h) \times C^0(\mathcal{M}_h)$ such that for all $t \in [0, T]$

$$\begin{cases} M_h\, \partial_t^2 \underline{y}_h + A_h\, \underline{y}_h + B_h^T p_h = \underline{f}_h & \text{in } \mathcal{X}_h, \\ B_h\, \underline{y}_h = 0 & \text{in } \mathcal{M}_h, \end{cases} \tag{IMh}$$

and

$$\underline{y}_h(t=0)=0,\ \partial_t\underline{y}_h(t=0)=0,$$

where $\underline{f}_h(t)\in X_h$ denotes some approximation of $\underline{f}$. Analogously to the pure incompressible mixed formulation, we can retrieve the space discretisation associated with (QIMv). It reads
Find $(\underline{y}_{\lambda,h},p_{\lambda,h})\in C^2(\mathcal{X}_h)\times C^0(\mathcal{M}_h)$ such that for all $t\in[0,T]$

$$\begin{cases} M_h\,\partial_t^2\underline{y}_{\lambda,h}+A_h\,\underline{y}_{\lambda,h}+B_h^T p_{\lambda,h}=\underline{f}_h & \text{in } \mathcal{X}_h,\\ B_h\,\underline{y}_{\lambda,h}=\lambda^{-1}I_h p_{\lambda,h} & \text{in } \mathcal{M}_h, \end{cases} \tag{QIMh}$$

and

$$\underline{y}_{\lambda,h}(t=0)=0,\ \partial_t\underline{y}_{\lambda,h}(t=0)=0.$$

The operator $I_h:\mathcal{M}_h\to\mathcal{M}_h$ is such that for all $(p_h,q_h)\in\mathcal{M}_h$

$$(I_h p_h,q_h)_{\mathcal{L}}=(p_h,q_h)_{\mathcal{L}_h},$$

where $(\cdot,\cdot)_{\mathcal{L}_h}$ stands for the approximation of the scalar product in $\mathcal{L}$ by quadrature formulae.
Finally, we are able to give the space discretisation associated with the novel formulation we propose (QIPv). It reads
Find $(\underline{\tilde{y}}_{\alpha,h},\tilde{p}_{\alpha,h})\in C^2(\mathcal{X}_h)\times C^0(\mathcal{M}_h)$ such that for all $t\in[0,T]$

$$\begin{cases} M_h\,\partial_t^2\underline{\tilde{y}}_{\alpha,h}+A_h\,\underline{\tilde{y}}_{\alpha,h}+B_h^T\tilde{p}_{\alpha,h}=\underline{f}_h & \text{in } \mathcal{X}_h,\\ B_h\,\underline{\tilde{y}}_{\alpha,h}=\alpha\,C_hC_h^T\tilde{p}_{\alpha,h} & \text{in } \mathcal{M}_h, \end{cases} \tag{QIPh}$$

and

$$\underline{\tilde{y}}_{\alpha,h}(t=0)=0,\ \partial_t\underline{\tilde{y}}_{\alpha,h}(t=0)=0.$$

Note that the operator $C_hC_h^T$ corresponds to a discrete laplacian operator on $\mathcal{M}_h$. Indeed, for all $(p_h,q_h)\in\mathcal{M}_h\times\mathcal{M}_h$

$$(C_hC_h^Tp_h,q_h)_{\mathcal{L}}=(C_h^Tp_h,C_h^Tq_h)_{\mathcal{Y}_h}=(\nabla p_h,\nabla q_h)_{\mathcal{Y}_h}.$$

Therefore, $C_hC_h^T:\mathcal{M}_h\to\mathcal{M}_h$ is invertible for any reasonable choice of finite element spaces and quadrature rule. This is obviously also true for I_h and M_h.
Let us insist on the importance of the introduction of the space $\mathcal{Y}_h$. First, it is related to the definition of the quadrature formulae in $\mathcal{H}$ in the definition of (4.8). Second, even if exact integration is performed, the introduction of the space $\mathcal{Y}_h$ allows us to take into account the fact that, in general, the gradient of functions in $\mathcal{M}_h$ does not belong to $\mathcal{X}_h$. Indeed, if this was the case, then C_h and B_h would be the same operator and the penalisation strategy would be useless in terms of computational efficiency (see the discussion of Section 4.4.1).

In the numerical results we present in this work we use high-order Spectral Finite Element, as in [Komatitsch and Vilotte, 1998] and [Cohen and Fauqueux, 2005]. Since we consider a simple geometry for our purposes, we construct a quasi-uniform triangulation of Ω composed of quadrangles or hexahedra

$$\overline{\Omega}=\bigcup_{i=1}^{N}\overline{K}_i,\quad K_i\cap K_j=\emptyset,\quad \mathbf{F}_i(\hat{K})=K_i,$$

where $\hat{K}$ is the unit square or the unit cube and $\forall\, i \in \{1, 2, .., N\}$, $\mathbf{F}_i$ denotes the invertible transformation of the reference element $\hat{K}$ to the deformed element K_i. Then, we define

$$\mathcal{X}_h = \left\{\phi \in C^0(\Omega)^d \mid \phi|_{K_i} \circ \mathbf{F}_i \in \mathcal{Q}_r(\hat{K})^d\right\},$$

where $\mathcal{Q}_r$ is the set of polynomials with degree $r \geq 1$ in each variable of space. To obtain mass-lumping (meaning that M_h can be inverted trivially) one must choose the quadrature points in the computation of $m_h(\cdot, \cdot)$ at the same location as the interpolation points (see [Cohen, 2001]). Sufficient accuracy is obtained if the interpolation and quadrature points correspond in the reference elements to the Gauss-Lobatto points of same order (r in our case, that gives $(r+1)^d$ quadrature/interpolation points in the reference elements). For the computation of $a_h(\cdot, \cdot)$ we use the same quadrature rule as for the computation of $m_h(\cdot, \cdot)$ (which gives sufficient accuracy on non-distorted mesh, see [Durufle et al., 2009]). Then, we choose

$$\mathcal{M}_h = \left\{\varphi \in C^0(\Omega) \mid \varphi|_{K_i} \circ \mathbf{F}_i \in \mathcal{Q}_{r-1}(\hat{K})\right\}.$$

Note that the major difference here is that we choose a lower-order finite element space, but $\mathcal{M}_h$ is still constructed using continuous finite element. It is mentioned in [Brezzi and Fortin, 2012] that this choice is compatible with $\mathcal{X}_h$ in the sense that a discrete inf-sup condition is satisfied (the importance of this condition is further detailed below). In addition, we assume that $(\cdot, \cdot)_{\mathcal{L}_h}$ is computed using Gauss-Lobatto quadrature points of order $r - 1$. Hence, mass-lumping is achieved and the operator I_h is easily invertible. Finally, we define

$$\mathcal{Y}_h = \mathcal{X}_h + \left\{\psi \in L^2(\Omega)^d \mid \psi|_{K_i} \circ \mathbf{F}_i \in \mathcal{Q}_{r-1}(\hat{K})^d\right\}$$

and $(\cdot, \cdot)_{\mathcal{Y}_h}$ is computed using the Gauss-Lobatto quadrature points of order $r - 1$. Note that we have the inclusion $\nabla\mathcal{M}_h \subset \mathcal{Y}_h$ only if all the $\mathbf{F}_i$ are affine. We believe that this is only a technical limitation. However, numerical results are provided only in that case.

4.4 Time discretisation

This section deals with the time discretisation of the semi-discrete formulations obtained by FE approximation in space. We consider only finite difference schemes that are centred, in order to preserve energy conservation at the discrete level. In what follows, the fully discrete schemes for the standard formulations (IM) and (QIM) are provided. Moreover, we propose the fully discrete scheme for the novel formulation (QIP).

4.4.1 Fully discrete schemes

Let us consider a time interval $[0, T]$, with $T > 0$, and define the partition $t^n = n\,\Delta t$, with $n \in \{0, 1, .., N\}$, and $\Delta\, t = T/N$. The fully discrete scheme corresponding to (IM) for $n \in \{0, 1, .., N\}$ is constructed based on a simple second-order finite difference scheme, namely a leapfrog scheme. We shall consider two sequences of approximate displacement fields $\{\underline{y}_h^n \in \mathcal{X}_h\}$ and pressures $\{p_h^n \in \mathcal{M}_h\}$ such that $(\underline{y}_h^0, \underline{y}_h^1)$ is given and for $n \in \{1, , N\}$

$$\begin{cases} M_h \dfrac{\underline{y}_h^{n+1} - 2\,\underline{y}_h^n + \underline{y}_h^{n-1}}{\Delta t^2} + A_h\,\underline{y}_h^n + B_h^T\,p_h^n = \underline{f}_h^n & \text{in } \mathcal{X}_h, \\ B_h \underline{y}_h^n = 0 & \text{in } \mathcal{M}_h, \end{cases} \tag{IMnh}$$

with $\underline{f}_h^n = \underline{f}_h(t^n)$. The implementation of scheme (IMnh) can be done using Schur complement techniques. It reads as follows: given $(\underline{y}_h^{n-1}, \underline{y}_h^n)$, first compute p_h^n from

$$(B_h\, M_h^{-1}\, B_h^T)\, p_h^n = B_h\, M_h^{-1}(\underline{f}_h^n - A_h \underline{y}_h^n); \tag{4.10}$$

then, $\underline{y}_h^{n+1}$ is given by

$$\underline{y}_h^{n+1} = \Delta t^2 M_h^{-1} \underline{f}_h^n + 2\,\underline{y}_h^n - \underline{y}_h^{n-1} - \Delta t^2 M_h^{-1}\, A_h\, \underline{y}_h^n - \Delta t^2 M_h^{-1}\, B_h^T\, p_h^n.$$

One can see that the pressure field is an intermediate unknown that acts as a Lagrange multiplier to enforce the constraint $B_h \underline{y}_h^{n+1} = 0$. Note that we use the notation p_h^n by analogy with the quasi-incompressible schemes that we present in what follows. Moreover, the system (4.10) is well-posed if B_h^T is injective and B_h surjective. This corresponds to verify that the LBB condition is satisfied, i.e. there exists a constant $c > 0$ such that

$$\inf_{q_h \in \mathcal{M}_h} \sup_{\underline{w}_h \in \mathcal{X}_h} \frac{(B_h \underline{w}_h, q_h)}{\|\underline{w}_h\|_{\mathcal{X}}\, \|q_h\|_{\mathcal{L}}} \geq c, \tag{4.11}$$

where, if c does not depend on the discretisation parameter, one recovers an optimal convergence behaviour. Note that for the incompressible, linear Stokes problem it is standard to show [Heywood and Rannacher, 1982, 1986, 1988, 1990] that standard second-order discrete space-time discretisation can be achieved as soon as the LBB condition holds. We assume that similar results hold for the elastodynamic problem (IMh). Finally, note that Eq. (4.10) can be solved at each time step by iterative algorithms and, since the underlying problem is symmetric, the Conjugate Gradient method is a good candidate. However, it is important to highlight the fact that the operator $B_h\, M_h^{-1}\, B_h^T = C_h\, i_h\, M_h^{-1}\, i_h^T C_h^T$ is much more complicated to invert than $C_h\, C_h^T$ due to the presence of the term $i_h\, M_h^{-1}\, i_h^T$ that has the effect to widen the bandwidth of the corresponding finite element matrix. Our aim is to specifically tackle this problem by avoiding – at each time step – the inversion of $B_h\, M_h^{-1}\, B_h^T$, and inverting instead $C_h\, C_h^T$, for which we have efficient solvers.

Remark If non-zero initial displacement $\underline{y}_\lambda(t=0) = \underline{y}_0$ and/or initial velocity $\partial_t \underline{y}_\lambda(t=0) = \underline{v}_0$ are considered, or if the source term $\underline{f}_h$ is not 0 at time $t = 0$, then, to preserve the expected second-order consistency, the computation of the first two iterates is performed as follows:

$$\underline{y}_h^0 = \underline{y}_{h,0}, \quad \underline{y}_h^1 = \underline{y}_{h,0} + \Delta t\, \underline{v}_{h,0} + \frac{\Delta t^2}{2} M_h \big(\underline{f}_h^0 - A_h\, \underline{y}_{h,0} - B_h^T\, p_h^0\big) \tag{4.12}$$

where p_h^0 is computed from (4.10) with $n = 0$, and $(\underline{y}_{h,0}, \underline{v}_{h,0})$ belong to $\mathcal{X}_h \times \mathcal{X}_h$ and correspond to an approximation of $(\underline{y}_0, \underline{v}_0)$.

In order to write the fully discrete scheme corresponding to (QIM) for $n \in \{1, .., N\}$, we define two sequences of approximate displacement fields $\{\underline{y}_{\lambda,h}^n \in \mathcal{X}_h\}$ and pressures $\{p_{\lambda,h}^n \in \mathcal{M}_h\}$ such that $(\underline{y}_{\lambda,h}^0, \underline{y}_{\lambda,h}^1)$ is given and for $n \in \{1, .., N\}$

$$\begin{cases} M_h \dfrac{\underline{y}_{\lambda,h}^{n+1} - 2\,\underline{y}_{\lambda,h}^n + \underline{y}_{\lambda,h}^{n-1}}{\Delta t^2} + A_h\, \underline{y}_{\lambda,h}^n + B_h^T\, p_{\lambda,h}^n = \underline{f}_h^n & \text{in } \mathcal{X}_h, \\ B_h \underline{y}_{\lambda,h}^n = \lambda^{-1} I_h\, p_{\lambda,h}^n & \text{in } \mathcal{M}_h. \end{cases} \tag{QIMnh}$$

Observe that the scheme (QIMnh) is fully explicit, due to the use of the mass-lumping technique (we recall that M_h and I_h are easily invertible). However, we show in the following section that, due to stability considerations, the maximum time step allowed is

considerably reduced by the fact that the pressure term is treated explicitly. Observe that the first two iterates can be computed using (4.12) with p_h^0 replaced by $p_{\lambda,h}^0 = \lambda I_h^{-1} B_h \underline{y}_0$.

Finally, we provide the fully discrete scheme corresponding to (QIP) for $n \in \{1, .., N\}$. We define two sequences of approximate displacement fields $\{\tilde{\underline{y}}_{\alpha,h}^n \in \mathcal{X}_h\}$ and approximate pressures $\{\tilde{p}_{\alpha,h}^n \in \mathcal{M}_h\}$ such that $(\tilde{\underline{y}}_{\alpha,h}^0, \tilde{\underline{y}}_{\alpha,h}^1)$ is given and for $n \in \{1, , N\}$

$$\begin{cases} M_h \dfrac{\tilde{\underline{y}}_{\alpha,h}^{n+1} - 2\,\tilde{\underline{y}}_{\alpha,h}^n + \tilde{\underline{y}}_{\alpha,h}^{n-1}}{\Delta t^2} + A_h\,\tilde{\underline{y}}_{\alpha,h}^n + B_h^T\,\tilde{p}_{\alpha,h}^n = \underline{f}_h^n & \text{in } \mathcal{X}_h, \\ B_h \tilde{\underline{y}}_{\alpha,h}^n = \alpha\,\Delta t^2\, C_h\, C_h^T\, \tilde{p}_{\alpha,h}^n & \text{in } \mathcal{M}_h. \end{cases} \tag{QIPnh}$$

Note that here, for consistency reasons, we have rescaled the penalisation parameter by Δt^2 and assume α is independent of Δt. This choice should guarantee the second-order consistency in time that is expected from the leapfrog time discretisation. Note that we can directly rewrite the second equation in (QIPnh) as

$$\tilde{p}_{\alpha,h}^n = \frac{(C_h\, C_h^T)^{-1}}{\alpha\,\Delta t^2}\, B_h \tilde{\underline{y}}_{\alpha,h}^n. \tag{4.13}$$

Consequently, this step is equivalent to solving a discrete Poisson problem for the pressure at each time step, with homogeneous Neumann boundary conditions on the boundary $\partial\Omega$. One of the main advantages of this formulation is that the Poisson problem is very standard and its solution can be retrieved by fast solvers. In addition, observe that the first two iterates can be computed using (4.12) with p_h^0 computed with Eq. (4.13) for $n = 0$ and $\tilde{\underline{y}}_{\alpha,h}^0 \equiv \underline{y}_{h,0}$. Finally, observe that by injecting (4.13) in (QIPnh), we retrieve

$$M_h \frac{\tilde{\underline{y}}_{\alpha,h}^{n+1} - 2\,\tilde{\underline{y}}_{\alpha,h}^n + \tilde{\underline{y}}_{\alpha,h}^{n-1}}{\Delta t^2} + A_h\,\tilde{\underline{y}}_{\alpha,h}^n + \frac{B_h^T (C_h\, C_h^T)^{-1} B_h}{\alpha\,\Delta t^2} \tilde{\underline{y}}_{\alpha,h}^n = \underline{f}_h^n. \tag{4.14}$$

Remark Finally, note that it is not obvious to see why the solution computed by the scheme (QIPnh) should satisfy $B_h \tilde{\underline{y}}_{\alpha,h}^n \simeq 0$ as Δt goes to 0, since $C_h\, C_h^T\, \tilde{p}_{\alpha,h}^n$ may explode with Δt. Among other objectives, the stability analysis below describes precisely in which sense $B_h \tilde{\underline{y}}_{\alpha,h}^n$ is small.

4.4.2 Stability analysis

The aim of this section is to find uniform estimates of the discrete energy of the different schemes, i.e.

$$\sup_{n \in \{0,1,..,N\}} \left| \mathcal{E}_h^{n+\frac{1}{2}} \right| \leq C, \tag{4.15}$$

where the constant C depends on the final time step $T = N\,\Delta t$ and on the data of the continuous problem, but is independent of Δt and h. However, if explicit schemes are employed for time discretisation, the time step is limited by a stability condition depending on h. We refer to [Joly, 2008] for further reading.
For the sake of simplicity, we consider a time t^n such that the source term has vanished (i.e. $\underline{f}_h(t) = \underline{0}, \quad \forall t \geq t^n$). Then, the energy of the continuous problem is constant in time. In order to retrieve a discrete counterpart of this energy, we consider for every formulation, as a test function, the centred discrete approximation of the time derivative of the displacement at time t^n.

Stability of scheme (IMnh)**.** Let us first consider formulation (IMnh). By scalar product in the first equation in (IMnh) with

$$\underline{v}_h = \frac{\underline{y}_h^{n+1} - \underline{y}_h^{n-1}}{2\,\Delta t} \tag{4.16}$$

as well as by discrete differentiation of the second equation in (IMnh) and by scalar product with p_h^n we obtain

$$\begin{cases} \Big(M_h \dfrac{\underline{y}_h^{n+1} - 2\,\underline{y}_h^n + \underline{y}_h^{n-1}}{\Delta t^2} + A_h\,\underline{y}_h^n + B_h^T\,p_h^n,\ \dfrac{\underline{y}_h^{n+1} - \underline{y}_h^{n-1}}{2\,\Delta t}\Big)_{\mathcal{H}} = \underline{0}, \\ \Big(B_h \dfrac{\underline{y}_h^{n+1} - \underline{y}_h^{n-1}}{2\,\Delta t},\ p_h^n\Big)_{\mathcal{L}} = 0. \end{cases} \tag{4.17}$$

Then, due to symmetry of B_h and Eq. (4.9), we can simplify the first equation in (4.17). We have

$$\Big(M_h \frac{\underline{y}_h^{n+1} - 2\,\underline{y}_h^n + \underline{y}_h^{n-1}}{\Delta t^2} + A_h\,\underline{y}_h^n,\ \frac{\underline{y}_h^{n+1} - \underline{y}_h^{n-1}}{2\,\Delta t}\Big)_{\mathcal{H}} = \underline{0}. \tag{4.18}$$

We define the discrete energy at time $n+\frac{1}{2}$ as

$$\mathcal{E}_h^{n+\frac{1}{2}} = \mathcal{E}_k^{n+\frac{1}{2}} - \frac{\Delta t^2}{4}\mathcal{E}_{kp}^{n+\frac{1}{2}} + \mathcal{E}_p^{n+\frac{1}{2}}, \tag{4.19}$$

where the kinetic energy reads

$$\mathcal{E}_k^{n+\frac{1}{2}} := \frac{1}{2}\Big(M_h\,\frac{\underline{y}_h^{n+1} - \underline{y}_h^n}{\Delta\, t},\ \frac{\underline{y}_h^{n+1} - \underline{y}_h^n}{\Delta\, t}\Big)_{\mathcal{H}},$$

the potential energy reads

$$\mathcal{E}_p^{n+\frac{1}{2}} := \frac{1}{2}\Big(A_h\,\frac{\underline{y}_h^{n+1} + \underline{y}_h^n}{2},\ \frac{\underline{y}_h^{n+1} + \underline{y}_h^n}{2}\Big)_{\mathcal{H}},$$

and the mixed energy term is defined as

$$\mathcal{E}_{kp}^{n+\frac{1}{2}} := \frac{1}{2}\Big(A_h\,\frac{\underline{y}_h^{n+1} - \underline{y}_h^n}{\Delta\, t},\ \frac{\underline{y}_h^{n+1} - \underline{y}_h^n}{\Delta\, t}\Big)_{\mathcal{H}}.$$

Then, after some computations, using the symmetry properties of the operators M_h and A_h, we obtain from (4.18) the discrete conservation property

$$\frac{\mathcal{E}_h^{n+\frac{1}{2}} - \mathcal{E}_h^{n-\frac{1}{2}}}{\Delta t} = 0.$$

It now remains to prove that $\mathcal{E}_h^{n+\frac{1}{2}}$ is positive.

Proposition 4.1. *A sufficient condition for the stability of scheme* (IMnh) *is*

$$\Delta t^2 \le 4\,\big\|M_h^{-1}A_h\big\|^{-1}, \tag{4.20}$$

with

$$\big\|M_h^{-1}A_h\big\| = \sup_{0\neq \underline{y}_h\in\mathfrak{X}_h} \frac{a_h(\underline{y}_h,\,\underline{y}_h)}{m_h(\underline{y}_h,\underline{y}_h)}. \tag{4.21}$$

Proof. The proof is very standard (see [Joly, 2008]). Consequently, we only prove the positivity of the energy. We provide here some details for the sake of completeness. Let us first consider the definition of $\mathcal{E}_h^{n+\frac{1}{2}}$. Since $\mathcal{E}_s^{n+\frac{1}{2}}$ is positive by definition, we can easily retrieve the lower bound for the energy

$$\mathcal{E}_h^{n+\frac{1}{2}} \geq \frac{1}{2}\left(\left(M_h - \frac{\Delta t^2}{4} A_h\right) \frac{\underline{y}_h^{n+1} - \underline{y}_h^n}{\Delta t}, \frac{\underline{y}_h^{n+1} - \underline{y}_h^n}{\Delta t} \right)_{\mathcal{H}}.$$

Hence, the energy is positive if

$$m_h(\underline{y}_h, \underline{y}_h) - \frac{\Delta t^2}{4} a_h(\underline{y}_h, \underline{y}_h) \geq 0, \qquad \forall \underline{y}_h \in \mathrm{X}_h. \tag{4.22}$$

Finally, Eq. (4.22) can be rewritten as

$$\frac{\Delta t^2}{4} \sup_{0 \neq \underline{y}_h \in \mathfrak{X}_h} \frac{a_h(\underline{y}_h, \underline{y}_h)}{m_h(\underline{y}_h, \underline{y}_h)} \leq 1,$$

concluding the proof. □

Remark Note that Proposition 4.1 introduces an abstract CFL condition. Moreover, we expect the following estimation

$$\left\| M_h^{-1} A_h \right\| \sim \frac{c_s^2}{h^2}, \tag{4.23}$$

with c_s a positive constant, depending on the elasticity tensor driving the shear wave propagation. Consequently, we obtain the sufficient stability condition

$$\Delta t \lesssim \frac{h}{c_s}. \tag{4.24}$$

Therefore, the time step is not affected by the pressure wave propagation, that is travelling at an "infinite" velocity at the incompressible limit.

Stability of the scheme (QIMnh)**.** By similar reasoning, we can retrieve en energy estimation for the formulation (QIMnh). We retrieve, after some computations,

$$\left(M_h \frac{\underline{y}_{\lambda,h}^{n+1} - 2\underline{y}_{\lambda,h}^n + \underline{y}_{\lambda,h}^{n-1}}{\Delta t^2} + A_h \underline{y}_{\lambda,h}^n + \lambda B_h^T B_h \underline{y}_{\lambda,h}^n, \frac{\underline{y}_{\lambda,h}^{n+1} - \underline{y}_{\lambda,h}^{n-1}}{2\,\Delta t} \right)_{\mathcal{H}} = \underline{0}. \tag{4.25}$$

We introduce $A_{h,\lambda} := A_h + \lambda B_h^T B_h$. Then, if we define the discrete energy $\mathcal{E}_h^{n+\frac{1}{2}}$ as in Eq. (4.19), with $A_{h,\lambda}$ instead of A_h, we can assert the following proposition.

Proposition 4.2. *A sufficient condition for the stability of scheme* (QIMnh) *is*

$$\Delta t^2 \leq 4 \left\| M_h^{-1} A_{h,\lambda} \right\|^{-1}, \tag{4.26}$$

with

$$\left\| M_h^{-1} A_{h,\lambda} \right\| = \sup_{0 \neq \underline{y}_h \in \mathfrak{X}_h} \frac{a_h(\underline{y}_h, \underline{y}_h) + \lambda \|B_h \underline{y}_h\|_{\mathfrak{L}}^2}{m_h(\underline{y}_h, \underline{y}_h)}. \tag{4.27}$$

Remark Note that, by definition,

$$\left\|M_h^{-1}A_{h,\lambda}\right\| \leq \left\|M_h^{-1}A_h\right\| + \lambda\left\|M_h^{-1}B_h^T\,B_h\right\|,$$

with

$$\left\|M_h^{-1}B_h^T\,B_h\right\| = \sup_{0\neq \underline{y}_h\in\mathcal{X}_h} \frac{\|B_h\underline{y}_h\|_{\mathcal{L}}^2}{m_h(\underline{y}_h\,,\underline{y}_h)}.$$

By similar reasoning to Eq. (4.23), we can now introduce a constant c_p, related to the maximum generalised eigenvalue of the operator $(B_h^T\,B_h, M_h)$ such that

$$\lambda\left\|M_h^{-1}B_h^T\,B_h\right\| \sim \frac{c_p^2}{h^2}.$$

Therefore, we can assert

$$\left\|M_h^{-1}A_{h,\lambda}\right\| \sim \frac{c_s^2+c_p^2}{h^2}. \tag{4.28}$$

Consequently, the stability condition (4.26) imposes a significant restriction on the time step.

$$\Delta t^2 \lesssim \frac{h^2}{c_s^2+c_p^2}$$

Note that, because of the non-dimensionalisation, we expect c_s to be close to the unity, whereas, c_p is given by the velocity ratio between pressure and shear waves. For soft tissues this ratio is around 10^3. This makes in practice the scheme (QIMnh) not efficient and justifies our need to formulate more adequate methods for the limit – incompressible – problem.

Stability of the scheme (QIPnh)**.** Finally, let us analyse the stability estimates related to the novel formulation (QIPnh). By analogous reasoning, we get from (4.14)

$$\left(M_h\frac{\tilde{\underline{y}}_{\alpha,h}^{n+1}-2\tilde{\underline{y}}_{\alpha,h}^{n}+\tilde{\underline{y}}_{\alpha,h}^{n-1}}{\Delta t^2}+\left(A_h+\frac{1}{\alpha\Delta t^2}Q_h\right)\tilde{\underline{y}}_{\alpha,h}^{n},\ \frac{\tilde{\underline{y}}_{\alpha,h}^{n+1}-\tilde{\underline{y}}_{\alpha,h}^{n-1}}{2\,\Delta t}\right)=\underline{0}, \tag{4.29}$$

where we have defined $Q_h \coloneqq B_h^T(C_h\,C_h^T)^{-1}B_h$. Then, the discrete energy at time $n+\frac{1}{2}$ reads

$$\mathcal{E}_h^{n+\frac{1}{2}} = \mathcal{E}_k^{n+\frac{1}{2}} - \frac{\Delta t^2}{4}\mathcal{E}_{kp}^{n+\frac{1}{2}} + \mathcal{E}_p^{n+\frac{1}{2}},$$

with kinetic energy

$$\mathcal{E}_k^{n+\frac{1}{2}} \coloneqq \left(M_h\,\frac{\tilde{\underline{y}}_{\alpha,h}^{n+1}-\tilde{\underline{y}}_{\alpha,h}^{n}}{\Delta\,t},\ \frac{\tilde{\underline{y}}_{\alpha,h}^{n+1}-\tilde{\underline{y}}_{\alpha,h}^{n}}{\Delta\,t}\right)_{\mathcal{H}},$$

potential energy

$$\mathcal{E}_p^{n+\frac{1}{2}} \coloneqq \left((A_h+\frac{1}{\alpha\Delta t^2}Q_h),\ \frac{\tilde{\underline{y}}_{\alpha,h}^{n+1}+\tilde{\underline{y}}_{\alpha,h}^{n}}{2},\ \frac{\tilde{\underline{y}}_{\alpha,h}^{n+1}+\tilde{\underline{y}}_{\alpha,h}^{n}}{2}\right)_{\mathcal{H}},$$

and mixed energy term

$$\mathcal{E}_{kp}^{n+\frac{1}{2}} \coloneqq \left((A_h+\frac{1}{\alpha\Delta t^2}Q_h)\,\frac{\tilde{\underline{y}}_{\alpha,h}^{n+1}-\tilde{\underline{y}}_{\alpha,h}^{n}}{\Delta\,t},\ \frac{\tilde{\underline{y}}_{\alpha,h}^{n+1}-\tilde{\underline{y}}_{\alpha,h}^{n}}{\Delta\,t}\right)_{\mathcal{H}}.$$

Before providing a stability estimate for (4.29), we introduce the following lemma.

Lemma 4.3. *Let* $P_h \coloneqq C_h^T (C_h\, C_h^T)^{-1} C_h : \mathcal{Y}_h \to \mathcal{Y}_h$. *Then* P_h *is a projection and*

$$\|P_h\|_{\mathcal{L}(\mathcal{Y}_h)} \leq 1.$$

Proof. The proof consists in demonstrating that $P_h^2 = P_h$. That follows easily by the definition of P_h. □

We are now able to assert a stability condition for scheme (QIPnh).

Proposition 4.4. *A sufficient condition for the stability of scheme* (QIPnh) *is*

$$\Delta t^2 \leq 4 \left(\sup_{0 \neq \underline{y}_h \in \mathcal{X}_h} \frac{4\,\alpha\, a_h(\underline{y}_h,\, \underline{y}_h)}{4\,\alpha\, m_h(\underline{y}_h, \underline{y}_h) - \|\underline{y}_h\|_{\mathcal{Y}_h}^2} \right)^{-1} \tag{4.30}$$

and

$$\alpha > \frac{1}{4} \sup_{0 \neq \underline{y}_h \in \mathcal{X}_h} \frac{\|\underline{y}_h\|_{\mathcal{Y}_h}^2}{m_h(\underline{y}_h, \underline{y}_h)}. \tag{4.31}$$

Proof. Again we prove the positivity of the energy $\mathcal{E}_h^{n+\frac{1}{2}}$. By definition of $\mathcal{E}_h^{n+\frac{1}{2}}$, since $\mathcal{E}_p^{n+\frac{1}{2}}$ is positive, we can obtain the estimation

$$\mathcal{E}_h^{n+\frac{1}{2}} \geq \left(\left(M_h - \frac{\Delta t^2}{4} A_h - \frac{1}{4\alpha} Q_h \right) \frac{\tilde{y}_{\alpha,h}^{n+1} - \tilde{y}_{\alpha,h}^{n}}{\Delta\, t},\, \frac{\tilde{y}_{\alpha,h}^{n+1} - \tilde{y}_{\alpha,h}^{n}}{\Delta\, t} \right)_{\mathcal{H}}.$$

Hence, we need to satisfy

$$m_h(\underline{y}_h,\, \underline{y}_h) - \frac{\Delta t^2}{4} a_h(\underline{y}_h,\, \underline{y}_h) - \frac{1}{4\alpha} (Q_h \underline{y}_h,\, \underline{y}_h)_{\mathcal{H}} \geq 0, \quad \forall\, \underline{y}_h \in \mathcal{X}_h. \tag{4.32}$$

However, by definition of P_h and Lemma 4.3, we find $Q_h = i_h^T P_h i_h$ and, since we easily deduce the inequality $\|i_h \underline{y}_h\|_{\mathcal{Y}_h} \leq \|\underline{y}_h\|_{\mathcal{Y}_h}$ from Eq. (4.8), we have

$$(Q_h\, \underline{y}_h,\, \underline{y}_h)_{\mathcal{H}} = (i_h^T P_h\, i_h\, \underline{y}_h,\, \underline{y}_h)_{\mathcal{H}} = (P_h\, i_h\, \underline{y}_h, i_h\, \underline{y}_h)_{\mathcal{Y}_h} \leq \|i_h \underline{y}_h\|_{\mathcal{Y}_h}^2 \leq \|\underline{y}_h\|_{\mathcal{Y}_h}^2.$$

Finally, if (4.30) holds, then Eq. (4.32) can be rewritten as

$$\frac{\Delta t^2}{4} \sup_{0 \neq \underline{y}_h \in \mathcal{X}_h} \frac{a_h(\underline{y}_h,\, \underline{y}_h)}{m_h(\underline{y}_h, \underline{y}_h) - \|\underline{y}_h\|_{\mathcal{Y}_h}^2/(4\alpha)} \leq 1,$$

concluding the proof. □

Corollary 4.1. *If exact integration is used and the density* ρ *is constant, then a sufficient condition for the stability of scheme* (QIPnh) *is*

$$\Delta t^2 \leq 4\,\rho\, \|A_h\|^{-1} \frac{4\,\alpha\,\rho - 1}{4\,\alpha\,\rho}, \quad \alpha > \frac{1}{4\,\rho}, \tag{4.33}$$

with

$$\|A_h\| = \sup_{\underline{y}_h \in \mathcal{X}_h\, \underline{y}_h \neq 0} \frac{a(\underline{y}_h,\, \underline{y}_h)}{\|\underline{y}_h\|_{\mathcal{H}}^2}.$$

Proof. If exact integration is used and $\rho = \text{const}$, then $m_h(\underline{y}_h, \underline{y}_h) = \rho \|\underline{y}_h\|_{\mathcal{H}}^2$ and $\|\underline{y}_h\|_{\mathcal{Y}_h} = \|\underline{y}_h\|_{\mathcal{H}}$. Consequently, we can simplify Eq. (4.30) to obtain the result of the corollary. □

Remark We observe that the CFL condition (4.33) is well-defined for $\alpha > 1/(4\,\rho)$. Moreover, it is slightly worse than condition (4.20), since

$$\frac{4\,\alpha\,\rho - 1}{4\,\alpha\,\rho} \leq 1$$

in the allowed range for α. Nevertheless, this condition depends only on the space discretisation and on the tensor $\underline{\underline{\mathbf{C}}}$ and the density ρ. Therefore, it is still very advantageous with respect to condition (4.26).

As a final comment, note that if the scheme (QIPnh) is stable, i.e. (4.15) holds and Δt is sufficiently small, then

$$\sup_{n\in\{0,1,..,N\}} \mathcal{E}_p^{n+\frac{1}{2}} \leq C,$$

with C independent of Δt. Therefore, denoting $\tilde{\underline{y}}_{\alpha,h}^{n+\frac{1}{2}} = (\tilde{\underline{y}}_{\alpha,h}^{n+1} + \tilde{\underline{y}}_{\alpha,h}^{n})/2$, we have

$$\sup_{n\in\{0,1,..,N\}} \big(Q_h \tilde{\underline{y}}_{\alpha,h}^{n+\frac{1}{2}}, \tilde{\underline{y}}_{\alpha,h}^{n+\frac{1}{2}}\big)_{\mathcal{H}} \leq \alpha\, C\, \Delta t^2.$$

As a consequence, there exists another constant C independent of Δt such that, by definition of Q_h, we have

$$\sup_{n\in\{0,1,..,N\}} \left\| (C_h\, C_h^T)^{-\frac{1}{2}} B_h \tilde{\underline{y}}_{\alpha,h}^{n+\frac{1}{2}} \right\|_{\mathcal{H}} \leq C\, \Delta t.$$

This shows that $B_h \tilde{\underline{y}}_{\alpha,h}^{n+\frac{1}{2}}$ goes to 0 with Δt, but for a weak norm that involves the inverse Laplace operator.

4.5 Two-dimensional numerical convergence results

In order to perform the numerical validation of the properties of scheme (QIPnh), we consider as a model problem the elastic wave propagation in a 2D medium, and we take into account different constitutive laws. In the interest of clarity, we provide the physical and numerical parameters used for the simulations with their original units of measure. For the sake of simplicity, we assume constant density $\rho = 1050\,\mathrm{kg\,m^{-1}}$ and homogeneous Dirichlet boundary conditions on all the boundaries of the domain. Space discretisation is performed by high-order Spectral Finite Elements (of order 7 for the displacement, 6 for the pressure). The computational grid is a $1\,\mathrm{m}^2$ square composed of N uniform elements of size $h = 1/N$ in each direction. Concerning time discretisation, we adopt the discretisation introduced in scheme (QIPnh) with penalisation coefficient $\alpha = 1/3\rho$ and we choose the time step as

$$\Delta t^2 = (1-\varepsilon)\left\| M_h^{-1} A_h \right\|^{-1}, \tag{4.34}$$

where we set $\varepsilon = 0.2$ to account for the fact that the expression above is an approximation of the CFL condition given by Eq. (4.30) when considering that $\rho\|\underline{y}_h\|_{\mathcal{Y}_h}^2 = m_h(\underline{y}_h, \underline{y}_h)$ and accounting for the approximation of the norm in (4.34) by a power iteration algorithm. Note that the value of this parameter is not tight: $\varepsilon = 0$ also gives stable results. For each iteration of this scheme, the scalar pressure field (4.13) is computed by means of an in-house fast solver for the Poisson problem, based on Higher-Order Fourier Transform. Note that even when the medium is heterogeneous, the problem for the pressure wave

remains homogeneous, due to incompressibility.
Henceforth, we present a space/time convergence analysis. To do so, we test scheme (QIPnh) against the pure incompressible scheme (IMnh) for different values of N in $[10, 40]$. For each time step of each simulation, the pressure field is evaluated in Eq. (4.10) by means of the Conjugate Gradient method, with euclidian norm of the residue lower than $1e-14$ and maximum number of iterations $N_{\text{iter}} = 2000$. The source term considered is a standard Gaussian profile in space multiplied by a profile in time corresponding to the first derivative of the Gaussian function. In greater detail, it reads

$$f(x,y,t) \coloneqq -\frac{2\,t}{\sigma_t^2}\exp^{-\frac{(t-t_{pulse})^2}{\sigma_t^2}} \cdot 100\exp^{-\left(\frac{(x-x_F)^2}{\sigma_s^2}+\frac{(y-y_F)^2}{\sigma_s^2}\right)}, \tag{4.35}$$

with centre $(x_F, y_F) = (0.5, 0.5)\,\text{m}$, covariance $\sigma_s^2 = 0.0005$, $\sigma_t^2 = 0.0005$ and mean $t_{pulse} = 0.6\,\text{s}$. We consider several constitutive laws, and we present four convergence curves for each example, that illustrate the error in $L^2(\Omega_T)$, $C^0(L^2(\Omega))$, $L^2(H^1(\Omega))$ and $C^0(H^1(\Omega))$ norms, respectively.

4.5.1 Homogeneous isotropic material

As a first example, we study a homogenous isotropic medium. A standard constitutive law for this type of medium is

$$\underline{\underline{\mathbf{C}}}\,\underline{\underline{\varepsilon}}(\underline{y}) \coloneqq \mu\,\underline{\underline{\varepsilon}}(\underline{y}). \tag{4.36}$$

with shear modulus $\mu = 80\,\text{kPa}$. Note that from Eq. (4.36) we retrieve in (QI) the standard elastodynamic problem for isotropic law. The convergence curves in Figure 4.1 and Figure 4.2 confirm that second-order convergence is preserved in $L^2(\Omega_T)$. Note that it is slightly degraded and L^∞ in time and L^2 norm in space. Furthermore, the error does not vary (or it varies marginally in $L^\infty(L^2(\Omega))$) if we consider a larger t_{end} such that the wave has reached the boundaries of the computational domain. If we consider H^1 norm in space, the error is slightly degraded with respect to the previous norms. Moreover, when we consider a larger time interval (so that we take into account the effects at the boundaries), the error increases. Figures 4.3 illustrates three snapshots at $t = 1.0\,\text{s}$, $t = 2.\,\text{s}$ and $t = 2.65\,\text{s}$, of the displacement. The mesh is composed by $N = 40$ elements in each direction. Furthermore, Figure 4.4 depicts the time evolution of the displacement in three locations, indicated in Figure 4.3. Figures 4.5 and 4.6 are related to the acceleration. We do not plot the results concerning the velocity, since they do not provide relevant information. Note that the time evolution profiles in x and y direction of the location denoted P_1 correspond to the profiles in y and x direction of the location denoted P_2, that is the symmetric to P_1, due to isotropy. Concerning the pressure, Figure 4.7 indicates that this term corresponds to a correction mostly at the boundaries of the medium. In addition, symmetric points correspond to the same pressure time evolution, as depicted in Figure 4.8.

4.5.2 Heterogeneous transverse isotropic material

In the perspective of an application to elastography imaging of biological tissues, we need to analyse more complex constitutive laws. For example, striated muscle tissue can be modelled as a transverse isotropic medium, i.e. there exists, at every point, a privileged direction represented by the unit vector $\underline{\tau_1}$, related to the collagen fibre. A simple transverse

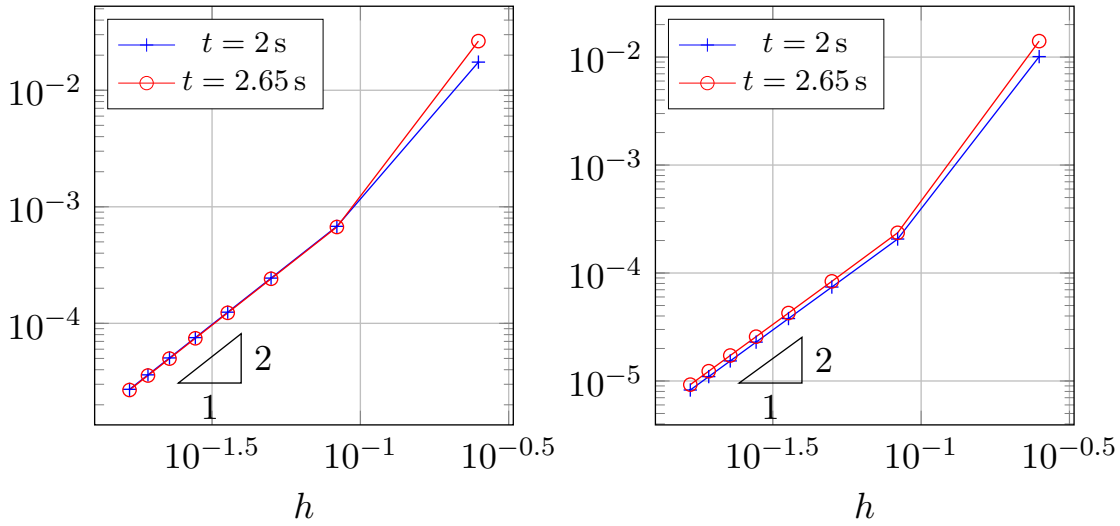

Figure 4.1 – Convergence of scheme (QIP) w.r.t. the space step h, for final time $t = 2\,\mathrm{s}$, $t = 2.65\,\mathrm{s}$ for a homogeneous isotropic material. Left: Relative $L^2(\Omega_T)$-error on the displacement. Right: Relative $L^\infty(L^2(\Omega))$-error on the displacement.

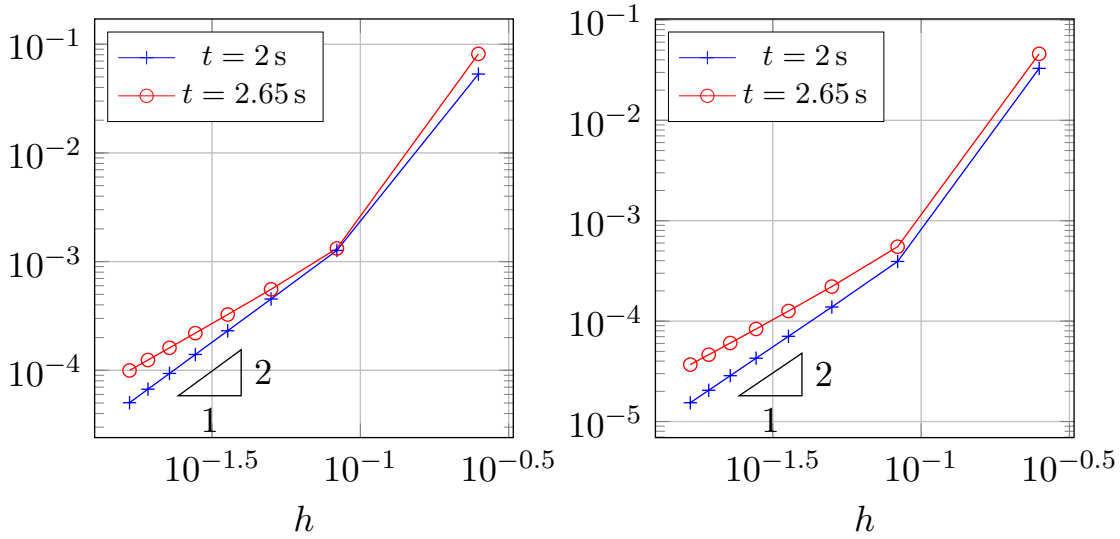

Figure 4.2 – Convergence of scheme (QIP) w.r.t. the space step h, for final time $t = 2\,\mathrm{s}$, $t = 2.65\,\mathrm{s}$ for a homogeneous isotropic material. Left: Relative $L^2(H^1(\Omega))$-error on the displacement. Right: Relative $L^\infty(H^1(\Omega))$-error on the displacement.

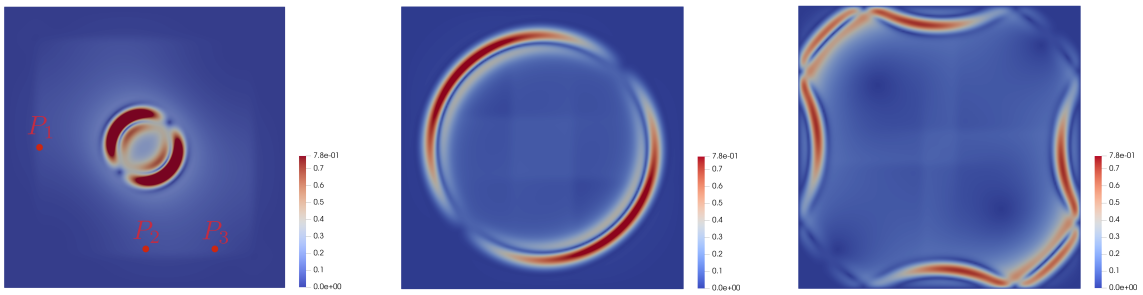

(a) $t = 1.\,\mathrm{s}$ (b) $t = 2.\,\mathrm{s}$ (c) $t = 2.65\,\mathrm{s}$

Figure 4.3 – Elastic wave propagation in a homogeneous isotropic medium (absolute value of the displacement field).

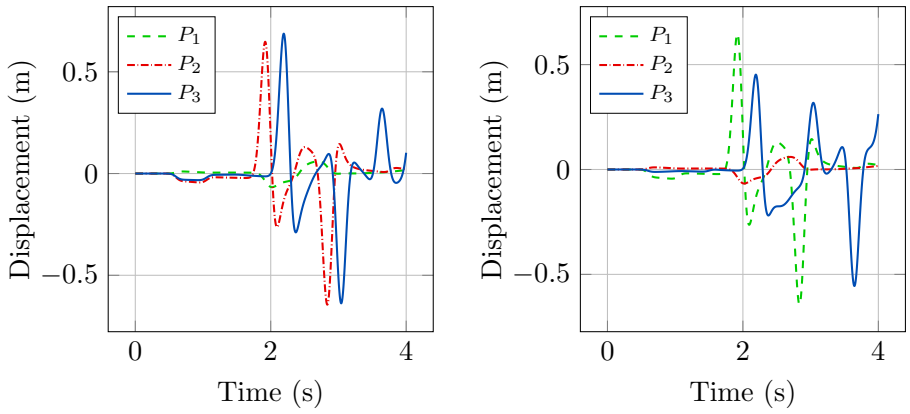

Figure 4.4 – Time evolution of the displacement field in a homogeneous isotropic medium in three locations (See Figure 4.3 for locations). Left : x direction. Right: y direction.

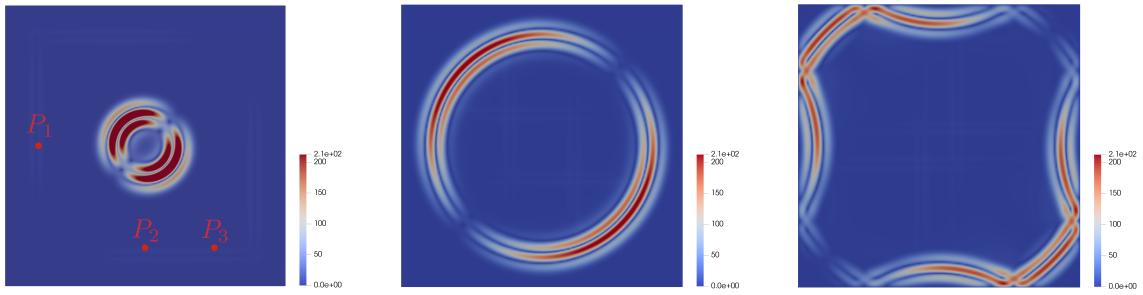

(a) $t = 1.\,\mathrm{s}$ (b) $t = 2.\,\mathrm{s}$ (c) $t = 2.65\,\mathrm{s}$

Figure 4.5 – Elastic wave propagation in a homogeneous isotropic medium (absolute value of the acceleration field).

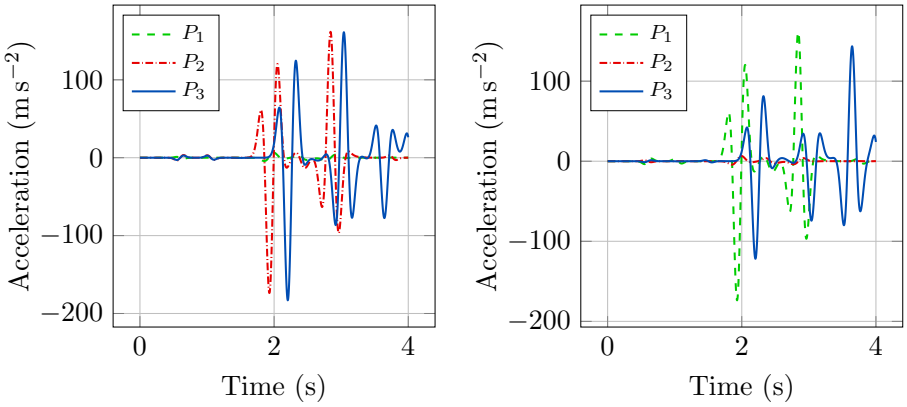

Figure 4.6 – Time evolution of the acceleration field in a homogeneous isotropic medium in three locations (See Figure 4.5 for locations). Left : x direction. Right: y direction.

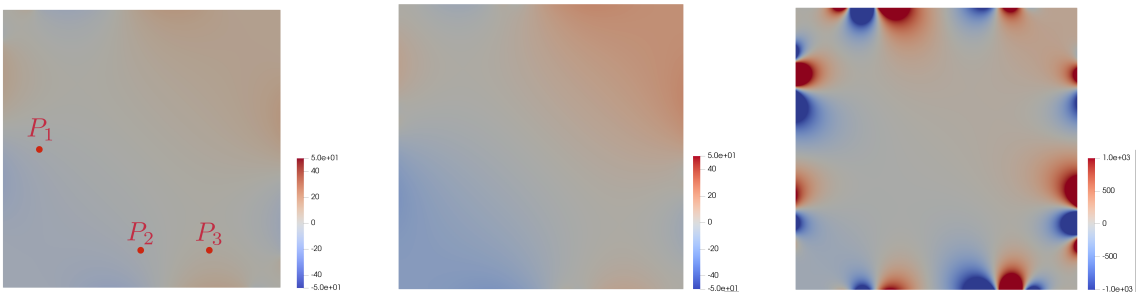

(a) $t = 1.\,\mathrm{s}$ (b) $t = 2.\,\mathrm{s}$ (c) $t = 2.65\,\mathrm{s}$

Figure 4.7 – Elastic wave propagation in a homogeneous isotropic medium (absolute value of the pressure field).

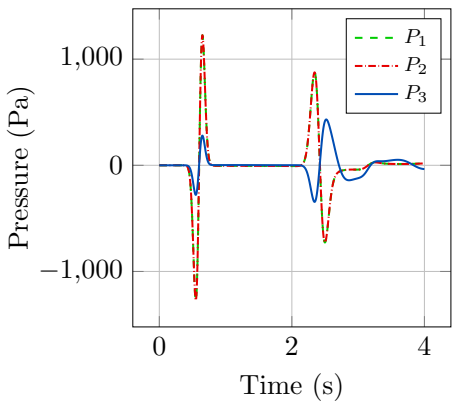

Figure 4.8 – Time evolution of the pressure field in a homogeneous isotropic medium in three locations (See Figure 4.7 for locations).

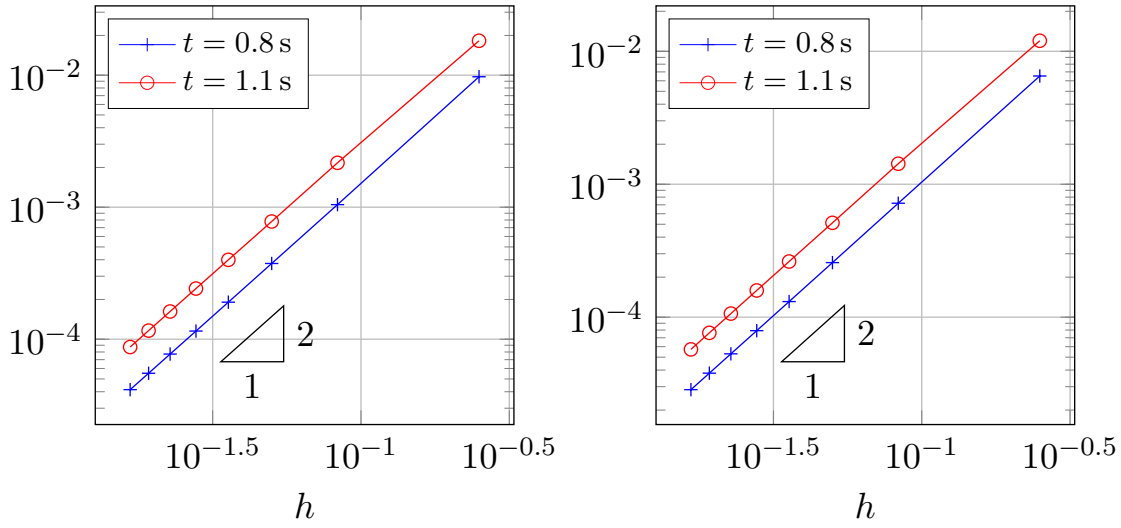

Figure 4.9 – Convergence of scheme (QIP) w.r.t. the space step h, for final time $t = 0.8\,\mathrm{s}$, $t = 1.1\,\mathrm{s}$ for a heterogeneous transverse isotropic material. Left: Relative $L^2(L^2(\Omega))$-error on the displacement. Right: Relative $L^\infty(L^2(\Omega))$-error on the displacement.

isotropic law, inspired by [Chapelle et al., 2012] is

$$\underline{\underline{\mathbf{C}}}\,\underline{\underline{\varepsilon}}(\underline{y}) \coloneqq \mu\,\underline{\underline{\varepsilon}}(\underline{y}) + \eta\left(\frac{1}{9}tr\big(\underline{\underline{\varepsilon}}(\underline{y})\big)\,\underline{\underline{\mathbb{1}}} - \frac{1}{3}tr\big(\underline{\underline{\varepsilon}}(\underline{y})\big)\,\underline{\tau_1}\otimes\underline{\tau_1} - \frac{1}{3}(\underline{\tau_1}\cdot\underline{\underline{\varepsilon}}(\underline{y})\cdot\underline{\tau_1})\,\underline{\underline{\mathbb{1}}} + (\underline{\tau_1}\cdot\underline{\underline{\varepsilon}}(\underline{y})\cdot\underline{\tau_1})\,\underline{\tau_1}\otimes\underline{\tau_1}\right), \quad (4.37)$$

with $\mu = 80\,\mathrm{kPa}$, $\eta = 3400\,\mathrm{kPa}$. In what follows, we present the results for a transverse isotropic medium in which the fibre direction $\underline{\tau_1}$ varies linearly along the direction y. This configuration is inspired by the structure of myocardial tissue. In fact, it has been experimentally validated that muscle fibres are arranged in laminar structures, denoted sheets, of three to four muscle fibres in the thickness, that are oriented transversely to the heart wall [Streeter et al., 1969; Lee et al., 2012]. Moreover, the fibre orientation in human left ventricle myocardium changes linearly throughout the wall thickness, from $-60°$ close to the epicardium to $+60°$ near the endocardium [Sommer et al., 2015]. In order to model such a material, we consider an orientation of $\underline{\tau_1}$ varying linearly from $-60°$ at the bottom of the domain ($y = 0$) to $+60°$ at the top of the domain ($y = 1$). The resulting medium is highly heterogeneous. Figures 4.9 and 4.10 show that the error worsens moderately in transverse isotropic media w.r.t. isotropic media. In addition, the order of convergence remains two for L^2 norm in space, and it is slightly degraded in $L^2(H^1(\Omega))$ and in $L^\infty(H^1(\Omega))$. Figure 4.11 illustrates three snapshots at $t = 0.5\,\mathrm{s}$, $t = 0.75\,\mathrm{s}$ and $t = 1.1\,\mathrm{s}$ of the displacement field., respectively. The mesh is composed by $N = 40$ elements in each direction. We do not provide the results concerning the velocity and the acceleration, since they not provide additional information. Note that the pressure field gives a significant contribution also in the interior of the domain, as it is illustrated in Figure 4.12, due to anisotropy.

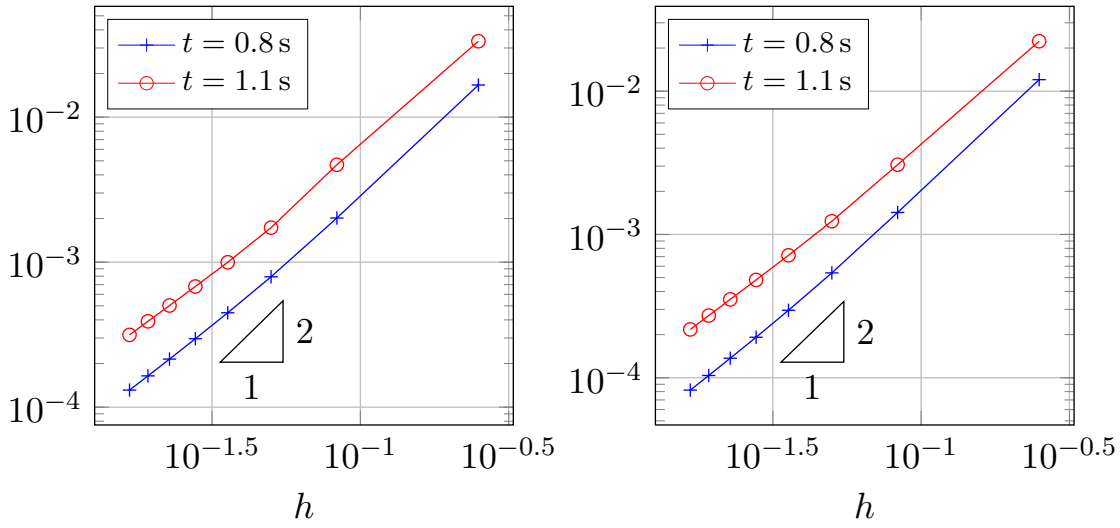

Figure 4.10 – Convergence of scheme (QIP) w.r.t. the space step h, for final time $t = 0.8\,\mathrm{s}$, $t = 1.1\,\mathrm{s}$ for a heterogeneous transverse isotropic material. Left: $L^2(H^1(\Omega))$-error on the displacement. Right: $L^\infty(H^1(\Omega))$-error on the displacement.

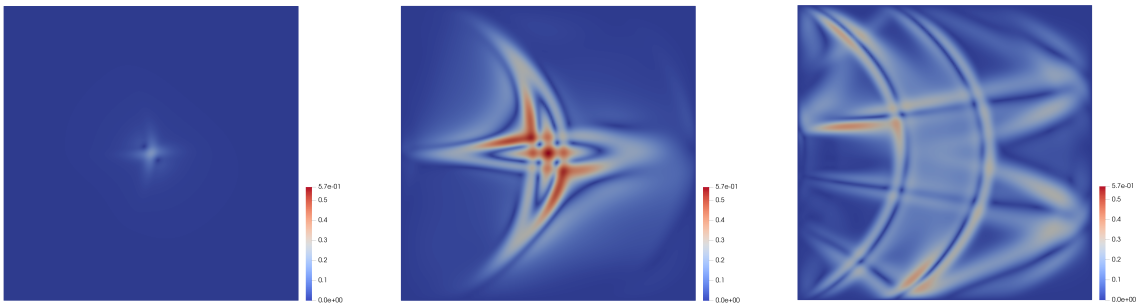

(a) $t = 0.5\,\mathrm{s}$ (b) $t = 0.75\,\mathrm{s}$ (c) $t = 1.1\,\mathrm{s}$

Figure 4.11 – Elastic wave propagation in a heterogeneous transverse isotropic medium (absolute value of the displacement field).

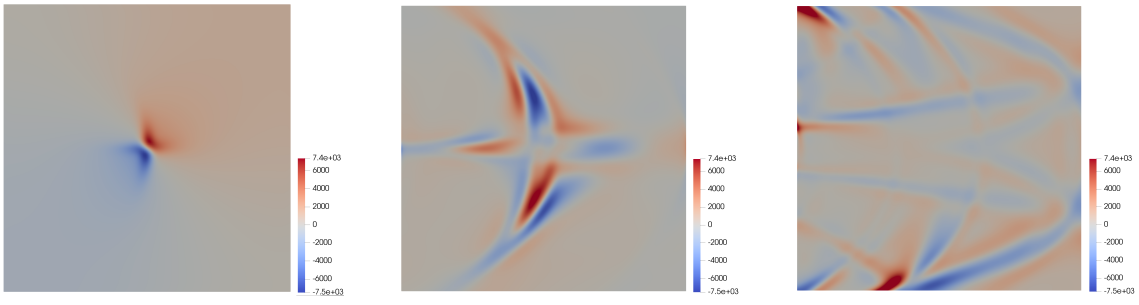

(a) $t = 0.5\,\mathrm{s}$ (b) $t = 0.75\,\mathrm{s}$ (c) $t = 1.1\,\mathrm{s}$

Figure 4.12 – Elastic wave propagation in a heterogeneous transverse isotropic medium (absolute value of the pressure field).

4.6 Approximations with improved accuracy by post-processing

It is possible to obtain more accurate approximations of the purely incompressible problem by post-processing of the solutions obtained with scheme (QIPnh). The strategy can be formulated easily at the continuous level. Recall that we have the decomposition (4.4)

$$\tilde{\underline{y}}_\alpha = \underline{y} + \alpha\tilde{\underline{y}}_1 + \alpha^2\tilde{\underline{y}}_2 + \cdots$$

and assume now that one can compute $\tilde{\underline{y}}_\alpha$ for different values of α, for instance $\alpha = \alpha_0$ and $\alpha = \alpha_1$. Then, by linear combination, we can write

$$\tilde{\underline{y}}_1 \simeq (\alpha_0 - \alpha_1)^{-1}\big(\tilde{\underline{y}}_{\alpha_0} - \tilde{\underline{y}}_{\alpha_1}\big),$$

and $\underline{y}$ can be approximated by

$$\underline{y} \simeq (1-\delta)(\tilde{\underline{y}}_{\alpha_0} - \alpha_0\tilde{\underline{y}}_1) + \delta\,(\tilde{\underline{y}}_{\alpha_1} - \alpha_1\tilde{\underline{y}}_1)$$

for any $\delta \in \mathbb{R}$. We apply the same principle to the discrete unknown $\{\tilde{\underline{y}}^n_{\alpha,h}\}$. We assume that

$$\tilde{\underline{y}}^n_{\alpha,h} = \underline{y}^n_h + \alpha\Delta t^2\tilde{\underline{y}}^n_{h,1} + \alpha^2\Delta t^4\tilde{\underline{y}}^n_{h,2} + \cdots$$

and solve scheme (QIPnh) for several values of $\alpha = \alpha_i$. We denote by $\tilde{\underline{y}}_{\alpha_i,h}$ the obtained solution. Then, a more accurate approximation of $\underline{y}^n_h$ – that we denote $\tilde{\underline{y}}^n_h$ – can be recovered from the first or second corrector by solving locally in space and time the algebraic system

$$\begin{pmatrix} 1 & \alpha_0 \\ 1 & \alpha_1 \end{pmatrix}\begin{pmatrix} \tilde{\underline{y}}^n_h \\ \Delta t^2\tilde{\underline{y}}^n_{h,1} \end{pmatrix} = \begin{pmatrix} \tilde{\underline{y}}^n_{\alpha_0,h} \\ \tilde{\underline{y}}^n_{\alpha_1,h} \end{pmatrix} \quad \text{or} \quad \begin{pmatrix} 1 & \alpha_0 & \alpha_0^2 \\ 1 & \alpha_1 & \alpha_1^2 \\ 1 & \alpha_2 & \alpha_2^2 \end{pmatrix}\begin{pmatrix} \tilde{\underline{y}}^n_h \\ \Delta t^2\tilde{\underline{y}}^n_{h,1} \\ \Delta t^4\tilde{\underline{y}}^n_{h,2} \end{pmatrix} = \begin{pmatrix} \tilde{\underline{y}}^n_{\alpha_0,h} \\ \tilde{\underline{y}}^n_{\alpha_1,h} \\ \tilde{\underline{y}}^n_{\alpha_2,h} \end{pmatrix}. \tag{4.38}$$

This process can be trivially generalised for an arbitrary number of correctors. However, note that, even though the system must be solved two or three times, the computation of the $\tilde{\underline{y}}_{\alpha_i,h}$ can be done completely in parallel. Furthermore, in order to solve the problem with different values of α with the same time step without generating instability, one should choose $\alpha_{i+1} > \alpha_i > \alpha_0$, and compute the stability condition based on the value of α_0. In addition, the system to solve has the form of a Vandermonde system

$$\begin{pmatrix} 1 & \alpha_0 & \alpha_0^2 & \cdots \\ 1 & \alpha_1 & \alpha_1^2 & \cdots \\ 1 & \alpha_2 & \alpha_2^4 & \cdots \\ \cdots & \cdots & \cdots & \cdots \end{pmatrix}\begin{pmatrix} \tilde{\underline{y}}^n_h \\ \Delta\tilde{t}^2\underline{y}^n_{h,1} \\ \Delta\tilde{t}^4\underline{y}^n_{h,2} \\ \cdots \end{pmatrix} = \begin{pmatrix} \tilde{\underline{y}}^n_{\alpha_0,h} \\ \tilde{\underline{y}}^n_{\alpha_1,h} \\ \tilde{\underline{y}}^n_{\alpha_2,h} \\ \cdots \end{pmatrix},$$

and is invertible when all the α_i are distinct. Moreover, $\tilde{\underline{y}}^n_h$ is a linear combination of the $\tilde{\underline{y}}^n_{\alpha_i,h}$ with coefficient independent of Δt. We expect, therefore, that all the convergence properties proved for scheme (QIPnh) are valid for the approximation $\tilde{\underline{y}}^n_h$. We have reiterated the test case presented in (4.5.2) with the choice $\alpha_0 = 1/3\rho$, $\alpha_1 = 2/5\rho$ and $\alpha_2 = 1/2\rho$. In more detail, we have compared the solution obtained with penalisation coefficient α_0 with approximations obtained by linear combination (by resolution of system (4.38)) of two solutions corresponding to α_0 and α_1, or three solutions associated with α_0, α_1 and α_2, respectively. The error obtained is shown in Figure 4.13. We observe that the approximation accuracy is improved by using more solutions of the problem (QIPnh). In particular, the more solutions are considered, the better is the accuracy in both $L^\infty(L^2(\Omega))$ norm and $L^\infty(H^1(\Omega))$ norm. Furthermore, note that the order of convergence corresponds to the number of combinations used, as shown in Figure 4.14.

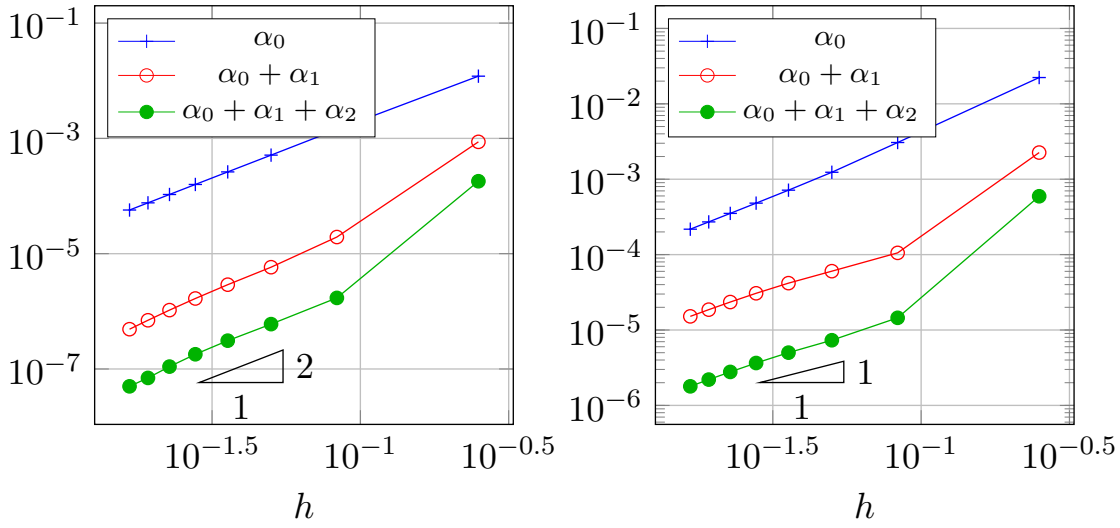

Figure 4.13 – Convergence of scheme (QIP) w.r.t. the space step h, for final time $t = 1.1\,\mathrm{s}$ for a heterogeneous transverse isotropic material. Comparison between the original scheme (with penalisation coefficient α_0) and improved extensions of the scheme solution obtained by linear combination of two solutions corresponding to α_0 and α_1, or three solutions associated with α_0, α_1 and α_2, respectively. Left: $L^\infty(L^2(\Omega))$-error on the displacement. Right: $L^\infty(H^1(\Omega))$-error on the displacement.

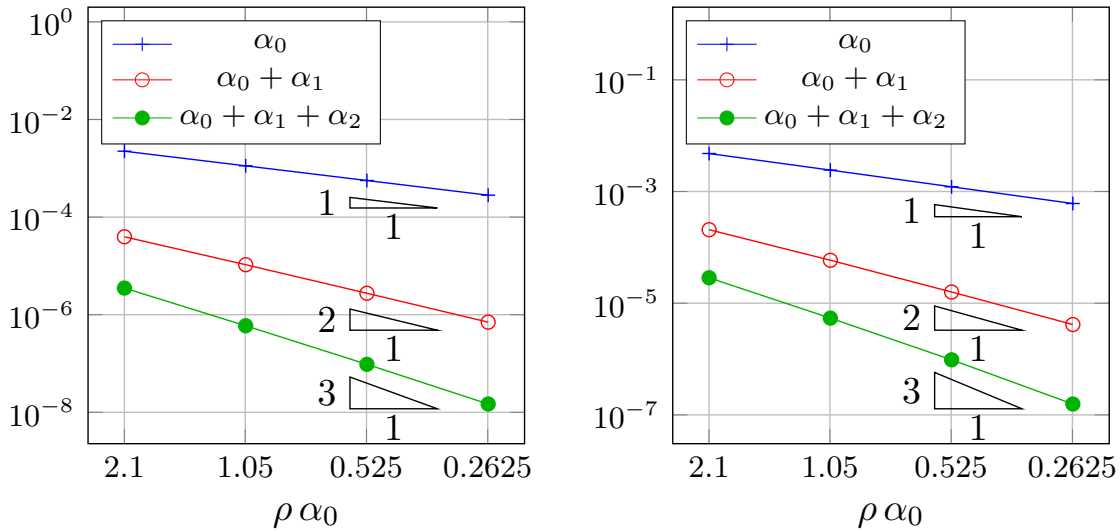

Figure 4.14 – Comparison for different values of α_0, for final time $t = 1.1\,\mathrm{s}$, $N = 12$ elements and for a heterogeneous transverse isotropic material. $\alpha_1 = 1.025 \cdot \alpha_0$. $\alpha_2 = 1.05 \cdot \alpha_0$. Comparison between the original scheme (with penalisation coefficient α_0) and improved extensions of the scheme solution obtained by linear combination of two solutions corresponding to α_0 and α_1, or three solutions associated with α_0, α_1 and α_2, respectively. Left: $L^\infty(L^2(\Omega))$-error on the displacement. Right: $L^\infty(H^1(\Omega))$-error on the displacement.

4.7 A three-dimensional test case

The main application we have in mind is the propagation of elastic waves in nearly-incompressible biological tissues in the context of ultrasound transient elastography [Sarvazyan et al., 1998; Bercoff et al., 2004]. Therefore, by way of illustration, we propose here a three-dimensional test case, inspired by elastography imaging of the myocardial tissue. Note that, due to dissipation, shear waves are fully attenuated in a few wavelength distance, i.e. some millimetres from the focal point of the ultrasonic beam [Sarvazyan et al., 2010]. As a consequence, we can consider a small region of interest and a simple geometry. However, there is a need for a fine space discretisation, compatible with the wavelength of shear waves.
In this example we consider a transverse isotropic domain (defined by Eq. (4.37)), with fibre direction $\underline{\tau_1}$ oriented in the xy-plane and varying linearly along the direction z from $-60°$ w.r.t. the x-axis at the bottom of the domain ($z = 0$) to $+60°$ at the top of the domain ($z = 0.02\,\mathrm{m}$). The geometry of the domain is a parallelepiped of length $0.04\,\mathrm{m}$ in x and y directions, and $0.02\,\mathrm{m}$ in z direction. This configuration represents an approximation of a region of interest in the left myocardium, selected in the anterior wall at the middle ventricular level. Density is set equal to $\rho = 1050\,\mathrm{kg\,m^{-1}}$ and homogeneous Neumann boundary conditions are imposed on all the boundaries of the domain. High-order Spectral Finite Elements (of order 7 for the displacement, 6 for the pressure) are used for the space discretisation. The computational grid is composed of 24 uniform elements of size $h = 1/24$ in each direction, for a total of 14480427 degrees of freedom (DOF) for the displacement field, and 3048625 DOF for the pressure field. We adopt the time discretisation introduced in scheme (QIPnh) with penalisation coefficient $\alpha = 1/3\rho$ and we choose the time step as in Eq. (4.34), with $\varepsilon = 0.2$, as in Section 4.5. For each time step of the scheme, the Poisson problem for the scalar pressure field (4.13) is computed by means of our in-house fast solver based on Higher-Order Fourier Transform, as in Section 4.5. In this way, the time step used in the explicit time discretisation is constrained by the shear wave velocity only. Figure 4.15 depicts four snapshots of the solution at different time steps.
Note that we have also considered an improved approximation by post-processing of the problem, by combination of the solutions associated with $\alpha_0 = 1/3\rho$ and $\alpha_1 = 2/5\rho$, respectively, considering $N = 24$ elements in each direction. Since we have not noticed a qualitative change in the behaviour of the solution, we are confident that the observed solution is a good approximation of the pure incompressible problem. Note also that, due to the resolution of the Poisson problem by our in-house fast solver, we have drastically reduced the computational cost of the scheme. In particular, the resolution of 1600 time steps of the problem on a 12-cores workstation (cores at 2.7 GHz and 64 GB of RAM at 1867 MHz), considering higher-order extension of the scheme (i.e. computation of the two solutions corresponding to α_0 and α_1) takes around 4 hours.

4.8 Conclusions

In this chapter we have outlined a new numerical scheme that is suitable for approximating elastic wave propagation in incompressible media, based on a mixed explicit/implicit time discretisation. We have demonstrated that the time step of the resulting algorithm is only constrained by the shear wave velocity, and it is not limited by the enforcement of incompressibility (as it is the case for fully-explicit time discretisation). Furthermore, if effective

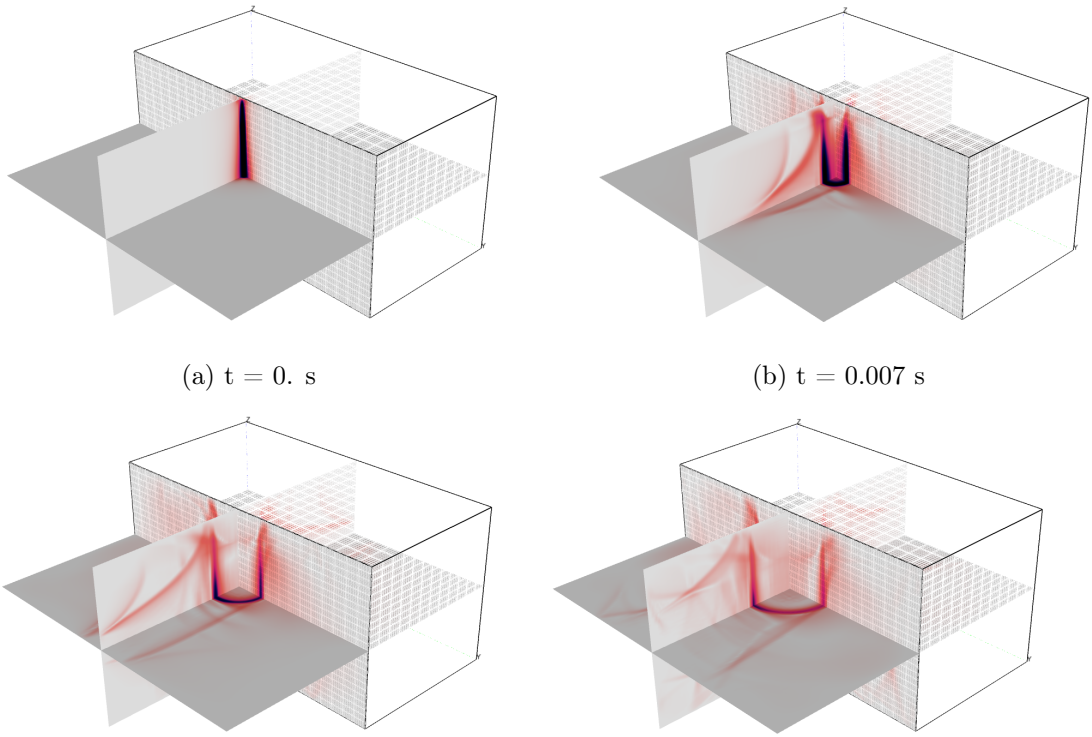

(a) t = 0. s (b) t = 0.007 s

(c) t = 0.014 s (d) t = 0.02 s

Figure 4.15 – Elastic wave propagation in a three-dimensional transverse isotropic medium (absolute value of the displacement field).

methods are adopted for explicit time-discretisation, our algorithm only entails at each time step one resolution of a scalar Poisson problem – that can be performed by various, efficient algorithms – and few matrix-vector multiplications for the explicit part of the scheme. Moreover, we have presented a two-dimensional numerical test case, to demonstrate the favourable convergence properties of the scheme, and one three-dimensional example, to illustrate a realistic application to elastography imaging. A theoretical demonstration of second-order convergence in time of the scheme is out of the scope of this chapter, and will be provided in Chapter 5.

Bibliography

Bathe, K.-J. [2006], *Finite element procedures*, Klaus-Jurgen Bathe.

Bercoff, J., Tanter, M. and Fink, M. [2004], 'Supersonic shear imaging: a new technique for soft tissue elasticity mapping', *IEEE transactions on ultrasonics, ferroelectrics, and frequency control* **51**(4), 396–409.

Boffi, D., Brezzi, F., Fortin, M. et al. [2013], *Mixed finite element methods and applications*, Vol. 44, Springer.

Brezzi, F. and Bathe, K.-J. [1990], 'A discourse on the stability conditions for mixed finite element formulations', *Computer methods in applied mechanics and engineering* **82**(1-3), 27–57.

Brezzi, F. and Falk, R. S. [1991], 'Stability of higher-order Hood–Taylor methods', *SIAM Journal on Numerical Analysis* **28**(3), 581–590.

Brezzi, F. and Fortin, M. [2012], *Mixed and hybrid finite element methods*, Vol. 15, Springer Science & Business Media.

Brezzi, F. and Pitkäranta, J. [1984], On the stabilization of finite element approximations of the Stokes equations, *in* 'Efficient solutions of elliptic systems', Springer, pp. 11–19.

Brooks, A. N. and Hughes, T. J. [1982], 'Streamline upwind/Petrov-Galerkin formulations for convection dominated flows with particular emphasis on the incompressible navier-stokes equations', *Computer methods in applied mechanics and engineering* **32**(1-3), 199–259.

Chapelle, D. and Bathe, K.-J. [1993], 'The inf-sup test', *Computers & structures* **47**(4-5), 537–545.

Chapelle, D., Le Tallec, P., Moireau, P. and Sorine, M. [2012], 'An energy-preserving muscle tissue model: formulation and compatible discretizations', *International Journal for Multiscale Computational Engineering* **10**(2), 189–211.

Chiumenti, M., Valverde, Q., De Saracibar, C. A. and Cervera, M. [2002], 'A stabilized formulation for incompressible elasticity using linear displacement and pressure interpolations', *Computer methods in applied mechanics and engineering* **191**(46), 5253–5264.

Chorin, A. J. [1968], 'Numerical solution of the Navier–Stokes equations', *Mathematics of computation* **22**(104), 745–762.

Chorin, A. J. [1969], 'On the convergence of discrete approximations to the Navier–Stokes equations', *Mathematics of computation* **23**(106), 341–353.

Cohen, G. [2001], *Higher-Order Numerical Methods for Transient Wave Equations*, Scientific Computation, Springer Berlin Heidelberg.

Cohen, G. and Fauqueux, S. [2005], 'Mixed spectral finite elements for the linear elasticity system in unbounded domains', *SIAM Journal on Scientific Computing* **26**(3), 864–884.

Durufle, M., Grob, P. and Joly, P. [2009], 'Influence of Gauss and Gauss-Lobatto quadrature rules on the accuracy of a quadrilateral finite element method in the time domain', *Numer. Methods Partial Differential Equations* **25**(3), 526–551.

Franca, L. P. and Frey, S. L. [1992], 'Stabilized finite element methods: Ii. the incompressible Navier–Stokes equations', *Computer Methods in Applied Mechanics and Engineering* **99**(2-3), 209–233.

Franca, L. P., Hughes, T. J., Loula, A. F. and Miranda, I. [1988], 'A new family of stable elements for nearly incompressible elasticity based on a mixed Petrov-Galerkin finite element formulation', *Numerische Mathematik* **53**(1-2), 123–141.

Guermond, J.-L., Minev, P. and Shen, J. [2006], 'An overview of projection methods for incompressible flows', *Computer methods in applied mechanics and engineering* **195**(44-47), 6011–6045.

Guermond, J.-L. and Quartapelle, L. [1998*a*], 'On stability and convergence of projection methods based on pressure Poisson equation', *International Journal for Numerical Methods in Fluids* **26**(9), 1039–1053.

Guermond, J.-L. and Quartapelle, L. [1998*b*], 'On the approximation of the unsteady Navier–Stokes equations by finite element projection methods', *Numerische Mathematik* **80**(2), 207–238.

Heywood, J. G. and Rannacher, R. [1982], 'Finite element approximation of the nonstationary Navier–Stokes problem. i. regularity of solutions and second-order error estimates for spatial discretization', *SIAM Journal on Numerical Analysis* **19**(2), 275–311.

Heywood, J. G. and Rannacher, R. [1986], 'Finite element approximation of the nonstationary Navier–Stokes problem, part ii: Stability of solutions and error estimates uniform in time', *SIAM journal on numerical analysis* **23**(4), 750–777.

Heywood, J. G. and Rannacher, R. [1988], 'Finite element approximation of the nonstationary Navier–Stokes problem iii. smoothing property and higher order error estimates for spatial discretization', *SIAM Journal on Numerical Analysis* **25**(3), 489–512.

Heywood, J. G. and Rannacher, R. [1990], 'Finite-element approximation of the nonstationary Navier–Stokes problem. part iv: Error analysis for second-order time discretization', *SIAM Journal on Numerical Analysis* **27**(2), 353–384.

Hughes, T. J. [1980], 'Generalization of selective integration procedures to anisotropic and nonlinear media', *International Journal for Numerical Methods in Engineering* **15**(9), 1413–1418.

Hughes, T. J. [2012], *The finite element method: linear static and dynamic finite element analysis*, Courier Corporation.

Hughes, T. J., Franca, L. P. and Balestra, M. [1986], 'A new finite element formulation for computational fluid dynamics: V. circumventing the Babuška-Brezzi condition: A stable Petrov-Galerkin formulation of the Stokes problem accommodating equal-order interpolations', *Computer Methods in Applied Mechanics and Engineering* **59**(1), 85–99.

Joly, P. [2008], *The mathematical model for elastic wave propagation. In "Effective Computational Methods for Wave Propagation"*, Numerical Insights, CRC Press.

Klaas, O., Maniatty, A. and Shephard, M. S. [1999], 'A stabilized mixed finite element method for finite elasticity.: Formulation for linear displacement and pressure interpolation', *Computer Methods in Applied Mechanics and Engineering* **180**(1-2), 65–79.

Komatitsch, D. and Vilotte, J.-P. [1998], 'The spectral element method: an efficient tool to simulate the seismic response of 2d and 3d geological structures', *Bulletin of the seismological society of America* **88**(2), 368–392.

Lahiri, S. K., Bonet, J., Peraire, J. and Casals, L. [2005], 'A variationally consistent fractional time-step integration method for incompressible and nearly incompressible Lagrangian dynamics', *International journal for numerical methods in engineering* **63**(10), 1371–1395.

Lee, W.-N., Pernot, M., Couade, M., Messas, E., Bruneval, P., Bel, A., Hagege, A. A., Fink, M. and Tanter, M. [2012], 'Mapping myocardial fiber orientation using echocardiography-based shear wave imaging', *IEEE transactions on medical imaging* **31**(3), 554–562.

Malkus, D. S. and Hughes, T. J. [1978], 'Mixed finite element methods. reduced and selective integration techniques: a unification of concepts', *Computer Methods in Applied Mechanics and Engineering* **15**(1), 63–81.

Maniatty, A. M., Liu, Y., Klaas, O. and Shephard, M. S. [2002], 'Higher order stabilized finite element method for hyperelastic finite deformation', *Computer methods in applied mechanics and engineering* **191**(13-14), 1491–1503.

Masud, A. and Truster, T. J. [2013], 'A framework for residual-based stabilization of incompressible finite elasticity: Stabilized formulations and F methods for linear triangles and tetrahedra', *Computer Methods in Applied Mechanics and Engineering* **267**, 359–399.

Neto, E., Pires, F. and Owen, D. [2005], 'F-bar-based linear triangles and tetrahedra for finite strain analysis of nearly incompressible solids. part i: formulation and benchmarking', *International Journal for Numerical Methods in Engineering* **62**(3), 353–383.

Orzechowski, G. and Frączek, J. [2015], 'Nearly incompressible nonlinear material models in the large deformation analysis of beams using ANCF', *Nonlinear Dynamics* **82**(1-2), 451–464.

Quarteroni, A. and Valli, A. [1994], *Numerical Approximation of Partial Differential Equations*, Springer.

Rossi, S., Abboud, N. and Scovazzi, G. [2016], 'Implicit finite incompressible elastodynamics with linear finite elements: A stabilized method in rate form', *Computer Methods in Applied Mechanics and Engineering* **311**, 208–249.

Sarvazyan, A. P., Rudenko, O. V. and Nyborg, W. L. [2010], 'Biomedical applications of radiation force of ultrasound: historical roots and physical basis', *Ultrasound in medicine & biology* **36**(9), 1379–1394.

Sarvazyan, A. P., Rudenko, O. V., Swanson, S. D., Fowlkes, J. B. and Emelianov, S. Y. [1998], 'Shear wave elasticity imaging: a new ultrasonic technology of medical diagnostics', *Ultrasound in medicine & biology* **24**(9), 1419–1435.

Scovazzi, G., Carnes, B., Zeng, X. and Rossi, S. [2016], 'A simple, stable, and accurate linear tetrahedral finite element for transient, nearly, and fully incompressible solid dynamics: a dynamic variational multiscale approach', *International Journal for Numerical Methods in Engineering* **106**(10), 799–839.

Scovazzi, G., Song, T. and Zeng, X. [2017], 'A velocity/stress mixed stabilized nodal finite element for elastodynamics: Analysis and computations with strongly and weakly enforced boundary conditions', *Computer Methods in Applied Mechanics and Engineering* **325**, 532–576.

Sommer, G., Schriefl, A. J., Andrä, M., Sacherer, M., Viertler, C., Wolinski, H. and Holzapfel, G. A. [2015], 'Biomechanical properties and microstructure of human ventricular myocardium', *Acta biomaterialia* **24**, 172–192.

Streeter, D. D., Spotnitz, H. M., Patel, D. P., Ross, J. and Sonnenblick, E. H. [1969], 'Fiber orientation in the canine left ventricle during diastole and systole', *Circulation research* **24**(3), 339–347.

Sussman, T. and Bathe, K.-J. [1987], 'A finite element formulation for nonlinear incompressible elastic and inelastic analysis', *Computers & Structures* **26**(1-2), 357–409.

Temam, R. [1968], 'Une méthode d'approximation de la solution des équations de Navier-Stokes', *Bull. Soc. Math. France* **98**(4), 115–152.

Temam, R. [2001], *Navier-Stokes equations: theory and numerical analysis*, Vol. 343, American Mathematical Soc.

Tezduyar, T. E. [1991], Stabilized finite element formulations for incompressible flow computations, *in* 'Advances in applied mechanics', Vol. 28, Elsevier, pp. 1–44.

Ye, W., Bel-Brunon, A., Catheline, S., Rochette, M. and Combescure, A. [2017], 'A selective mass scaling method for shear wave propagation analyses in nearly incompressible materials', *International Journal for Numerical Methods in Engineering* **109**(2), 155–173.

Zienkiewicz, O. C., Taylor, R. L. and Taylor, R. L. [2000], *The finite element method: solid mechanics*, Vol. 2, Butterworth-heinemann.

CHAPTER 5

Mathematical analysis of numerical schemes for wave propagation in incompressible media

Summary

In this chapter we provide some results of existence and uniqueness of solution of the formulations introduced in Chapter 4, for elastic wave propagation in incompressible media. Furthermore, we derive a convergence analysis in time and space of the continuous formulations and the fully discrete numerical schemes proposed through Chapter 4 for the approximation of the pure incompressible elastodynamic problem.

Contents

5.1 Introduction

The principal aim of this work is to provide some results of existence and uniqueness of solution of the formulations introduced in Chapter 4, for wave propagation in incompressible solids, and outline a convergence analysis in time and space of the adapted numerical schemes proposed through Chapter 4 for the approximation of those formulations. We recall that the proposed method is based on the extension to incompressible elasticity of existing numerical schemes adapted to viscous incompressible flows, due to the strong similarities between the respective governing equations. Indeed, when the bulk modulus λ of an elastic material is very large, this constraint corresponds in some sense to enforcing the divergence of the displacement to be zero. Furthermore, at the limit $\lambda \to \infty$, the pressure can be introduced as a Lagrange multiplier associated with the incompressibility constraint [Boffi et al., 2013].
For this reason, we have developed a new numerical scheme inspired by fractional-step algorithms and stabilisation techniques (see Chorin [1968, 1969]; Temam [1968, 2001]; Guermond and Quartapelle [1998*b*,*a*]; Guermond et al. [2006]) for the resolution of incompressible elasticity. In particular, in Chapter 4 we propose a conservative time discretisation that treats implicitly only the terms corresponding to "information" travelling at infinite velocity (i.e. the incompressibility constraint). Therefore, if efficient methods for explicit time-discretisation are used (e.g. Spectral Finite Elements with mass lumping), our algorithm requires at each time step the resolution of a scalar Poisson problem (that can be done by efficient algorithms, as in Chapter 7) and few matrix-vector multiplications for the explicit methods.
The work is organised as follows. In Section 5.2 we provide two standard formulations of the continuous elastodynamic problem for quasi-incompressible and pure incompressible media, as well as a formulation for the treatment of incompressibility by penalisation. We demonstrate existence and uniqueness results for each formulation. The description of the variational formulation associated with each problem concludes this section. Section 5.3 is devoted to convergence estimates between the penalised formulations proposed in Chapter 4 and the standard pure incompressible problem in the continuous framework at the limit $\lambda \to \infty$. In order to retrieve optimal convergence error estimates in L^2-norm, we introduce the elasto-static operator associated with the elastodynamic problem and use intrinsic regularity properties of this operator [Brenner and Sung, 1992], following a similar approach to the one presented by Guermond [1999] for the Stokes problem. Through Section 5.4 the abstract framework for space discretisation of the incompressible elastodynamics equation is outlined, and a discrete elasto-static operator is introduced, whereas Section 5.5 is devoted to the brief description of the fully discrete schemes introduced in Chapter 4. Finally, in Section 5.6 we provide the convergence analysis between the fully discrete schemes associated with the penalised formulations.

5.2 Continuous framework

5.2.1 Preliminaries and notations

Given a bounded, Lipschitz domain $\Omega \subset \mathbb{R}^d$ with $d \leq 3$, we introduce the following notations to define Hilbert spaces for the elastic displacements

$$\mathcal{H} := \{\underline{v} \in L^2(\Omega)^d\}, \quad \mathcal{X} := H_0^1(\Omega)^d, \quad \mathcal{X}' = H^{-1}(\Omega)^d.$$

For the sake of simplicity, we consider homogenous Dirichlet conditions on the boundary of the propagation domain. We also need to consider divergence-free displacements. Hence, we introduce the following subspace of $\mathcal{X}$:

$$\mathcal{V} \coloneqq \{\underline{v} \in \mathcal{X} \mid \operatorname{div} \underline{v} = 0\}.$$

Another space that we need to introduce is the following subspace of $\mathcal{X}'$:

$$\mathcal{V}^0 = \{\underline{v} \in \mathcal{X}' \mid \langle \underline{v}, \underline{\phi} \rangle = 0 \ \forall \underline{\phi} \in \mathcal{V}\}.$$

We recall that $-\underline{\nabla} \in \mathscr{L}\big(L^2(\Omega); \mathcal{X}'\big)$ is the dual operator of $\operatorname{div} \in \mathscr{L}\big(\mathcal{X}; L^2(\Omega)\big)$. It is possible to prove that, due to the closed range theorem of Banach [Girault and Raviart, 1979],

$$\mathcal{R}(\underline{\nabla}) = \big(\operatorname{Ker}(\operatorname{div})\big)^{\perp} = \mathcal{V}^0.$$

Pressure is a variable of interest and is sought in the spaces

$$\mathcal{L} \coloneqq L^2_0(\Omega) = \left\{ q \in L^2(\Omega) \mid \int_\Omega q = 0 \right\}, \quad \mathcal{M} = \{q \in H^1(\Omega) \mid q \in \mathcal{L}\}.$$

As usual, we identify $\mathcal{L}$ and $\mathcal{H}$ with their dual spaces in what follows. Moreover, for the sake of conciseness, we define, given a function space A on Ω,

$$C^k(A) \coloneqq C^k([0,T]; A), \quad k \in \{0, 1, 2, ..\},$$

where $T > 0$ is a given final time of observation. Furthermore, we introduce

$$\Omega_T \coloneqq \Omega \times (0,T).$$

Finally, we introduce the standard Sobolev spaces, for all $k \in \mathbb{N}^*$,

$$W^k_0\big(0,T\big) \coloneqq \big\{\underline{v} \in W^{k,1}\big(0,T\big) \mid \partial_t^p \underline{v}(t=0) = \underline{0} \ \ \forall p < k\big\}.$$

Note that this definition is well-posed since, for all $k \in \mathbb{N}^*$, there exists an imbedding from $W^{k+1,1}_0\big(0,T\big)$ to $C^k\big(0,T\big)$ [Adams and Fournier, 2003]. Furthermore, given a function space A on Ω, we define the set of functions in $W^k_0\big(0,T\big)$ with values in A, namely

$$W^k_0(A) \coloneqq W^k_0\big(0,T;A\big).$$

5.2.2 Equations of the problem

Our aim is to analyse the propagation of elastic waves in heterogenous, anisotropic and incompressible solids. The main application we have in mind is the propagation of elastic waves in nearly-incompressible biological tissues (e.g. the heart) in the context of transient elastography. For the sake of simplicity, we assume that all quantities in the elastodynamic problem are non-dimensional.
We consider as a reference model the elastic wave propagation in an incompressible solid, that is described by the following partial differential equation (PDE) system:
For $\underline{f}$ given and sufficiently regular, find $\underline{y}_\lambda \in C^2(\mathcal{H}) \cap C^1(\mathcal{X})$ such that

$$\begin{cases} \rho\, \partial_t^2 \underline{y}_\lambda - \underline{\operatorname{div}}\left(\underline{\underline{\mathbf{C}}}\, \underline{\underline{\varepsilon}}(\underline{y}_\lambda)\right) - \lambda\, \underline{\nabla} \operatorname{div} \underline{y}_\lambda = \underline{f} & \text{in } \Omega_T, \\ \underline{y}_\lambda(t=0) = \underline{0}, \quad \partial_t \underline{y}_\lambda(t=0) = \underline{0} & \text{in } \Omega, \end{cases} \tag{QI}$$

with $\lambda \in \mathbb{R}^+$ the bulk modulus, that is assumed to be large, due to nearly-incompressibility, $\rho(\underline{x})$ the positive density of the medium and $\underline{\underline{\mathbf{C}}}(\underline{x})$ the elasticity fourth-order tensor, that is symmetric, coercive and bounded, i.e. there exist two strictly positive scalars c, C such that

$$c\left|\underline{\underline{\varepsilon}}\right|^2 \leq \underline{\underline{\mathbf{C}}}(\underline{x})\underline{\underline{\varepsilon}} : \underline{\underline{\varepsilon}} \leq C\left|\underline{\underline{\varepsilon}}\right|^2, \quad \forall\, \underline{\underline{\varepsilon}}.$$

Note that the tensor $\underline{\underline{\mathbf{C}}}$ accounts for a general anisotropic medium. For the sake of simplicity, we take $\rho \equiv 1$ in what follows. Existence and uniqueness results for problem (QI) are well-known. As an illustration, it is proved in Joly [2008] that the following proposition holds:

Proposition 5.1. *Let $\underline{f} \in L^1(\mathcal{H})$. Then, the solution $\underline{y}_\lambda$ of (QI) exists and it is unique, and it satisfies*

$$\underline{y}_\lambda \in C^1(\mathcal{H}) \cap C^0(\mathcal{X}). \tag{5.1}$$

As a corollary of Proposition 5.1, one can show the following energy estimates. In particular, we can state:

$$\frac{\mathrm{d}}{\mathrm{d}t}\mathcal{E}_{\underline{y}_\lambda}(t) = \int_\Omega \underline{f}\,\partial_t \underline{y}_\lambda \,\mathrm{d}\Omega,$$

with

$$\mathcal{E}_{\underline{y}_\lambda}(t) = \frac{1}{2}\int_\Omega \left|\partial_t \underline{y}_\lambda\right|^2 \mathrm{d}\Omega + \frac{1}{2}\int_\Omega \underline{\underline{\mathbf{C}}}(\underline{x})\underline{\underline{\varepsilon}}(\underline{y}_\lambda) : \underline{\underline{\varepsilon}}(\underline{y}_\lambda)\,\mathrm{d}\Omega + \frac{\lambda}{2}\int_\Omega \left|\operatorname{div} \underline{y}_\lambda\right|^2 \mathrm{d}\Omega.$$

It is standard to show, using the Grönwall lemma, that there exists a constant $C > 0$ independent of λ such that

$$\mathcal{E}^{\frac{1}{2}}_{\underline{y}_\lambda} := \sup_{t\in[0,T]} \mathcal{E}^{\frac{1}{2}}_{\underline{y}_\lambda}(t) \leq C\int_0^T \left\|\underline{f}\right\|_{\mathcal{H}} \mathrm{d}s. \tag{5.2}$$

Therefore, we can assert by the Korn inequality that there exists another $C > 0$ independent of λ such that

$$\left\|\partial_t \underline{y}_\lambda\right\|_{L^\infty(\mathcal{H})} + \left\|\underline{y}_\lambda\right\|_{L^\infty(\mathcal{X})} + \lambda^{\frac{1}{2}}\left\|\operatorname{div} \underline{y}_\lambda\right\|_{L^\infty(\mathcal{H})} \leq C. \tag{5.3}$$

Under further regularity assumptions on $\underline{f}$ in time, we can formally differentiate (QI) with respect to time and apply Proposition 5.1 again. As a consequence, we can state the following corollary.

Corollary 5.1. *Let $\underline{f} \in W_0^k(\mathcal{H})$. Then, the solution $\underline{y}_\lambda$ of (QI) exists and it is unique, and it satisfies*

$$\underline{y}_\lambda \in C^{k+1}(\mathcal{H}) \cap C^k(\mathcal{X}).$$

Moreover, there exists $C > 0$ independent of λ such that

$$\left\|\partial_t^{k+1} \underline{y}_\lambda\right\|_{L^\infty(\mathcal{H})} + \left\|\partial_t^k \underline{y}_\lambda\right\|_{L^\infty(\mathcal{X})} + \lambda^{\frac{1}{2}}\left\|\operatorname{div} \partial_t^k \underline{y}_\lambda\right\|_{L^\infty(\mathcal{L})} \leq C,$$

Assume $\underline{f} \in W_0^1(\mathcal{H})$. An alternative formulation to (QI) consists in introducing a scalar function p_λ such that the couple $(\underline{y}_\lambda, p_\lambda) \in C^2(\mathcal{H}) \cap C^1(\mathcal{X}) \times C^1(\mathcal{L})$ satisfies

$$\begin{cases} \partial_t^2 \underline{y}_\lambda - \underline{\operatorname{div}}\,(\underline{\underline{\mathbf{C}}}(\underline{x})\underline{\underline{\varepsilon}}(\underline{y}_\lambda)) - \underline{\nabla}\, p_\lambda = \underline{f} & \text{in } \Omega_T, \\ \operatorname{div} \underline{y}_\lambda = \lambda^{-1} p_\lambda & \text{in } \Omega_T, \\ \underline{y}_\lambda(t=0) = \underline{0}, \quad \partial_t \underline{y}_\lambda(t=0) = \underline{0} & \text{in } \Omega. \end{cases} \tag{QIM}$$

Note that the mixed formulation (QIM) is obtained from (QI) by imposing $p_\lambda = \lambda \operatorname{div} \underline{y}_\lambda$, and therefore existence and uniqueness results for (QIM) can be deduced straightforwardly.

Corollary 5.2. *Let $\underline{f} \in W_0^k(\mathcal{H})$. Then, the solution $(\underline{y}_\lambda, p_\lambda)$ of (QIM) exists and it is unique, and it satisfies*

$$\underline{y}_\lambda \in C^{k+1}(\mathcal{H}) \cap C^k(\mathcal{X}) \times C^k(\mathcal{L}),$$

and $\underline{y}_\lambda$ solution of (QI). Moreover, there exists $C > 0$ independent of λ such that

$$\left\|\partial_t^{k+1} \underline{y}_\lambda\right\|_{L^\infty(\mathcal{H})} + \left\|\partial_t^k \underline{y}_\lambda\right\|_{L^\infty(\mathcal{X})} + \lambda^{-\frac{1}{2}} \left\|\partial_t^k p_\lambda\right\|_{L^\infty(\mathcal{L})} \leq C,$$

Since λ is large, it is natural to approximate the solution of (QIM) by the solution obtained at the limit as $\lambda \to \infty$. In more detail, if we define $(\underline{y}, p)$ and some corrector functions $(\underline{y}_1, p_1)$ and $(\underline{y}_2, p_2)$ such that

$$\underline{y}_\lambda = \underline{y} + \lambda^{-1} \underline{y}_1 + \lambda^{-2} \underline{y}_2 + \cdots, \quad p_\lambda = p + \lambda^{-1} p_1 + \lambda^{-2} p_2 + \cdots, \tag{5.4}$$

then a standard asymptotic analysis procedure shows that $(\underline{y}, p)$ satisfies a pure incompressible problem, that reads
Given $\underline{f} \in W_0^1(\mathcal{H})$, find $(\underline{y},\, p) \in C^2(\mathcal{H}) \cap C^1(\mathcal{V}) \times C^0(\mathcal{L})$, $T > 0$, such that

$$\begin{cases} \partial_t^2 \underline{y} - \underline{\operatorname{div}}\,(\underline{\underline{\mathbf{C}}}(\underline{x})\underline{\underline{\varepsilon}}(\underline{y})) - \underline{\nabla}\, p = \underline{f} & \text{in } \Omega_T, \\ \operatorname{div} \underline{y} = 0 & \text{in } \Omega_T, \\ \underline{y}(t=0) = \underline{0}, \quad \partial_t \underline{y}(t=0) = \underline{0} & \text{in } \Omega. \end{cases} \tag{IM}$$

Note that $\partial_t^2 \underline{y}$ is continuous with values in

$$\{\underline{v} \in H(\operatorname{div}; \Omega) \mid \operatorname{div} \underline{v} = 0 \text{ in } \Omega, \underline{v} \cdot \underline{n} = 0 \text{ on } \partial\Omega\}.$$

Moreover, note that p is sought in $C^0(\mathcal{L})$, although one could have expected $C^1(\mathcal{L})$. This is a consequence of the definition of p_λ and the limit process. Moreover, we do not need to add initial conditions on p (as it was the case of (QIM), due to the definition of p_λ), since at $t = 0$ we have

$$\partial_t^2 \underline{y}(t=0) = \underline{\nabla}\, p(t=0) \quad \text{in } \Omega, \qquad \operatorname{div} \partial_t^2 \underline{y}(t=0) = 0 \quad \text{in } \Omega.$$

As a consequence,

$$\begin{cases} \Delta\, p(t=0) = 0 & \text{in } \Omega \\ \underline{\nabla}\, p \cdot \underline{n}(t=0) = 0 & \text{on } \partial\Omega \end{cases} \implies p(t=0) = 0.$$

Problem (QIM) can be seen as a penalised formulation of (IM). Existence and uniqueness of the solution of system (IM) are deduced from (QI) by taking the limit as $\lambda \to \infty$, and they are stated in the following proposition.

Proposition 5.2. *Let $\underline{f} \in W_0^1(\mathcal{H})$. Then, there exists a unique couple $(\underline{y},\, p) \in C^2(\mathcal{H}) \cap C^1(\mathcal{V}) \times C^0(\mathcal{L})$ solution of (IM). Furthermore, there exists $C > 0$ independent of λ such that*

$$\left\|\partial_t^2 \underline{y}\right\|_{L^\infty(\mathcal{H})} + \left\|\partial_t \underline{y}\right\|_{L^\infty(\mathcal{X})} + \left\|\underline{y}\right\|_{L^\infty(\mathcal{X})} + \|p\|_{L^\infty(\mathcal{L})} \leq C. \tag{5.5}$$

Before detailing the proof of Proposition 5.2, we introduce the energy associated with (IM). If we consider the variational formulation associated with (IM), multiply the first equation by $\partial_t \underline{y} \in \mathbb{C}^0(\mathcal{V})$ and differentiate the second with respect to time, we retrieve

$$\begin{cases} \dfrac{1}{2}\dfrac{\mathrm{d}}{\mathrm{d}t}\left(\left\|\partial_t \underline{y}\right\|_{\mathcal{H}}^2 + \left(\underline{\underline{\mathbf{C}}}(\underline{x})\underline{\underline{\varepsilon}}(\underline{y}), \underline{\underline{\varepsilon}}(\underline{y})\right)\right) + (p, \operatorname{div} \partial_t \underline{y}) = (\underline{f}, \partial_t \underline{y}), \\ \operatorname{div} \partial_t \underline{y} = \underline{0}, \end{cases} \tag{5.6}$$

that implies

$$\frac{1}{2}\frac{\mathrm{d}}{\mathrm{d}t}\left(\left\|\partial_t \underline{y}\right\|_{\mathcal{H}}^2 + \left(\underline{\underline{\mathbf{C}}}(\underline{x})\underline{\underline{\varepsilon}}(\underline{y}), \underline{\underline{\varepsilon}}(\underline{y})\right)\right) = (\underline{f}, \partial_t \underline{y}).$$

Therefore, if we define the energy

$$\mathcal{E}_{\underline{y}} \coloneqq \frac{1}{2} \sup_{t\in[0,T]} \left(\left\|\partial_t \underline{y}\right\|_{\mathcal{H}}^2 + \left(\underline{\underline{\mathbf{C}}}(\underline{x})\underline{\underline{\varepsilon}}(\underline{y}(t)), \underline{\underline{\varepsilon}}(\underline{y}(t))\right)\right),$$

noting that there exists $C > 0$ such that

$$(\underline{f}, \partial_t \underline{y}) \leq \left\|\underline{f}\right\|_{\mathcal{H}} \left\|\partial_t \underline{y}\right\|_{\mathcal{H}} \leq C \left\|\underline{f}\right\|_{\mathcal{H}} \mathcal{E}_{\underline{y}}^{\frac{1}{2}},$$

by the Grönwall inequality in integral form there exists another constant $C > 0$ such that

$$\mathcal{E}_{\underline{y}}^{\frac{1}{2}} \leq C \int_0^T \left\|\underline{f}\right\|_{\mathcal{H}} \mathrm{d}s. \tag{5.7}$$

Note that Eq. (5.7) is not sufficient to deduce Eq. (5.5).

Proof. **Existence.** First, let us consider the variational formulation associated with (QI) with $\underline{f} \in W_0^2(\mathcal{H})$. Then, due to Corollary 5.1, there exists $C > 0$ such that for all $\lambda > 0$ there exists $\underline{y}_\lambda \in C^3(\mathcal{H}) \cap C^2(\mathcal{X})$ (that is a subspace of $H^3(\mathcal{H}) \cap H^2(\mathcal{X})$) satisfying

$$\left\|\underline{y}_\lambda\right\|_{H^3(\mathcal{H})} + \left\|\underline{y}_\lambda\right\|_{H^2(\mathcal{X})} \leq C.$$

Taking the limit $\lambda \to \infty$, by compactness arguments we can assert that, up to a subsequence, there exists $\underline{y} \in H^3(\mathcal{H}) \cap H^2(\mathcal{X})$, such that the following weak convergence holds:

$$\underline{y}_\lambda \overset{\lambda\to\infty}{\rightharpoonup} \underline{y} \quad \text{in } H^3(\mathcal{H}) \cap H^2(\mathcal{X}). \tag{5.8}$$

Let us now use a test function $\underline{v} \in C^0(\mathcal{V})$. Due to the fact that $\operatorname{div} \underline{v} = 0$, we obtain from (IM)

$$(\partial_t^2 \underline{y}_\lambda, v)_{L^2(\Omega_T)} + \left(\underline{\underline{\mathbf{C}}}(\underline{x})\underline{\underline{\varepsilon}}(\underline{y}_\lambda), \underline{\underline{\varepsilon}}(\underline{v})\right)_{L^2(\Omega_T)} = (\underline{f}, \underline{v})_{L^2(\Omega_T)}.$$

and therefore, at the limit $\lambda \to \infty$,

$$(\partial_t^2 \underline{y}, v)_{L^2(\Omega_T)} + \left(\underline{\underline{\mathbf{C}}}(\underline{x})\underline{\underline{\varepsilon}}(\underline{y}), \underline{\underline{\varepsilon}}(\underline{v})\right)_{L^2(\Omega_T)} = (\underline{f}, \underline{v})_{L^2(\Omega_T)}. \tag{5.9}$$

We can rewrite Eq. (5.9) as a duality pairing, namely

$$\langle \partial_t^2 \underline{y} - \underline{\operatorname{div}}\, \underline{\underline{\mathbf{C}}}(\underline{x})\underline{\underline{\varepsilon}}(\underline{y}) - f, \underline{v}\rangle_{\mathcal{V}'\times\mathcal{V}} = 0, \quad \forall t \in [0, T]. \tag{5.10}$$

From Eq. (5.10) we retrieve that $\partial_t^2 \underline{y} - \underline{\operatorname{div}}\, \underline{\underline{\mathbf{C}}}(\underline{x}) - f$ is orthogonal to every function v with zero-divergence. Therefore, there exists a scalar function $p \in C^0(\mathcal{L})$ such that the first

equation in (IM) holds [Girault and Raviart, 1979]. Furthermore, since from Eq. (5.3) we have

$$\left\|\operatorname{div} \underline{y}_\lambda\right\|_{L^\infty(\mathcal{H})} \leq \lambda^{-\frac{1}{2}}\, C,$$

we recover that $\underline{y}$ is divergence-free by taking the limit as $\lambda \to \infty$. We now demonstrate that $\underline{y}$ satisfies adequate initial conditions, i.e. $\underline{y}(t=0) = \underline{0}$, and $\partial_t \underline{y}(t=0) = \underline{0}$.
Let us define a function $\underline{v} \in C^1(\mathcal{H})$ such that, for any $\underline{v}_0 \in \mathcal{H}$, $\underline{v} = (T-t)\underline{v}_0$. Then, since $\underline{y}_\lambda$ vanishes at $t=0$, we have

$$\int_0^T \int_\Omega \underline{y}_\lambda \cdot \partial_t \underline{v} \,\mathrm{d}\Omega \,\mathrm{d}t = -\int_0^T \int_\Omega \partial_t \underline{y}_\lambda \cdot \underline{v} \,\mathrm{d}\Omega \,\mathrm{d}t.$$

Due to weak convergence, we derive $\forall \underline{v}_0$

$$\int_0^T \int_\Omega \underline{y} \cdot \partial_t \underline{v} \,\mathrm{d}\Omega \,\mathrm{d}t = -\int_0^T \int_\Omega \partial_t \underline{y} \cdot \underline{v} \,\mathrm{d}\Omega \,\mathrm{d}t \implies \int_\Omega \underline{y}(0) \cdot \underline{v}_0 \,\mathrm{d}\Omega = 0.$$

Hence, we obtain $\underline{y}(t=0) = \underline{0}$. Similar results can be shown for $\partial_t \underline{y}(t=0)$.
Uniqueness. Let us consider $\underline{f} = \underline{0}$. Due to Eq. (5.7) and the hypothesis of zero initial conditions, we retrieve that the only solution of (IM) is $\underline{y} = 0$. It now remains to demonstrate $p = 0$. This is directly retrieved by injecting $\underline{y} = \underline{0}$ in the first equation in (IM). We obtain

$$\underline{\nabla}\, p = \underline{0} \implies p = c,$$

for some $c \in \mathbb{R}$. Since $p \in L^2(\mathcal{L})$ (it has zero average), the only solution is $p = 0$. Therefore, the solution is unique.
Regularity. We can demonstrate more optimal regularity results on the solution $\underline{y}$. In more detail, it is possible to prove that, if $\underline{f} \in W_0^1(\mathcal{H})$, the solution $\underline{y}$ of (IM) is in $C^2(\mathcal{H}) \cap C^1(\mathcal{V})$. Indeed, let us consider a sequence $\{\underline{f}_n\}_{n\in\mathbb{N}} \in W_0^2(\mathcal{H})$ such that

$$f_n \to f \quad \text{in } W_0^1(\mathcal{H}).$$

Consequently, this sequence is a Cauchy sequence. Let $\underline{y}_n$ be the solution of (IM) associated with source term $\underline{f}_n$ and zero initial conditions. We define $\underline{e}_{n,m} \coloneqq \underline{y}_n - \underline{y}_m$, with $n,\ m \in \mathbb{N}$. Then, from Eq. (5.2), for all $\varepsilon > 0$ there exists $N \in \mathbb{N}$ such that, for all $n,\ m > N$,

$$\begin{aligned} \mathcal{E}^{\frac{1}{2}}_{\underline{e}_{n,m}} = \frac{1}{2} \sup_{t\in[0,T]} \left(\int_\Omega \left|\partial_t \underline{e}_{n,m}\right|^2 \mathrm{d}\Omega + \int_\Omega \underline{\underline{\mathbf{C}}}\, \underline{\underline{\varepsilon}}(\underline{e}_{n,m}) : \underline{\underline{\varepsilon}}(\underline{e}_{n,m}) \mathrm{d}\Omega \right)^{\frac{1}{2}} \\ \leq C \int_0^T \left\|\underline{f}_n - \underline{f}_m\right\|_{\mathcal{H}} \mathrm{d}s < \varepsilon. \end{aligned} \tag{5.11}$$

By differentiating Eq. (5.9) with respect to time, and considering the energy associated with the problem (there is no difficulty here since $\underline{e}_{n,m} \in H^3(\mathcal{H}) \cap H^2(\mathcal{X})$), we have

$$\begin{aligned} \mathcal{E}^{\frac{1}{2}}_{\partial_t \underline{e}_{n,m}} = \frac{1}{2} \sup_{t\in[0,T]} \left(\int_\Omega \left|\partial_t^2 \underline{e}_{n,m}\right|^2 \mathrm{d}\Omega + \int_\Omega \underline{\underline{\mathbf{C}}}\, \underline{\underline{\varepsilon}}(\partial_t \underline{e}_{n,m}) : \underline{\underline{\varepsilon}}(\partial_t \underline{e}_{n,m}) \mathrm{d}\Omega \right)^{\frac{1}{2}} \\ \leq C \int_0^T \left\|\partial_t \underline{f}_n - \partial_t \underline{f}_m\right\|_{\mathcal{H}} \mathrm{d}s < \varepsilon. \end{aligned} \tag{5.12}$$

Due to Eqs. (5.11) and (5.12), the regularity assumptions on $\underline{f}_n$ and the Korn inequality, the sequence $\{\underline{y}_n\}_{n\in\mathbb{N}}$ is a Cauchy sequence in the Banach space $C^2(\mathcal{H}) \cap C^1(\mathcal{V})$, and therefore

$$\underline{y}_n \to \underline{y} \quad \text{in } C^2(\mathcal{H}) \cap C^1(\mathcal{V}).$$

Consequently,

$$\underline{\mathrm{div}}\left(\underline{\underline{\mathbf{C}}}(\underline{x})\underline{\underline{\varepsilon}}(\underline{y})\right) \in C^1(\mathcal{X}').$$

This implies (since $\underline{f} \in C^0(\mathcal{H})$ up to a zero-measure set) that

$$\underline{\nabla} p_n = -\partial_t^2 \underline{y}_n - \underline{\mathrm{div}}\left(\underline{\underline{\mathbf{C}}}(\underline{x})\underline{\underline{\varepsilon}}(\underline{y}_n)\right) + \underline{f}_n \in C^0(\mathcal{X}') \implies p_n \in C^0(\mathcal{L}), \tag{5.13}$$

and it is uniquely defined (see Evans [2010, Chap 5.9]).
Then, we consider problem (IM) associated with $(\underline{e}_{n,m}, p_{n,m})$, with $p_{n,m} = p_n - p_m$. First, we can estimate, due to Eq. (5.13),

$$\|\underline{\nabla} p_{n,m}\|_{\mathcal{X}'} \leq \left\|\underline{\mathrm{div}}\,\underline{\underline{\mathbf{C}}}\,\underline{\underline{\varepsilon}}(\underline{e}_{n,m})\right\|_{\mathcal{X}'} + \left\|\underline{f}_n - \underline{f}_m\right\|_{\mathcal{X}'} + \left\|\partial_t^2 \underline{e}_{n,m}\right\|_{\mathcal{X}'}, \quad \forall t \in [0,T].$$

Due to the Riesz-Fréchet Theorem [Brezis, 2010], we can assert that there exists $C > 0$ such that

$$\left\|\underline{f}\right\|_{\mathcal{X}'} \leq C\left\|\underline{f}\right\|_{\mathcal{H}}, \quad \left\|\partial_t^2 \underline{e}_{n,m}\right\|_{\mathcal{X}'} \leq C\left\|\partial_t^2 \underline{e}_{n,m}\right\|_{\mathcal{H}}. \tag{5.14}$$

Furthermore, from the Cauchy-Schwarz and Korn inequalities, there exists a scalar $C > 0$ such that

$$\begin{aligned}\left\|\underline{\mathrm{div}}\,\underline{\underline{\mathbf{C}}}\,\underline{\underline{\varepsilon}}(\underline{e}_{n,m})\right\|_{\mathcal{X}'} &:= \sup_{\underline{v}\in\mathcal{X}} \frac{\left|\langle \underline{\mathrm{div}}\,\underline{\underline{\mathbf{C}}}\,\underline{\underline{\varepsilon}}(\underline{e}_{n,m}), \underline{v}\rangle\right|}{\|\underline{v}\|_{\mathcal{X}}} \leq \sup_{\underline{v}\in\mathcal{X}} \frac{\left|\left(\underline{\underline{\mathbf{C}}}\,\underline{\underline{\varepsilon}}(\underline{e}_{n,m}), \underline{\underline{\varepsilon}}(\underline{v})\right)_{\mathcal{H}}\right|}{\|\underline{v}\|_{\mathcal{X}}} \\ &\leq C\frac{\left\|\underline{\underline{\varepsilon}}(\underline{e}_{n,m})\right\|_{\mathcal{H}}\left\|\underline{\underline{\varepsilon}}(\underline{v})\right\|_{\mathcal{H}}}{\|\underline{v}\|_{\mathcal{X}}} \leq C\frac{\left\|\underline{e}_{n,m}\right\|_{\mathcal{X}}\|\underline{v}\|_{\mathcal{X}}}{\|\underline{v}\|_{\mathcal{X}}} = C\left\|\underline{e}_{n,m}\right\|_{\mathcal{X}}.\end{aligned} \tag{5.15}$$

In addition, since the gradient operator is an isomorphism of $\mathcal{L}$ onto $\mathcal{V}^0$, [Girault and Raviart, 1979, Cor. 2.4], we can assert that there exists $C > 0$ such that

$$\|p_{n,m}\|_{\mathcal{L}} \leq C\|\underline{\nabla} p_{n,m}\|_{\mathcal{X}'}. \tag{5.16}$$

Finally, by Eqs. (5.14), (5.15), (5.16), we can assert that there exists $C > 0$ independent of n such that

$$\|p_{n,m}\|_{L^\infty(\mathcal{L})} \leq C\left(\left\|\underline{e}_{n,m}\right\|_{L^\infty(\mathcal{X})} + \left\|\underline{f}_n - \underline{f}_m\right\|_{L^\infty(\mathcal{H})} + \left\|\partial_t^2 \underline{e}_{n,m}\right\|_{L^\infty(\mathcal{H})}\right).$$

Consequently, p_n is a Cauchy sequence in the Banach space $C^0(\mathcal{L})$. Hence, there exists $p \in C^0(\mathcal{L})$ such that $p_n \to p$ in $C^0(\mathcal{L})$. Then, we retrieve the equation satisfied by the couple $(\underline{y}, p)$ by a standard limit process on the weak formulation associated with (QIM).
Energy Estimate. In order to obtain an estimate on the couple $(\underline{y}, p)$ solution of (IM), we consider the sequence $\{(\underline{y}_n, p_n)\}_{n\in\mathbb{N}}$. Analogously to Eq. (5.12), we can provide the following estimate: there exists $C > 0$ such that

$$\mathcal{E}^{\frac{1}{2}}_{\partial_t \underline{y}_n} = \frac{1}{2}\sup_{t\in[0,T]}\left(\int_\Omega \left|\partial_t^2 \underline{y}_n\right|^2 \mathrm{d}\Omega + \int_\Omega \underline{\underline{\mathbf{C}}}\,\underline{\underline{\varepsilon}}(\partial_t \underline{y}_n) : \underline{\underline{\varepsilon}}(\partial_t \underline{y}_n)\mathrm{d}\Omega\right)^{\frac{1}{2}} \leq C,$$

similarly, we retrieve $\|p_n\|_{L^\infty(\mathcal{L})} \leq C$. By taking the limit $n \to \infty$, we deduce, by strong convergence, Eq. (5.5). □

More in general, it is possible to deduce the following corollary.

Corollary 5.3. *Let $\underline{f} \in W_0^k(\mathcal{H})$. Then, there exists a unique couple $(\underline{y}, p) \in C^{k+1}(\mathcal{H}) \cap C^k(\mathcal{V}) \times C^{k-1}(\mathcal{L})$ solution of (IM). Furthermore, there exists $C > 0$ independent of λ such that*

$$\left\|\partial_t^{k+1}\underline{y}\right\|_{L^\infty(\mathcal{H})} + \left\|\partial_t^{k}\underline{y}\right\|_{L^\infty(\mathcal{X})} + \left\|\partial_t^{k-1}\underline{y}\right\|_{L^\infty(\mathcal{X})} + \left\|\partial_t^{k-1}p\right\|_{L^\infty(\mathcal{L})} \leq C. \tag{5.17}$$

The other formulation we consider is the one introduced in Chapter 4, called (QIP). It corresponds to an approximation by penalisation of the problem (IM), inspired from existing formulations for incompressible fluid dynamics [Boffi et al., 2013]:
Given $\underline{f} \in W_0^1(\mathcal{H})$, find $(\tilde{\underline{y}}_\alpha, \tilde{p}_\alpha) \in C^2(\mathcal{H}) \cap C^1(\mathcal{X}) \times C^1(\mathcal{M})$ s.t.

$$\begin{cases} \partial_t^2 \tilde{\underline{y}}_\alpha - \underline{\mathrm{div}}\,(\underline{\underline{\mathbf{C}}}(\underline{x})\underline{\underline{\varepsilon}}(\tilde{\underline{y}}_\alpha)) - \underline{\nabla}\,\tilde{p}_\alpha = \underline{f} & \text{in } \Omega_T, \\ \mathrm{div}\,\tilde{\underline{y}}_\alpha = -\alpha\,\Delta\tilde{p}_\alpha & \text{in } \Omega_T, \\ \tilde{\underline{y}}_\alpha(t=0) = \underline{0}, \quad \partial_t\tilde{\underline{y}}_\alpha(t=0) = \underline{0} & \text{in } \Omega. \end{cases} \tag{QIP}$$

We note that (QIP) differs from (QIM) for the introduction of the laplacian operator in the second equation. Consequently, (QIP) corresponds to another approximation of the pure incompressible mixed formulation (IM). Moreover, note that (QIP) differs from the other formulations by several aspects. First, the pressure $\tilde{p}_\alpha$ is sought in a more regular space , in order to give an appropriate meaning to the introduced Laplace operator. Second, a boundary condition is required for the second equation for the pressure, that now has a trace (we recall that we use homogeneous Dirichlet conditions on the displacement). A common but arbitrary choice is to use homogenous Neumann boundary conditions

$$\underline{\nabla}\,\tilde{p}_\alpha \cdot \underline{n} = 0 \quad \text{on } \partial\Omega \times (0,T). \tag{5.18}$$

Using the same arguments as before, i.e., writing

$$\tilde{\underline{y}}_\alpha = \underline{y} + \alpha\,\tilde{\underline{y}}_1 + \alpha^2\tilde{\underline{y}}_2 + \cdots, \quad \tilde{p}_\alpha = p + \alpha\,\tilde{p}_1 + \alpha^2\tilde{p}_2 + \cdots, \tag{5.19}$$

one can see that $(\tilde{\underline{y}}_\alpha, \tilde{p}_\alpha)$ can be approximated by $(\underline{y}, p)$, solution of the pure incompressible mixed formulation (IM). In addition, if we eliminate $\tilde{p}_\alpha$ in the first equation in (QIP), we retrieve

$$\partial_t^2\tilde{\underline{y}}_\alpha - \underline{\mathrm{div}}\,(\underline{\underline{\mathbf{C}}}(\underline{x})\underline{\underline{\varepsilon}}(\tilde{\underline{y}}_\alpha)) - \alpha^{-1}\underline{\nabla}\big(-\Delta^{-1}\big)\mathrm{div}\tilde{\underline{y}}_\alpha = \underline{f}, \tag{5.20}$$

where $\Delta^{-1} : \mathcal{L} \to \mathcal{M}$ stands for the inverse Laplace operator on $\mathcal{M}$, equipped with a homogeneous Neumann boundary condition. It is possible to prove that the operator $-\underline{\mathrm{div}}\,(\underline{\underline{\mathbf{C}}}(\underline{x})\underline{\underline{\varepsilon}}(\cdot)) - \alpha^{-1}\underline{\nabla}\big(-\Delta^{-1}\big)\mathrm{div}(\cdot)$ is a self-adjoint and positive bilinear form. Consequently, existence and uniqueness of the solution can be retrieved from Eq. (QIP) by standard theory. Moreover, we can infer

$$\alpha^{-1}\big(\Delta^{-1}\mathrm{div}\tilde{\underline{y}}_\alpha, \mathrm{div}\tilde{\underline{y}}_\alpha\big)_{\mathcal{L}} = \alpha\big(\underline{\nabla}\tilde{p}_\alpha, \underline{\nabla}\tilde{p}_\alpha\big)_{\mathcal{L}}.$$

As a consequence, we can state the following proposition:

Proposition 5.3. *Let $\underline{f} \in W_0^k(\mathcal{H})$. Then, there exists a unique couple $(\tilde{\underline{y}}_\alpha, \tilde{p}_\alpha) \in C^{k+1}(\mathcal{H}) \cap C^k(\mathcal{X}) \times C^k(\mathcal{M})$ solution of (QIP). Moreover, there exists a strictly positive constant C independent of α such that*

$$\left\|\partial_t^{k+1}\tilde{\underline{y}}_\alpha\right\|_{L^\infty(\mathcal{H})} + \left\|\partial_t^{k}\tilde{\underline{y}}_\alpha\right\|_{L^\infty(\mathcal{X})} + \alpha^{\frac{1}{2}}\left\|\underline{\nabla}\,\partial_t^k\tilde{p}_\alpha\right\|_{L^\infty(\mathcal{H})} \leq C. \tag{5.21}$$

Remark We emphasize that, instead of the laplacian operator, we could define

$$\operatorname{div} \underline{\tilde{y}}_\alpha = -\alpha \operatorname{\underline{div}}(\underline{\underline{A}} \underline{\nabla} \tilde{p}_\alpha) \quad \text{in } \Omega_T, \qquad \text{with } \underline{\underline{A}} \underline{\nabla} \tilde{p}_\alpha \cdot \underline{n} = 0 \quad \text{on } \partial\Omega \times (0,T),$$

and $\underline{\underline{A}} \in L^\infty(\Omega)^{d\times d}$ a coercive and symmetric operator. This may have a practical interest when computing $\tilde{p}_\alpha$ in a discrete setting.

5.3 Convergence estimates

The objective of this section is to provide an error estimate between formulations (QIM) and (QIP). To do so, we consider (IM) as reference formulation, and we derive the error estimates associated with the approximation of formulation (IM) by (QIM) or (QIP), respectively, in order to infer the sought estimate using the triangular inequality. The analysis in continuous framework is preliminary to the convergence analysis in the discrete setting.

5.3.1 First convergence estimates

Our aim is to provide a first convergence result with respect to λ, based on standard energy estimates. We first compute the error between formulations (IM) and (QIM). Let us define the quantities

$$\underline{e}_\lambda \coloneqq \underline{y}_\lambda - \underline{y}, \qquad q_\lambda = p_\lambda - p. \tag{5.22}$$

Let $\underline{f} \in W_0^1(\mathcal{H})$. The couple $(\underline{e}_\lambda, q_\lambda) \in C^2(\mathcal{H}) \cap C^1(\mathcal{X}) \times C^0(\mathcal{L})$ satisfies

$$\begin{cases} \partial_t^2 \underline{e}_\lambda - \underline{\nabla} q_\lambda - \operatorname{div} \underline{\underline{\mathbf{C}}}\, \underline{\underline{\varepsilon}}(\underline{e}_\lambda) = \underline{0} & \text{in } \Omega_T, \\ \operatorname{div} \underline{e}_\lambda = \lambda^{-1}\, q_\lambda + \lambda^{-1}\, p & \text{in } \Omega_T, \\ \underline{e}_\lambda(t=0) = \underline{0}, \quad \partial_t \underline{e}_\lambda(t=0) = \underline{0} & \text{in } \Omega. \end{cases} \tag{5.23}$$

Proposition 5.4. *Let $\underline{f} \in W_0^2(\mathcal{H})$. Then, the couple $(\underline{e}_\lambda, q_\lambda) \in C^3(\mathcal{H}) \cap C^2(\mathcal{X}) \times C^1(\mathcal{L})$ solution of (5.23), satisfies*

$$\boxed{\sup_{t\in[0,T]} \left(\|\partial_t \underline{e}_\lambda\|_{\mathcal{H}} + \|\underline{e}_\lambda\|_{\mathcal{X}} + \lambda^{-\frac{1}{2}} \|q_\lambda\|_{\mathcal{L}} \right) \leq \lambda^{-\frac{1}{2}}\, C.} \tag{5.24}$$

Moreover,

$$\boxed{\sup_{t\in[0,T]} \|p_\lambda\|_{\mathcal{L}} \leq C.} \tag{5.25}$$

Proof. The energy associated with Eq. (5.23) reads

$$\mathcal{E}_{\underline{e}_\lambda}(t) = \frac{1}{2} \int_\Omega |\partial_t \underline{e}_\lambda|^2 \mathrm{d}\Omega + \frac{1}{2} \int_\Omega \underline{\underline{\mathbf{C}}}\, \underline{\underline{\varepsilon}}(\underline{e}_\lambda) : \underline{\underline{\varepsilon}}(\underline{e}_\lambda) \mathrm{d}\Omega + \frac{\lambda^{-1}}{2} \int_\Omega |q_\lambda|^2 \mathrm{d}\Omega.$$

Using the second equation in (5.23), we derive

$$(q_\lambda, \operatorname{div} \partial_t \underline{e}_\lambda)_{\mathcal{L}} = \lambda^{-1} (q_\lambda, \partial_t q_\lambda)_{\mathcal{L}} + \lambda^{-1} (q_\lambda, \partial_t p)_{\mathcal{L}}.$$

Then, if we perform a scalar product of the first equation in (5.23) with $\partial_t \underline{e}_\lambda$, we retrieve

$$\frac{1}{2}\frac{\mathrm{d}}{\mathrm{d}t}\int_\Omega |\partial_t \underline{e}_\lambda|^2 \mathrm{d}\Omega + \frac{1}{2}\frac{\mathrm{d}}{\mathrm{d}t}\int_\Omega \underline{\underline{\mathbf{C}}}\,\underline{\underline{\varepsilon}}(\underline{e}_\lambda) : \underline{\underline{\varepsilon}}(\underline{e}_\lambda)\mathrm{d}\Omega + \lambda^{-1}\int_\Omega q_\lambda \cdot \overline{\partial_t q_\lambda}\,\mathrm{d}\Omega + \lambda^{-1}\int_\Omega q_\lambda \cdot \overline{\partial_t p}\,\mathrm{d}\Omega = 0.$$

As a consequence, we deduce that

$$\frac{\mathrm{d}}{\mathrm{d}t}\mathcal{E}_{\underline{e}_\lambda}(t) = -\lambda^{-1}(q_\lambda, \partial_t p)_{\mathcal{L}} \leq \lambda^{-\frac{1}{2}}\|q_\lambda\|_{\mathcal{L}}\lambda^{-\frac{1}{2}}\|\partial_t p\|_{\mathcal{L}} \leq \lambda^{-\frac{1}{2}}\|\partial_t p\|_{\mathcal{L}}\mathcal{E}^{\frac{1}{2}}_{\underline{e}_\lambda}(t).$$

By the Grönwall lemma, we retrieve

$$\mathcal{E}^{\frac{1}{2}}_{\underline{e}_\lambda}(t) \leq C\lambda^{-\frac{1}{2}}\int_0^t \|\partial_t p\|_{\mathcal{L}}\mathrm{d}s, \tag{5.26}$$

with $C > 0$. Note that, due to the assumption $\underline{f} \in W^2_0(\mathcal{H})$ we can assert, due to Corollary 5.3, that there exists a scalar $C > 0$ independent of λ such that

$$\int_0^t \|\partial_t p\|_{\mathcal{L}}\mathrm{d}s \leq C. \tag{5.27}$$

Consequently, from Eq. (5.26) we obtain the estimation (5.24). Since $\|p\|_{\mathcal{L}}$ is bounded, due to the regularity assumption on $\underline{f}$, we can easily deduce Eq. (5.25). □

Corollary 5.4. *Let $\underline{f} \in W^k_0(\mathcal{H})$, $k > 1$. Then, the couple $(\underline{e}_\lambda, q_\lambda) \in C^{k+1}(\mathcal{H}) \cap C^k(\mathcal{X}) \times C^{k-1}(\mathcal{L})$ solution of (5.23), satisfies*

$$\sup_{t\in[0,T]}\left(\left\|\partial_t^{k-1}\underline{e}_\lambda\right\|_{\mathcal{H}} + \left\|\partial_t^{k-2}\underline{e}_\lambda\right\|_{\mathcal{X}} + \lambda^{-\frac{1}{2}}\left\|\partial_t^{k-2}q_\lambda\right\|_{\mathcal{L}}\right) \leq \lambda^{-\frac{1}{2}}\,C. \tag{5.28}$$

Moreover,

$$\sup_{t\in[0,T]}\left\|\partial_t^{k-2}p_\lambda\right\|_{\mathcal{L}} \leq C. \tag{5.29}$$

The proof of Corollary 5.4 follows by similar considerations as the proof of Proposition 5.4. We only emphasize that, due to the additional regularity assumption on $\underline{f}$, we can derive that $\left\|\partial_t^{k-2}p\right\|_{\mathcal{L}}$ is also bounded, that implies Eq. (5.29).

We now compare formulations (IM) and (QIP). Let us consider $\underline{f} \in W^1_0(\mathcal{H})$. To this aim, we analyse the problem for the error

$$\tilde{\underline{e}}_\alpha \coloneqq \tilde{\underline{y}}_\alpha - \underline{y}, \qquad \tilde{q}_\alpha = \tilde{p}_\alpha - p, \tag{5.30}$$

where $(\tilde{\underline{y}}_\alpha, \tilde{p}_\alpha) \in C^2(\mathcal{H})\cap C^1(\mathcal{X})\times C^0(\mathcal{M})$ is solution of (QIP) and $(\underline{y}, p) \in C^2(\mathcal{H})\cap C^1(\mathcal{X})\times C^0(\mathcal{L})$ is solution of (IM). It reads

$$\begin{cases} \partial_t^2\tilde{\underline{e}}_\alpha - \underline{\nabla}\tilde{q}_\alpha - \operatorname{div}\underline{\underline{\mathbf{C}}}\,\underline{\underline{\varepsilon}}(\tilde{\underline{e}}_\alpha) = \underline{0} & \text{in } \Omega_T, \\ \operatorname{div}\tilde{\underline{e}}_\alpha = -\alpha\,\Delta\,\tilde{q}_\alpha + -\alpha\,\Delta\,p & \text{in } \Omega_T, \\ \tilde{\underline{e}}_\alpha(t=0) = \underline{0}, \quad \partial_t\tilde{\underline{e}}_\alpha(t=0) = \underline{0} & \text{in } \Omega. \end{cases} \tag{5.31}$$

Proposition 5.5. *Let $\underline{f} \in W^2_0(\mathcal{H})$ and $p \in C^1(\mathcal{M})$. Then, there exists a constant $C > 0$ independent of α such that the couple $(\tilde{\underline{e}}_\alpha, \tilde{q}_\alpha) \in C^3(\mathcal{H})\cap C^2(\mathcal{X})\times C^1(\mathcal{M})$ solution of (5.31), satisfies*

$$\boxed{\sup_{t\in[0,T]}\left(\|\partial_t\tilde{\underline{e}}_\alpha\|_{\mathcal{H}} + \|\tilde{\underline{e}}_\alpha\|_{\mathcal{X}} + \alpha^{\frac{1}{2}}\|\underline{\nabla}\tilde{q}_\alpha\|_{\mathcal{H}}\right) \leq \alpha^{\frac{1}{2}}\,C.} \tag{5.32}$$

Moreover,

$$\boxed{\sup_{t\in[0,T]} \|\underline{\nabla}\tilde{p}_\alpha\|_{\mathcal{H}} \leq C.} \tag{5.33}$$

Proof. The energy associated with Eq. (5.31) reads

$$\mathcal{E}_{\underline{\tilde{e}}_\alpha}(t) = \frac{1}{2}\int_\Omega |\partial_t \underline{\tilde{e}}_\alpha|^2 \mathrm{d}\Omega + \frac{1}{2}\int_\Omega \underline{\underline{\mathbf{C}}}\,\underline{\underline{\varepsilon}}(\underline{\tilde{e}}_\alpha) : \underline{\underline{\varepsilon}}(\underline{\tilde{e}}_\alpha)\mathrm{d}\Omega + \frac{\alpha}{2}\int_\Omega |\underline{\nabla}\tilde{q}_\alpha|^2 \mathrm{d}\Omega,$$

and it satisfies

$$\frac{\mathrm{d}}{\mathrm{d}t}\mathcal{E}_{\underline{\tilde{e}}_\alpha}(t) = -\alpha(\underline{\nabla}\tilde{q}_\alpha, \partial_t\underline{\nabla}p) \leq \alpha^{\frac{1}{2}}\|\underline{\nabla}\tilde{q}_\alpha\|_{\mathcal{H}}\alpha^{\frac{1}{2}}\|\partial_t\underline{\nabla}p\|_{\mathcal{H}} \leq \alpha^{\frac{1}{2}}\|\partial_t\underline{\nabla}p\|_{\mathcal{H}}\,\mathcal{E}^{\frac{1}{2}}_{\underline{\tilde{e}}_\alpha}(t).$$

This implies, by the Grönwall lemma, that there exists $C > 0$ such that

$$\mathcal{E}^{\frac{1}{2}}_{\underline{\tilde{e}}_\alpha}(t) \leq C\alpha^{\frac{1}{2}}\int_0^t \|\partial_t\underline{\nabla}p\|_{\mathcal{H}}\mathrm{d}s. \tag{5.34}$$

Consequently, under regularity assumptions on $\partial_t\underline{\nabla}p$, from Eq. (5.34) we obtain the estimation (5.32). Moreover, since p vanishes at $t = 0$, one can show that

$$\sup_{t\in[0,T]} \|\underline{\nabla}\,p\|_{\mathcal{H}} \leq C\int_0^T \|\partial_t\underline{\nabla}\,p\|_{\mathcal{H}}\ \mathrm{d}t.$$

As a consequence, we can directly derive (5.33).

□

Note that here we also require regularity on the spatial derivatives of the field $\partial_t p$, in order to have a control on the energy. Assuming additional regularity on the source term, it is possible to retrieve the following result.

Corollary 5.5. *Let $\underline{f} \in W_0^k(\mathcal{H})$, $k > 1$, and let $p \in C^{k-1}(\mathcal{M})$. Then there exists a constant $C > 0$ independent of α such that the couple $(\underline{\tilde{e}}_\alpha, \tilde{q}_\alpha) \in C^{k+1}(\mathcal{H}) \cap C^k(\mathcal{X}) \times C^{k-1}(\mathcal{M})$, solution of (5.31), satisfies*

$$\sup_{t\in[0,T]} \left(\left\| \partial_t^{k-1}\underline{\tilde{e}}_\alpha \right\|_{\mathcal{H}} + \left\| \partial_t^{k-2}\underline{\tilde{e}}_\alpha \right\|_{\mathcal{X}} + \alpha^{\frac{1}{2}} \left\| \partial_t^{k-2}\tilde{q}_\alpha \right\|_{\mathcal{H}} \right) \leq \alpha^{\frac{1}{2}}\, C. \tag{5.35}$$

In addition,

$$\sup_{t\in[0,T]} \left\| \partial_t^{k-2}\underline{\nabla}\tilde{p}_\alpha \right\|_{\mathcal{H}} \leq C. \tag{5.36}$$

Therefore, we are able to provide a first estimate on the error between the formulations (QIM) and (QIP).

Corollary 5.6. *Let $\underline{f} \in W_0^2(\mathcal{H})$, and let $p \in C^1(\mathcal{M})$. Let the couple $(\underline{y}_\lambda, p_\lambda)$ be the solution of problem (QIM) and $(\underline{\tilde{y}}_\alpha, \tilde{p}_\alpha)$ be the solution of problem (QIP). Then, there exists a constant $C > 0$ independent of λ and α such that*

$$\sup_{t\in[0,T]} \left(\left\| \partial_t\underline{y}_\lambda - \partial_t\underline{\tilde{y}}_\alpha \right\|_{\mathcal{H}} + \left\| \underline{y}_\lambda - \underline{\tilde{y}}_\alpha \right\|_{\mathcal{X}} \right) \leq (\lambda^{-\frac{1}{2}} + \alpha^{\frac{1}{2}})\, C. \tag{5.37}$$

5.3.2 Additional regularity of the pure incompressible problem

First, note that the hypothesis of Corollary 5.5 is not satisfying, since it involves an a priori regularity property on the solution of the problem (IM). Furthermore, estimations (5.28) and (5.35) are not complete, since they involve a control on the H^1-norm, and it is possible to retrieve a higher order of convergence with respect to λ and α if we consider a weaker norm. To do so, we introduce the elasto-static operator associated with the underlying elastodynamic problem.

Introduction of the elasto-static operator. Following the approach proposed in Guermond [1999], we define a continuous operator $S : \mathcal{H} \to \mathcal{V}$ such that

$$\underline{r} \in \mathcal{H} \mapsto S\underline{r} \in \mathcal{V}, \tag{5.38}$$

and the couple $(S\underline{r}, q_r) \in \mathcal{V} \times \mathcal{L}$ is solution of

$$\begin{cases} -\underline{\mathrm{div}}\left(\underline{\underline{\mathbf{C}}}(\underline{x})\underline{\underline{\varepsilon}}(S\underline{r})\right) + \underline{\nabla}\, q_r = \underline{r} & \text{in } \Omega, \\ \mathrm{div}\, S\underline{r} = 0 & \text{in } \Omega. \end{cases} \tag{5.39}$$

It can be proved that S is a positive and self-adjoint operator with respect to the scalar product in $\mathcal{H}$. Problem (5.39) is well posed if the operator $\underline{\mathrm{div}}\,(\underline{\underline{\mathbf{C}}}(\underline{x})\underline{\underline{\varepsilon}}(\cdot))$ is coercive, and in this case it admits a unique solution $(S\underline{r}, q_r)$. The variational formulation of Eq. (5.39) reads
Find $(\underline{s}, q) \in \mathcal{V} \times \mathcal{L}$ solution of

$$\begin{cases} \left(\underline{\underline{\mathbf{C}}}(\underline{x})\underline{\underline{\varepsilon}}(\underline{s}), \underline{\underline{\varepsilon}}(\underline{w})\right)_{\mathcal{H}} - (q, \mathrm{div}\,\underline{w})_{\mathcal{L}} = (\underline{r}, \underline{w})_{\mathcal{H}} & \forall \underline{w} \in \mathcal{V}, \\ (\mathrm{div}\,\underline{s}, z)_{\mathcal{L}} = 0 & \forall z \in \mathcal{L}. \end{cases} \tag{5.40}$$

For $(\underline{w}, z) = (\underline{s}, q)$, we have

$$\begin{cases} \left(\underline{\underline{\mathbf{C}}}(\underline{x})\underline{\underline{\varepsilon}}(\underline{s}), \underline{\underline{\varepsilon}}(\underline{s})\right)_{\mathcal{H}} - (q, \mathrm{div}\,\underline{s})_{\mathcal{L}} = (\underline{r}, \underline{s})_{\mathcal{H}}, \\ (\mathrm{div}\,\underline{s}, q)_{\mathcal{L}} = 0, \end{cases} \tag{5.41}$$

and from the Cauchy-Schwarz inequality we can estimate that there exists a constant $C > 0$ such that

$$\left(\underline{\underline{\mathbf{C}}}(\underline{x})\underline{\underline{\varepsilon}}(\underline{s}), \underline{\underline{\varepsilon}}(\underline{s})\right)_{\mathcal{H}} \leq C\|\underline{r}\|_{\mathcal{H}}\|\underline{s}\|_{\mathcal{H}}.$$

Therefore, from the Korn inequality, we can assert

$$\|\underline{s}\|_{\mathcal{X}} \leq C\|\underline{r}\|_{\mathcal{H}}.$$

In addition, from inf-sup conditions, we can also infer that there exists $C > 0$ such that

$$\|q\|_{\mathcal{L}} \leq C\|\underline{r}\|_{\mathcal{H}}.$$

Returning to Eq. (5.39), we retrieve that there exists $C > 0$ such that

$$\|S\underline{r}\|_{\mathcal{X}} + \|q_r\|_{\mathcal{L}} \leq C\|\underline{r}\|_{\mathcal{H}}. \tag{5.42}$$

Note that C only depends on the domain Ω and the constitutive law considered.

Additional regularity of the elasto-static operator. In what follows, we use the following assumption.

Assumption 5.6. *Let $S : \mathcal{H} \to \mathcal{V}$ such that Eqs. (5.38) and (5.39) hold. Then, there exists $C > 0$ such that, for all $\underline{r} \in \mathcal{H}$,*

$$\left\|\underline{\operatorname{div}}\,\underline{\underline{\mathbf{C}}}(x)\underline{\underline{\varepsilon}}(S\underline{r})\right\|_{\mathcal{H}} + \|q_r\|_{\mathcal{M}} \leq C\|\underline{r}\|_{\mathcal{H}}.$$

It is shown in Brenner and Sung [1992] that Assumption 5.6 holds in the case of an isotropic medium in a convex polyhedron. To our knowledge, this property has not been proved yet for anisotropic media.

Hidden regularity of the pure incompressible problem.

Proposition 5.7. *Let Assumption 5.6 hold, and let $\underline{f} \in W_0^k(\mathcal{H})$. Then, p solution of problem (IM) belongs to $C^{k-1}(\mathcal{M})$.*

Proof. We observe that $\big(\underline{y}, p\big) = \big(S\underline{r}, q_r\big)$, with $\underline{r} = \underline{f} - \partial_t^2 \underline{y} \in C^{k-1}(\mathcal{H})$, up to modifications on zero-measure sets. The result follows due to Assumption 5.6. □

Note that, due to Proposition 5.7, if Assumption 5.6 holds, then the result of Corollary 5.5 holds if $\underline{f} \in W_0^k(\mathcal{H})$ and the result of Corollary 5.6 holds if $\underline{f} \in W_0^2(\mathcal{H})$.

5.3.3 Higher-order error estimates

The objective of this section is to obtain optimal estimates in weaker norms (namely, on $\mathcal{H}$) of the error performed if we approximate (IM) by (QIM) and (QIP), respectively. In what follows, we show that the error due to the approximation of (IM) by one of the aforementioned penalisation techniques is proportional to λ^{-1} and α, respectively.

First, we analyse again the approximation of (IM) by formulation (QIM) from a new perspective, in order to improve Proposition 5.4. Preliminarily, let us consider a Helmholtz decomposition of the solution $\underline{y}_\lambda$ of formulation (QIM) [Monk et al., 2003]. We can introduce a scalar field $\hat{p}_\lambda$ such that

$$\begin{cases} \underline{y}_\lambda = \lambda^{-1}\underline{\nabla}\hat{p}_\lambda + \underline{y}_\lambda^0 & \text{in } \Omega_T, \\ \operatorname{div}\underline{y}_\lambda^0 = 0 & \text{in } \Omega_T, \\ \underline{y}_\lambda^0 \cdot \underline{n} = \underline{0} & \text{in } \partial\Omega \times (0,T), \end{cases} \tag{5.43}$$

with $\underline{y}_\lambda^0(t) \in \mathcal{H}$ and $\hat{p}_\lambda(t) \in \mathcal{M}$ given by

$$\begin{cases} \Delta\hat{p}_\lambda = p_\lambda & \text{in } \Omega_T, \\ \underline{\nabla}\hat{p}_\lambda \cdot \underline{n} = 0 & \text{in } \partial\Omega \times (0,T). \end{cases} \tag{5.44}$$

We introduce $\underline{r}_\lambda \coloneqq \underline{y}_\lambda^0 - \underline{y}$. We underline that, if $\underline{f} \in W_0^k(\mathcal{H})$, then we obtain

$$(\underline{y}, \underline{y}_\lambda, p_\lambda) \in C^k(\mathcal{H}) \times C^k(\mathcal{H}) \times C^k(\mathcal{L}) \implies (\underline{r}_\lambda, \hat{p}_\lambda) \in C^k(\mathcal{H}) \times C^k(\mathcal{M}).$$

We choose, for the sake of simplicity, $k = 1$. If $\underline{f} \in W_0^1(\mathcal{H})$, then the couple $(\underline{e}_\lambda, q_\lambda) \in C^2(\mathcal{H}) \cap C^1(\mathcal{X}) \times C^0(\mathcal{L})$ solution of (5.23) also satisfies

$$\begin{cases} \partial_t^2 \underline{e}_\lambda - \underline{\mathrm{div}}\,(\underline{\underline{\mathbf{C}}}(\underline{x})\underline{\underline{\varepsilon}}(\underline{e}_\lambda)) - \underline{\nabla}\, q_\lambda = \underline{0} & \text{in } \Omega_T, \\ \mathrm{div}\, \underline{r}_\lambda = 0, \ \Delta \hat{p}_\lambda = p_\lambda & \text{in } \Omega_T, \\ \underline{e}_\lambda = \lambda^{-1} \underline{\nabla} \hat{p}_\lambda + \underline{r}_\lambda & \text{in } \Omega_T, \\ \underline{r}_\lambda \cdot \underline{n} = 0 & \text{in } \partial\Omega \times (0,T), \\ \underline{e}_\lambda(t=0) = \underline{0}, \quad \partial_t \underline{e}_\lambda(t=0) = \underline{0} & \text{in } \Omega. \end{cases} \tag{5.45}$$

We now consider the error associated with Eq. (5.45). It satisfies the following proposition.

Proposition 5.8. *Let $\underline{f} \in W_0^k(\mathcal{H})$, $k > 2$. Then, $\underline{e}_\lambda$ defined by Eq. (5.22) satisfies*

$$\boxed{\left\| \partial_t^{k-3} \underline{e}_\lambda \right\|_{L^2(\Omega_T)} \leq C \lambda^{-1},} \tag{5.46}$$

for some $C > 0$ independent of λ.

Proof. Note that the value of C will change along the proof, for the sake of simplicity. Moreover, we choose $k = 3$ without loss of generality. We recall that, in this case, we have

$$(\underline{e}_\lambda, q_\lambda) \in C^4(\mathcal{H}) \cap C^3(\mathcal{X}) \times C^2(\mathcal{L}).$$

A same property holds for $(\underline{y}_\lambda, p_\lambda)$ with, in addition, $p_\lambda \in C^3(\mathcal{L})$ (due to the second equation in (QIM)) and, therefore,

$$(\underline{r}_\lambda, \hat{p}_\lambda) \in C^3(\mathcal{H}) \times C^3(\mathcal{L}).$$

In order to compute the energy of Eq. (5.45), we consider the corresponding variational formulation and we take $S\partial_t \underline{r}_\lambda \in C^2(\mathcal{V}) \subset C^0(\mathcal{X})$ as a test function. From the first equation, we get

$$(\partial_t^2 \underline{e}_\lambda, S\partial_t \underline{r}_\lambda)_{\mathcal{H}} + \left(\underline{\underline{\mathbf{C}}}(\underline{x})\underline{\underline{\varepsilon}}(\underline{e}_\lambda), \underline{\underline{\varepsilon}}(S\partial_t \underline{r}_\lambda) \right)_{\mathcal{H}} = \langle \underline{\nabla} q_\lambda, S\partial_t \underline{r}_\lambda \rangle_{\mathcal{X}' \times \mathcal{X}}. \tag{5.47}$$

Boundary terms vanish here, due to the assumptions on the operator S (i.e. $S\underline{r}_\lambda = \underline{0}$ on $\partial\Omega$), even though the function $\underline{r}_\lambda$ is not required to be zero at boundaries. Note also that the right-hand side of Eq. (5.47) vanishes, due to the fact that $\mathrm{div}\, S\partial_t \underline{r}_\lambda = 0$ in Ω. Note that we can rewrite for all $t \in [0,T]$, from Eq. (5.40),

$$\begin{aligned} \left(\underline{\underline{\mathbf{C}}}(\underline{x})\underline{\underline{\varepsilon}}(\underline{e}_\lambda), \underline{\underline{\varepsilon}}(S\partial_t \underline{r}_\lambda) \right)_{\mathcal{H}} &= -\langle \underline{\mathrm{div}}\,(\underline{\underline{\mathbf{C}}}(\underline{x})\underline{\underline{\varepsilon}}(S\partial_t \underline{r}_\lambda)), \underline{e}_\lambda \rangle_{\mathcal{X}' \times \mathcal{X}} \\ &= -\langle \underline{\nabla} \partial_t q_{r_\lambda}, \underline{e}_\lambda \rangle_{\mathcal{X}' \times \mathcal{X}} + (\partial_t \underline{r}_\lambda, \underline{e}_\lambda)_{\mathcal{H}}. \end{aligned} \tag{5.48}$$

We emphasize that the first term at the right-hand side of Eq. (5.48) is a duality pairing in $\mathcal{X}$, since $\partial_t q_{r_\lambda}(t) \in \mathcal{L}$ by hypothesis. Using the third equation in the system (5.45) and Eq. (5.48), we can rewrite Eq. (5.47) as

$$(\lambda^{-1} \partial_t^2 \underline{\nabla} \hat{p}_\lambda + \partial_t^2 \underline{r}_\lambda, S\partial_t \underline{r}_\lambda)_{\mathcal{H}} - \langle \underline{\nabla} \partial_t q_{r_\lambda}, \underline{e}_\lambda \rangle_{\mathcal{X}' \times \mathcal{X}} + (\partial_t \underline{r}_\lambda, \underline{e}_\lambda)_{\mathcal{H}} = 0. \tag{5.49}$$

Using again the fact that by definition $\mathrm{div}\, S\partial_t \underline{r}_\lambda = 0$, Eq. (5.49) further simplifies into

$$(\partial_t^2 \underline{r}_\lambda, S\partial_t \underline{r}_\lambda)_{\mathcal{H}} + (\partial_t \underline{r}_\lambda, \underline{e}_\lambda)_{\mathcal{H}} = \langle \underline{\nabla} \partial_t q_{r_\lambda}, \underline{e}_\lambda \rangle_{\mathcal{X}' \times \mathcal{X}}. \tag{5.50}$$

We use again the second and the third equations in (5.45) to infer that Eq. (5.50) is equivalent to

$$(\partial_t^2 \underline{r}_\lambda, S\partial_t \underline{r}_\lambda)_{\mathcal{H}} + (\partial_t \underline{r}_\lambda, \underline{r}_\lambda)_{\mathcal{H}} = \langle \underline{\nabla} \partial_t q_{r_\lambda}, \lambda^{-1} \underline{\nabla} \hat{p}_\lambda \rangle_{\mathcal{X}' \times \mathcal{X}}. \tag{5.51}$$

We now define the norm $\|\cdot\|_*$ as

$$\|S\underline{r}\|_*^2 := (\underline{r}, S\underline{r})_{\mathcal{H}}.$$

Then, Eq. (5.51) can be reformulated as

$$\frac{1}{2}\frac{\mathrm{d}}{\mathrm{d}t}\Big(\|\partial_t \underline{r}_\lambda\|_*^2 + \|\underline{r}_\lambda\|_{\mathcal{H}}^2 \Big) = \lambda^{-1} \langle \underline{\nabla} \partial_t q_{r_\lambda}, \underline{\nabla} \hat{p}_\lambda \rangle_{\mathcal{X}' \times \mathcal{X}}. \tag{5.52}$$

Let us now integrate with respect to time. We obtain

$$\|\partial_t \underline{r}_\lambda\|_*^2 + \|\underline{r}_\lambda\|_{\mathcal{H}}^2 = 2 \int_0^t \lambda^{-1} \langle \underline{\nabla} \partial_t q_{r_\lambda}, \underline{\nabla} \hat{p}_\lambda \rangle_{\mathcal{X}' \times \mathcal{X}} \, \mathrm{d}s.$$

By integration by parts (IPP) in time, considering zero initial conditions, we retrieve

$$\|\partial_t \underline{r}_\lambda\|_*^2 + \|\underline{r}_\lambda\|_{\mathcal{H}}^2 = -2 \int_0^t \lambda^{-1} \langle \underline{\nabla} q_{r_\lambda}, \underline{\nabla} \partial_t \hat{p}_\lambda \rangle_{\mathcal{X}' \times \mathcal{X}} \, \mathrm{d}s + 2\lambda^{-1} \langle \underline{\nabla} q_{r_\lambda}(t), \underline{\nabla} \hat{p}_\lambda(t) \rangle_{\mathcal{X}' \times \mathcal{X}}.$$

By the Green Formula in space, due to Eq. (5.44), we obtain

$$\begin{aligned} \|\partial_t \underline{r}_\lambda\|_*^2 + \|\underline{r}_\lambda\|_{\mathcal{H}}^2 &= 2 \int_0^t \lambda^{-1} (q_{r_\lambda}, \Delta \partial_t \hat{p}_\lambda)_{\mathcal{L}} \, \mathrm{d}s - 2\lambda^{-1} \big(q_{r_\lambda}(t), \Delta \hat{p}_\lambda(t) \big)_{\mathcal{L}} \\ &= 2 \int_0^t \lambda^{-1} (q_{r_\lambda}, \partial_t p_\lambda)_{\mathcal{L}} \, \mathrm{d}s - 2\lambda^{-1} \big(q_{r_\lambda}(t), p_\lambda(t) \big)_{\mathcal{L}}. \end{aligned} \tag{5.53}$$

Taking into account the Cauchy-Schwarz inequality and Eq. (5.42), there exists $C > 0$ independent of λ s.t.

$$\begin{aligned} \|\partial_t \underline{r}_\lambda\|_*^2 + \|\underline{r}_\lambda\|_{\mathcal{H}}^2 &\le C \int_0^t \lambda^{-1} \|q_{r_\lambda}\|_{\mathcal{L}} \|\partial_t p_\lambda\|_{\mathcal{L}} \, \mathrm{d}s + C\lambda^{-1} \|q_{r_\lambda}(t)\|_{\mathcal{L}} \|p_\lambda(t)\|_{\mathcal{L}} \\ &\le C \int_0^t \lambda^{-1} \|\underline{r}_\lambda\|_{\mathcal{H}} \|\partial_t p_\lambda\|_{\mathcal{L}} \, \mathrm{d}s + C\lambda^{-1} \|\underline{r}_\lambda(t)\|_{\mathcal{H}} \|p_\lambda(t)\|_{\mathcal{L}}. \end{aligned} \tag{5.54}$$

We now define

$$c(t) := \|\underline{r}_\lambda(t)\|_{\mathcal{H}}, \quad b_0(t) := \|p_\lambda(t)\|_{\mathcal{L}}, \quad b_1(t) := \|\partial_t p_\lambda\|_{\mathcal{L}}.$$

Therefore, from Eq. (5.54) we can derive

$$c^2(t) \le C \, \lambda^{-1} \Big(\int_0^t c(s) b_1(s) \mathrm{d}s + c(t) b_0(t) \Big). \tag{5.55}$$

By integrating again with respect to time, we obtain

$$\begin{aligned} \int_0^T c^2(t) \mathrm{d}t &\le C \, \lambda^{-1} \Big(\int_0^T \int_0^t c(s) \, b_1(s) \, \mathrm{d}s \, \mathrm{d}t + \int_0^T c(t) \, b_0(t) \, \mathrm{d}t \Big) \\ &\le C \, \lambda^{-1} \Big(\int_0^T c(t) \big(T \, b_1(t) + b_0(t) \big) \mathrm{d}t \Big). \end{aligned} \tag{5.56}$$

From the Cauchy-Schwarz inequality, we have

$$\int_0^T c^2(t)\mathrm{d}t \leq C\lambda^{-1}\left(\int_0^T c^2(t)\right)^{\frac{1}{2}}\left(\int_0^T (b_1(t)+b_0(t))^2\mathrm{d}t\right)^{\frac{1}{2}}. \tag{5.57}$$

We get

$$\|\underline{r}_\lambda\|_{L^2(\Omega_T)} = \left(\int_0^T c^2(t)\mathrm{d}t\right)^{\frac{1}{2}} \leq C\lambda^{-1}\left(\int_0^T (b_1(t)+b_0(t))^2\mathrm{d}t\right)^{\frac{1}{2}}, \tag{5.58}$$

and therefore, due to Eqs. (5.25) and (5.29), there exists $C>0$ such that

$$\|\underline{r}_\lambda\|_{L^2(\Omega_T)} \leq C\lambda^{-1}.$$

In order to retrieve an estimation on $\underline{e}_\lambda$, we recall that $\underline{e}_\lambda = \lambda^{-1}\underline{\nabla}\hat{p}_\lambda + \underline{r}_\lambda$. Furthermore, since $\Delta\hat{p}_\lambda = p_\lambda$, by the Poincaré-Wirtinger inequality there exists $C>0$ such that

$$\|\underline{\nabla}\hat{p}_\lambda(t)\|_{\mathcal{H}} \leq C\|p_\lambda(t)\|_{\mathcal{H}}, \quad \forall t\in[0,T].$$

Consequently, we obtain from Eq. (5.58) the following estimate on $\underline{e}_\lambda$:

$$\|\underline{e}_\lambda\|_{L^2(\Omega_T)} \leq \lambda^{-1}\|\underline{\nabla}\hat{p}_\lambda\|_{L^2(\Omega_T)} + \|\underline{r}_\lambda\|_{L^2(\Omega_T)} \leq C\lambda^{-1}, \tag{5.59}$$

since there exists $C>0$ such that

$$\|p_\lambda\|_{L^2(\Omega_T)} \leq \|q_\lambda\|_{L^2(\Omega_T)} + \|p\|_{L^2(\Omega_T)} \leq C.$$

□

We now consider the error between the solution $\tilde{\underline{y}}_\alpha$ of problem (QIP) and $\underline{y}$, solution of the pure incompressible mixed problem (IM). Our aim is to improve the estimation provided in Proposition 5.5.
In an analogous way to Eq. (5.43), we can introduce the Helmholtz decomposition for the solution $\tilde{\underline{y}}_\alpha$ of formulation (QIP). We obtain

$$\begin{cases} \tilde{\underline{y}}_\alpha = \alpha\underline{\nabla}\tilde{p}_\alpha + \tilde{\underline{y}}^0_\alpha & \text{in } \Omega_T, \\ \operatorname{div}\tilde{\underline{y}}^0_\alpha = 0 & \text{in } \Omega_T, \\ \tilde{\underline{y}}^0_\alpha\cdot\underline{n} = \underline{0} & \text{in } \partial\Omega\times(0,T). \end{cases} \tag{5.60}$$

with $\tilde{\underline{y}}^0_\alpha(t)\in\mathcal{H}$. We also define $\tilde{\underline{r}}_\alpha := \tilde{\underline{y}}^0_\alpha - \underline{y}$. Note that, under the assumption $\underline{f}\in W^k_0(\mathcal{H})$, we have that

$$(\underline{y},\tilde{\underline{y}}_\alpha,\tilde{p}_\alpha)\in C^k(\mathcal{H})\times C^k(\mathcal{H})\times C^k(\mathcal{M}) \implies \tilde{\underline{r}}_\alpha\in C^k(\mathcal{H}).$$

Let now $k=1$. If $\underline{f}\in W^1_0(\mathcal{H})$, then the couple $(\tilde{\underline{e}}_\alpha,\tilde{q}_\alpha)\in C^2(\mathcal{H})\cap C^1(\mathcal{X})\times C^0(\mathcal{M})$, solution of (5.31), also satisfies

$$\begin{cases} \partial_t^2\tilde{\underline{e}}_\alpha - \underline{\operatorname{div}}\,(\underline{\underline{\mathbf{C}}}(\underline{x})\underline{\underline{\varepsilon}}(\tilde{\underline{e}}_\alpha)) - \underline{\nabla}\,\tilde{q}_\alpha = \underline{0} & \text{in } \Omega_T, \\ \tilde{\underline{e}}_\alpha = \alpha\underline{\nabla}\tilde{p}_\alpha + \tilde{\underline{r}}_\alpha & \text{in } \Omega_T, \\ \operatorname{div}\tilde{\underline{r}}_\alpha = 0 & \text{in } \Omega_T, \\ \tilde{\underline{r}}_\alpha\cdot\underline{n} = 0 & \text{in } \partial\Omega\times(0,T), \\ \tilde{\underline{e}}_\alpha(t=0) = \underline{0}, \quad \partial_t\tilde{\underline{e}}_\alpha(t=0) = \underline{0} & \text{in } \Omega. \end{cases} \tag{5.61}$$

Similarly to Proposition 5.8, we can state the following proposition.

Proposition 5.9. *Let $\underline{f} \in W_0^k(\mathcal{H})$, $k > 2$. Let Assumption 5.6 hold. Then, $\underline{\tilde{e}}_\alpha$ defined by Eq. (5.30) satisfies*

$$\boxed{\left\| \partial_t^{k-3} \underline{\tilde{e}}_\alpha \right\|_{L^2(\Omega_T)} \leq C\alpha,} \tag{5.62}$$

for some $C > 0$ independent of α.

Proof. The proof of Proposition 5.9 follows the main arguments of the previous proof. Therefore, we only provide the main ideas of the proof. We choose $k = 3$ and we introduce the couple $(S\underline{\tilde{r}}_\alpha, \tilde{q}_{r_\alpha}) \in C^3(\mathcal{X}) \times C^3(\mathcal{L})$ solution of

$$\begin{cases} -\underline{\operatorname{div}} \left(\underline{\underline{\mathbf{C}}}(\underline{x}) \underline{\underline{\varepsilon}}(S\underline{\tilde{r}}_\alpha) \right) + \underline{\nabla}\, \tilde{q}_{r_\alpha} = \underline{\tilde{r}}_\alpha & \text{in } \Omega_T, \\ \operatorname{div} S\underline{\tilde{r}}_\alpha = 0 & \text{in } \Omega_T. \end{cases} \tag{5.63}$$

Note however that, by Assumption 5.6, $\tilde{q}_{r_\alpha} \in C^3(\mathcal{M})$. First, we retrieve an analogous estimation to Eq. (5.53) that is suitable for this formulation. To do so, we multiply the first equation in Eq. (5.61) by $S\partial_t \underline{\tilde{r}}_\alpha$. After similar considerations to the ones outlined in the previous proof, we derive

$$\|\partial_t \underline{\tilde{r}}_\alpha\|_*^2 + \|\underline{\tilde{r}}_\alpha\|_{\mathcal{H}}^2 = -2 \int_0^t \alpha (\underline{\nabla} \tilde{q}_{r_\alpha}, \underline{\nabla} \partial_t \tilde{p}_\alpha)_{\mathcal{H}} \, \mathrm{d}s + 2\alpha (\underline{\nabla} \tilde{q}_{r_\alpha}(t), \underline{\nabla} \tilde{p}_\alpha(t))_{\mathcal{H}}. \tag{5.64}$$

Using the Cauchy-Schwarz inequality and Assumption 5.6 again, we obtain

$$\|\partial_t \underline{\tilde{r}}_\alpha\|_*^2 + \|\underline{\tilde{r}}_\alpha\|_{\mathcal{H}}^2 \leq C \int_0^t \alpha \|\underline{\tilde{r}}_\alpha\|_{\mathcal{H}} \|\partial_t \underline{\nabla} \tilde{p}_\alpha\|_{\mathcal{H}} \, \mathrm{d}s + C\alpha \|\underline{\tilde{r}}_\alpha(t)\|_{\mathcal{H}} \|\underline{\nabla} \tilde{p}_\alpha(t)\|_{\mathcal{H}}. \tag{5.65}$$

Since $k = 3$, from Corollary 5.5 we retrieve that there exists $C > 0$ such that

$$\sup_{t \in [0,T]} \left(\|\partial_t \underline{\nabla} \tilde{p}_\alpha\|_{\mathcal{H}} + \|\underline{\nabla} \tilde{p}_\alpha\|_{\mathcal{H}} \right) \leq C.$$

By similar reasoning to the previous proof, we get

$$\|\underline{\tilde{r}}_\alpha\|_{L^2(\Omega_T)} \leq C\alpha \implies \|\underline{\tilde{e}}_\alpha\|_{L^2(\Omega_T)} \leq \alpha \|\underline{\nabla} \tilde{p}_\alpha\|_{L^2(\Omega_T)} + \|\underline{\tilde{r}}_\alpha\|_{L^2(\Omega_T)} \leq C\alpha,$$

since $\|\underline{\nabla} \tilde{p}_\alpha\|_{L^2(\Omega_T)}$ is bounded. □

Finally, we can provide the following estimate by triangular inequality.

Corollary 5.7. *Let $\underline{f} \in W_0^k(\mathcal{H})$, $k > 2$. Let $(\underline{y}_\lambda, p_\lambda)$ be the solution of problem (QIM) and $(\underline{\tilde{y}}_\alpha, \tilde{p}_\alpha)$ the solution of problem (QIP). Let also Assumption 5.6 hold. Then, there exists a constant $C > 0$ independent of λ and α such that*

$$\boxed{\left\| \partial_t^{k-3} \underline{y}_\lambda - \partial_t^{k-3} \underline{\tilde{y}}_\alpha \right\|_{L^2(\Omega_T)} \leq C(\lambda^{-1} + \alpha).} \tag{5.66}$$

5.4 Space discretisation

Let us now consider a regular, quasi-uniform triangulation τ_h of Ω parametrised by a small parameter h devoted to tend to 0. We define the finite-dimensional spaces $\mathcal{X}_h \subset \mathcal{X}$ and

$\mathcal{M}_h \subset \mathcal{M}$, obtained by finite element approximation. For the analysis, we need to introduce the additional Hilbert space

$$\mathcal{C} := \{\underline{v} \in \mathcal{X} \mid \underline{\mathrm{div}}\, \underline{\underline{\mathbf{C}}}(x)\underline{\underline{\varepsilon}}(\underline{v}) \in \mathcal{H}\},$$

equipped with the scalar product

$$(\underline{v}, \underline{w})_{\mathcal{C}} := (\underline{v}, \underline{w})_{\mathcal{X}} + \left(\underline{\mathrm{div}}\, \underline{\underline{\mathbf{C}}}(x)\underline{\underline{\varepsilon}}(\underline{v}), \underline{\mathrm{div}}\, \underline{\underline{\mathbf{C}}}(x)\underline{\underline{\varepsilon}}(\underline{w})\right)_{\mathcal{H}}, \quad \forall (\underline{v}, \underline{w}) \in \mathcal{C} \times \mathcal{C}.$$

The norm in $\mathcal{C}$ is straightforwardly defined as

$$\|\underline{v}\|_{\mathcal{C}} := (\underline{v}, \underline{v})_{\mathcal{C}} \quad \forall \underline{v} \in \mathcal{C}.$$

It is assumed that the following properties hold [Quarteroni and Valli, 1994; Guermond and Quartapelle, 1998*b*]

Assumption 5.10. *There exists $c \geq 0$, independent of h, such that*

$$\inf_{\underline{v}_h \in \mathcal{X}_h} \{\|\underline{v} - \underline{v}_h\|_{\mathcal{H}} + h\|\underline{v} - \underline{v}_h\|_{\mathcal{X}}\} \leq c\, h^2 \|\underline{v}\|_{\mathcal{C}}, \quad \forall \underline{v} \in \mathcal{C},$$

and

$$\sup_{\underline{w}_h \in \mathcal{X}_h} \frac{\|\underline{w}_h\|_{\mathcal{X}}}{\|\underline{w}_h\|_{\mathcal{H}}} \leq c\, h^{-1}, \quad \forall \underline{w}_h \in \mathcal{X}_h.$$

Furthermore, there exists another constant $c \geq 0$, independent of h, such that $\forall q \in \mathcal{M}$,

$$\inf_{q_h \in \mathcal{M}_h} \|q - q_h\|_{\mathcal{L}} \leq c\, h \|q\|_{\mathcal{M}}.$$

It was shown in Chapter 4 that problem (IM) can be recast as
find $(\underline{y}_h, p_h) \in C^2(\mathcal{X}_h) \times C^0(\mathcal{M}_h)$ s.t.

$$\begin{cases} \partial_t^2 \underline{y}_h + A_h\, \underline{y}_h + B_h^T p_h = \underline{f}_h & \text{in } \mathcal{X}_h, \\ B_h\, \underline{y}_h = 0 & \text{in } \mathcal{M}_h, \\ \underline{y}_h(t=0) = 0,\ \partial_t \underline{y}_h(t=0) = 0 & \text{in } \mathcal{X}_h, \end{cases} \tag{IMh}$$

where $\underline{f}_h \in W_0^1(\mathcal{X}_h)$ is for each time t the projection of $\underline{f}(t)$ in $\mathcal{X}_h$ for the scalar product in $\mathcal{H}$. We recall that the symmetric, positive operator $A_h : \mathcal{X}_h \longrightarrow \mathcal{X}_h$ is such that $\forall\, (\underline{y}_h, \underline{w}_h) \in \mathcal{X}_h \times \mathcal{X}_h$

$$(A_h \underline{y}_h, \underline{w}_h)_{\mathcal{H}} := \int_\Omega \underline{\underline{\mathbf{C}}}(x)\underline{\underline{\varepsilon}}(\underline{y}_h) : \underline{\underline{\varepsilon}}(\underline{w}_h)\, \mathrm{d}\Omega,$$

and there exists $c_a > 0$, independent of h, such that

$$(A_h \underline{y}_h, \underline{y}_h)_{\mathcal{H}} \geq c_a \left\|\underline{y}_h\right\|_{\mathcal{X}}^2, \quad \forall\, \underline{y}_h \in \mathcal{X}_h.$$

In addition, there exists a strictly positive constant C_a such that

$$\left|(A_h \underline{y}_h, \underline{w}_h)_{\mathcal{H}}\right| \leq C_a \left\|\underline{y}_h\right\|_{\mathcal{X}} \|\underline{w}_h\|_{\mathcal{X}}, \quad \forall\, (\underline{y}_h, \underline{w}_h) \in \mathcal{X}_h \times \mathcal{X}_h.$$

The linear operator $B_h : \mathcal{X}_h \longrightarrow \mathcal{M}_h$ and its transpose $B_h^T : \mathcal{M}_h \longrightarrow \mathcal{X}_h$ are such that $\forall\ (\underline{y}_h, q_h) \in \mathcal{X}_h \times \mathcal{M}_h$

$$(B_h \underline{y}_h, q_h)_{\mathcal{L}} = \int_\Omega q_h \operatorname{div} \underline{y}_h \, \mathrm{d}\Omega = (\underline{y}_h, B_h^T q_h)_{\mathcal{H}}.$$

and there exists a strictly positive constant C_b such that

$$\left|(B_h \underline{y}_h, q_h)_{\mathcal{L}}\right| \leq C_b \left\|\underline{y}_h\right\|_{\mathcal{X}} \|q_h\|_{\mathcal{L}}, \quad \forall\, (\underline{y}_h, q_h) \in \mathcal{X}_h \times \mathcal{M}_h.$$

Assumption 5.11. *The operator B_h is surjective, moreover the discrete inf-sup condition is satisfied uniformly, i.e. there exists a constant $c_b \geq 0$, independent of h, s.t.*

$$\inf_{q_h \in \mathcal{M}_h} \sup_{\underline{v}_h \in \mathcal{X}_h} \frac{(B_h \underline{y}_h, q_h)_{\mathcal{L}}}{\|\underline{v}_h\|_{\mathcal{X}} \, \|q\|_{\mathcal{H}}} \geq c_b.$$

Following Chapter 4 and Guermond and Quartapelle [1998*b*], we first introduce the finite-dimensional space $\mathcal{Y}_h \subset \mathcal{H}$ endowed with the norm of $L^2(\Omega)^d$. We recall that $\mathcal{X}_h \subset \mathcal{Y}_h$ and $\nabla \mathcal{M}_h \subset \mathcal{Y}_h$, and we define the embedding $i_h : \mathcal{X}_h \longrightarrow \mathcal{Y}_h$; note that the transpose $i_h^T : \mathcal{Y}_h \longrightarrow \mathcal{X}_h$ corresponds to the L^2 projection of $\mathcal{Y}_h$ onto $\mathcal{X}_h$. We also introduce the subspace $\mathcal{V}_h \subset \mathcal{X}_h$ such that

$$\mathcal{V}_h \coloneqq \{\underline{v}_h \in \mathcal{X}_h \mid B_h \, \underline{v}_h = 0\}.$$

Note that, even though $\mathcal{X}_h \subset \mathcal{X}$, in general $\mathcal{V}_h$ is not a subspace of $\mathcal{V}$. We also recall that the discrete divergence operator $C_h : \mathcal{Y}_h \longrightarrow \mathcal{M}_h$ is such that

$$C_h \, i_h = B_h, \quad i_h^T \, C_h^T = B_h^T,$$

and, therefore, the following commutative diagrams hold

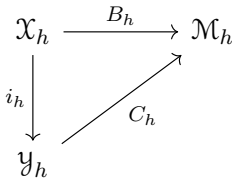

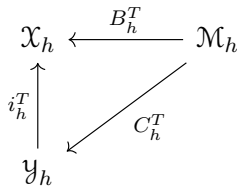

We emphasize that the operator C_h is surjective, due to surjectivity of B_h. We are now able to give the space discretisation associated with Eq. (QIP). It reads
find $(\underline{\tilde{y}}_{\alpha,h}, \tilde{p}_{\alpha,h}) \in C^2(\mathcal{X}_h) \times C^0(\mathcal{M}_h)$ s.t.

$$\begin{cases} \partial_t^2 \underline{\tilde{y}}_{\alpha,h} + A_h \, \underline{\tilde{y}}_{\alpha,h} + B_h^T \tilde{p}_{\alpha,h} = \underline{f}_h & \text{in } \mathcal{X}_h, \\ B_h \, \underline{\tilde{y}}_{\alpha,h} = \alpha C_h C_h^T \tilde{p}_{\alpha,h} & \text{in } \mathcal{M}_h, \\ \underline{\tilde{y}}_{\alpha,h}(t=0) = 0, \ \partial_t \underline{\tilde{y}}_{\alpha,h}(t=0) = 0 & \text{in } \mathcal{X}_h. \end{cases} \tag{QIPh}$$

Note that the operator $C_h C_h^T$ corresponds to a discrete laplacian operator on $\mathcal{M}_h$.

In order to perform the convergence analysis of the discrete schemes, we need to define the discrete counterpart of the operator S introduced in Eq. (5.38). Inspired by Guermond [1999], we define $S_h : \mathcal{Y}_h \to \mathcal{X}_h$, such that for every $\underline{r}_h \in \mathcal{Y}_h$, the couple $(S_h \underline{r}_h, q_{r_h}) \in \mathcal{V}_h \times \mathcal{M}_h$ is the solution of the discrete problem

$$\begin{cases} A_h(S_h \underline{r}_h) + B_h^T(q_{r_h}) = i_h^T \underline{r}_h & \text{in } \mathcal{X}_h, \\ B_h S_h \underline{r}_h = 0 & \text{in } \mathcal{M}_h. \end{cases} \tag{5.67}$$

Note that proof of the following lemma is not provided, since it is given in Guermond [1999].

Lemma 5.12. *For all* $(\underline{r}_h, \underline{v}_h) \in \mathcal{Y}_h \times \mathcal{Y}_h$, *we have*

$$(S_h\underline{v}_h, \underline{r}_h)_{\mathcal{H}} = (A_h S_h \underline{v}_h, S_h\underline{r}_h)_{\mathcal{H}} = (A_h S_h \underline{r}_h, S_h\underline{v}_h)_{\mathcal{H}}.$$

Moreover, there exists $C > 0$ *such that for all* $v_h \in \mathcal{Y}_h$

$$\|S_h\underline{r}_h\|_{\mathcal{X}} \leq C(\underline{r}_h, S_h\underline{r}_h)^{\frac{1}{2}}.$$

Note that S_h^T can be interpreted as the left pseudo-inverse operator of A_h. In addition, the linear form that associates $\underline{r}_h \mapsto (\underline{r}_h, S_h\underline{r}_h)$, with $\underline{r}_h \in \mathcal{Y}_h$, is a norm on $\mathcal{Y}_h$. We will denote

$$\|\underline{r}_h\|_{*,h} \coloneqq (\underline{r}_h, S_h\underline{r}_h)_{\mathcal{H}}^{\frac{1}{2}} \quad \forall\, \underline{r}_h \in \mathcal{Y}_h. \tag{5.68}$$

Lemma 5.13. *If Assumptions 5.6 and 5.10 hold, then there exists* $C > 0$ *such that for all* $r_h \in \mathcal{Y}_h$

$$\|A_h S_h \underline{r}_h\|_{\mathcal{H}} + \left\|C_h^T q_{r_h}\right\|_{\mathcal{H}} \leq C\|\underline{r}_h\|_{\mathcal{H}}.$$

Proof. We introduce the unique couple $(\underline{s}, q)$ solution of

$$\begin{cases} -\underline{\operatorname{div}}\left(\underline{\underline{\mathbf{C}}}(\underline{x})\underline{\underline{\varepsilon}}(\underline{s})\right) + \underline{\nabla}\, q = i_h^T \underline{r}_h & \text{in } \mathcal{X}, \\ \operatorname{div} \underline{s} = 0 & \text{in } \mathcal{L}. \end{cases} \tag{5.69}$$

Note that Problem (5.69) is well defined, since $i_h^T\underline{r}_h \in \mathcal{X}_h \subset \mathcal{X}$, and it represents the continuous counterpart of the discrete problem defined in Eq. (5.67). Due to Assumption 5.6, there exists $C > 0$ such that, for all $\underline{r} \in \mathcal{Y}_h$,

$$\left\|\underline{\operatorname{div}}\, \underline{\underline{\mathbf{C}}}(\underline{x})\underline{\underline{\varepsilon}}(\underline{s})\right\|_{\mathcal{H}} + \|q\|_{\mathcal{M}} \leq C\left\|i_h^T\underline{r}_h\right\|_{\mathcal{H}} = C\|\underline{r}_h\|_{\mathcal{H}}, \tag{5.70}$$

since i_h^T is a projection and, as a consequence, $\|\underline{s}\|_{\mathcal{C}} \leq C\|\underline{r}_h\|_{\mathcal{H}}$. In addition, due to Brezzi and Fortin [1991, Prop. 2.6 and 2.7], we have

$$\|\underline{s} - S_h\underline{r}_h\|_{\mathcal{X}} \leq \left(1 + \frac{C_a}{c_a}\right)\left(1 + \frac{C_b}{c_b}\right) \inf_{\underline{w}_h \in \mathcal{X}_h} \|\underline{s} - \underline{w}_h\|_{\mathcal{X}} + \frac{C_b}{c_a} \inf_{q_h \in \mathcal{M}_h} \|q - q_h\|_{\mathcal{L}}, \tag{5.71}$$

and

$$\|q - q_{r_h}\|_{\mathcal{L}} \leq \left(1 + \frac{C_b}{c_b}\right) \inf_{q_h \in \mathcal{M}_h} \|q - q_h\|_{\mathcal{L}} + \frac{C_a}{c_b} \inf_{\underline{w}_h \in \mathcal{X}_h} \|\underline{s} - S_h\underline{r}_h\|_{\mathcal{X}}. \tag{5.72}$$

Combining Eqs. (5.70), (5.71) and (5.72), as well as Assumption 5.10, we obtain that there exists $C > 0$ such that

$$\|\underline{s} - S_h\underline{r}_h\|_{\mathcal{X}} + \|q - q_{r_h}\|_{\mathcal{L}} \leq C\, h\|\underline{r}_h\|_{\mathcal{H}}.$$

Now, note that

$$\begin{aligned} \|A_h S_h \underline{r}_h\|_{\mathcal{H}} &= \sup_{\underline{w}_h \in \mathcal{X}_h} \frac{(A_h S_h \underline{r}_h, \underline{w}_h)_{\mathcal{H}}}{\|\underline{w}_h\|_{\mathcal{H}}} = \sup_{\underline{w}_h \in \mathcal{X}_h} \int_\Omega \underline{\underline{\mathbf{C}}}(x)\underline{\underline{\varepsilon}}(S_h\underline{r}_h) : \frac{\underline{\underline{\varepsilon}}(\underline{w}_h)}{\|\underline{w}_h\|_{\mathcal{H}}}\, \mathrm{d}\Omega \\ &\leq \sup_{\underline{w}_h \in \mathcal{X}_h} \int_\Omega \underline{\underline{\mathbf{C}}}(x)\underline{\underline{\varepsilon}}(S_h\underline{r}_h - \underline{s}) : \frac{\underline{\underline{\varepsilon}}(\underline{w}_h)}{\|\underline{w}_h\|_{\mathcal{H}}}\, \mathrm{d}\Omega + \sup_{\underline{w}_h \in \mathcal{X}_h} \int_\Omega \underline{\underline{\mathbf{C}}}(x)\underline{\underline{\varepsilon}}(\underline{s}) : \frac{\underline{\underline{\varepsilon}}(\underline{w}_h)}{\|\underline{w}_h\|_{\mathcal{H}}}\, \mathrm{d}\Omega. \end{aligned}$$

By the Green formula and using the Cauchy-Schwarz inequality, there exists a strictly positive constant C such that

$$\|A_h S_h \underline{r}_h\|_{\mathcal{H}} \leq C\|S_h \underline{r}_h - \underline{s}\|_{\mathcal{X}} \sup_{\underline{w}_h \in \mathcal{X}_h} \frac{\|\underline{w}_h\|_{\mathcal{X}}}{\|\underline{w}_h\|_{\mathcal{H}}} + \left\|\underline{\mathrm{div}}\left(\underline{\underline{\mathbf{C}}}(\underline{x})\underline{\underline{\varepsilon}}(\underline{s})\right)\right\|_{\mathcal{H}}.$$

Then, using the inverse inequality and the approximation property of Assumption 5.10, we obtain

$$\|A_h S_h \underline{r}_h\|_{\mathcal{H}} \leq C\big(\|\underline{s}\|_{\mathcal{C}} + \|q\|_{\mathcal{M}}\big) \implies \|A_h S_h \underline{r}_h\|_{\mathcal{H}} \leq C\|\underline{r}_h\|_{\mathcal{H}}.$$

In addition, note that

$$\big\|C_h^T q_h\big\|_{\mathcal{H}} = \big\|B_h^T q_h\big\|_{\mathcal{H}} = \sup_{\underline{w}_h \in \mathcal{X}_h} \frac{(B_h q_h, \underline{w}_h)_{\mathcal{H}}}{\|\underline{w}_h\|_{\mathcal{H}}} = \sup_{\underline{w}_h \in \mathcal{X}_h} \int_\Omega q_h \frac{\mathrm{div}\,\underline{w}_h}{\|\underline{w}_h\|_{\mathcal{H}}}\,\mathrm{d}\Omega$$

$$\leq \sup_{\underline{w}_h \in \mathcal{X}_h} \int_\Omega (q_h - q) \frac{\mathrm{div}\,\underline{w}_h}{\|\underline{w}_h\|_{\mathcal{H}}}\,\mathrm{d}\Omega + \sup_{\underline{w}_h \in \mathcal{X}_h} \int_\Omega q \frac{\mathrm{div}\,\underline{w}_h}{\|\underline{w}_h\|_{\mathcal{H}}}\,\mathrm{d}\Omega$$

Using again the Green formula and the Cauchy-Schwarz inequality, there exists a strictly positive constant C such that

$$\big\|C_h^T q_h\big\|_{\mathcal{H}} \leq C\|q_h - q\|_{\mathcal{L}} \sup_{\underline{w}_h \in \mathcal{X}_h} \frac{\|\underline{w}_h\|_{\mathcal{X}}}{\|\underline{w}_h\|_{\mathcal{H}}} + \|\underline{\nabla}\, q\|_{\mathcal{H}}.$$

Then, using the inverse inequality and the approximation property of Assumption 5.10, we obtain

$$\big\|C_h^T q_h\big\|_{\mathcal{H}} \leq C\big(\|\underline{r}_h\|_{\mathcal{C}} + \|q\|_{\mathcal{M}}\big) \implies \big\|C_h^T q_h\big\|_{\mathcal{H}} \leq C\|\underline{r}_h\|_{\mathcal{H}},$$

which concludes the proof. □

5.5 Time discretisation

This section deals with the time discretisation of the semi-discrete formulations obtained by FE approximation in space. First, we will recall the fully discrete schemes provided in Chapter 4, and in the second sub-section we detail the stability property of the discrete solution.

5.5.1 Fully discrete schemes

Henceforth, we recall the fully discrete schemes for the standard formulation (IM) and the novel formulation (QIP) presented in Chapter 4. Let us consider a time interval $[0, T]$, with $T > 0$, and define the partition $t^n = n\,\Delta t$, $n \in \{0, 1, .., N\}$, and $\Delta t = T/N$. Henceforth, we define with $\mathcal{N} = \{1, .., N\}$. The fully discrete scheme corresponding to (IM) for $n \in \mathcal{N}$ is constructed based on a simple second-order finite difference scheme, namely a leapfrog scheme. We shall consider two sequences of approximate displacement fields $\{\underline{y}_h^n \in \mathcal{X}_h\}$ and pressures $\{p_h^n \in \mathcal{L}_h\}$ such that $(\underline{y}_h^0, \underline{y}_h^1)$ is given and for $n \in \mathcal{N}$

$$\begin{cases} \dfrac{\underline{y}_h^{n+1} - 2\,\underline{y}_h^n + \underline{y}_h^{n-1}}{\Delta t^2} + A_h\,\underline{y}_h^n + B_h^T\,p_h^n = \underline{f}_h^n & \text{in } \mathcal{X}_h, \\ B_h \underline{y}_h^n = 0 & \text{in } \mathcal{M}_h, \end{cases} \tag{IMnh}$$

where $\underline{f}_h^n = \underline{f}_h(t^n)$. Finally, we provide the fully discrete scheme corresponding to (QIP) for $n \in \mathcal{N}$. We define two sequences of approximate displacement fields $\{\tilde{\underline{y}}_{\alpha,h}^n \in \mathcal{X}_h\}$ and approximate pressures $\{\tilde{p}_{\alpha,h}^n \in \mathcal{M}_h\}$ such that $(\tilde{\underline{y}}_{\alpha,h}^0, \tilde{\underline{y}}_{\alpha,h}^1)$ is given and for $n \in \mathcal{N}$

$$\begin{cases} \dfrac{\tilde{\underline{y}}_{\alpha,h}^{n+1} - 2\,\tilde{\underline{y}}_{\alpha,h}^n + \tilde{\underline{y}}_{\alpha,h}^{n-1}}{\Delta t^2} + A_h\,\tilde{\underline{y}}_{\alpha,h}^n + B_h^T\,\tilde{p}_{\alpha,h}^n = \underline{f}_h^n & \text{in } \mathcal{X}_h, \\ B_h \tilde{\underline{y}}_{\alpha,h}^n = \alpha\,\Delta t^2\,C_h\,C_h^T\,\tilde{p}_{\alpha,h}^n & \text{in } \mathcal{M}_h. \end{cases} \tag{QIPnh}$$

Note that here, for consistency reasons, we have rescaled the penalisation parameter by Δt^2 and assume α is independent of Δt.

5.5.2 Stability analysis

Preliminaries. Note that we assume that $\underline{f} \in W_0^k(\mathcal{H})$, $k \geq 1$. From $\underline{f}$, we have constructed the discrete field $\underline{f}_h \in W_0^k(\mathcal{X}_h)$ as the L^2 projection in $\mathcal{H}$ at every time t. In order to simplify the analysis, we assume that $\underline{f}_h(t)$ vanishes identically in a neighbourhood of $t = 0$, and that the initial data are zero. Furthermore, by definition, $\underline{f}_h^n = \underline{f}_h(t^n)$, $\forall n \in \{0, 1, .., N\}$. As a consequence, if Δt is sufficiently small, then one can consider that $\underline{f}_h^n$, $\underline{y}_h^n$, $\tilde{\underline{y}}_{\alpha,h}^n$ vanish at the first iterates. In more detail, we define $\tau_0 > 0$, and the functional space

$$W_c^k(\mathcal{H}) := \{\underline{f} \in W_0^k(\mathcal{H}) \mid \underline{f}(t) = \underline{0}, \forall t \leq M\tau_0\},$$

with M sufficiently large. Then, if $\Delta t < \tau_0$, then the first M iterates of $\underline{f}_h^n$, $\underline{y}_h^n$, $\tilde{\underline{y}}_{\alpha,h}^n$ are null.

If we assume that $\underline{f} \in W_c^1(\mathcal{H})$, then we retrieve that there exists $C > 0$ independent of Δt such that

$$\Delta t \sum_{n=0}^{N} \left\| \underline{f}_h^n \right\|_{\mathcal{H}} + \Delta t \sum_{n=0}^{N-1} \left\| \frac{\underline{f}_h^{n+1} - \underline{f}_h^n}{\Delta t} \right\|_{\mathcal{H}} \leq C.$$

In addition, if we assume that $\underline{f} \in W_c^2(\mathcal{H})$, then we retrieve that there exists $C > 0$ independent of Δt such that

$$\Delta t \sum_{n=0}^{N-1} \left\| \frac{\underline{f}_h^{n+1} - 2\underline{f}_h^n + \underline{f}_h^{n-1}}{\Delta t^2} \right\|_{\mathcal{H}} \leq C.$$

In the following proofs, we will introduce a constant C that is independent of Δt, for every $\Delta t < \tau_0$.

Stability analysis of the scheme (IMnh)**.** It is proved in Chapter 4 that the discrete energies associated with the scheme (IMnh) is preserved. Furthermore, this energy is positive if a CFL condition is satisfied. First, we consider scheme (IMnh). We define the discrete energy at time $n + \frac{1}{2}$ as

$$\mathcal{E}_h^{n+\frac{1}{2}} = \mathcal{E}_k^{n+\frac{1}{2}} - \frac{\Delta t^2}{4}\mathcal{E}_{kp}^{n+\frac{1}{2}} + \mathcal{E}_p^{n+\frac{1}{2}}, \tag{5.73}$$

where the kinetic energy reads

$$\mathcal{E}_k^{n+\frac{1}{2}} := \frac{1}{2}\left(\frac{\underline{y}_h^{n+1} - \underline{y}_h^n}{\Delta t}, \frac{\underline{y}_h^{n+1} - \underline{y}_h^n}{\Delta t} \right)_{\mathcal{H}},$$

the potential energy reads

$$\mathcal{E}_p^{n+\frac{1}{2}} := \frac{1}{2}\left(A_h \frac{\underline{y}_h^{n+1}+\underline{y}_h^n}{2}, \frac{\underline{y}_h^{n+1}+\underline{y}_h^n}{2}\right)_{\mathcal{H}},$$

and the mixed energy term is defined as

$$\mathcal{E}_{kp}^{n+\frac{1}{2}} := \frac{1}{2}\left(A_h \frac{\underline{y}_h^{n+1}-\underline{y}_h^n}{\Delta t}, \frac{\underline{y}_h^{n+1}-\underline{y}_h^n}{\Delta t}\right)_{\mathcal{H}}.$$

Then, after some computations, using the symmetry properties of the operator A_h, we obtain the discrete conservation property

$$\frac{\mathcal{E}_h^{n+\frac{1}{2}}-\mathcal{E}_h^{n-\frac{1}{2}}}{\Delta t} = \left(\underline{f}_h^n, \frac{\underline{y}_h^{n+1}-\underline{y}_h^{n-1}}{2\Delta t}\right)_{\mathcal{H}},$$

for all sequence $\{\underline{y}_h^n \in \mathcal{X}_h\}$ solution of scheme (IMnh).

Proposition 5.14. *Assume that the following CFL condition is satisfied:*

$$\Delta t^2 \leq (1-\varepsilon)4\left\|A_h\right\|^{-1}, \quad \text{with } \left\|A_h\right\| = \sup_{0\neq \underline{y}_h\in\mathcal{X}_h} \frac{(A_h\underline{y}_h, \underline{y}_h)_{\mathcal{H}}}{\left\|\underline{y}_h\right\|_{\mathcal{H}}^2}, \tag{5.74}$$

where $\varepsilon \in (0,1)$. Then, for all sequence $\{\underline{y}_h^n \in \mathcal{X}_h\}$, we have $\mathcal{E}_h^{n+\frac{1}{2}} \geq 0$ and $\forall n \in \mathcal{N}$ and there exists $C_\varepsilon > 0$ independent of Δt such that

$$\left\|\frac{\underline{y}_h^{n+1}-\underline{y}_h^n}{\Delta t}\right\|_{\mathcal{H}} + \left\|\frac{\underline{y}_h^n+\underline{y}_h^{n+1}}{2}\right\|_{\mathcal{X}} \leq C_\varepsilon\sqrt{\mathcal{E}_h^{n+\frac{1}{2}}}. \tag{5.75}$$

We can now state the following stability corollary of scheme (IMnh).

Corollary 5.8. *Assume that $\underline{f} \in W_c^2(\mathcal{H})$. Then, there exists $C > 0$ such that for all $\Delta t < \tau_0$ satisfying condition (5.74), then*

$$\boxed{\sup_{n\in\{1,2,..,N\}}\sqrt{\mathcal{E}_h^{n+\frac{1}{2}}} + \sup_{n\in\{1,2,..,N-1\}}\left\|C_h^T\frac{p_h^{n+1}-p_h^n}{\Delta t}\right\|_{\mathcal{H}} \leq C.} \tag{5.76}$$

Proof. We give the main ideas of the proof, since it is very standard.

$$\mathcal{E}_h^{n+\frac{1}{2}} - \mathcal{E}_h^{n-\frac{1}{2}} \leq \Delta t\left\|\underline{f}_h^n\right\|_{\mathcal{H}}\left\|\frac{\underline{y}_h^{n+1}-\underline{y}_h^{n-1}}{2\Delta t}\right\|_{\mathcal{H}} \leq C\,\Delta t\left\|\underline{f}_h^n\right\|_{\mathcal{H}}\left(\sqrt{\mathcal{E}_h^{n-\frac{1}{2}}}+\sqrt{\mathcal{E}_h^{n+\frac{1}{2}}}\right).$$

As a consequence,

$$\sqrt{\mathcal{E}_h^{n+\frac{1}{2}}} \leq \sqrt{\mathcal{E}_h^{\frac{1}{2}}} + C\,\Delta t\sum_{k=1}^{n}\left\|\underline{f}_h^k\right\|_{\mathcal{H}}, \quad \forall n \in \mathcal{N}. \tag{5.77}$$

This gives the first part of the inequality, since we consider zero initial data, and f is sufficiently regular. Hence, using Proposition 5.14, there exists a constant $C > 0$ such that

$$\sup_{n\in\{1,2,..,N\}}\left\|\frac{\underline{y}_h^{n+1}-\underline{y}_h^n}{\Delta t}\right\|_{\mathcal{H}} \leq C, \qquad \sup_{n\in\{0,1,..,N+1\}}\left\|\underline{y}_h^n\right\|_{\mathcal{H}} \leq C. \tag{5.78}$$

We now consider problem (IMnh) with source term

$$\delta_t^2 \underline{f}_h^n := \frac{\underline{f}_h^{n+1} - 2\underline{f}_h^n + \underline{f}_h^{n-1}}{\Delta t^2}.$$

Due to the regularity assumption on the source term, using (5.78) we retrieve that

$$\sup_{n\in\{2,3,..,N-1\}} \left\| \frac{\delta_t^2 \underline{y}_h^{n+1} - \delta_t^2 \underline{y}_h^n}{\Delta t} \right\|_{\mathcal{H}} \leq C, \qquad \sup_{n\in\{1,2,..,N\}} \left\| \delta_t^2 \underline{y}_h^n \right\|_{\mathcal{H}} \leq C. \tag{5.79}$$

Observe that we can rewrite the scheme (IMnh) as

$$\begin{cases} A_h\, \underline{y}_h^n + B_h^T\, p_h^n = \underline{f}_h^n - \delta_t^2 \underline{y}_h^n & \text{in } \mathcal{X}_h, \\ B_h \underline{y}_h^n = 0 & \text{in } \mathcal{M}_h, \end{cases} \tag{5.80}$$

Then, if we set $\underline{r}_h = i_h\, \underline{f}_h^n - i_h\, \delta_t^2 \underline{y}_h^n$, we observe that $(\underline{y}_h^n, p_h^n) = (S_h \underline{r}_h, q_{r_h})$ Therefore, using Lemma 5.13 and estimation (5.79), we retrieve that there exists $C > 0$ such that

$$\sup_{n\in\{1,2,..,N\}} \left\| C_h^T p_h^n \right\|_{\mathcal{H}} \leq C.$$

We now apply the same procedure for the discrete time derivative of p_h^n. First, we introduce the notation

$$\delta_t p_h^n := \frac{p_h^{n+1} - p_h^n}{\Delta t}.$$

Then, we note that $\delta_t p_h^n$ is solution of problem (IMnh) with source term given by $\delta_t \underline{f}_h^n$. Then, if we set

$$\underline{r}_h = i_h\, \delta_t \underline{f}_h^n - i_h\, \frac{\delta_t^2 \underline{y}_h^{n+1} - \delta_t^2 \underline{y}_h^n}{\Delta t},$$

we retrieve that $(\delta_t \underline{y}_h^n, \delta_t p_h^n) = (S_h \underline{r}_h, q_{r_h})$. Hence, using again Lemma 5.13 and estimation (5.79), we retrieve that there exists $C > 0$ such that

$$\sup_{n\in\{2,3,..,N-1\}} \left\| C_h^T \delta_t p_h^n \right\|_{\mathcal{H}} \leq C,$$

thus concluding the proof. □

Corollary 5.9. *Assume that $\underline{f} \in W_c^3(\mathcal{H})$. Then, there exists $C > 0$ such that for all $\Delta t < \tau_0$ satisfying condition (5.74), then*

$$\boxed{\sup_{n\in\{1,2,..,N-1\}} \left\| C_h^T \frac{p_h^{n+1} - 2p_h^n + p_h^{n-1}}{\Delta t^2} \right\|_{\mathcal{H}} \leq C.} \tag{5.81}$$

Proof. We define

$$\delta_t^2 p_h^n := \frac{p_h^{n+1} - 2p_h^n + p_h^{n-1}}{\Delta t^2}.$$

Then, we note that $\delta_t^2 p_h^n$ is solution of problem (IMnh) with source term given by $\delta_t^2 \underline{f}_h^n$. In particular, we can rewrite

$$\begin{cases} A_h\, \delta_t^2 \underline{y}_h^n + B_h^T\, \delta_t^2 p_h^n = \underline{r}_h & \text{in } \mathcal{X}_h, \\ B_h \delta_t^2 \underline{y}_h^n = 0 & \text{in } \mathcal{M}_h, \end{cases} \tag{5.82}$$

with

$$\underline{r}_h \coloneqq i_h \delta_t^2 \underline{f}_h^n - i_h \frac{\delta_t^3 \underline{y}_h^{n+1} - \delta_t^3 \underline{y}_h^n}{\Delta t},$$

where we have defined

$$\delta_t^3 \underline{y}_h^n \coloneqq \frac{\underline{y}_h^{n+1} - 3\underline{y}_h^n + 3\underline{y}_h^{n-1} - \underline{y}_h^{n-2}}{\Delta t^3}.$$

Note that $\delta_t^3 \underline{y}_h^n$ corresponds to a discrete third derivative in time of $\underline{y}_h^n$. Then, we retrieve that $(\delta_t^2 \underline{y}_h^n, \delta_t^2 p_h^n) = (S_h \underline{r}_h, q_{r_h})$. Then, considering (IMnh) with source term $\delta_t^3 \underline{f}_h^n$, one can show, using Corollary 5.8, that

$$\sup_{n \in \{2,3,..,N-1\}} \left\| \frac{\delta_t^3 \underline{y}_h^{n+1} - \delta_t^3 \underline{y}_h^{n-1}}{2\Delta t} \right\|_{\mathcal{H}} \leq C.$$

Hence, using again Lemma 5.13, we retrieve that there exists $C > 0$ such that

$$\sup_{n \in \{2,3,..,N-1\}} \left\| C_h^T \delta_t^2 p_h^n \right\|_{\mathcal{H}} \leq C,$$

thus concluding the proof. □

Stability analysis of the scheme (QIPnh)**.** We now provide the energy identity associated with scheme (QIPnh). Let us define $Q_h \coloneqq B_h^T (C_h C_h^T)^{-1} B_h$. Then, the discrete energy at time $n + \frac{1}{2}$ reads

$$\tilde{\mathcal{E}}_h^{n+\frac{1}{2}} = \mathcal{E}_k^{n+\frac{1}{2}} - \frac{\Delta t^2}{4} \tilde{\mathcal{E}}_{kp}^{n+\frac{1}{2}} + \tilde{\mathcal{E}}_p^{n+\frac{1}{2}},$$

with kinetic energy

$$\tilde{\mathcal{E}}_k^{n+\frac{1}{2}} \coloneqq \frac{1}{2} \left(\frac{\tilde{\underline{y}}_{\alpha,h}^{n+1} - \tilde{\underline{y}}_{\alpha,h}^n}{\Delta t}, \frac{\tilde{\underline{y}}_{\alpha,h}^{n+1} - \tilde{\underline{y}}_{\alpha,h}^n}{\Delta t} \right)_{\mathcal{H}},$$

potential energy

$$\tilde{\mathcal{E}}_p^{n+\frac{1}{2}} \coloneqq \frac{1}{2} \left(\left(A_h + \frac{1}{\alpha \Delta t^2} Q_h \right), \frac{\tilde{\underline{y}}_{\alpha,h}^{n+1} + \tilde{\underline{y}}_{\alpha,h}^n}{2}, \frac{\tilde{\underline{y}}_{\alpha,h}^{n+1} + \tilde{\underline{y}}_{\alpha,h}^n}{2} \right)_{\mathcal{H}},$$

and mixed energy term

$$\tilde{\mathcal{E}}_{kp}^{n+\frac{1}{2}} \coloneqq \frac{1}{2} \left(\left(A_h + \frac{1}{\alpha \Delta t^2} Q_h \right) \frac{\tilde{\underline{y}}_{\alpha,h}^{n+1} - \tilde{\underline{y}}_{\alpha,h}^n}{\Delta t}, \frac{\tilde{\underline{y}}_{\alpha,h}^{n+1} - \tilde{\underline{y}}_{\alpha,h}^n}{\Delta t} \right)_{\mathcal{H}}.$$

Then, after some computations, using the symmetry properties of the operator A_h, we obtain the discrete conservation property

$$\frac{\tilde{\mathcal{E}}_h^{n+\frac{1}{2}} - \tilde{\mathcal{E}}_h^{n-\frac{1}{2}}}{\Delta t} = \left(\underline{f}_h^n, \frac{\underline{y}_h^{n+1} - \underline{y}_h^{n-1}}{2\Delta t} \right)_{\mathcal{H}}. \tag{5.83}$$

It now remains to prove that $\mathcal{E}_h^{n+\frac{1}{2}}$ and $\tilde{\mathcal{E}}_h^{n+\frac{1}{2}}$ are positive.

Proposition 5.15. *Assume that the following CFL condition is satisfied:*

$$\Delta t^2 \leq (1-\varepsilon)4\,\rho\,\|A_h\|^{-1}\frac{4\,\alpha\,\rho-1}{4\,\alpha\,\rho}, \quad \alpha > \frac{1}{4\,\rho}, \quad \text{with } \|A_h\| = \sup_{0\neq \underline{y}_h\in\mathcal{X}_h}\frac{(A_h\underline{y}_h,\,\underline{y}_h)_{\mathcal{H}}}{\|\underline{y}_h\|^2_{\mathcal{H}}}, \tag{5.84}$$

with $\varepsilon \in (0,1)$. *Then, for all sequence* $\{\tilde{\underline{y}}_h^n \in \mathcal{X}_h\}$, *we have* $\tilde{\mathcal{E}}_h^{n+\frac{1}{2}} \geq 0$ *and* $\forall n \in \mathcal{N}$ *there exists a strictly positive constant* C_ε *independent of* Δt *such that*

$$\left\|\frac{\tilde{\underline{y}}_h^{n+1}-\tilde{\underline{y}}_h^{n-1}}{2\Delta t}\right\|_{\mathcal{H}} + \left\|\frac{\tilde{\underline{y}}_h^{n}+\tilde{\underline{y}}_h^{n+1}}{2}\right\|_{\mathcal{X}} \leq C_\varepsilon\sqrt{\tilde{\mathcal{E}}_h^{n+\frac{1}{2}}}. \tag{5.85}$$

Furthermore, if $\underline{f} \in W_c^1(\mathcal{H})$, *then there exists* $C>0$ *such that for all* $\Delta t < \tau_0$ *satisfying condition* (5.74), *then , we have*

$$\sup_{n\in\{1,2,..,N\}}\sqrt{\tilde{\mathcal{E}}_h^{n+\frac{1}{2}}} \leq C.$$

The proof is omitted, since it follows the first arguments of the proof of Corollary 5.8. Moreover, some elements are given in Chapter 4.

5.6 Discrete error estimates

At this point of our analysis, we are able to provide the discrete counterpart of the error estimates given in Section 5.3. Given $\underline{f}$ sufficiently regular, we want to estimate, given $\underline{y}_\lambda$ solution of scheme (QIM) and $\tilde{\underline{y}}_{\alpha,h}^n$ solution of scheme (QIPnh), the quantity

$$\left\|\underline{y}_\lambda - \tilde{\underline{y}}_{\alpha,h}^n\right\|^2_{\ell^2(\mathcal{H})} := \Delta t\sum_{k=0}^{N}\left\|\underline{y}_\lambda(t^k) - \tilde{\underline{y}}_{\alpha,h}^k\right\|^2_{\mathcal{H}}.$$

This estimate will be retrieved by triangular inequality. First, we can state that there exists a constant $C>0$ independent of λ, h and Δt, such that

$$\left\|\underline{y}_\lambda - \tilde{\underline{y}}_{\alpha,h}^n\right\|_{\ell^2(\mathcal{H})} \leq C\left\|\underline{y}_\lambda - \underline{y}\right\|_{L^2(\Omega_T)} + \left\|\underline{y} - \underline{y}_h^n\right\|_{\ell^2(\mathcal{H})} + \left\|\underline{y}_h^n - \tilde{\underline{y}}_{\alpha,h}^n\right\|_{\ell^2(\mathcal{H})}.$$

Note that, given $\underline{f} \in W_0^3(\mathcal{H})$ we have demonstrated in Proposition 5.8 that $\underline{y}_\lambda$ and $\underline{y}$ belong to $C^4(\mathcal{H})$ and there exists $C>0$ independent of λ such that

$$\left\|\underline{y}_\lambda - \underline{y}\right\|_{L^2(\Omega_T)} \leq C\lambda^{-1}.$$

Note that for the incompressible, linear Stokes problem it is standard to show [Heywood and Rannacher, 1982, 1986, 1988, 1990] that standard second-order discrete space-time discretisation can be achieved as soon as the inf-sup condition holds. We assume that similar results hold for the elastodynamic problem (IM), under the assumption that the CFL condition (5.74) is satisfied.
Hence, we can assume that there exists another $C>0$ independent of h and Δt such that

$$\left\|\underline{y} - \underline{y}_h^n\right\|_{\ell^2(\mathcal{H})} \leq C(h^2+\Delta t^2).$$

As a consequence, we just need to obtain an adequate estimate for $\left\|\underline{y}_h^n - \tilde{\underline{y}}_{\alpha,h}^n\right\|_{\ell^2(\mathcal{H})}$.

5.6.1 A first-order error estimate

First, we derive first-order convergence results in time. The first error we compute is the one between formulations (IMnh) and (QIPnh). Let us define the quantities

$$\tilde{\underline{e}}^n_{\alpha,h} \coloneqq \tilde{\underline{y}}^n_{\alpha,h} - \underline{y}^n_h, \qquad \tilde{q}^n_{\alpha,h} \coloneqq \tilde{p}^n_{\alpha,h} - \mathrm{p}^n_h, \quad n \in \mathcal{N}. \tag{5.86}$$

The sequence $\{(\tilde{\underline{e}}^n_{\alpha,h}, \tilde{q}^n_{\alpha,h}) \in \mathcal{X}_h \times \mathcal{M}_h\}$ satisfies

$$\begin{cases} \dfrac{\tilde{\underline{e}}^{n+1}_{\alpha,h} - 2\,\tilde{\underline{e}}^n_{\alpha,h} + \tilde{\underline{e}}^{n-1}_{\alpha,h}}{\Delta t^2} + A_h\,\tilde{\underline{e}}^n_{\alpha,h} + B_h^T\,\tilde{q}^n_{\alpha,h} = \underline{0} & \text{in } \mathcal{X}_h, \\ B_h \tilde{\underline{e}}^n_{\alpha,h} = \alpha \Delta t^2 C_h\, C_h^T\,(\tilde{q}^n_{\alpha,h} + p^n_h) & \text{in } \mathcal{M}_h. \end{cases} \tag{5.87}$$

From Eq. (5.87) we retrieve

$$\frac{\tilde{\underline{e}}^{n+1}_{\alpha,h} - 2\,\tilde{\underline{e}}^n_{\alpha,h} + \tilde{\underline{e}}^{n-1}_{\alpha,h}}{\Delta t^2} + \left(A_h + \frac{1}{\alpha \Delta t^2} Q_h\right) \tilde{\underline{e}}^n_{\alpha,h} = B_h^T\, p^n_h. \tag{5.88}$$

Proposition 5.16. *Assume that $\underline{f} \in W^2_c(\mathcal{H})$. Then, there exists $C > 0$ such that for all $\Delta t < \tau_0$ satisfying condition (5.74), then*

$$\boxed{\sup_{n \in \mathcal{N}} \left(\left\| \frac{\tilde{\underline{e}}^{n+1}_{\alpha,h} - \tilde{\underline{e}}^n_{\alpha,h}}{\Delta t} \right\|_{\mathcal{H}} + \left\| \frac{\tilde{\underline{e}}^{n+1}_{\alpha,h} + \tilde{\underline{e}}^n_{\alpha,h}}{2} \right\|_{\mathcal{X}} \right) \leq C \Delta t.} \tag{5.89}$$

Moreover,

$$\boxed{\sup_{n \in \mathcal{N}} \left\| C_h^T \frac{\tilde{p}^{n+1}_{\alpha,h} + \tilde{p}^n_{\alpha,h}}{2} \right\|_{\mathcal{H}} \leq C.}$$

Proof. The proof is based on energy considerations. First, note that, by L^2-scalar product of (5.87) with $(\tilde{\underline{e}}^{n+1}_{\alpha,h} - \tilde{\underline{e}}^{n-1}_{\alpha,h})/(2\Delta t)$, we have

$$\frac{\tilde{\mathcal{E}}_h^{n+\frac{1}{2}} - \tilde{\mathcal{E}}_h^{n-\frac{1}{2}}}{\Delta t} = \left(\frac{\tilde{\underline{e}}^{n+1}_{\alpha,h} - \tilde{\underline{e}}^{n-1}_{\alpha,h}}{2\Delta t}, B_h^T p^n_h \right)_{\mathcal{H}} \implies \tilde{\mathcal{E}}_h^{n+\frac{1}{2}} = \Delta t \sum_{k=1}^{n} \left(\frac{\tilde{\underline{e}}^{k+1}_{\alpha,h} - \tilde{\underline{e}}^{k-1}_{\alpha,h}}{2\Delta t}, B_h^T p^n_h \right)_{\mathcal{H}},$$

since the term $\tilde{\mathcal{E}}_h^{\frac{1}{2}}$ is zero due to the null initial conditions. Now, we use the Abel summation, and we retrieve

$$\tilde{\mathcal{E}}_h^{n+\frac{1}{2}} = \left(\frac{\tilde{\underline{e}}^{n+1}_{\alpha,h} + \tilde{\underline{e}}^n_{\alpha,h}}{2}, B_h^T p^n_h \right)_{\mathcal{H}} + \Delta t \sum_{k=1}^{n-1} \left(\frac{\tilde{\underline{e}}^{k+1}_{\alpha,h} + \tilde{\underline{e}}^k_{\alpha,h}}{2}, B_h^T \frac{p^{k+1}_h - p^k_h}{\Delta t} \right)_{\mathcal{H}}. \tag{5.90}$$

Note that the first term in the right-hand side of Eq. (5.90) can be rewritten

$$\left(\frac{\tilde{\underline{e}}^{n+1}_{\alpha,h} + \tilde{\underline{e}}^n_{\alpha,h}}{2}, B_h^T p^n_h \right)_{\mathcal{H}} = \sqrt{\alpha} \Delta t \left(\frac{(C_h C_h^T)^{-\frac{1}{2}}}{\sqrt{\alpha}\Delta t} B_h \frac{\tilde{\underline{e}}^{n+1}_{\alpha,h} + \tilde{\underline{e}}^n_{\alpha,h}}{2}, (C_h C_h^T)^{\frac{1}{2}} p^n_h \right)_{\mathcal{H}}.$$

Then, by the Cauchy-Schwarz inequality, and using the definition of the energy, we obtain

$$\left| \left(\frac{\tilde{\underline{e}}^{n+1}_{\alpha,h} + \tilde{\underline{e}}^n_{\alpha,h}}{2}, B_h^T p^n_h \right)_{\mathcal{H}} \right| \leq \sqrt{2\alpha} \Delta t \sqrt{\tilde{\mathcal{E}}_p^{n+\frac{1}{2}}} \left\| (C_h C_h^T)^{\frac{1}{2}} p^n_h \right\|_{\mathcal{H}} \leq C \Delta t \sqrt{\tilde{\mathcal{E}}_h^{n+\frac{1}{2}}} \left\| C_h^T p^n_h \right\|_{\mathcal{H}}.$$

With similar arguments, we can derive the following estimation: there exists $C > 0$ independent of Δt such that

$$\tilde{\mathcal{E}}_h^{n+\frac{1}{2}} \leq C\Delta t\sqrt{\tilde{\mathcal{E}}_h^{n+\frac{1}{2}}}\left\|C_h^T p_h^n\right\|_{\mathcal{H}} + C\Delta t^2 \sum_{k=1}^{n-1} \sqrt{\tilde{\mathcal{E}}_h^{k+\frac{1}{2}}}\left\|C_h^T \frac{p_h^{k+1}-p_h^k}{\Delta t}\right\|_{\mathcal{H}}.$$

It is then standard to prove by the discrete Grönwall lemma, using Corollary 5.8, that there exists $C > 0$ such that

$$\sup_{n\in\mathcal{N}} \sqrt{\mathcal{E}^{n+\frac{1}{2}}} \leq C\Delta t,$$

and therefore estimation (5.89) holds, due to the stability estimate of Corollary 5.8. Furthermore, from this estimate we deduce that

$$\sup_{n\in\mathcal{N}}\left\|(C_h C_h^T)^{-\frac{1}{2}} B_h \frac{\underline{\tilde{e}}_{\alpha,h}^{n+1}+\underline{\tilde{e}}_{\alpha,h}^{n}}{2}\right\|_{\mathcal{H}} \leq C\Delta t^2 \implies \sup_{n\in\mathcal{N}}\left\|C_h^T \frac{\tilde{p}_{\alpha,h}^{n+1}+\tilde{p}_{\alpha,h}^{n}}{2}\right\|_{\mathcal{H}} \leq C,$$

thus concluding the proof. □

We give without proof the following Corollary, since it is similar to the proof of Proposition 5.16. Note that it not assessed if this result is optimal or not, but it is sufficient for our analysis.

Corollary 5.10. *Assume that $\underline{f} \in W_c^4(\mathcal{H})$. Then, there exists $C > 0$ such that for all $\Delta t < \tau_0$ satisfying condition (5.74), then*

$$\boxed{\sup_{n\in\mathcal{N}}\left(\left\|\frac{\underline{\tilde{e}}_{\alpha,h}^{n+1}-\underline{\tilde{e}}_{\alpha,h}^{n}}{\Delta t}\right\|_{\mathcal{X}} + \Delta t \sup_{n\in\mathcal{N}}\left\|C_h^T\frac{\tilde{p}_{\alpha,h}^{n+1}-\tilde{p}_{\alpha,h}^{n}}{\Delta t}\right\|_{\mathcal{H}}\right) \leq C\Delta t.} \tag{5.91}$$

5.6.2 A second-order error estimate

We now retrieve an higher-order estimate on the error performed if we approximate (IMnh) by (QIPnh). Preliminarily, we consider a Helmholtz decomposition of the solution $\underline{y}_{\lambda,h}^n$ of formulation (QIPnh). We can introduce a vectorial field $\underline{w}_{\lambda,h}^n \in \mathcal{Y}_h$ such that, $\forall n \in \mathcal{N}$,

$$\begin{cases} i_h \underline{\tilde{y}}_{\alpha,h}^n = \alpha\Delta t^2 C_h^T \tilde{p}_{\alpha,h}^n + \underline{\tilde{w}}_{\alpha,h}^n & \text{in } \mathcal{Y}_h, \\ C_h\, \underline{\tilde{w}}_{\alpha,h}^n = 0 & \text{in } \mathcal{M}_h. \end{cases} \tag{5.92}$$

We introduce $\underline{\tilde{r}}_{\alpha,h}^n \coloneqq \underline{\tilde{w}}_{\alpha,h}^n - i_h \underline{y}_h^n$. The sequence $\{(\underline{\tilde{e}}_{\alpha,h}^n, \tilde{q}_{\alpha,h}^n)\}_{n\in\mathcal{N}}$ defined in Eq. (5.86) also satisfies

$$\begin{cases} \dfrac{\underline{\tilde{e}}_{\alpha,h}^{n+1} - 2\,\underline{\tilde{e}}_{\alpha,h}^{n} + \underline{\tilde{e}}_{\alpha,h}^{n-1}}{\Delta t^2} + A_h\,\underline{\tilde{e}}_{\alpha,h}^n + B_h^T\,\tilde{q}_{\alpha,h}^n = \underline{0} & \text{in } \mathcal{X}_h, \\ i_h \underline{\tilde{e}}_{\alpha,h}^n = \alpha\Delta t^2 C_h^T \tilde{p}_{\alpha,h}^n + \underline{\tilde{r}}_{\alpha,h}^n & \text{in } \mathcal{X}_h, \\ C_h\,\underline{\tilde{r}}_{\alpha,h}^n = 0, & \text{in } \mathcal{X}_h. \end{cases} \tag{5.93}$$

We now use Eq. (5.93) as a basic ingredient to derive the following proposition.

Proposition 5.17. *Assume that* $\underline{f} \in W_c^4(\mathcal{H})$. *Then, there exists* $C > 0$ *such that for all* $\Delta t < \tau_0$ *satisfying condition* (5.74), *then*

$$\boxed{\left\| \frac{\underline{\tilde{e}}_{\alpha,h}^{n+1} + \underline{\tilde{e}}_{\alpha,h}^{n}}{2} \right\|_{\ell^2(\mathcal{H})} \leq C\Delta t^2.}$$

Proof. First, we introduce the sequence $\{(S_h\underline{\tilde{r}}_{\alpha,h}^n, \tilde{q}_{r_{\alpha,h}}^n) \in \mathcal{X}_h \times \mathcal{M}_h\}$, solution of the dual discrete problem

$$\begin{cases} A_h(S_h\underline{\tilde{r}}_{\alpha,h}^n) + B_h^T(\tilde{q}_{r_{\alpha,h}}^n) = i_h^T\underline{\tilde{r}}_{\alpha,h}^n, \\ B_hS_h\underline{\tilde{r}}_{\alpha,h}^n = 0. \end{cases} \tag{5.94}$$

We consider the first equation in (5.93). Then, we the L^2-scalar product of Eq. (5.94) with $(S_h(\underline{\tilde{r}}_{\alpha,h}^{n+1} - \underline{\tilde{r}}_{\alpha,h}^{n-1}))/(2\,\Delta t)$, and we obtain

$$\left(\frac{\underline{\tilde{e}}_{\alpha,h}^{n+1} - 2\,\underline{\tilde{e}}_{\alpha,h}^{n} + \underline{\tilde{e}}_{\alpha,h}^{n-1}}{\Delta t^2}, \frac{S_h(\underline{\tilde{r}}_{\alpha,h}^{n+1} - \underline{\tilde{r}}_{\alpha,h}^{n-1})}{2\,\Delta t} \right) + \left(A_h\,\underline{\tilde{e}}_{\alpha,h}^{n}, \frac{S_h(\underline{\tilde{r}}_{\alpha,h}^{n+1} - \underline{\tilde{r}}_{\alpha,h}^{n-1})}{2\,\Delta t} \right) = 0,$$

since $B_hS_h\underline{\tilde{r}}_{\alpha,h}^n = 0$. Furthermore, from Eq. (5.94), we get, for all $n > 1$,

$$\left(A_h(S_h\underline{\tilde{r}}_{\alpha,h}^n), \underline{v}_h \right)_{\mathcal{H}} + \left(B_h^T\tilde{q}_{r_{\alpha,h}}^n, \underline{v}_h \right)_{\mathcal{H}} = \left(i_h^T\underline{\tilde{r}}_{\alpha,h}^n, \underline{v}_h^n \right)_{\mathcal{H}}, \quad \forall \underline{v}_h \in \mathcal{X}_h. \tag{5.95}$$

As a consequence, we can rewrite

$$\begin{aligned} \left(A_h\,\underline{\tilde{e}}_{\alpha,h}^n, \frac{S_h(\underline{\tilde{r}}_{\alpha,h}^{n+1} - \underline{\tilde{r}}_{\alpha,h}^{n-1})}{2\,\Delta t} \right)_{\mathcal{H}} &= \left(\underline{\tilde{e}}_{\alpha,h}^n, i_h^T\frac{\underline{\tilde{r}}_{\alpha,h}^{n+1} - \underline{\tilde{r}}_{\alpha,h}^{n-1}}{2\,\Delta t} \right)_{\mathcal{H}} - \left(\underline{\tilde{e}}_{\alpha,h}^n, B_h^T\frac{\tilde{q}_{r_{\alpha,h}}^{n+1} - \tilde{q}_{r_{\alpha,h}}^{n-1}}{2\,\Delta t} \right)_{\mathcal{H}} \\ &= \left(\underline{\tilde{r}}_{\alpha,h}^n, \frac{\underline{\tilde{r}}_{\alpha,h}^{n+1} - \underline{\tilde{r}}_{\alpha,h}^{n-1}}{2\,\Delta t} \right)_{\mathcal{H}} - \alpha\Delta t^2 \left(C_h^T\tilde{p}_{\alpha,h}^n, C_h^T\frac{\tilde{q}_{r_{\alpha,h}}^{n+1} - \tilde{q}_{r_{\alpha,h}}^{n-1}}{2\,\Delta t} \right)_{\mathcal{H}}, \end{aligned}$$

since $C_h\underline{r}_\lambda^n = 0$. Therefore, we have

$$\begin{aligned} \left(\frac{\underline{\tilde{r}}_{\alpha,h}^{n+1} - 2\,\underline{\tilde{r}}_{\alpha,h}^{n} + \underline{\tilde{r}}_{\alpha,h}^{n-1}}{\Delta t^2}, \frac{S_h(\underline{\tilde{r}}_{\alpha,h}^{n+1} - \underline{\tilde{r}}_{\alpha,h}^{n-1})}{2\,\Delta t} \right)_{\mathcal{H}} + \left(\underline{\tilde{r}}_{\alpha,h}^n, \frac{\underline{\tilde{r}}_{\alpha,h}^{n+1} - \underline{\tilde{r}}_{\alpha,h}^{n-1}}{2\,\Delta t} \right)_{\mathcal{H}} \\ = \alpha\Delta t^2 \left(C_h^T\tilde{p}_{\alpha,h}^n, C_h^T\frac{\tilde{q}_{r_{\alpha,h}}^{n+1} - \tilde{q}_{r_{\alpha,h}}^{n-1}}{2\,\Delta t} \right)_{\mathcal{H}}. \end{aligned} \tag{5.96}$$

We now define, using Definition 5.68,

$$\mathcal{E}_r^{n+\frac{1}{2}} := \frac{1}{2}\left\| \frac{\underline{\tilde{r}}_{\alpha,h}^{n+1} - \underline{\tilde{r}}_{\alpha,h}^{n}}{\Delta t} \right\|_{*,h}^2 + \frac{1}{2}\left\| \frac{\underline{\tilde{r}}_{\alpha,h}^{n+1} + \underline{\tilde{r}}_{\alpha,h}^{n}}{2} \right\|_{\mathcal{H}}^2 - \frac{\Delta t^2}{8}\left\| \frac{\underline{\tilde{r}}_{\alpha,h}^{n+1} - \underline{r}_\lambda^n}{\Delta t} \right\|_{\mathcal{H}}^2.$$

It can be shown that this energy is positive under the CFL condition (5.74). Then, we can rewrite Eq. (5.96) as

$$\frac{\mathcal{E}_r^{n+\frac{1}{2}} - \mathcal{E}_r^{n-\frac{1}{2}}}{\Delta t} = \alpha\Delta t^2 \left(C_h^T\hat{p}_{\lambda,h}^n, C_h^T\frac{\tilde{q}_{r_{\alpha,h}}^{n+1} - \tilde{q}_{r_{\alpha,h}}^{n-1}}{2\,\Delta t} \right)_{\mathcal{H}}.$$

Using the Abel summation, we obtain

$$\begin{aligned}\mathcal{E}_r^{n+\frac{1}{2}} =&\alpha\Delta t^2\left(C_h^T\tilde{p}_{\alpha,h}^n, C_h^T\frac{\tilde{q}_{r_{\alpha,h}}^{n+1}+\tilde{q}_{r_{\alpha,h}}^n}{2}\right)\\ &+\alpha\Delta t^2\sum_{k=0}^{n-1}\left(C_h^T\frac{\tilde{q}_{r_{\alpha,h}}^{k+1}+\tilde{q}_{r_{\alpha,h}}^k}{2}, C_h^T\frac{\tilde{p}_{\alpha,h}^{k+1}-\tilde{p}_{\alpha,h}^{k-1}}{\Delta t}\right)\Delta t.\end{aligned} \tag{5.97}$$

Now, as a consequence of Lemma 5.13, we can assert that there exists $C>0$ such that

$$\left\|C_h^T\tilde{q}_{r_{\alpha,h}}^n\right\|_{\mathcal{H}}\leq C\left\|\underline{\tilde{r}}_{\alpha,h}^n\right\|_{\mathcal{H}},\quad \forall n\in\{0,1,..,N+1\}.$$

Therefore, from (5.97) we derive

$$\begin{aligned}\mathcal{E}_r^{n+\frac{1}{2}} \leq& C\,\Delta t^2\left\|C_h^T\tilde{p}_{\alpha,h}^n\right\|_{\mathcal{H}}\left\|\frac{\underline{\tilde{r}}_{\alpha,h}^{n+1}+\underline{\tilde{r}}_{\alpha,h}^n}{2}\right\|_{\mathcal{H}}\\ &+C\,\Delta t^3\sum_{k=0}^{n-1}\left\|\frac{\underline{\tilde{r}}_{\alpha,h}^{k+1}+\underline{\tilde{r}}_{\alpha,h}^k}{2}\right\|_{\mathcal{H}}\left\|C_h^T\frac{\tilde{p}_{\alpha,h}^{k+1}-\tilde{p}_{\alpha,h}^k}{\Delta t}\right\|_{\mathcal{H}}.\end{aligned} \tag{5.98}$$

Note that, thanks to Proposition 5.16, we have that there exists a constant $C>0$ independent of t such that

$$\sup_{n\in\mathcal{N}}\left\|C_h^T\frac{\tilde{p}_{\alpha,h}^{n+1}-\tilde{p}_{\alpha,h}^{n-1}}{2\Delta t}\right\|_{\mathcal{H}}\leq C\implies\sup_{n\in\mathcal{N}}\left\|C_h^T\tilde{p}_{\alpha,h}^n\right\|_{\mathcal{H}}\leq C.$$

We define

$$c(n):=\left\|\frac{\underline{\tilde{r}}_{\alpha,h}^{n+1}+\underline{\tilde{r}}_{\alpha,h}^n}{2}\right\|_{\mathcal{H}},\quad b_0(n):=\left\|C_h^T\tilde{p}_{\alpha,h}^n\right\|_{\mathcal{H}},\quad b_1(n):=\left\|C_h^T\frac{\tilde{p}_{\alpha,h}^{n+1}-\tilde{p}_{\alpha,h}^{n-1}}{2\Delta t}\right\|_{\mathcal{H}}.$$

Then, Eq.(5.98) implies that

$$c^2(n)\leq C\,\Delta t^2c(n)+C\,\Delta t^3\sum_{k=0}^{n-1}c(k).$$

This implies that

$$\Delta t\sum_{n=0}^{N}c^2(n)\leq C\,\Delta t^2\left(\Delta t\sum_{n=0}^{N}c(n)+\Delta t^2\sum_{n=0}^{N}\sum_{k=0}^{n-1}c(k)\right)\leq C\,\Delta t^2\big(1+(N+1)\Delta t\big)\Delta t\sum_{n=0}^{N}c(n).$$

Using the Cauchy-Schwarz inequality in $\ell^2(\mathcal{H})$, we can assert that there exists $C>0$ such that

$$\left\|\frac{\underline{\tilde{r}}_{\alpha,h}^{n+1}+\underline{\tilde{r}}_{\alpha,h}^n}{2}\right\|_{\ell^2(\mathcal{H})}=\left(\sum_{n=0}^{N}c^2(n)\Delta t\right)^{\frac{1}{2}}\leq C\,\Delta t^2.$$

Therefore, we can conclude that

$$\left\|\frac{\underline{\tilde{e}}_{\alpha,h}^{n+1}+\underline{\tilde{e}}_{\alpha,h}^n}{2}\right\|_{\ell^2(\mathcal{H})}\leq\left\|\frac{\underline{\tilde{r}}_{\alpha,h}^{n+1}+\underline{\tilde{r}}_{\alpha,h}^n}{2}\right\|_{\ell^2(\mathcal{H})}+\alpha\Delta t^2\left\|C_h^T\frac{\tilde{p}_{\alpha,h}^{n+1}+\tilde{p}_{\alpha,h}^n}{2}\right\|_{\ell^2(\mathcal{H})}\leq C\Delta t^2,$$

thus concluding the proof. □

Bibliography

Adams, R. A. and Fournier, J. J. [2003], *Sobolev spaces*, Vol. 140, Elsevier.

Boffi, D., Brezzi, F., Fortin, M. et al. [2013], *Mixed finite element methods and applications*, Vol. 44, Springer.

Brenner, S. C. and Sung, L.-Y. [1992], 'Linear finite element methods for planar linear elasticity', *Mathematics of Computation* **59**(200), 321–338.

Brezis, H. [2010], *Functional analysis, Sobolev spaces and partial differential equations*, Springer Science & Business Media.

Brezzi, F. and Fortin, M. [1991], 'Mixed and hybrid finite element methods'.

Chorin, A. J. [1968], 'Numerical solution of the Navier–Stokes equations', *Mathematics of computation* **22**(104), 745–762.

Chorin, A. J. [1969], 'On the convergence of discrete approximations to the Navier–Stokes equations', *Mathematics of computation* **23**(106), 341–353.

Evans, L. C. [2010], 'Partial differential equations'.

Girault, V. and Raviart, P.-A. [1979], Finite element approximation of the Navier–Stokes equations, Technical report, Springer-Verlag.

Guermond, J.-L. [1999], 'Un résultat de convergence d'ordre deux en temps pour l'approximation des équations de Navier–Stokes par une technique de projection incrémentale', *ESAIM: Mathematical Modelling and Numerical Analysis* **33**(1), 169–189.

Guermond, J.-L., Minev, P. and Shen, J. [2006], 'An overview of projection methods for incompressible flows', *Computer methods in applied mechanics and engineering* **195**(44-47), 6011–6045.

Guermond, J.-L. and Quartapelle, L. [1998*a*], 'On stability and convergence of projection methods based on pressure Poisson equation', *International Journal for Numerical Methods in Fluids* **26**(9), 1039–1053.

Guermond, J.-L. and Quartapelle, L. [1998*b*], 'On the approximation of the unsteady Navier–Stokes equations by finite element projection methods', *Numerische Mathematik* **80**(2), 207–238.

Heywood, J. G. and Rannacher, R. [1982], 'Finite element approximation of the nonstationary Navier–Stokes problem. i. regularity of solutions and second-order error estimates for spatial discretization', *SIAM Journal on Numerical Analysis* **19**(2), 275–311.

Heywood, J. G. and Rannacher, R. [1986], 'Finite element approximation of the nonstationary Navier–Stokes problem, part ii: Stability of solutions and error estimates uniform in time', *SIAM journal on numerical analysis* **23**(4), 750–777.

Heywood, J. G. and Rannacher, R. [1988], 'Finite element approximation of the nonstationary Navier–Stokes problem iii. smoothing property and higher order error estimates for spatial discretization', *SIAM Journal on Numerical Analysis* **25**(3), 489–512.

Heywood, J. G. and Rannacher, R. [1990], 'Finite-element approximation of the nonstationary Navier–Stokes problem. part iv: Error analysis for second-order time discretization', *SIAM Journal on Numerical Analysis* **27**(2), 353–384.

Joly, P. [2008], *The mathematical model for elastic wave propagation. In "Effective Computational Methods for Wave Propagation"*, Numerical Insights, CRC Press.

Monk, P. et al. [2003], *Finite element methods for Maxwell's equations*, Oxford University Press.

Quarteroni, A. and Valli, A. [1994], *Numerical Approximation of Partial Differential Equations*, Springer.

Temam, R. [1968], 'Une méthode d'approximation de la solution des équations de Navier-Stokes', *Bull. Soc. Math. France* **98**(4), 115–152.

Temam, R. [2001], *Navier-Stokes equations: theory and numerical analysis*, Vol. 343, American Mathematical Soc.

CHAPTER 6

Numerical modelling of a Shear Wave Elastography experiment

Summary

This chapter is devoted to the description of a complete three-dimensional mathematical and numerical model of the propagation of elastic waves in the myocardial tissue in the context of an SWE experiment. In more detail, we consider that the medium is governed by visco-hyperelasticity and that it is fibered, i.e. heterogeneous and transversely isotropic. Furthermore, we assume that the medium is subject to an active stress, and we consider realistic conditions of an SWE experiment. The numerical approximation of this model consists in high-order Spectral Element method in space and an adapted implicit/explicit time discretisation.

Contents

6.1 Introduction

Remote generation of shear waves induced by a radiation force of a focused ultrasound beam has been recently used in numerous biomedical applications. The main area of application is represented by elasticity imaging, e.g. Shear Wave Elastography Imaging (SWEI) [Sarvazyan et al., 1998], Acoustic Radiation Force Imaging (ARFI) [Nightingale et al., 2003] and Supersonic Shear Imaging (SSI) [Bercoff et al., 2004]. In fact, by measuring the velocity of propagation of the generated shear waves, it is possible to assess mechanical properties of biological tissues and fluids of great clinical interest. Furthermore, a relevant advantage of this approach is the complete attenuation of shear waves in a few wavelengths distance from the focal point of the ultrasonic beam, causing a narrowing of the induced strain, augmenting the spatial resolution and excluding interactions with longitudinal waves at the surface of the tissue.
Numerous models of SWE have been developed in the last decade, mostly oriented toward the applications. The first models were based on the simplifying assumption of a linear and isotropic material, that could represent for example an approximation of the hepatic tissue or other isotropic soft tissues. One of the first FEM models of the dynamic response of the tissue to an impulsive radiation force excitation was presented by Palmeri et al. [2005]. The tissue modelled in this work was isotropic, elastic and linear; two different simulations were presented, accounting for a homogeneous material and a medium with stiffer spherical inclusion. Subsequently, Lee, Szajewski, Hah, Parker and Maniatty [2012] included the effects of viscoelasticity. In more detail, they performed FE simulations with a linear, viscoelastic, isotropic phantom with stiffer cylindrical inclusion undergoing ARF excitation. Shear viscosity was included by a Generalised Maxwell two-element model. Then, the effect of the geometry was explored by Caenen et al. [2017]. In particular, the adopted geometry represented an ellipsoid, and a viscoelastic, linear, isotropic model was adopted by the authors to investigate shear wave physics. The viscosity on the shear was modelled using a two-element Prony model. One of the first models taking into account anisotropy was proposed by Rouze et al. [2013]. In particular, they adopted an FEM model of shear wave propagation in a quasi-incompressible, transversely isotropic, linear, elastic material undergoing impulsive ARF excitation. More recently, Qiang et al. [2015] analysed shear wave propagation in the plane of symmetry of a transversely isotropic, viscoelastic, nearly-incompressible linear material. An impulse traction force was applied at the centre of the cylindrical domain, and a small rod-shape source was considered, so that the generated wave could be assumed as a cylindrical wave; shear viscosity was inserted by a Voigt model. More recent contributions in this context concern the 2D FE simulation proposed by Ye et al. [2017], accounting for a visco-hyperelastic, isotropic, nearly-incompressible Landau's model, and the work of Caenen et al. [2018], who studied an FEM model for shear wave mechanics in an orthotropic material, in combination with uniaxial mechanical loading. In all the aforementioned works, fully explicit time discretisation was adopted and, except for Ye et al. [2017], the software Abaqus was used to solve the resulting system of equations. In fact, the approach of the authors is more oriented towards the application rather than the development of adapted numerical schemes for these problems. Furthermore, in all models an approximation of the body force resulting from the ARF is used. In particular, the acoustic intensity field was simulated with the software program FIELD II and/or modelled as a 3D Gaussian distribution, and in most cases the FE simulation results were compared with in vitro experimental data. On the contrary, our target is to develop a mathematical model of shear wave propagation in SWE and an adequate discretisation of the resulting equations, that is suitable for this specific problem and can enable efficient simulations of an SWE experiment. Furthermore, we aim at exploring the

approximation error that is induced when the approximation of the ARF source term is used instead of the exact expression, that we have derived in Chapter 2. The end-goal of this work is to formally validate transient elastography in the context of cardiac imaging. In particular, we propose a formal 3D mathematical model for elastic wave propagation in a pre-stressed, hyperelastic, viscoelastic, heterogeneous, transversely isotropic medium, that is also subject to an active stress. We hypothesise that the source term, composed of piezoelectric sensors, is high frequency and of small amplitude, and we use the detailed description of the ARF excitation, based on Chapter 2. Note that, in the cardiac setting, the wave propagation induced by the ARF is superposed to the nonlinear mechanics associated with the heart deformation during the cardiac cycle. Moreover, as we are dealing with a soft tissue, the moduli associated with quasi-incompressibility are several orders of magnitude greater than those corresponding to the shear term in the constitutive law. This is reflected by the fact that the velocity of propagation of shear waves (1–$10\,\mathrm{m\,s^{-1}}$) is at least two orders of magnitude lower that the velocity of pressure waves ($1500\,\mathrm{m\,s^{-1}}$). As a consequence, in a fully explicit time discretisation, the choice of the time step is dramatically affected by the fastest wave. On the contrary, a fully implicit time discretisation would not be suitable for our applications, due to the large size of the matrices to invert. In order to overcome this problem, we propose an adapted numerical method for an FEM simulation of the wave propagation, according to the scheme proposed in Chapter 4, based on a mixed implicit/explicit time discretisation.
The chapter is organised as follows. Section 6.2 is devoted to the description of the mathematical model. In particular, in Section 6.2.1, the constitutive laws of the tissue under consideration are recalled, whereas the initial and boundary conditions are defined in Section 6.2.2. Section 6.2.3 is dedicated to the description of the governing equations of the term corresponding to:

- the underlying non-linear mechanics of heart deformation,
- a fast-oscillating pressure wave excited by the probes,
- the shear wave propagation generated by ARF.

The second part of the chapter deals with the numerical approximation of the model for shear wave propagation. In particular, Section 6.3 is devoted to the description of the high-order spectral element method adopted for the discretisation in space of the resulting system of equation; then, in Section 6.4 the implicit/explicit approach is presented for time discretisation. In addition, the stability analysis of the scheme is performed in Section 6.4.1. Finally, Section 6.5 contains some details on the implementation of the numerical scheme and the physical parameters considered for the simulations. Some final remarks and perspectives in Section 6.6 conclude the chapter.

6.2 A 3D non-linear model for wave propagation in the myocardial tissue

6.2.1 Constitutive law

We recall here the main elements in cardiac modelling for the sake of completeness (see Chapter 1 for further detail). Henceforth, we will consider an elastic finite strain dynamic formulation in total Lagrangian form. The Principle of Virtual Work (PVW) reads, in the

reference configuration Ω_0:

$$\forall \underline{w} \in V(\Omega_0), \qquad \int_{\Omega_0} \rho_0 \, \partial_t^2 \underline{y} \cdot \underline{w} \, \mathrm{d}\Omega_0 + \int_{\Omega_0} \underline{\underline{\Sigma}}(\underline{\underline{e}}) : d_{\underline{y}} \underline{\underline{e}} \cdot \underline{w} \, \mathrm{d}\Omega_0 = \int_{\Gamma_{N,0}} \underline{\mathrm{t}}_0 \cdot \underline{w} \, \mathrm{d}S_0, \quad (6.1)$$

where ρ_0 is the density of the medium in the reference configuration, $\underline{y}$ is the displacement field, $\underline{\underline{\Sigma}}$ the Second Piola-Kirchhoff stress tensor, $\underline{\underline{e}}$ the Green-Lagrange strain tensor given by

$$\underline{\underline{e}} = \frac{1}{2}(\underline{\underline{\nabla}} \underline{y} + \underline{\underline{\nabla}}^T \underline{y} + \underline{\underline{\nabla}}^T \underline{y} \cdot \underline{\underline{\nabla}} \underline{y}).$$

Furthermore, $\underline{\mathrm{t}}_0$ accounts for the surfacic force on the boundary $\Gamma_{N,0} \subset \partial\Omega$, generated by the piezoelectric probes. $V(\Omega_0)$ represents the space of admissible test functions, to be defined. We assume that no volumic source term $\underline{f}$ is present and we consider null initial conditions. We have

$$d_{\underline{y}} \underline{\underline{e}} \cdot \underline{w} = \frac{1}{2}\Big(\underline{\underline{\nabla}}_{\underline{\xi}}^T \underline{w} \cdot \underline{\underline{F}} + \underline{\underline{F}}^T \cdot \underline{\underline{\nabla}}_{\underline{\xi}} \underline{w}\Big) = \frac{1}{2}\Big((\mathrm{d}_{\underline{y}} \underline{\underline{F}} \cdot \underline{w})^T \cdot \underline{\underline{F}} + \underline{\underline{F}}^T \cdot \mathrm{d}_{\underline{y}} \underline{\underline{F}} \cdot \underline{w}\Big), \quad (6.2)$$

with $\underline{\underline{F}}$ the deformation tensor. Eq. (6.2) gives the differential of the Green-Lagrange strain tensor with respect to displacement in the space $V(\Omega_0)$. For our purposes, we shall choose with care the expression for $\underline{\underline{\Sigma}}(\underline{\underline{e}})$. In the context of cardiac modelling, we decompose it into two terms, accounting for passive and active stress: $\underline{\underline{\Sigma}} = \underline{\underline{\Sigma}}^P + \underline{\underline{\Sigma}}^A$, where

$$\underline{\underline{\Sigma}}^P := \frac{\partial W^e}{\partial \underline{\underline{e}}} + \frac{\partial W^{\mathrm{VS}}}{\partial \dot{\underline{\underline{e}}}},$$

with W^e hyperelastic potential and W^{VS} viscous pseudo-potential.
In order to consider a realistic passive constitutive law for the myocardium, which is crucial for the analysis of wave propagation and the identification of mechanical parameters, we need to take into account the fibered structure of the tissue. In fact, it has been experimentally validated that muscle fibres are arranged in laminar structures, called sheets, of three to four muscle fibres in the thickness, that are oriented transversely to the heart wall [Streeter et al., 1969; Lee, Pernot, Couade, Messas, Bruneval, Bel, Hagege, Fink and Tanter, 2012]. Moreover, the fibre orientation in human left ventricle myocardium changes smoothly throughout the wall thickness, from $-60°$ close to the epicardium to $+60°$ near the endocardium [Sommer et al., 2015]. Therefore, we propose to model the medium as transversely isotropic, i.e. we suppose that there exists, at every point, a privileged direction represented by the unit vector $\underline{\tau_1}$, related to the muscle fibre, varying smoothly throughout the computational domain. For example, we can consider a hyperelastic potential composed of a term corresponding to a transversely isotropic (TI) law and a penalisation term accounting for nearly-incompressibility (NI) [Chapelle et al., 2012]. In particular, we define

$$W^e := W^{\mathrm{TI}} + W^{\mathrm{NI}},$$

where

$$W^{\mathrm{TI}} := \kappa_1 e^{\kappa_2 (J_1 - 3)^2} + \kappa_3 e^{\kappa_4 (J_4 - 1)^2} + \kappa_5 (J_2 - 3), \quad (6.3)$$

$$W^{\mathrm{NI}} := \frac{\kappa}{2}\big((J^2 - 1) - \log(J^2)\big). \quad (6.4)$$

Eqs. (6.3) and (6.4) are written as functions of *reduced invariants*

$$J_1 = I_1 \, I_3^{-\frac{1}{3}}, \; J_2 = I_2 \, I_3^{-\frac{1}{3}}, \; J \equiv J_3 = I_3^{\frac{1}{2}}, \; J_4 = I_4 \, I_3^{-\frac{1}{3}},$$

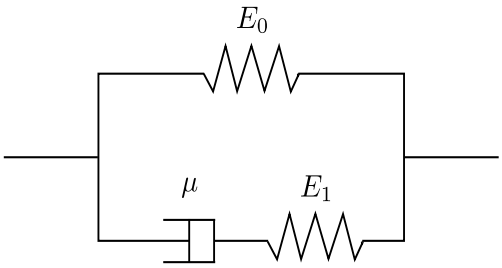

Figure 6.1 – Zener model.

where

$$I_1 = \|\underline{\underline{F}}\|^2 = \mathrm{tr}(\underline{\underline{C}}),\ I_2 = \frac{1}{2}\left((\mathrm{tr}(\underline{\underline{C}}))^2 - \mathrm{tr}(\underline{\underline{C}}^2)\right),\ I_3 = \det \underline{\underline{C}} = \left(\det \underline{\underline{F}}\right)^2,\ I_4 \coloneqq \underline{\tau_1} \cdot \underline{\underline{C}} \cdot \underline{\tau_1}.$$

Note that the myocardium is a soft tissue, therefore it is quasi-incompressible. Consequently, the bulk modulus κ is classically assumed to be several orders of magnitude higher than the coefficients accounting for the other terms in the stress tensor. Henceforth, we define the second Piola-Kirchhoff stress tensors

$$\underline{\underline{\Sigma}}^{\mathrm{TI}} \coloneqq \frac{\partial W^{\mathrm{TI}}}{\partial \underline{\underline{e}}} \quad \text{and} \quad \underline{\underline{\Sigma}}^{\mathrm{NI}} \coloneqq \frac{1}{2}\frac{\partial W^{\mathrm{NI}}}{\partial \underline{\underline{e}}}.$$

On the other hand, we define the second Piola-Kirchhoff stress tensor associated with the active term along the fibre direction $\underline{\tau_1}$ as

$$\underline{\underline{\Sigma}}^{A} = \Sigma_{1d}\, \underline{\tau_1} \otimes \underline{\tau_1},$$

where Σ_{1d} is a prescribed constant. Note that the assumption of a simple active law is justified by our application (see Chapter 1 for further detail).
Viscoelasticity is modelled by adding two separate contributions, acting on pressure and shear term, respectively. Therefore, the viscous second Piola-Kirchhoff stress tensor is defined as

$$\underline{\underline{\Sigma}}^{\mathrm{VS}} \coloneqq \underline{\underline{\Sigma}}^{\mathrm{VS,P}} + \underline{\underline{\Sigma}}^{\mathrm{VS,S}}. \tag{6.5}$$

We can introduce a scalar potential $W^{\mathrm{VS,P}}$ such that

$$\underline{\underline{\Sigma}}^{\mathrm{VS,P}} \coloneqq \frac{\partial W^{\mathrm{VS,P}}}{\partial \underline{\underline{\dot{e}}}},\ \text{with } W^{\mathrm{VS,P}} \coloneqq \frac{\zeta}{2}\left(\mathrm{tr}(\underline{\underline{\dot{e}}})\right)^2$$

Note that we have introduced $\underline{\underline{\dot{e}}} \coloneqq d_{\underline{y}}\underline{\underline{e}} \cdot \partial_t \underline{y} = \frac{1}{2}\Big(\left(\underline{\underline{\nabla}}\partial_t \underline{y}\right)^T \cdot \underline{\underline{F}} + \underline{\underline{F}}^T \cdot \underline{\underline{\nabla}}\partial_t \underline{y}\Big)$. As a consequence, $\underline{\underline{\Sigma}}^{\mathrm{VS,P}}$ reads

$$\underline{\underline{\Sigma}}^{\mathrm{VS,P}} \coloneqq \zeta\ \mathrm{tr}(\underline{\underline{\dot{e}}})\ \underline{\underline{\mathbb{1}}}. \tag{6.6}$$

Note that the viscous coefficient ζ is also assumed to be large. Moreover, On the contrary, the second contribution $\underline{\underline{\Sigma}}^{\mathrm{VS,S}}$ describes the nonlinear, time-dependent behaviour of the shear modulus. Here, we consider a generalisation of the Maxwell model, namely a Zener Model, inspired by Ezziani [2005]. In a rheological representation, we assume that two elements are in parallel (see Figure 6.1), one composed only by a spring with elastic modulus E_0, and the second one consisting in one dashpot with viscosity μ and elastic modulus

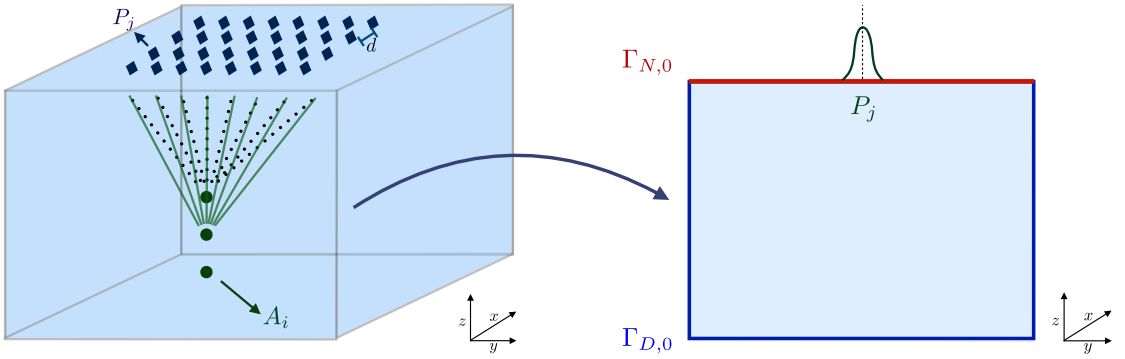

Figure 6.2 – Focalisation of piezoelectric probes at different foci A_i in depth.

E_1. We will define the relaxation time $\tau_1 = \mu/E_1$ and the relaxation modulus ratio $g_1 = E_1/(E_{\text{tot}})$, with $E_{\text{tot}} = E_0 + E_1$. Then, the component $\underline{\underline{\Sigma}}^{\text{VS,S}}$ is defined as

$$\underline{\underline{\Sigma}}^{\text{VS,S}} \coloneqq E_{\text{tot}} \int_0^t \left(1 - g_1\left(1 - e^{-\frac{t-s}{\tau_1}}\right)\right) \underline{\underline{\dot{e}}}(s)\,\mathrm{d}s. \tag{6.7}$$

Note that we can rewrite $\underline{\underline{\Sigma}}^{\text{VS,S}}$ as

$$\underline{\underline{\Sigma}}^{\text{VS,S}} = E_{\text{tot}}\,(1 - g_1)\,\underline{\underline{e}}(t) + E_{\text{tot}}\,g_1 \int_0^t e^{-\frac{t-s}{\tau_1}}\,\underline{\underline{\dot{e}}}\,\mathrm{d}s = \underline{\underline{\Sigma}}^{V}(t) + \underline{\underline{\Sigma}}^{\text{D}}(t),$$

with

$$\underline{\underline{\Sigma}}^{V}(t) \coloneqq E_0\,\underline{\underline{e}}(t), \quad \underline{\underline{\Sigma}}^{\text{D}}(t) \coloneqq E_1 \int_0^t e^{-\frac{t-s}{\tau_1}}\,\underline{\underline{\dot{e}}}\,\mathrm{d}s.$$

As a consequence, we can introduce a potential W^V such that $\underline{\underline{\Sigma}}^{V} = \frac{\partial W^V}{\partial \underline{\underline{e}}}$. From the Duhamel principle, we see that $\underline{\underline{\Sigma}}^{\text{D}}(t)$ is solution of the inhomogeneous linear evolution equation

$$\begin{cases} \partial_t \underline{\underline{\Sigma}}^{\text{D}}(t) + \tau_1^{-1}\,\underline{\underline{\Sigma}}^{\text{D}}(t) = E_1\,\partial_t\,\underline{\underline{e}}(t), \\ \underline{\underline{\Sigma}}^{\text{D}}(0) = \underline{\underline{0}}. \end{cases} \tag{6.8}$$

6.2.2 Boundary conditions

In experiments, shear waves are fully attenuated within a few wavelengths distance, i.e. some millimetres, due to viscosity, and the region of interest taken into account is of some centimetres in each direction. As a consequence, we assume homogeneous Dirichlet boundary conditions on the whole boundary, except for the surface where the piezoelectric probes are located. We denote this boundary as $\Gamma_{D,0}$.
In what follows, we assume that our reference domain is a rectangular slab, and that the probes P_j occupy a surface $\Gamma_{N,0}$ on the upper face of the slab and are equally distributed at distance d, as shown in Figure 6.2. We model this source term as a high-frequency, small-amplitude periodic pressure applied normally to the surface of the slab during a certain pulse time, with focalisation at different foci A_i. Therefore, it reads

$$\underline{\mathrm{t}}_0(\underline{\xi}, t) = \sum_{i=1}^{N_{foci}} \sum_{j=1}^{N_{probes}} g_{i,j}(t)\mathrm{p}_j(\underline{\xi}) \cos\left(\hat{\omega}\,\sqrt{\kappa}\,(t - \tau_{i,j})\right) \underline{\underline{F}}^{-T} \cdot \underline{n}_0 \text{ on } \Gamma_{N,0},$$

where $\mathrm{p}_j(\underline{\xi}) \in H^{\frac{1}{2}}(\Gamma_{N,0})$ are normalised pressures, representing the action of the probes P_j, and modelled as smooth functions with compact support, centred in P_j. Furthermore, $g_{i,j}$ are continuous functions of time with compact support (e.g. a Gaussian profile), and $\underline{\underline{F}}^{-T}\,\underline{n}_0$ is the outward normal of the domain $\Omega(t)$ written in Lagrangian framework. The values of the time delays $\tau_{i,j}$ are computed as

$$\tau_{i,j} = \frac{1}{c}\|A_i - P_j\|.$$

Note that the coefficients $\hat{\omega}$ and $\tau_{i,j}$ represent the parameters to tune to generate shear waves of satisfying amplitude and achieve a good Signal-to-Noise ratio.

6.2.3 Cascade of approximate problems

First, we introduce the following functional spaces:

$$\mathcal{X} := \left\{\underline{v} \in H^1(\Omega_0) \mid \underline{v} = 0 \text{ in } \Gamma_{D,0}\right\}, \quad \mathcal{W} := \left\{\underline{\underline{V}} \in L^2(\Omega_0, \mathscr{L}^{sym}(\mathbb{R}^d))\right\},$$

$$\mathcal{L} := \left\{q \in L^2(\Omega_0) \mid \int_{\Omega_0} q = 0\right\}, \quad \mathcal{M} := \left\{q \in H^1(\Omega_0) \mid q \in \mathcal{L}\right\}.$$

We look for a solution $(\underline{y}, \underline{\underline{\Sigma}}^{\mathrm{D}}) \in \mathcal{X}_{\mathrm{adm}} \times \mathcal{W}_{\mathrm{adm}}$, with $\mathcal{X}_{\mathrm{adm}} \subset \mathcal{X}$, $\mathcal{W}_{\mathrm{adm}} \subset \mathcal{W}$, such that $\forall \underline{w} \in \mathcal{X}_{\mathrm{adm}}$, $\forall t \in [0,T]$,

$$\begin{cases} \displaystyle\int_{\Omega_0} \rho_0\, \partial_t^2 \underline{y} \cdot \underline{w}\, \mathrm{d}\Omega_0 + \int_{\Omega_0} \left(\underline{\underline{\Sigma}}^{\mathrm{TI}} + \underline{\underline{\Sigma}}^{\mathrm{NI}} + \underline{\underline{\Sigma}}^{\mathrm{VS,P}} + \underline{\underline{\Sigma}}^{V} + \underline{\underline{\Sigma}}^{\mathrm{D}} + \underline{\underline{\Sigma}}^{A}\right) : d_{\underline{y}}\underline{\underline{e}} \cdot \underline{w}\, \mathrm{d}\Omega_0 = \\ \qquad\qquad\qquad\qquad\qquad\qquad\qquad\qquad\qquad\qquad \displaystyle\int_{\Gamma_{N,0}} \underline{\mathrm{t}}_0 \cdot \underline{w}\, \mathrm{d}S_0, \\ \partial_t \underline{\underline{\Sigma}}^{\mathrm{D}}(t) + \tau_1^{-1}\, \underline{\underline{\Sigma}}^{\mathrm{D}}(t) = E_1\, \partial_t\, \underline{\underline{e}}(t), \quad \text{in } \Omega_0, \\ \underline{y}(0) = \underline{0}, \quad \partial_t \underline{y}(0) = \underline{0}, \quad \underline{\underline{\Sigma}}^{\mathrm{D}}(0) = \underline{\underline{0}}, \quad \text{in } \Omega_0. \end{cases} \tag{6.9}$$

From the nonlinear problem (6.9) it is possible to retrieve the equations governing the pressure and shear propagation in SWE, as we have shown in Chapter 2 and recall in what follows. To our knowledge, there is no proof of existence and uniqueness of solutions for this problem. However, it is possible to demonstrate that the energy of the problem is non-increasing in absence of external source terms, if the problem is set in a space $\mathcal{X}_{\mathrm{adm}} \times \mathcal{W}_{\mathrm{adm}}$ regular enough.

Energy identity. We assume that a sufficiently smooth solution $\underline{y}$ of Problem (6.9) exists. Then, the energy associated with problem (6.9) reads

$$\mathcal{E} = \mathcal{K} + \mathcal{E}^{\mathrm{int}}, \tag{6.10}$$

where

$$\mathcal{K} := \frac{1}{2}\int_{\Omega_0} \rho_0 \left|\partial_t \underline{y}\right|^2 \mathrm{d}\Omega_0,$$

$$\mathcal{E}^{\mathrm{int}} := \frac{1}{2}\int_{\Omega_0} \left(W^{\mathrm{TI}} + W^{\mathrm{NI}} + W^{V}\right) \mathrm{d}\Omega_0 + \frac{1}{2}\int_{\Omega_0} E_1^{-1} \underline{\underline{\Sigma}}^{\mathrm{D}}(t) : \underline{\underline{\Sigma}}^{\mathrm{D}}(t)\, \mathrm{d}\Omega_0.$$

Proposition 6.1. *The energy satisfies, for all* $t \in [0,T]$:

$$\frac{\mathrm{d}}{\mathrm{d}t}\mathcal{E} = \mathcal{P}^{ext} - \int_{\Omega_0} \frac{\partial W^{VS,P}}{\partial \underline{\underline{\dot{e}}}} : \partial_t \underline{\underline{e}}\, \mathrm{d}\Omega_0 - \int_{\Omega_0} \tau_1^{-1}\, E_1^{-1} \underline{\underline{\Sigma}}^D : \underline{\underline{\Sigma}}^D\, \mathrm{d}\Omega_0,$$

with

$$\mathcal{P}^{ext} := \int_{\Omega_0} \underline{\underline{\Sigma}}^A : \partial_t \underline{\underline{e}}\ \mathrm{d}\Omega_0 + \int_{\Gamma_{N,0}} \underline{t}_0 \cdot \partial_t \underline{y}\, \mathrm{d}S_0.$$

Note that from Proposition 6.1 we deduce that, in absence of external source terms, the energy is non-increasing.

Proof. We consider as test function in the first equation in (6.9) the field $\underline{w} = \partial_t \underline{y}$. We obtain, using Eq. (6.10),

$$\frac{\mathrm{d}}{\mathrm{d}t}\mathcal{K} + \frac{1}{2}\frac{\mathrm{d}}{\mathrm{d}t}\int_{\Omega_0} \left(W^{\mathrm{TI}} + W^{\mathrm{NI}} + W^{V}\right) \mathrm{d}\Omega_0 = \mathcal{P}^{\mathrm{ext}} - \int_{\Omega_0} \frac{\partial W^{\mathrm{VS,P}}}{\partial \underline{\underline{\dot{e}}}} : \partial_t \underline{\underline{e}}\, \mathrm{d}\Omega_0 - \int_{\Omega_0} \underline{\underline{\Sigma}}^{\mathrm{D}} : \partial_t \underline{\underline{e}}\, \mathrm{d}\Omega_0. \tag{6.11}$$

Furthermore, we can rewrite the second equation in (6.9) in the variational formulation, considering a test function $\underline{\underline{W}} \in \mathcal{W}_{\mathrm{adm}}$, and we retrieve

$$\int_{\Omega_0} E_1^{-1} \partial_t \underline{\underline{\Sigma}}^{\mathrm{D}}(t) : \underline{\underline{W}}\, \mathrm{d}\Omega_0 + \int_{\Omega_0} \tau_1^{-1}\, E_1^{-1} \underline{\underline{\Sigma}}^{\mathrm{D}} : \underline{\underline{W}}\, \mathrm{d}\Omega_0 = \int_{\Omega_0} \partial_t \underline{\underline{e}} : \underline{\underline{W}}\, \mathrm{d}\Omega_0. \tag{6.12}$$

If we use as test function $\underline{\underline{W}} = \underline{\underline{\Sigma}}^{\mathrm{D}}$ in Eq. (6.12) and we combine it with Eq. (6.11), we obtain the result of the proposition. □

Preliminaries. The propagation of an elastic wave corresponds to the perturbation of the dynamics defined by Eq. (6.9) on a small time scale t. Therefore, we can assume that the elastic wave propagation is decoupled from the heart dynamics, i.e. we can introduce a slow time scale s associated with the heart deformation and perform a quasi-static approximation of the underlying non-linear mechanics of the heart deformation. Then, since the myocardial tissue is quasi-incompressible, we can define two timescales: one fast, corresponding to the pressure wave propagation, and the scale of the observation, related to the shear wave propagation. We introduce a small and dimensionless parameter ε related to the velocity ratio between the two wave velocities. Then, we rescale

$$\kappa = \varepsilon^{-2}\hat{\kappa}, \quad \zeta = \varepsilon^{-1}\hat{\zeta}, \quad \omega = \varepsilon^{-1}\hat{\omega}.$$

After some considerations issued from asymptotic analysis of the problem (see Chapter 2 for more details), we can assert that, for small t and small ε,

$$\underline{y}(\underline{\xi}, s+t) \approx \underline{y}_0(\underline{\xi}, s) + \varepsilon^2\, \underline{y}_f\big(\underline{\xi}, t, t/\varepsilon\big) + \varepsilon^2\, \underline{y}_S(\underline{\xi}, t), \tag{6.13}$$

where $\underline{y}_0$ is the solution of the underlying non-linear mechanics, $\underline{y}_f$ is a curl-free pressure wave, accounting for the ARF, and $\underline{y}_S$ accounts for the elastic wave propagation. Consequently, we can define a fast time variable $\tau \propto t/\varepsilon$, and a slow time variable t. See Figure 6.3 for a graphical illustration. As a consequence, we assume that $\partial_t \underline{y}_0 \approx \underline{0}$.
Henceforth, we define

$$\begin{aligned}
\underline{\underline{e}}_0 &:= \frac{1}{2}\big(\underline{\underline{F}}_0^T \cdot \underline{\underline{F}}_0 - \underline{\underline{\mathbb{1}}}\big) = \frac{1}{2}\big(\underline{\underline{\nabla}}\, \underline{y}_0 + \underline{\underline{\nabla}}\, \underline{y}_0^T + \underline{\underline{\nabla}}\, \underline{y}_0^T \cdot \underline{\underline{\nabla}}\, \underline{y}_0\big),\\
\underline{\underline{e}}_0(\underline{v}) &:= \frac{1}{2}\big(\underline{\underline{F}}_0^T \cdot \underline{\underline{\nabla}}\, \underline{v} + \underline{\underline{\nabla}}\, \underline{v}^T \cdot \underline{\underline{F}}_0\big) = \frac{1}{2}\big(\underline{\underline{\nabla}}\, \underline{v} + \underline{\underline{\nabla}}\, \underline{v}^T + \underline{\underline{\nabla}}\, \underline{y}_0^T \cdot \underline{\underline{\nabla}}\, \underline{v} + \underline{\underline{\nabla}}\, \underline{v}^T \cdot \underline{\underline{\nabla}}\, \underline{y}_0\big),\\
\underline{\underline{e}}_S(\underline{w}) &:= \frac{1}{2}\big(\underline{\underline{\nabla}}^T \underline{y}_S \cdot \underline{\underline{\nabla}}\, \underline{w} + \underline{\underline{\nabla}}^T \underline{w} \cdot \underline{\underline{\nabla}}\, \underline{y}_S\big),
\end{aligned}$$

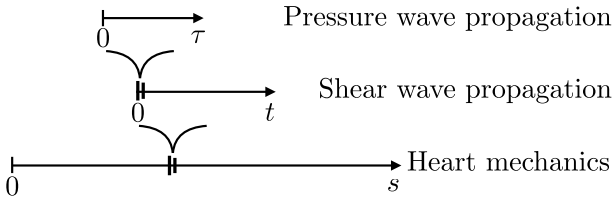

Figure 6.3 – Graphical illustration of the three timescales involved in the problem, accounting for the underlying heart mechanics, the shear wave propagation and the pressure wave propagation.

with $\underline{\underline{F}}_0 := \underline{\underline{\mathbb{1}}} + \underline{\nabla} \underline{y}_0$. Following the approach of Chapter 2, we denote

$$\underline{\underline{C}}_0 := \underline{\underline{\mathbb{1}}} + 2\,\underline{\underline{e}}_0, \quad \underline{\underline{C}}_S := \underline{\underline{e}}_0(\underline{y}_S).$$

Henceforth, we introduce

$$\underline{\underline{C}}_0^{-1} = (\underline{\underline{\mathbb{1}}} + 2\,\underline{\underline{e}}_0)^{-1}, \quad \underline{\underline{G}}_S := -2\,\underline{\underline{C}}_0^{-1} \cdot \underline{\underline{e}}_0(\underline{y}_S) \cdot \underline{\underline{C}}_0^{-1}.$$

We recall here the main results given in Chapter 2, adapted to the specific problem considered.

The nonlinear problem. The leading term $\underline{y}_0$ in the expansion (6.13) satisfies the problem
Find $\left(\underline{y}_0(s), \mathrm{p}_0(s), \underline{\underline{\Sigma}}_0^D(s)\right) \in \mathcal{X} \times \mathcal{L} \times \mathcal{W}$ *s.t.* $\forall \underline{w} \in \mathcal{X}, \forall s \in [0, T^*]$,

$$\begin{cases} \displaystyle\int_{\Omega_0} \rho_0\, \partial_s^2 \underline{y}_0 \cdot \underline{w}\, \mathrm{d}\Omega_0 + \int_{\Omega_0} \left(\underline{\underline{\Sigma}}_0^{\mathrm{TI}} + E_0\, \underline{\underline{e}}_0^D + \underline{\underline{\Sigma}}_0^D\right) : \underline{\underline{e}}_0(\underline{w})\ \mathrm{d}\Omega_0 \\ \qquad\qquad + \displaystyle\int_{\Omega_0} \mathrm{p}_0\, \mathrm{tr}\left(\underline{\underline{C}}_0^{-1} \cdot \underline{\underline{e}}_0(\underline{w})\right)\ \mathrm{d}\Omega_0 = -\int_{\Omega_0} \underline{\underline{\Sigma}}^A : \underline{\underline{e}}_0(\underline{w})\ \mathrm{d}\Omega_0, \\ \partial_s \underline{\underline{\Sigma}}_0^D(t) + \tau_1^{-1}\, \underline{\underline{\Sigma}}_0^D(s) = E_1\, \partial_s\, \underline{\underline{e}}_0(s), \quad \text{in } \Omega_0 \\ \det\left(\underline{\underline{F}}_0^T \cdot \underline{\underline{F}}_0\right) = 1, \quad \text{in } \Omega_0 \end{cases} \tag{6.14}$$

Note that p_0 represents a Lagrange multiplier to enforce incompressibility.

Pressure field and Acoustic Radiation Force The term $\underline{y}_f \in \mathcal{X}$ satisfies $\forall t \in [0, T]$

$$\underline{y}_f(\underline{\xi}, t, \tau) = g(t) \left(Re\big(\hat{\underline{y}}_f(\underline{\xi}, t)\big)\, \cos(\hat{\omega}\,\tau) + Im\big(\hat{\underline{y}}_f(\underline{\xi}, t)\big)\, \sin(\hat{\omega}\,\tau)\right),$$

and

$$\mathrm{div}_{\underline{x}}\, \hat{\underline{y}}_f = \hat{p}_f,$$

where $\hat{p}_f$ satisfies

$$\begin{cases} \Delta\, \hat{p}_f + \alpha\, \hat{p}_f = 0 & \text{in} \quad \Omega(s), \\ \underline{\nabla}_{\underline{x}}\, \hat{p}_f \cdot \underline{n} = 0 & \text{on} \quad \Gamma_{D,s}, \\ \hat{p}_f = \frac{\alpha}{\rho_0\, \hat{\omega}^2} p & \text{on} \quad \Gamma_{N,s}, \end{cases} \tag{6.15}$$

with

$$\alpha \coloneqq \frac{\rho_0\,\hat{\omega}^2}{\hat{\kappa} - i\,\hat{\omega}\,\hat{\zeta}} \in \mathbb{C}. \tag{6.16}$$

Moreover, the pressure field $\hat{p}_f$ is responsible for the Acoustic Radiation Force, that corresponds to a source term for the shear wave field $\underline{y}_S$, and it reads

$$\begin{aligned} s(t,w) = -\frac{\hat{\zeta}\,\hat{\omega}}{2}\int_{\Omega(s)} Im\Big(\hat{p}_f\,\underline{\nabla}_{\underline{x}}\overline{\hat{p}_f}\Big)\cdot\underline{w}\,\mathrm{d}\Omega - \frac{\rho_0\,\hat{\omega}^2}{2|\alpha|^2}\int_{\Gamma_N(t)}\Big(\mathrm{Re}\,\big(\hat{p}_f\,\underline{\underline{H}}_{\underline{x}}\big(\overline{\hat{p}_f}\big)\big)\cdot\underline{n}\Big)\cdot\underline{w}\,\mathrm{d}\Gamma \\ + \frac{1}{4|\alpha|^2}\int_{\Gamma_N(t)}\big(\,\rho_0\,\hat{\omega}^2|\underline{\nabla}_{\underline{x}}\hat{p}_f|^2 - \hat{\kappa}\,|\alpha|^2\,|\hat{p}_f|^2\,\big)\underline{w}\cdot\underline{n}\,\mathrm{d}\Gamma, \end{aligned} \tag{6.17}$$

with $\underline{\underline{H}}_{\underline{x}}\big(\hat{p}_f\big)$ the Hessian matrix of $\hat{p}_f$.

Equation of elastic wave propagation The second corrector $\underline{y}_S$ corresponds to the elastic wave propagating in the medium. The problem satisfied by this field reads
Find $\big(\underline{y}_S, \mathrm{p}_S, \underline{\underline{U}}_S\big) \in \mathcal{X}\times\mathcal{M}\times\mathcal{W}$ *s.t.* $\forall\,(\underline{w}, q, \underline{\underline{W}}) \in \mathcal{X}\times\mathcal{M}\times\mathcal{W}$, $\forall\, t\in[0,T]$,

$$\begin{cases} m(\partial_t^2\underline{y}_S, \underline{w}) + a(\underline{y}_S, \underline{w}) + b(\mathrm{p}_S, \underline{w}) - d(\underline{w}, \underline{\underline{U}}_S) = s(t, \underline{w}), \\ b(q, \underline{y}_S) = g(q) + \alpha\, c(\mathrm{p}_S, q), \\ m_U(\partial_t\underline{\underline{U}}_S, \underline{\underline{W}}) + m_\tau(\underline{\underline{U}}_S, \underline{\underline{W}}) + d(\partial_t\underline{y}_S, \underline{\underline{W}}) = 0, \end{cases} \tag{6.18}$$

with

$$\begin{cases} \underline{y}_S\Big|_{\Gamma_{D,s}} = \underline{0}, \\ \underline{y}_S(0) = \underline{0}, \quad \partial_t\underline{y}_S(0) = \underline{0}, \quad \underline{\underline{U}}_S(0) = \underline{\underline{0}}, \end{cases}$$

we have defined, $\forall(\underline{v},\underline{w}) \in \mathcal{X}\times\mathcal{X}$, $\forall(\underline{\underline{V}},\underline{\underline{W}}) \in \mathcal{W}\times\mathcal{W}$, $\forall(p,q)\in\mathcal{M}\times\mathcal{M}$,

$$\begin{aligned} m(\underline{v},\underline{w}) &= \int_{\Omega_0}\rho_0\,\underline{v}\cdot\underline{w}\,\mathrm{d}\Omega_0, \\ a(\underline{v},\underline{w}) &= \int_{\Omega_0}\Big(\underline{\underline{\Sigma}}_S^{\mathrm{TI}} + E_0\,\underline{\underline{e}}_0(\underline{v})\Big) : \underline{\underline{e}}_0(\underline{w})\;\mathrm{d}\Omega_0 \\ &\quad + \int_{\Omega_0}\Big(\underline{\underline{\Sigma}}_0^{\mathrm{TI}} + E_0\,\underline{\underline{e}}_0 + \underline{\underline{\Sigma}}^A + \mathrm{p}_0\underline{\underline{C}}_0^{-1}\Big) : \underline{\underline{e}}_S(\underline{w})\;\mathrm{d}\Omega_0 \\ &\quad - 2\int_{\Omega_0}\mathrm{p}_0\,\underline{\underline{C}}_0^{-1}\cdot\underline{\underline{e}}_0(\underline{v}) : \underline{\underline{C}}_0^{-1}\cdot\underline{\underline{e}}_0(\underline{w})\;\mathrm{d}\Omega_0, \end{aligned}$$

$$b(q,\underline{w}) = \int_{\Omega_0} \underline{\underline{C}}_0^{-1} : \underline{\underline{e}}_0(\underline{w})\, q \,\mathrm{d}\Omega_0,$$

$$g(q) = \frac{1}{\hat{\kappa}} \int_{\Omega_0} \mathrm{p}_0\, q \,\mathrm{d}\Omega_0,$$

$$c(p,q) = \int_{\Omega_0} \underline{\nabla}\,\mathrm{p} \cdot \underline{\nabla}\, q \,\mathrm{d}\Omega_0,$$

$$m_U(\underline{\underline{V}},\underline{\underline{W}}) = E_1^{-1} \int_{\Omega_0} \underline{\underline{V}} : \underline{\underline{W}} \,\mathrm{d}\Omega_0,$$

$$m_\tau(\underline{\underline{V}},\underline{\underline{W}}) = \tau_1^{-1}\, E_1^{-1} \int_{\Omega_0} \underline{\underline{V}} : \underline{\underline{W}} \,\mathrm{d}\Omega_0 = \tau_1^{-1}\, m_U(\underline{\underline{V}},\underline{\underline{W}}),$$

$$d(\underline{w},\underline{\underline{W}}) = \int_{\Omega_0} \underline{\underline{W}} : \underline{\underline{e}}_0(\underline{w}) \,\mathrm{d}\Omega_0.$$

Furthermore, p_S is a Lagrange multiplier enforcing incompressibility, and $s(t,\underline{w})$ is the non-linear source term depending on $\hat{p}_f$ introduced before. We emphasize that the term $s(t,\underline{w})$ in Eq. (6.17) is written in deformed configuration for the sake of clarity (since some expressions are drastically simplified in deformed configuration), but the problem is solved in reference configuration.
Note also that $\underline{\underline{\Sigma}}_0^{\mathrm{TI}}$ and $\underline{\underline{\Sigma}}_S^{\mathrm{TI}}$ are obtained by linearisation of the tensor $\underline{\underline{\Sigma}}^{\mathrm{TI}}$ around $\underline{y}_0$:

$$\underline{\underline{\Sigma}}^{\mathrm{TI}}(\underline{y}) \approx \underline{\underline{\Sigma}}^{\mathrm{TI}}(\underline{y}_0) + \varepsilon^2 \frac{\partial \underline{\underline{\Sigma}}^{\mathrm{TI}}}{\partial \underline{y}}(\underline{y}_0) : \underline{\underline{e}}_0(\underline{y}_S),$$

and

$$\underline{\underline{\Sigma}}_0^{\mathrm{TI}} := \underline{\underline{\Sigma}}^{\mathrm{TI}}(\underline{y}_0), \quad \underline{\underline{\Sigma}}_S^{\mathrm{TI}} := \frac{\partial \underline{\underline{\Sigma}}^{\mathrm{TI}}}{\partial \underline{y}}(\underline{y}_0) : \underline{\underline{e}}_0(\underline{y}_S).$$

Furthermore, from Eq. (6.18) we can see that the solution has a prescribed divergence, and incompressibility is imposed by penalisation, with a parameter α (see Chapter 4 for further detail).

6.3 Discretisation in space

For spatial discretisation, we introduce the finite-dimensional spaces

$$\mathcal{X}_h \subset \mathcal{X},\ \mathcal{M}_h \subset \mathcal{M} \text{ and } \mathcal{W}_h \subset \mathcal{W},$$

obtained by standard finite element approximation of the spaces $\mathcal{X}$, $\mathcal{M}$, $\mathcal{W}$, respectively. For the sake of simplicity, we denote $\Omega \equiv \Omega(s)$ and $\Gamma_N \equiv \Gamma_{N,s}$ in what follows. We consider here a general framework of finite element approximation with high-order Spectral Elements as proposed by Cohen [2001]. We take a quasi-uniform triangulation $\mathcal{K}$ of Ω composed of quadrangle or hexahedra such that

$$\mathcal{K} = \bigcup_{i=1}^{N} \bar{K}_i, \quad K_i \cap K_j = \emptyset \quad \forall i \neq j.$$

We denote the reference element $\hat{K} = [0,1]^d$, $d = 2, 3$, and the bijective maps $\underline{\phi}_i \in Q_1(\hat{K})^d$ such that

$$\forall i \in \{1, 2, .., N\}, \qquad \underline{\phi}_i(\hat{K}) = K_i,$$

and we define the Jacobian matrix $\underline{\underline{F}}_i = \underline{\nabla}\,\underline{\phi}_i$ and the Jacobian $J_i = \det \underline{\underline{F}}_i$. We also define a triangulation $\mathcal{F}$ of Γ_N composed of elements of dimension $d-1$ such that

$$\mathcal{F} = \bigcup_{i=1}^{N_F} \bar{F}_i.$$

The space discretisation associated with Eq. (6.18) reads
given $(\underline{y}_{0,h}, \mathrm{p}_{0,h}, \underline{\underline{\Sigma}}_0^D) \in \mathcal{X}_h \times \mathcal{M}_h \times \mathcal{W}_h$ and $\hat{p}_{f,h} \in \mathcal{M}_h$, find $\left(\underline{y}_h, \mathrm{p}_h, \underline{\underline{U}}_h\right) \in \mathcal{X}_h \times \mathcal{M}_h \times \mathcal{W}_h$ such that

$\forall\, \underline{w}_h \in \mathcal{X}_h, \forall\, q_h \in \mathcal{M}_h, \forall\, \underline{\underline{W}}_h \in \mathcal{W}_h$

$$\begin{cases} m_h(\partial_t^2 \underline{y}_h, \underline{w}_h) + a_h(\underline{y}_h, \underline{w}_h) + b_h(\mathrm{p}_h, \underline{w}_h) - d_h(\underline{w}_h, \underline{\underline{U}}_h) = s_h(t, \underline{w}_h), \\ b_h(q_h, \underline{y}_h) = g_h(q_h) + \alpha\, c_h(\mathrm{p}_h, q_h), \\ m_{U,h}(\partial_t \underline{\underline{U}}_h, \underline{\underline{W}}_h) + m_{\tau,h}(\underline{\underline{U}}_h, \underline{\underline{W}}_h) + d_h(\partial_t \underline{y}_h, \underline{\underline{W}}_h) = 0, \end{cases} \tag{6.19}$$

with

$$\underline{y}_h(0) = \underline{0}, \quad \partial_t \underline{y}_h(0) = \underline{0}, \quad \underline{\underline{U}}_h(0) = \underline{\underline{0}},$$

and we have approximated

$$m(\underline{y}_h, \underline{w}_h) \approx m_h(\underline{y}_h, \underline{w}_h) = \sum_{\hat{K}_i \in \hat{\mathfrak{K}}} \oint_{\hat{K}_i}^{Q} \rho_0\, \underline{y}_h \cdot \underline{w}_h \,\mathrm{d}\hat{K}_i,$$

$$\begin{aligned} a(\underline{y}_h, \underline{w}_h) \approx a_h(\underline{y}_h, \underline{w}_h) = &\sum_{\hat{K}_i \in \hat{\mathfrak{K}}} \oint_{\hat{K}_i}^{Q} \left(\underline{\underline{\Sigma}}_S^{\mathrm{TI}} + E_0\, \underline{\underline{e}}_0(\underline{y}_h)\right) : \underline{\underline{e}}_0(\underline{w}_h)\ \mathrm{d}\hat{K}_i \\ &+ \sum_{\hat{K}_i \in \hat{\mathfrak{K}}} \oint_{\hat{K}_i}^{Q} \left(\underline{\underline{\Sigma}}_0^{\mathrm{TI}} + E_0\, \underline{\underline{e}}_0 + \underline{\underline{\Sigma}}^A + \mathrm{p}_0 \underline{\underline{C}}_0^{-1}\right) : \underline{\underline{e}}_S(\underline{w}_h)\ \mathrm{d}\hat{K}_i \\ &- 2 \sum_{\hat{K}_i \in \hat{\mathfrak{K}}} \oint_{\hat{K}_i}^{Q} \mathrm{p}_0\, \underline{\underline{C}}_0^{-1} \cdot \underline{\underline{e}}_0(\underline{y}_h) : \underline{\underline{C}}_0^{-1} \cdot \underline{\underline{e}}_0(\underline{w}_h)\ \mathrm{d}\hat{K}_i, \end{aligned}$$

$$b(q_h, \underline{w}_h) \approx b_h(q_h, \underline{w}_h) = \sum_{\hat{K}_i \in \hat{\mathfrak{K}}} \oint_{\hat{K}_i}^{Q} \underline{\underline{C}}_0^{-1} : \underline{\underline{e}}_0(\underline{w}_h)\, q_h \,\mathrm{d}\hat{K}_i,$$

$$g(q_h) \approx g_h(q_h) = \frac{1}{\hat{\kappa}} \sum_{\hat{K}_i \in \hat{\mathfrak{K}}} \oint_{\hat{K}_i}^{Q} \mathrm{p}_{0,h}\, q_h \,\mathrm{d}\hat{K}_i,$$

$$c(\mathrm{p}_h, q_h) \approx c_h(\mathrm{p}_h, q_h) = \sum_{\hat{K}_i \in \hat{\mathfrak{K}}} \oint_{\hat{K}_i}^{Q} \underline{\nabla}\, \mathrm{p}_h \cdot \underline{\nabla}\, q_h \,\mathrm{d}\hat{K}_i,$$

$$m_U(\underline{\underline{U}}_h, \underline{\underline{W}}_h) \approx m_{U,h}(\underline{\underline{U}}_h, \underline{\underline{W}}_h) = E_1^{-1} \sum_{\hat{K}_i \in \hat{\mathfrak{K}}} \oint_{\hat{K}_i}^{Q} \underline{\underline{U}}_h : \underline{\underline{W}}_h \,\mathrm{d}\hat{K}_i,$$

$$m_\tau(\underline{\underline{U}}_h, \underline{\underline{W}}_h) \approx m_{\tau,h}(\underline{\underline{U}}_h, \underline{\underline{W}}_h) = \tau_1^{-1} E_1^{-1} \sum_{\hat{K}_i \in \hat{\mathfrak{K}}} \oint_{\hat{K}_i}^{Q} \underline{\underline{U}}_h : \underline{\underline{W}}_h \,\mathrm{d}\hat{K}_i,$$

and

$$d(\underline{\underline{U}}_h, \underline{w}_h) \approx d_h(\underline{\underline{U}}_h, \underline{w}_h) = \sum_{K_i \in \mathcal{K}} \oint_{K_i}^{Q} \underline{\mathrm{div}}_{\underline{x}}(\underline{\underline{U}}_h) \cdot \underline{w}_h \, \mathrm{d}K_i,$$

$$\begin{aligned} s(t, \underline{w}_h) \approx s_h(t, \underline{w}_h) = & -\frac{\hat{\zeta}\,\hat{\omega}}{2} \sum_{K_i \in \mathcal{K}} \oint_{K_i}^{Q} Im\Big(\hat{p}_{f,h}\, \underline{\nabla}_{\underline{x}} \overline{\hat{p}_{f,h}} \Big) \cdot \underline{w}_h \, \mathrm{d}K_i \\ & - \frac{\rho_0\, \hat{\omega}^2}{2|\alpha|^2} \sum_{F_i \in \mathcal{F}} \oint_{F_i}^{Q} \Big(\mathrm{Re}\left(\hat{p}_{f,h}\, \underline{\underline{H}}_{\underline{x}}(\overline{\hat{p}_{f,h}}) \right) \cdot \underline{n} \Big) \cdot \underline{w}_h \, \mathrm{d}F_i \\ & + \frac{1}{4|\alpha|^2} \sum_{F_i \in \mathcal{F}} \oint_{F_i}^{Q} \left(\rho_0\, \hat{\omega}^2 |\underline{\nabla}_{\underline{x}} \hat{p}_{f,h}|^2 - \hat{\kappa}\, |\alpha|^2\, |\hat{p}_{f,h}|^2 \right) \underline{w}_h \cdot \underline{n} \, \mathrm{d}F_i. \end{aligned}$$

Note that we have identified, for simplicity of notation,

$$\underline{\underline{e}}_0 \equiv \frac{1}{2}\Big(\underline{\underline{\nabla}}\, \underline{y}_{0,h} + \underline{\underline{\nabla}}\, \underline{y}_{0,h}^T + \underline{\underline{\nabla}}\, \underline{y}_{0,h}^T \cdot \underline{\underline{\nabla}}\, \underline{y}_{0,h} \Big), \quad \underline{\underline{C}}_0 \equiv \underline{\underline{\mathbb{1}}} + 2\, \underline{\underline{e}}_{0,h},$$

$$\underline{\underline{\Sigma}}_0^{\mathrm{TI}} \equiv \underline{\underline{\Sigma}}^{\mathrm{TI}}(\underline{y}_{0,h}), \quad \underline{\underline{\Sigma}}_S^{\mathrm{TI}} \equiv \frac{\partial \underline{\underline{\Sigma}}^{\mathrm{TI}}}{\partial \underline{y}}(\underline{y}_{0,h}) : \underline{\underline{e}}_0(\underline{y}_h).$$

The symbol $\oint^{Q}$ stands for the evaluation of the integral by quadrature rule.

Let $r \geq 1$, $d = 3$. We define the space of approximation

$$\mathcal{X}_h = \left\{ \underline{w}_h \in C^0(\Omega)^3 \ s.t. \ \ \underline{w}_h|_{K_i} \circ \underline{\phi}_i \in Q_r(\hat{K})^3 \ \forall i \in \{1, 2, .., N\} \right\},$$

where

$$Q_r(\hat{K}) = \left\{ p(\underline{\xi}) = \sum_{l=0}^{r} \sum_{m=0}^{r} \sum_{n=0}^{r} a_{l,m,n}\, \xi_1^l\, \xi_2^m\, \xi_3^n, \ a_{l,m,n} \in \mathbb{R} \right\}.$$

The basis functions of $\mathcal{X}_h$ are defined from the basis functions of $Q_r(\hat{K})$. We choose for $Q_r(\hat{K})$ the classical Lagrange basis functions $(\hat{\varphi}_{l,m,n})_{l,m,n \in \{1,2,..,r+1\}}$, that satisfy

$$\hat{\varphi}_{l,m,n}\Big(\hat{\underline{\xi}}_{p,q,s} \Big) = \delta_{lp}\, \delta_{mq}\, \delta_{ns},$$

where the points

$$\hat{\underline{\xi}}_{p,q,s} = \left(\underline{\xi}_p, \underline{\xi}_q, \underline{\xi}_s \right), \ p \in \{1, 2, .., r+1\}, \ q \in \{1, 2, .., r+1\}, \ s \in \{1, 2, .., r+1\},$$

are the Legendre-Gauss-Lobatto quadrature points defined on $\hat{K}$ ($\underline{\xi}_p$, $\underline{\xi}_q$, $\underline{\xi}_s$ correspond to the zeros of the derivatives of the Legendre polynomials on $]0, 1[$ plus the extrema 0 and 1), and δ_{lp} is the Kronecker symbol.

Now, since the functions w_h in $\mathcal{X}_h$ satisfy the condition $w_h|_{K_i} \circ \underline{\phi}_i \in Q_r(\hat{K})$, we can assert that, for all basis functions $\varphi_j \in \mathcal{X}_h$, there exists a basis function $\hat{\varphi}_{p,q,s} \in Q_r(\hat{K})$ such that

$$\varphi_j|_{K_i} \circ \underline{\phi}_i = \hat{\varphi}_{p,q,s}, \ \forall K_i \subset supp(\varphi_j).$$

Note that the scalar Degrees Of Freedom (DOFs) for $(y_{h,i})_{i=1,2,3}$ correspond to the components of $y_{h,i}$ in the basis defined by the images by $\underline{\phi}_i$ of the interpolation points $\hat{\underline{\xi}}_{p,q,s}$.

We highlight that, in order to obtain mass-lumping, the quadrature points for the evaluation of the form $m_h(\cdot, \cdot)$ must coincide with the interpolation points. Furthermore,

sufficient accuracy is achieved if such points correspond in the reference elements to the Gauss-Lobatto points of order r. Consequently, we obtain $(r+1)^3$ quadrature/interpolation points in each reference element. We choose the same quadrature for $a_h(\cdot,\cdot)$, in order to obtain sufficient accuracy on non-distorted mesh (see Durufle et al. [2009] for further reading). Then, we consider

$$\mathcal{M}_h = \left\{ q_h \in C^0(\Omega) \; s.t. \;\; q_h|_{K_i} \circ \underline{\phi}_i \in Q_{r-1}(\hat{K}) \; \forall i \in \{1,2,..,N\} \right\}.$$

By definition, $\mathcal{M}_h$ is constructed using continuous finite elements in a lower finite element space. This definition ensures that a discrete inf-sup condition is satisfied (see Boffi et al. [2013]).
Finally, we define

$$\mathcal{W}_h = \left\{ \underline{\underline{W}}_h \in C^0(\Omega)^{3\times 3} \; s.t. \;\; \underline{\underline{W}}_h\Big|_{K_i} \circ \underline{\phi}_i \in Q_r(\hat{K})^{3\times 3} \; \forall i \in \{1,2,..,N\} \right\},$$

For the sake of simplicity, we introduce $B_{N_1} = \{\underline{\omega}_i \mid i = 1,2,..,N_1\}$, with $N_1 = \dim\mathcal{X}_h$, basis functions of $\mathcal{X}_h$. Analogously, we define $B_{N_2} = \{\phi_i \mid i = 1,2,..,N_2\}$ and $B_{N_3} = \{\underline{\underline{\psi}}_i \mid i = 1,2,..,N_3\}$, basis functions of $\mathcal{M}_h$ and $\mathcal{W}_h$, respectively, with $N_2 = \dim\mathcal{M}_h$, $N_3 = \dim\mathcal{W}_h$. We define $Y_h = (Y_{h,1}, Y_{h,2}, .., Y_{h,N_1})$, $P_h = (P_{h,1}, P_{h,2}, .., P_{h,N_2})$ and $U_h = (U_{h,1}, U_{h,2}, .., U_{h,N_3})$ coordinates of $\underline{y}_h$, p_h and $\underline{\underline{U}}_h$ on these bases. Then, we can define the matrices

$$\begin{aligned}
(\mathbf{M}_y)_{i,j} &\coloneqq m_h(\underline{\omega}_i, \underline{\omega}_j), && i,j \in \{1,2,N_1\},\\
(\mathbf{A}_h)_{i,j} &\coloneqq a_h(\underline{\omega}_i, \underline{\omega}_j), && i,j \in \{1,2,N_1\},\\
(\mathbf{B}_h)_{i,j} &\coloneqq b_h(\phi_i, \underline{\omega}_j), && i \in \{1,2,N_2\},\ j \in \{1,2,N_1\},\\
(\mathbf{D}_h)_{i,j} &\coloneqq d_h(\underline{\underline{\psi}}_i, \underline{\omega}_j), && i \in \{1,2,N_3\},\ j \in \{1,2,N_1\},\\
(\mathbf{M}_U)_{i,j} &\coloneqq m_{U,h}(\underline{\underline{\psi}}_i, \underline{\underline{\psi}}_j), && i,j \in \{1,2,N_3\},\\
(\mathbf{M}_\tau)_{i,j} &\coloneqq m_{\tau,h}(\underline{\underline{\psi}}_i, \underline{\underline{\psi}}_j), && i,j \in \{1,2,N_3\},\\
(\mathbf{K}_h)_{i,j} &\coloneqq b_h(\phi_i, \phi_j), && i,j \in \{1,2,N_2\}\\
(G_h)_i &\coloneqq g_h(\phi_i), && i \in \{1,2,N_2\},\\
(S_h)_i &\coloneqq s_h(t, \underline{\omega}_i), && i \in \{1,2,N_1\}.
\end{aligned}$$

The semi-discrete formulation (6.19) reads, in matrix form,

$$\begin{cases}
\mathbf{M}_y \ddot{Y}_h + \mathbf{A}_h Y_h + \mathbf{B}_h^T P_h - \mathbf{D}_h U_h = S_h,\\
\mathbf{M}_U \dot{U}_h + \mathbf{M}_\tau U_h = \mathbf{D}_h \dot{Y}_h,\\
\mathbf{B}_h Y_h = \alpha \mathbf{K}_h P_h + G_h,
\end{cases} \tag{6.20}$$

with

$$Y_h(t=0) = 0, \quad \dot{Y}_h(t=0) = 0, \quad U_h(0) = 0.$$

6.4 Discretisation in time

Soft media, such as the myocardial tissue, are quasi-incompressible. Therefore, a total explicit discretisation in time is not efficient, since the CFL stability condition is highly affected by the enforcement of incompressibility. On the other hand, a total implicit

time discretisation would also be unsuitable, since the matrix to invert would have size $\left(3 \times N_{dof}\right)^2$, too large to be efficiently computed.
In order to solve this problem, we have developed in Chapter 4 a numerical scheme that carefully takes into account the intrinsic properties of the wave equation. In more detail, only the terms corresponding to "informations" travelling at infinite velocity (i.e. the incompressibility constraint) are treated implicitly, by solving a Poisson problem. Therefore, if effective methods for explicit time- discretisation are used, our algorithm requires at each iteration one resolution of a scalar Poisson problem and few matrix-vector multiplications for the explicit methods. Note that we choose here only finite difference scheme. In more detail, we adopt centred finite difference schemes, in order to preserve energy conservation in the discrete framework.
We consider a time interval $[0, T]$, $T > 0$, and introduce a time discretisation $t^n = n\,\Delta t$, $n \in \{0, 1, .., N\}$, with $\Delta t = T/N$. Then, the fully discrete scheme corresponding to Eq. (6.20) reads

$$\begin{cases} \mathbf{M}_y \dfrac{Y_h^{n+1} - 2\,Y_h^n + Y_h^{n-1}}{\Delta\, t^2} + \mathbf{A}_h\, Y_h^n + \mathbf{B}_h^T\, P_h^n - \mathbf{D}_h\, U_h^n = S_h^n, \\ \mathbf{B}_h\, Y_h^n = \alpha \Delta t^2 \mathbf{K}_h\, P_h^n + G_h, \\ \mathbf{M}_U \dfrac{U_h^{n+1} - U_h^n}{\Delta\, t} + \mathbf{M}_\tau \dfrac{U_h^{n+1} + U_h^n}{2} + \mathbf{D}_h^T \dfrac{Y_h^{n+1} - Y_h^n}{\Delta\, t} = 0, \end{cases} \tag{6.21}$$

with $\{Y_h^n \in \mathcal{X}_h\}$, $\{P_h^n \in \mathcal{M}_h\}$, $\{U^n \in \mathcal{W}_h\}$ for $n \in \{1, .., N\}$, and (Y_h^0, P_h^0, U_h^0) given. Note that here, for consistency reasons, we have rescaled the penalisation parameter by Δt^2 and assume that α is independent of Δt. Note that G_h has no time evolution, since this term depends on the field p_0, that is independent of t. Note that the scalar field P_h^n is computed at each time step as

$$P_h^n = \frac{\mathbf{K}_h^{-1}\mathbf{B}_h}{\alpha\, \Delta\, t^2}\, Y_h^n - G_h. \tag{6.22}$$

Using Eq. (6.22), we can reformulate the first equation in (6.21) as

$$\mathbf{M}_y \frac{Y_h^{n+1} - 2\,Y_h^n + Y_h^{n-1}}{\Delta\, t^2} + \mathbf{A}_h^*\, Y_h^n - \mathbf{D}_h\, U_h^n = S_h^n + \mathbf{B}_h^T\, G_h,$$

with

$$\mathbf{A}_h^* = \mathbf{A}_h + \frac{\mathbf{B}_h^T \mathbf{K}_h^{-1} \mathbf{B}_h}{\alpha\, \Delta\, t^2}.$$

Note that the first and second equations in (6.21) are centred at time step t^n, while the third one is centred at $t^{n+\frac{1}{2}}$.

6.4.1 Stability analysis

The objective of this section is to retrieve a uniform estimate of the discrete energy associated with Eq. (6.21). For the sake of simplicity, we consider that

$$S_h^n + \mathbf{B}_h^T\, G_h = \underline{0},\ \forall n \geq 0.$$

The discrete energy at time $n + \frac{1}{2}$ reads

$$\mathcal{E}^{n+\frac{1}{2}} = \mathcal{E}_k^{n+\frac{1}{2}} - \frac{\Delta t^2}{4} \mathcal{E}_{kp}^{n+\frac{1}{2}} + \mathcal{E}_p^{n+\frac{1}{2}} + \mathcal{E}_U^{n+\frac{1}{2}} + \frac{\Delta\, t^2}{4} \mathcal{C}^{n+\frac{1}{2}}, \tag{6.23}$$

with

$$\mathcal{E}_k^{n+\frac{1}{2}} := \frac{1}{2}\left(\frac{Y_h^{n+1}-Y_h^n}{\Delta t}\right)^T \mathbf{M}_y \frac{Y_h^{n+1}-Y_h^n}{\Delta t}, \tag{6.24}$$

$$\mathcal{E}_{kp}^{n+\frac{1}{2}} := \frac{1}{2}\left(\frac{Y_h^{n+1}-Y_h^n}{\Delta t}\right)^T \mathbf{A}_h^* \frac{Y_h^{n+1}-Y_h^n}{\Delta t}, \tag{6.25}$$

$$\mathcal{E}_p^{n+\frac{1}{2}} := \frac{1}{2}\left(\frac{Y_h^{n+1}+Y_h^n}{2}\right)^T \mathbf{A}_h^* \frac{Y_h^{n+1}+Y_h^n}{2}, \tag{6.26}$$

$$\mathcal{E}_U^{n+\frac{1}{2}} := \frac{1}{4}\left(\|U_h^{n+1}\|_{\mathbf{M}_U}^2 + \|U_h^n\|_{\mathbf{M}_U}^2\right), \tag{6.27}$$

$$\mathcal{C}^{n+\frac{1}{2}} := \frac{1}{2}\left(\frac{U_h^{n+1}-U_h^n}{\Delta t}\right)^T \mathbf{D}_h^T \frac{Y_h^{n+1}-Y_h^n}{\Delta t}. \tag{6.28}$$

Proposition 6.2. *Let us define the following dissipative term:*

$$\mathcal{D}_U^n := \frac{1}{4}\left\|\frac{U_h^{n+1}+U_h^n}{2}\right\|_{M_\tau}^2 + \frac{1}{4}\left\|\frac{U_h^n+U_h^{n-1}}{2}\right\|_{M_\tau}^2. \tag{6.29}$$

Then, the discrete energy $\mathcal{E}^{n+\frac{1}{2}}$ satisfies

$$\frac{\mathcal{E}^{n+\frac{1}{2}}-\mathcal{E}^{n-\frac{1}{2}}}{\Delta t} = -\mathcal{D}_U^n \leq 0.$$

Therefore, the energy associated with Eq. (6.21) is decreasing.

Proof. First, let us multiply the first equation in (6.21) by $\dfrac{Y_h^{n+1}-Y_h^{n-1}}{2\,\Delta t}$. We obtain, using Eqs. (6.24) and (6.26),

$$\begin{aligned}\frac{1}{\Delta t}\left(\mathcal{E}_k^{n+\frac{1}{2}} - \mathcal{E}_k^{n-\frac{1}{2}} + \mathcal{E}_p^{n+\frac{1}{2}} - \mathcal{E}_p^{n-\frac{1}{2}} - \frac{\Delta t^2}{4}\mathcal{E}_{kp}^{n+\frac{1}{2}} + \frac{\Delta t^2}{4}\mathcal{E}_{kp}^{n-\frac{1}{2}}\right)\\ -\left(\frac{Y_h^{n+1}-Y_h^{n-1}}{2\,\Delta t}\right)^T \mathbf{D}_h^T U_h^n = 0.\end{aligned} \tag{6.30}$$

Now, let us multiply the third equation in (6.21) by $\dfrac{U_h^{n+1}+U_h^n}{2}$. We get

$$\begin{aligned}\frac{1}{2\,\Delta t}\left((U_h^{n+1})^T \mathbf{M}_U U_h^{n+1} - (U_h^n)^T \mathbf{M}_U U_h^n\right) + \left(\frac{U_h^{n+1}+U_h^n}{2}\right)^T \mathbf{M}_\tau \frac{U_h^{n+1}+U_h^n}{2}\\ +\left(\frac{U_h^{n+1}+U_h^n}{2}\right)^T \mathbf{D}_h^T \frac{Y_h^{n+1}-Y_h^n}{\Delta t} = 0.\end{aligned} \tag{6.31}$$

We now average Eq. (6.31) between the two time instants $t^{n+\frac{1}{2}}$ and $t^{n-\frac{1}{2}}$. We can write

$$\begin{aligned}\frac{1}{4\,\Delta t}\left((U_h^{n+1})^T \mathbf{M}_U U_h^{n+1} - (U_h^{n-1})^T \mathbf{M}_U U_h^{n-1}\right) + \frac{1}{2}\left(\frac{U_h^{n+1}+U_h^n}{2}\right)^T \mathbf{M}_\tau \frac{U_h^{n+1}+U_h^n}{2}\\ +\frac{1}{2}\left(\frac{U_h^n+U_h^{n-1}}{2}\right)^T \mathbf{M}_\tau \frac{U_h^n+U_h^{n-1}}{2} + \Delta t\left(\frac{U_h^{n+1}-U_h^n}{2\Delta t}\right)^T \mathbf{D}_h^T \frac{Y_h^{n+1}-Y_h^n}{2\Delta t}\\ -\Delta t\left(\frac{U_h^n-U_h^{n-1}}{2\Delta t}\right)^T \mathbf{D}_h^T \frac{Y_h^n-Y_h^{n-1}}{2\Delta t} + \left(U_h^n\right)^T \mathbf{D}_h^T \frac{Y_h^{n+1}-Y_h^{n-1}}{2\Delta t} = 0.\end{aligned}$$

Consequently, we can rewrite, using Eqs. (6.27) and (6.28),

$$-\left(U_h^n\right)^T \mathbf{D}_h^T \frac{Y_h^{n+1}-Y_h^{n-1}}{2\Delta t} = \frac{1}{\Delta t}\left(\mathcal{E}_U^{n+\frac{1}{2}} - \mathcal{E}_U^{n-\frac{1}{2}}\right) + \mathcal{D}_U^n + \frac{1}{\Delta t}\left(\mathcal{C}^{n+\frac{1}{2}} - \mathcal{C}^{n-\frac{1}{2}}\right). \quad (6.32)$$

By injecting Eq. (6.32) in Eq. (6.30), and taking into account the definition of $\mathcal{E}^{n+\frac{1}{2}}$, we obtain the desired result. □

It now remains to prove the positivity of discrete energy $\mathcal{E}^{n+\frac{1}{2}}$.

Proposition 6.3. *A sufficient condition for the stability of the scheme (6.21) in $L^2(\Omega)$ is*

$$\frac{\Delta t^2}{4} \sup_{Y_h \neq 0} \frac{4\,\alpha\, Y_h^T \mathbf{R}_h\, Y_h}{4\,\alpha\, Y_h^T \mathbf{M}_y\, Y_h - Y_h^T \mathbf{Q}_h Y_h} \leq 1, \quad (6.33)$$

with

$$\mathbf{R}_h := \mathbf{A}_h + \mathbf{D}_h\, \mathbf{M}_U^{-1}\, \mathbf{D}_h^T, \quad \mathbf{Q}_h := \mathbf{B}_h^T \mathbf{K}_h^{-1} \mathbf{B}_h. \quad (6.34)$$

Proof. Let us first note that

$$\left\|U_h^{n+1}\right\|_{\mathbf{M}_U}^2 + \left\|U_h^n\right\|_{\mathbf{M}_U}^2 = \frac{1}{2}\left(\left\|U_h^{n+1} + U_h^n\right\|_{\mathbf{M}_U}^2 + \left\|U_h^{n+1} - U_h^n\right\|_{\mathbf{M}_U}^2\right).$$

We rewrite the definition of $\mathcal{E}^{n+\frac{1}{2}}$ as

$$\mathcal{E}^{n+\frac{1}{2}} = \mathcal{E}_1^{n+\frac{1}{2}} + \mathcal{E}_2^{n+\frac{1}{2}},$$

with

$$\mathcal{E}_1^{n+\frac{1}{2}} = \frac{1}{4}\left\|U_h^{n+1} + U_h^n\right\|_{\mathbf{M}_U}^2 + \left(\frac{Y_h^{n+1}+Y_h^n}{2}\right)^T \mathbf{A}_h^* \frac{Y_h^{n+1}+Y_h^n}{2},$$

$$\mathcal{E}_2^{n+\frac{1}{2}} = \left(\frac{Y_h^{n+1}-Y_h^n}{\Delta t}\right)^T \left(\mathbf{M}_y - \frac{\Delta t^2}{4}\mathbf{A}_h^*\right) \frac{Y_h^{n+1}-Y_h^n}{\Delta t} + \frac{\Delta t^2}{4}\left\|\frac{U_h^{n+1}-U_h^n}{\Delta t}\right\|_{\mathbf{M}_U}^2 + \frac{\Delta t^2}{2}\left(\frac{U_h^{n+1}-U_h^n}{\Delta t}\right)^T \mathbf{D}_h^T \frac{Y_h^{n+1}-Y_h^n}{\Delta t}.$$

Since $\mathcal{E}_1^{n+\frac{1}{2}} \geq 0$, we need to find the sufficient condition that ensures $\mathcal{E}_2^{n+\frac{1}{2}} \geq 0$, in order to infer stability.

Note that, from the Cauchy-Schwarz and triangular inequality, we have

$$\left|\left(\frac{U_h^{n+1}-U_h^n}{\Delta t}\right)^T \mathbf{M}_U^{\frac{1}{2}} \mathbf{M}_U^{-\frac{1}{2}} \mathbf{D}_h^T \frac{Y_h^{n+1}-Y_h^n}{\Delta t}\right| \leq \frac{1}{2}\left(\frac{U_h^{n+1}-U_h^n}{\Delta t}\right)^T \mathbf{M}_U \frac{U_h^{n+1}-U_h^n}{\Delta t} + \frac{1}{2}\left(\frac{Y_h^{n+1}-Y_h^n}{\Delta t}\right)^T \mathbf{D}_h \mathbf{M}_U^{-1} \mathbf{D}_h^T \frac{Y_h^{n+1}-Y_h^n}{\Delta t}.$$

Consequently, we get

$$\mathcal{E}_2^{n+\frac{1}{2}} \geq \left(\frac{Y_h^{n+1}-Y_h^n}{\Delta t}\right)^T \left(\mathbf{M}_y - \frac{\Delta t^2}{4}\mathbf{A}_h^*\right) \frac{Y_h^{n+1}-Y_h^n}{\Delta t} - \frac{\Delta t^2}{4}\left(\frac{Y_h^{n+1}-Y_h^n}{\Delta t}\right)^T \mathbf{D}_h \mathbf{M}_U^{-1} \mathbf{D}_h^T \frac{Y_h^{n+1}-Y_h^n}{\Delta t}$$

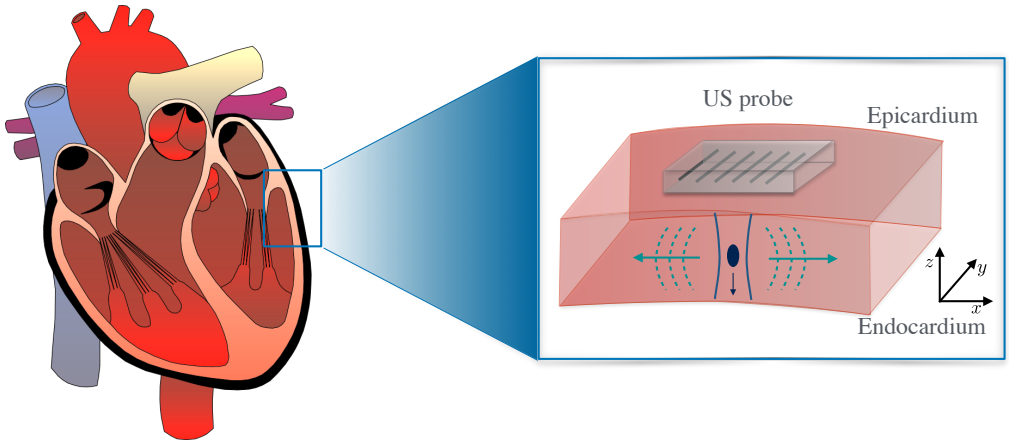

Figure 6.4 – Graphical illustration of the region of interest.

Finally, we need to satisfy

$$Y_h^T \mathbf{M}_y Y_h - \frac{\Delta t^2}{4} Y_h^T (\mathbf{A}_h^* + \mathbf{D}_h \mathbf{M}_U^{-1} \mathbf{D}_h^T) Y_h \geq 0, \ \forall Y_h \in \mathcal{X}_h.$$

By definition of A_h^*, this corresponds to verify

$$Y_h^T \mathbf{M}_y Y_h - \frac{\Delta t^2}{4} Y_h^T (\mathbf{A}_h + \mathbf{D}_h \mathbf{M}_U^{-1} \mathbf{D}_h^T) Y_h - \frac{1}{4\,\alpha} Y_h^T \mathbf{Q}_h Y_h \geq 0, \ \forall Y_h \in \mathcal{X}_h, \tag{6.35}$$

with $\mathbf{Q}_h$ defined as in Eq. (6.34). Therefore, taking into account Eq. (6.34), Eq. (6.35) can be rewritten as

$$\frac{\Delta t^2}{4} \sup_{Y_h \neq 0} \frac{4\,\alpha\, Y_h^T \mathbf{R}_h \underline{y}_h}{4\,\alpha\, Y_h^T \mathbf{M}_y Y_h - Y_h^T \mathbf{Q}_h Y_h} \leq 1,$$

thus concluding the proof. □

6.5 Perspective results

In the perspective of an application to elastography imaging of myocardial tissue by means of ARF-based SWE, we need to consider three-dimensional simulation of elastic wave propagation in an heterogeneous, anisotropic, viscoelastic, nearly-incompressible, pre-stressed medium, as proposed in Section 6.2.1.

Physical parameters. The geometry of the domain to be considered is a parallelepiped of length 0.04 m in x and y directions, and 0.02 m in z direction. This configuration represents an approximation of a region of interest in the left myocardium, selected at the middle ventricular level, see Figure 6.4 for a graphical illustration. Furthermore, the orientation of $\underline{\tau_1}$ is in the xy-plane, and it varies linearly along the direction z from $-60°$ w.r.t. the x-axis at the bottom of the domain ($z = 0$) to $+60°$ at the top of the domain ($z = L$). The resulting medium is highly heterogeneous. Density is set equal to $\rho = 1050\,\mathrm{kg\,m^{-1}}$. The coefficients in Eqs. (6.3), (6.4) and (6.6) read $\kappa_1 = 80\,\mathrm{kPa}$, $\kappa_2 = 2$, $\kappa_3 = 170\,\mathrm{kPa}$, $\kappa_4 = 2.5$, $\kappa_5 = 80\,\mathrm{Pa}$, $\kappa = 10\,\mathrm{MPa}$ and $\mu = 80\,\mathrm{kPa}$.
Two different expressions of the source term will be used: one is the exact expression

of the Acoustic Radiation Force, obtained in Chapter 2, whereas the other expression is represented by the volumic body force used in standard modeling of SWE [Nightingale et al., 2002; Palmeri et al., 2005]. This source term consists is an approximation of the term $s(t, w)$ by standard Gaussian profile in space multiplied by a Gaussian profile in time. In particular, it reads

$$\underline{f}(x, y, z, t) \coloneqq A_{max} \exp^{-\left(\frac{(x-x_F)^2}{\sigma_x^2}+\frac{(y-y_F)^2}{\sigma_y^2}+\frac{(z-z_F)^2}{\sigma_z^2}\right)} \cdot \exp^{-\frac{(t-t_{pulse})^2}{\sigma_t^2}}, \tag{6.36}$$

with centre $(x_F, y_F, z_F) = (0., 0., 0.02)\,\mathrm{m}$, covariance $(\sigma_x^2, \sigma_y^2, \sigma_z^2) = (4e{-}4, 4e{-}4, 1e{-}1)\,\mathrm{m}$, $\sigma_t^2 = 5e-5\,\mathrm{s}$ and mean $t_{pulse} = 1.25e-4\,\mathrm{s}$. The coefficient A_{max} is a maximal amplitude, and it is derived from the expression [Nightingale et al., 2002]

$$A_{max} = \frac{2\,\alpha\,I}{v_p}, \tag{6.37}$$

with absorption coefficient $\alpha = 0.4\,\mathrm{dB/cm/MHz}$, time-averaged acoustic intensity $I = 1500\,\mathrm{W/cm^2}$ and longitudinal wave speed $v_p = 1540\,\mathrm{m/s}$.

Numerical parameters. High-order Spectral Finite Elements of order R for the displacement and $R-1$ for the pressure will be used for space discretisation. The computational grid is composed of N uniform elements of size $h = 1/N$ in each direction. We will adopt the time discretisation introduced in scheme (6.21) with penalisation coefficient $\alpha = 1/3\rho$ and we choose the time step as

$$\Delta t^2 \leq (1-\varepsilon)\,4\,\rho\,\|A_h\|^{-1}\frac{4\,\alpha\,\rho-1}{4\,\alpha\,\rho},$$

with $\varepsilon \in (0, 1)$, to account for the fact that the expression above is an approximation of the CFL condition when quadrature formulae are used. For each iteration of the scheme, the Poisson problem for the scalar pressure field (6.22) is computed by means of our in-house fast solver based on high-order Fourier Transform (see Chapter 7). This is possible since, due to incompressibility, the problem for the pressure wave remains homogeneous, although the medium is heterogeneous. Consequently, the time step used in the explicit time discretisation is only limited by the shear wave velocity.

6.6 Discussions and conclusions

One of the end-objectives of this ongoing work is to simulate an SWE experiment in realistic conditions. Moreover, we aim at using the exact term accounting for the ARF, in order to analyse the effect of the approximation of this source term by the volumic body force that is usually implemented in the literature [Nightingale et al., 2002; Palmeri et al., 2005].
In addition, we aim at considering the effect of more complex viscous laws in the propagation of shear waves. In this chapter, we have considered a Zener model, but other choices could be envisaged. We also emphasize that a further complexity is represented by the assumption of a prestressed medium (i.e. $\underline{y}_0 \neq \underline{0}$).
Another aspect concerns the boundary conditions. Due to the full attenuation of shear waves in a few millimetres, it is reasonable to consider a small region of interest. The

simplest choice is to consider transparent boundary conditions everywhere except for the surface where the probes are positioned. However, it would be of interest to use Perfectly Matched Layers (PML) [Berenger, 1994]. These techniques have proven to be efficient in the treatment of wave propagation in anisotropic acoustic media [Demaldent and Imperiale, 2013; Fliss and Joly, 2012] and in elastic materials [Bécache et al., 2003; Chew and Liu, 1996], but they need to be extended to incompressible elasticity. The main challenge consists in the adequate treatment of the large ratio between the shear wave and pressure wave velocity. However, the proper definition of the specific configuration of the domain (e.g. geometry, heterogeneity, viscosity) and the mathematical analysis of the obtained equations are key-steps to define adapted and stable variants of these techniques.

Bibliography

Bécache, E., Fauqueux, S. and Joly, P. [2003], 'Stability of perfectly matched layers, group velocities and anisotropic waves', *Journal of Computational Physics* **188**(2), 399–433.

Bercoff, J., Tanter, M. and Fink, M. [2004], 'Supersonic shear imaging: a new technique for soft tissue elasticity mapping', *IEEE transactions on ultrasonics, ferroelectrics, and frequency control* **51**(4), 396–409.

Berenger, J.-P. [1994], 'A perfectly matched layer for the absorption of electromagnetic waves', *Journal of computational physics* **114**(2), 185–200.

Boffi, D., Brezzi, F., Fortin, M. et al. [2013], *Mixed finite element methods and applications*, Vol. 44, Springer.

Caenen, A., Pernot, M., Peirlinck, M., Mertens, L., Swillens, A. and Segers, P. [2018], 'An in silico framework to analyze the anisotropic shear wave mechanics in cardiac shear wave elastography', *Physics in Medicine & Biology* **63**(7), 075005.

Caenen, A., Pernot, M., Shcherbakova, D. A., Mertens, L., Kersemans, M., Segers, P. and Swillens, A. [2017], 'Investigating shear wave physics in a generic pediatric left ventricular model via in vitro experiments and finite element simulations', *IEEE transactions on ultrasonics, ferroelectrics, and frequency control* **64**(2), 349–361.

Chapelle, D., Le Tallec, P., Moireau, P. and Sorine, M. [2012], 'An energy-preserving muscle tissue model: formulation and compatible discretizations', *International Journal for Multiscale Computational Engineering* **10**(2), 189–211.

Chew, W. and Liu, Q. [1996], 'Perfectly matched layers for elastodynamics: a new absorbing boundary condition', *Journal of Computational Acoustics* **4**(04), 341–359.

Cohen, G. [2001], *Higher-Order Numerical Methods for Transient Wave Equations*, Scientific Computation, Springer Berlin Heidelberg.

Demaldent, E. and Imperiale, S. [2013], 'Perfectly matched transmission problem with absorbing layers: Application to anisotropic acoustics in convex polygonal domains', *International Journal for Numerical Methods in Engineering* **96**(11), 689–711.

Durufle, M., Grob, P. and Joly, P. [2009], 'Influence of Gauss and Gauss-Lobatto quadrature rules on the accuracy of a quadrilateral finite element method in the time domain', *Numer. Methods Partial Differential Equations* **25**(3), 526–551.

Ezziani, A. [2005], Modélisation mathématique et numérique de la propagation d'ondes dans les milieux viscoélastiques et poroélastiques, PhD thesis, Mathématiques [math]. ENSTA ParisTech. Français. $\langle NNT : 2005PA090019\rangle.\langle tel - 00009179v3\rangle$.

Fliss, S. and Joly, P. [2012], 'Wave propagation in locally perturbed periodic media (case with absorption): Numerical aspects', *Journal of Computational Physics* **231**(4), 1244–1271.

Lee, K. H., Szajewski, B. A., Hah, Z., Parker, K. J. and Maniatty, A. M. [2012], 'Modeling shear waves through a viscoelastic medium induced by acoustic radiation force', *International journal for numerical methods in biomedical engineering* **28**(6-7), 678–696.

Lee, W.-N., Pernot, M., Couade, M., Messas, E., Bruneval, P., Bel, A., Hagege, A. A., Fink, M. and Tanter, M. [2012], 'Mapping myocardial fiber orientation using echocardiography-based shear wave imaging', *IEEE transactions on medical imaging* **31**(3), 554–562.

Nightingale, K., McAleavey, S. and Trahey, G. [2003], 'Shear-wave generation using acoustic radiation force: in vivo and ex vivo results', *Ultrasound in medicine & biology* **29**(12), 1715–1723.

Nightingale, K., Soo, M. S., Nightingale, R. and Trahey, G. [2002], 'Acoustic radiation force impulse imaging: in vivo demonstration of clinical feasibility', *Ultrasound in medicine & biology* **28**(2), 227–235.

Palmeri, M. L., Sharma, A. C., Bouchard, R. R., Nightingale, R. W. and Nightingale, K. R. [2005], 'A finite-element method model of soft tissue response to impulsive acoustic radiation force', *IEEE transactions on ultrasonics, ferroelectrics, and frequency control* **52**(10), 1699–1712.

Qiang, B., Brigham, J. C., Aristizabal, S., Greenleaf, J. F., Zhang, X. and Urban, M. W. [2015], 'Modeling transversely isotropic, viscoelastic, incompressible tissue-like materials with application in ultrasound shear wave elastography', *Physics in medicine and biology* **60**(3), 1289.

Rouze, N. C., Wang, M. H., Palmeri, M. L. and Nightingale, K. R. [2013], 'Finite element modeling of impulsive excitation and shear wave propagation in an incompressible, transversely isotropic medium', *Journal of biomechanics* **46**(16), 2761–2768.

Sarvazyan, A. P., Rudenko, O. V., Swanson, S. D., Fowlkes, J. B. and Emelianov, S. Y. [1998], 'Shear wave elasticity imaging: a new ultrasonic technology of medical diagnostics', *Ultrasound in medicine & biology* **24**(9), 1419–1435.

Sommer, G., Schriefl, A. J., Andrä, M., Sacherer, M., Viertler, C., Wolinski, H. and Holzapfel, G. A. [2015], 'Biomechanical properties and microstructure of human ventricular myocardium', *Acta biomaterialia* **24**, 172–192.

Streeter, D. D., Spotnitz, H. M., Patel, D. P., Ross, J. and Sonnenblick, E. H. [1969], 'Fiber orientation in the canine left ventricle during diastole and systole', *Circulation research* **24**(3), 339–347.

Ye, W., Bel-Brunon, A., Catheline, S., Combescure, A. and Rochette, M. [2017], 'Simulation of non-linear transient elastography: finite element model for the propagation of shear waves in homogeneous soft tissues', *International Journal for Numerical Methods in Biomedical Engineering* .

CHAPTER 7

High-order Discrete Fourier Transform for the resolution of the Poisson equation

Summary

The aim of this chapter is to show a novel, fast, matrix-free solver for the Poisson problem discretised with high-order Spectral Element Methods (HO-SEM). This method is based on the use of Discrete Fourier Transform to rewrite the problem as the inversion of the symbol of the operator in frequency space. When first-order FE elements are adopted, the symbol is scalar, and the solution is retrieved by Fast Fourier Transform (FFT). If HO-SEM are adopted, the inversion of the symbol can be very costly, and efficient implementation is required. The solver proposed is endowed with several properties. First, it preserves the efficiency of standard FFT algorithm; then, the matrix storing is minimised; a pseudo-explicit Singular Value Decomposition (SVD) is used for inversion of the symbol; finally, it can be easily extended to multiple dimensions and non-periodic boundary conditions. In particular, due to the underlying HO-SEM discretisation, the multi-dimensional symbol of the operator can be efficiently computed from the one-dimensional symbol by tensorisation. Dirichlet or Neumann boundary conditions can be treated by performing a periodic, symmetric extension of the source term, odd for Dirichlet and even for Neumann boundary conditions. However, due to symmetry properties of the extended source term and intrinsic properties of the DFT, we are able to restrict most computations to the frequencies associated with the original (not extended) source term, preserving the efficiency of the algorithm. *This chapter is in the form of a paper – coauthored by F. Caforio and S. Imperiale – already submitted for publication in an international journal.*

Contents

7.1 Introduction

The objective of this work is to provide a matrix-free, high-order, fast method to solve the Poisson partial differential equation (PDE) in bounded domains. This topic has already been largely addressed in the literature (see [Van Loan, 1992; Gustafsson, 2011] or more recently [Lyon and Bruno, 2010; Amlani and Bruno, 2016]). However, to our best knowledge, there is no efficient algorithm that is adequate for the specific applications we target. In more detail, we require a fast method that is compatible (in a sense that will be specified in what follows) with high-order Finite Element (FE) discretisations. The main application is the treatment of the incompressibility condition for transient elastodynamic or Navier-Stokes PDEs (see [Guermond and Quartapelle, 1998; Guermond et al., 2006]). In these PDEs, although parameters may be heterogeneous and/or anisotropic, the treatment of the incompressibility constraint is reduced to the resolution of a Poisson equation for a scalar unknown, i.e. the pressure, thanks to penalisation techniques.
Advanced methods involve the resolution of these PDEs (Stokes or elastodynamics) with high-order FE methods, and it can be shown (see [Guermond and Quartapelle, 1998]) that the pressure must be solved in an suitable High-Order (HO) FE space, in order to satisfy a stability condition, namely the inf-sup condition, also known as Ladyzhenskaya-Babŭska-Brezzi (LBB) condition (we refer to [Brezzi and Fortin, 2012; Brezzi and Falk, 1991] for further details).
A well-known FE method for Stokes flow and transient elastodynamic problems is the so-called Spectral Element Method (SEM) (see [Maday and Patera, 1989] for Stokes equation, [Komatitsch and Vilotte, 1998] for seismic wave equations and [Cohen and Fauqueux, 2005] for elastodynamics). Two main assets of this type of FE methods are the optimal rate of convergence achieved and mass-lumping. Therefore, they represent a privileged choice for explicit discretisation of transient problems. Furthermore, they are constructed in one-dimension from Lagrangian basis functions supported on Gauss-Lobatto points, and their extension to two- and three-dimensions is straightforward, since it is based on tensorisation.
Due to the aforementioned inf-sup condition, the choice of space discretisation for the main unknown restricts the choice for the auxiliary variable, i.e. the pressure. In more detail, it is shown in [Brezzi and Falk, 1991] that if R-order continuous SEM are used for the main unknown, and a regular rectangular mesh is considered, it is possible to use $R-1$ continuous SEM for the pressure, still keeping the optimal order of convergence, and the inf-sup constant does not depend on the size of the mesh. Note, however, that [Ainsworth and Coggins, 2002] have provided numerical evidence that the inf-sup constant decays as the order of polynomials increases. We also refer to [Pena, 2009] for a numerical analysis concerning different choices for the pressure space.
Hexahedral finite elements represent a suitable framework for the very specific applications we are interested in, namely the local propagation of elastographic waves in soft biological tissues ([Bercoff et al., 2004; Palmeri et al., 2005; Caenen et al., 2018]). In fact, in this configuration the propagation medium can be assumed to be unbounded, and computations are restricted to a cube, that can be locally discretised with regular hexahedral meshes.
In this work we construct a fast, matrix-free solver for the Poisson problem discretised with HO-SEM on uniform meshes. The main peculiarity of this method is that it corresponds to the explicit computation of the inverse of the discrete Laplace operator (computed with HO-SEM), hence accuracy and convergence properties of the solver are directly inherited from those of the SEM.
The proposed method relies on the use of the Fast Fourier Transform (FFT), to reduce the problem in the inversion of the – frequency-dependent – symbol of the operator. When

first-order finite elements are adopted, the symbol is scalar, its inversion is trivial and the solution is recovered using inverse FFT (this is the classical fast method presented in many textbooks, see for instance [Gustafsson, 2011; Iserles, 2009]). When high-order FE are used, the symbol is no-longer scalar, and its inversion is no longer trivial. The definition of this symbol has been first introduced in ([Cohen, 2001; Ainsworth, 2004]) for the discrete analysis of wave propagation phenomena in periodic domains but, surprisingly, it has never been used as an actual solver for the Poisson equation. The solver we construct has the following algorithmic properties: first, it preserves the efficiency of standard FFT algorithm; then, it minimises matrix storage; a pseudo-explicit Singular Value Decomposition (SVD) is used for inversion of the symbols; finally, it is extended to the treatment of Neumann and Dirichlet boundary conditions.
This paper is organised as follows. Section 7.2.1 contains the main features of the Poisson-like partial differential equation that we aim to solve and its numerical approximation by standard Spectral Element Methods. Then, in Section 7.2.2 a well-known method based on FFT is presented for the resolution of the problem when linear polynomials are adopted for space approximation and periodic conditions are imposed at the boundaries. In Section 7.3 a novel, efficient method for the resolution of the problem with high-order space approximation and periodic boundary conditions (BCs) is described. This method is derived as a generalisation of the aforementioned algorithm associated with linear interpolation. This section also contains further details on the practical implementation of the method. Sections 7.3.2 and 7.4 are devoted to the generalisation to other BCs, e.g. Dirichlet and Neumann, and the extension to multiple dimensions, respectively. Numerical results are shown in Section 7.5, along with some remarks on the complexity of the solver – which is shown to be in $O(R^{d+1}\,N^d\,\log N)$ in dimension d – and its parallelisability.

7.2 Statement of the problem and standard results

7.2.1 Variational formulation for the Poisson problem

Let us consider a generalisation of the Poisson equation in $\Omega \subset \mathbb{R}^d$

$$\rho\, u - \Delta u = f, \tag{7.1}$$

with u and f scalar functions, and $\rho \in \mathbb{C}$ is a constant. We do not specify the conditions imposed on the boundary of Ω for the moment. Given an admissible subspace $\mathcal{V} \subset H^1(\Omega)$, we want to solve the following variational formulation related to Eq. (7.1):
Find $u \in \mathcal{V}$ such that

$$\rho\, m(u,v) + a(u,v) = \ell(v), \quad \forall v \in \mathcal{V}, \tag{7.2}$$

where

$$m(u,v) = \int_\Omega u\,\overline{v}\,\mathrm{d}\Omega, \quad a(u,v) = \int_\Omega \underline{\nabla} u \cdot \overline{\underline{\nabla} v}\,\mathrm{d}\Omega, \quad \ell(v) = \int_\Omega f\,\overline{v}\,\mathrm{d}\Omega. \tag{7.3}$$

By definition, $a : \mathcal{V}\times\mathcal{V} \to \mathbb{C}$ is a bilinear form (i.e. linear and continuous in each variable), while $\ell : \mathcal{V} \to \mathbb{C}$ is a linear form (i.e. linear and continuous) by hypothesis.
For the discretisation in space, we introduce a finite-dimensional subspace $\mathcal{V}_h \subset \mathcal{V}$, according to standard continuous Galerkin methods. We denote by N the dimension of this space. The discrete problem reads
Find $u_h \in \mathcal{V}_h$ such that

$$\rho\, m_h(u_h,v_h) + a_h(u_h,v_h) = \ell_h(v_h), \quad \forall\, v_h \in \mathcal{V}_h, \tag{7.4}$$

where

$$m_h(u_h, v_h) = \int_\Omega^Q u_h\, \overline{v_h}\, \mathrm{d}\Omega, \quad a_h(u_h, v_h) = \int_\Omega^Q \underline{\nabla} u_h \cdot \overline{\underline{\nabla} v_h}\, \mathrm{d}\Omega, \quad \ell_h(f_h, v_h) = \int_\Omega^Q f_h\, \overline{v_h}\, \mathrm{d}\Omega. \tag{7.5}$$

Note that the superscript Q on the integral signs denotes integral approximation by quadrature rule. We recall that in one-dimension, given a function f, an $(R_Q+1)-$points quadrature rule is based on the definition of a suitable set of points $\{\eta_k\}_{k=0}^{R_Q}$ in $[0,1]$ and weights $\{\omega_k\}_{k=0}^{R_Q}$ such that

$$\int_{[0,h]} f(x)\, \mathrm{d}x \approx \int_{[0,h]}^Q f(x)\, \mathrm{d}x \coloneqq h \sum_{k=0}^{R_Q} f(\eta_k\, h)\, \omega_k. \tag{7.6}$$

We recall that if Gauss-Lobatto nodes are used (i.e. the end-points of the integration interval are included in the set of quadrature points), this formula is exact for polynomials up to degree $2R_Q - 1$, and R_Q integration points (see for instance [Quarteroni et al., 2010] for more details). For the sake of simplicity, we assume that there exists $f_h \in \mathcal{V}_h$ such that $\ell_h(v_h) = m_h(f_h, v_h)$. Standard Galerkin methods are based on the decomposition of the discrete solution u_h, the test function v_h and the source term f_h on basis functions $\{\varphi_j\}_{j=0}^N$. They can be rewritten, in one-dimension for example, as

$$u_h(x) = \sum_{j=0}^N u_j \varphi_j(x), \quad v_h(x) = \sum_{j=0}^N v_j \varphi_j(x), \quad f_h(x) = \sum_{j=0}^N f_j \varphi_j(x). \tag{7.7}$$

The discrete problem then reads

$$\underline{V}^*(\rho\, M + A)\underline{U} = \underline{V}^* M \underline{F}, \tag{7.8}$$

where $\underline{U}$, $\underline{V} \in \mathbb{C}^N$, $\underline{F} \in \mathbb{C}^N$ are defined as

$$\underline{U} = \big(u_0, u_1, .., u_{N-1}\big)^T, \quad \underline{V} = \big(v_0, v_1, .., v_{N-1}\big)^T, \quad \underline{F} = \big(f_0, f_1, .., f_{N-1}\big)^T,$$

and M, $A \in \mathcal{M}_N(\mathbb{C})$ read

$$M_{i\,j} = \int_\Omega^Q \varphi_i\, \overline{\varphi_j}\, \mathrm{d}\Omega, \quad A_{i\,j} = \int_\Omega^Q \underline{\nabla}\varphi_i \cdot \overline{\underline{\nabla}\varphi_j}\, \mathrm{d}\Omega.$$

Note that the symbol $(\cdot)^*$ denotes transpose conjugate. Matrices M and A are commonly called mass and stiffness matrix, respectively. If an adequate $\mathcal{V}_h$ is chosen for discretisation, the matrix $\rho\, M + K$ is invertible and, in practice, the discrete solution $\underline{U}$ is retrieved as

$$\underline{U} = (\rho\, M + A)^{-1}\, M \underline{F}. \tag{7.9}$$

Matrix inversion can imply a significant computational cost, especially if the problem is multi-dimensional and/or high-order space approximation is used. Several strategies exist in the literature to deal with the inversion of large matrices. In general, iterative methods as the Conjugate Gradient (first proposed in [Hestenes and Stiefel, 1952]) are employed, with suitable preconditioners, see for example [Spillane, 2016]. Alternatively, fast methods can be used, see for example the hierarchical matrix (H-matrix) method ([Hackbusch, 2015]), that is an efficient algorithm to compute approximate inverse matrices based on data-sparse approximations of non-sparse matrices. Within this family of methods, the most efficient one relies on the use of the Fast Fourier Transform (FFT). The use of the FFT Poisson solver is, however, restricted to some assumptions on the computational domain. The next section is devoted to a recap of this solver (in one-dimension) for linear approximation. The solver we propose in this work represents a generalisation of the aforementioned algorithm for high-order discretisation.

7.2.2 A fast solver based on FFT in one-dimension

The standard Fast Fourier Transform (FFT) can be used to solve elliptic partial differential equations (PDEs) in multiple dimensions when linear polynomials are used for space approximation (i.e. Q1 finite elements) and Ω is a rectangle in 2-D, or a parallelepiped in 3-D, see for example [Gustafsson, 2011; Iserles, 2009]. To briefly recall the method, we consider the one-dimensional case, with periodic boundary conditions, i.e. $u_N \equiv u_0$ and P1 Lagrange shape functions.
We assume that the computational domain is $[0, L]$, the source term f_h is L-periodic and its values $f_n \coloneqq f_h(x_n)$ are given at the grid points

$$x_n = n\,h, \quad n \in \mathcal{N}, \quad N\,h = L,$$

where we have defined $\mathcal{N} = \{0, 1, .., N-1\}$. Based on these known values, we can construct an interpolation function

$$\tilde{f}_h(x) = \frac{1}{N} \sum_{k \in \mathcal{N}} \hat{f}_k \, e^{\frac{i2\pi x k}{N}}, \tag{7.10}$$

that should agree with f_h at the grid points. This is guaranteed by the use of the Discrete Fourier Transform (DFT) of the function f_h and its inverse, called Inverse Discrete Fourier Transform (IDFT). It is possible to prove the following standard result ([Gustafsson, 2011]):

Property 7.1. *Let $f_h \in C^0_\sharp([0, L])$ and $\tilde{f}_h \in C^0_\sharp([0, L])$ be defined by Eq. (7.10). Then, denoting*

$$f_n \coloneqq f_h(x_n), \quad \tilde{f}_n \coloneqq \tilde{f}_h(x_n),$$

we have

$$\begin{aligned} f_n = \tilde{f}_n, \ \forall n \in \mathcal{N} \iff \hat{f}_k &= \sum_{n \in \mathcal{N}} f_n \, e^{-\frac{ik2\pi nh}{L}}, \ \forall n \in \mathcal{N} \\ \iff f_n &= \frac{1}{N} \sum_{k \in \mathcal{N}} \hat{f}_k \, e^{\frac{ik2\pi nh}{L}}, \ \forall k \in \mathcal{N}. \end{aligned}$$

The basic ingredient to prove this property is the following orthogonality property:

$$\sum_{\ell \in \mathcal{N}} e^{-\frac{i\ell 2\pi nh}{L}} \, e^{-\frac{ik2\pi nh}{L}} = \delta_{k,\ell}, \quad \forall k, n \in \mathcal{N}. \tag{7.11}$$

Derivation of the symbol of the operator. If we adopt for each integral the simple quadrature formula below (known as midpoint rule), on an interval $[a, b]$, $a < b$,

$$\int_{[a,b]}^{Q} g(x)dx = \frac{b-a}{2}\big(g(0) + g(1)\big),$$

then we end up with the finite-difference scheme (with the convention $u_{-1} = u_{N-1}$)

$$\rho\, u_n\, h - \frac{1}{h}\Big(u_{n+1} + u_{n-1} - 2\, u_n\Big) = f_n\, h \quad n \in \mathcal{N}. \tag{7.12}$$

Analogously, we can construct an interpolation function for the solution $u_h(x)$, that reads

$$\tilde{u}_h(x) = \frac{1}{N} \sum_{k \in \mathcal{N}} \hat{u}_k \, e^{\frac{i2\pi x k}{N}}, \tag{7.13}$$

where the coefficients $\hat{u}_k$ satisfy Property 7.1, i.e. they are given by

$$\hat{u}_k = \sum_{n\in\mathcal{N}} u_n \, e^{-\frac{ik2\pi nh}{L}}, \ \forall n \in \mathcal{N},$$

and, therefore $\tilde{u}_n := \tilde{u}(x_n) = u_n$, for all $n \in \mathcal{N}$. Assuming again that $\tilde{u}_{-1} = \tilde{u}_{N-1}$, we obtain that

$$\rho \, \tilde{u}_n \, h - \frac{1}{h}\Big(\tilde{u}_{n+1} + \tilde{u}_{n-1} - 2\,\tilde{u}_n\Big) = \tilde{f}_n \, h \quad n \in \mathcal{N}. \tag{7.14}$$

By definition of the interpolation functions in Eqs. (7.10) and (7.13) and due to the orthogonality property (7.11), we get

$$\mathcal{S}_k \hat{u}_k = \hat{f}_k, \quad \mathcal{S}_k := \Big(\rho - \frac{2}{h^2}(\cos(2\pi kh/L) - 1)\Big), \ \forall k \in \mathcal{N},$$

where $\mathcal{S}_k$ is called the symbol of the operator associated with Eq. (7.9).

The algorithm. The complete algorithm for the resolution of problem (7.9) by means of Fourier Transform can be resumed in three main steps:

1. Perform a DFT of the discrete source term for each element

$$\hat{f}_k = \sum_{n\in\mathcal{N}} f_n \, e^{-\frac{ik2\pi nh}{L}}, \ \forall k \in \mathcal{N};$$

2. Apply the inverse symbol of the operator

$$\hat{u}_k = \mathcal{S}_k^{-1} \hat{f}_k, \quad k \in \mathcal{N};$$

3. Perform an inverse DFT of the solution for each frequency

$$u_n = \frac{1}{N} \sum_{k\in\mathcal{N}} \hat{u}_k \, e^{\frac{ik2\pi nh}{L}}, \ \forall n \in \mathcal{N}.$$

This algorithm has several advantages. First, the operator is explicitly computed, without requiring any inversion, nor storage of assembled matrices as for Eq. (7.9). Furthermore, the problem for each frequency k is decoupled. Therefore, operations at each step can be performed in parallel on the frequencies. At last, the first and third steps can be performed by Fast Fourier Transform (FFT) algorithm. This algorithm is very efficient: the computation of a FFT of N points requires $O(N \log N)$ arithmetical operations, whereas standard DFT takes $O(N^2)$ operations.

7.3 The High-Order Spectral Element FFT solver in one-dimension

7.3.1 Periodic boundary conditions

If higher-order approximation in space is considered for the numerical resolution of Eq. (7.1), the Fourier-based method described above is not suitable and needs to be generalised. In this section we present a novel, efficient method based on High-Order DFT (HO-DFT)

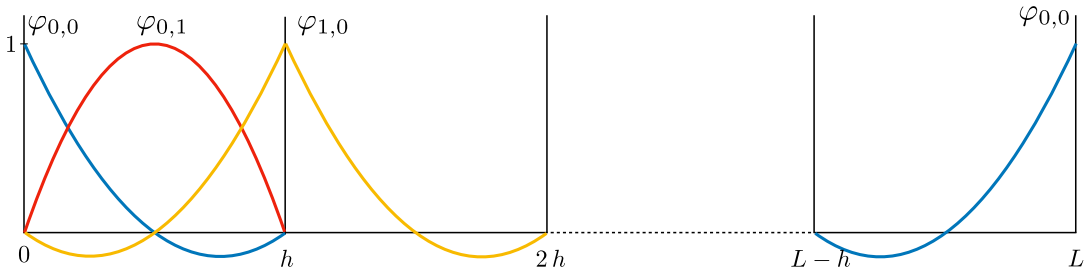

Figure 7.1 – Shape functions for quadratic Lagrange polynomial interpolation on Gauss-Lobatto nodes in $[0, L]$.

for the resolution of elliptic PDEs.
First, we introduce the framework for higher-order spatial approximation of Eq. (7.1). This formulation is inspired by [Ainsworth, 2004] and [Cohen, 2001]. For the sake of clarity, we consider a one-dimensional domain of size $[0, L]$ and impose periodic boundary conditions (BCs) at first. We refer the reader to Sections 7.3.2 and 7.4 for the extension to Neumann and Dirichlet BCs and to multiple dimensions, respectively.
Let $\mathcal{V}_{h,R}$ be the approximation space for continuous piecewise R-order polynomials in $[0, L]$. We introduce a basis of shape functions

$$\left\{\varphi_{n,j}\right\}_{n\in\mathcal{N},\, j\in\mathcal{R}} \tag{7.15}$$

with $\mathcal{N} = \{0, 1, .., N-1\}$, $\mathcal{R} = \{0, 1, .., R-1\}$, such that

$$\mathrm{Supp}(\varphi_{n,0}) = [(n-1)h, (n+1)h], \quad \mathrm{Supp}(\varphi_{n,j}) = [nh, (n+1)h], \forall n \in \mathcal{N}^*,$$

with $\mathcal{N}^* \coloneqq \mathcal{N} \setminus \{0\}$. In order to take into account periodicity, we also have

$$\mathrm{Supp}(\varphi_{0,0}) = [0, h] \cup [L-h, L].$$

Moreover, we assume that the shape functions are obtained by translation, namely

$$\forall x \in [0,h],\ \forall n \in \mathcal{N}^*,\ \forall j \in \mathcal{R}^*, \quad \begin{cases} \varphi_{n,0}(x + n\,h) = \varphi_{0,0}(x) & \in \mathcal{P}^R([0,h]), \\ \varphi_{n,0}(x + (n-1)\,h) = \varphi_{1,0}(x) & \in \mathcal{P}^R([0,h]), \\ \varphi_{n,j}(x + n\,h) = \varphi_{0,j}(x) & \in \mathcal{P}^R([0,h]), \end{cases} \tag{7.16}$$

where $\mathcal{P}^R([0,h])$ denotes the set of polynomials of degree R on $[0,h]$ and with $\mathcal{R}^* \coloneqq \mathcal{R}\setminus\{0\}$, and where, by periodicity again, $\varphi_{0,0}(x + L - h) = \varphi_{1,0}(x)$, for $x \in [0,h]$. We introduce a set of nodes $\left\{\xi_j\right\}_{j=0}^{R}$, s.t. $\xi_j \in [0,1]\ \forall j \in \mathcal{R}$ and, by definition of shape functions, we have

$$\varphi_{m,i}((\xi_j + n)h) = \delta_{m\,n}\,\delta_{i\,j},\ \forall i, j \in \mathcal{R},\ \forall m, n \in \mathcal{N}.$$

Note that $\xi_0 = 0$ by construction (this is a necessary condition in order to have continuous finite elements), and we assume $\xi_R = 1$. Henceforth, we adopt Lagrange basis functions on Gauss-Lobatto nodes. By way of illustration, Lagrange basis functions for $R = 2$ are depicted in Figure 7.1. Then, $f_h, u_h \in \mathcal{V}_{h,R}$ can be rewritten as

$$f_h(x) = \sum_{n\in\mathcal{N}}\sum_{j\in\mathcal{R}} f_{n,j}\,\varphi_{n,j}(x), \quad u_h(x) = \sum_{n\in\mathcal{N}}\sum_{j\in\mathcal{R}} u_{n,j}\,\varphi_{n,j}(x),$$

with coefficients

$$f_{n,j} \coloneqq f_h((\xi_j + n)h), \quad u_{n,j} \coloneqq u_h((\xi_j + n)h) \quad \forall j \in \mathcal{R}, \forall n \in \mathcal{N},$$

and an analogous decomposition holds for $v_h \in \mathcal{V}_{h,R}$. We can introduce an interpolation function of f_h defined as

$$\tilde{f}_h(x) = \frac{1}{N} \sum_{k \in \mathcal{N}} \Big(\sum_{j \in \mathcal{R}} \hat{f}_{k,j}\, e^{\frac{i2\pi(x - h\xi_j)k}{L}} \sum_{n \in \mathcal{N}} \varphi_{n,j}(x) \Big). \tag{7.17}$$

As a consequence of our definition, we obtain

$$\tilde{f}_h((\xi_j + n)h) = \frac{1}{N} \sum_{k \in \mathcal{N}} \hat{f}_{k,j}\, e^{\frac{i2\pi nk}{N}}, \ \forall j \in \mathcal{R}, \tag{7.18}$$

since $h\,N = L$. Eq. (7.18) represents a generalisation of Eq. (7.10) for higher-order spatial approximation. Therefore, the coefficients $\hat{f}_{k,j}$, $\forall j \in \mathcal{R}$, can be computed by means of classical DFT. In particular, the following property holds.

Property 7.2. *Let $f_h \in C^0_\sharp([0, L])$ and $\tilde{f}_h \in C^0_\sharp([0, L])$ be defined by Eq. (7.17). Let us denote*

$$\tilde{f}_{n,j} \coloneqq \tilde{f}_h((\xi_j + n)h) \quad \forall j \in \mathcal{R}, \forall n \in \mathcal{N}.$$

Then, we have, for all j fixed in $\mathcal{R}$,

$$\begin{aligned} f_{n,j} = \tilde{f}_{n,j} \iff \hat{f}_{k,j} &= \sum_{n \in \mathcal{N}} f_{n,j}\, e^{-\frac{i2\pi nk}{N}}, \ \forall k \in \mathcal{N}, \\ \iff f_{n,j} &= \frac{1}{N} \sum_{k \in \mathcal{N}} \hat{f}_{k,j}\, e^{\frac{i2\pi nk}{N}}, \ \forall n \in \mathcal{N}. \end{aligned} \tag{7.19}$$

Property 7.2 is a straightforward consequence of Property 7.1 and Eq. (7.18).
Following the approach in Section 7.2.2, we introduce the interpolation function of the discrete solution u_h such that

$$\tilde{u}_{n,j} \coloneqq \tilde{u}_h((\xi_j + n)h) = \frac{1}{N} \sum_{k \in \mathcal{N}} \hat{u}_{k,j}\, e^{\frac{i2\pi nk}{N}}, \ \forall j \in \mathcal{R}, \tag{7.20}$$

where the coefficients $\hat{u}_{k,j}$ are given by

$$\hat{u}_{k,j} = \sum_{n \in \mathcal{N}} u_{n,j}\, e^{-\frac{i2\pi nk}{N}}, \ \forall k \in \mathcal{N}, \ \forall j \in \mathcal{R}. \tag{7.21}$$

As a consequence of Eqs. (7.20) and (7.21), we derive

$$u_{n,j} = \tilde{u}_{n,j}, \quad \forall k \in \mathcal{N}, \ \forall j \in \mathcal{R}. \tag{7.22}$$

We now manipulate the bilinear forms in Eq. (7.4). Due to invariance of the bilinear forms with respect to translations, we assume that the same quadrature formula is used for each segment of size h. Therefore, we can rewrite the integrals

$$m_h(u_h, v_h) = \sum_{n \in \mathcal{N}} \int_{[nh,(n+1)h]}^{Q} u_h(x)\, \overline{v_h(x)}\, \mathrm{d}x = \sum_{n \in \mathcal{N}} \int_{[0,h]}^{Q} u_h(x + nh)\, \overline{v_h(x + nh)}\, \mathrm{d}x.$$

Consequently, by quadrature rule (Eq. (7.6)) and the definition of shape functions, we obtain

$$\int_{[0,h]}^{Q} u_h(x+nh)\,\overline{v_h(x+nh)}\,\mathrm{d}x = h\sum_{k=0}^{R_Q}\sum_{i,j=0}^{R}\omega_k\varphi_{0,i}(\eta_k\,h)\varphi_{0,j}(\eta_k\,h)u_{n,j}\,\overline{v_{n,i}},$$

where, for the sake of conciseness, we have set $\varphi_{0,R}(x) = \varphi_{1,0}(x)$, $u_{n,R} = u_{n+1,0}$, $v_{n,R} = v_{n+1,0}$ and, by periodicity, $u_{N-1,R} = u_{N,0} = u_{0,0}$ and $v_{N-1,R} = v_{N,0} = v_{0,0}$. Note that this implies

$$\hat{u}_{k,R} = \hat{u}_{k+1,0}, \quad \hat{f}_{k,R} = \hat{f}_{k+1,0}. \tag{7.23}$$

Finally, one can show that

$$m_h(u_h, v_h) = \sum_{n\in\mathcal{N}}\sum_{i,j=0}^{R}\hat{m}_{i,j}u_{n,j}\,\overline{v_{n,i}},$$

where $\hat{m}_{i,i}$ denote the coefficients of the mass matrix in the reference element $[0,h]$. Similar treatment of the bilinear form a_h gives

$$a_h(u_h, v_h) = \sum_{n\in\mathcal{N}}\sum_{i,j=0}^{R}\hat{a}_{i,j}u_{n,j}\,\overline{v_{n,i}}.$$

Note that the coefficients $\hat{a}_{i,j}$ and $\hat{m}_{i,i}$ do not depend on the index n, as a consequence of the invariance of the discrete bilinear forms with respect to translations. This property is fundamental for the derivation of the symbol of the operator. Furthermore, due to the use of Gauss-Lobatto nodes both for the interpolation and the quadrature rule (i.e. $\{\eta_k\} = \{\xi_k\}$), the mass matrix is diagonal. This property, named mass lumping, is a fundamental feature of Spectral Element Methods (SEM), first proposed by [Maday and Patera, 1989]. We make this choice for the rest of the chapter. Consequently, we obtain

$$m_h(u_h, v_h) = \sum_{n\in\mathcal{N}}\sum_{i=0}^{R}\hat{m}_{i,i}u_{n,i}\,\overline{v_{n,i}},$$

and the algebraic system to solve is

$$\sum_{n\in\mathcal{N}}\sum_{i=0}^{R}\hat{m}_{i,i}u_{n,i}\,\overline{v_{n,i}} + \sum_{n\in\mathcal{N}}\sum_{i,j=0}^{R}\hat{a}_{i,j}u_{n,j}\,\overline{v_{n,i}} = \sum_{n\in\mathcal{N}}\sum_{i=0}^{R}\hat{m}_{i,i}f_{n,i}\,\overline{v_{n,i}}. \tag{7.24}$$

Since Eq. (7.4) must be true for any $v_h \in \mathcal{V}_h$, it must hold true for any choice of $v_{n,i}$, $v \in \mathcal{N}$, $i \in \{0,1,..,R\}$.
In particular, for $v_{n,i} = \delta_{i\,q}\,\delta_{n\,\ell}$, with $q \in \mathcal{R}$ and $\ell \in \mathcal{N}$, due to Eq. (7.23) we derive

$$\hat{m}_{q,q}\,u_{l,q} + \sum_{j\in\mathcal{R}^*}\hat{a}_{q,j}\,u_{l,j} + \hat{a}_{q,0}\,u_{l,0} + \hat{a}_{q,R}\,u_{l+1,0} = \hat{m}_{q,q}\,f_{l,q}. \tag{7.25}$$

Furthermore, if $q = R$ we obtain

$$\begin{aligned}
&\hat{m}_{R,R}\,u_{l+1,0} + \sum_{j\in\mathcal{R}^*}\hat{a}_{R,j}\,u_{l,j} + \hat{a}_{R,0}\,u_{l,0} + \hat{a}_{R,R}\,u_{l+1,0} = \hat{m}_{R,R}\,f_{l+1,0}, \text{ i.e.}\\
&\hat{m}_{R,R}\,u_{l,0} + \sum_{j\in\mathcal{R}^*}\hat{a}_{R,j}\,u_{l-1,j} + \hat{a}_{R,0}\,u_{l-1,0} + \hat{a}_{R,R}\,u_{l,0} = \hat{m}_{R,R}\,f_{l,0}.
\end{aligned} \tag{7.26}$$

Note that Eq. (7.24) is still true when we replace $u_{l,j}$ by $\tilde{u}_{l,j}$ and $f_{l,j}$ by $\tilde{f}_{l,j}$, due to Eq. (7.22). Following the strategy of Section 7.2.2, we further replace $\tilde{u}_{l,j}$ by their expression in terms of $\hat{u}_{k,j}$ (Eq. (7.20)) and $\tilde{f}_{l,j}$ by their expression in terms of $\hat{f}_{k,j}$ (Eq. (7.18)), for all $j \in \mathcal{R}$, observing that $\tilde{u}_{l,R} = \tilde{u}_{l+1,0}$ and $\tilde{f}_{l,R} = \tilde{f}_{l+1,0}$. Therefore, Eq. (7.25) becomes, $\forall q \in \mathcal{R}$,

$$\sum_{k\in\mathcal{N}} \left(\hat{m}_{q,q}\, \hat{u}_{k,q}\, e^{\frac{i2\pi k\ell}{N}} + \sum_{j\in\mathcal{R}^*} \hat{a}_{q,j}\, \hat{u}_{k,j}\, e^{\frac{i2\pi k\ell}{N}} + \big(\hat{a}_{q,0} + \hat{a}_{q,R}\, e^{\frac{i2\pi k}{N}}\big)\hat{u}_{k,0}\, e^{\frac{i2\pi k\ell}{N}} \right) = \sum_{k\in\mathcal{N}} \hat{m}_{q,q}\, \hat{f}_{k,q}\, e^{\frac{i2\pi k\ell}{N}}. \tag{7.27}$$

In particular, if $q = 0$, we obtain

$$\sum_{k\in\mathcal{N}} \left(\hat{m}_{0,0}\, \hat{u}_{k,0}\, e^{\frac{i2\pi k\ell}{N}} + \sum_{j\in\mathcal{R}^*} \hat{a}_{0,j}\, \hat{u}_{k,j}\, e^{\frac{i2\pi k\ell}{N}} + \big(\hat{a}_{0,0} + \hat{a}_{0,R}\, e^{\frac{i2\pi k}{N}}\big)\hat{u}_{k,0}\, e^{\frac{i2\pi k\ell}{N}} \right) = \sum_{k\in\mathcal{N}} \hat{m}_{0,0}\, \hat{f}_{k,0}\, e^{\frac{i2\pi k\ell}{N}}. \tag{7.28}$$

Furthermore, if $q = R$, Eq. (7.26) can be rewritten as

$$\sum_{k\in\mathcal{N}} \left(\hat{m}_{R,R}\, \hat{u}_{k,0}\, e^{\frac{i2\pi k\ell}{N}} + \sum_{j\in\mathcal{R}^*} \hat{a}_{R,j}\, \hat{u}_{k,j}\, e^{\frac{i2\pi(k-1)\ell}{N}} + \big(\hat{a}_{R,0}\, e^{\frac{-i2\pi k}{N}} + \hat{a}_{R,R}\big)\hat{u}_{k,0}\, e^{\frac{i2\pi k\ell}{N}} \right) = \sum_{k\in\mathcal{N}} \hat{m}_{R,R}\, \hat{f}_{k,0}\, e^{\frac{i2\pi k\ell}{N}}. \tag{7.29}$$

Let us now define the vectors $\underline{\hat{U}}_k, \underline{\hat{F}}_k \in \mathbb{C}^R$, such that

$$\underline{\hat{U}}_k = (\hat{u}_{k,0}\,, \hat{u}_{k,1}, .., \hat{u}_{k,R-1})^T, \quad \underline{\hat{F}}_k = (\hat{f}_{k,0}\,, \hat{f}_{k,1}, .., \hat{f}_{k,R-1})^T,$$

and the matrices $\boldsymbol{\mathcal{A}}_k, \boldsymbol{\mathcal{M}} \in M_R(\mathbb{C})$ such that

$$\boldsymbol{\mathcal{A}}_k = \begin{bmatrix} \mathrm{a}_k & \underline{\mathcal{B}}_k \\ \underline{\mathcal{B}}_k^* & \mathring{\boldsymbol{\mathcal{A}}} \end{bmatrix}, \quad \boldsymbol{\mathcal{M}} = \begin{bmatrix} \mathcal{M} & 0 \\ 0 & \mathring{\boldsymbol{\mathcal{M}}} \end{bmatrix}, \tag{7.30}$$

where a_k, $\mathcal{M} \in \mathbb{C}$, $\underline{\mathcal{B}}_k \in \mathbb{C}^{R-1}$, $\mathring{\boldsymbol{\mathcal{A}}}$, $\mathring{\boldsymbol{\mathcal{M}}} \in M_{R-1}(\mathbb{C})$ read

$$\mathrm{a}_k = \hat{a}_{0,0} + \hat{a}_{R,R} + 2\,\hat{a}_{0,R}\,\cos(2\pi k/N), \quad \mathcal{M} = \hat{m}_{0,0} + \hat{m}_{R,R},$$

$$\mathcal{B}_{k,q\,1} = \hat{a}_{0,q} + \hat{a}_{R,q}\, e^{i2\pi k/N}, \quad \mathring{\boldsymbol{\mathcal{M}}}_{q\,q^*} = \hat{m}_{q,q^*}\,\delta_{q\,q^*}, \quad \mathring{\boldsymbol{\mathcal{A}}}_{q\,q^*} = \hat{a}_{q,q^*},\ q, q^* \in \mathcal{R}^*.$$

Thereupon, Eqs. (7.27), (7.28) and (7.29) can be rewritten in compact form as

$$\sum_{k\in\mathcal{N}} e^{\frac{i2\pi k\ell}{N}} (\rho\,\boldsymbol{\mathcal{M}} + \boldsymbol{\mathcal{A}}_k)\,\underline{\hat{U}}_k = \sum_{k\in\mathcal{N}} e^{\frac{i2\pi k\ell}{N}}\, \boldsymbol{\mathcal{M}}\,\underline{\hat{F}}_k,\ \forall l \in \mathcal{N}. \tag{7.31}$$

By orthogonality of the factors $e^{\frac{i2\pi kl}{N}}$ (Eq. (7.11)), we can further simplify Eq. (7.31) as

$$(\rho\,\boldsymbol{\mathcal{M}} + \boldsymbol{\mathcal{A}}_k)\,\underline{\hat{U}}_k = \boldsymbol{\mathcal{M}}\,\underline{\hat{F}}_k,\ \forall k \in \mathcal{N}.$$

Ultimately, the solution $\hat{U}_k$, for every frequency $k \in \mathcal{N}$, is computed as

$$\underline{\hat{U}}_k = \boldsymbol{\mathcal{S}}_k^{-1}\,\underline{\hat{F}}_k\ \forall k \in \mathcal{N}, \tag{7.32}$$

where the symbol of the operator $\boldsymbol{\mathcal{S}}_k$ reads

$$\boldsymbol{\mathcal{S}}_k = (\rho\,\mathbf{I} + \boldsymbol{\mathcal{M}}^{-1}\,\boldsymbol{\mathcal{A}}_k).$$

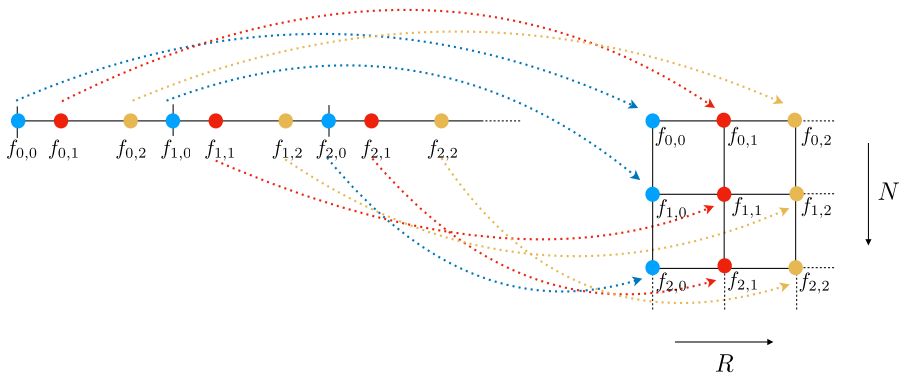

Figure 7.2 – Redistribution of the source term in matrix form. Row index corresponds to the element, column index refers to the Gauss-Lobatto node in the reference element.

The algorithm. In order to compute the discrete solution at the Gauss-Lobatto nodes, i.e. $u_{n,j}$, we can derive an algorithm based on Eqs. (7.19), (7.32) and (7.21). The main steps of this algorithm read:

1. Perform a DFT of the discrete source term for each order j fixed in $\mathcal{R}$
$$\hat{f}_{k,j} = \sum_{n \in \mathcal{N}} f_{n,j}\, e^{-\frac{i2\pi nk}{N}}, \ \forall k \in \mathcal{N};$$
2. Apply the inverse symbol of the operator
$$\underline{\hat{U}}_k = \boldsymbol{\mathcal{S}}_k^{-1}\, \underline{\hat{F}}_k, \ \forall k \in \mathcal{N}; \tag{7.33}$$
3. Perform an inverse DFT for each order j fixed in $\mathcal{R}$
$$u_{n,j} = \frac{1}{N} \sum_{k \in \mathcal{N}} \hat{u}_{k,j}\, e^{\frac{i2\pi nk}{N}}, \ \forall n \in \mathcal{N}.$$

A crucial aspect of this method concerns the definition of an efficient algorithm to compute the coefficients $f_{n,j}$ and $\hat{f}_{k,j}$. To this end, we re-organise the source term vector in matrix form, in which the row index corresponds to the element, whereas the column index refers to the Gauss-Lobatto point in the reference element of size h. Then, the terms $\hat{f}_{k,j}$ are obtained by DFT column by column (using the FFT algorithm). See Figure 7.2 for a schematic illustration of the procedure.

Inversion of the symbol by SVD. In this section we anticipate the difficulties that will be encountered in multiple dimensions, namely the inversion of the symbol of the operator $\boldsymbol{\mathcal{S}}_k$ in Eq. (7.33). In fact, an important advantage of the proposed algorithm is the explicit computation of the inverse symbol. For simplicity of notation, we fix a frequency $k \in \mathcal{N}$. The system that has to be solved is
$$\boldsymbol{\mathcal{S}}_k\, \underline{\hat{U}}_k = \underline{\hat{F}}_k,$$
with $\boldsymbol{\mathcal{S}}_k \coloneqq (\rho\, I + \boldsymbol{\mathcal{M}}^{-1} \boldsymbol{\mathcal{A}}_k)$. We now derive a pseudo-explicit inversion of $\boldsymbol{\mathcal{S}}_k$ by means of Singular Value Decomposition (SVD). For this purpose, let us denote by $\{\underline{V}_{k,i}, \lambda_{k,i}\}_{i \in \mathcal{R}}$ the eigenvectors and eigenvalues of $\boldsymbol{\mathcal{S}}_k$. They satisfy the eigenvalue problem
$$(\rho\, \boldsymbol{\mathcal{M}} + \boldsymbol{\mathcal{A}}_k)\, \underline{V}_{k,i} = \lambda_{k,i}\, \boldsymbol{\mathcal{M}}\, \underline{V}_{k,i} \qquad \forall i \in \mathcal{R}.$$

Since $\boldsymbol{\mathcal{S}}_k$ is hermitian and positive-definite, all eigenvalues $\lambda_{k,i}$ are positive and real for all $k > 0$, and all eigenvectors $\underline{V}_{k,i}$ are orthonormal with respect to the scalar product by $\boldsymbol{\mathcal{M}}$, i.e.

$$\underline{V}_{k,j}^* \, \boldsymbol{\mathcal{M}} \, \underline{V}_{k,i} = \delta_{ij}, \ \forall i, j \in \mathcal{R}.$$

After some standard algebra, we obtain

$$\boldsymbol{\mathcal{S}}_k = \sum_{i \in \mathcal{R}} \lambda_{k,i} \, \underline{V}_{k,i} \, \underline{V}_{k,i}^* \, \boldsymbol{\mathcal{M}} \implies \boldsymbol{\mathcal{S}}_k^{-1} = \sum_{i \in \mathcal{R}} \lambda_{k,i}^{-1} \, \underline{V}_{k,i} \, \underline{V}_{k,i}^* \, \boldsymbol{\mathcal{M}}.$$

Therefore, Eq. (7.33) can be rewritten as

$$\underline{\hat{U}}_k = \sum_{i \in \mathcal{R}} \lambda_{k,i}^{-1} \, \underline{V}_{k,i} \, \underline{V}_{k,i}^* \, \boldsymbol{\mathcal{M}} \, \underline{\hat{F}}_k. \tag{7.34}$$

At this stage, Eq. (7.34) requires the same computational cost as Eq. (7.33), since the computation of the eigenvalues and eigenvectors of a matrix implies the same number of operations as the multiplication by an inverse matrix. Nevertheless, we will show in Section 7.4 that the generalisation to higher dimensions becomes very efficient, due to tensorisation.

7.3.2 Extension to Neumann and Dirichlet Boundary conditions

Care is required when Neumann or Dirichlet conditions are imposed at the boundaries. When linear interpolation is used, it is standard to use, in the definition of the interpolation function (7.10), the Discrete Sine Transform (DST) for Dirichlet BCs, or Discrete Cosine Transform (DCT) for Neumann BCs. Note that sine (cosine) transforms are equivalent to the imaginary part (real part) of a DFT of twice the length of f, operating on real data with odd (even) symmetry. In other words, DST (DCT) coefficients correspond to DFT coefficients of a periodically and anti-symmetrically (symmetrically) extended sequence. If a high-order approximation is used, a generalisation of the Poisson solver by HO-DFT must be performed to satisfy the assumptions under which the interpolation conditions (7.19) hold. Instead of using DCT or DST, we explicitly "double" the computational domain and the discrete source term f_h in order to extend it into a periodic one and perform DFT. According to the BC imposed, we perform an even (for Neumann BCs) or odd (for Dirichlet BCs) extension of our source term (that is set to 0 at the end-points of the interval for antisymmetric extensions). See Figure 7.3 for a graphical illustration of this procedure in one-dimension. Therefore, we need to take into account $2N$ frequencies for each direction, instead of N frequencies for the periodic case. However, thanks to symmetry properties of the DFT, we are able to restrict most operations to $N + 1$ frequencies, as shown in what follows.

Henceforth, we extend the analysis for a one-dimensional, complex-valued discrete source term f_h. Note that, after doubling the computational domain and performing an even (or odd) extension of the source term, depending on the BCs considered, the sequence $\left\{f_{n,R-j}\right\}_{n \in \mathcal{N}, j \in \mathcal{R}}$ satisfies, for any given $n \in \mathcal{N}$,

$$\begin{cases} f_{n,R-j} = f_{2N-n-1,j}, & \text{if } j \in \mathcal{R}^*, \\ f_{n,0} = f_{2N-n,0}, \end{cases} \tag{7.35}$$

for an even extension, and

$$\begin{cases} f_{n,R-j} = -f_{2N-n-1,j}, & \text{if } j \in \mathcal{R}^*, \\ f_{n,0} = -f_{2N-n,0}, \end{cases} \tag{7.36}$$

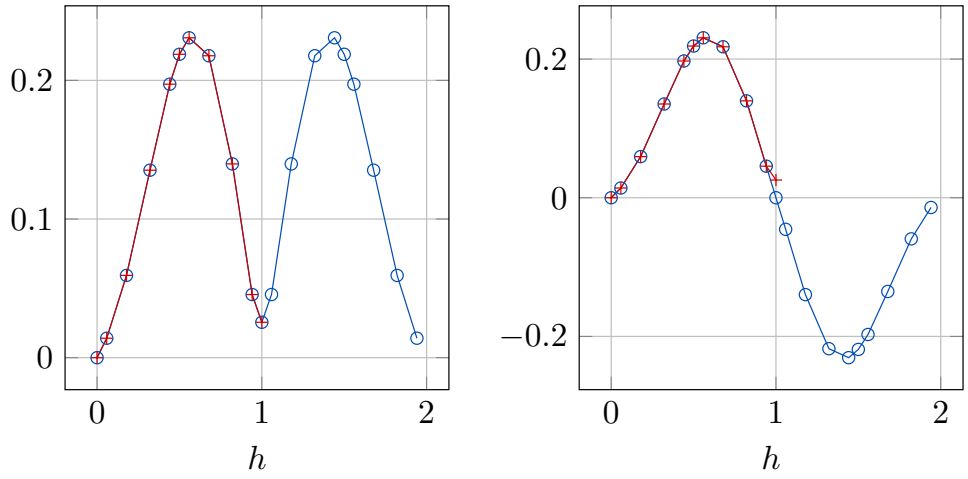

Figure 7.3 – Illustration of a periodic extension of a discrete, one-dimensional function at Gauss-Lobatto nodes. Left: comparison between original function and its even expansion (for Neumann BCs); right: comparison between original function and its odd expansion (for Dirichlet BCs). Gauss-Lobatto nodes for N=2 elements, 5^{th}-Order Lagrange polynomials.

for an odd extension. Henceforth, we use the symbol $\pm$ for the sake of conciseness, where $+$ is associated with Neumann conditions, whereas $-$ corresponds to Dirichlet conditions. We define the coefficients $\hat{f}_{k,j}$ following Eq. (7.19). Given $j \in \mathcal{R}$, they read

$$\hat{f}_{k,j} = \sum_{n=0}^{2N-1} f_{n,j}\, e^{-\frac{i\pi nk}{N}}, \quad \forall k \in \{0, 1, .., 2N-1\}. \tag{7.37}$$

From the properties of the sequence $\left\{f_{n,j}\right\}_{n\in\mathcal{N},j\in\mathcal{R}}$ we can deduce some symmetry properties of the coefficients $\hat{f}_{k,j}$, as stated in the following lemma. These properties allow to reduce the number of frequencies considered for the construction of the symbol of the operator. Due to the use of high-order polynomial interpolation, this symmetry is not trivial.

Lemma 7.1. *Let $\left\{f_{n,j}\right\}_{n\in\mathcal{N},j\in\mathcal{R}}$ be a complex-valued sequence.*
If the sequence satisfies Eq. (7.35) or Eq. (7.36), the coefficients $\hat{f}_{k,j}$ read, $\forall k \in \mathcal{N}^*$

$$\begin{cases} \hat{f}_{2N-k,j} = \pm e^{\frac{-i\pi k}{N}} \hat{f}_{k,R-j}, & \text{if } \; j \in \mathcal{R}^*, \\ \hat{f}_{2N-k,0} = \pm \hat{f}_{k,0}, \end{cases} \tag{7.38}$$

with the established convention for the plus and minus signs.

Proof. Let us consider an even extension of the discrete source term, and fix $j \in \mathcal{R}^*$. On the one hand, due to Eq. (7.35), Eq. (7.36) and Lemma 7.1, we are able to retrieve that, for $k \in \mathcal{N} \cup \{N\}$,

$$\begin{aligned} \hat{f}_{k,R-j} &= \sum_{n=0}^{2N-1} f_{n,R-j}\, e^{-\frac{i\pi nk}{N}} = \sum_{n=0}^{2N-1} f_{2N-n-1,j}\, e^{-\frac{i\pi nk}{N}} \\ &= \sum_{m=0}^{2N-1} f_{m,j}\, e^{\frac{-i2N\pi k}{N}} e^{\frac{i\pi mk}{N}} e^{\frac{ik}{N}} = e^{\frac{ik}{N}} \sum_{m=0}^{2N-1} f_{m,j}\, e^{\frac{i\pi mk}{N}}. \end{aligned}$$

On the other hand, due to a standard property of DFT, we have that

$$\hat{f}_{2N-k,j} = \sum_{m=0}^{2N-1} f_{m,j}\, e^{\frac{-i\pi m(2N-k)}{N}} = \sum_{m=0}^{2N-1} f_{m,j}\, e^{\frac{i\pi mk}{N}},\ \forall j \in \mathcal{R}.$$

Hence, we deduce that

$$\hat{f}_{k,R-j} = e^{\frac{i\pi k}{N}}\, \hat{f}_{2N-k,j}. \tag{7.39}$$

In addition, for $j = 0$ and $k \in \mathcal{N} \cup \{N\}$, we obtain

$$\begin{aligned} \hat{f}_{k,0} &= \sum_{n=0}^{2N-1} f_{n,0}\, e^{-\frac{i\pi nk}{N}} = \sum_{n=0}^{2N-1} f_{2N-n,0}\, e^{-\frac{i\pi nk}{N}} \\ &= \sum_{m=1}^{2N} f_{m,0}\, e^{\frac{-i2N\pi k}{N}} e^{\frac{i\pi mk}{N}} = \sum_{m=0}^{2N-1} f_{m,0}\, e^{\frac{i\pi mk}{N}} \\ &= \hat{f}_{2N-k,0}, \end{aligned} \tag{7.40}$$

since, by periodicity, $f_{2N,0} = f_{0,0}$. The proof for odd extension of the discrete source term is analogous. □

Furthermore, we state the following property:

Property 7.3. *Let us consider Problem (7.1), with $\Omega \in \mathbb{R}^d$, $d \geq 1$. Then, if the source term f is periodic and even (odd), the solution u is endowed with the same properties, i.e. it is periodic and even (odd).*

Note that Property 7.3 also holds true for the discrete problem (7.4), and f_h, u_h. From Lemma 7.1 and Property 7.3, we deduce that the discrete solution u_h satisfies Eq.(7.38). For this reason, we can construct an efficient algorithm for the resolution of a Poisson problem by HO-DFT that consists in three steps:

1. Perform a DFT of the discrete source term for each order j fixed in $\mathcal{R}^*$

$$\hat{f}_{k,j} = \sum_{n=0}^{2N-1} f_{n,j}\, e^{-\frac{i\pi nk}{N}},\ \forall k \in \mathcal{N} \cup \{N\};$$

2. Apply the inverse symbol of the operator for each frequency

$$\underline{\hat{U}}_k = \boldsymbol{\mathcal{S}}_k^{-1}\, \underline{\hat{F}}_k,\ \forall k \in \mathcal{N} \cup \{N\};$$

3. Perform an inverse DFT for each order j fixed in $\mathcal{R}^*$

$$u_{n,j} = \frac{1}{2N} \sum_{k=0}^{2N-1} \hat{u}_{k,j}\, e^{\frac{i\pi nk}{N}},\ \forall n \in \mathcal{N} \cup \{N\}.$$

This algorithm relies on the evaluation of the symbol of the operator of the first $N+1$ frequencies only. Note, however, that the standard implementation of DFT (or its inverse) by FFT algorithm implies the evaluation of all 2N frequencies. Consequently, the main gain in one-dimension is reduced to Step 2. However, we will show in what follows that in multi-dimensions it is possible to optimise Steps 1 and 3, by considering an *ad hoc* extension of the sequence "dimension by dimension" when the FFT (or its inverse) is performed.

Remark Note that the $\boldsymbol{\mathcal{A}}_k$ are all invertible, except for the case $k = 0$. Indeed, if $k = 0$, the constant vector is an eigenvector of $\boldsymbol{\mathcal{A}}_0$ associated with the eigenvalue 0. Therefore, if $\rho = 0$, then $\boldsymbol{\mathcal{S}}_k = \boldsymbol{\mathcal{A}}_k$ and $\underline{\hat{U}}_k$ is computed using a pseudoinverse of $\boldsymbol{\mathcal{A}}_k$, i.e.

$$\underline{\hat{U}}_k = \sum_{\substack{i \in \mathcal{R} \\ \lambda_{k,i} \neq 0}} \lambda_{k,i}^{-1} \, \underline{V}_{k,i} \, \underline{V}_{k,i}^* \, \boldsymbol{\mathcal{M}} \, \underline{\hat{F}}_k. \tag{7.41}$$

Eq. (7.41) corresponds to setting the mean value of the solution equal to zero.

7.4 Extension to higher dimensions

The generalisation to two (or higher) dimensions is performed by tensorisation from the one-dimensional case. Therefore, most of the properties are directly inherited from the one-dimensional case, and we do not provide the proofs, for the sake of conciseness. Henceforth, we denote by $d > 1$ the dimension of the computational domain. Our formulation is valid for every $d > 1$, but we mostly focus on $d = 2, 3$ for our purposes.

7.4.1 Periodic boundary conditions

First, let us define $\mathcal{N}^d = \{0, 1, .., N-1\}^d$ and $\mathcal{R}^d = \{0, 1, .., R-1\}^d$. We introduce the set of points in the reference element $[0, 1]^d$ as

$$\underline{\xi}_{\mathbf{j}} = [\xi_{j_1}, \xi_{j_2}, .., \xi_{j_r}],$$

where ξ_i corresponds to a 1-D Gauss-Lobatto node $\forall i \in \mathcal{R}$, and $\mathbf{j}$ is a multi-index in $\mathcal{R}^d$. Let us introduce the multi-index $\mathbf{n} = [n_1, n_2, .., n_d] \in \mathcal{N}^d$. Then, the d-dimensional shape functions defined on $\underline{x} = [x_1, x_2, .., x_d] \in [0, L]^d$ read

$$\Phi_{\mathbf{n},\mathbf{j}}(\underline{x}) = \prod_{r=1}^{d} \varphi_{n_r, j_r}(x_r), \tag{7.42}$$

where $\varphi_{n_r,j_r}(x_r)$ are defined as in Eq. (7.15). As in 1-D, the shape functions satisfy, $\forall \mathbf{p} \in \mathcal{R}^d$, $\mathbf{m} \in \mathcal{N}^d$,

$$\begin{aligned} \Phi_{\mathbf{m},\mathbf{p}}((\underline{\xi}_{\mathbf{j}} + \mathbf{n})h) &= \Phi_{\mathbf{m},\mathbf{p}}((\xi_{j_1} + n_1)h, (\xi_{j_2} + n_2)h, .., (\xi_{j_d} + n_d)h) \\ &= \prod_{r=1}^{d} \varphi_{n_r,p_r}(\xi_{j_r}) \delta_{m_r \, n_r} = \prod_{r=1}^{d} \delta_{p_r \, j_r} \delta_{m_r \, n_r}. \end{aligned}$$

For simplicity of notation, we denote

$$\sum_{\mathbf{n}} \coloneqq \sum_{n_1=0}^{N-1} \sum_{n_2=0}^{N-1} \cdots \sum_{n_d=0}^{N-1}, \quad \sum_{\mathbf{j}} \coloneqq \sum_{j_1=0}^{R-1} \sum_{j_2=0}^{R-1} \cdots \sum_{j_d=0}^{R-1}.$$

From Eq. (7.42) we derive the following decomposition for the discrete source term f_h and the discrete solution u_h:

$$f_h(\underline{x}) = \sum_{\mathbf{n},\mathbf{j}} f_{\mathbf{n},\mathbf{j}} \, \Phi_{\mathbf{n},\mathbf{j}}(\underline{x}), \quad u_h(\underline{x}) = \sum_{\mathbf{n},\mathbf{j}} u_{\mathbf{n},\mathbf{j}} \, \Phi_{\mathbf{n},\mathbf{j}}(\underline{x}),$$

with

$$f_{\mathbf{n},\mathbf{j}} \coloneqq f_h\big((\underline{\xi}_{\mathbf{j}} + \mathbf{n})h\big) \quad u_{\mathbf{n},\mathbf{j}} \coloneqq u_h\big((\underline{\xi}_{\mathbf{j}} + \mathbf{n})h\big), \quad \forall \mathbf{n} \in \mathcal{N}^d,\, \forall \mathbf{j} \in \mathcal{R}^d.$$

Let $\mathbf{k} \in \mathcal{N}^d$. Since the source term is periodic in $[0, L]^d$, we can generalise the definition of an interpolation function (7.17) for higher dimensions as

$$\tilde{f}_h(\underline{x}) = \frac{1}{N^d} \sum_{\mathbf{k}} \left(\sum_{\mathbf{j}} \hat{f}_{\mathbf{k},\mathbf{j}}\, e^{\frac{i2\pi(\underline{x} - h\underline{\xi}_{\mathbf{j}})\cdot\mathbf{k}}{L}} \sum_{\mathbf{n}} \varphi_{\mathbf{n},\mathbf{j}}(\underline{x}) \right), \tag{7.43}$$

with

$$e^{\frac{i2\pi(\underline{x} - h\underline{\xi}_{\mathbf{j}})\cdot\mathbf{k}}{L}} = e^{\frac{i2\pi(x_1 - h\xi_{j_1})\,k_1}{L}}\, e^{\frac{i2\pi(x_2 - h\xi_{j_2})\,k_2}{L}} \cdots e^{\frac{i2\pi(x_d - h\xi_{j_d})\,k_d}{L}}.$$

Note that this formula can be easily extended to more general hexahedral meshes by considering a different length L depending on the direction. Eq. (7.43) is a generalisation of Eq. (7.17) to the multi-dimensional case. Therefore, the coefficients $\hat{f}_{k,j}$, $\forall j \in \mathcal{R}$, can be computed by DFT, as stated in the following property.

Property 7.4. *Let $f_h \in C^0_\sharp([0, L]^d)$ and $\tilde{f}_h \in C^0_\sharp([0, L]^d)$ defined by Eq. (7.43). Let us denote*

$$\tilde{f}_{\mathbf{n},\mathbf{j}} \coloneqq \tilde{f}_h\big((\underline{\xi}_{\mathbf{j}} + \mathbf{n})h\big) \quad \forall \mathbf{j} \in \mathcal{R}^d,\ \forall \mathbf{n} \in \mathcal{N}^d.$$

Then, for all $\mathbf{j}$ fixed in $\mathcal{R}^d$,

$$\begin{aligned} f_{\mathbf{n},\mathbf{j}} = \tilde{f}_{\mathbf{n},\mathbf{j}} \iff \hat{f}_{\mathbf{k},\mathbf{j}} &= \sum_{\mathbf{n}} f_{\mathbf{n},\mathbf{j}}\, e^{\frac{-i2\pi\mathbf{n}\cdot\mathbf{k}}{N}},\ \forall \mathbf{k} \in \mathcal{N}^d, \\ \iff f_{\mathbf{n},\mathbf{j}} &= \frac{1}{N^d} \sum_{\mathbf{k}} \hat{f}_{\mathbf{k},\mathbf{j}}\, e^{\frac{i2\pi\mathbf{n}\cdot\mathbf{k}}{N}},\ \forall \mathbf{n} \in \mathcal{N}^d, \end{aligned} \tag{7.44}$$

since $h\,N = L$.

Similarly, we introduce the interpolation function of the discrete solution u_h such that, $\forall \mathbf{j} \in \mathcal{R}^d$ fixed,

$$\tilde{u}_{\mathbf{n},\mathbf{j}} \coloneqq \tilde{u}_h\big((\xi_{\mathbf{j}} + \mathbf{n})h\big) = \frac{1}{N^d} \sum_{\mathbf{k}} \hat{u}_{\mathbf{k},\mathbf{j}}\, e^{\frac{i2\pi\mathbf{n}\cdot\mathbf{k}}{N}},\ ,\forall \mathbf{n} \in \mathcal{N}^d, \tag{7.45}$$

where

$$\hat{u}_{\mathbf{k},\mathbf{j}} = \sum_{\mathbf{n}} u_{\mathbf{n},\mathbf{j}}\, e^{-\frac{i2\pi\mathbf{n}\cdot\mathbf{k}}{N}},\ \forall \mathbf{k} \in \mathcal{N}^d. \tag{7.46}$$

Due to Eqs. (7.45) and (7.46), we retrieve

$$u_{\mathbf{n},\mathbf{j}} = \tilde{u}_{\mathbf{n},\mathbf{j}}, \quad \forall \mathbf{n} \in \mathcal{N}^d.$$

As a straightforward generalisation of the one-dimensional case, the main steps of the algorithm read:

1. Perform a DFT of the discrete source term for each order $\mathbf{j}$ fixed in $\mathcal{R}^d$

$$\hat{f}_{\mathbf{k},\mathbf{j}} = \sum_{\mathbf{n}} f_{\mathbf{n},\mathbf{j}}\, e^{\frac{-i2\pi\mathbf{n}\cdot\mathbf{k}}{N}},\ \forall \mathbf{k} \in \mathcal{N}^d;$$

2. Solve for each frequency $\mathbf{k} \in \mathcal{N}^d$

$$\boldsymbol{\mathcal{S}}_{\mathbf{k}}\, \underline{\hat{U}}_{\mathbf{k}} = \underline{\hat{F}}_{\mathbf{k}}; \tag{7.47}$$

3. Perform an inverse DFT for each order $\mathbf{j}$ fixed in $\mathcal{R}^d$

$$u_{\mathbf{n},\mathbf{j}} = \frac{1}{N^d} \sum_{\mathbf{k}} \hat{u}_{\mathbf{k},\mathbf{j}}\, e^{\frac{i2\pi \mathbf{n}\cdot\mathbf{k}}{N}}, \ \forall \mathbf{n} \in \mathcal{N}^d.$$

We emphasize that the multi-dimensional DFT is implemented recursively from the one-dimensional DFT. Furthermore, step 2 must be implemented with care. In fact, one possibility is to inverse the symbol $\boldsymbol{\mathcal{S}}_{\mathbf{k}}$ for each frequency, and then perform a matrix-vector multiplication to obtain $\underline{\hat{U}}_{\mathbf{k}}$. Note, however, that such an algorithm would imply a substantial computational cost. To give an idea, in 2-D the matrix inversion would require $O(R^6)$ operations ($O(R^{3d})$ in general), while matrix-vector multiplication requires $O(R^4)$ operations. In what follows, we propose a method that requires neither matrix inversion nor storage and drastically reduces the complexity of the algorithm, based on SVD and tensorisation.
For the sake of conciseness, we denote $\boldsymbol{\mathcal{N}}_k = \boldsymbol{\mathcal{M}}^{-1}\boldsymbol{\mathcal{A}}_k$, with $\boldsymbol{\mathcal{M}}$ and $\boldsymbol{\mathcal{A}}_k$ associated with the 1-D case, and defined in Eq. (7.30). We also can rewrite $\boldsymbol{\mathcal{S}}_k \coloneqq \rho\,\mathbf{I} + \boldsymbol{\mathcal{N}}_k$, with $\mathbf{I}$ the identity matrix of size R^2. The following theorem can be proven ([Cohen, 2001]):

Proposition 7.2. *Let $\boldsymbol{\mathcal{S}}_{\mathbf{k}}(\boldsymbol{\ell},\mathbf{m})$ denote the term located at line $\boldsymbol{\ell}$ and column $\mathbf{m}$, with $\boldsymbol{\ell},\mathbf{m} \in \mathcal{R}^d$. Then*

$$\boldsymbol{\mathcal{S}}_{\mathbf{k}}(\boldsymbol{\ell},\mathbf{m}) = \rho \prod_{r=1}^{d} \delta_{l_r\, m_r} + \sum_{r=1}^{d} \boldsymbol{\mathcal{N}}_{k_r}(\ell_r, m_r) \prod_{q\neq r} \delta_{\ell_q\, m_q}. \tag{7.48}$$

For example, when $d = 2$, the symbol reads

$$\boldsymbol{\mathcal{S}}_{\mathbf{k}}(\boldsymbol{\ell},\mathbf{m}) = \rho\,\delta_{l_1\, m_1}\,\delta_{l_2\, m_2} + \boldsymbol{\mathcal{N}}_{k_1}(\ell_1, m_1)\,\delta_{\ell_2\, m_2} + \boldsymbol{\mathcal{N}}_{k_2}(\ell_2, m_2)\,\delta_{\ell_1\, m_1}.$$

This result is a direct consequence of the use of the Gauss-Lobatto nodes for quadrature formulae. Due to Proposition 7.2, it is possible to compute the eigenvalues and eigenvectors of the multi-dimensional symbol $\boldsymbol{\mathcal{S}}_{\mathbf{k}}$ starting from eigenvalues and eigenvectors of the one-dimensional symbols $\boldsymbol{\mathcal{S}}_{k_r}$, $r \in \{1,2,..,d\}$. We recall that, given $\mathbf{k} \in \mathcal{N}^d$, $\left\{\lambda_{\mathbf{k},\mathbf{i}}, \underline{V}_{\mathbf{k},\mathbf{i}}\right\}_{\mathbf{i}\in\mathcal{R}^d}$ is the set of eigenvalues and eigenvectors of $\boldsymbol{\mathcal{S}}_{\mathbf{k}}$ if they satisfy

$$\boldsymbol{\mathcal{S}}_{\mathbf{k}}\, \underline{V}_{\mathbf{k},\mathbf{i}} = \lambda_{\mathbf{k},\mathbf{i}}\, \underline{V}_{\mathbf{k},\mathbf{i}}, \quad \forall \mathbf{k} \in \mathcal{N}^d, \ \forall \mathbf{i} \in \mathcal{R}^d.$$

Corollary 7.1. *Let $\left\{\nu_{k_r,i_r}, \underline{W}_{k_r,i_r}\right\}_{i_r\in\mathcal{R}}$ be the eigenvalues and eigenvectors of $\boldsymbol{\mathcal{N}}_{k_r}$, $r \in \{1,2,..,d\}$, and let $\left\{\lambda_{\mathbf{k},\mathbf{i}}, \underline{V}_{\mathbf{k},\mathbf{i}}\right\}_{\mathbf{i}\in\mathcal{R}^d}$ be the eigenvalues and eigenvectors of $\boldsymbol{\mathcal{S}}_{\mathbf{k}}$. Let $\mathbf{i} \in \mathcal{R}^d$. Then*

$$\begin{cases} \lambda_{\mathbf{k},\mathbf{i}} = \rho + \displaystyle\sum_{r=1}^{d} \nu_{k_r,i_r}, \\ V_{\mathbf{k},\mathbf{i}}(\mathbf{m}) = \displaystyle\prod_{r=1}^{d} W_{k_r,i_r}(m_r). \end{cases}$$

As an illustration, when $d = 2$ we obtain

$$\begin{cases} \lambda_{\mathbf{k},\mathbf{i}} = \rho + \nu_{k_1,i_1} + \nu_{k_2,i_2}, \\ \underline{V}_{\mathbf{k},\mathbf{i}} = \underline{W}_{k_1,i_1} \otimes \underline{W}_{k_2,i_2}, \end{cases}$$

where $\otimes$ denotes the tensor product.

Proof. This corollary is deduced from [Cohen, 2001] and some classical results in linear algebra. First, it is possible to prove (see [Cohen, 2001]) that, given $\left\{\nu_{k_r,i_r}, \underline{W}_{k_r,i_r}\right\}_{i_r\in\mathcal{R}}$ the eigenvalues and eigenvectors of $\boldsymbol{\mathcal{N}}_{k_r}$, $r \in \{1,2,..,d\}$, and $\left\{\nu_{\mathbf{k},\mathbf{i}}, \underline{W}_{\mathbf{k},\mathbf{i}}\right\}_{\mathbf{i}\in\mathcal{R}^d}$ the eigenvalues and eigenvectors of $\boldsymbol{\mathcal{N}}_{\mathbf{k}}$, then

$$\begin{cases} \nu_{\mathbf{k},\mathbf{i}} = \displaystyle\sum_{r=1}^{d} \nu_{k_r,i_r}, \\ W_{\mathbf{k},\mathbf{i}}(\mathbf{m}) = \displaystyle\prod_{r=1}^{d} W_{k_r,i_r}(m_r). \end{cases}$$

Furthermore, it is straightforward to demonstrate that, given an identity matrix of order n, every vector of size equal to n is an eigenvector for this matrix, with eigenvalue equal to 1. Finally, it is trivial to show that, given $\mathbf{A}$, $\mathbf{B} \in M_n(\mathbb{C})$, and $\underline{W} \in \mathbb{C}^n$, ν_A, $\nu_B \in \mathbb{C}$ such that

$$\begin{cases} \mathbf{A}\,\underline{W} = \nu_A\,\underline{W}, \\ \mathbf{B}\,\underline{W} = \nu_B\,\underline{W}, \end{cases}$$

then

$$(\mathbf{A}+\mathbf{B})\,\underline{W} = (\nu_A+\nu_B)\,\underline{W}.$$

The result of the corollary follows immediately. □

As a result of Eq. (7.1), the solution $\underline{\hat{U}}_{\mathbf{k}}$ in the frequency domain can be computed with an optimised algorithm that we give henceforth. It is based on tensorisation and the use of internal variables.

Inversion of the symbol by SVD. Let us fix a frequency $\mathbf{k} \in \mathcal{N}^d$, and define $\mathbf{p}, \mathbf{j}, \mathbf{r} \in \mathcal{R}^d$. For the sake of simplicity, we use in this section the notation $\hat{F}_{\mathbf{k}}(\mathbf{j}) \coloneqq \hat{f}_{\mathbf{k},\mathbf{j}}$ and $\hat{U}_{\mathbf{k}}(\mathbf{j}) \coloneqq \hat{u}_{\mathbf{k},\mathbf{j}}$.
As for the one-dimensional case, Eq. (7.47) can be rewritten as

$$\underline{\hat{U}}_{\mathbf{k}} = \boldsymbol{\mathcal{S}}_{\mathbf{k}}^{-1}\,\underline{\hat{F}}_{\mathbf{k}} = \sum_{\mathbf{p}} \lambda_{\mathbf{k},\mathbf{p}}^{-1}\,\underline{V}_{\mathbf{k},\mathbf{p}}\,\underline{V}_{\mathbf{k},\mathbf{p}}^{*}\,\boldsymbol{\mathcal{M}}_d\,\underline{\hat{F}}_{\mathbf{k}}. \tag{7.49}$$

i.e.

$$\begin{aligned} \hat{U}_{\mathbf{k}}(\mathbf{j}) &= \sum_{\mathbf{p}}\sum_{\mathbf{r}} \lambda_{\mathbf{k},\mathbf{p}}^{-1} V_{\mathbf{k},\mathbf{p}}(\mathbf{j})\,\overline{V_{\mathbf{k},\mathbf{p}}(\mathbf{r})}\,\boldsymbol{\mathcal{M}}_d(\mathbf{r})\hat{F}_{\mathbf{k}}(\mathbf{r}) \\ &= \sum_{\mathbf{p}} \lambda_{\mathbf{k},\mathbf{p}}^{-1} V_{\mathbf{k},\mathbf{p}}(\mathbf{j}) \sum_{\mathbf{r}} \overline{V_{\mathbf{k},\mathbf{p}}(\mathbf{r})}\,\boldsymbol{\mathcal{M}}_d(\mathbf{r})\hat{F}_{\mathbf{k}}(\mathbf{r}), \end{aligned} \tag{7.50}$$

where $\boldsymbol{\mathcal{M}}_d$ denotes the symbol of the mass matrix in d-dimensions, and it can be rewritten as

$$\boldsymbol{\mathcal{M}}_d(\mathbf{i},\mathbf{m}) = \prod_{r=1}^{d} \boldsymbol{\mathcal{M}}(i_r, m_r).$$

From Eq. (7.50), note that the total number of operations required to compute all the components of $\underline{\hat{U}}_{\mathbf{k}}$ is $O(R^{3d})$, that is comparable to the cost of symbol inversion by standard algorithms (e.g. by Gaussian elimination). As an illustration, this inversion would require $O(R^6)$ operations in 2 dimensions, $O(R^9)$ in 3 dimensions. However, the eigenvalues and eigenvectors in higher dimensions can be directly derived by tensorisation from those in 1-D. For the moment, we fix the frequency $\mathbf{k} \in \mathcal{N}$ for the sake of clarity. First, we introduce two intermediate variables, and we split Eq. (7.50) into three main operations:

- We define $\alpha_{\mathbf{k}}(\mathbf{p})$ as

$$\alpha_{\mathbf{k}}(\mathbf{p}) = \sum_{\mathbf{r}} \overline{V_{\mathbf{k},\mathbf{p}}(\mathbf{r})}\, \boldsymbol{\mathcal{M}}_d(\mathbf{r}) \hat{F}_{\mathbf{k}}(\mathbf{r}); \tag{7.51}$$

- Then, we compute the scalar coefficients $\gamma_{\mathbf{k}}(\mathbf{p})$ as

$$\gamma_{\mathbf{k}}(\mathbf{p}) \coloneqq \lambda_{\mathbf{k},\mathbf{p}}^{-1}\, \alpha_{\mathbf{k}}(\mathbf{p}) = (\rho + \lambda_{k_1,p_1} + \lambda_{k_2,p_2})^{-1}\, \alpha_{\mathbf{k}}(p_1,p_2);$$

- Finally, the components $\hat{u}_{\mathbf{k}}(\mathbf{j})$ are retrieved as

$$\hat{u}_{\mathbf{k}}(\mathbf{j}) = \sum_{\mathbf{p}} \gamma_{\mathbf{k}}(\mathbf{p})\, V_{\mathbf{k},\mathbf{p}}(\mathbf{j}). \tag{7.52}$$

Now, we can take advantage of the properties of the eigenvalues $V_{\mathbf{k},\mathbf{p}}(\mathbf{j})$. Due to Eq.(7.1), we can reduce the two multi-dimensional sums in Eq. (7.51) and Eq. (7.52) in successions of one-dimensional sums. In order to avoid cumbersome expressions, we consider $d = 2$ henceforth. Note, however, that the extension of our analysis for $d > 2$ is straightforward.

$$\begin{aligned}
\alpha_{\mathbf{k}}(\mathbf{p}) = \alpha_{\mathbf{k}}(p_1,p_2) &\coloneqq \sum_{r_1,r_2\in\mathcal{R}} \boldsymbol{\mathcal{M}}_d(r_1,r_2) \hat{F}_{\mathbf{k}}(r_1,r_2)\, \overline{V_{k_1,p_1}(r_1)}\, \overline{V_{k_2,p_2}(r_2)} \\
&= \sum_{r_2\in\mathcal{R}} \overline{V_{k_2,p_2}(r_2)} \sum_{r_1\in\mathcal{R}} \boldsymbol{\mathcal{M}}_d(r_1,r_2) \hat{F}_{\mathbf{k}}(r_1,r_2)\, \overline{V_{k_1,p_1}(r_1)} \\
&= \sum_{r_2\in\mathcal{R}} \overline{V_{k_2,p_2}(r_2)}\, \beta_{\mathbf{k}}(p_1,r_2),
\end{aligned}$$

where

$$\beta_{\mathbf{k}}(\mathbf{p}) = \beta_{\mathbf{k}}(p_1,p_2) \coloneqq \sum_{r_1\in\mathcal{R}} \boldsymbol{\mathcal{M}}_d(r_1,p_2)\, \hat{F}_{\mathbf{k}}(r_1,p_2) \overline{V_{k_1,p_1}(r_1)}.$$

Analogously, $\hat{u}_{\mathbf{k}}(\mathbf{j})$ are obtained as

$$\begin{aligned}
\hat{u}_{\mathbf{k}}(\mathbf{j}) = \hat{u}_{\mathbf{k}}(j_1,j_2) &= \sum_{p_1,p_2\in\mathcal{R}} \gamma_{\mathbf{k}}(p_1,p_2)\, V_{k_1,p_1}(j_1)\, V_{k_2,p_2}(j_2) \\
&= \sum_{p_2\in\mathcal{R}} V_{k_2,p_2}(j_2) \sum_{p_1\in\mathcal{R}} \gamma_{\mathbf{k}}(p_1,p_2)\, V_{k_1,p_1}(j_1) \\
&= \sum_{p_2\in\mathcal{R}} V_{k_2,p_2}(j_2)\, \mu_{\mathbf{k}}(j_1,p_2),
\end{aligned}$$

with

$$\mu_{\mathbf{k}}(\mathbf{j}) = \mu_{\mathbf{k}}(j_1,j_2) \coloneqq \sum_{p_1\in\mathcal{R}} \gamma_{\mathbf{k}}(p_1,j_2)\, V_{k_1,p_1}(j_1).$$

Consequently, the overall complexity of the algorithm for the symbol inversion for each frequency decreases to $O(R^{d+1})$. For example, only $O(R^3)$ operations are needed in 2-D for the computation of $\hat{\underline{U}}_{\mathbf{k}}$, instead of $O(R^6)$ as in Eq. (7.50). In an analogous way, in 3-D only $O(R^4)$ operations are required, instead of $O(R^9)$.

7.4.2 Neumann or Dirichlet boundary conditions

The algorithm in the d-dimensional case can be directly deduced by tensorisation also when Dirichlet or Neumann conditions are imposed at the boundaries. In order to perform the DFT, the source term is periodically and symmetrically extended in d directions. This leads to the evaluation of a computational domain that is potentially 2^d times larger than the original domain. However, due to the symmetry properties of the extended source term, we will be able to reduce the main computations to the first $(N+1)^d$ frequencies. The extended discrete source term $\left\{f_{\mathbf{n},\mathbf{j}}\right\}$ satisfies, for all $r \in \{1, \cdots, d\}$,

$$\begin{cases} f_{\mathbf{n}+\mathbf{n}_r,\mathbf{j}} = \pm f_{\mathbf{n},\mathbf{j}+\mathbf{j}_r}, & j_r \neq 0, \quad \mathbf{n}_r = \mathbf{e}_r(2N-1-n_r),\ \mathbf{j}_r = \mathbf{e}_r(R-j_r), \\ f_{\mathbf{n}+\mathbf{n}_r,\mathbf{j}} = \pm f_{\mathbf{n},\mathbf{j}}, & j_r = 0, \quad \mathbf{n}_r = \mathbf{e}_r(2N-n_r), \end{cases} \tag{7.53}$$

where $\mathbf{e}_r$ is the $r-$th vector of the canonical basis of $\mathbb{R}^d$ and (n_r, j_r) is such that

$$\mathbf{n} + \mathbf{n}_r \in \{0, \cdots, 2N-1\}^d, \quad \mathbf{j} + \mathbf{j}_r \in \{0, \cdots R-1\}^d,$$

and where the even extension corresponds to Neumann BCs, while the odd extension is associated with Dirichlet BCs, as before.

Lemma 7.3. *The DFT of the extended sequence $\left\{f_{\mathbf{n},\mathbf{j}}\right\}$ satisfies, $\forall r \in \{1, \cdots, d\}$,*

$$\begin{cases} \hat{f}_{\mathbf{k}+\mathbf{k}_r,\mathbf{j}} = \pm \hat{f}_{\mathbf{k},\mathbf{j}+\mathbf{j}_r}\, e^{\frac{-i\pi k}{N}}, & \text{if } \ j_r \neq 0, \quad \mathbf{k}_r = \mathbf{e}_r(2N-k_r),\ \mathbf{j}_r = \mathbf{e}_r(R-j_r), \\ \hat{f}_{\mathbf{k}+\mathbf{k}_r,\mathbf{j}} = \pm \hat{f}_{\mathbf{k},\mathbf{j}}, & \text{if } \ j_r = 0, \quad \mathbf{k}_r = \mathbf{e}_r(2N-k_r), \end{cases}$$

with (k_r, j_r) such that

$$\mathbf{k} + \mathbf{k}_r \in \{0, \cdots, 2N-1\}^d, \quad \mathbf{j} + \mathbf{j}_r \in \{0, \cdots R-1\}^d$$

and with the usual convention for the plus and minus signs.

By way of illustration, we give the explicit expression of the DFT of the discrete, even-extended source term in $\mathbb{R}^2$. It satisfies, for $k_1, k_2 \in \mathcal{N}^*$,

$$\begin{cases} \hat{f}_{2N-k_1,k_2,j_1,j_2} = e^{\frac{-i\pi k_1}{N}} \hat{f}_{k_1,k_2,R-j_1,j_2}, & \text{if } \ j_1 \neq 0, \\ \hat{f}_{k_1,2N-k_2,j_1,j_2} = e^{\frac{-i\pi k_2}{N}} \hat{f}_{k_1,k_2,j_1,R-j_2}, & \text{if } \ j_2 \neq 0, \\ \hat{f}_{2N-k_1,2N-k_2,j_1,j_2} = e^{\frac{-i\pi (k_1+k_2)}{N}} \hat{f}_{k_1,k_2,R-j_1,R-j_2}, & \text{if } \ j_1 \neq 0, j_2 \neq 0, \\ \hat{f}_{2N-k_1,2N-k_2,j_1,0} = e^{\frac{-i\pi k_1}{N}} \hat{f}_{k_1,k_2,R-j_1,0}, & \text{if } \ j_1 \neq 0,\ j_2 = 0, \\ \hat{f}_{2N-k_1,2N-k_2,0,j_2} = e^{\frac{-i\pi k_2}{N}} \hat{f}_{k_1,k_2,0,R-j_2}, & \text{if } \ j_1 = 0,\ j_2 \neq 0, \\ \hat{f}_{2N-k_1,2N-k_2,0,0} = f_{k_1,k_2,0,0}, & \text{if } \ j_2 = 0,\ j_2 = 0. \end{cases} \tag{7.54}$$

Therefore, given a direction $i \in [1, 2, .., d]$, the value of the DFT coefficients for the last $N-1$ coefficients in that direction are directly retrieved from the first N coefficients, and the relationship depends on the frequency and the Gaussian point taken into account.
Eventually, due to Lemma 7.3 and Property 7.3, the solution $\hat{u}_{\mathbf{k},\mathbf{j}}$ inherits the same properties of $\hat{f}_{\mathbf{k},\mathbf{j}}$. Therefore, the optimised algorithm for resolution of a complex Poisson problem in $\Omega_h \subset \mathbb{R}^d$ reads:

1. Perform a DFT of the discrete source term for each order $\mathbf{j}$ fixed in $\mathcal{R}$

$$\hat{f}_{\mathbf{k},\mathbf{j}} = \sum_{\mathbf{n}=0}^{(2N-1)^d} f_{\mathbf{n},\mathbf{j}}\, e^{\frac{-i\pi\mathbf{n}\cdot\mathbf{k}}{N}},\ \forall \mathbf{k} \in (\mathcal{N} \cup \{N\})^d,$$

   using Eq. (7.53);

2. Solve for each frequency

$$\boldsymbol{\mathcal{S}}_{\mathbf{k}}\, \underline{\hat{U}}_{\mathbf{k}} = \underline{\hat{F}}_{\mathbf{k}},\ \forall \mathbf{k} \in (\mathcal{N} \cup \{N\})^d;$$

3. Perform an inverse DFT for each order $\mathbf{j}$ fixed in $\mathcal{R}$

$$u_{\mathbf{n},\mathbf{j}} = \frac{1}{(2N)^d} \sum_{\mathbf{k}=0}^{(2N-1)^d} \hat{u}_{\mathbf{k},\mathbf{j}}\, e^{\frac{i\pi\mathbf{n}\cdot\mathbf{k}}{N}},\ \forall \mathbf{n} \in (\mathcal{N} \cup \{N\})^d,$$

   where

$$\begin{cases} \hat{u}_{\mathbf{k}+\mathbf{k}_r,\mathbf{j}} = \pm \hat{u}_{\mathbf{k},\mathbf{j}+\mathbf{j}_r}\, e^{\frac{-i\pi k}{N}}, & \text{if } j_r \neq 0, \quad \mathbf{k}_r = \mathbf{e}_r(2N - k_r),\ \mathbf{j}_r = \mathbf{e}_r(R - j_r), \\ \hat{u}_{\mathbf{k}+\mathbf{k}_r,\mathbf{j}} = \pm \hat{u}_{\mathbf{k},\mathbf{j}}, & \text{if } j_r = 0, \quad \mathbf{k}_r = \mathbf{e}_r(2N - k_r), \end{cases}$$

   with the usual convention for signs, and with (k_r, j_r) such that

$$\mathbf{k} + \mathbf{k}_r \in \{0, \cdots, 2N-1\}^d, \quad \mathbf{j} + \mathbf{j}_r \in \{0, \cdots R-1\}^d.$$

7.5 Numerical Results, complexity and parallelisation

7.5.1 Convergence analysis

In order to demonstrate that the HO-DFT method preserves the order of convergence of the underlying SEM discretisation, the method is tested against an exact solution of Problem (7.1) with homogeneous Dirichlet Boundary conditions, that reads

$$u(\underline{x}) = \prod_{i=1}^{d} (1 - x_i)^3\, x_i^3\, \cos(k\, x_i), \quad \forall \underline{x} \in \Omega = [0,1]^d,\ d = 2, 3,$$

with $k = 10$. Figures 7.4 and 7.5 show the convergence error between the exact solution and the output of the HO-SEM algorithm in relative $L^2(\Omega)$ and $H^1(\Omega)$ norm w.r.t. the space step h in two and three dimensions, for different values of order R. We note some superconvergence effects associated with the $L^2(\Omega)$-error, whereas the convergence rate of the error in $H^1(\Omega)$-norm corresponds to the chosen order R. We do not show the last coordinates (accounting for h =0.0385 m) associated with order $R = 7$, since the estimation of the error is biased by the fact that the precision of the machine is reached.

7.5.2 Complexity of the algorithm

As it has been stated in the previous sections, this algorithm is remarkably efficient in multiple dimensions, for multiple reasons. First, the regularity of the computational domain

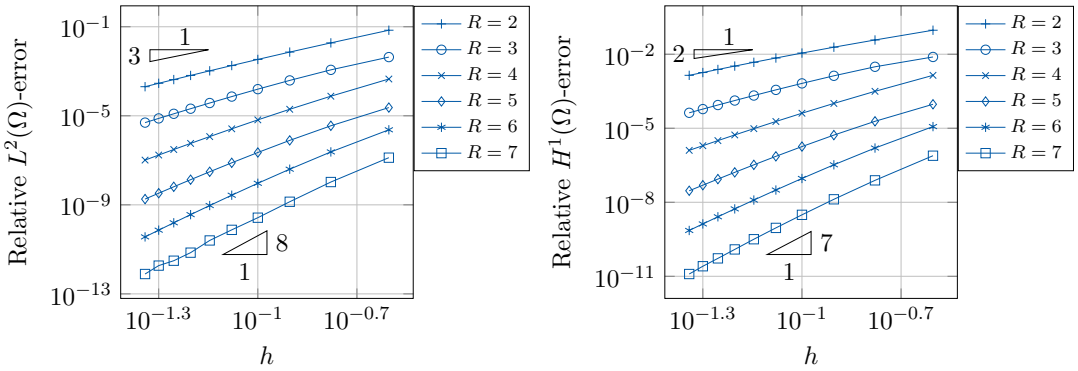

Figure 7.4 – Convergence of the two-dimensional scheme w.r.t. the space step h, for different values of order R. Left: Relative $L^2(\Omega)$-error. Right: Relative $H^1(\Omega)$-error.

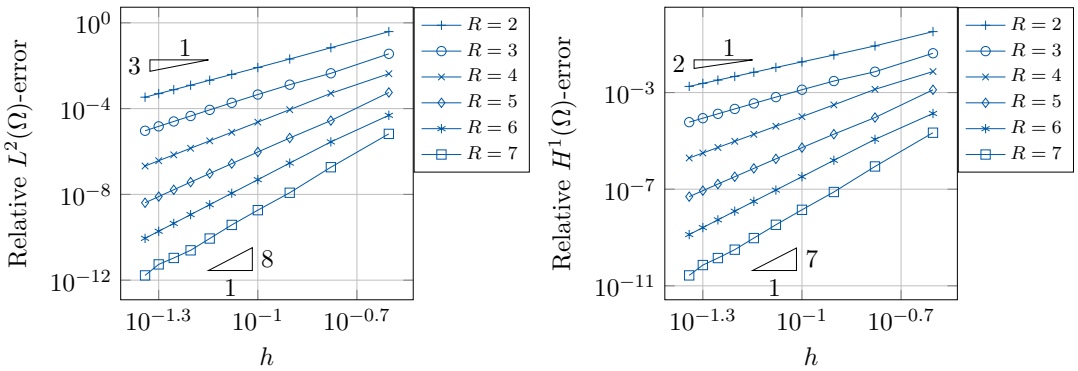

Figure 7.5 – Convergence of the three-dimensional scheme w.r.t. the space step h, for different values of order R. Left: Relative $L^2(\Omega)$-error. Right: Relative $H^1(\Omega)$-error.

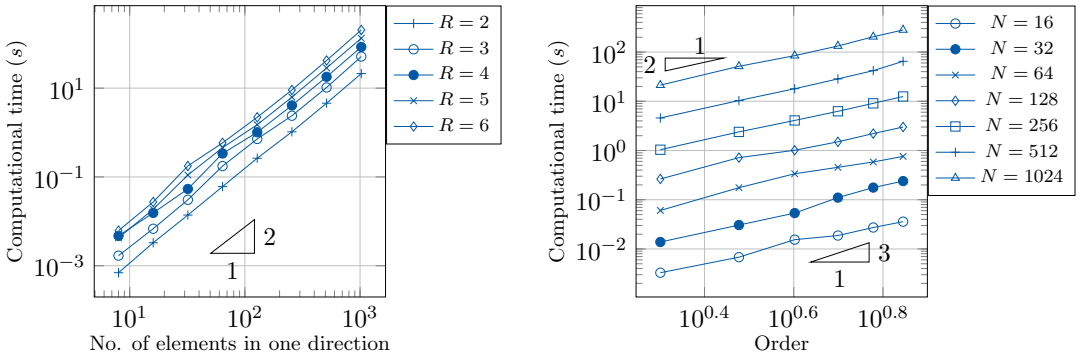

Figure 7.6 – Computational cost of the two-dimensional scheme. Left: comparison for different values of elements N (in every direction). comparison for different values of order R.

and the underlying use of HO-SEM for the discretisation of the Poisson problem enable the direct generalisation of Step 2 to multiple dimensions by tensorisation. Moreover, it is possible to rewrite the symbol inversion in terms of an eigenvalue problem. Therefore, in order to compute the solution in frequency domain, it is necessary to compute the eigenvalues and eigenvectors only of the symbol in 1-D. Consequently, this step of the algorithm requires for each frequency only $O(R^3)$ operations (instead of $O(R^6)$) in two dimensions, and $O(R^4)$ operations (instead of $O(R^9)$) in three dimensions.
In addition, Steps 1 and 3 can be performed by FFT. Since d-dimensional FFT corresponds to a 1-D FFT having the size of the product of the dimensions, its complexity is $d(\log N)N^d$ (if the domain is divided into the same number of elements N for each direction). Consequently, the implementation of FFT causes a further, sensible reduction of the computational cost.
We emphasize that this method is not limited to the resolution of the Poisson-like problem with periodic boundary conditions. In fact, we have shown that, in case of Dirichlet or Neumann BCs, it is possible to employ HO-DFT after extending symmetrically or antisymmetrically the computational domain – i.e. the number of frequencies considered – in each dimension. However, thanks to symmetry properties of the sequence considered and Fourier Transform, most operations only involve the first $N+1$ frequencies, and therefore the complexity of the algorithm remains approximatively the same as the one associated with the periodic case. Besides, the DFT and IDFT (steps 1 and 3) are disjoint for each order, whereas the operations involved in the inversion of the symbol (step 2) are disjoint for each frequency. Therefore, the algorithm is extremely well-adapted to parallelisation. In particular, Steps 1 and 3 can be run in parallel for each order, whereas Step 2 can be performed in parallel for each frequency. Figures 7.6 and 7.7 show the computational cost of the sequential resolution of the problem with homogeneous Dirichlet Boundary conditions in two and three dimensions on a 4-cores workstation (cores at 3.1 GHz and 16 GB of RAM at 1867 MHz). The computational time is accordance with the expected complexity with respect to number of elements N and the order R. Furthermore, the memory storage is also linear with the number of elements. We do not show any result concerning the memory for the sake of conciseness.

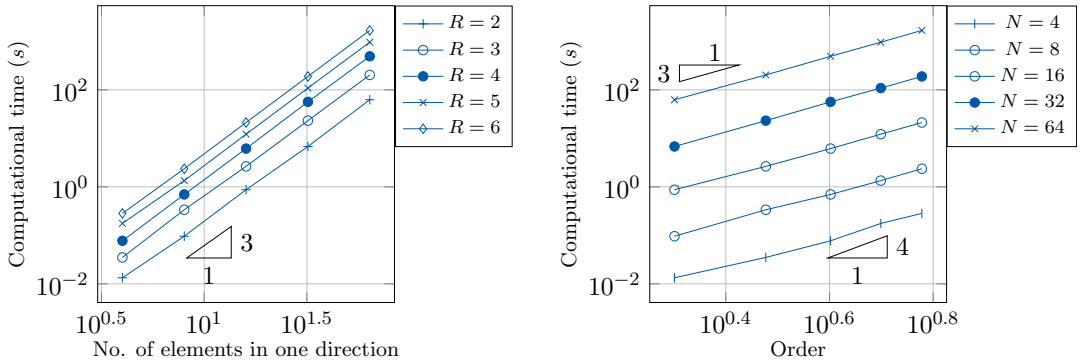

Figure 7.7 – Computational cost of the three-dimensional scheme. Left: comparison for different values of elements N (in every direction). comparison for different values of order R.

7.6 Conclusions

In this work we have proposed a new, efficient, matrix-free solver for the solution of the Poisson problem in Cartesian geometry discretised with HO-SEM, based on the used of the Discrete Fourier Transform. In particular, we have developed an efficient implementation of the problem that consists in the resolution of the symbol of the operator in the frequency domain. We have shown that the proposed algorithm can be extended in a straightforward manner to multiple dimensions and Dirichlet or Neumann boundary conditions, without affecting its efficiency. Furthermore, we have provided numerical evidence that the order of convergence of the underlying HO-SEM discretisation is preserved. In addition, the computational cost is linear with the total number of elements, and it is proportional to $O(R^3)$ (instead of $O(R^6)$) in two dimensions, and $O(R^4)$ (instead of $O(R^9)$) in three dimensions, R being the order of the basis function used for the HO-SEM discretisation.

Bibliography

Ainsworth, M. [2004], 'Discrete dispersion relation for hp-version finite element approximation at high wave number', *SIAM Journal on Numerical Analysis* **42**(2), 553–575.

Ainsworth, M. and Coggins, P. [2002], 'A uniformly stable family of mixed hp-finite elements with continuous pressures for incompressible flow', *IMA journal of numerical analysis* **22**(2), 307–327.

Amlani, F. and Bruno, O. P. [2016], 'An FC-based spectral solver for elastodynamic problems in general three-dimensional domains', *Journal of Computational Physics* **307**, 333 – 354.

Bercoff, J., Tanter, M. and Fink, M. [2004], 'Supersonic shear imaging: a new technique for soft tissue elasticity mapping', *IEEE transactions on ultrasonics, ferroelectrics, and frequency control* **51**(4), 396–409.

Brezzi, F. and Falk, R. S. [1991], 'Stability of higher-order Hood–Taylor methods', *SIAM Journal on Numerical Analysis* **28**(3), 581–590.

Brezzi, F. and Fortin, M. [2012], *Mixed and hybrid finite element methods*, Vol. 15, Springer Science & Business Media.

Caenen, A., Pernot, M., Peirlinck, M., Mertens, L., Swillens, A. and Segers, P. [2018], 'An in silico framework to analyze the anisotropic shear wave mechanics in cardiac shear wave elastography', *Physics in Medicine & Biology* **63**(7), 075005.

Cohen, G. [2001], *Higher-Order Numerical Methods for Transient Wave Equations*, Scientific Computation, Springer Berlin Heidelberg.

Cohen, G. and Fauqueux, S. [2005], 'Mixed spectral finite elements for the linear elasticity system in unbounded domains', *SIAM Journal on Scientific Computing* **26**(3), 864–884.

Guermond, J.-L., Minev, P. and Shen, J. [2006], 'An overview of projection methods for incompressible flows', *Computer methods in applied mechanics and engineering* **195**(44-47), 6011–6045.

Guermond, J.-L. and Quartapelle, L. [1998], 'On the approximation of the unsteady Navier–Stokes equations by finite element projection methods', *Numerische Mathematik* **80**(2), 207–238.

Gustafsson, B. [2011], *Fundamentals of Scientific Computing*, Texts in Computational Science and Engineering, Springer Berlin Heidelberg.

Hackbusch, W. [2015], *Hierarchical matrices: algorithms and analysis*, Vol. 49, Springer.

Hestenes, M. R. and Stiefel, E. [1952], *Methods of conjugate gradients for solving linear systems*, Vol. 49, NBS Washington, DC.

Iserles, A. [2009], *A first course in the numerical analysis of differential equations*, number 44, Cambridge university press.

Komatitsch, D. and Vilotte, J.-P. [1998], 'The spectral element method: an efficient tool to simulate the seismic response of 2d and 3d geological structures', *Bulletin of the seismological society of America* **88**(2), 368–392.

Lyon, M. and Bruno, O. P. [2010], 'High-order unconditionally stable FC-AD solvers for general smooth domains ii. elliptic, parabolic and hyperbolic pdes; theoretical considerations', *Journal of Computational Physics* **229**(9), 3358 – 3381.

Maday, Y. and Patera, A. T. [1989], Spectral element methods for the incompressible Navier-Stokes equations, *in* 'State-of-the-art surveys on computational mechanics (A90-47176 21-64). New York, American Society of Mechanical Engineers. Research supported by DARPA.', pp. 71–143.

Palmeri, M. L., Sharma, A. C., Bouchard, R. R., Nightingale, R. W. and Nightingale, K. R. [2005], 'A finite-element method model of soft tissue response to impulsive acoustic radiation force', *IEEE transactions on ultrasonics, ferroelectrics, and frequency control* **52**(10), 1699–1712.

Pena, G. [2009], Spectral element approximation of the incompressible Navier-Stokes equations in a moving domain and applications, PhD thesis, Ecole Polytechnique Fédérale de Lausanne (EPFL).

Quarteroni, A., Sacco, R. and Saleri, F. [2010], *Numerical mathematics*, Vol. 37, Springer Science & Business Media.

Spillane, N. [2016], 'An adaptive multipreconditioned conjugate gradient algorithm', *SIAM journal on Scientific Computing* **38**(3), A1896–A1918.

Van Loan, C. [1992], *Computational frameworks for the fast Fourier transform*, Vol. 10, Siam.

Conclusions and perspectives

Elastography techniques have raised a growing interest in clinical applications for soft tissue characterisation over the past decades, the tissue stiffness being highly sensitive to structural changes associated with physiological and pathological processes [Sarvazyan et al., 2010; Gennisson, 2003]. In particular, very recent elastographic techniques, like Acoustic Radiation Force Imaging (ARFI) [Nightingale et al., 2003], Shear Wave Elasticity Imaging (SWEI) [Sarvazyan et al., 1998] and Supersonic Shear Imaging (SSI) [Bercoff et al., 2004], are based on the propagation of shear waves, the measurement of which is often referred to as "transient elastography". We can refer to this family of methods by Shear Wave Elastography (SWE). These techniques are based on the use of emitted and back-scattered ultrasounds at a very high frequency to image the propagation of generated shear waves in the tissue. The generation of shear waves is remotely induced by the radiation force of an acoustic pulse, and this phenomenon is called Acoustic Radiation Force (ARF). Then, the mechanical properties of the medium are retrieved from the velocity of propagation of the generated shear wave at a very fine scale, using inverse problem strategies.
Experimental studies such as those presented in [Couade et al., 2011; Correia et al., 2017; Lee et al., 2012; Papadacci et al., 2012; Pernot et al., 2011, 2016] show the potential of the extension of transient elastography to cardiac imaging. This opens new perspectives in the patient-specific monitoring of the mechanical properties of the myocardium, and can potentially yield qualitative and quantitative informations on several pathologies, helping medical doctors in the definition of an accurate and reliable diagnosis.

The objective of this thesis was the development of a rigorous mathematical and numerical background for the extension of this new transient elastography modality to the cardiac setting. This interest was also justified by the fact that, to our knowledge, there is no study in the applied mathematics literature of this methodology for application to the myocardium. This is due to the fact that accurate and realistic mechanical models for the heart deformation are relatively new [Chapelle et al., 2012], and are of fundamental importance to define an appropriate modeling framework for the elastic wave propagation. Moreover, a major challenge is associated with the fact that, even though all the physical phenomena (heart contraction, ultrasound and shear wave propagation) can be derived from the governing equations of the underlying nonlinear mechanics of the heart deformation, they take place at different time scales, and the linearisation must be performed around the deformed (prestressed) state of the tissue.

In the recent years, several models of SWE have been developed, mostly oriented toward the applications. As a consequence, these models are based on simplifying assumptions on the constitutive law of the medium and the source term resulting from the ARF, and ready-made softwares were used for the Finite Element simulations. On the contrary, our approach is more methodological. In more detail, the aim of this work was to study the elastic (pressure and shear) propagation generated by an impulsive source in the beating heart and propose new mathematical modeling and adapted numerical strategies for the efficient simulation of an SWE experiment, taking into account the involved multi-scale and multi-physics phenomena. Furthermore, we aimed at deriving an accurate expression of the source term corresponding to the ARF. Among the intrinsic difficulties related to our problem, we needed to take into account the underlying nonlinear mechanics of heart contraction (passive and active stress) and the fact that the heart tissue is heterogeneous, nearly-incompressible and viscoelastic. To do so, we also focused on the development of novel scientific computing strategies for incompressible elastodynamics.
The main achievements of this thesis can be categorised into the following two topics.

1. Mathematical modeling.

- We have proposed a **novel methodological approach to characterise elastographic shear wave propagation** for a general constitutive behaviour of the myocardium, starting from an accurate biomechanical model of the heart. In addition, we have studied the contribution of active stress on the elastographic wave propagation, and we have demonstrated that it is dominated by the prestress effect. Furthermore, we have applied this approach to the biomechanical heart model [Chapelle et al., 2012], and we have compared some detailed results with published experimental measurements.

- We have derived an **original mathematical model of the acoustic radiation force phenomenon**. We emphasize that the proposed model dispenses with the simplifying hypotheses that are usually made on the properties of the solution (e.g. plane wave assumption). In greater detail, based on asymptotic analysis, we have derived the governing equation of the pressure field and the shear wave field remotely induced by the ARF, and we have computed an analytical expression of the source term responsible for the generation of shear waves from an acoustic pressure pulse. As a by-product of our analysis, we have shown that it is associated with the viscosity and the tissue nonlinearities. In addition, we have derived a proof of convergence of the approximation of solution in a quasi-static linear configuration.

2. Numerical approximation.

- We have developed a **novel numerical scheme suitable for approximating elastic wave propagation in incompressible media**, based on a mixed explicit/implicit time discretisation. We have demonstrated that the time step of the resulting algorithm is only constrained by the shear wave velocity (unlike fully-explicit time schemes). Furthermore, our algorithm only entails at each time step one resolution of a scalar Poisson problem and few matrix-vector multiplications for the explicit part of the scheme. Additionally, we have shown that more accurate approximations of the purely incompressible problem can be retrieved by post-processing of the solutions obtained with the scheme. Moreover, we have presented a two-dimensional numerical test case, to demonstrate the favourable convergence properties of the scheme, and one three-dimensional example, to illustrate a realistic application to elastography imaging. Finally, we have provided a theoretical demonstration of second-order convergence in time of the scheme.

- We have developed a **novel, fast, matrix-free solver for the Poisson problem discretised with High-Order Spectral Element Methods** in simple geometries. We have constructed an efficient implementation of the problem that consists in the resolution of the symbol of the operator in the frequency domain. We have demonstrated that the proposed algorithm can be extended straightforwardly to multiple dimensions and Dirichlet or Neumann boundary conditions, without affecting its efficiency. Furthermore, we have provided numerical evidence that the order of convergence of the underlying HO-SEM discretisation is preserved.

- We have outlined a **three-dimensional mathematical model for the propagation of elastic waves** in a pre-stressed, hyperelastic, viscoelastic, heterogeneous, anisotropic medium, that is also subject to an active stress, under realistic conditions of an SWE experiment. The discretisation in space is based on high-order Spectral

Elements, whereas the novel adapted implicit/explicit time discretisation is used for time discretisation.

These results represent a significant step forward in the **modeling and simulation of transient elastography in the cardiac setting** and, more generally, in the study of **elastic wave propagation in incompressible, anisotropic and heterogeneous media**. Moreover, we have constructed an adapted and efficient numerical framework for problems in incompressible elastodynamics that is prone to numerous applications, apart from transient elastography. However, numerous aspects can still be tackled and improved in this topic, of course, both from the modeling and from the numerical perspective. The main open questions and perspectives can be summarised in the following aspects:

- Further investigate the quasi-static assumption that is performed to decouple pressure and shear waves. In more detail, the end-goal of this work is to study when the principle of limiting amplitude takes place, i.e. when it is reasonable to consider that, at every time of the slow time scale, it is possible to solve a Helmholtz equation associated with the fast time scale of the pressure field.

- Compare the exact term accounting for the ARF that has been derived in this work with the approximation of this source term by a volumic body force that is usually considered in the literature [Palmeri et al., 2005], in order to analyse the effect of this approximation on the propagation of the shear waves.

- Simulate an SWE experiment under realistic conditions. Moreover, we aim at considering the effect of more complex viscous laws in the propagation of shear waves. In this work, we have considered a Zener model, but other choices could be considered. Note also that a further complexity is represented by the assumption of a prestressed medium. One of the end-goals would be to validate the model against in vitro and in vivo experiments.

Furthermore, in the perspective of a realistic application to SWE elastographic reconstruction, further aspects should be tackled:

- The construction of efficient solvers for the inversion of the high-order discrete Laplace operator (required in the proposed scheme for incompressible elastodynamics) in case of non-simple geometries. A possible solution could be represented by hierarchical solvers [Börm et al., 2003] in order to perform an adequate preconditioning in the iterative inversion of the Laplace operator.

- The truncation of the computational domain. Due to the full attenuation of shear waves in a few millimetres, it is reasonable to consider a small region of interest. For the moment, we assume transparent boundary conditions everywhere except for the surface where the probes are located. However, it would be of interest to extend some existing methods, e.g. Perfectly Matched Layers (PML) [Bécache et al., 2003], to incompressible elasticity in prestressed media. Nonetheless, to our knowledge standard PML techniques only work for isotropic elastic media, but fail for general anisotropic media. As a consequence, the proper definition of the specific configuration of the domain (e.g. geometry, heterogeneity, viscosity) and the mathematical analysis of the obtained equations are key-steps to define adapted and stable variants of these techniques. Another approach that could be investigated consists in the extension of the Halfspace Matching Method [Dhia et al., 2018] to anisotropic elastic problems.

- The modeling of the backscattering of the ultrasound waves by small scatterers, that generates the speckle, i.e. the signal that is measured by the probes after

sending an ultrasound wave in the tissue during the imaging modality. This step is crucial, since the speckle is then processed to estimate the shear wave propagation for the elastographic reconstruction. As scatterers can be assumed to be random perturbations of the mechanical parameters of the tissue, the scattering phenomenon could be modelled by means of adapted homogenisation procedures.

- The derivation of advanced and stable inverse problem strategies for the reconstruction of the mechanical properties of the tissue from the backscattered signals. This aspect is a major challenge, due to the intrinsic complexity of the underlying physical phenomena. In particular, the methodology needs to take into account the physical coupling between shear wave propagation and backscattering of ultrasounds that takes place in transient elastography. A possible strategy could be represented by observer-based data assimilation techniques [Moireau and Chapelle, 2011; Chabiniok et al., 2012].

The end-goal is to construct a simulation framework that can allow to measure in silico the outcome of an SWE experiment in a given configuration (e.g. the position of the sensors, the frequency and profile of the excitation), in order to optimise the Signal-to-noise ratio of the experiment, and to apply efficient identification strategies for the parameter reconstruction. That would optimise the existing transient ultrasound elastography techniques and hopefully improve the dissemination of these methodologies in clinical applications.

Bibliography

Bécache, E., Fauqueux, S. and Joly, P. [2003], 'Stability of perfectly matched layers, group velocities and anisotropic waves', *Journal of Computational Physics* **188**(2), 399–433.

Bercoff, J., Tanter, M. and Fink, M. [2004], 'Supersonic shear imaging: a new technique for soft tissue elasticity mapping', *IEEE transactions on ultrasonics, ferroelectrics, and frequency control* **51**(4), 396–409.

Börm, S., Grasedyck, L. and Hackbusch, W. [2003], 'Introduction to hierarchical matrices with applications', *Engineering analysis with boundary elements* **27**(5), 405–422.

Chabiniok, R., Moireau, P., Lesault, P.-F., Rahmouni, A., Deux, J.-F. and Chapelle, D. [2012], 'Estimation of tissue contractility from cardiac cine-MRI using a biomechanical heart model', *Biomechanics and modeling in mechanobiology* **11**(5), 609–630.

Chapelle, D., Le Tallec, P., Moireau, P. and Sorine, M. [2012], 'An energy-preserving muscle tissue model: formulation and compatible discretizations', *International Journal for Multiscale Computational Engineering* **10**(2), 189–211.

Correia, M., Podetti, I., Villemain, O., Baranger, J., Tanter, M. and Pernot, M. [2017], 'Non-invasive myocardial shear wave elastography device for clinical applications in cardiology', *IRBM* **38**(6), 357–362.

Couade, M., Pernot, M., Messas, E., Bel, A., Ba, M., Hagege, A., Fink, M. and Tanter, M. [2011], 'In vivo quantitative mapping of myocardial stiffening and transmural anisotropy during the cardiac cycle', *IEEE transactions on medical imaging* **30**(2), 295–305.

Dhia, A.-S. B.-B., Fliss, S. and Tonnoir, A. [2018], 'The halfspace matching method: A new method to solve scattering problems in infinite media', *Journal of Computational and Applied Mathematics* **338**, 44–68.

Gennisson, J.-L. [2003], Le palpeur acoustique: un nouvel outils d'investigation des tissus biologiques, PhD thesis, Université Pierre et Marie Curie-Paris VI.

Lee, W.-N., Pernot, M., Couade, M., Messas, E., Bruneval, P., Bel, A., Hagege, A. A., Fink, M. and Tanter, M. [2012], 'Mapping myocardial fiber orientation using echocardiography-based shear wave imaging', *IEEE transactions on medical imaging* **31**(3), 554–562.

Moireau, P. and Chapelle, D. [2011], 'Reduced-order Unscented Kalman Filtering with application to parameter identification in large-dimensional systems', *ESAIM: Control, Optimisation and Calculus of Variations* **17**(2), 380–405.

Nightingale, K., McAleavey, S. and Trahey, G. [2003], 'Shear-wave generation using acoustic radiation force: in vivo and ex vivo results', *Ultrasound in medicine & biology* **29**(12), 1715–1723.

Palmeri, M. L., Sharma, A. C., Bouchard, R. R., Nightingale, R. W. and Nightingale, K. R. [2005], 'A finite-element method model of soft tissue response to impulsive acoustic radiation force', *IEEE transactions on ultrasonics, ferroelectrics, and frequency control* **52**(10), 1699–1712.

Papadacci, C., Pernot, M., Couade, M., Fink, M. and Tanter, M. [2012], Shear wave imaging of the heart using a cardiac phased array with coherent spatial compound, *in* 'Ultrasonics Symposium (IUS), 2012 IEEE International', IEEE, pp. 2023–2026.

Pernot, M., Couade, M., Mateo, P., Crozatier, B., Fischmeister, R. and Tanter, M. [2011], 'Real-time assessment of myocardial contractility using shear wave imaging', *Journal of the American College of Cardiology* **58**(1), 65–72.

Pernot, M., Lee, W.-N., Bel, A., Mateo, P., Couade, M., Tanter, M., Crozatier, B. and Messas, E. [2016], 'Shear wave imaging of passive diastolic myocardial stiffness: stunned versus infarcted myocardium', *JACC: Cardiovascular Imaging* **9**(9), 1023–1030.

Sarvazyan, A. P., Rudenko, O. V. and Nyborg, W. L. [2010], 'Biomedical applications of radiation force of ultrasound: historical roots and physical basis', *Ultrasound in medicine & biology* **36**(9), 1379–1394.

Sarvazyan, A. P., Rudenko, O. V., Swanson, S. D., Fowlkes, J. B. and Emelianov, S. Y. [1998], 'Shear wave elasticity imaging: a new ultrasonic technology of medical diagnostics', *Ultrasound in medicine & biology* **24**(9), 1419–1435.

université PARIS-SACLAY | École doctorale de mathématiques Hadamard (EDMH)

Titre : Modélisation mathématique et simulation numérique de la propagation d'ondes élastiques dans les tissus mous avec application à l'élastographie cardiaque

Mots Clefs : propagation d'ondes élastiques – élastographie impulsionnelle – sciences de la vie – simulation numérique – informatique scientifique

Résumé : Les objectifs de cette thèse sont la modélisation mathématique et la simulation numérique de l'élastographie impulsionnelle basée sur la force de radiation acoustique (FRA) dans un tissu mou précontraint, et en particulier le myocarde. La première partie du manuscript concerne la modélisation mathématique de la FRA, la propagation d'ondes de cisaillement qui en résulte et la caractérisation de la vitesse des ondes de cisaillement pour une loi de comportement générale du tissu myocardique. Nous montrons aussi des applications pour l'estimation de l'orientation des fibres cardiaques dans le myocarde et l'évaluation de "pathologies synthétiques ". Une des contributions principales de ce travail est le développement d'un modèle mathématique original de la FRA. En particulier, à partir d'un modèle biomécanique tridimensionnel du coeur, nous obtenons, à travers une approche asymptotique, les équations qui régissent les champs de pression et de cisaillement induits par la FRA. De plus, nous calculons une expression analytique du terme source responsable de la génération des ondes de cisaillement à partir d'une impulsion acoustique en pression. Dans la deuxième partie de la thèse, nous proposons des outils numériques efficaces pour une simulation numérique réaliste d'une expérience d'élastographie impulsionnelle dans un tissu quasi-incompressible, précontraint et fibré. La discrétisation en espace se base sur des éléments finis spectraux d'ordre élevé. Pour la discrétisation en temps, nous proposons une nouvelle méthode adaptée à l'élasticité incompressible. En particulier, seuls les termes correspondant à des vitesses infinies, associés à la contrainte d'incompressibilité, sont traités implicitement, à travers la resolution d'un problème de Poisson à chaque pas de temps de l'algorithme. En outre, nous proposons une nouvelle méthode d'ordre élevé et efficace pour la résolution d'un problème de Poisson, qui se base sur la transformée de Fourier discrète.

Title : Mathematical modelling and numerical simulation of elastic wave propagation in soft tissues with application to cardiac elastography

Key words : elastic wave propagation – Shear Wave Elastography – life sciences – numerical simulation – scientific computing

Abstract : This PhD thesis concerns the mathematical modelling and numerical simulation of impulsive Acoustic Radiation Force (ARF)-driven Shear Wave Elastography (SWE) imaging in a prestressed soft tissue, with a specific reference to the cardiac setting. The first part of the manuscript deals with the mathematical modelling of the ARF, the resulting shear wave propagation, and the characterisation of the shear wave velocity in a general constitutive law for the myocardial tissue. We also show some applications to the extraction of fibre orientation in the myocardium and the detection of "synthetic pathologies". One of the main contributions of this work is the derivation of an original mathematical model of the ARF. In more detail, starting from an accurate biomechanical model of the heart, and based on asymptotic analysis, we infer the governing equation of the pressure and the shear wave field remotely induced by the ARF, and we compute an analytical expression of the source term responsible for the generation of shear waves from an acoustic pressure pulse. In the second part of the PhD thesis, we propose efficient numerical tools for a realistic numerical simulation of an SWE experiment in a nearly-incompressible, pre-stressed, fibered soft tissue. The spatial discretisation is based on high-order Spectral Finite Elements (HO-SEM). Concerning time discretisation, we propose a novel method adapted to incompressible elasticity. In particular, only the terms travelling at infinite velocity, associated with the incompressibility constraint, are treated implicitly by solving a scalar Poisson problem at each time step of the algorithm. Furthermore, we provide a novel matrix-free, high-order, fast method to solve the Poisson problem, based on the use of the Discrete Fourier Transform.